585

CRANFIELD INSTITUTE OF TECHNOLOGY

DEPARTMENT OF FLUID ENGINEERING AND INSTRUMENTATION

PhD THESIS

Academic Year 1984-5

J H MOSLEY

A Study of the Tyre/Road Interface Under Wet Conditions

Supervisor: J R Heritage

February 1985

SUMMARY

This work addresses the problem of tyre tread pattern design for optimum wet grip performance.

A mathematical model of tyre behaviour on wet roads has been developed. This utilizes the finite element method in the representation of tread pattern geometry. The performance of a particular tread pattern is found in terms of the fluid pressures and film thicknesses existing within the contact patch, under wet conditions.

Many modern tread patterns are based on 'blocks', and a computer model has been developed specifically to assist the tyre designer in the design of these blocks for improved wet grip. Numerical results are presented both for complete contact patches and for individual tread blocks. To allow the use of the computer models by the tyre designer, with no specialist knowledge of the finite element method, special purpose mesh generation and plotting programs have been developed.

Experiments have been undertaken whereby the fluid pressures and film thicknesses existing in the tyre contact patch have been measured under high speed conditions in the wet. These measurements were made on an indoor testing machine, and the techniques developed can be used in the routine evaluation of tyre wet grip performance. Some results of experiments performed on plain and simple patterned tyres are presented.

The main purpose of this work was the development of the mathematical models which can be used for future research into, and design of, tyres for improved wet grip. However, some conclusions are made as to possible features which could be utilized in future tyre designs.

ACKNOWLEDGEMENTS

As this was a Total Technology PhD (hence the inclusion of Chapters 2 and 7), a support panel was used to monitor its progress. The following people contributed to the activities of the support panel :-

Professor R.C. Baker Dr. J.R. Heritage Dr. K. Enever	Dept. of Fluid Engineering and Instrumentation.
Mr. B. Fielden Mr. J. Mapes	Cranfield School of Management.
Dr. C.W. Barson Dr. J.C. Walker	SP Tyres UK Limited.

I would like to thank SP Tyres UK Limited (formerly part of Dunlop Limited) for employing me during the period of this research.

I am indebted to my supervisor Dr. J.R. Heritage for his advice and support during the research, and also for his thorough reading and constructive criticism of this thesis, whilst in draft form.

Thanks are due to Professor R.C. Baker for making available facilities within the Department of Fluid Engineering and Instrumentation, and also for his enthusiastic chairing of support panel meetings. I would also like to thank any other members of the Department of Fluid Engineering and Instrumentation and of the British Hydromechanics Research Association, who have contributed to this work in any way.

Acknowledgements are also due to Mr. J. Mapes and the late Mr. B. Fielden for their advice and assistance with the non-technical aspects of this work.

I would like to thank all members of Tyre Research and Indoor Tyre Testing Departments, and any other members of the Tyre Technical Division of SP Tyres UK Limited who have contributed to this work in any way. Particular thanks are due to Dr. C.W. Barson, Dr. J.C. Walker and Dr. A.R. Williams for their help and advice during this work.

The funding for this project was provided jointly by SP Tyres UK Limited (formerly part of Dunlop Limited), and the Science and Engineering Research Council.

The opinions, findings and conclusions expressed in this thesis are those of the author and not necessarily those of SP Tyres UK Limited.

CONTENTS

FIGURES

NOTATION

The following list (which is not comprehensive) gives the most common usage of variables. Where other meanings are used they are explained at the appropriate point in the text.

Symbol	Description	Dimensions
A	(element) Area	L^2
d	Road surface water depth	L
E	Tread elastic modulus	$M\ L^{-1}\ T^{-2}$
E'	Tread effective elastic modulus	$M\ L^{-1}\ T^{-2}$
E_s'	Tread effective elastic modulus in semi-infinite model	$M\ L^{-1}\ T^{-2}$
F	Force	$M\ L\ T^{-2}$
F_F	Groove flow factor	-
$\{F\}$	Global force vector	-
$\{F_L\}$	Local force vector	-
g	Acceleration due to gravity	$L\ T^{-2}$
h	Fluid film thickness	L
h_i	Inlet fluid film thickness	L
h_o	Outlet fluid film thickness	L
H_1, H_2, H_3	Fluid film thickness at local nodes 1,2 and 3	L
I	Integral formed by variational principle	-
I_E	Integral formed by variational principle for one element only	-
i,j,k	Local node numbers	-
$[K]$	Global stiffness matrix	-
$[K_L]$	Local stiffness matrix	-
L	Contact patch length	L
L_A	Additional length at front of contact patch	L
N_1, N_2, N_3	Area co-ordinates	-
p	Fluid pressure	$M\ L^{-1}\ T^{-2}$
P_i, p_i	Inlet fluid pressure	$M\ L^{-1}\ T^{-2}$
P_o, p_o	Outlet fluid pressure	$M\ L^{-1}\ T^{-2}$

Symbol	Description	Dimensions
P_1, P_2, P_3	Fluid pressures at local nodes 1,2 and 3	$M\ L^{-1}\ T^{-2}$
$\overline{p}$	Non-dimensional fluid pressure	-
$\{p\}$	Column vector of unknown fluid pressures	-
Q	Volume flow rate	$L^3\ T^{-1}$
q	Volume flow rate per unit width	$L^2\ T^{-1}$
r_r	Tyre rolling radius	L
Re	Reynolds number	-
s	Tyre slip	-
S	Boundary of the domain	-
U,u	Velocity (road speed from Browne)	$L\ T^{-1}$
$\overline{U}$	Mean flow velocity	$L\ T^{-1}$
V	Velocity	$L\ T^{-1}$
V_x	Velocity in the x direction	$L\ T^{-1}$
V_y	Velocity in the y direction	$L\ T^{-1}$
V_h	Velocity in the -h direction	$L\ T^{-1}$
V_s	Slip velocity	$L\ T^{-1}$
V_{ROAD}	Vehicle road speed	$L\ T^{-1}$
W	Load carrying capacity	$M\ L\ T^{-2}$
$\overline{W}$	Non-dimensionalload carrying capacity	-
x	Co-ordinate axis (front to rear of contact patch)	-
y	Co-ordinate axis (across width of contact patch)	-
z	Co-ordinate axis (normal to contact patch - also known as 'h' axis)	-
δ	Tread surface deflection (damping factor in section 4.5.4)	L
ρ	Water density	$M\ L^{-3}$
ϕ	Tyre slip angle	-
μ	Water dynamic viscosity	$M\ L^{-1}\ T^{-1}$
ν	Poisson's ratio	-
ω	Angular velocity	-

CHAPTER 1 - INTRODUCTION AND LITERATURE REVIEW

1.1 INTRODUCTION

Wet grip refers to the study of tyres operating on wet roads. There are, therefore, three component parts:-

The Tyre.
The Road.
The Water in the Tyre/Road Interface.

This work is mainly concerned with the tyre and its interaction with the water.

When a vehicle is moving along the road in the wet, there will always be some penetration of water into the tyre/road contact patch (or contact area) which is the part of the tyre flattened into contact with the road due to loading from the vehicle. This water penetration reduces the friction level between the tyre and the road, and the object of improving wet grip is to minimise this reduction in friction level. Friction is caused by the tyre tread surface interacting with road surface asperities. A road surface can be characterised by its microtexture and macrotexture levels, which are defined thus: (see figure 1.1.1).

Macrotexture - is the characteristic which determines the bulk water drainage capability of the road surface.

Microtexture - is the characteristic which determines the magnitude of the frictional force generated at the tyre/road surface interface.

This work is concerned with the amount of water and the fluid pressures existing between the tyre and the road surface. Therefore, friction levels are not considered and macrotexture is the only road surface property of importance in this work.

SURFACE	MACROTEXTURE	MICROTEXTURE
	OPEN	HARSH
	OPEN	POLISHED
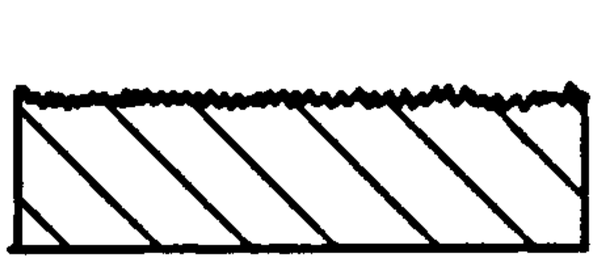	SMOOTH	HARSH
	SMOOTH	POLISHED

FIGURE 1.1.1 - ROAD SURFACE
MACROTEXTURE & MICROTEXTURE

Similarly, there are two tyre properties which determine the wet grip level; namely, tread pattern geometry and tread compound. The tread pattern geometry determines the bulk water drainage capability of the tyre and is analogous to the macrotexture of the road surface. The tread compound determines the level of friction between the tyre and road surface and is analogous to the road surface microtexture. As friction levels are not being considered in this work, then tyre tread compound effects will also not be considered.

The two features which govern the amount of water penetration into the contact patch are, therefore, the tyre tread pattern geometry and the road surface macrotexture.

The purpose of this work (see Chapter 2) was to produce a computer model which could be used at the design stage to assist in the development of tyres with improved wet grip. Detailed geometry of individual road surface macrotextures need not, therefore, be considered, and the road surface is characterised by its overall drainage capacity only.

The tyre tread pattern requires to be modelled in terms of its geometry and groove depth. The depth of grooves in tyre tread patterns has a very large effect on wet grip levels as shown in figure 1.1.2(2), where the effect of reducing groove depth on peak brake force co-efficient is shown. It can be seen that at higher speeds, the level of braking obtainable on tyres worn to the legal limit (1mm) is only approximately 25% of that of a new tyre. Whilst the data for figure 1.1.2 were obtained on a smooth macrotextured surface (such as worn concrete), therefore exaggerating the effect of tyre tread pattern, the results still show the importance of a tread pattern performing as well as possible, particularly when worn. They also illustrate the case for an increase in the legal minimum tread depth.

It would not be possible however to raise the legal minimum tread depth to the level needed to maintain an acceptable level of brake force coefficient on smooth road surfaces as this would mean a minimum tread depth of at least 4mm.

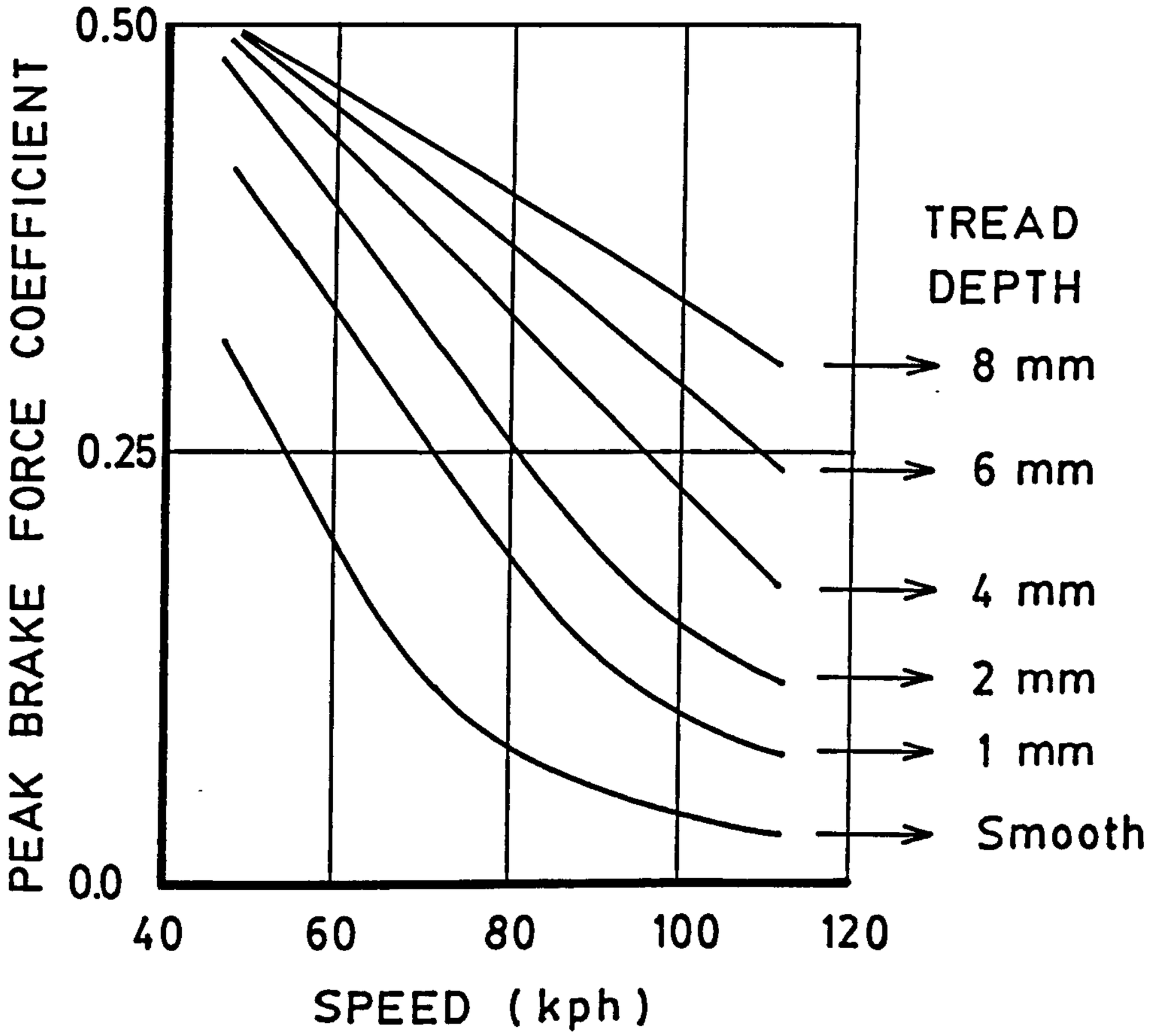

FIGURE 1.1.2 - THE EFFECT OF TREAD PATTERN DEPTH ON PEAK BRAKE FORCE COEFFICIENT ;IN THE WET

Whilst this would be a boost to tyre sales, it is unlikely to happen; therefore, it is important that road surfaces can provide an adequate amount of texture. Some work has been performed in the past within Dunlop on the development of a road surface which has a good macrotexture and a microtexture which resists polishing. The practical value of this is limited by the need to resurface large amounts of the country's roads. Therefore, improvements to the tyre tread pattern have a much larger potential for the improvement of wet grip levels than do improvements to road surfaces.

1.2 LITERATURE REVIEW

The areas of interest for this project can be split into three distinct groups:-

1. Tyre Wet Grip
2. Fluid Mechanics
3. The Finite Element Method

The literature reviewed can also be split this way, and it is convenient to consider each area separately.

1.2.1 Tyre Wet Grip

There is much published literature on tyre wet grip, but a large portion of it is not of direct relevance to the current project, being primarily concerned with the testing of specific tyres under specific conditions. To allow a mathematical model of the tyre/road interface under wet conditions to be developed, an understanding of the fundamental behaviour of tyres under wet conditions is required and it is literature that deals with this that is concentrated on.

The behaviour of the tyres on wet roads was noted in the mid-1960's (1). A range of peak brake force coefficients for the extreme cases of smooth and new patterned tyres and road surfaces with open macrotexture/harsh microtexture and smooth macrotexture/polished microtexture are shown in figure 1.2.1(2). The contribution that the tread pattern makes to the overall wet grip level can be seen. The tread pattern used to obtain these results was based on longitudinal ribs, and a modern tyre with a block tread pattern would probably show a greater contribution to the overall wet grip level due to the tread pattern.

A common method used for the visualisation of tyre behaviour under wet conditions is the three zone concept. This is discussed in (1) and in the much more recent paper by Moore (3). Figure 1.2.2 shows a diagrammatic representation of this concept and the three zones are defined thus:

Zone 1 - Sinkage or Squeeze-Film Zone

The forward part of the contact patch is completely separated from the road surface by a film of water, the thickness of which decreases as individual tread elements pass further into the contact patch. When the tyre is rolling freely on the road surface, the water is squeezed, due to the action of load on the contact patch.

Zone 2 - Draping or Transition Zone

The film thickness in this zone is very small and the tyre tread elements are starting to drape over the major asperities of the road surface. The larger asperities make contact with the contact patch.

1——1 SURFACE: Open macrotexture, harsh microtexture
TYRE: Patterned (new)

1- - -2 SURFACE: Open macrotexture, harsh microtexture
TYRE: Plain tread

2——3 SURFACE: Smooth macrotexture, polished microtexture
TYRE: Patterned (new)

3- - -4 SURFACE: Smooth macrotexture, polished microtexture
TYRE: Plain tread

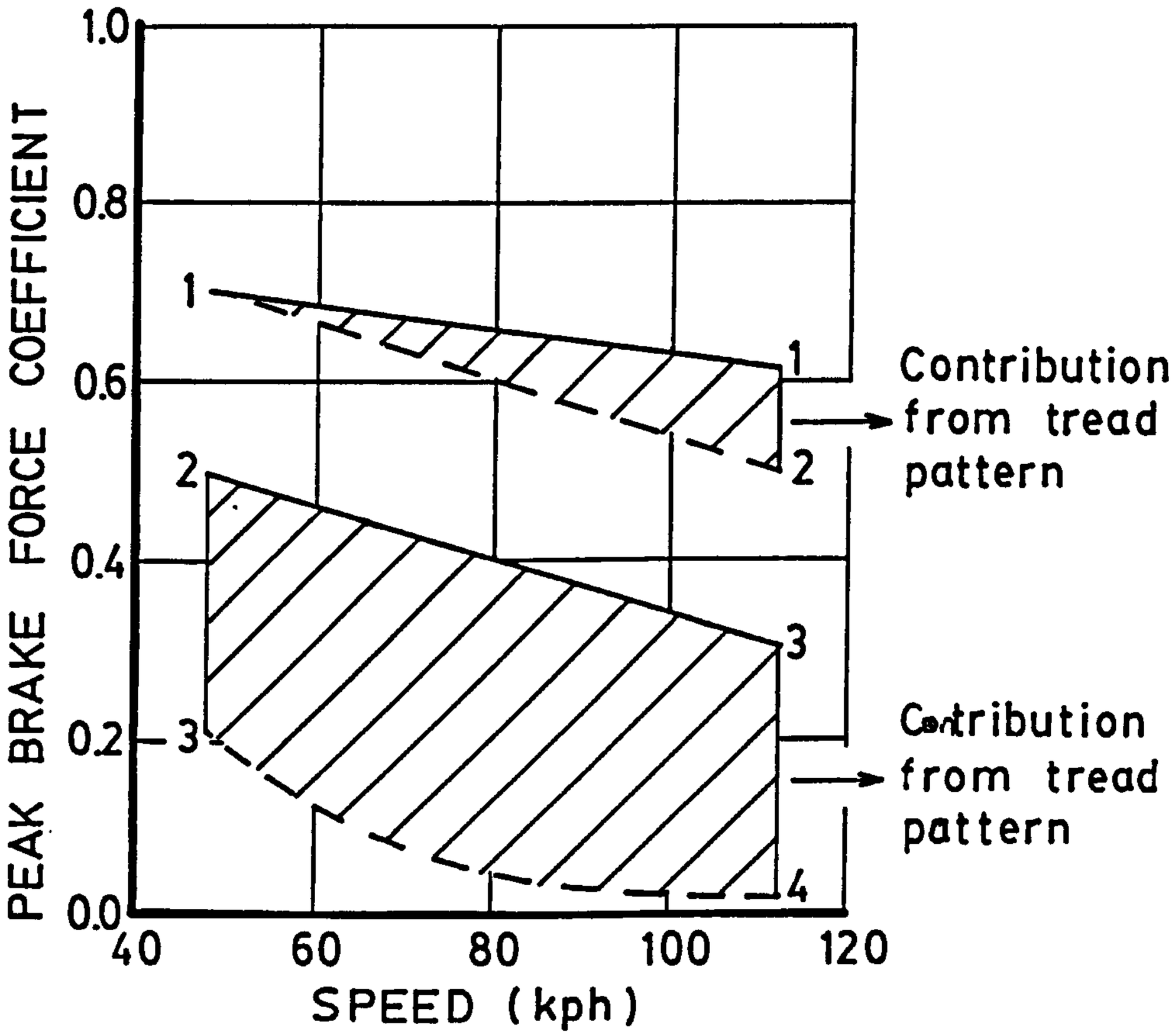

FIGURE 1.2.1 - FRICTION LEVELS ATTAINABLE IN THE WET

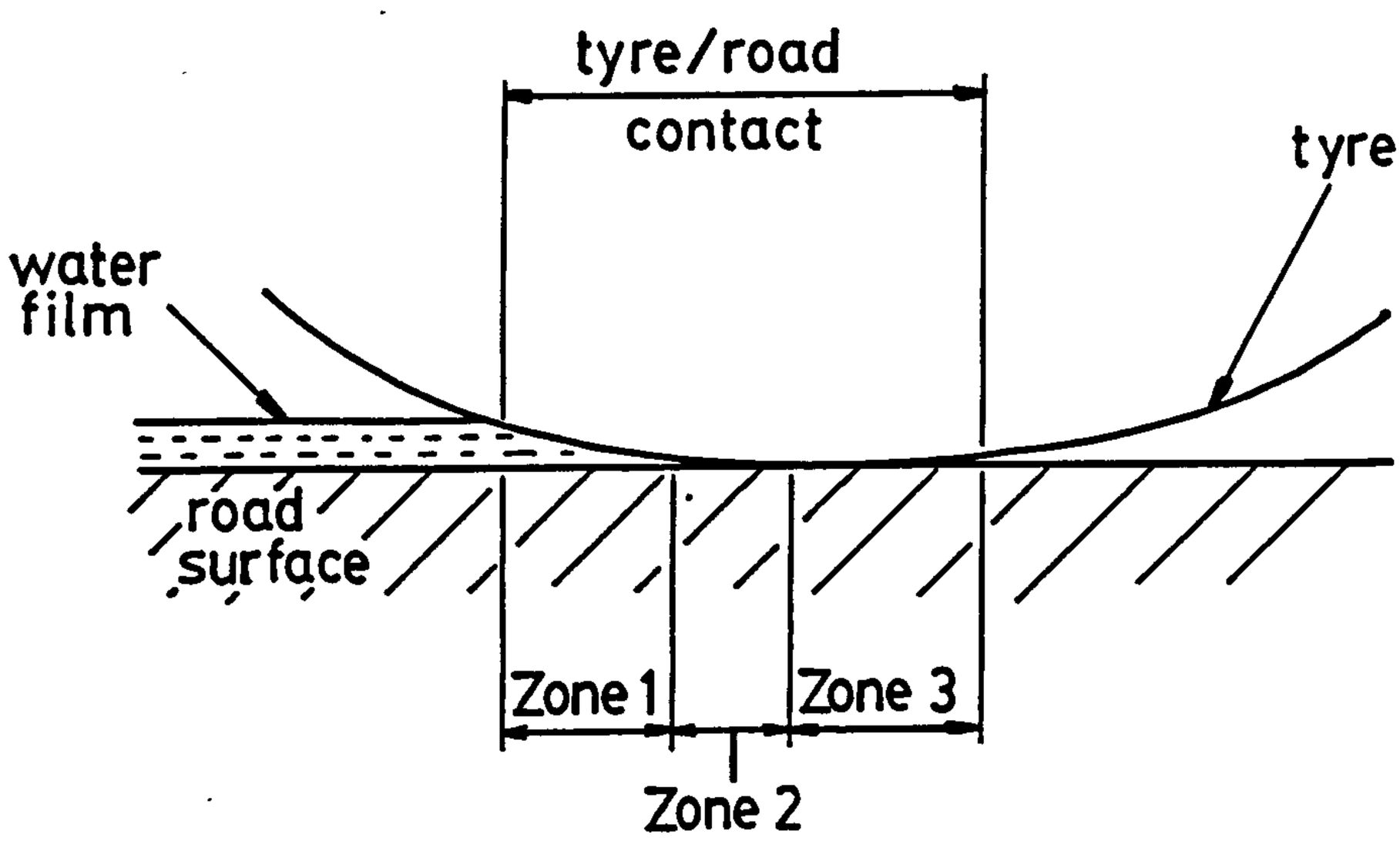

FIGURE 1.2.2 - THE THREE ZONE CONCEPT

Zone 3 - Actual Contact or Traction Zone

This is the rearmost part of the contact patch and exists under all conditions, except total aquaplaning. The tread elements are mostly in contact with the road surface and almost all the tyres skid-resistance is developed in this zone.

Gough (4) proposed a similar three zone concept and suggested that the overall coefficient of friction between the tyre and road surface could be expressed as μ_{FRICT} where:-

$$\mu_{FRICT} = \frac{A_1 (a + b) + A_2 (c + b) + A_3 (d + b)}{LOAD}$$

and

A_1 = area of contact of zone 1.

A_2 = area of contact of zone 2.

A_3 = area of contact of zone 3.

a = hydrodynamic drag/unit area of unbroken water film.

b = tyre hysteresis loss/unit area.

c = drag/unit area of partial breakdown of lubricant film.

d = the friction force/unit area of dry contact.

The coefficients a, b and c are small compared to d, thus allowing the assumption that the coefficient of friction is proportional to the area of the contact zone (zone 3). A prediction of the area of actual contact between the tyre and road surface will, therefore, give a relative measure of wet grip friction level.

A number of papers have been presented (e.g. (5) and (6)) which attempt to simplify the tyre/road problem so that an analytical solution can be found. Boness (5) makes the assumption that lateral flow out of the side of the tyre can be neglected. He justifies this on the basis of observations on glass plate photographs. However, Bathelt (6) neglects longitudinal flow through the tyre contact patch on the basis that until complete aquaplaning is achieved, the backward flow of water through the contact patch is prevented by tyre/road contact at the rear of the contact patch.

There is obviously an element of truth in both these statements but this serves to illustrate the importance of treating the flow within the contact patch by a 2-dimensional model.

In (6) Bathelt treats the effect of the road surface texture by using an equivalent water depth based on the polishing depth of the road surface asperities (as per DIN4762). Bathelt concludes that the road surface texture (as represented by a polishing depth) has a very large part to play in determining the overall level of friction. For example, he states that the effect of doubling the road surface polishing depth from 0.15mm to 0.30mm has a much larger effect on the hydroplaning speed than does the doubling of the tyre tread pattern depth from 1mm to 2mm. He also shows that water pockets ("puddles") should be avoided as their effect cannot be counteracted even by new (unworn) tyre tread patterns.

Golden (7) also uses the approach of treating the road surface as an effective water depth. He also treats the tyre as acting as a 'balloon', as does Moore (3). When a 'balloon' model for the tyre is used, the dry contact pressure is assumed equal to the tyre inflation pressure throughout the contact patch. This does not appear to be so, and it is shown in (8) that the contact pressure is higher in the shoulder regions. In chapter 6, some dry contact pressures are presented which clearly show their wide variation at different points within the contact patch.

To allow the development of a mathematical model for tyre wet grip, one must have a method of modelling tyre deformation under the action of the fluid pressure. Browne et al (9) overcome this problem by using an experimentally determined fluid film thickness (from (10)) and assume that this remains constant. The tyre used for the measurement in (10) is plain treaded and the effects of tread pattern are added to the model developed in (9) in a further report (11), also by Browne. The tread pattern is added, basically by superimposing the additional water film thickness at the appropriate points to the thickness gained from (10).

Treating the tyre surface as rigid in this way will severely restrict the value of any results gained. In a later paper (12), Browne has introduced a deflection model into the fluid model developed for (11). This deflection model utilises a full 3-dimensional finite element model for the tyre construction. Browne notes that there are problems with both the stability of this model and with the generation of the finite element model of the tyre structure. Browne in (12) also shows a tyre deflection model based on a semi-infinite elastic half space, but notes that tyre constructional details cannot be modelled by this. A semi-infinite deflection model has also been used by Boness (5).

A paper by Agrawal and Henry (13) concerns itself entirely with the subject of developing a simple tyre deflection model. The method chosen is based on a semi-infinite method and is shown to give close agreement with experimental results from (14), provided appropriate values for the material properties are chosen.

In (13) the elastic modulus of the tyre is found from:-

$$E = \frac{64LR}{\pi(CA)^2}$$

where: CA = contact area length.

L = load per unit width.

R = cylinder (tyre) radius.

This is also proposed in (5) and is originally derived from the theory of Hertz in Timoshenko (15) by considering the contact between an elastic cylinder and a rigid plane. This method of calculating elastic modulus is intended to include the effect of tyre preload (due to both inflation pressure and normal load). This is thought to be a poor way of doing this and an alternative method is proposed in this work.

The above mentioned experimental results for water depth (14) are found by a method utilising capacitance plates inside a tyre and measuring the change in capacitance due to tyre deformation. The main disadvantages with a method of this type are: that only locked wheel conditions can be used, the tyre has to be specially modified and, the accuracy of the results must be suspect due to the necessity of subtracting the measured deflection, plus a constant from the measured variable axle height to obtain the actual water film thickness. Other methods of measuring the water film thickness between a tyre and road surface are based on glass plate photographs, such as already discussed (10), where Browne has used a Moiré fringe technique. Moiré fringe techniques are also discussed by Browne in (16) and by Roberts in (17).

From the tests performed by Browne in (10), some very important points can be raised which will have a large effect on the results, and, subsequently, on the work in (9) and (11). Because of problems with the light level reflected from the tyre, Browne used a special tyre with the tread moulded from white sidewall rubber.

The properties of this rubber would be quite different from those of actual tread rubber. The vehicle speed was limited to a maximum of 18.8 m/s for safety; therefore the inflation pressure was chosen to allow total aquaplaning at this speed by applying an approximate formula developed by Horne (18):-

$$V_H = 1.764 \sqrt{p}$$

where V_H is the hydroplaning velocity in m/s and p is the tyre inflation pressure in kilopascals.

The above relationship was determined by Horne for aircraft tyres. Browne used an inflation pressure of 1.3 bar on a H78 - 15 steel-belted bias ply tyre at a load of 591 Kg. A tyre of this size at this load should have an inflation pressure of approximately 2.0 bar (19), and Browne has purposely under-inflated the tyre. The effect of under-inflation is to reduce the contact pressure (and stiffness) in the centre of the contact patch, with a corresponding increase in contact pressure in the shoulder regions. The fluid film thickness resulting from this work is shown in figure 1.2.3. The film thickness in the centre of the contact patch is larger than would be expected at this relatively low speed (68 Kph), and is of the magnitude normally found at 96 Kph. This would seem to be explained by the fact that the tyre was under-inflated. As this fluid film thickness is used as the basis of the work in (9) and (11), the results from these must be treated with a certain amount of suspicion.

A good review of the early work of Browne, and others, can be found in the paper "Mathematical Analysis for Pneumatic Tire Hydroplaning" (20), although the present author would disagree to some extent with the opinions of the usefulness of sipes expressed within this publication. If one refers to (1), it is clearly shown that the addition of sipes does improve the level of grip attainable in the wet. The effect of sipes is, however, most noticeable on smooth road surfaces, but also has some beneficial effects on even rough surfaces.

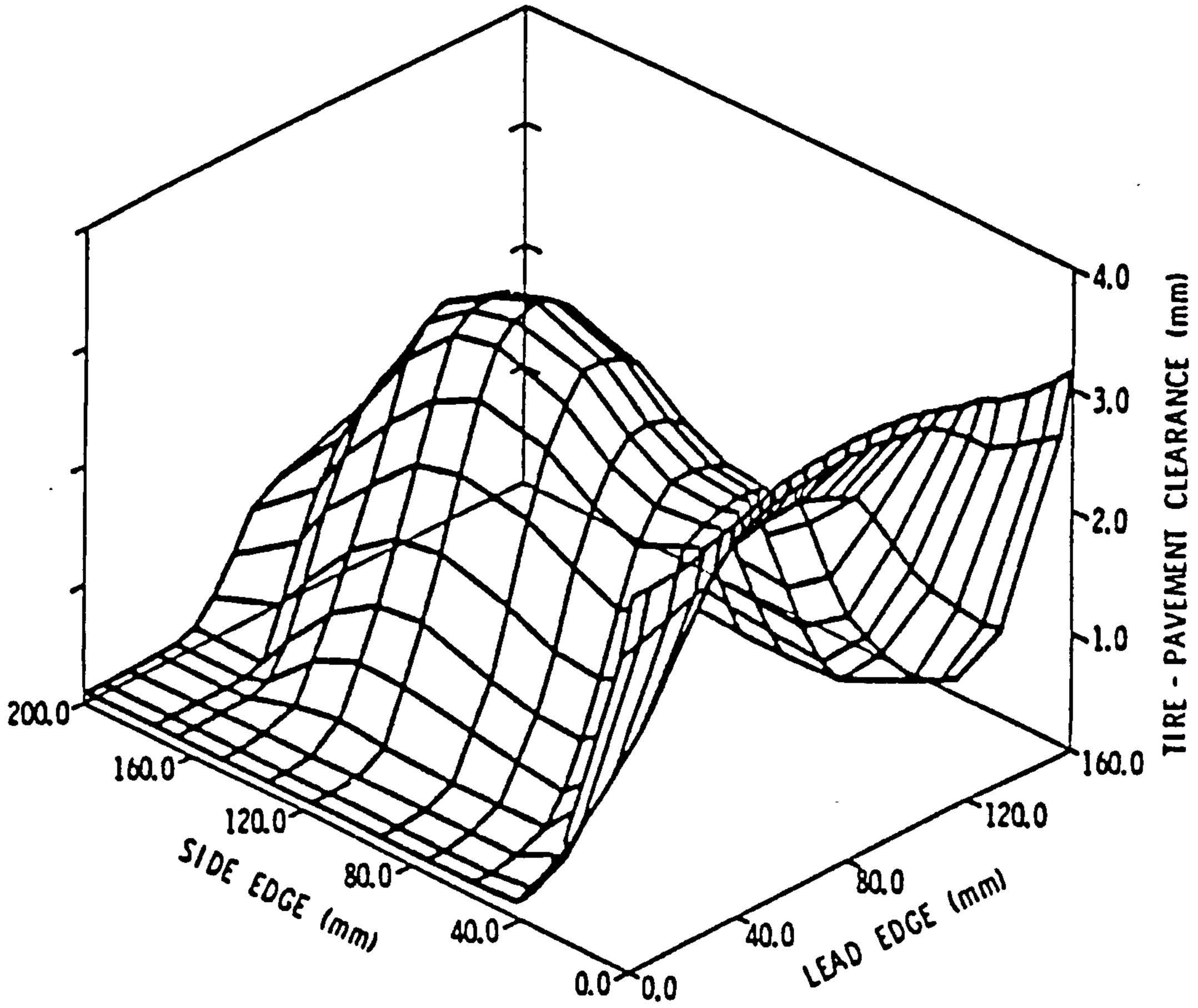

FIGURE 1.2.3 - FLUID FILM SHAPE (from (10))

A paper (21) by Yeager and Tuttle uses a glass plate facility in the study of tyres under wet conditions. In this work a tri-axial load pin was positioned at the lead edge of the glass plate and a photograph taken to record the position of the tyre as it passed over the load pin. Unfortunately, the results presented for the interfacial fluid pressure are for a specific ribbed tyre which makes it difficult to draw general conclusions.

Another method of using a glass plate facility is to add fluorescent dye to the water so that the fluid film between the tyre and the glass plate will be visible. A fairly commonly stated fact is that the water film thickness can be determined from photographs taken under such conditions. Some work has been undertaken to improve this technique (22) and is discussed later.

If one is to produce a mathematical model of the tyre contact patch under wet conditions, then the choice of fluid boundary conditions becomes an important one. Browne in (9) has produced a thorough discussion of this. At both the side edges and rear of the contact patch, Browne proposes a pressure boundary condition of $p = 0$ (atmospheric), whilst the pressure is assumed to be symmetrical about the tyre centre line. The last assumption restricts the type of tread patterns which may be modelled, but will suffice for many simple patterns. The front edge of the contact patch, is, however, more difficult to specify a boundary condition for.

Browne proposed two treatments:-

Treatment 1 - $V_x = U$ and $p = 0$ implies that all fluid in the path of the tyre passes through the lead edge of the contact patch.

Treatment 2 - $V_y = 0$ $p = \frac{1}{2}\rho (U^2 - V_x^2)$ corresponds to no side flow and a pressure determined by Bernoulli's equation.

There seems to be some contradication in these two treatments. Treatment 1 states that all the fluid in the patch of the tyre enters the lead edge of the contact patch. Therefore, there can be no side flow actually at the front edge (although there may be side flow just inside the front of the contact patch) and Treatment 2 also seems to state the same($V_y = 0$), yet the pressures are specified differently in the two cases. A method is proposed in the present work which allows the pressure of the leading edge of the contact patch to be determined by flow boundary conditions.

Browne, with others (23) and (24), has undertaken some work investigating the properties of individual tyre tread elements. (23) considers only rectangular tread elements, whilst (24) considers both rectangular and circular tread elements. Two further papers have been published by the same authors (25) and (26) which cover the same work, but are directed at the more general case of elastohydrodynamic squeeze films rather than specifically at tyre tread elements.

As this work concerns itself only with simple shapes, no direct evaluation of actual tyre tread elements was performed, although a few general conclusions about elast ohydrodynamic squeeze films were made.

The pressure distribution of a rigid tread element and that of a flexible tread element are compared in (23), and it is shown that the flexible tread element gives a more uniform pressure distribution.

In (25), the pocket of water trapped as a flexible element approaches the rigid surface, is shown, and the significance of this to tyre wet grip is discussed in (24). The contact between the tread element and the road surface will be established sooner with a flexible element rather than with a rigid element, but this contact will only be around the perimeter of the tread element. There must, therefore, be sufficient road surface macrotexture to allow this trapped pocket of water to escape to allow full contact between the tread element and the road surface.

In (24), a comparison is also made between a rectangular tread element and a circular tread element with the same surface area.

From the curves presented in (24), it can be seen that the time to contact is slightly increased in the case of the circular tread element. However, the most important feature of changing to a circular tread element is that the maximum pocket depth at the time of contact (at the element edge) is substantially increased, as shown.

	Time to Contact	Max. Pocket Depth
SQUARE 19.1 x 19.1	0.612	0.519
CIRCULAR rad. 10.8	0.637	0.657

Browne and Whicker suggest that it is due to a circular tread block simultaneously contacting with the road surface at all points on its perimeter, whilst the square tread element will have its sides bowed and only contact the road surface at the corners. When acting on an actual road surface with macrotexture, there will be no sealing action by the circular block. However, the greater pocket depth may mean that it takes longer for the circular block to clear all the water from the tyre/road interface.

Browne and Whicker in (24) also show the effect of different road surface asperities on the minimum film thickness for square tread elements.

The experimental techniques so far discussed have, with the exception of (14), been based on outdoor testing facilities. Indoor testing, again with the exception of (14), tends to be concerned with the measurement of overall tyre properties, such as braking or cornering forces. A description of a typical machine of this type is given in (27).

Indoor tyre testing machines tend to be based on one of three principles: Internal Drum, External Drum, or Flat Belt. The Calspan machine (27) is of the latter type. The advantage of a flat belt tester is that no errors are introduced due to the effects of drum curvature. The main disadvantage of this type of machine is that it is not possible to test tyres on realistic road surfaces. This is because of the need for the belt to flex as it passes around the two drums; see Fig. 1.2.4(a).

The internal drum type machine (figure 1.2.4(b)), as described in (28), can be used for wet grip testing and has the principal advantage that real road surfaces can be utilised. On an external drum (figure 1.2.4(c)) (1), it is only possible to use fibre glass replica surfaces because the centrifugal force acting on the surface would tend to throw the stones out of the surface. On the internal drum machine, centrifugal force acts to put the road surface in compression. Therefore, real surfaces can be used with safety. Internal drums also have the advantage that only a low flow rate of water is required to maintain a given water depth in front of the tyre, in contrast to the external drum (and flat belt) machine where a large flow of water is required to compensate for the water thrown off the drum by centrifugal force.

Another area of work which is relevant to tyre wet grip, is that of road surface texture measurement. If the effect of road surface texture is to be included as an effective water depth as in (6) and (7), then some measurement of this depth needs to be made on various road surfaces. The use of a so called "outflow meter" is described by Henry and Hegmon (29). The outflow meter is based on loading a rubber ring against the road surface and measuring the length of time for a fixed volume of water to flow from the inside to the outside through gaps between the road surface and the rubber. Some outflow meters, such as the one in (30) are only lightly loaded onto the road surface. The mean contact pressure of a car tyre is approximately 0.3 N/mm^2, (based on measurement of the

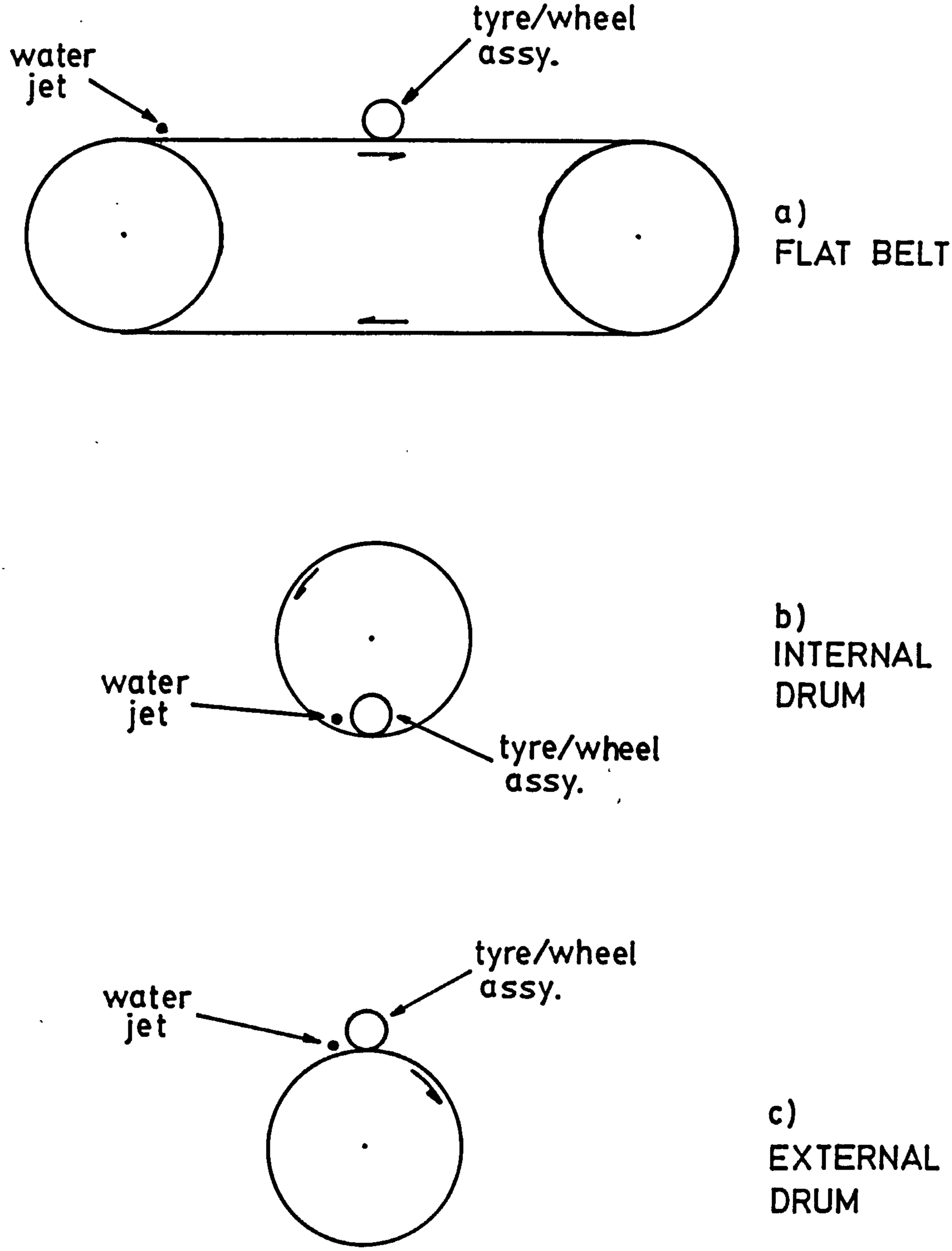

FIGURE 1.2.4 - ALTERNATIVE ARRANGEMENTS FOR TYRE WET TESTING MACHINES

actual 'land' area in the tyre contact patch), and the outflow meter used in (30) has a contact pressure of only 0.012 N/mm^2. This means that the outflow meter tends to 'sit' on the top of the road surface asperities and allow drainage much easier than below a tyre contact patch. The outflow meter used in (29) was loaded to 0.14 N/mm^2 which is still rather low, but should give some realistic results. Also in (29), the water is pressurised to reduce the out flow time. This will tend to cause the rubber to deform and further reduce the outflow time and introduce an error in the method. From the outflow time and making some assumptions about the viscosity of the water, the effective water depth (mean hydraulic radius) can be found from (33).

$$h = \sqrt[3]{\frac{6\mu Q \ln(r_o/r_i)}{\pi P_i}}$$

where h = effective water depth

Q = volume flow (volume/out-flow time)

μ = water viscosity

r_i = rubber ring inner radius

r_o = rubber ring outer radius

P_i = pressure applied to water in outflow meter.

Effective water depths calculated from the data of Henry and Hegmon (29) range from 0.35mm to 1.3mm, depending on the road surface, but for the reasons described above these are probably high.

In both (29) and (30), there seems to be some attempt to correlate out'fow meter results with friction levels (skid resistance). As the outflow meter only measures road surface macrotexture and not microtexture, then a prediction of friction level cannot be possible by use of the outflow meter alone. In the present work and that of Bathelt (6), the effective water depth for the road surface is only being used as a measure of the road surface's drainage capacity and not its friction level.

1.2.2 Fluid Mechanics

The fluid mechanics background for this work falls into the areas of hydrodynamic and elast. hydrodynamic lubrication and their application to turbulent fluid films.

Basic thin film lubrication theory (Reynolds equation) is covered in many text books, e.g. (31), (32), (33) and (34), where the derivation from first principles can be found.

Solution of Reynolds equation for all but very simple geometry necessitates the use of a numerical technique. For this reason much work tends to concentrate on the case of one-dimensional flow (side leakage neglected) for which there is an analytical solution. It seems to be generally accepted (33) that in bearings, if the width is at least four times the length, then the effect of side leakage can be neglected with sufficient accuracy. It is clear that the case of tyres on wet roads does not fall into this category and two-dimensional fluid flow will have to be considered.

A number of approximate methods for finding the load carrying capacity of bearings of finite width exist (33) and (35), and these will be discussed in Chapter 4. These methods do not give information on pressure distribution and are only applicable to rectangular slider bearings of certain width to length and inlet film thickness to outlet film thickness ratios. The above work concerns itself only with rigid bearings, but to model a tyre under wet conditions the bearing surface has to be allowed to deform under the action of fluid pressure, the so called elasto hydrodynamic effect. Solutions to the elasto hydrodynamic problem for specific cases of simple geometry can be found in (36), (37) and (38).

The case of a tyre on a road is, as well as being elasto hydrodynamic, preloaded and there seems to be very little literature on this subject. One paper that does cover this subject is (39).

Gupta (39) postulates that because of the interference fit in a preloaded bearing, no fluid flows until a certain pressure is reached, at which point the bearing will instantly lift off and at this point the fluid pressure will be just equal to the preload pressure.

Reynolds equation is generally used for problems where Reynolds Number is low and the flow is laminar. When Reynolds Number is high, the flow will tend to become turbulent. A bearing with water as the lubricant (low Kinematic Viscosity) will, compared to a bearing with oil as the lubricant and the same velocity and dimensions, have a higher Reynolds Number and it is, therefore, more likely to operate in the turbulent regime. A tyre on a wet road can be considered as a water lubricated bearing. A number of papers (40), (41), (42), (43), (44), (45) and (46), concern themselves with the application of Reynolds equation to problems where turbulence is likely.

The basic principle on which all the above papers work, is that the effect of turbulence can be included in Reynolds equation by the use of an "effective" viscosity, which is dependent on the Reynolds Number. The net result of turbulence is, therefore, the same as using a fluid with a greater viscosity, i.e. larger film thickness, high pressure, etc.

In (46), Wilcock examines the special case of designing turbulent thrust bearings, which is fairly close to the model of a tyre on a wet road. Unfortunately, Wilcock concerns himself only with bearings in which side leakage can be neglected (i.e. wide bearings). As has already been discussed, this is not the case for either a tyre contact patch as a whole or an individual tread element. Therefore, the model by Wilcock cannot be used in this case.

The turbulent models developed by different authors concern themselves with either Poiseuille flow, where the flow is due to pressure only, or with Couette flow, where the flow is due to the movement of one of the surfaces (see figure 3.6.1).

Typically, for the case of a tyre under operating conditions on a wet road, the flow will be neither of these extremes, but a combination of the two. Constantinescu (41) suggested a way in which this could be incorporated into a model of turbulent flow. He states that the values found for Couette flow should be used provided that it will give a larger increase in viscosity than there would be by using the Poiseuille values. In other words, the value giving the largest increase in viscosity is used.

The different turbulent lubrication theories are reviewed by Taylor and Dowson (42), where the result of work by Ng and Pan for dominant Couette flow is presented. This is in either graphical or tabular form, but Constantinescu (47) has devised empirical expressions to fit this data. These expressions give separate factors for the flow in two-dimensions and the viscosity in each direction can be multiplied by the appropriate factor. The factors depend only on the Couette Reynolds Number based on sliding velocity. Also presented in the review by Taylor and Dowson (42) is a turbulence factor for dominant Poiseuille flow,which was developed by Constantinescu (41) using data from (40). As there is no relative movement between the surfaces with Poiseuille flow, then the turbulence factor is found from the same equation for both directions and is based on the Poiseuille Reynolds Number utilising mean flow velocity in that direction. In both cases the empirical formulae give close agreement with the graphical results over a very wide range of Reynolds Numbers.

1.2.3 The Finite Element Method

It has already been noted that a numerical solution technique will be required for the solution of Reynolds equation in two-dimensions. At the start of the project the decision to use the finite element method had already been made, and it had been recognised that this type of problem could be solved without any extension to the finite element method.

There are many text books available which cover the finite element method, e.g. (48), (49) and (50) which are typical of these. In the main, text books concern themselves with the application of the finite element method to the solution of structural problems. This is not surprising, as the method was first applied, and is now widely used, for this type of problem. However, text books are now becoming available on other specific applications of the finite element method, such as (51), which deals entirely with the application of finite elements to a solution of the Navier-Stokes equations.

Almost all text books on finite elements present some computer programs, and (52) in particular, is devoted mainly to the practical problems of implementing the finite element method on a digital computer.

If one were developing a finite element model of a structural system, then the information in the above text books would probably be sufficient. However, it was necessary to search the literature for more details on the application of finite elements to lubrication problems.

Two papers by Reddi (53) and (54) use the finite element method to solve incompressible (53) and compressible (54) lubrication problems. In (54), Reddi states that the compressible problem can be handled by an iterative solution to allow for the non-linearity of the equations. In (53), the boundary conditions that apply to lubrication problems are discussed. There are two basic types of boundary conditions available, pressure and flow, and either or none of these may be applied to nodes on the boundary of the domain. Some results are given in (53) which show that the finite element method gives close agreement with the exact solution for a number of simple slider bearing cases.

Reddi notes that the finite element method is initially more difficult to implement than the finite-difference method, but that once a suitable computer program has been developed, the finite element method is simpler to use than the finite-difference method.

Reddi also discussed some of the computational implications of the bandwidth in the matrix of the final system of equations. The variational principle required for the formulation of the basic equations is proved in (53) and is also shown in (55).

The papers (53), (54) and (55), concern themselves with two-dimensional lubrication problems, but (56) develops the method for the solution of one-dimensional problems where analytical solutions are known. Wada et al (56) then show comparisons of finite element solutions with varying numbers of elements with the exact solution. Typical of these is the table below where the pressure in a journal bearing at x = 90 degrees with an eccentricity ratio of 0.2 is shown.

No. of Elements	Exact Sol.	F. Diff. Sol.	F.E. Sol.
2		1.397	1.132
4		1.233	1.170
6	1.176	1.201	1.174
12		1.183	1.176
18		1.179	1.176
24		1.178	1.176
36		1.177	1.176

This illustrates the need to use sufficient elements to ensure an accurate soltuion. It can also be seen that the finite element solution will give accurate results for a much more coarse mesh than the finite-difference solution. For example, the finite element method will give a solution within 0.5% of the exact solution with only 4 elements, where the finite difference method requires 12 elements to achieve the same degree of accuracy.

Wada and Hayashi extended the work from (56) to include finite width (two-dimensional) bearings in (57), and again present results comparing finite element solutions with finite-difference solutions. These show that the finite element solution for finite width bearings can be made with less elements than the finite difference solution, in a similar way to the infinite width bearings in (56).

Part of the work in (57) is with Reynolds equation transformed into an ordinary differential equation, which is applicable when the film thickness changes in the sliding direction only. When the film thickness changes in the direction normal to movement also, the finite element method has to be applied to a partial differential equation. Obviously, for the case of tyres on wet roads, the full partial differential equation has to be solved, as film thickness changes are required in both directions.

Allaire et al (58) presented a paper which was concerned primarily with the size of mesh required to get accurate results in , lubrication problems. They note that by using the mesh with the optimum node positions, and thence minimum number of elements, the amount of computer time (hence cost) to solve the problem will be substantially reduced.

An example is given of a plain journal bearing with a mesh of 4 x 31 nodes which are spaced on a variable grid with the element diagonals aligned with the pressure gradient direction. This gives similar accuracy to a mesh with 5 x 31 nodes on a uniform grid and all the diagonals orientated in one direction. In numbering the nodes to achieve a low bandwidth, Allaire et al numbered the nodes in assending order across the smallest side. Therefore, the above increase in mesh size will also cause an increase of one in the bandwidth. According to Allaire et al, the first solution will require 50 percent less computer time than the second. Therefore, the size of the bandwidth will have a very marked effect on the computer time required. The bandwidth is not only dependent on the size of the problem however, it is also dependant on the node numbering scheme employed, and the work of Allaire et al was intended to be using the minimum bandwidth for the particular mesh size.

The application of the finite element method to elastohydrodynamic problems has been shown by Taylor and O'Callaghan (59) for the case of lightly loaded elastic cylinders. This uses an iterative technique for the simultaneous solution of the fluid and elastic equations. A similar technique is also used by Oh and Huebner (60) and Rohde and Oh (61).

In (61), it is noted that better convergence was found by using higher order interpolation functions (in their case cubic) rather than linear interpolation functions in the finite element formulation.

In using the finite element method to solve any type of problem, one of the main difficulties (and the most time consuming) is the preparation of the numerical input data.

A common way of easing the mesh generation problem, is to use a computer program into which the domain to be represented is idealised as a number of quadrilaterals input by the user. The mesh generation program then sub-divides each quadrilateral into a number of elements as specified by the user. The element sub-divisions can usually be unequal by specified input weighting factors. A simple mesh generation program which uses this method is given in (52). The mesh generation program given in (50) is similar, except that the domain may be sub-divided into triangular regions as well as quadrilaterals.

The use of a mesh generation program, such as those above, significantly reduces the effort required to produce accurate finite element mesh data. However, they still require a relatively large amount of data to define the sub-regions and the density of the mesh required. This sub-dividing method also restricts the type of mesh that can be generated, and Frederick et al (62) in noting this, proposed an alternative method. Their method requires the x-y co-ordinates of each node in the mesh to be specified, along with the material type to allow different materials to be used in the same object. The computer program will then automatically form the mesh by joining points to produce triangles which are as near to equilateral as possible. In this method, there is a problem in defining the boundary, and so called 'ghost' points are formed outside the domain. The elements formed with ghost points are deleted later in the mesh generation process. A large disadvantage with this method is that all the node points have to be specified in terms of their x-y co-ordinates, and although this can be done on a digitising table, it is still a time consuming activity.

The precise position of a node is rarely of importance in finite element analysis (62), particularly if it is in the interior of the domain.

The above methods, particularly the domain sub-dividing method, are most suitable when a mesh is to be produced of a large geometrically simple domain. This allows only a few sub-domains to be used to specify the whole domain. When a more complex (geometrically)domain needs to be meshed, the number of sub-domains that would need to be specified would become prohibitive. In the present context, the tread blocks within the tyre contact patch are complex geometrically and the above methods of mesh generation are not particularly suitable. The method proposed in (62) is similarly thought to be unsuitable in the present context, due to the amount of data the user is required to input to define the x-y co-ordinates of all node points.

The introduction of Computer-Aided-Design (CAD) opens up new possibilities in the generation of meshes for finite element analysis (63). If a CAD system has been used in design, then the necessary geometric information is already stored in the computer and the finite element mesh can be produced without the need for the user to input this data. The user can then concentrate on producing a suitable mesh and can easily display the mesh graphically for checking.

1.3 CONCLUSIONS FROM THE LITERATURE REVIEW

From the information gained in the literature review, a number of conclusions, which will serve to direct the rest of the work, can be drawn.

Whilst there have been a number of attempts at producing a mathematical model of a tyre under wet conditions, there appears to be none that will satisfy the current requirements for providing the tyre designer with a tool which he can use to aid his selection of tyre tread patterns for improved wet grip. There is a need for two types of design aid:-

i) to allow study at the contact patch level to assist in the layout of the individual tread elements within the contact patch.

ii) to allow study at the individual block level to allow the detail design of blocks to be optimised for wet grip.

It is important to model the flow of water as fully as possible, but the modelling of the tyre structure can be simplified as it is not necessary to assess the effect of changes in tyre construction within the model. The effects of tyre construction can be represented by a preload (contact pressure) and a stiffness at all points within the contact patch.

As the object is to aid the geometric design of tread patterns, it is not necessary to include the effects of either the tread compound or the road surface microtexture on friction levels. The capability of a tread pattern can, therefore, be determined from fluid pressure and film thickness distributions. The component parts of such a model are developed in Chapter 3.

The implementation of the theory into computer programs for both tyre contact patch analysis and individual block analysis is shown in Chapter 4.

On the experimental side, there is a lack of detailed fluid pressure and water film thickness measurements for tyres moving at high speed in wet conditions. No facilities are available for this, and the development of an existing test facility to allow these measurements to be made is discussed in Chapter 5. Results from these measurements are presented in Chapter 6 and their comparison with results produced by the computer programs are discussed.

It should be stressed that this work is only a first step towards the detailed study of the tyre/road interface under wet conditions. Chapter 8 presents many suggestions for further work, both in the mathematical modelling and experimental fields, as well as drawing conclusion from the present work.

CHAPTER 2 - "NON-TECHNICAL"WORK

2.1 INTRODUCTION TO "NON-TECHNICAL"SECTIONS

The purpose of this chapter is to document some of the non-technical work which was undertaken as part of the Total Technology PhD. The work can be considered as falling into three main categories:-

1. Study of the Tyre Design Process.

2. Cost/Benefit Analysis of the Project.

3. Network Analysis of the Project.

1 & 2 are linked to a certain extent and will be covered in this chapter. The third category is concerned with the monitoring of the project and is covered in chapter 7.

The study of the tyre design process was undertaken in order to identify the areas in which a computer model could assist the design of the tyres for improved wet grip. This was particularly important as the underlying object of this project was to produce a design, rather than a research tool. An understanding of the tyre design process was necessary to allow the computer model to be directed to those areas which would have the greatest impact on tyre design for wet grip.

To assess the financial implications of undertaking this project, a Cost/Benefit Analysis was performed. The costs of the conventional design process were assessed for typical design activities. The benefits which could be gained by using an improved method of design for wet grip were also assessed. The costs of actually undertaking the project are estimated, and making assumptions based on the benefits analysis, a decision on how worthwhile the project was can be made.

2.2 STUDY OF THE TYRE DESIGN PROCESS

2.2.1 Introduction to the Tyre Design Study

The main purpose of the tread pattern on a tyre is for the improvement of wet grip. It is unfortunate that the tread pattern has a detrimental effect on most other properties of tyres, such as:

Noise Generation - the generation of noise as a tyre rolls along a road is largely determined by the number of air/rubber transitions. Therefore, a plain treaded tyre will produce very little noise compared to a patterned tyre, particularly if the pattern is based on blocks rather than ribs.

Wear - the tread pattern influences the wear of the tyre, both in terms of the overall wear rate and the evenness of wear. The unevenness of wear can cause particular tread patterns to promote high wear in, say, the shoulder regions.

Handling & Stability - the addition of a tread pattern to a tyre causes the loss of some structural rigidity.

The design of the tyre tread pattern, therefore, has to be a compromise between the conflicting requirements of different properties. The technical work in this project is concerned only with the optimisation of tread patterns with respect to wet grip. Therefore, it is essential that as a design tool it fits into the overall design process where other factors of tyre performance can be considered. This study of the tyre design process was undertaken with this aim in mind.

2.2.2 The Design Specification

The development of a new tyre may be initiated in a number of ways:

(i) The introduction of a new vehicle range by an original equipment (O.E.) manufacturer.

(ii) Noted deficiencies in the performance of a current range of tyres.

(iii) The desire for the Company to enter a new section of the market.

When the need for a new range of tyres has been identified, the marketing department set out a series of specifications based on one or more current production tyres. This rates the requirements of the proposed tyre for all the relevant tyre properties. For example the specification for a winter tyre may be:-

	Current	Proposed
Handling	100	95
Wet Grip	100	110
Performance on Ice	100	105
Performance on Snow	100	105
Noise	100	85
Wear	100	90

Liaison between marketing and design departments ensure that targets set are realistic.

Once targets have been set in terms of a current tyre's performance, there may be additional constraints imposed on how these targets can be met. For instance, a certain style of tread pattern may be required, depending on market fashion, or an O.E. manufacturer may have a preference for a certain style of tyre, possibly to fit in with the image of the vehicle, or possibly because a particular style of tyre has performed well in the past.

2.2.3 Tyre Structural Design

The type of structural design used will largely be determined by the type of tyre required by the design specification. Factors, such as if the tyre is for the performance or economy market, the aspect ratio (60 series, 70 series, etc.), will influence the type of construction used.

The overall dimensions of the tyre for any particular rim size and width, are given in European Standards (ETRTO). Therefore, the designer is left mainly with the decision about the type of construction required. One of the main variables in radial tyre construction are the breakers. The number and type of breakers affect the profile of the tyre and also the speed rating. Higher speed ratings require more complex breaker arrangements and are more costly to produce.

Once the construction and size of the new tyres have been determined then plain tread moulds can be designed and manufactured. These moulds cost approximately £10,000 each and allow the production of plain tread development tyres.

2.2.4 Initial Tread Pattern Design

Whilst the plain tread moulds are being manufactured, the overall type of tread pattern required is worked out. The starting point for this is the performance specification which should suggest a particular style of pattern. It is here that the experience of the designer is used to allow some tread patterns to be sketched out, and then drawn accurately to scale. The tread pattern consists of a series of "building blocks" which are placed together to form the total pattern. These "building blocks" or segments are usually specified in 'short', 'medium' and 'long' lengths, so that the pattern is not repeated at a regular frequency around the tyre, which is detrimental for the generation of noise.

Masks are made of these segments so that the pattern can be marked out on plain tread development tyres. At this stage, a computer model can be used to select the best arrangement of segments for lowest noise generation.

It is usual at this stage to cut the tread pattern on only a section of plain tread tyre so that the designer can see the pattern on the tyre's curved surface. Any possible weaknesses in the pattern can be visually identified and the tyre can also be loaded onto a glass plate, so that the contact patch under load can be seen. This process is repeated until a number of versions of the tread pattern are found which look satisfactory. These will then be fully hand-cut onto plain tread tyres.

2.2.5 Testing Hand Cut Tyres

The hand cut tyres are tested along with one or two standard production tyres as controls. Because there is only one tyre of each variant available, machine testing can only be performed at this stage.

Using the results from these machine tests, modifications may be made to the designs, and the testing procedure repeated. When satisfactory results have been obtained from the machine tests, more tyres are hand cut to allow on-vehicle testing. The on-vehicle testing is much more thorough than the machine testing, and, again, modifications may be required followed by re-testing. On the basis of these vehicle tests, one tread pattern will be chosen for use in the development mould.

2.2.6 Development Mould Tyres

A development mould is manufactured using the construction from the plain tread mould and the pattern determined from the testing of hand cut tyres. This stage in the tyre design process is both expensive (approx. £30,000 per mould) and time consuming (6 to 8 months), and it is unlikely that there will be time to make any changes to the design once this stage has been reached. It is, therefore, important that the design is optimised before this stage is reached.

2.2.7 O.E. Approval

Providing the results of tests on the development mould tyres are satisfactory, tyres are then supplied to the O.E. customer for evaluation. The tyres must meet specified standards set by the O.E. manufacturer and must be available at the time when the O.E. manufacturer is evaluating tyres from all the different suppliers. The subject of O.E. approval is again discussed in Section 2.3.11 when the effect of technical quality on sales performance is considered.

2.2.8 Conclusions From The Tyre Design Study

From the submssion of tyres for O.E. approval until going into full-scale production, generally takes ten to twelve months, making the total time from specification to production two to three years. This can have a significant effect on the design process, as the increased performance continually being demanded from tyres makes it more difficult to meet the dead-line for O.E. approval. The requirements and style of a tyre may also change over this period. Therefore, it is desirable to reduce the design lead time if at all possible.

The critical time in the design is at the early stage when hand cut tyres are being used, as once the development mould specification has been set, there is little opportunity for major change to either the tread pattern or construction without serious time penalties. This stage of the tyre design lasts for up to six months and is really the only stage that can vary in length, as other stages are governed by such factors as machine shop lead times in mould manufacture.

This initial design process is basically an iterative procedure, particularly with the detail design of tread blocks. It was thought that this is the area in which computer modelling would be most useful.

The design of tyre tread blocks has become more important in recent years with the switch from rib based patterns to block based patterns, as construction has changed from cross-ply to radial.

Whilst "blocky" tread patterns have detrimental effects on other tyre properties, in particular noise, they do provide the potential for improved wet grip levels. A method of assessing individual block designs would, therefore, be desirable and should reduce the number of design variations which have to be evaluated by testing.

Given the present structure of the tyre design process, a computer model for wet grip could be used in a number of different ways. For example, it could be used to reduce the number of design variations which require testing, and hence reduce the overall design time. This could allow a deadline for O.E. approval to be met which otherwise would not. A second way of using a computer model would be to allow more design ideas to be evaluated and, as a result, to produce a tyre with improved wet grip properties. In doing so, the actual time taken, and the amount of testing, may be increased, because the results of computer modelling could not be used without verification using traditional testing methods. In this case, the computer model would be used to decide which designs were worth progressing and which should be modified at an early stage.

2.3 COST-BENEFIT ANALYSIS OF THE PROJECT

2.3.1 Introduction to Cost-Benefit Analysis

The cost side of this study can be split into two areas: cost of the current project, and cost of the tyre design process; in particular the cost of testing development tyres. The benefits side is approached by identifying the areas where possible benefits, due to the introduction of computer modelling for wet grip, may be gained.

An attempt has then been made to quantify the value of these benefits so that a comparison with the costs incurred in undertaking the project can be made.

2.3.2 The Cost of Undertaking the Project

The actual costs which can be attributed to the undertaking of the current project have been calculated and are shown in figure 2.3.1. The details of how these figures were obtained are now shown:

i) Direct Labour - this is based on the time for one person over the full three year period, including a notional amount of £2,000 to cover expenses. The actual hourly rates used were £15.93 for year 1: £16.73 for year 2 and £17.57 for year 3. These figures include overheads, such as heat, light, etc., and the number of working days per year was taken as 250.

ii) Computing (IBM) - this is the cost associated with the use of the IBM mainframe computer for both development and use of the program. The actual cost varies, depending on what peripherals are used by a particular job, and is between £300 and £500 per CPU hour. The figure here is based on an average CPU cost of £400/hour and an estimated usage of 50 CPU hours over the three year period.

iii) Cornering Force Machine - the cost for use of the cornering force machine is based on the cost of performing standard tests on that machine. When the time to perform each of these tests is taken into consideration, a figure of £900 per day for use of the machine is gained. This cost includes direct labour (one technician), overheads and depreciation of capital

FIGURE 2.3.1 - ESTIMATED TOTAL COST FOR WET GRIP PROJECT

(COST TOLERANCES SHOWN ON VARIOUS ITEMS)

			£	
i)	Direct Labour (including £2,000 expenses)		94,181	± 5%
ii)	Computing (IBM)		20,000	+ 30% − 10%
iii)	Cornering Force Machine		36,000	+ 0% − 50%
iv)	Image Analyser			
	Depreciation	4,615		+ 0% − 10%
	Operator	4,779		+ 5% − 20%
		9,394	9,394	
v)	Glass Plate Photographs		1,075	± 5%
vi)	Testing of Nozzle at Cranfield		2,000	± 10%
vii)	Electronics Engineer		1,884	+ 5% − 30%
viii)	Capital Expenditure:			
	Radio Telemetry	1,106		
	Surface Shells	2,750		
	Pressure Transducer	421		
	Fibre Optic Probe	61		
	Electronic Components	80		
	Nozzle (complete)	273		
	Test Tyres	100		
a)	Extra Ends for Nozzle	160		
b)	Transmitter Mountings	50		
c)	Pressure Calibration Rig	200		
		5,201	5,201	
		TOTAL COST:	169,735	

ESTIMATE BASED ON HIGHEST COST £181,031

ESTIMATE BASED ON LOWEST COSTS £142,792

equipment. However, the figure of £900 per day seems rather excessive as the machine is 25 years old and has, therefore, been completely written off for depreciation purposes. There will, of course, be high maintenance costs. Therefore, as no other figures are available, the one above will be used. In the duration of the project, the machine was used for a total of 40 days, which included the time taken to set the machine up for testing.

iv) Image Analyser - the image analyser was used for a total of 16 weeks over the duration of the project. For 8 of these weeks an operator was also used with the machine. The machine cost is based on a purchase price of £75,000, which is to be depreciated over 5 years, giving a depreciation cost attributable to this project of £4,600. The operator cost at £15.93 per hour (operator used in first year of project) is £4,779.

v) Glass Plate Photographs - as no information is available on the cost of the glass plate facility, then the cost of the glass plate photographs is based entirely on the labour cost of 3 people for 3 days. Again, these photographs were taken in the first year. Therefore, the hourly rate was £15.93.

vi) Testing of Nozzle at Cranfield - the cost was estimated based on equipment used and labour costs for 4 days.

vii) Electronics Engineer - the assistance of an Electronics Engineer was used for a total of 3 weeks, spread throughout the project.

viii) Capital Expenditure - this is based on the actual purchase price of equipment obtained specifically for this project. Items a, b and c were manufactured 'in house'. Therefore, their cost was estimated.

2.3.3 Discussion of Project Costs

The greatest component of cost is labour, which is included not only in the major single item of direct labour, but also in other items such as cornering force machine and electronics engineer. To a certain extent, these labour costs are misleading in that if the project were not undertaken then this amount would not be saved. However, that would then free the people involved to undertake alternative work, which may or may not be directly profitable. Therefore, the true total cost of labour must be used as has been done here.

In a similar way, the cost of use of the IBM computer is not directly payable by the Company, as it is leased on a fixed charge. Therefore, if the computing work in this project had not been undertaken, then the Company would not have saved any money.

However, the lease cost has to be divided amongst the users; therefore, this is done on the basis of time used by each user and the computing cost shown in figure 2.3.1 should be attributed to this project.

The actual costs incurred by the Company in undertaking this project are mainly those due to capital expenditure, but these are a relatively small proportion of the total project cost. The total cost of this project can be used as a basis of comparison with the possible benefits detailed in Section 2.3.6. By also comparing the cost of this project with the normal costs incurred with routine testing, it is possible to make a judgement as to whether the project was worthwile undertaking.

The costs shown in figure 2.3.1 have tolerance figures attached where appropriate. These are based on discussion with people involved with the setting of costs in the appropriate areas.

Some of the cost figures are also inaccurate because of time estimates. In particular, the amount of CPU time used on the IBM mainframe computer is only an estimate. Therefore, the tolerance will represent this as well as the tolerance on the cost.

2.3.4 Tyre Testing Costs

The actual amount of testing to which a series of development tyres is subjected, depends on the number of changes that have been made from a previous standard design. When a range of tyres is being developed, a number of design variants are put through the testing process and the most suitable chosen, depending on the test results.

Initial tests are performed with hand cut tyres on machines and, as the variants progress, their number will be reduced and a smaller number subjected to the full range of on-vehicle tests. Usually, the testing commences with 6 to 8 variants, plus 1 or 2 standard control tyres; this would be reduced to 1 or 2 variants in the later (more expensive) stages of testing.

A typical series of tests to which a new range of tyres would be subjected is:-

Noise

Cornering Force (wet grip)

Rolling Resistance

Thermovision (wear)

Structural Durability

Structural - High Speed

On-Vehicle Braking (wet grip)

On-Vehicle Handling

On-Vehicle Wear

In addition to the above, if during development a particular type of problem arises, then specific tests will be designed to investigate it.

The order in which these tests are performed will vary and it is usual to perform the tests which the tyres are expected to perform badly at first.

The actual cost of these tests vary enormously, and as would be expected, the on-vehicle tests tend to be the most expensive. The costs of individual tests are shown in the table below:-

TEST	COST PER VARIANT
	£
Noise	85
Cornering Force	310
Rolling Resistance	120
Thermovision	45
Structural Durability	1,040
Structural - High Speed	66
On-Vehicle Braking	480
On-Vehicle Handling	256
On-Vehicle Wear	15,600
TOTAL COST PER VARIANT:	18,002

The above costs take into account that for certain tests more than one tyre of a particular variant has to be tested to obtain average values. The cost of these tests include the depreciation of capital equipment, plus direct labour costs and overheads.

2.3.5 Discussion of Testing Costs

The tyre testing costs outlined above are incurred during the normal iterative tyre design process. As was discussed in section 2.2.8, the design process would last for up to 2 or 3 years and would include a team of 2 or 3 designers. The labour cost incurred over this period could, therefore, be as much as £800,000. The actual cost of producing the hand cut test tyres is approximately £600 per tyre. Therefore, initial tyre costs (for a range of variants) would be approximately £4,000, with additional costs of the same magnitude when extra tyres are required for on-vehicle testing.

The cost of performing tests is, therefore, only part of the total design cost. The actual cost in a specific case will vary depending on the amount of design time and re-testing required, and also on the number of development moulds required. Unfortunately, it is not possible to quantify the design costs for specific cases as figures are not available.

2.3.6 Possible Benefits Attributable to this Project

The benefits to the Company, due to work performed in this project will depend on how the mathematical model for tyre wet grip is used. If the model is used to reduce the amount of iterative testing, then there would be savings, both in testing and design time costs. It would also help in meeting O.E. manufacturers' dead-lines and may mean that an O.E. supply contract is gained that would otherwise not be. The model could also be used to improve the performance of tyres in the wet with little or no effect on design time or testing costs. The benefit here would be in increased sales and, to assess the possible benefits to be gained, a study of the effect of technical quality on sales performance was undertaken.

A further area where possible benefits may be gained is in a reduction of wet skidding accidents. Government statistics give the cost of various types of accidents and, therefore, the potential for saving to the Country can be assessed.

The benefits can be divided into four main categories:-

1. Savings in Design & Testing Costs.
2. Increased Credibility with O.E. Manufacturers.
3. Increased Sales.
4. Savings to the Country due to a reduction in accidents.

2 and 3 are similar in that they both concern the level of sales, and, in particular, sales to O.E. Manufacturers. The effect of technical quality on sales performance is covered in Section 2.3.11.

2.3.7 Savings in Design & Testing Costs

The magnitude of any cost saving in the design function, due to the introduction of a computer model for wet grip, depends largely on how that model would be used. The most likely use would be in the early stages of design where unsuitable tread patterns could be identified before any testing were carried out. This would save both design time costs and testing costs.

The actual cost savings are fairly hard to determine, as the amount of re-design time and the quantity of re-testing would vary in each specific case. However, the typical sort of detail change to a tread block design would be, say, the addition of a 'cut-out'. In this case the additional costs incurred would typically be:-

	£
Re-design time - 1 week	2,000
Hand cut new pattern	600
Test Tyre	25
Cornering Force Tests	500
TOTAL:	3,125

The above only includes re-testing for wet grip properties, but it is possible that other testing, such as noise or thermovision would have to be repeated, further increasing the additional costs.

Within the total design time of a tyre, there may be many such re-designs, and the above assumes that they are made before the original design had progressed further than the first stage of testing. If it had, then the re-testing costs would be very much higher (Section 2.3.4), especially if on-vehicle tests had to be repeated.

The above case outlines the regular savings that could be made during the normal iterative design process. Sometimes modifications will be made to a design after the development mould has been made, and if a re-design of this type could be avoided then the savings would be £30,000 for the mould, plus re-design and testing costs. Bearing in mind that more testing would have to be repeated in this case, then the total cost may be as high as £50,000.

2.3.8 Increased Credibility with O.E. Manufacturers

The development and use of a computer model for wet grip can be viewed in terms of overall improvements in the understanding of tyre technology and in the use of new methods to aid the design process. The O.E. Manufacturers themselves are continually developing the understanding of their products, and it is, therefore, reasonable for them to expect their component suppliers to do likewise. It is, therefore, important for the supplier to be able to exhibit to the O.E. Manufacturer, both his current technical understanding and his developments towards improved understanding.

In many cases the speed of response of its supplier in answer to an enquiry is important to an O.E. Manufacturer. Therefore, a supplier who can provide a fast service places himself in a

favourable position when negotiating future contracts. The effect of gaining an additional O.E. supply contract is discussed in Section 2.3.11.

2.3.9 Increased Sales

One aspect of increased sales has already been discussed in Section 2.3.8, in that gaining O.E. contracts amounts to an increase in sales. The other area in which increased sales can be had is in the replacement market. It is important in the replacement market to keep ahead of one's competitors and to be able to provide a tyre which performs well in all aspects.

Tyres sold for the replacement market are generally more profitable than tyres sold for O.E. fitment. However, without O.E. fitment, the number of replacement tyres sold will be greatly reduced. This is discussed in Section 2.3.11, where an example is given showing the total effect on replacement sales over a 5 year period of gaining one O.E. supply contract.

2.3.10 Saving to the Country Due to a Reduction in Accidents

Wet skidding is a major cause of road accidents, and, therefore, any improvement in tyre performance in the wet is likely to reduce the number of accidents. It is very difficult to predict what reduction in accident rate could be achieved by a given improvement in technical performance. However, the cost of road accidents can be found from reference (73). The latest available figures are for 1981, when a total of 25,342 vehicles were involved in skidding accidents on wet roads. The severity of these accidents varies enormously, but, again from (73), the average cost of all injury accidents is £6,060, and damage only accidents £460. The actual cost for injury accidents of different categories is made up as follows (73):-

	Fatal	Serious	Slight
Lost Output	105,470	1,430	20
Medical & Ambulance	500	870	50
Police, Insurance & Admin.	240	190	150
Damage to Property	1,390	1,120	770
Pain, Grief & Suffering	41,600	4,280	90
TOTAL:	£149,200	£7,890	£1,080

As can be seen from the above table, the spread of costs which give rise to the average cost per accident are very large. The total cost of wet skidding accidents in Great Britain in 1981 was approximately £153M, and any reduction in the total number of accidents would represent a very large potential saving to the Country.

2.3.11 The Effect of Technical Quality on Sales Performance

There are two distinct markets in which tyres are sold; Original Equipment (O.E.) and replacement. The O.E. sales are by far the most important to the tyre manufacturer and, as is shown in this section, also have a very great effect on the level of replacement sales.

When selecting which tyres to fit, O.E. Manufacturers use a number of factors to rank them: figure 2.3.2.

Wet grip comes very high in priority for both performance orientated and economy orientated categories. Therefore, a tyres wet grip performance will have a large influence on its acceptability. The exact weighting placed on different attributes is not disclosed by the O.E. Manufacturers, as this tends to encourage suppliers to build tyres to satisfy the ranking requirements rather than service requirements.

Figure 2.3.2 - ASSESSED AVERAGE PRODUCT BENEFIT PRIORITIES OF O.E.M's.

Performance Orientated

1. Handling
2. Wet Grip
3. Structural Integrity
4. Directional Stability
5. Comfort
6. Mileage
7. Low Rolling Resistance

Economy Orientated

1. Wet Grip
2. Low Rolling Resistance
3. Structural Integrity
4. Handling
5. Comfort
6. Directional Stability
7. Mileage

Before a tyre can be considered for O.E. fitment, samples must be supplied for acceptance tests, where minimum standards in the categories shown in figure 2.3.2 must be met. It should be noted that it is becoming increasingly more difficult to meet these standards. The acceptance tests will also only normally be carried out at the time of introduction of a new vehicle model, so it is very important to be able to supply sample tyres at this time, as missing the acceptance date could mean missing out on O.E. fitment for the whole of that vehicle's life.

Once a tyre has been accepted as meeting the minimum standards, then, depending on its overall position in the ranking compared to other suppliers tyres, the percentage of supply for that particular vehicle will be determined. However, this ranking, based on technical performance, can be upset by a tyre manufacturer who offers to supply tyres at a low price; although these tyres would still have to meet the minimum performance standards.

On a large volume fitment there may be as many as 6 or 7 different tyre manufacturers who will each get a different percentage of the fitment, dependent upon their position in the ranking. For a low volume fitment there may be only 1 or 2 suppliers. The actual position in the ranking can have a large influence on the percentage of tyres supplied and the difference between third and first in the ranking can mean a difference of 10% volume of fitment.

The full implications of gaining O.E. fitment can be seen if a 5 year period is considered when the original tyres on a vehicle are being replaced. If a tyre manufacturer has his tyres fitted as original equipment, then he can expect, according to the Marketing Department of S.P. Tyres U.K. Limited (manufacturing and marketing Dunlop tyres in the U.K.) to sell 45 replacement tyres for each 100 sold as original fitment.

If he did not get original fitment, then he could only expect to gain 6% of replacement sales. In the high volume market it is these replacements which represent the most profit, as tyres for O.E. fitment may be sold for cost price or even at a small loss, so that the benefits of replacement sales can be gained in a few years time. In the supply of low volume HR and VR tyres the situation may be different and a substantial profit may be made on tyres supplied for O.E. fitment.

To give an indication as to how important this 'knock-on' effect on replacement sales is, an example of the case for supply of 155SR13 tyres for fitment to a high volume selling car will be considered.

Assuming that in one year 140,000 vehicles of this model are produced, then there is a need for 700,000 tyres, and Dunlop may aim to obtain, say, 20% of this fitment, i.e.140,000 tyres. Therefore, if we consider the effect on replacement sales over 5 years, of 1 year's O.E. fitment, then the number of replacement units it is anticipated will be supplied is approximately 45,000. This is detailed in the table below.

	YEAR				
	1	2	3	4	5
Fraction replaced in that year.	0.2	0.4	0.8	1.1	1.1
Number of units replaced if O.E. fitment to 28,000 cars	5,600	11,200	22,400	30,800	30,800
Number of replacement units can expect to achieve on 45% replacement rate	2,500	5,040	10,808	13,860	13,860

From the table it can be seen that the fraction of tyres replaced after 1 year is 0.2, and if Dunlop obtains a fitment rate of 20%, then Dunlop tyres will have been fitted to 28,000 vehicles, and, assuming that 45% of tyres are replaced with those fitted as original equipment, then Dunlop can expect sales of 2,520 units after 1 year. If a 5 year period is considered, the total replacement sales due to O.E. fitment for 1 year on this vehicle is 45,360. The total amount of profit that this represents to the tyre supplier obviously varies, depending on how much profit is made on each individual tyre. As an example, if say £5 profit were made per tyre, then the above would represent £227,000 over 5 years.

This assumes that Dunlop achieves a 20% fitment rate, and it is this which will be affected by the technical performance of the tyre. If a tyre does not get O.E. fitment, then any technical improvement will have very little affect on the level of sales, as the motorist tends to assume that all tyres perform equally well and the normal influences, such as cost and advertising, have a much greater influence than technical performance.

2.3.12 Conclusions from the Cost-Benefit Analysis

The preceding sections have identified areas where a mathematical model to aid tyre design for wet grip could give benefits.

In Section 2.3.7 it was shown that the cost of a small modification, in the iterative design process, would cost approximately £3,000. This type of change is occurring at the rate of approximately 10 per month in the U.K.. Similar design activities are also being carried out at Dunlop in Germany, and since the take-over of Tyre Technical Division by Sumitomo Rubber Industries, in Japan; any savings in design costs by use of the wet grip model will also apply to these centres. The cost per year in the U.K. of iterative design and testing would, therefore, be approximately £360,000.

Given the content of this type of iterative design process, it is thought that as much as 30% of this could be saved by using the wet grip model to eliminate poor designs before any testing was performed. The saving from this could, therefore, be as high as £120,000 per year.

Design changes at a later stage in the design process are hard to determine, both in their cost and frequency of occurrence. The worst case when a mould has to be scrapped and all the testing on development tyres repeated, is a fairly rare occurrence, say twice a year, but the cost of this is high. The saving of one such re-design would be approximately £50,000.

From the above, it can be seen that the cost of the project (£170,000) could be recouped in one year by savings in design costs. However, given the uncertainty of the savings figures, it is probably safer to assume that the project would pay for itself in under 3 years by savings in design and testing costs. This alone makes the project worthwile.

The items discussed in Sections 2.3.8 & 2.3.9 are both connected with obtaining additional O.E. supply contracts, and the relationship between O.E. supply and replacement sales was discussed in Section 2.3.11.

An extra O.E. supply contract could be gained if a deadline to submit tyres was met that would not have been possible had the current amount of testing and re-design been needed. Also, as wet grip is very near the top in importance in the ranking of tyres by O.E. manufacturers, then an improvement in wet grip performance could easily change the position in the ranking and mean an extra 10%, or more, of the fitment. The example given in Section 2.3.11 shows that an extra 10% fitment would represent an extra 23,000 tyres sold over a 5 year period on one vehicle model alone. Any small gains in the level of O.E. sales would be able to cover the cost of undertaking this project from the profit from these extra sales.

The final area of possible benefits, discussed in Section 2.3.10, of saving to the country could also give very large potential savings. In 1981 the total cost of wet skidding accidents was £153M; therefore, a saving of just 0.1% in wet skidding accidents would represent £150,000. To put this into context, it would only mean the saving of one fatal accident, or 20 serious accidents. It would seem that any improvement in wet grip performance, no matter how small, could have this potential.

The costs and possible benefits attributable to this project can, therefore, be summarised as in the table below:-

Total Cost of Project	£170,000
Benefit Type	Benefit per annum £
Saving in design and testing costs (iterative + saving 1 mould scrapping)	170,000
Additional sales to O.E.M. (on one vehicle model only - 10% higher fitment)	4,500 per £1 profit on each unit
Saving to Country (0.1% reduction in wet skidding accidents)	150,000

CHAPTER 3 - THEORETICAL DEVELOPMENT

3.1 INTRODUCTION TO THEORETICAL DEVELOPMENT

The object of this chapter is to develop the individual aspects of the mathematical model which can then be used in a computer program to analyse the wet grip properties of various tyre tread pattern configurations. The mathematics developed allow analysis of both individual tyre tread blocks and complete tyre tread contact patches with any tread patterns.

3.2 GENERAL ASSUMPTIONS & SIMPLIFICATIONS

Because of the complex nature of tyre/road interaction, particularly under wet conditions, it was necessary to make a number of assumptions to simplify the problem before it could be expressed mathematically.

The nature of some of these assumptions was dictated by the object of developing the mathematical model; i.e. that the model should treat in as full a way as possible the tyre tread pattern and the flow of water within the contact patch.

The problem is complicated by the fact that it involves interaction between fluid in the tyre/road interface and the tread material, which deforms under the action of fluid pressure. To allow this to be mathematically modelled, the problem is split so that a solution is obtained on an iterative basis between a fluid problem with explicit values of film thickness and a solid problem where the fluid pressures determine new film thicknesses for the next iteration.

The tread pattern mainly influences the bulk water drainage, as does the road surface macrotexture. Therefore, these features can be represented by an analysis of fluid flow and pressure existing in the tyre/road interface.

The tyre tread compound and the road surface microtexture determine the level of friction between the tyre and the road surface under wet conditions and will have little effect on the bulk water drainage. As the analysis developed here is not concerned with friction levels, then these features need not be considered.

The magnitude of the water film thickness is known to be generally less than 1 to 2mm, although at the leading edge of the contact patch, film thicknesses greater than this may exist. As the film thickness is mostly less than, say, 1mm (excluding grooves) and, in many cases, much lower than 0.1mm, the water film will be treated as "thin", and a 2-dimensional Reynolds equation will be used to represent the water film between the tyre tread and the road surface. Other mathematical models of tyre/road interaction in the wet have used Reynolds equation (3), (4), (5) & (6).

In the derivation of Reynolds equation itself, a number of assumptions are made which are covered in the literature (particularly (31)). However, two important assumptions in the current context are: that the pressure is constant throughout the thickness of the fluid film and that the fluid flow is laminar. Constant pressure through the thickness of the film is reasonable because of the thinness of the film.

Under certain circumstances, it will, however, be possible for turbulence to exist. An extreme case would be when a tyre was sliding (locked wheel) with a velocity of, say, 96 Kph and an average fluid film thickness of 0.1mm between the tyre tread and the road surface. Under these circumstances Reynolds Number would be given by:

$$Re = \rho \frac{ud}{\mu} = 2342$$

It should be emphasised however, that in certain parts of the contact patch, Reynolds Number may be very much lower than this, particularly if the tyre were freely rolling, (when Reynolds Number is based on mean flow velocity and not sliding velocity).

In lubrication, it is normal to neglect turbulent effects for low Reynolds Numbers (say < 1000) (42). In pipe flow analysis, it is usual to take Reynolds Numbers of greater than 2,000 to be indicative of turbulence. Because in practical tyres Reynolds Number may be higher than these limits, a method of adding turbulent effects, when required, into Reynolds equation will be used. This method is described in detail in section 3.6 and basically involves multiplying the fluid viscosity by a factor which is dependent on Reynolds Number.

Assumptions also have to be made about boundary conditions at the edges of the contact patch. This is covered fully in section 3.7.

The progress of a tyre on a road can be defined by two extreme cases; when the wheel is rotating; free rolling, and when the wheel is not rotating - locked or sliding. The movements of the tyre tread surface, due to either rolling or sliding, are modelled as follows:-

Rolling: the portion of the wet contact patch ahead of the front of the dry contact patch is assumed to rotate about the front of the dry contact patch.

Sliding: all points on the tyre tread will slide relative to the road surface.

The tyre may be completely rolling or completely sliding, or any relative proportion of the two. The subject of contact patch movements is discussed in section 3.8.

Probably the area where the most sweeping simplifications are made, is that of contact patch deformations. Tyre construction is relatively complex and is built up from a number of components as shown in figure 3.2.1.

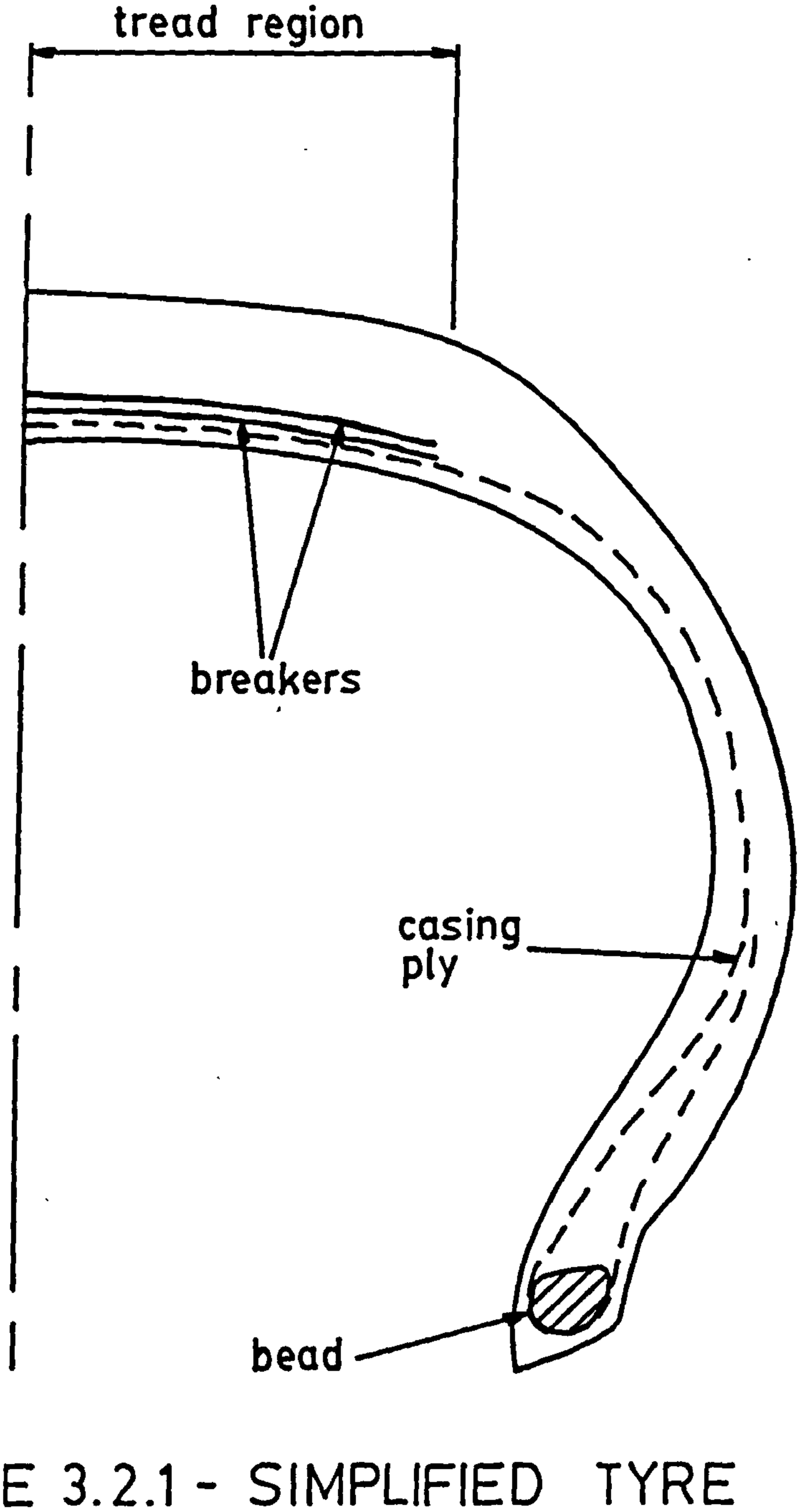

FIGURE 3.2.1 - SIMPLIFIED TYRE CROSS-SECTION

To make an attempt at modelling this fully is a very large problem and is beyond the scope of this project. The method chosen is thought to be adequate to allow the study of different tyre tread patterns, which is the overall aim of the project. The effect on wet grip levels of tyre construction changes cannot, of course, be studied directly when using a simplified model of tyre construction, but can be studied indirectly. For example, changes in the tyre construction would largely, as far as wet grip levels are concerned, affect the contact patch shape, the contact pressure between the tyre and the road, and the contact patch vertical stiffness. The current mathematical model allows all these factors to be varied, and therefore, given that the effect of tyre construction changes on these parameters is known, then their effect on wet grip levels can be assessed using the model. This is not such a disadvantage as it would at first seem, because during the normal tyre design process, the tyre construction is one of the first things to be determined. A mould is then manufactured to allow tyres with the appropriate construction, but with plain treads, to be produced. Simple tests on these tyres can then give the required information on contact patch shape, contact pressure and vertical stiffness.

The actual details of the deflection method used and other methods which were evaluated, are given in section 3.10.

3.3 THE BASIC FLUID MECHANICS PROBLEM

As was stated in section 3.2 the fluid mechanics problem will be treated as one of thin film lubrication, and will be represented by Reynolds equation. A number of previous mathematical models of tyre/road interaction in the wet ((3), (4), (5), (6) etc.) have used Reynolds equation to represent the behaviour of the water, but some of them treated the problem as one-dimensional flow and neglected, for various reasons, the flow in either the longitudinal or lateral directions. These are discussed in the 'Literature Review', section 1.2.1. The current model will treat the problem as two-dimensional.

The fluid mechanics problem is, therefore, considered basically as two surfaces separated by a fluid film, as shown in figure 3.3.1, where the upper surface represents the tyre tread and the lower surface represents the road.

The relevant form of Reynolds equation is, therefore, given by equation 3.3.1.

$$\frac{\partial}{\partial x}\left(\frac{h^3}{12\mu_x}\cdot\frac{\partial p}{\partial x}\right) + \frac{\partial}{\partial y}\left(\frac{h^3}{12\mu_y}\cdot\frac{\partial p}{\partial y}\right) = \frac{1}{2}\cdot\frac{\partial}{\partial x}(V_x h) + \frac{1}{2}\cdot\frac{\partial}{\partial y}(V_y h) + \frac{\partial h}{\partial t} \quad - 3.3.1.$$

The derivation of this equation from first principles can be found in many text books, such as (31). In its present form, this equation is difficult to solve, and for any realistic geometry cannot be solved explicitly; resort to a numerical technique must, therefore, be made.

3.4 THE SOLUTION OF REYNOLDS EQUATION BY THE FINITE ELEMENT METHOD

The Finite Element Method is a numerical technique for solving differential equations and relies on the fact that any continuous quantity (in this case pressure) varying over a region can be approximated by discretising that region into a number of sub-domains. These sub-domains are known as elements, and the way in which the unknown quantity varies over that element is specified by a polynomial. This polynominal is known as a shape function or an interpolation function, and is such that the value of the unknown within an element can be defined by the values at the interconnection points between elements which are known as nodes. The solution, therefore, need only be found at the nodes, and by using the interpolation function, the values at other points may be found if required. It is usual though only to calculate values at the nodes and if a value is required at a specific point then a node would be placed at that point.

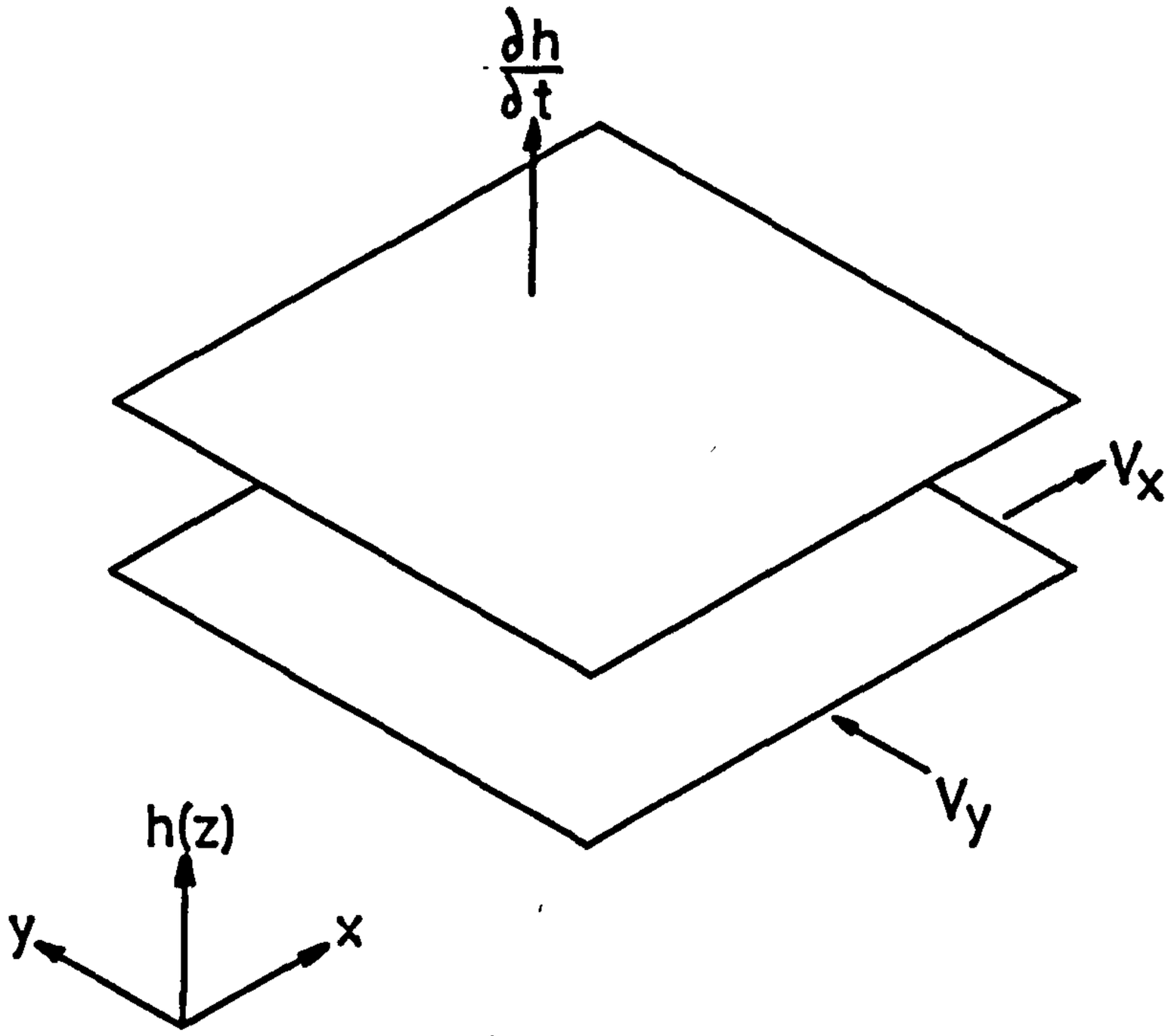

FIGURE 3.3.1- FLUID MECHANICS COORDINATE SYSTEM

Throughout this work, the type of element used is triangular with nodes at each of the three vertices. As there are three points defined for each triangular element, then the pressure within each element must vary linearly and be represented by the equation of a plane surface. A typical three noded element is shown in figure 3.4.1.

Any number of triangular elements can be combined to form more complex shapes. Therefore, there is very little restriction on the geometry that can be modelled, although a high concentration of elements may be needed to model certain highly curved boundaries.

The spacing of elements and nodes within the domain will, to some extent, affect the accuracy of the results. To improve the results, it is generally recognised that a higher concentration of elements should be placed in areas of high pressure gradient. This can be difficult because these areas may not be know before the solution is attempted. The normal procedure in such a case would be to produce a uniformly spaced mesh and obtain a trial solution. The results of the trial solution would then indicate the areas of high pressure gradient and the mesh could be refined in these areas and the problem solved using the new mesh.

This procedure has not been generally used in this work as the accuracy of the finite element solution is thought not to be the limiting factor in the present model of tyres under wet conditions, but these points should be considered if one is attempting an optimum finite element solution.

The problem, in terms of nodal pressures, can now be solved by Reynolds equation. When the finite element method is used to solve structural problems, where the relationship between stress and strain (displacement) is sought, the finite element properties can be formulated by minimising the potential energy within the system.

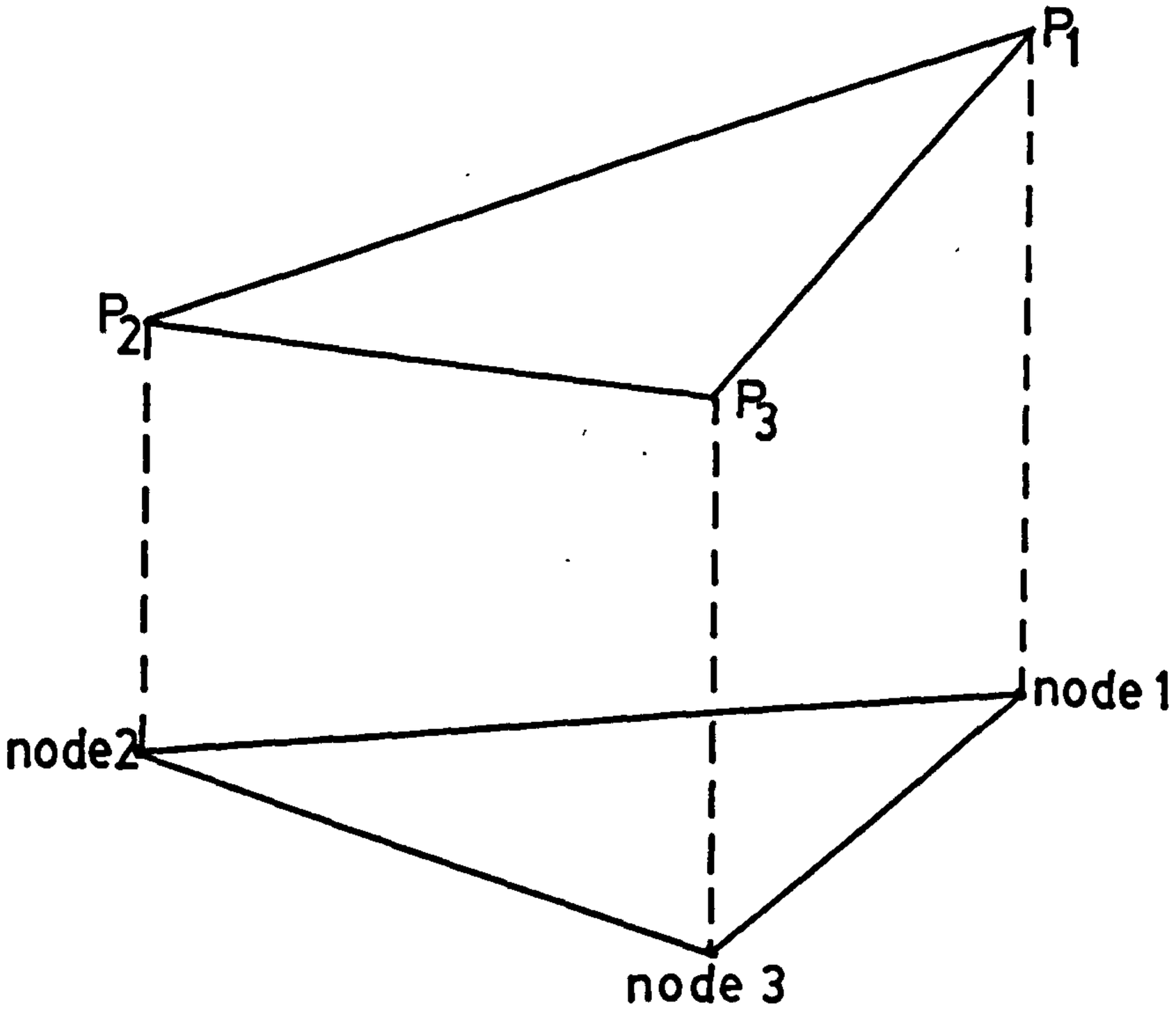

FIGURE 3.4.1 - TYPICAL THREE NODED ELEMENT

When a problem such as the solution of Reynolds equation is being attempted, then an integral is used, which when minimised will form the solution. This integral is obtained by a variational method, and for the case of Reynolds equation can be found in much of the literature. In particular, Booker and Heubner (55) or Reddi (53) and will be stated here without any proof.

$$I = \int \left\{ \frac{h^3}{24}\mu_x\left(\frac{\partial p}{\partial x}\right)^2 + \frac{h^3}{24}\mu_y\left(\frac{\partial p}{\partial y}\right)^2 - \frac{1}{2}\,hV_x\frac{\partial p}{\partial x} - \frac{1}{2}\,hV_y\frac{\partial p}{\partial y} + p\frac{\partial h}{\partial t} \right\} dA$$

$$+ \int_c qp\, dS \qquad \text{-----3.4.1}$$

The second integral of equation 3.4.1 represents flow boundary conditions over the boundary 'c'.

The appropriate interpolation function for three noded triangles can be substituted into equation 3.4.1 and the equation minimised over the whole domain. This procedure is discussed in detail in Appendix A.

The resulting set of equations for the whole domain can be expressed in the usual finite element matrix notation as,

$$[K] \cdot \{p\} = \{F\} \qquad \text{-----3.4.2}$$

where $[K]$ is known as the global stiffness matrix, $\{p\}$ is a column vector of the unknown nodal pressures, and $\{F\}$ is the generalised force vector.

Equation 3.4.2 is obtained by considering each element separately and forming the local stiffness matrix and local generalised force vector for each element. The local stiffness matrix defines the physical properties of that particular element and includes the x and y co-ordinates of the nodes, the properties of the fluid (in terms of its viscosity), and also the fluid film thickness over that element. The local generalised force vector includes the terms which 'generate' the fluid pressure, such as the sliding or squeezing velocities, and in the case of elements on the edge of the mesh, any flow into or out of the domain.

When the local generalised force vector is being assembled, the term representing fluid flow into or out of the domain is only used for elements which have at least one of their sides on the edge of the domain, and then it is only used for those nodes within that element which are actually on the edge of the domain.

Once the local stiffness matrices and the local generalised force vectors have been formed for each element, they are added into the global stiffness matrix and generalised force vector, taking into consideration the continuity of pressure across element boundaries. The stiffness matrix and force vector can then be considered as forming, along with the unknown pressures, equation 3.4.2. Before solving equation 3.4.2, it is necessary to add any geometric boundary conditions which, in this case, will be pressures. The solution of equation 3.4.2 can then be carried out by one of the standard methods of solving large orders of simultaneous equations.

The foregoing section has given a general outline of how the finite element method can be used to solve Reynolds equation. Some of the practical details of this will be covered in chapter 4 and the complete details of the computer programs, which perform the calculations, are given in Appendix B.

The reader who is unfamiliar with, or who requires more details of, the finite element method is referred to the many text books on the subject, such as (48), (49), (50) and (51), as some aspects of the method have not been covered here.

The solution of Reynolds equation is in terms of fluid pressures, but it is also useful to know the fluid flow velocities within the domain, and the calculation of these is covered in the next section.

3.5 CALCULATION OF FLUID FLOW

The volume flow per unit width in the x and y directions can be expressed as (31).

$$q_x = \frac{V_x h}{2} - \frac{h^3}{12\mu_x} \cdot \frac{\partial p}{\partial x} \qquad \text{------3.5.1}$$

$$q_y = \frac{V_y h}{2} - \frac{h^3}{12\mu_y} \cdot \frac{\partial p}{\partial y} \qquad \text{------3.5.2}$$

The pressure gradients $\frac{\partial p}{\partial x}$ and $\frac{\partial p}{\partial y}$ can be found from the element interpolation functions. As in this case linear interpolation functions are being used then the pressure gradients will be constant over each element.

It follows, therefore, that there is a discontinuity in pressure gradient between elements, and thus a discontinuity in fluid flow. This feature could be avoided if higher order elements were used which possessed interelement continuity of the derivative of the primary variable.

If the fluid flows are calculated at nodes, then a different value will be obtained, depending on which of the elements surrounding that node is used for the calculation. It is possible to smooth this difference by various methods, ranging upwards in complexity from a simple averaging of the different values for flow. This problem of interelement discontinuity is discussed in a paper by Hinton and Campbell (65).

Based on suggestions made by Hinton and Campbell, the method used here is to find the value of fluid flow at the centroid of each element. This has the attraction that it is known that the interpolation functions perform badly at the edges of elements (and hence better at the centres of elements), and also the fluid flow velocity at the centroid of each element is required in the modelling of turbulence. The fluid flow velocity is found from the volume flow per unit width (equations 3.5.1 and 3.5.2) by dividing by the mean fluid film thickness for that element.

To check the effect of interelement discontinuities on fluid flow, and the extent to which using centroid values overcomes this, values of flow predicted by the computer program for one-dimensional cases were compared with analytical solutions. Figure 3.5.1 shows the result of such a comparison for a case using velocities and fluid film thicknesses appropriate to a tyre under wet conditions. It can be seen that the use of centroid values for the fluid flow gives close agreement with analytical results.

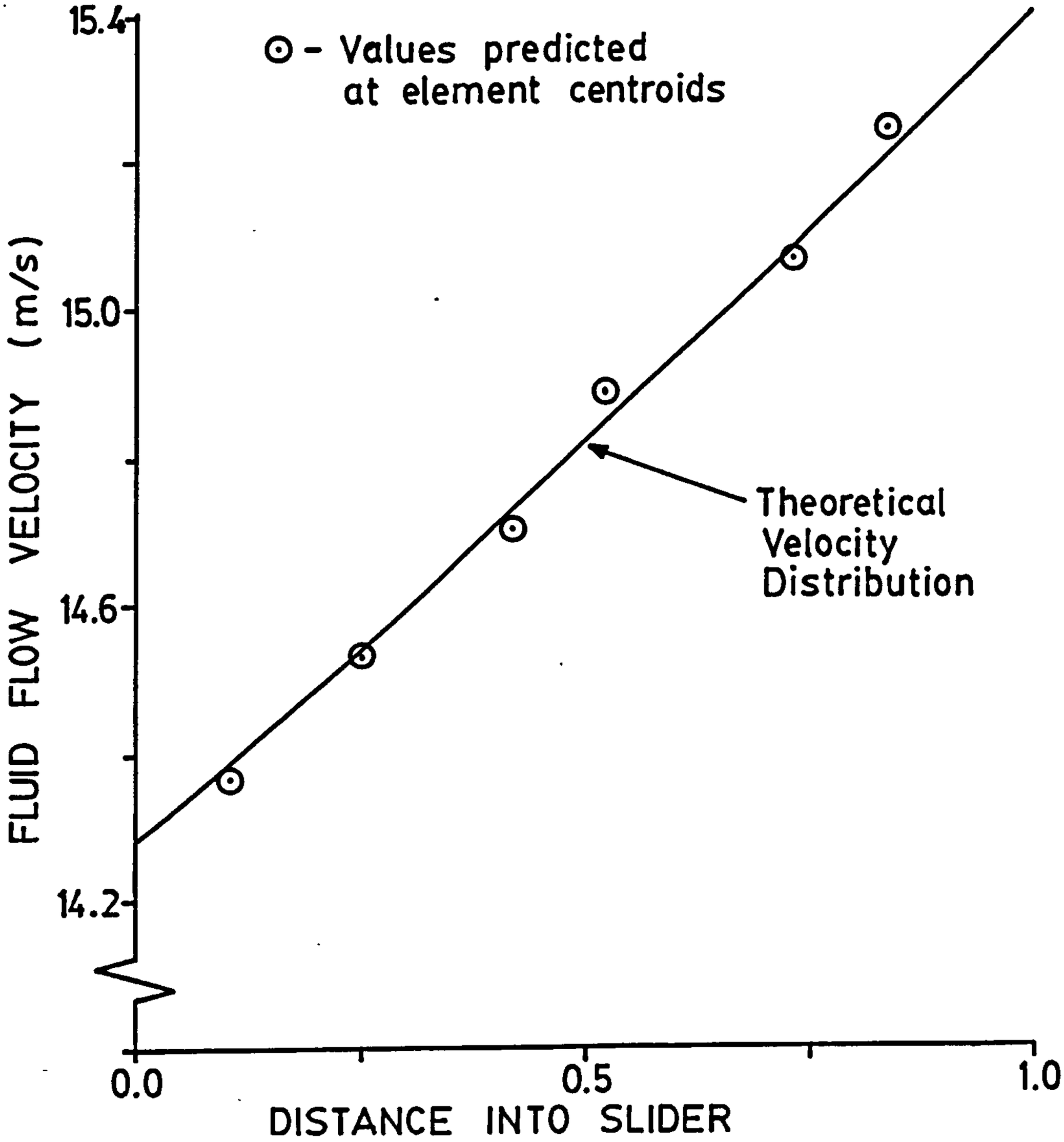

FIGURE 3.5.1 - VELOCITIES AT ELEMENT CENTROIDS FOR ONE-DIMENSIONAL SLIDER

3.6 TURBULENCE MODELLING

As was discussed in section 3.2, tyres under wet conditions (particularly when locked) may operate in the turbulent region; therefore, some form of modelling turbulence is necessary. When a tyre is free rolling, then there is less likely to be turbulence, and the model should only add turbulent effects where appropriate.

A number of papers discussing turbulence modelling found in the literature (40), (41), (42), (43), (44), (45) and (46) (discussed in section 1.2.2), all take basically the same form in providing a "factor" by which the fluid viscosity may be multiplied (or divided) to provide an "effective viscosity". This factor is in all cases a function of Reynolds Number and the different theories apply to either Couette or Poiseuille flow.

In the case of modelling a tyre under wet conditions, the degree of slip between the tyre and road surface will vary. If the wheel is freely rolling, there will be dominant Poiseuille flow, and if the wheel is locked there will be dominant Couette flow. In most cases there will be a combination of these two flows, as shown in figure 3.6.1.

When turbulence is to be modelled, Reynolds equation is modified slightly from the form shown in equation 3.3.1 giving,

$$\frac{\partial}{\partial x}\left(\frac{h^3}{12 j_x \mu_x}\frac{\partial p}{\partial x}\right) + \frac{\partial}{\partial y}\left(\frac{h^3}{12 j_y \mu_y}\frac{\partial p}{\partial y}\right) = \frac{1}{2}\frac{\partial}{\partial x}(V_x h) + \frac{1}{2}\frac{\partial}{\partial y}(V_y h) + \frac{\partial h}{\partial t} \quad \text{-----3.6.1}$$

where 'j_x' and 'j_y' are 'x' and 'y' factors, dependent on Reynolds Number. The purpose of the turbulent lubrication theories presented in the following two sections is to specify values for 'j_x' and 'j_y' under specific conditions. If 'j_x' and 'j_y' are equal to unity, then equation 3.6.1 represents the laminar case.

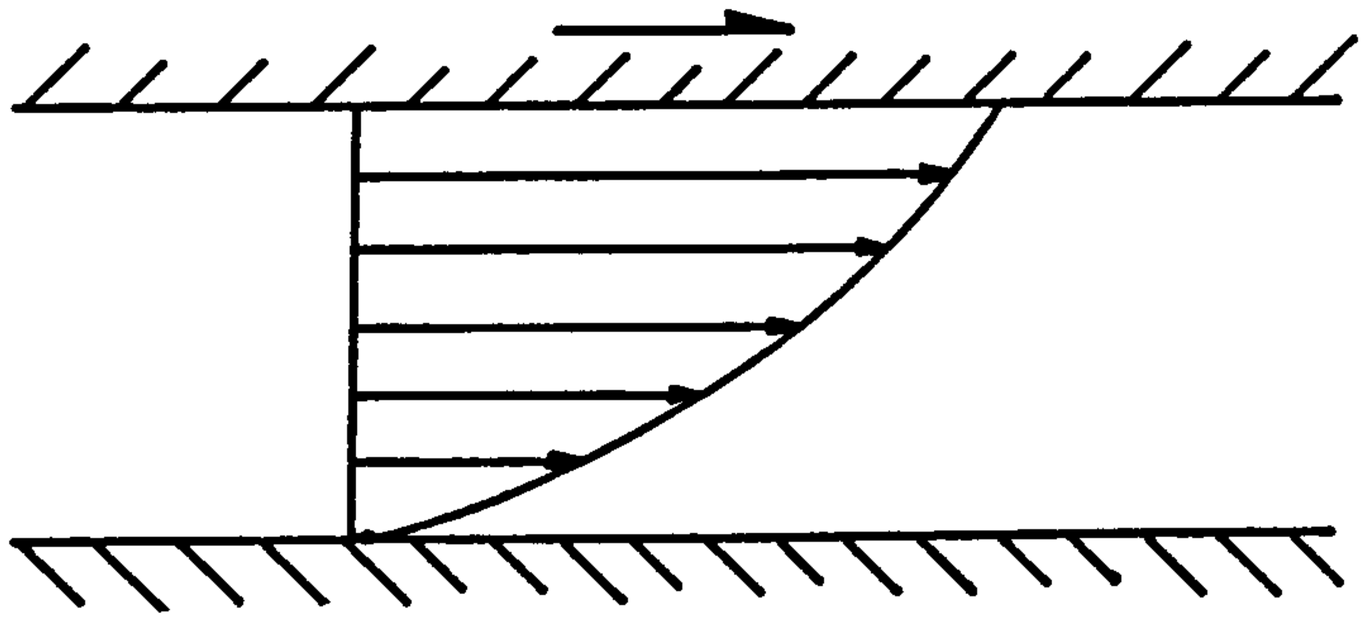

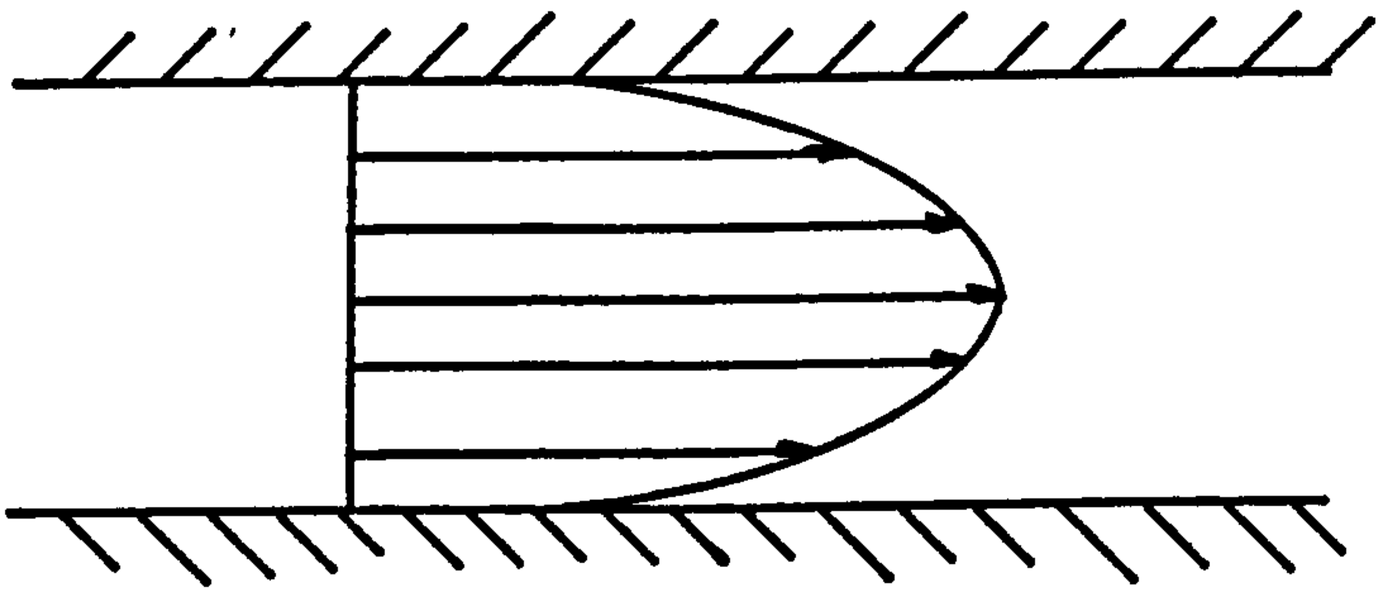

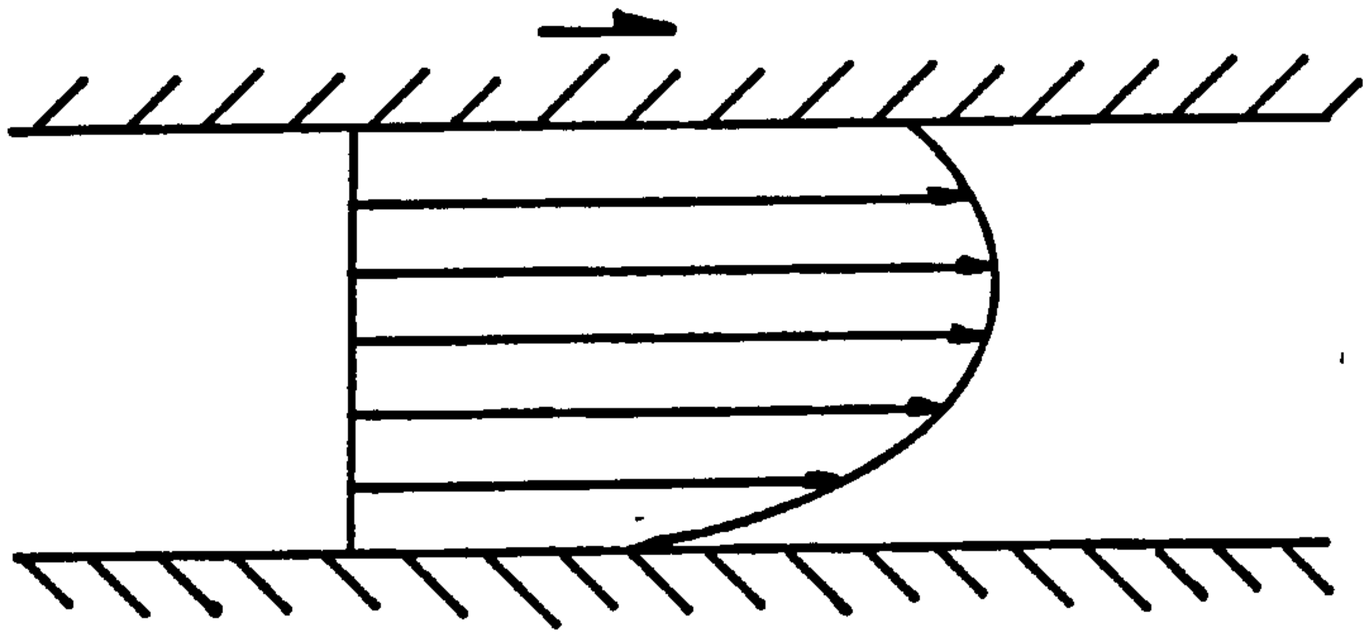

FIGURE 3.6.1 - FLUID FLOW TYPES

The turbulence theories used here are described in full by Taylor and Dowson (42) in their review of existing turbulent lubrication theories. We shall consider the cases of Couette and Poiseuille flow separately.

3.6.1 Turbulence Theory for Couette Flow

The Couette flow turbulence theory used here will be that derived by Ng and Pan and discussed in (42). The results of Ng and Pan's work is presented in graphical form,from which empirical expressions have been developed by curve fitting (42), (66) to yield:

$$j_x = 1 + K_x Re_c^{n_x} \quad \text{----------3.6.2}$$

$$j_y = 1 + K_y Re_c^{n_y} \quad \text{----------3.6.3}$$

This theory is for dominant Couette flow, therefore, Reynolds number is based on the slider velocity. The theory also assumes that there is a sliding velocity in only one direction (the x direction). In the application to tyres on wet roads, with the x direction defined as from front to rear of the contact patch, it is possible, when a slip angle is applied to the tyre, to have sliding in both the x and y directions. However, as the slip angles obtained in practice on the road are small (typically<3°), the y component of sliding velocity will be neglected as far as its effect on turbulence modelling.

The terms K_x, n_x and K_y, n_y in equations 3.6.2 and 3.6.3 are expressed in tabular form in (42). However, for the purpose of calculation, it is more convenient to have the data in an explicit form, and this has been achieved by Constantinescu (47),

$$j_x = 1 + 0.001133\ (Re_c)^{0.9} \quad \text{------3.6.4}$$

$$j_y = 1 + 0.000358\ (Re_c)^{0.96} \quad \text{------3.6.5}$$

where Re_c is the Couette Reynolds Number, based on slider velocity in the x direction. The limiting case for j_x and j_y must be that their value cannot fall below unity, i.e. that the 'effective viscosity' cannot fall below the laminar viscosity. This condition is automatically fulfilled in equations 3.6.4 and 3.6.5.

3.6.2 Turbulence Theory for Poiseuille Flow

The Poiseuille turbulent lubrication theory used here is that derived by Constantinescu (41). In (41), Constantinescu noted that for pressure (Poiseuille) flow, the factors j_x and j_y would be functions of the pressure gradient and hence the flow velocity. Constantinescu then used existing theoretical data from (40) to express j_x and j_y as functions of the Poiseuille Reynolds Number. In Poiseuille flow there are no sliding velocities, therefore, j_x is based on the mean flow velocity in the x direction and j_y is based on the mean flow velocity in the y direction.

$$j_x = 0.01225\ (Re_{px})^{0.681} \quad \text{------3.6.6}$$

$$j_y = 0.01225\ (Re_{py})^{0.681} \quad \text{------3.6.7.}$$

where $Re_{px} = \frac{\rho U_x h}{\mu}$ and $Re_{py} = \frac{\rho U_y h}{\mu}$

Care must be taken when using 3.6.6 and 3.6.7 to ensure that the values j_x and j_y do not fall below unity.

3.6.3 Use of the Turbulent Theories

As has already been discussed, the proportions of Couette and Poiseuille flow existing in the case of tyres on wet roads will vary. A scheme has been used which was suggested by Constantinescu (41), where the maximum value of the j_x or j_y factor, found by either Couette or Poiseuille methods, is used. This allows the automatic handling of the case of mixed flows.

3.7 BOUNDARY CONDITIONS

There are two types of boundary conditions which can be used in this type of problem: flow boundary conditions and pressure boundary conditions. As was discussed in section 1.2.1, a number of different methods have been used in the past to specify boundary conditions in wet grip models, particularly on the front edge of the contact patch. In addition to boundary conditions applied on the edges of the tyre contact patch, it is also necessary to consider boundary conditions on the centre line, so that if the tyre is symmetrical about this line, only half the contact patch need be modelled.

3.7.1 Side Edges of the Contact Patch

At the side edges of the contact patch the pressure is assumed to be zero (atmospheric). This can be justified by the fact that outside the contact patch the water on the road must have a free surface, and therefore, must be at atmospheric pressure. At the edge of the contact patch there is also an abrupt change in the film thickness which will tend to cause the flow to separate and hence the pressure to fall to atmospheric.

3.7.2 Rear of the Contact Patch

The pressure at the rear edge of the contact patch is also assumed to be zero. The reasons for this are similar to those for the side edges of the contact patch. At the rear of the contact patch there is, however, not such an abrupt change in the film thickness as at the side edges, but behind the contact patch there is water with a free surface which must be at atmospheric pressure.

The thickness of the film of water on the road surface, behind the contact patch, will be very small because the majority of the water will have been removed to the sides by the passing of the tyre. This situation can be seen in glass plate photographs, such as those in figure 5.3.1. Therefore, the point at which the tyre tread surface meets the free surface of the water will be very close to the actual rear edge of the contact patch; it will be considered for this work to be actually at the rear edge of the contact patch. Because of this, the pressure at the rear edge of the contact patch will be atmospheric.

When the wheel is rotating, there will be some upward movement at the rear of the contact patch, which will tend to promote separation and, under certain circumstances, cavitation. This is a further argument in favour of making the pressure atmospheric at the rear edge of the contact patch. Browne in (9) uses similar arguments to these for the boundary conditions at both the rear and sides of the contact patch.

3.7.3 Centre Line of the Contact Patch

If the possible existence of symmetry about the contact patch centre line is to be taken advantage of, then it is necessary to specify zero flow across this boundary. This method of introducing an axis of symmetry into a fluid problem is equivalent to the centre line being a streamline.

It is worth mentioning here that when using the finite element method to solve both fluids and structural problems, where a line of symmetry is used, the correct solution is not always obtained. This is due to the discretisation process, introducing errors and distorting the results near to the axis of symmetry. Because of this possible distortion of results, it is best to model the whole of the contact patch whenever possible.

3.7.4 Front Edge of the Contact Patch

The front edge boundary conditions are the most difficult to specify. Two strategies are discussed, the second of which has been developed here and is implemented in the computer program.

The first is included as being typical of the type that has been used in past work. (e.g. Browne (9)). This is based on the assumption that fluid impinging on the front of the contact patch has its velocity changed. It is convenient to consider the wheel axle stationary with the road surface moving beneath it, as shown in figure 3.7.1.

Considering the energy at position ①-① neglecting elevation,

$$E_{①} = \frac{V_1^2}{2g} + \frac{p_1}{\rho g}$$

as there is a free surface at ①-① then $p_1 = 0$, also $V_1 = V_{ROAD}$, therefore:

$$E_{①} = \frac{V_{ROAD}^2}{2g} \qquad \text{----------3.7.1}$$

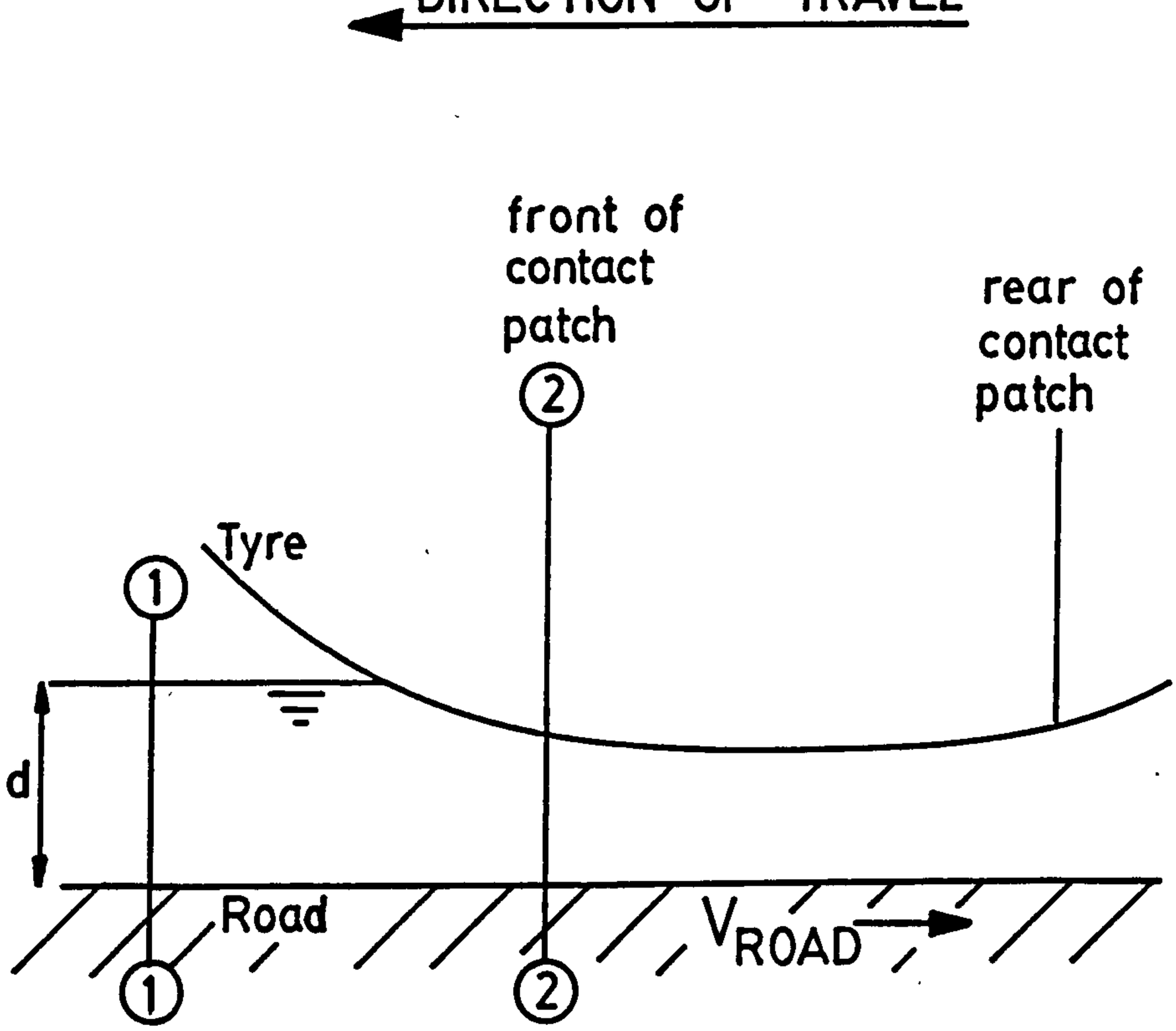

FIGURE 3.7.1 - FLUID FLOW FOR FRONT EDGE PRESSURE BOUNDARY CONDITIONS

Similarly, considering the energy at position ②-②

$$E_{②} = \frac{V_2^2}{2g} + \frac{p_2}{\rho g} \qquad \text{----------3.7.2}$$

If it is assumed that there is no loss of energy between ①-① and ②-②; in this case, mainly assuming that there is no side flow, then

$$E_{①} = E_{②}$$

and 3.7.1 and 3.7.2 give

$$p_2 = \frac{\rho}{2} (V_{ROAD}^2 - V_2^2) \qquad \text{---------3.7.3}$$

If one is to use the above representation of the front edge boundary conditions, it should be noted that the pressure P_2 is dependent on the velocity V_2, the average flow velocity into the front edge of the contact patch. V_2 is unknown and, in turn, will depend on the level of the pressure P_2. An iterative solution of equation 3.7.3 would, therefore, be necessary.

The second strategy which has been developed here is based on the fact that there cannot be any side flow at the front edge of the contact patch. This can be shown to be so by considering the water, which has a free surface ahead of the front of the contact patch. The wave propogation speed in that water is governed by the critical velocity (34).

$$U_{CRIT} = \sqrt{gd}$$

which is equivalent to a Froude Number of unity.

Typical conditions on a road surface would be with water depths ('d') of 1 to 3mm, and taking the 3mm case this gives a critical velocity of:

$$U_{CRIT} = 0.17 \text{ m/s}$$

The implication of this is that if the vehicle road speed is greater than the wave propagation speed in the road surface water, then water cannot be deflected around the sides of the contact patch, and all water in the path of the tyre must enter the front of the contact patch.

A critical velocity of 0.17 m/s represents a vehicle road speed of 0.6 Kph. Therefore, under all conditions of relevance the vehicle will be travelling at a speed very much greater than the wave propagation speed in the road surface water.

The neglect of side flow in the formulation of equation 3.7.3 is therefore valid, providing the front of the contact patch (position ②) is defined as the point where the free surface film meets the tyre tread surface. If position ② were to be taken further into the contact patch then there would no longer be a free surface and there could be side flow. Under these circumstances the fluid velocity at ② must be equal to the road speed, and equation 3.7.3 gives $p_2 = 0$ (atmospheric). This must also be true because there is a free surface immediately ahead of the front of the contact path.

Pressure equal to atmospheric could therefore be used as a boundary condition at the front of the contact patch, but the limitation on flow at the front of the contact patch was thought to be more important; and, as it is only possible to use either flow or pressure boundary conditions at one point, then flow boundary conditions were imposed at the front of the contact patch.

As all the water in the road surface film must enter the front of the contact patch, it is simply a matter of using flow boundary conditions within the finite element method to obtain a representation of this. The details of how flow boundary conditions are included in the finite element method are given in section 3.4 and Appendix A. Flow boundary conditions are specified as volumetric flow per unit width normal to the boundary at that point.

In this case we have

$$q_x = V_{ROAD}\, d \cos \emptyset \quad \text{----------3.7.4}$$

$$q_y = V_{ROAD}\, d \sin \emptyset \quad \text{----------3.7.5.}$$

where $\emptyset$ is the tyre slip angle and 'd' the road surface water depth. For the straight ahead position,

$$q_x = V_{ROAD}\, d$$

and $$q_y = 0$$

By specifying q_x and q_y separately, they can be entered as such into the finite element formulation without the need to calculate their resultant normal to the front edge of the contact patch. In the computer program velocities are measured relative to the contact patch and not the axle as here, therefore equations 3.7.4 and 3.7.5 are modified slightly when used in the program.

In (9) Browne only considers tyres with square fronted contact patches, and presumably, with zero slip angle, although this is not explicitly stated. By using the flow boundary conditions developed here, contact patches of any shape and with any slip angle can be modelled realistically.

The position of the front of the wet contact patch also follows from the preceding argument. If all the fluid enters the front of the contact patch, then the front of the contact patch will be defined as

the point where the tyre surface and the free water surface meet, as shown in figure 3.7.2.

Therefore, in the wet there is an extra region to the contact patch which is capable of supporting a load. This region is also important in determining the movements in the contact patch when the tyre is rolling. This is covered in section 3.8.

3.8 MOVEMENT WITHIN THE CONTACT PATCH

It is the movement of the tyre tread surface relative to the road surface, together with water flow at the front of the contact patch, that causes a pressure to exist between the tyre and the road surface. These movements can be classified by the two extreme conditions of free rolling and locked wheel.

Free rolling is defined as the condition when a vehicle is moving with no relative slip between the tyre and road surface. When rolling, as a point on the tyre circumference enters the contact patch, the radius of the tyre at that point reduces; therefore, the linear velocity of the tyre periphery must also reduce as the front of the contact patch is entered.

The converse is true at the rear of the contact patch with the linear velocity increasing as the contact patch is exited. This situation means that there must be some slippage between parts of the tyre and the road surface, and this is known as 'microslip'. In the context of this work, microslip will be neglected.

The other extreme condition, locked wheel, is when the wheel is not rotating and all vehicle movement is reflected in slip between the tyre contact patch and the road surface.

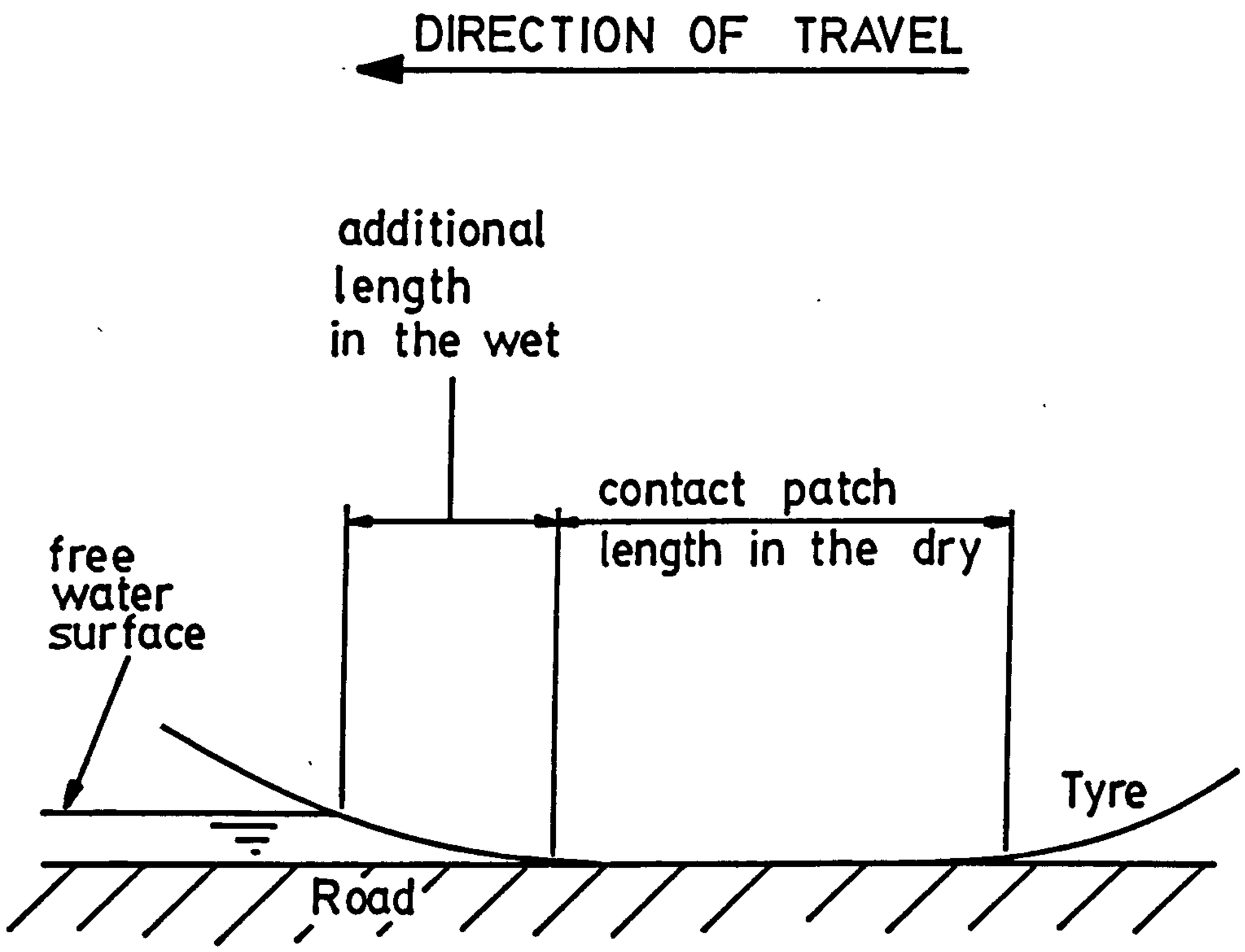

FIGURE 3.7.2 - ADDITIONAL CONTACT PATCH LENGTH IN THE WET

There are a number of slightly differing definitions of slip, but the one which will be used here is:

$$s = \frac{V_s}{V_{ROAD}} \qquad \text{----------3.8.1}$$

where V_s is the relative velocity between the tyre contact patch and the road surface, i.e. the slip velocity. The value of s therefore varies between 0.0 (free rolling) and 1.0 (locked wheel).

3.8.1. Sliding

Where the tyre is sliding on the road surface, the x and y components of slip velocity are given by,

$$V_x = V_s \cos \phi \qquad \text{----------3.8.2.}$$

$$V_y = V_s \sin \phi \qquad \text{----------3.8.3.}$$

where Ø is the tyre slip angle.

Therefore, combining equations 3.8.1., 3.8.2 and 3.8.3 gives:

$$V_x = s\ V_{ROAD} \cos \phi \qquad \text{----------3.8.4}$$

$$V_y = s\ V_{ROAD} \sin \phi \qquad \text{----------3.8.5}$$

These are the x and y components of sliding velocity as functions of vehicle road speed, slip and slip angle.

The x and y components of relative velocities are now specified requiring only the h (vertical) component to be specified to describe completely movement within the contact patch.

3.8.2 Rolling

It has already been stated that under rolling conditions, the rear of the contact patch will tend to separate from the road surface with a vertical velocity. Under these circumstances the water film will tend to break-up; therefore, upward movement of the tread behind the contact patch need not be included in the model.

At the front of the contact patch, the converse is true, the tyre tread is approaching the road surface with a vertical velocity which acts as a 'squeeze film'.

As has already been discussed in section 3.7.4, there is an area in front of the dry contact patch which is considered in the application of boundary conditions. When the tyre tread is undeformed and there is no water film thickness between the dry contact patch and the road surface, then only this additional part of the wet contact patch is able to approach the road surface with a vertical velocity.

The whole aspect of vertical movements within the contact patch is little understood. Therefore, a very much simplified method of treating these movements is used here, as a full study of this is outside the scope of this project (see section 8.3.1).

It is shown in (72) that a rolling tyre can be considered to be instantaneously rotating about a point 'R' beneath the road surface, as shown in figure 3.8.1.

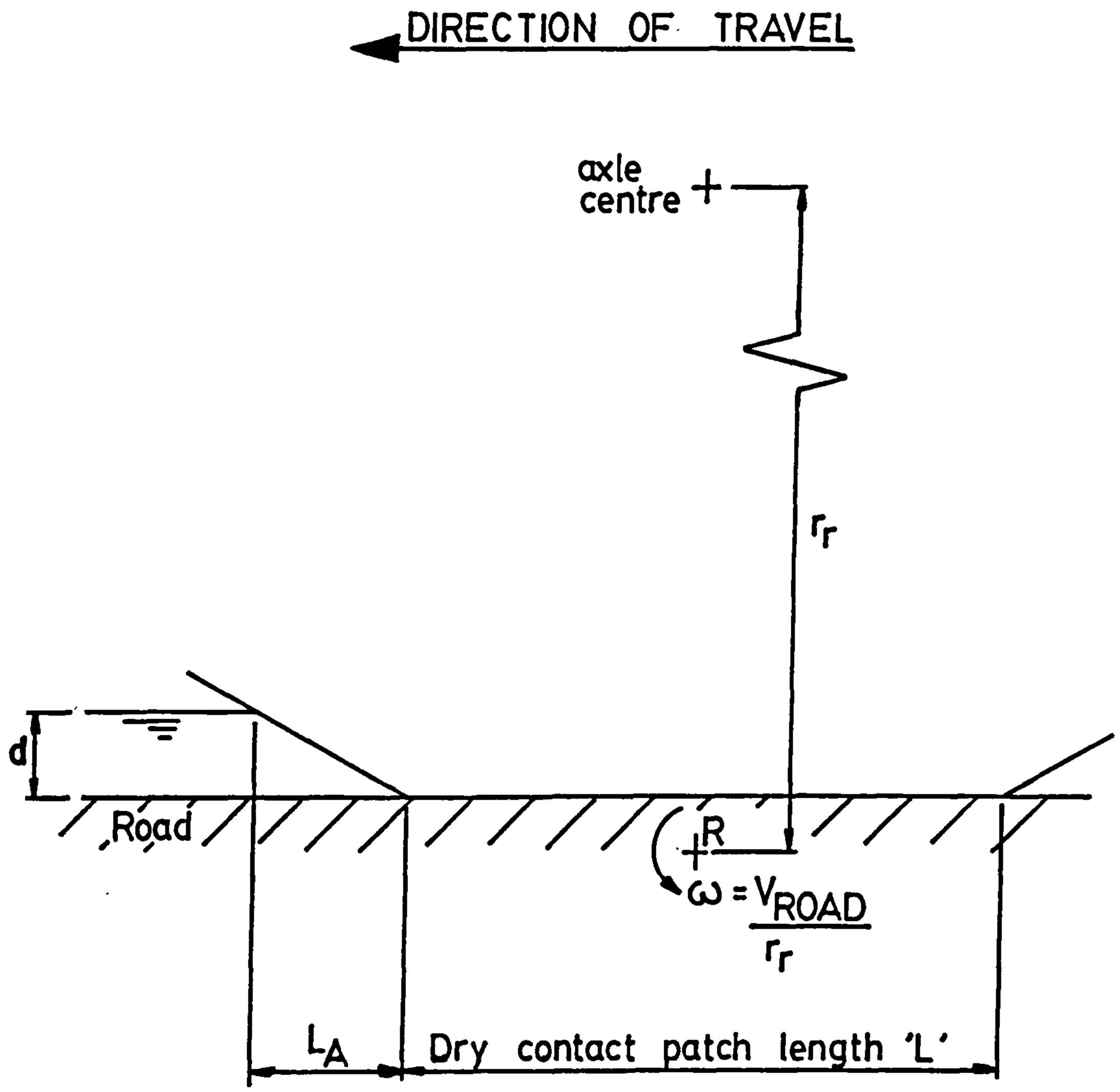

FIGURE 3.8.1 - CONTACT PATCH ROTATION

The front of the wet contact patch is defined in section 3.7.4 as the point when the tyre tread surface meets the free surface of the road surface water. By considering the geometry of the situation shown in figure 3.8.1., it can be shown that the treadsurface at the front of the wet contact patch will be on the undeformed tyre circumference. Therefore, this point is rotating about 'R' and its vertical velocity (V_{VERT}) is given by (notation as figure 3.8.1).

$$V_{VERT} = \left(\frac{L}{2} + L_A\right) \frac{V_{ROAD}}{r_r} \qquad \text{----3.8.6}$$

Further into the front of the wet contact patch, the tread surface deviates from the circumference of the tyre. At the front of the dry contact patch, the vertical component of velocity must be zero. The variation of velocity from that given by equation 3.8.6, at the front of the wet contact patch, to zero at the front of the dry contact patch is however not linear. The overall constraint is that a point on the tyre surface must move down by a distance 'd' (figure 3.8.1) in the time taken for the tyre to move forward a distance 'L_A'. The mean velocity must, therefore, be

$$V_{MEAN} = \frac{d}{L_A} V_{ROAD} \qquad \text{------3.8.7}$$

The vertical velocity variation in the front of the contact patch is shown diagrammatically in figure 3.8.2.

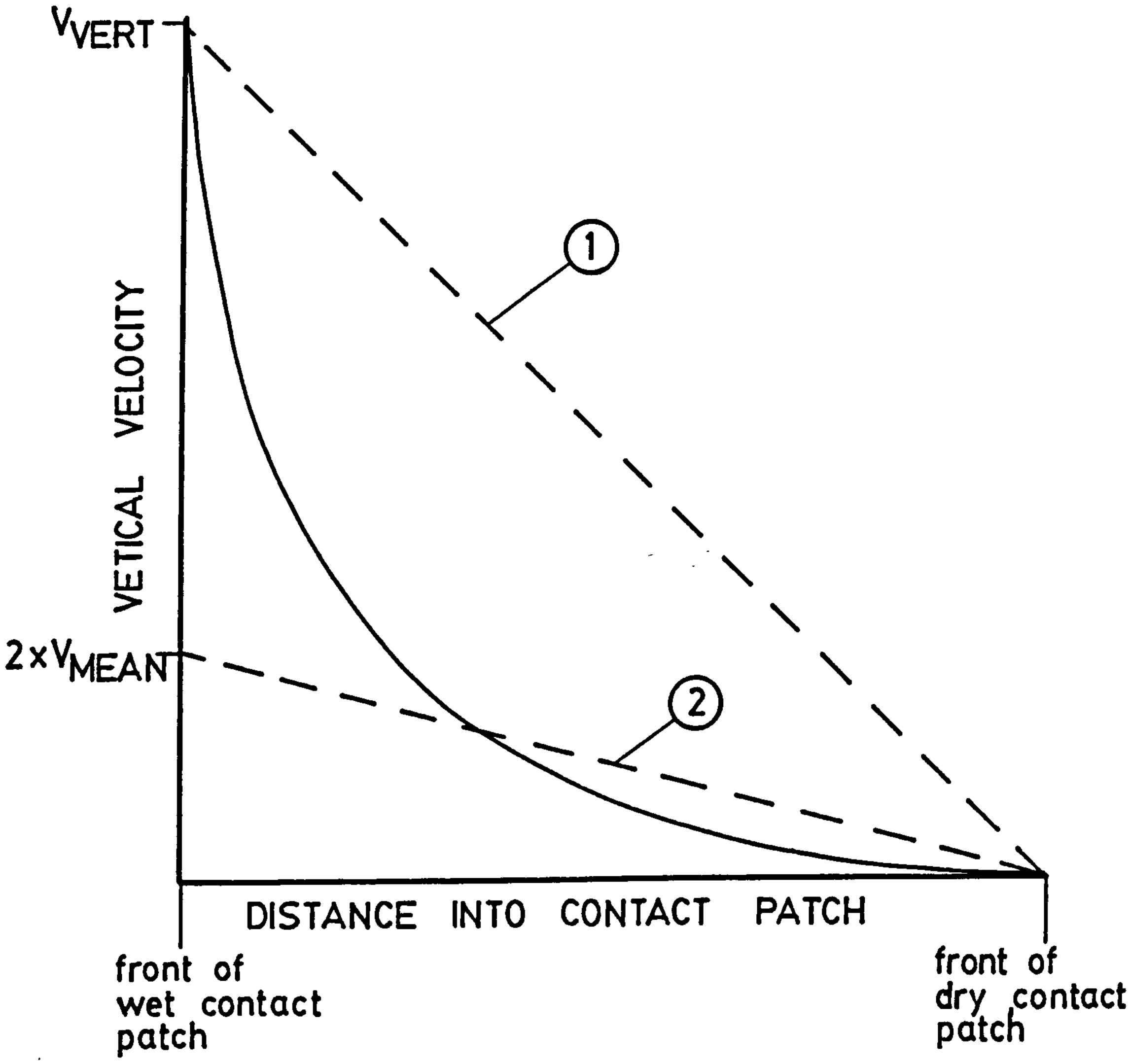

FIGURE 3.8.2 - VERTICAL VELOCITIES AT THE FRONT OF THE CONTACT PATCH

The exact nature of the curve shown in figure 3.8.2 is not known. If one were to use a linear velocity distribution based on the velocity in equation 3.8.6, then the velocity profile would be as shown by the dashed line ① in figure 3.8.2. In this case, the overall movements (area under curve) would be greatly exaggerated. Alternatively, one could use a velocity distribution based on the mean velocity given by equation 3.8.7, i.e. 2 x V_{MEAN} at the front of the wet contact patch and linearly tapering to zero at the front of the dry contact patch, as shown by the dashed line ②. In this case, the effect of the high velocities at the front of the wet contact patch is ignored.

In practice, neither of the above methods proved satisfactory and a simplified technique was used based on considering the additional length 'L_A' to be rotating, with angular velocity ω , about the front of the dry contact patch as shown in figure 3.8.3.

The resulting vertical velocity distribution falls between those by the above two methods, and gives a compromise between high front edge velocities and correct overall movement. The vertical velocity at any point in this area is, therefore, given by

$$V_h = \frac{a}{r_r} V_{ROAD} \qquad \text{--------3.8.8}$$

where 'a' is the distance from the point to the front of the dry contact patch. Equation 3.8.8 is valid only for a freely rotating tyre and for the more general case of a tyre under any slip condition,

$$V_h = \frac{a}{r_r} V_{ROAD} \quad (1 - s) \qquad \text{------3.8.9}$$

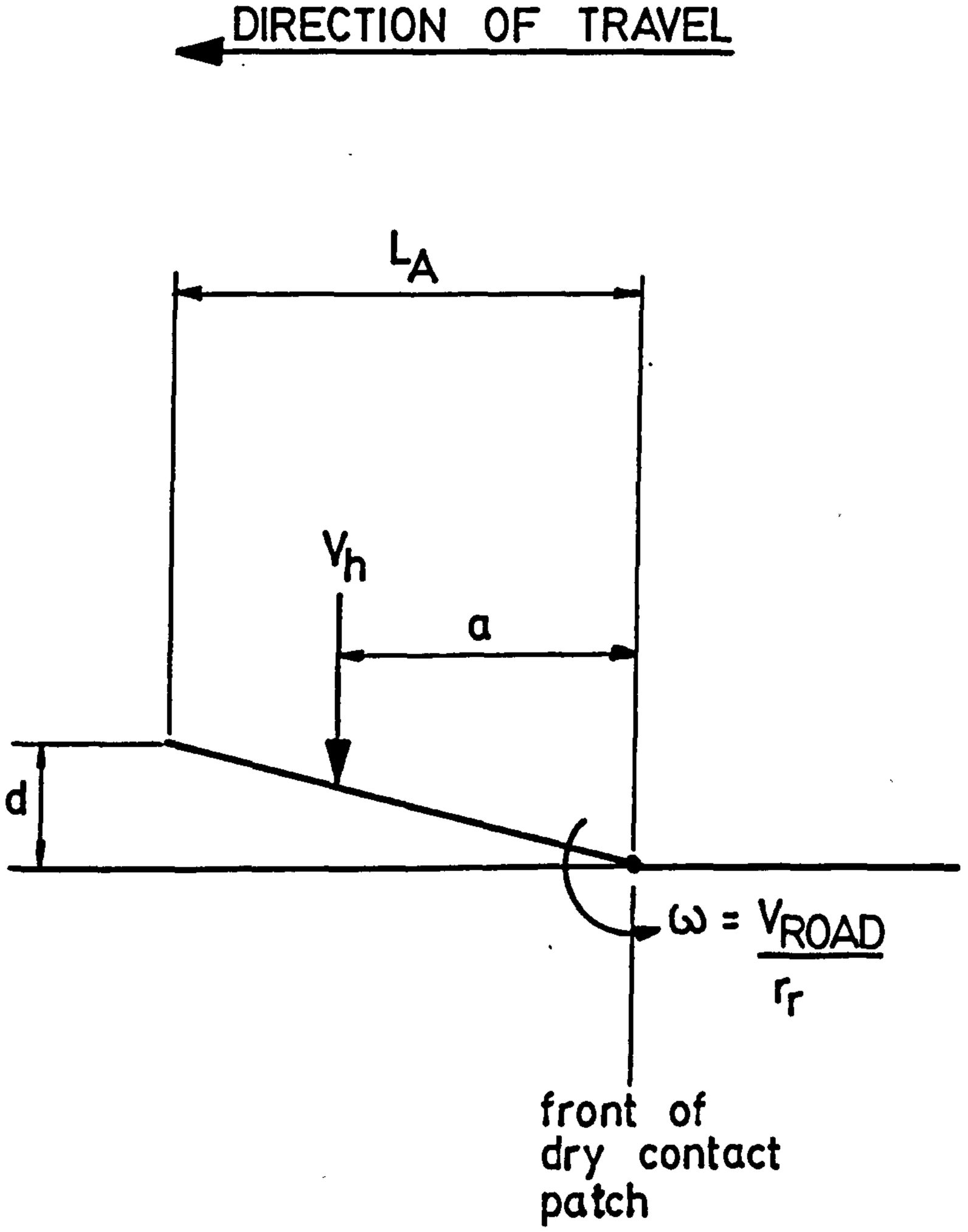

FIGURE 3.8.3 - SIMPLIFIED VERTICAL MOVEMENTS IN THE CONTACT PATCH

By considering tyre data (19), an approximate value for the length 'L_A' can be found for various values of road surface water depth. For a 155R13 tyre, this was estimated to be between 38 and 42mm for water depth ranging from 1 to 3mm. 'L_A' can also be estimated from static glass plate photographs where the water surface/tyre surface contact can be seen. The values of 'L_A' found by these two methods agree well.

In reality, the vertical movements of the tyre contact patch will be much more complex than have so far been considered. It was stated that the only portion of the wet contact patch that can have a vertical velocity is the area ahead of the front of the dry contact patch. When a film of water exists between the tyre and the road, then it is possible that other areas of the contact patch also have vertical velocities.

The expected velocity profile shown in figure 3.8.2 is based on a tyre undeformed due to fluid pressure, but the deformation due to fluid pressure will alter the shape of the tyre in this region. If the tyre is 'flattened' by the fluid pressure so that its rate of approach to the road surface is less in this region, then there will be a vertical velocity further to the rear of the contact patch. In fact, one could consider that the tyre will, to some extent, rotate about the furthest point forward, which is in contact with the road surface.

Having vertical velocities further to the rear of the contact patch, with velocities of lower magnitude at the front of the contact patch, will cause there to be higher fluid pressures to the rear of the contact patch. Considering the experimental values of fluid pressure for a free rolling tyre, given in chapter 6, it can be seen that this will give better correlation between analytical and experimental results.

If the vertical velocity modelling is to be improved, then as discussed above, it will be dependent to some extent on the fluid film thickness shape of the deformed tyre. The vertical velocities would, therefore, need to be calculated at each iteration through the solution procedure. Before this can be done however, more experimental work is required, studying the vertical movements of tyres, both in, and on entry to the contact patch. For this reason, the simplified method of considering rotation about the front of the dry contact patch has been used in the present version of the computer program. The tyre tread block analysis computer program treats the velocities differently, as these are local velocities within the contact patch. Therefore, the user explicitly specifies the three components of velocity for the block when using this program.

3.9 GROOVE FLOW FACTOR

A "groove flow factor" is used to modify the fluid flow for elements which are defined to be the tyre grooves. This is necessary because of the very different magnitudes of water film thickness found under a tyre tread block and in the grooves of a tyre. Typically, a groove in a new tyre would be 8mm deep, and the fluid film under the block of a tyre would be, say, 0.1mm. As well as this difference in film thickness, the side walls of a groove effect the flow and no allowance is made for side walls in an analysis using Reynolds equation.

The numerical analysis used here is two-dimensional using Reynolds equation for fluid film lubrication. A more appropriate method of analysing the flow in tyre grooves would be to treat the grooves as rectangular 'pipes'. Pipe flow is essentially one-dimensional, i.e. flow is along the axis of the pipe, but in the case of tyre grooves, there will be some flow into or out of the grooves along their length - a leaky pipe! This 'leakage' will, however, be small compared to the flow along the groove because of the large difference in film thickness between a groove and a block.

A flow factor F_F will now be developed which can be used in the finite element formulation for elements which are in tyre grooves to modify the flow properties within these elements.

If we consider flow through a rectangular slot, as given by a one-dimensional Reynolds equation, then the volume flow per unit width q is given by (31).

$$q = \frac{Vh}{2} - \frac{h^3}{12\mu} \cdot \frac{dp}{dx} \qquad \text{----------3.9.1}$$

To allow a direct comparison with the properties of a rectangular pipe, it will be assumed that there is no relative movement between the two surfaces, i.e. V = 0, and that the water film thickness is constant; therefore, 3.9.1 becomes,

$$q = - \frac{h^3}{12\mu} \cdot \frac{dp}{dx} \qquad \text{----------3.9.2}$$

As the two surfaces through which flow takes place are parallel, the volume flow per unit width must be constant through the slot. Therefore $\frac{dp}{dx}$ must also be a constant, from equation 3.9.2.

$\frac{dp}{dx}$ constant implies that there is a linear pressure drop through the slot, i.e.

$$p = P_i - \frac{x}{l} (P_i - P_o) \qquad \text{----------3.9.3}$$

where the particular notation is shown in figure 3.9.1.

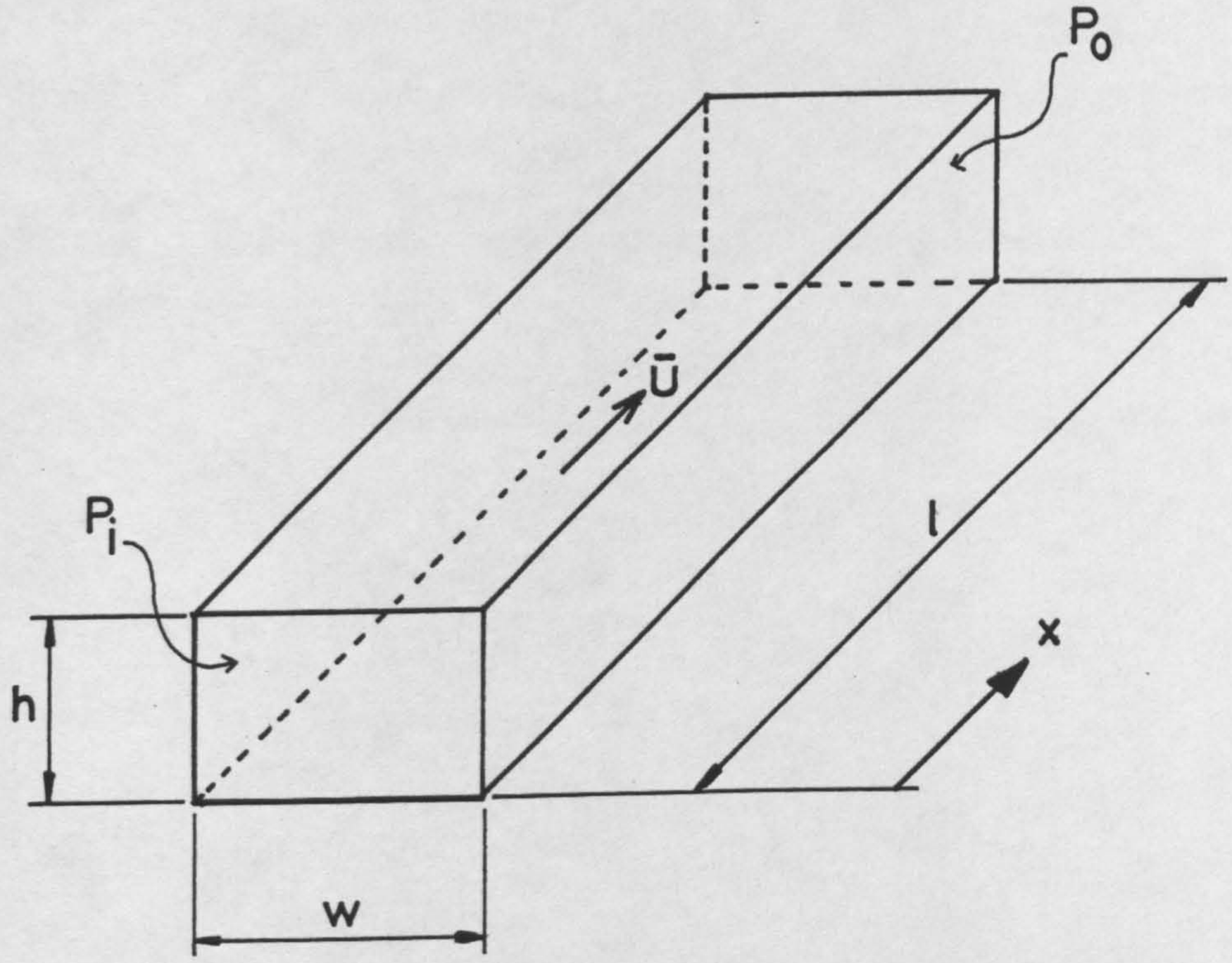

FIGURE 3.9.1 - SLOT GEOMETRY AND NOTATION

Differentiating equation 3.9.3 gives,

$$\frac{dp}{dx} = - \frac{(P_i - P_o)}{l} \qquad \text{----------3.9.4}$$

and if we let $\Delta_{p_R} = P_i - P_o$ and substitute 3.9.4 in 3.9.2, then

$$q = \frac{h^3 \Delta p_R}{12 \mu l} \qquad \text{----------3.9.5}$$

Equation 3.9.5 gives the volume flow per unit width, but if the slot has a width of w (figure 3.9.1) then

$$Q = \frac{h^3 w \Delta p_R}{12 \mu l} \qquad \text{----------3.9.6}$$

where Q is the total volume flow through the slot.

Equation 3.9.6 is the relationship between pressure drop and volume flow given by Reynolds equation and is only really applicable for slots where $w >> h$, so that the effect of the slot's sidewalls may be neglected.

The flow in a pipe is given by Darcy's equation (34),

$$\frac{\Delta p_D}{\rho g} = \frac{f l \bar{U}^2}{m 2g} \qquad \text{----------3.9.7}$$

(Note that the 'f' here incorporates the constant '4')

In equation 3.9.7, 'm' is the hydraulic mean depth and for a rectangular pipe, using the notation of figure 3.9.1,

$$m = \frac{\text{cross-sectional area}}{\text{perimeter}} = \frac{wh}{2(w+h)} \qquad \text{----------3.9.8}$$

To allow a direct comparison between the pressure drop/flow relationship given by Reynolds equation (3.9.6), and the similar relationship given by Darcy's equation for pipe flow, the flow in the pipe will be considered laminar, i.e. (34),

$$f = \frac{16}{Re} \qquad \text{----------3.9.9}$$

where Re is Reynolds Number in the pipe based on mean flow velocity. For a rectangular pipe, Re is given by

$$Re = \frac{\rho \bar{U} 4m}{\mu} \qquad \text{----------3.9.10}$$

where '4m' replaces 'd', the pipe diameter as normally found for circular pipes. Equations 3.9.9 and 3.9.10 give

$$f = \frac{4\mu}{Um\rho} \; ; \qquad \text{----------3.9.11}$$

substituting 3.9.11 in 3.9.7 gives

$$\Delta p_D = \frac{2\mu l \bar{U}}{m^2} \qquad \text{----------3.9.12}$$

In equation 3.9.12, $\bar{U}$ is the mean flow velocity. Therefore, the mean volumetric flow through the rectangular pipe is given by

$$Q = \bar{U}A;$$

therefore

$$\bar{U} = \frac{Q}{A} = \frac{Q}{wh} \qquad \text{----------3.9.13}$$

Substituting equation 3.9.13 onto equation 3.9.12 gives,

$$\Delta p_D = \frac{2\mu l Q}{m^2 wh} \qquad \text{----------3.9.14}$$

and equation 3.9.8 in equation 3.9.14 gives

$$\Delta p_D = \frac{8\mu lQ(w+h)^2}{w^3h^3} \quad \text{-----3.9.15}$$

Equation 3.9.15 is the relationship between pressure drop and volume flow given by Darcy's equation for pipe flow.

If equation 3.9.6 for Reynolds equation flow is re-arranged to be of the same form as 3.9.15, then 3.9.6 gives

$$\Delta p_R = \frac{12\mu lQ}{h^3 w} \quad \text{-----3.9.16}$$

Re-arranging equation 3.9.15 gives

$$\Delta p_D = \frac{2}{3}\frac{(w+h)^2}{w^2} \cdot \frac{12\mu lQ}{h^3 w} \quad \text{-----3.9.17}$$

If we compare equations 3.9.16 and 3.9.17, we see that the pressure drop Δp_D, given by Darcy's equation for pipe flow, is greater than Δp_R given by Reynolds equation, by a factor of $\frac{2}{3}\frac{(w+h)^2}{w^2}$

As the analysis developed in section 3.3 and 3.4 uses Reynolds equation, then to effectively use pipe flow theory for elements within a groove it is necessary to multiply the pressure drop by the factor $\frac{2}{3}\frac{(w+h)^2}{w^2}$

Let $$F_F = \frac{2}{3}\frac{(w+h)^2}{w^2} \quad \text{------3.9.18}$$

Referring to equation 3.9.16 and 3.9.17, it is convenient to consider F_F to be a factor by which the viscosity in Reynolds equation should be multiplied. This should not be confused with the effective viscosity calculations described in section 3.6. Equation 3.3.1 (section 33) could be re-written to include the groove flow factor.

$$\frac{\partial}{\partial x}\left(\frac{h^3}{12F_F\mu_x}\frac{\partial p}{\partial x}\right) + \frac{\partial}{\partial y}\left(\frac{h^3}{12F_F\mu_y}\frac{\partial p}{\partial y}\right) = \frac{1}{2}\frac{\partial}{\partial x}(V_x h) + \frac{1}{2}\frac{\partial}{\partial y}(V_y h) + \frac{\partial h}{\partial t} \quad \text{-----3.9.19}$$

F_F is applied to flow in both the x and y directions, as the axis of a groove may be orientated in any direction. If, for example, a groove ran from front to rear of the contact patch, the x direction, then F_F would also be applied to flow in the y direction. However, as was stated earlier, the flow is predominantly along the axis of the groove, therefore, in this case there would be little flow in the y direction. The use of F_F in the y direction would therefore only have a small effect on the result compared with its effect in the x direction.

3.9.1 The Limiting Case for the Groove Flow Factor

The limiting case for the use of the groove flow factor is when $F_F = 1$. That is to say, when $F_F \leqslant 1$ then Reynolds equation is applicable and when $F_F > 1$ Darcy's pipe flow equation is applicable.

Limiting case when,

$$\frac{2}{3}\left(\frac{w + h}{w^2}\right)^2 = 1$$

$$\text{i.e.} \quad \frac{w}{h} = 4.45 \quad \text{-----3.9.20}$$

Equation 3.9.20 states that grooves with a width of less than approximately 4½ times their depth will need to use the groove flow factor to correctly predict the relationship between pressure drop and fluid flow. $w < 4.45h$ covers all the grooves normally found in tyres, except for the case of very worn tyres.

The variation of F_F for different values of $\frac{w}{h}$ is shown in figure 3.9.2.

3.9.2 The Physical Significance of the Groove Flow Factor

With reference to figure 3.9.2, it can be seen that for tyre grooves in the region of practical interest the value of F_F is sensitive to changes in $\frac{w}{h}$. If one considers just the drainage capacity of tyre grooves, then by examining equation 3.9.17, the pressure drop in a section of groove, due to changes in groove depth, is

$$\Delta p \propto \frac{F_F}{h^3 w} = \frac{2}{3} \frac{(w + h)^2}{h^3 w^3}$$

The drainage capacity can be expressed as

$$\text{drainage capacity} \propto \frac{1}{\Delta p}$$

therefore,

$$\text{drainage capacity} \propto \frac{h^3 w^3}{(h+w)^2} \qquad \text{------3.9.21}$$

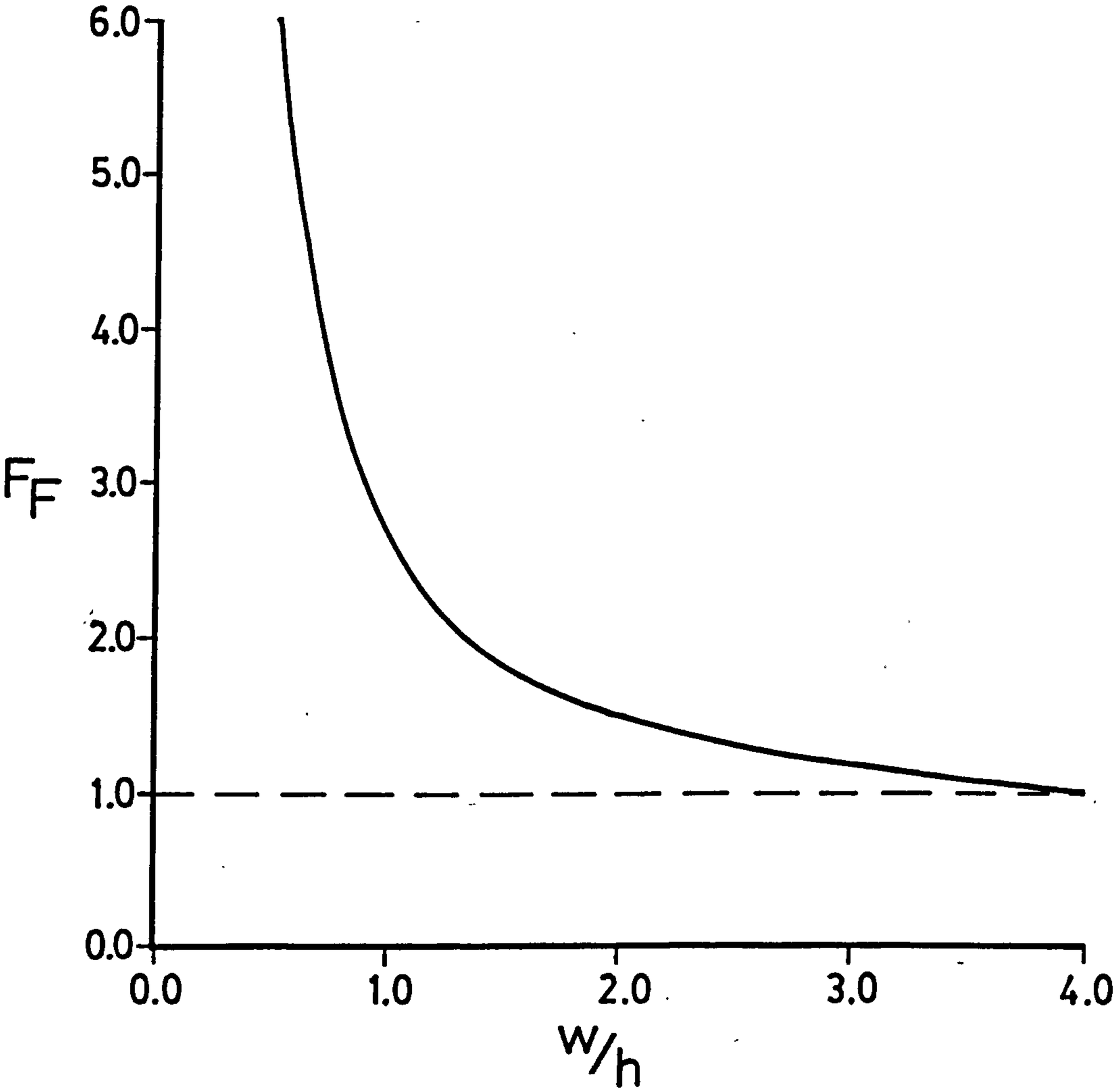

FIGURE 3.9.2 - GROOVE FLOW FACTOR AGAINST GROOVE ASPECT RATIO

The approximate relationship (3.9.21) between drainage capacity and groove depth and width can be used to show the effects on drainage of a reducing groove depth. Figure 3.9.3 shows such a relationship with the drainage expressed as a proportion of the new tyre (8mm deep groove) drainage capacity. Also shown on figure 3.9.3 are figures showing the reduction in peak brake force coefficient. The brake force coefficient figures are taken for a tyre travelling at high speed. This is because in the formulation of the fluid problem, it is assumed that the area under consideration (in this case the grooves) is flooded with water, and when the tyre is moving at high speed there will be the greatest tendency for the contact patch to be flooded with water.

In the model when the contact patch is not flooded (specified by the user), the elements which have been defined as being in grooves are removed from the mesh and zero pressure boundary conditions are applied to nodes on the edges of all the blocks. This can be done because if a groove is not flooded there must be a free surface within the groove and therefore the pressure must be atmospheric. The use of the groove flow factor developed here is, therefore, limited to the case of flooded contact patches.

		with 4mm wide grooves	
Groove depth (mm)	w/h	Drainage Capacity Relative to New Tyre	Brake Force Co-efficient Relative to New Tyre
8	0.5	100%	100%
6	0.667	61%	79%
4	1.0	28%	55.5%
2	2.0	6%	47%
1	4.0	1.1%	24%
0	∞	0%	9%

FIGURE 3.9.3 - DRAINAGE CAPACITY

AND BRAKE FORCE COEFFICIENT

FOR DIFFERENT GROOVE ASPECT RATIOS

3.10 CONTACT PATCH DEFORMATIONS

As a tyre is constructed mainly from rubber, it will tend to deform elastically under the influence of fluid pressure. This has the effect of modifying the fluid film thickness, and thus the fluid pressures in the tyre/road contact area. It is, therefore, essential that any model of tyre behaviour in the wet should include tyre deformation under the action of fluid pressure. However, the complex nature of a tyre's construction makes a detailed analysis of tyre deformation difficult. To overcome this, in some past work a rigid shape has been chosen for the tyre under typical operating conditions. The complexity of this has ranged from a simple tapering wedge shape to the complex shape used by Browne in (11) and much of his other work.

The shape used by Browne was estimated from glass plate photographs of a plain tread tyre under typical operating conditions (10). This deformation is for a steel belted bias ply tyre under free rolling conditions, but Browne (11) states that the data can be used with reasonable accuracy on tyres of different construction and under different operating conditions. As the deformation used in (11) is for a plain tread tyre, when grooves are required the additional film thickness due to the grooves is superimposed on these deformations.

This method of incorporating tyre deformation into a model of tyre behaviour under wet conditions, is thought by the present author to be inadequate. In fairness though, Browne in a later paper (12) has introduced tyre deformation into tyre/fluid model developed for (11). In (12), Browne appears to use a full three-dimensional finite element model of the complete tyre structure using a commercially available computer package (NASTRAN). Browne (12) notes that it is very complex (expensive) to generate the stiffness matrix for the tyre structure, and also that there are convergence problems with the model.

In modelling the complete tyre structure to get any reasonable accuracy the various components within the tyre, such as cords, breakers, etc., have to be included in the model. It is also necessary to have finite element programs which can handle large deflections and non-linear materials. The analysis of tyre structures by the finite element method therefore requires special purpose computer programs, such as the ones available within Dunlop and described in (67).

These special computer programs only handle axi-symmetric and plane strain problems in two-dimensions and are, therefore, unsuitable for calculating the deflections of the contact patch surface due to fluid pressure. Because of the need to handle large deflections and non-linear materials, the deflections would have to be found by an incremental/iterative method in addition to the iterations between fluid pressure and deflection. The possibility of obtaining a stable converging solution under such conditions is small; therefore, a full finite element solution of the tyre structure was not attempted, and the deflections of the contact patch, due to fluid pressure, were approximated by a simplified model.

One approach would be to use a simplified model using the finite element method, where only the tyre contact patch is modelled. The problem with modelling only the tyre contact patch is in the specification of boundary conditions for the structural model. The only part of the tyre which does not deform is the bead area, which is in contact with the wheel rim. Therefore at no point within the contact patch can a fixed deflection be specified. If only the contact patch is being modelled then there must be some deflection specified, and, in effect, the finite element model of the tyre contact patch becomes a model of a slab of rubber on a rigid backing. With this simplification, the effect of internal detail within the tyre's structure is lost. This means that the effects on wet grip of changing the tyre's internal construction cannot be evaluated. This is not too much of a disadvantage as the object of this work is to allow evaluation of tyre tread patterns, and not construction, for wet grip properties.

As a finite element model of only the tyre contact patch simplifies the model to the extent that internal construction is not modelled, then there is little to be gained by using this method over other simplified models. Three different methods of modelling the contact patch deformation were evaluated.

3.10.1 The Strip Method

The strip method is a very simple method of modelling tyre contact patch deformations and was only used early on in the project.

The tyre contact patch is divided into strips which run from the front to the rear of the contact patch. These strips coincide with 'lines' of nodes in a rectangular grid based finite element mesh. The front edge of the contact patch is given a fixed film thickness and initially all 'strips' form a tapering film thickness from front to rear of the contact patch. The contact point for each strip is defined, and this point can move from front to rear of the contact patch. The geometry of an individual strip can, therefore, be varied as shown in figure 3.10.1.

The fluid film thickness ahead of the contact point therefore tapers from the fixed film thickness at the front of the contact patch to zero film thickness at the contact point. If a base line film thickness to simulate road surface drainage is required, then this must be added to the film thickness at all points.

The position of the contact point is determined by the pressures at nodes along the strip. The contact point is moved to the node on the strip whose fluid pressure is nearest to the dry contact pressure at that node.

The above process is repeated for each of the strips across the tyre, and each strip will therefore show the extent of water penetration into the contact patch as illustrated in figure 3.10.2.

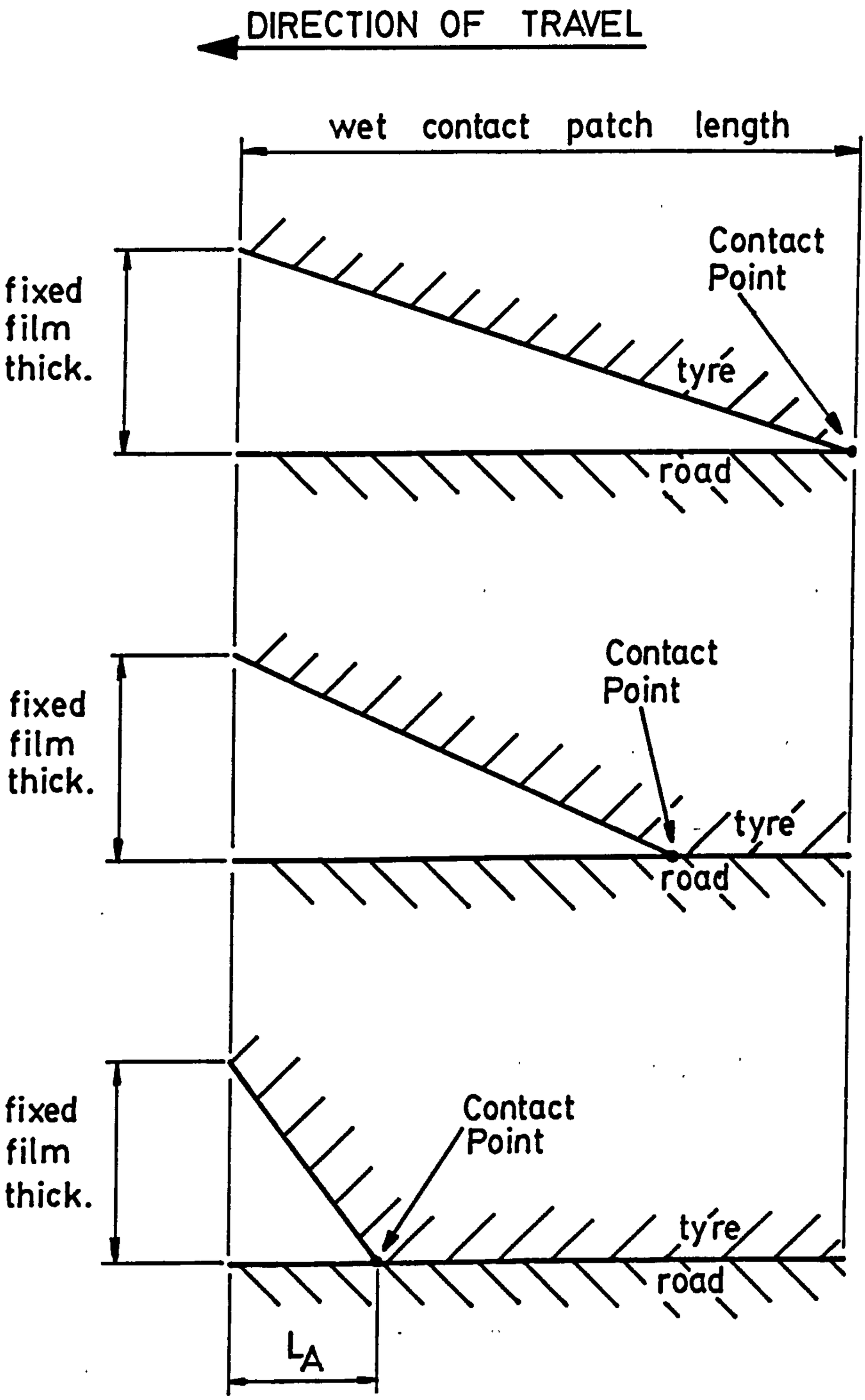

FIGURE 3.10.1 - CONTACT POINT POSITION

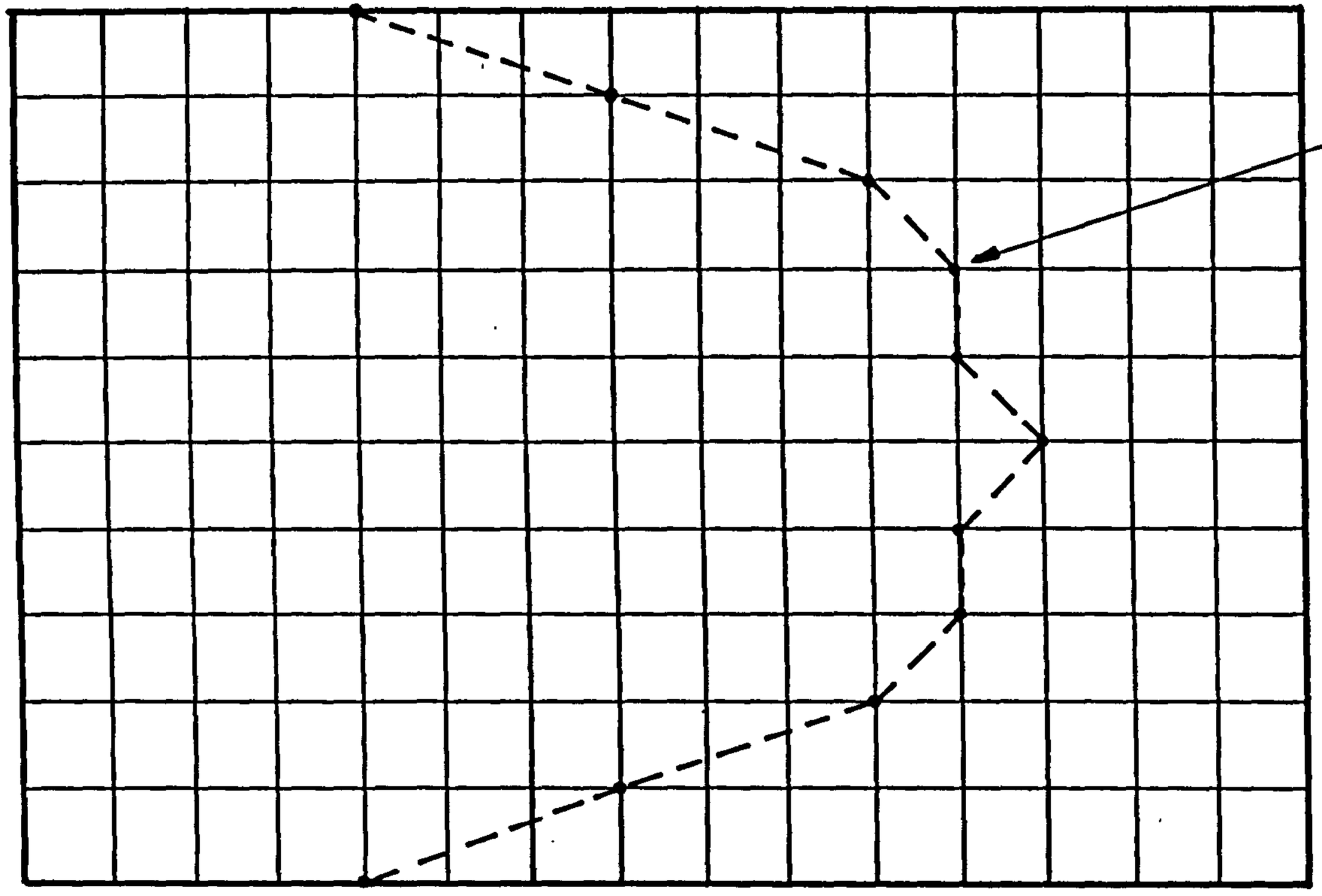

FIGURE 3.10.2 - WATER PENETRATION BY THE STRIP METHOD

Considering the very great simplifying assumptions made in this deflection model, the results obtained by it were remarkably good, exhibiting the classic "horse-shoe" type of water penetration into the front of the contact patch.

The restrictions on the type of fluid film that can be formed by this method seriously limit its usefulness and the need for a more realistic model was quickly identified.

3.10.2 'Column' Method

The column method of tyre contact patch deflection is based on the principle of treating each element as an independent column of material which compresses under the action of fluid pressure. The different deflections at each node due to the deflections of surrounding elements are then averaged to find the actual deflection of a particular node.

If we consider pressure acting over a triangular element, as shown in figure 3.10.3, then the mean pressure acting on that element will be,

$$P_m = \frac{(P_1 + P_2 + P_3)}{3} \qquad \text{----------3.10.1}$$

P_m can also be considered as the pressure acting at the centroid of the triangle. The total force acting on that element would, of course, be

$$F = P_m A \qquad \text{----------3.10.2}$$

Under equalibrium conditions, we can consider that the stress in the tyre normal to the tread surface is equal to the fluid pressure in the tyre/road interface. If we use the normal stress/strain relationship of

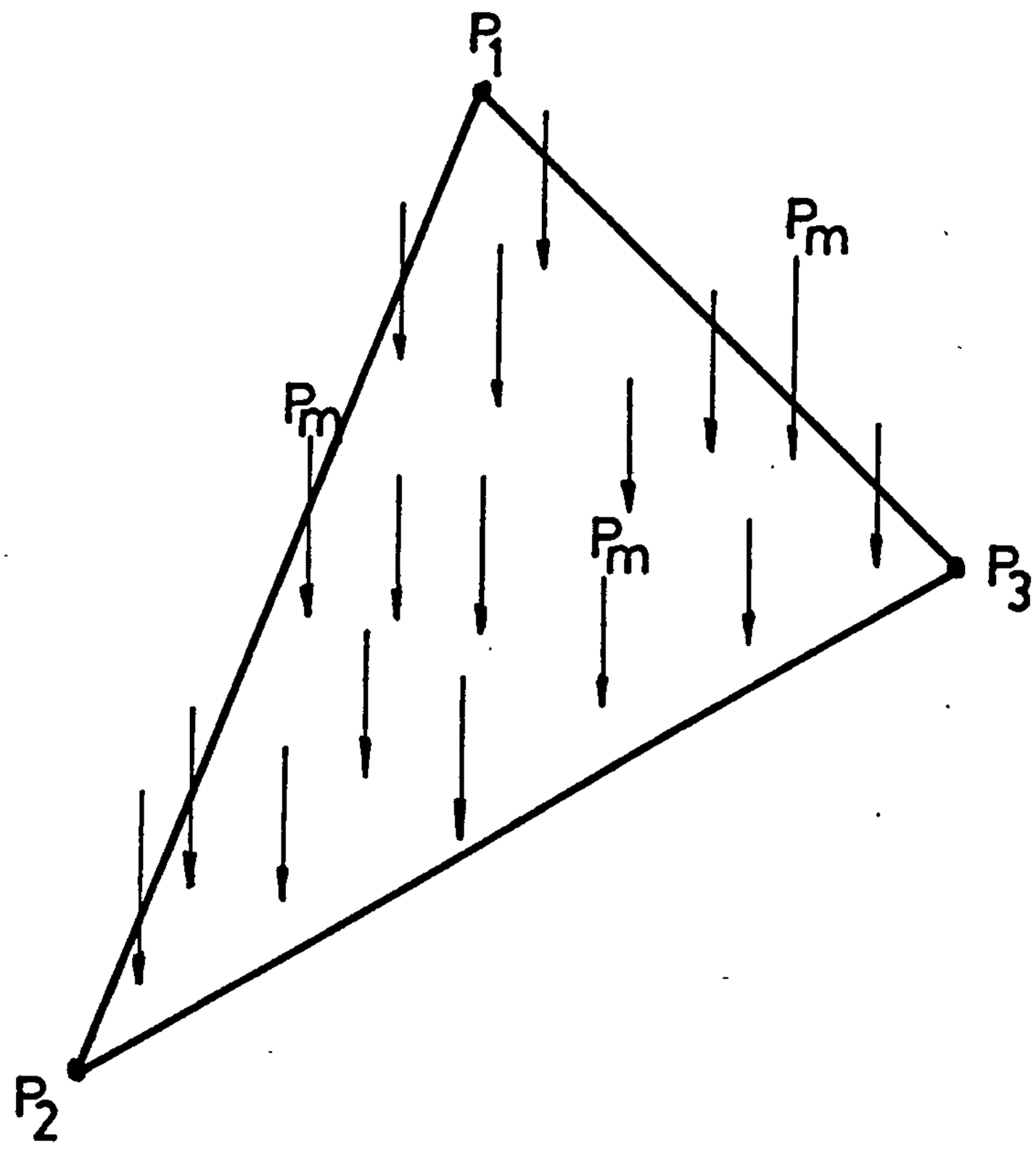

FIGURE 3.10.3 - PRESSURES ACTING ON A SINGLE ELEMENT

$$E' = \frac{\text{stress (or fluid pressure)}}{\text{strain}}$$

where E' is the effective elastic modulus of the material and strain is given by

$$\text{strain} = \frac{\delta}{t}$$

where δ is the vertical deflection of the element and t is the effective thickness of the material, we can therefore write

$$\delta = \frac{P_m t}{E'}$$

As δ is the mean deflection of an element, the deflection of a node can be found by averaging.

If this method is used, both the effective modulus and the effective material thickness must be known. Dowson & Taylor (37) show a method of finding the effective modulus for this type of problem, resulting in,

$$\frac{1}{E'} = \frac{1}{E}\left[1 - \frac{2\nu^2}{1-\nu}\right] \quad \text{-----3.10.4}$$

Care must be taken when applying equation 3.10.4 as Poisson's ratio for rubber is close to 0.5 and when $\nu = 0.5$ equation 3.10.4 will give an infinite effective modulus. The effective material thickness t is the thickness of rubber that can be considered attached to a rigid backing. In the case of a tyre contact patch, there is no such rigid backing, but the breakers within the tyre casing (figure 3.2.1) form a relatively stiff portion of the tyre; therefore, the effective thickness can be taken as the thickness of the tread rubber to the breakers. In most radial ply car tyres, this would given an effective material thickness of approximately 15mm. It is felt that for the purpose of this work the exact values taken for E, ν and t are not critical, as the main purpose of this work is to evaluate tyre tread patterns.

At the design stage various tread patterns can be analysed and their results compared; provided that the same values of E, ν and t are used in all cases (and that the values chosen are realistic), the comparison will be valid.

This type of simple structural model, therefore, only allows limited analysis of the effects of tyre construction. Construction effects, such as the overall effect of stiffening the contact patch can be evaluated by either increasing the elastic modulus or reducing the effective material thickness. This effect may, however, be gained by a totally different method in practice, such as changing the type of breaker construction, and not by changing either material properties or thickness.

As the properties of each element are formed separately and the deflection for each element calculated, it is possible for the values of E, ν or t to be different for each element. This allows some parts (such as the shoulders) of the tyre contact area to be stiffer than others (such as the crown), allowing a more realistic representation of the tyre structure.

So far we have not considered the effects of the tyre preload (contact pressure) on the deflections, but as this effect is the same for both the 'column' method and the 'semi-infinite' method it will be considered later in section 3.11.

3.10.3 The 'Semi-Infinite' Method

As an alternative to the 'column' method, a semi-infinite body method of calculating tyre contact patch deformation can be used. This method treats the tyre contact patch material as a semi-infinite half space, i.e. the material is infinitely thick in the z(h) direction, and stretches to infinity in both positive and negative x and y directions.

The x, y plane, therefore, is the only free surface of the material. The tyre contact patch is clearly not a true semi-infinite half space, but a number of physical factors of tyres make this assumption a valid approximation.

In a model of tyre deflection, such as the 'column' model already discussed, the tyre contact patch is idealised as a thickness of rubber on a rigid backing, and a value for that thickness must be given. Because there is actually no solid backing in a tyre contact patch, it can be argued that the semi-infinite method is more appropriate. The most rigid part of the contact patch is the breaker package which will deform, but more stiffly than the rubber. Some of the load will ultimately be supported by air pressure inside the tyre, although the tyre in no way behaves as a "balloon".

Near the edges of the contact patch it would initially seem that the semi-infinite method would give a poor approximation to contact patch behaviour. At the front and rear edges of the contact patch the tyre perifery continues outside the contact patch.

The semi-infinite method considers the material to extend to infinity in the plane of the free surface; therefore, at the front and rear of the contact patch this is not a bad approximation, and in fact, it is a better approximation than the alternative of considering that the contact patch material ends suddenly at the front and rear of the contact patch, which use of the 'column' method would imply.

The sides of the contact patch are rather more of a problem. As was discussed with reference to boundary conditions (section 3.7.1) there is an abrupt change in the fluid film thickness and tyre shape here.

The side edges of the contact patch are greatly influenced by effects from the side walls of the tyre which tends to restrict lateral movement of the contact patch material. This is a similar

effect to the presence of more contact patch material outside the side edge of the contact patch, and therefore approximates to a certain extent the situation required for using a semi-infinite model. It must be stressed however that the use of a semi-infinite model of tyre contact patch deformation will inevitably introduce some errors into the model, particularly in the region of the shoulders.

As was stressed earlier, the deflection methods presented here are not intended to model accurately the tyre structure, but are intended to give an approximate deformation model which can be used on a comparative basis in the full model to allow the evaluation of tyre tread patterns for wet grip performance.

A semi-infinite method of predicting tyre contact patch deformation is used in reference (13) which is discussed in section 1.2.1. In (13), the deflection at a point is found as the sum of the deflection at that point due to pressure at the area immediately surrounding it, and the deflection due to pressure at areas a specified distance away. To facilitate this, Agrawal and Henry subdivide the contact patch into a rectangular grid, as shown in figure 3.10.4, and then assign an area (shown dotted) to each node formed by the grid.

A uniform pressure is then assumed over each of these areas, and it is this pressure which is used to calculate the surface deflection.

The method of implementing the semi-infinite model used here is slightly different from that used by Agrawal and Henry. The requirement here is for a deflection method which will work with any mesh built up of triangular elements. As the method used by Agrawal and Henry requires a weighting factor dependent on the shape of the area associated with each node, then it is not suitable for use with a mesh built up of 'random' sized elements.

To overcome this problem here, the method used is to calculate the deflection of nodes due to loads at the centroids of elements, and

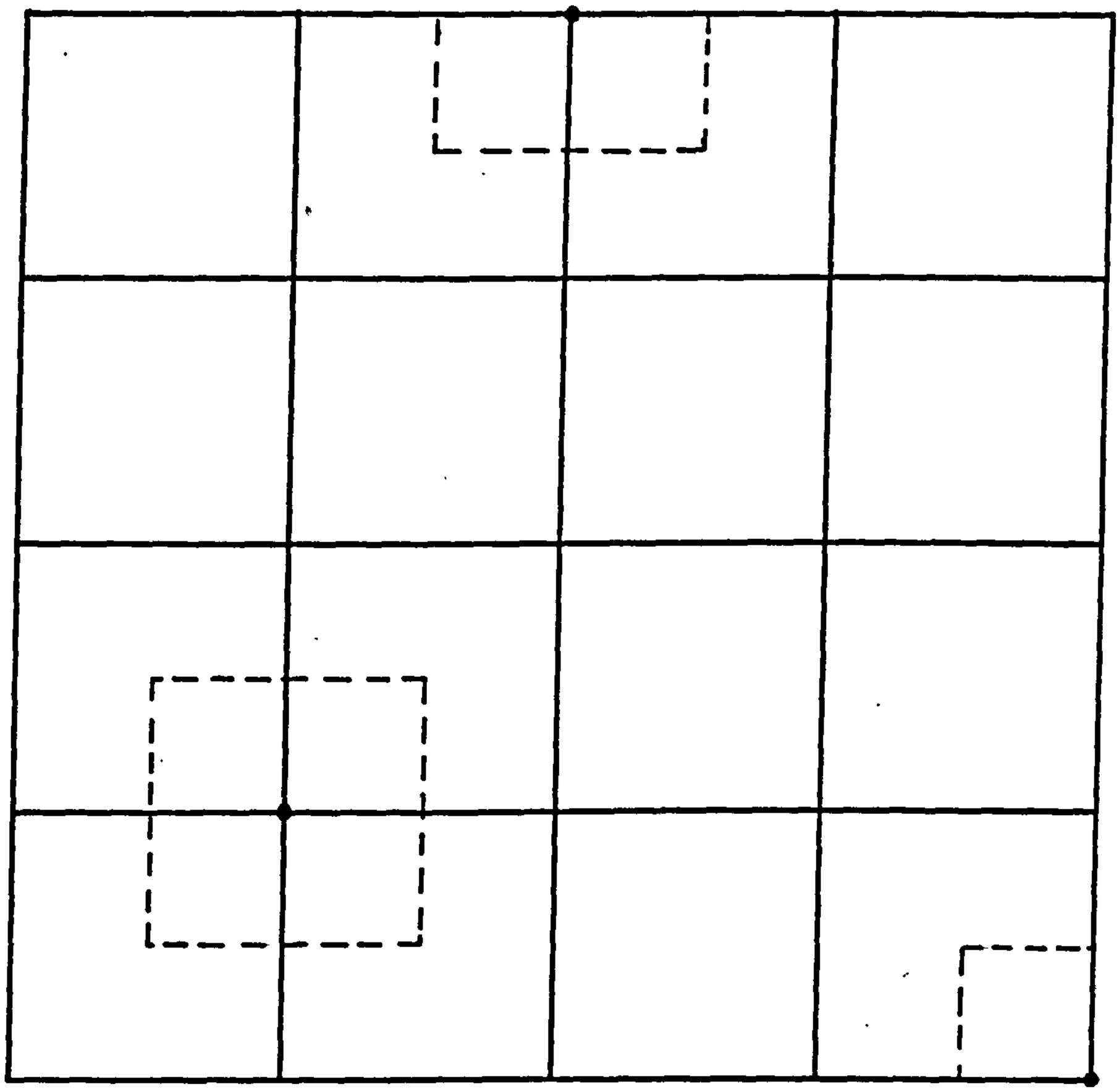

FIGURE 3.10.4 - AREAS ASSOCIATED WITH NODES FOR THE DISTRIBUTION OF PRESSURE

therefore, the case of deflection at a point due to load at that point never arises. The loading at the centre of each element is found in the same way as in the 'column' method, i.e.

$$P_m = \frac{(P_1 + P_2 + P_3)}{3} \qquad \text{(see figure 3.10.3)}$$

and the total force acting on that element would be

$$F = P_m A$$

The assumption is now made that the pressure acting over the contact patch can be treated as a series of point loads applied at the centroids of each element. F is therefore the load at the centroid of the element under consideration. The deflection of a node due to the force at the centroid of one element can, therefore, be found from semi-infinite body theory (Timoshenko 15).

$$\delta = \frac{F(1 - \nu^2)}{\pi E_s' r} \qquad \text{----------3.10.5}$$

where E_s' is the effective elastic modulus and r is the distance from the point at which δ is measured to the point where the load (F) is applied. The total deflection of a node, due to the loads at the centroids of all elements, can be found by assuming that the principle of superposition is valid and that the total deflection can be found by summing the deflections due to the load on each element in a similar way to Agrawal and Henry (13).

From Timoshenko (15), the displacement u, in the plane of the surface is

$$u = - \frac{(1 - 2\nu)(1 + \nu)F}{2\pi E_s' r} \qquad \text{----------3.10.6}$$

where the notation is as for equation 3.10.5. It can be seen from equation 3.10.6 that as ν tends to 0.5, then u tends to zero. For rubber, poissons ratio is almost 0.5 (denoting that rubber is almost incompressible), and therefore u is very small; movements of nodes in the plane of the contact patch can thus reasonably be neglected.

The calculation of vertical deflection δ, using equation 3.10.5 requires both E_s' and ν to be known. From 3.10.5 it can be seen that δ is insensitive to values of ν close to 0.5, and $\nu = 0.5$ can be used safely. The physical reasoning behind this is that equation 3.10.5 assumes infinite thickness of the material, making deflections less sensitive to the compressibility of the material. The elastic modulus of the material has been denoted here by E_s', the effective elastic modulus. Because the tyre contact patch is not infinitely thick, some form of correction should be applied to equation 3.10.5 to allow for this. The method chosen is to modify the value of the elastic modulus. In the case of the 'column' model, the elastic modulus was modified to allow the effects of Poissons ratio to be included. Poissons ratio effects are already included in equation 3.10.5; therefore, this need not be done in this case, and the modification of the modulus is solely to make allowance for the fact that the contact patch material has a finite thickness.

A number of different approaches could be used to find a value for E_s'. Bond (2) in his study of the penetration into tread rubber of idealised road surface asperities, used a semi-infinite model of the tyre contact patch with spherical road asperities. To account for the finite thickness of the tread rubber, Bond conducted experiments indenting different diameter spheres into various thicknesses of rubber and obtained the load/deflection curves. These were then compared with the theoretical case and a correction factor determined which was a function of sphere radius and material thickness. Figure 3.10.5 shows a typical one of these load/

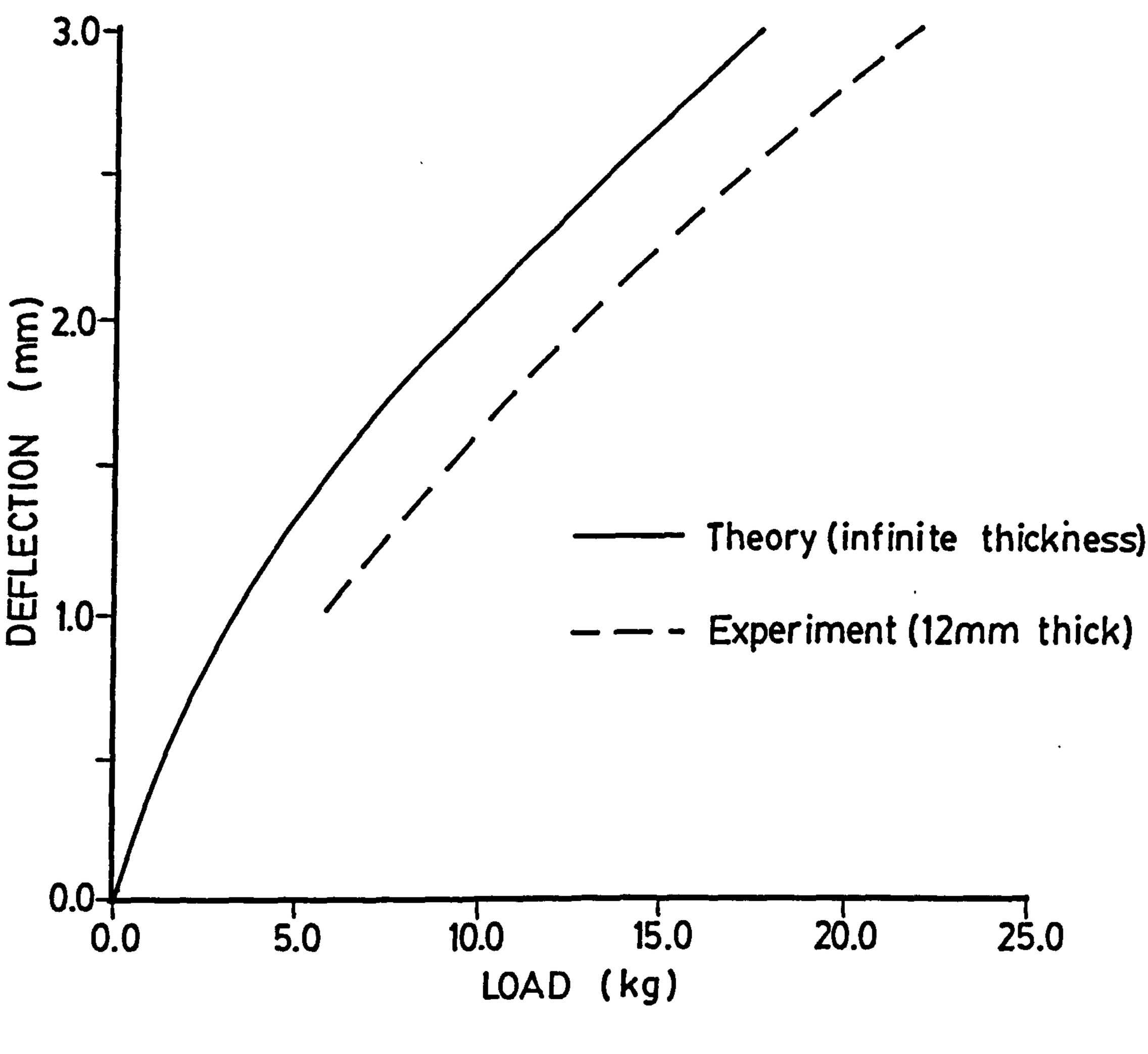

FIGURE 3.10.5 - LOADING OF A SPHERICAL INDENTER (from (2))

deflection curves. As can be seen, the deviation from theory at a material thickness of 12mm, is 10 or 15%, but this is obtained by indenting a sphere of radius 9.5mm. Bond has also indented spheres of 6.4mm radius and the deviation from theory at 12mm material thickness is then only 5%. The indenter radius therefore, has a large effect on the deviation from theory, and, as in this case there is no spherical indenter this correction cannot be used. The nearest analogy with Bonds work would be to consider that the fluid pressure acting on the tread surface was like an indenter of large radius. The effect of the finite thickness of the contact patch in this case will therefore, have a much larger effect on the deformation,than that found by Bond.

If one were to attempt to find a correction factor by experiment using a flat indenter, then the area of the indenter chosen would affect the value of the correction factor in the same way as Bond found the radius of the sphere affected the correction factor, as well as the thickness of the material. Also, as has been discussed earlier, there is no actual rigid backing to the contact patch, but rather the steel breaker which, whilst being much stiffer than the tread rubber, still deforms to some extent. It would therefore, be more appropriate that any experiments to determine a correction factor for deflection would take place on an actual tyre. This is discussed in section 8.8.1.

To get a feel for the magnitude by which the modulus would be modified, a theoretical comparison between the deflection predicted by the 'column' method (which includes material thickness) and the deflection predicted by the semi-infinite method, was performed. Combining equations 3.10.2, 3.10.3 and 3.10.4 gives the deflection by the 'column' method as

$$\delta = \frac{Ft}{EA}\left[1 - \frac{2\nu^2}{1-\nu}\right] \qquad \text{----------3,10.7}$$

Equation 3.10.7 gives the deflection over an area due to a force applied over that area. A similar equation based on semi-infinite theory can be found in (15) and is

$$\delta_{AV} = \frac{mF\ (1 - \nu^2)}{E'_s\ \sqrt{A}} \qquad \text{----------3.10.8}$$

where δ_{AV} is the average deflection over the area A, and E'_s is the effective elastic modulus. 'm' is a numerical factor dependent on the shape of area A and can be found from (15).

Assuming $\delta = \delta_{AV}$ and combining equations 3.10.7 and 3.10.8 gives

$$E'_s = E \cdot \frac{m\sqrt{A}}{t} \cdot \frac{(1 - \nu)^2}{(1 - 2\nu)} \qquad \text{----------3.10.9}$$

The relationship between E_s' and E can now be found for specific cases.

In (37), it is shown that the use of a 'column' model with an effective modulus gives good results for Poissons ratio up to 0.45; therefore, this value of Poissons ratio will be used in 3.10.9. The two extreme cases are to consider the whole area of a typical contact patch, and to consider only one small block within the contact patch.

Whole Contact Patch:

length = 150mm

width = 100mm

$A = 15{,}000mm^2$ and m = 0.94 (15)

therefore $E_s' = \frac{348}{t} \cdot E$

Single Block:

length = 20mm

width = 20mm

$A = 400mm^2$ and $m = 0.95$ (15)

therefore $E_s' = \frac{57.5}{t} . E$

A typical thickness for the tread rubber is 15mm. Therefore E_s' ranges from approximately 23E to approximately 4E. Because the backing is not rigid (i.e.'t' could be considered effectively larger), then the low end of this range would seem most appropriate.

In conclusion, therefore, the value entered into the computer program for the modulus of the material (when using the semi-infinite deflection method) should be treated as an effective modulus. When more experience of the program has been gained or experiments on the stiffness of tyre contact patches performed, a more exact method of determining the effective modulus can be found. The actual value of modulus chosen is not critical as the results from the computer program will be used on a comparative basis, and, to a large extent, the effects of tyre preload dominate over the effects of tyre modulus.

3.11 TYRE PRELOAD

The tyre contact patch is preloaded onto the road surface owing to the weight of the vehicle. This preloading causes the toroidal shape of the tyre to be flattened where it contacts with the road surface to form the contact patch.

The value of the tyre/road preload is known as the contact pressure and can be measured by rolling a tyre over a load sensor. If we consider the case of a tyre loaded onto a road surface (figure 3.11.1),

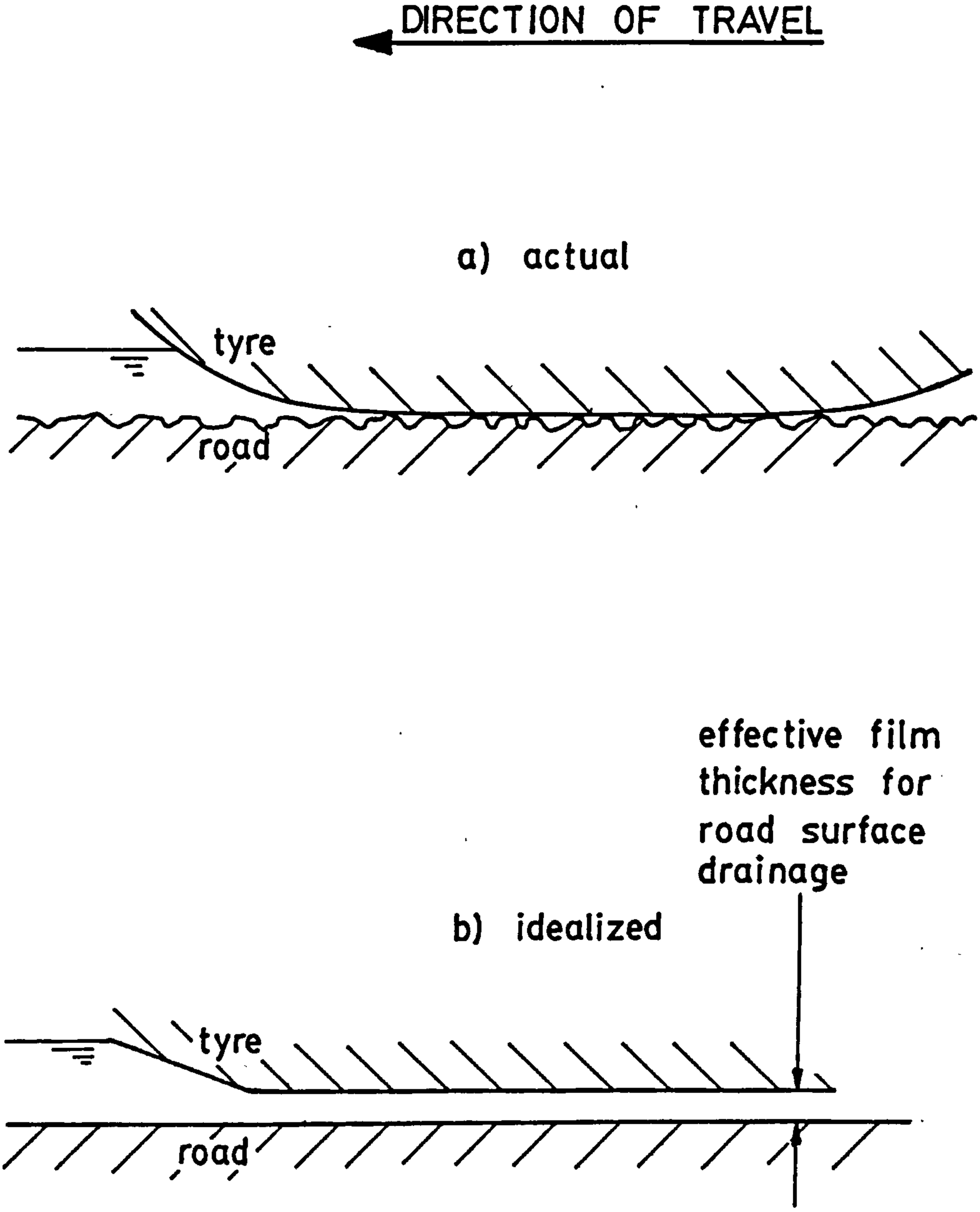

FIGURE 3.11.1 - ACTUAL AND IDEALIZED TYRE/ROAD INTERFACE

the drainage capacity of the road surface can be represented as an effective film thickness and the simplified representation shown in figure 3.11.1(b) given.

Before the tyre tread surface can deform, the fluid pressure of the water in the tyre/road interface must exceed the local contact pressure. If the tyre then deforms linearly with increasing fluid pressure, the response of one point on the contact patch to fluid pressure will be as shown in figure 3.11.2.

From figure 3.11.2 it can be seen that the fluid pressure used in the deflection model should have had the contact pressure subtracted from it. In practice, the fluid pressure is averaged over an element; therefore, the contact pressure is also averaged over an element and the difference between these two values is used in the deflection model.

If the vehicle axle were fixed, then the tyre contact pressure would remain constant. It follows that any deformation of the tyre contact patch by fluid pressure would cause an increase in the load supported by that tyre. This is not the case for a tyre on a vehicle as the load on the tyre is fixed by the vehicle mass; therefore the axle height must vary. The case of fixed axle height can be simulated on a test machine and can be useful, as this allows the variation in load carrying capacity of the tyre under various wet conditions to be examined.

The modelling of the tyre with the type of response in figure 3.11.2 would give this fixed axle height case and the computer model can use this to find the predicted load carrying capacity under wet conditions. Obviously, it is desirable that the tyre should have as low a load carrying capacity as possible under wet conditions.

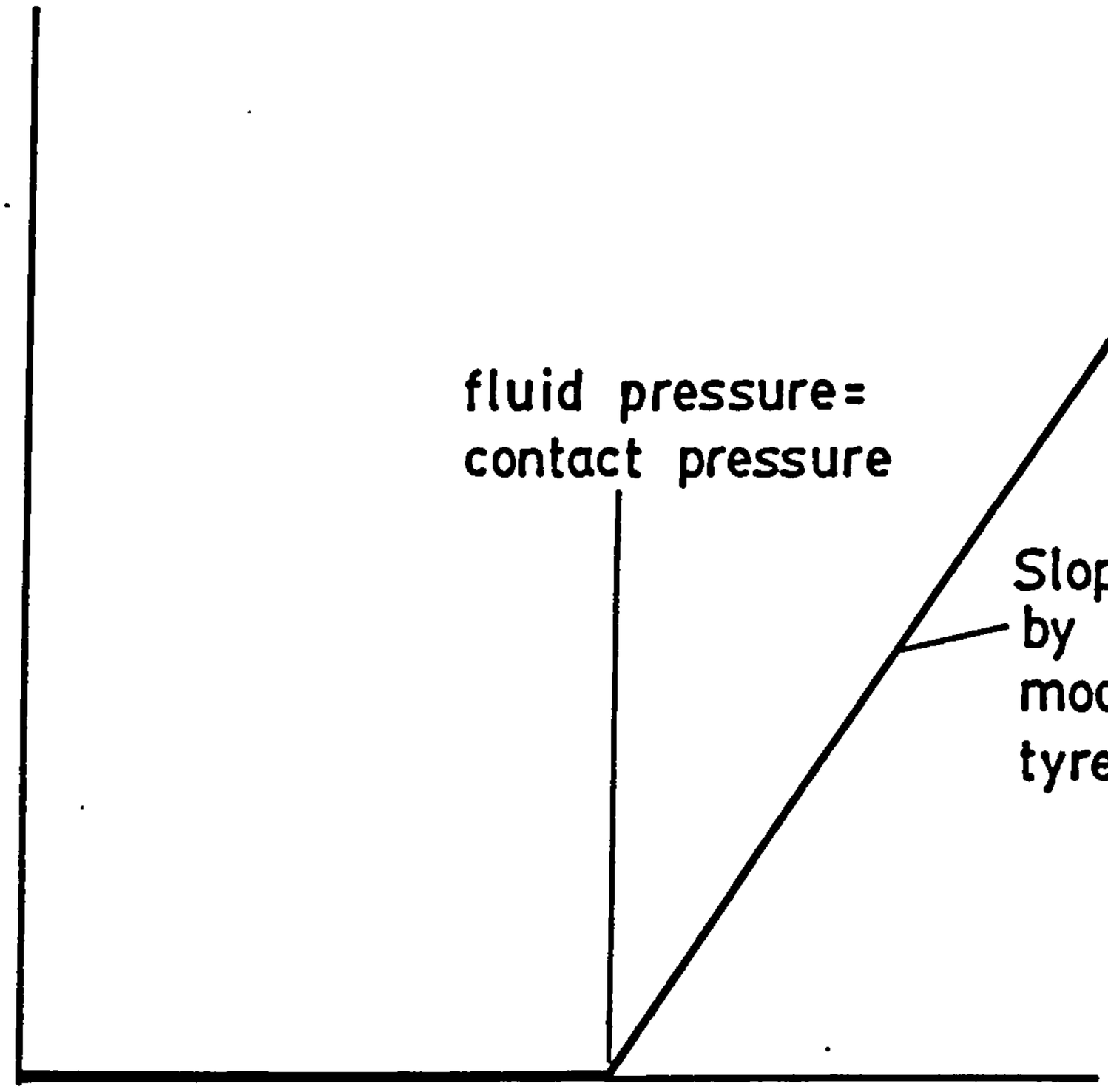

FIGURE 3.11.2 - FLUID PRESSURE / DEFLECTION FOR ONE POINT IN THE CONTACT PATCH

To allow modelling of the situation of a tyre on a vehicle, the axle height has to be allowed to vary and the total load on the contact patch remain constant, at the value found by integrating the dry contact pressure over the area of the contact patch. If one considers only the tyre contact patch, then the effect of varying the axle height reflects itself in changes in the contact pressure. If the axle is raised, the contact pressure will reduce and, if the axle is lowered, the contact pressure will increase. As well as changes in contact pressure, changing the axle height will also alter the contact patch size. Tests have shown that the width of the contact patch is virtually independent of the axle height and also that the length of the contact patch only varies by a small amount for changes in the axle height near to the height at schedule load. As a result of this, the area of the contact patch will be considered not to vary with changes in the contact pressure caused by adjusting the axle height.

To allow the constant load situation to be modelled, one can consider that changes in axle height will affect, as far as fluid in the tyre/road interface is concerned, only the contact pressure. To aid the convergence of the computer program, the contact pressure is applied in a number of steps, as discussed in section 4.5.5. This procedure has been extended, allowing the contact pressure level to be modified, to achieve matching of the total load in the wet with the total load in the dry. In practice, the contact pressure level required to achieve this is close to the dry contact pressure level; confirming that the assumption of constant contact patch area, due to variation in axle height, is valid.

CHAPTER 4 - COMPUTING DEVELOPMENT

4.1 INTRODUCTION TO COMPUTING DEVELOPMENT

The purpose of this chapter is to describe the operation of the computer programs which form an integral part of this project. The finite element programs, one for contact patch analysis and one for individual tread block analysis, basically differ only in their input, the loading procedure and the boundary conditions. The overall structure of the two programs is similar, and the initial work shown here on their verification applies equally to both. Later on in this chapter operating procedures and flow diagrams for the two programs are presented; the actual source listings are in Appendix B.

The other computer programs which have been developed in conjunction with this project are for finite element mesh generation and for the plotting of results from the finite element programs. The mesh generation program in particular will be described later in this chapter. The source listings for both the mesh generation and the plotting programs are also in Appendix B.

The finite element programs are written in FORTRAN IV and are implemented on an IBM 3031. The mesh generation and plotting programs are also written in FORTRAN IV, but are implemented on DEC PDP11 computers. The mesh generation program also requires the use of the special facilities of a Cambridge Instruments Quantimet image analyser with image store.

4.2 1-DIMENSIONAL VERIFICATION OF THE FINITE ELEMENT COMPUTER PROGRAMS

These verification tests were performed using the block design program, with modifications to allow the viscosity to be held constant rather than to use an effective viscosity (section 3.6). This was to enable the results to be easily compared with theory.

The tests performed fall into the following categories and allow the verification of the fluid dynamical parts of the computer programs.

1. Slider with taper.
2. Composite slider with taper + parallel.
3. Squeezing - parallel.
4. Squeezing - tapered.

All cases are for rigid bearings with no elastic deformation. The viscosity used was 1.0 Ns/mm^2, and where appropriate the sliding velocity was 1.0 mm/s. Therefore, the actual pressure values predicted were not realistic, but allowed verification of the computer programs by comparison with the analytical solution of Reynolds equation. The mathematical details of the analytical solutions are not presented here, but can be derived relatively easily from information in the literature (31), (32), (33), (34).

4.2.1 1-Dimensional Slider

The 1-Dimensional slider is the simplest case of hydrodynamic lubrication. A convenient way of characterising a slider bearing is by the ratio of inlet to outlet film thickness $\bar{h}_i$. (see figure 4.2.1).

$$\bar{h}_i = \frac{h_i}{h_o} \qquad \text{---------} \quad 4.2.1$$

The results for three different values of $\bar{h}_i$ are shown in Figure 4.2.2(a) - (c). The three values of $\bar{h}_i$ represent a shallow, medium and steeply sloping bearing.

The outlet film thickness h_o is arbitary and will not affect the pressure distribution, only the overall magnitude of the pressures. For this, and the reasoning given earlier, the graphs presented do not have any units on the pressure axis. Similarly, the bearing length is presented with respect to the maximum length.

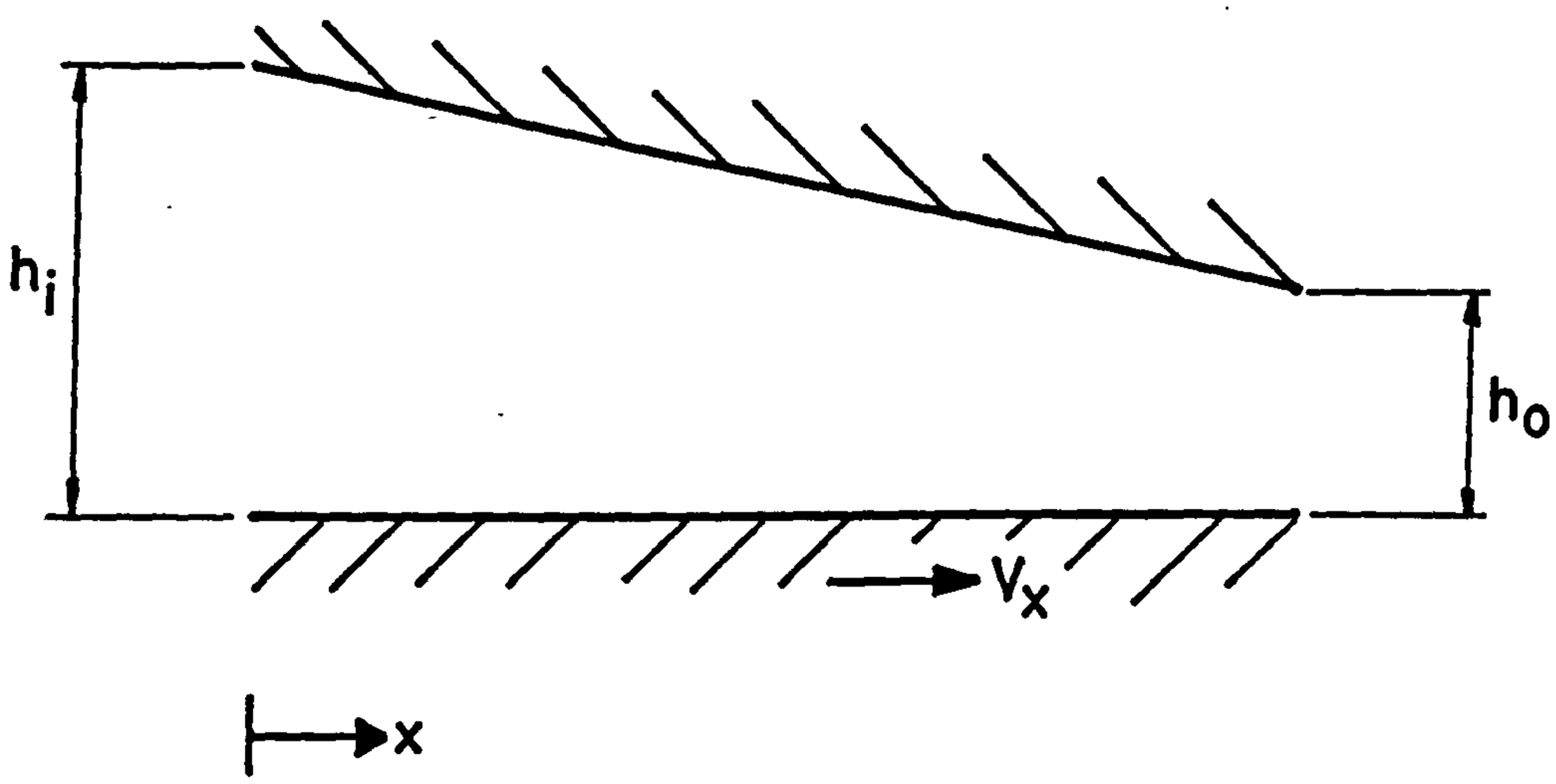

FIGURE 4.2.1 - 1-DIMENSIONAL SLIDER - GEOMETRY AND NOTATION

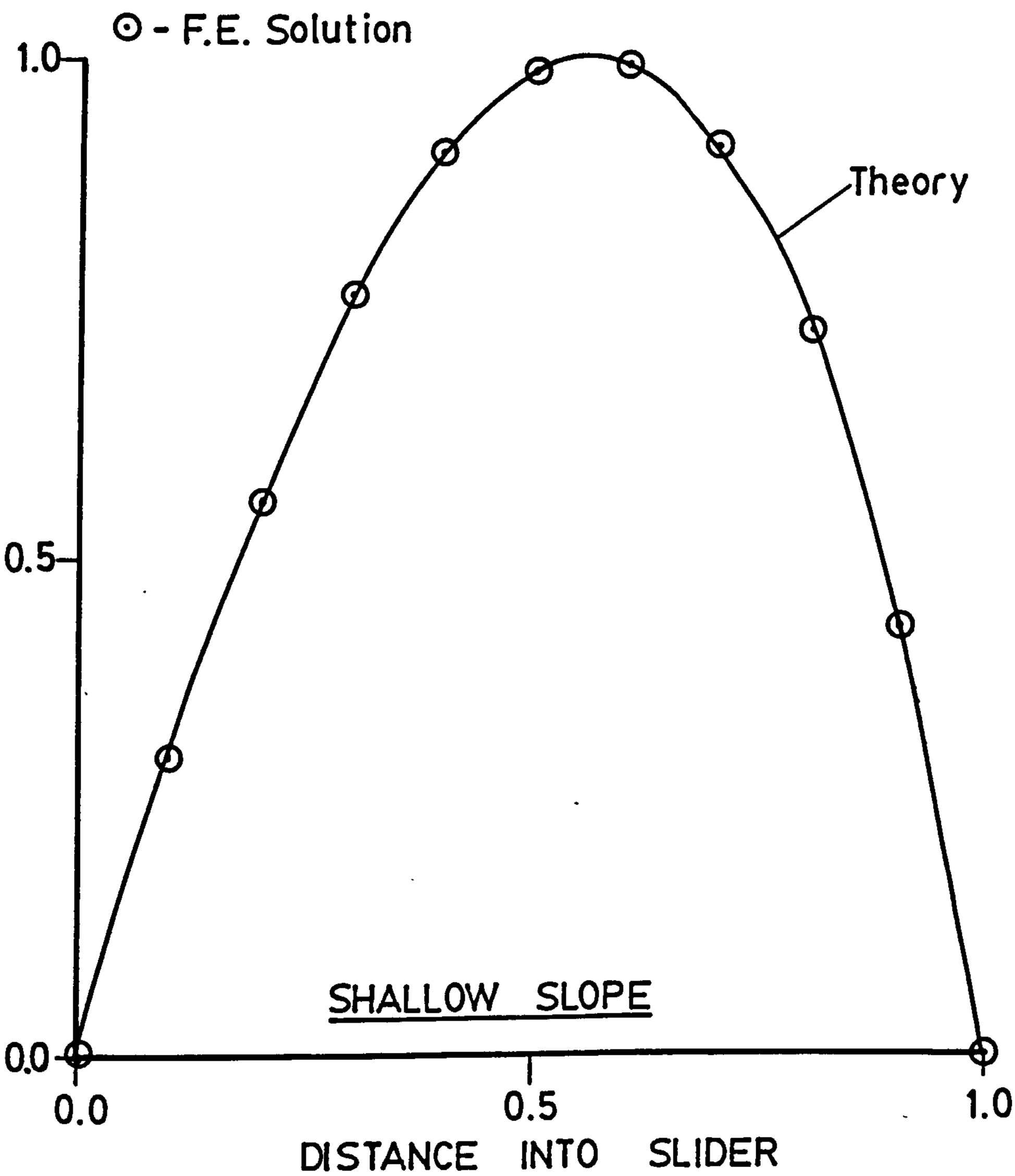

FIGURE 4.2.2a - 1-DIMENSIONAL SLIDER - COMPARISON BETWEEN THEORETICAL AND NUMERICAL SOLUTIONS

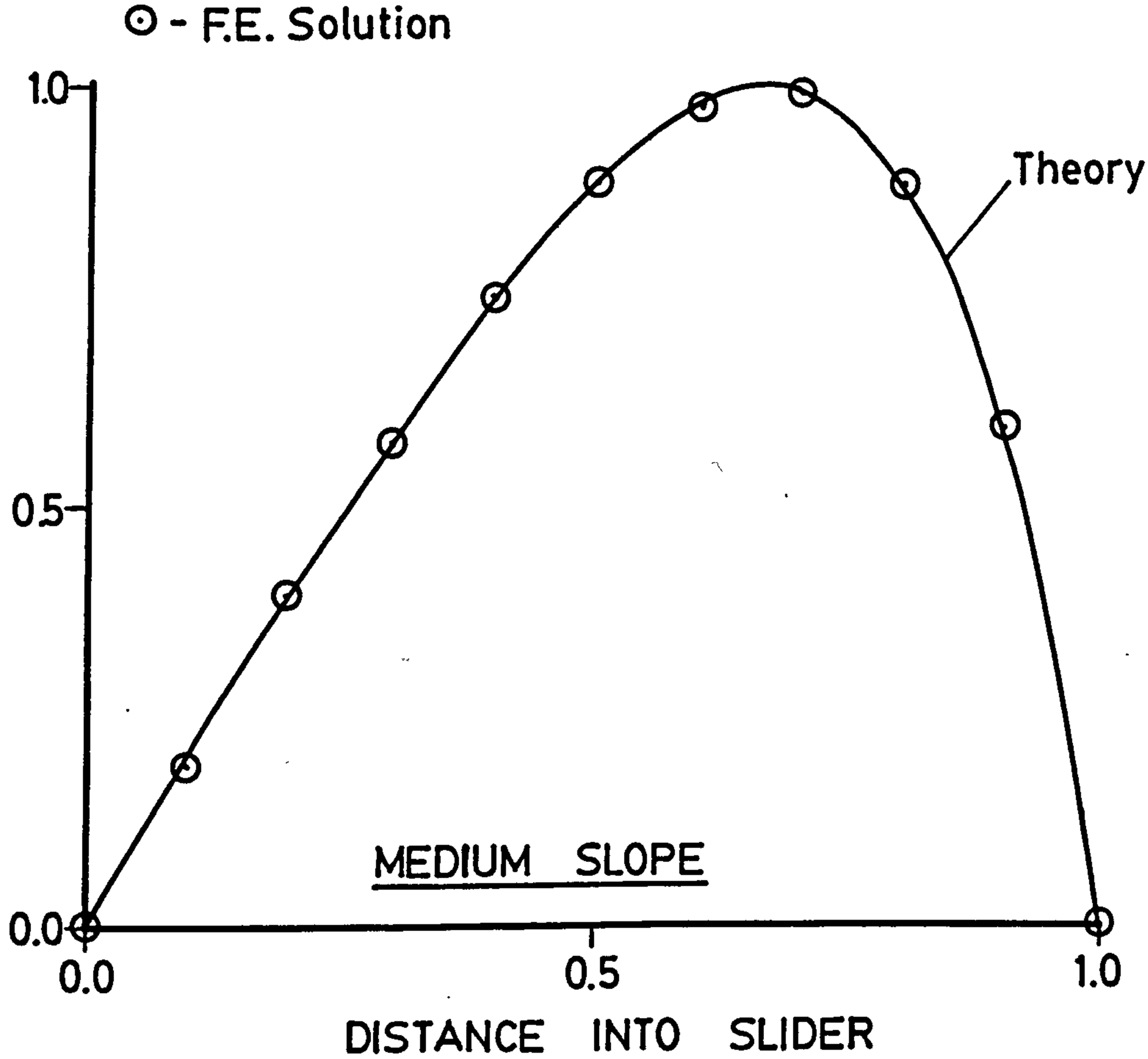

FIGURE 4.2.2b - 1-DIMENSIONAL SLIDER - COMPARISON BETWEEN THEORETICAL AND NUMERICAL SOLUTIONS

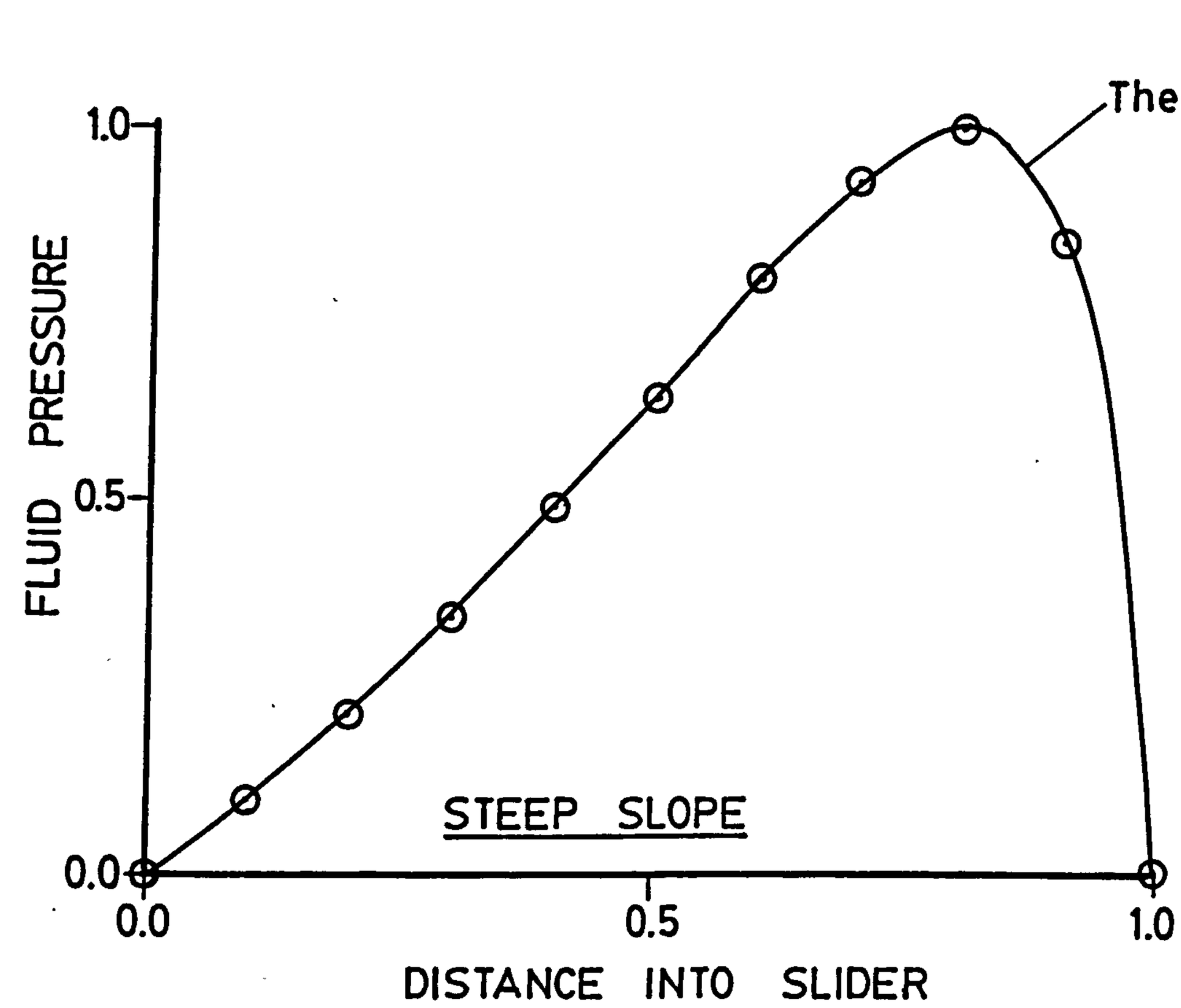

FIGURE 4.2.2c - 1-DIMENSIONAL SLIDER - COMPARISON BETWEEN THEORETICAL AND NUMERICAL SOLUTIONS

From figure 4.2.2 it can be seen that the finite element results agree very closely with the theoretical solutions. However, a little more insight can be gained by looking at the percentage error between theory and finite element at the mid-point ($\bar{x} = 0.5$). The mid-point was chosen as this is furthest from the influence of the fixed boundary conditions at the ends. The errors are shown below:-

$\bar{h}_i$	% error at $\bar{x} = 0.5$
4.0	-0.412
2.0	-0.101
1.25	-0.011

The error here is defined as:

$$\% \text{ error} = \left(\frac{\text{finite element solution} - \text{theoretical solution}}{\text{theoretical solution}}\right) \times 100 \qquad \text{----4.2.2}$$

The error is greatest for the steeply sloping case. This will generally occur for plain slider bearings and the accuracy with $\bar{h}_i = 4.0$ could be improved to the level attained with $\bar{h}_i = 1.25$ by increasing the number of nodes in the $\bar{x}$ direction. The accuracy in all the above cases is more than adequate and if a lower degree of accuracy could be tolerated, the number of nodes in the $\bar{x}$ direction could be substantially reduced. This would give a saving in computer cost and illustrates the general trade-off between accuracy and costs when dealing with finite element solutions.

4.2.2 1-Dimensional Composite Slider

The geometry of the composite slider bearing is shown in figure 4.2.3.

The results of the finite element and theoretical solutions are given in figure 4.2.4(a) and (b).

Again, the finite element solutions agree well with the theoretical solutions. In this case, it is not possible to draw any firm conclusions about the nature of the errors because in this case there is a discontinuity in the surface, and the error level is dependent on the position within the slider (value of $\bar{x}$). Also the behaviour cannot be entirely defined by the value of $\bar{h}_i$ (equation 4.2.1) because the value of h_o alone will determine the behaviour in the parallel region. For comparison, the error levels at the mid-point position ($x = 0.5$) are shown for two values of $\bar{h}_i$.

$\bar{h}_i$	% error at $\bar{x} = 0.5$ (equation 4.2.2)
2.0	0.327
1.1	0.599

The error in this case is greater for the smallest value of $\bar{h}_i$; however, noting that the errors are now positive, (i.e. the finite element solution over-estimates the pressure), the trend is the same as in the case of the slider in the previous section. That is to say, the smaller the value of $\bar{h}_i$, the greater the pressure predicted, with respect to the theoretical pressure at that point, and the actual bearing configuration will determine whether the finite element solution will over or under estimate the theoretical solution.

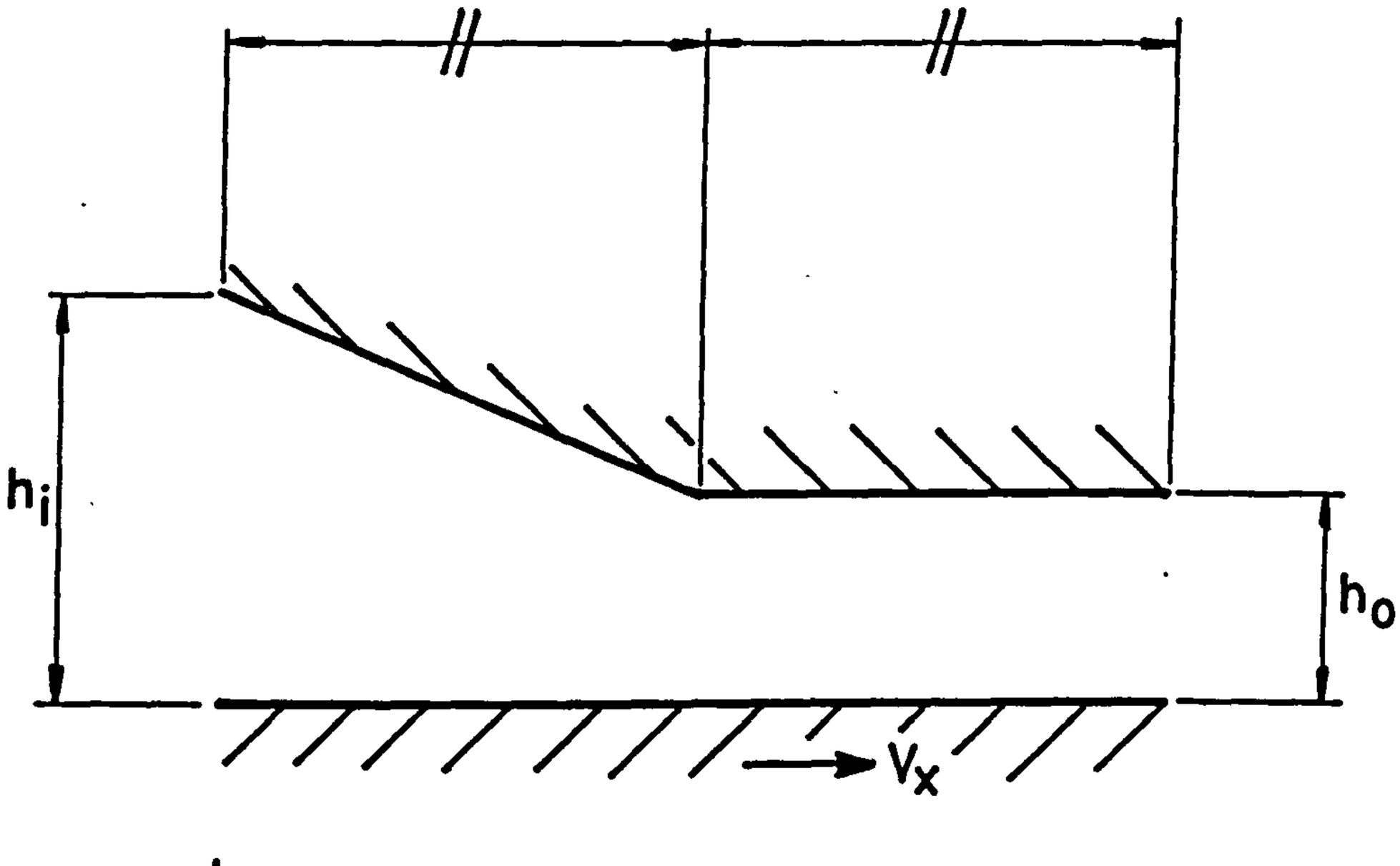

FIGURE 4.2.3 - 1-DIMENSIONAL COMPOSITE SLIDER - GEOMETRY AND NOTATION

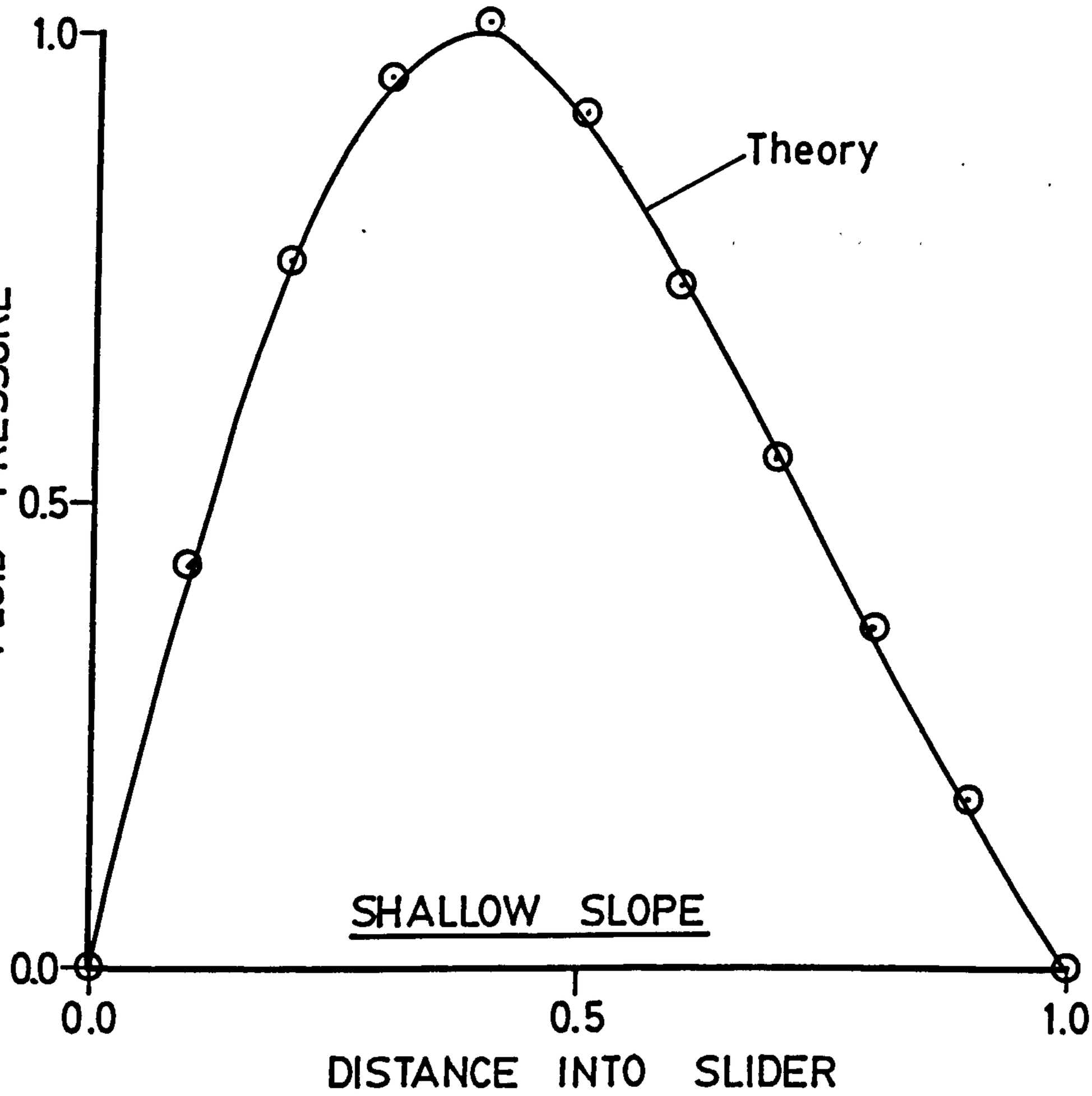

FIGURE 4.2.4a - 1-DIMENSIONAL COMPOSITE SLIDER - COMPARISON BETWEEN THEORETICAL AND NUMERICAL SOLUTIONS

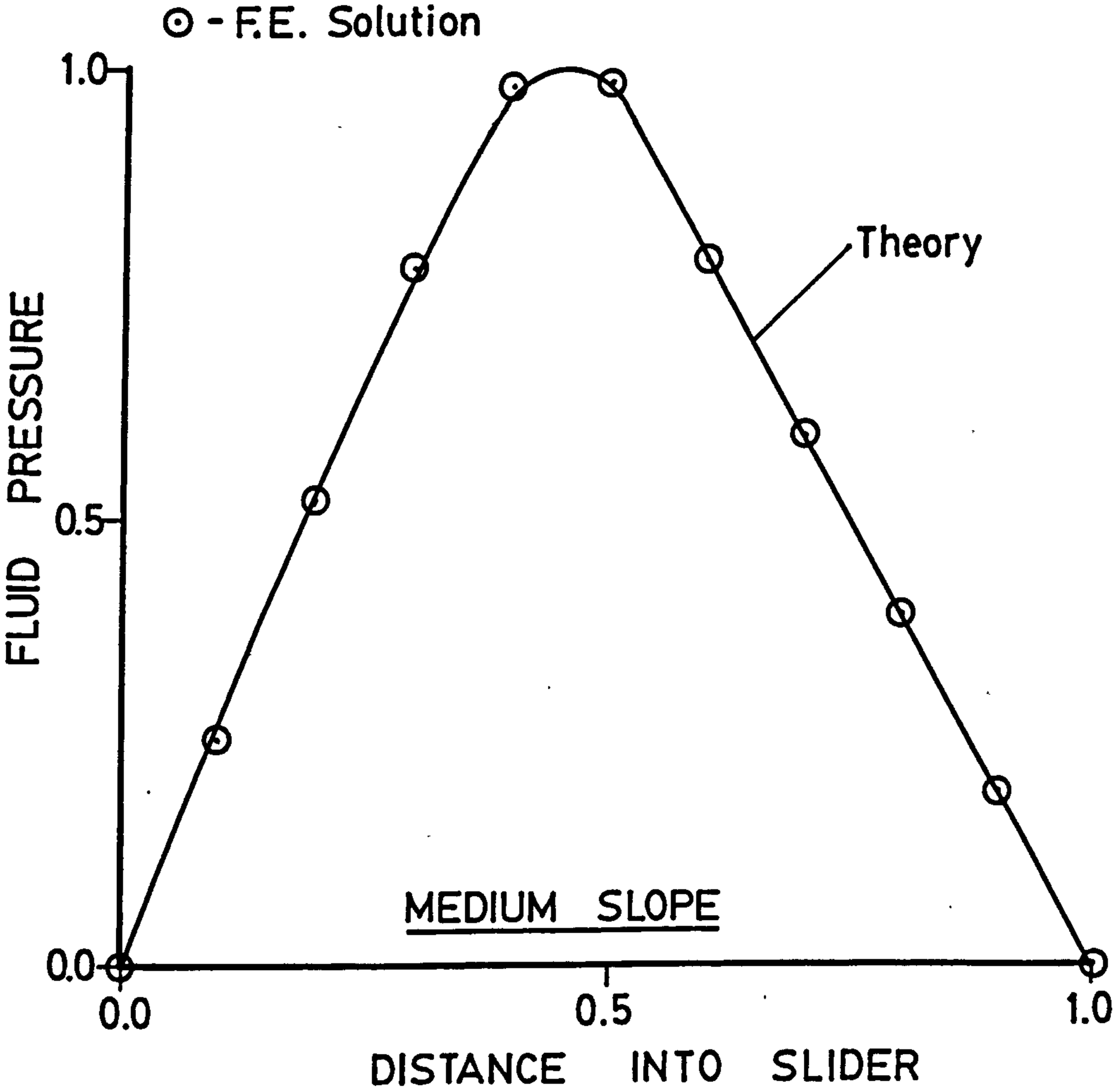

FIGURE 4.2.4b - 1-DIMENSIONAL COMPOSITE SLIDER - COMPARISON BETWEEN THEORETICAL AND NUMERICAL SOLUTIONS

4.2.3 1-Dimensional Squeezing (parallel)

In this case the sliding velocity is zero, as effects of squeezing the two surfaces of the bearing are being considered (figure 4.2.5).

Because the surfaces are parallel ($\bar{h}_i = 1.0$), only one case is considered, and the squeezing velocity will be taken as 1mm/s, with the instantaneous film thickness 1mm. The results of both the finite element and the theoretical solutions are shown in figure 4.2.6.

The finite element values agree exactly (within the limits of computer accuracy) with the theoretical solution. From figure 4.2.6 it can be seen that the pressure profile is symmetrical about the point $\bar{x} = 0.5$, as would be expected.

4.2.4 1-Dimensional Squeezing (tapered)

This is similar to the previous case, except that the two surfaces are not parallel (figure 4.2.7).

The same constants were used as in the previous case, except that $\bar{h}_i$ was taken as 2.0 and 1.1 with $h_o = 1.0$mm. The results of these tests are shown in figure 4.2.8(a) and (b).

The errors $\bar{x} = 0.5$ for the two values of $\bar{h}_i$ are shown below:

$\bar{h}_i$	% error at $\bar{x} = 0.5$
2.0	-0.451
1.1	-0.008

As usual, the finite element solution is close to the theoretical solution, and, as with the tapered slider, the error is less for the case with the lower value of $\bar{h}_i$.

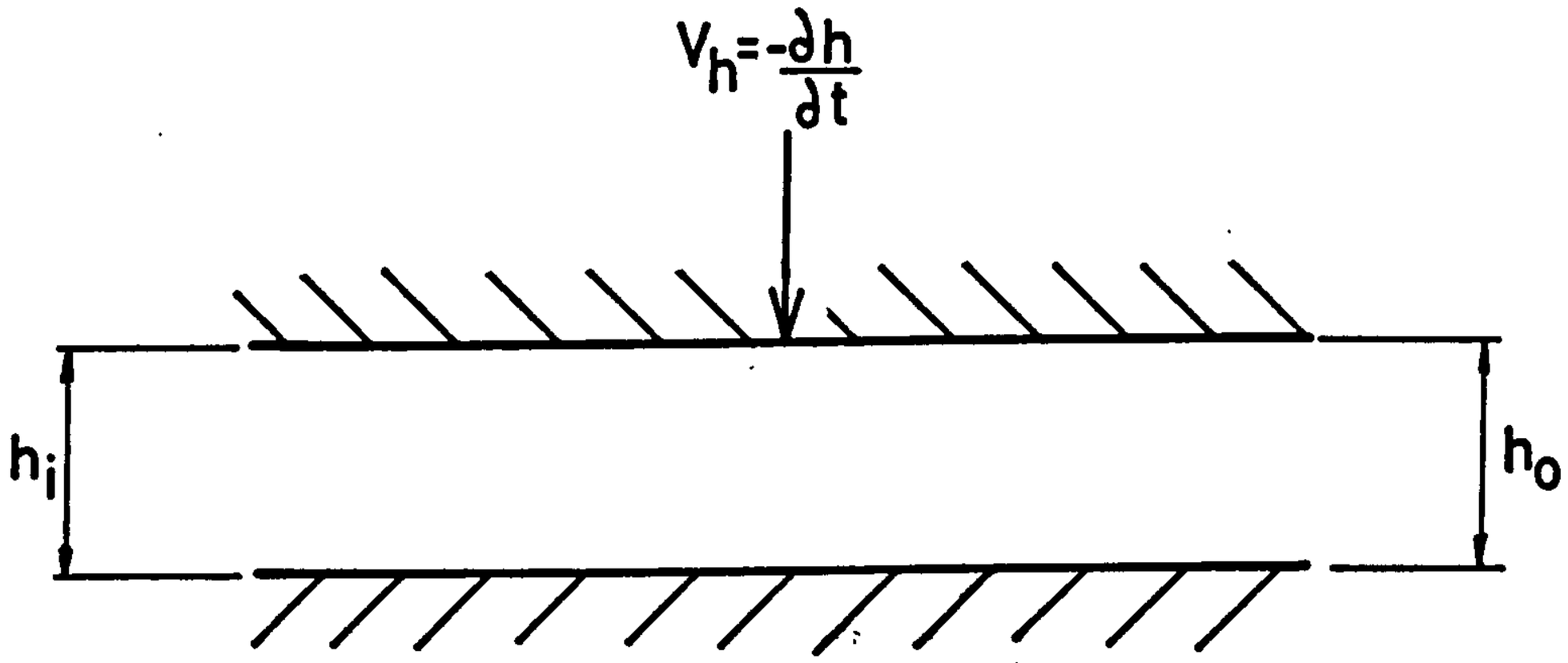

FIGURE 4.2.5 - 1-DIMENSIONAL SQUEEZING (PARALLEL) - GEOMETRY AND NOTATION

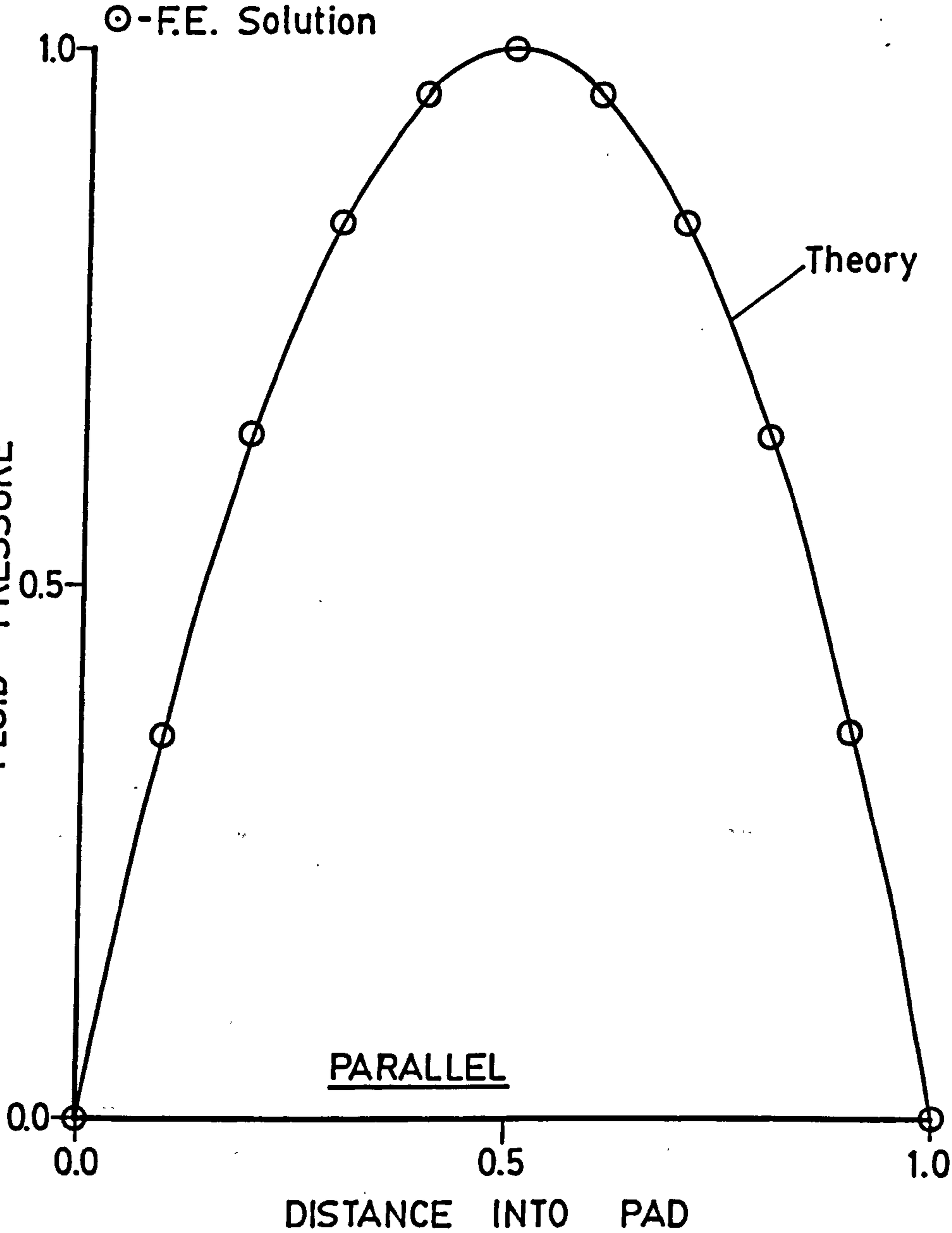

FIGURE 4.2.6 - 1-DIMENSIONAL SQUEEZING - COMPARISON BETWEEN THEORETICAL AND NUMERICAL SOLUTIONS

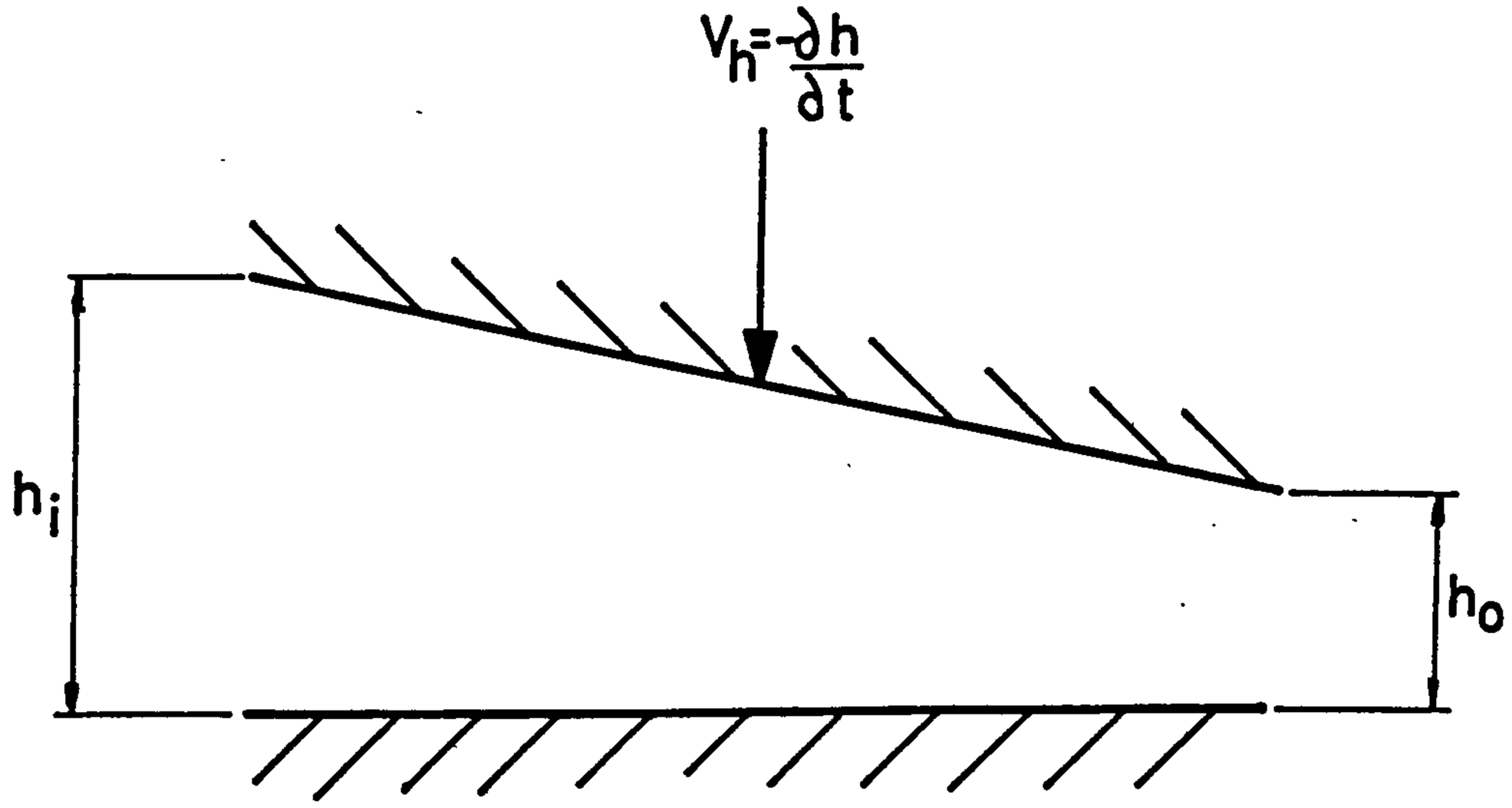

FIGURE 4.2.7- 1-DIMENSIONAL SQUEEZING (TAPERED) - GEOMETRY AND NOTATION

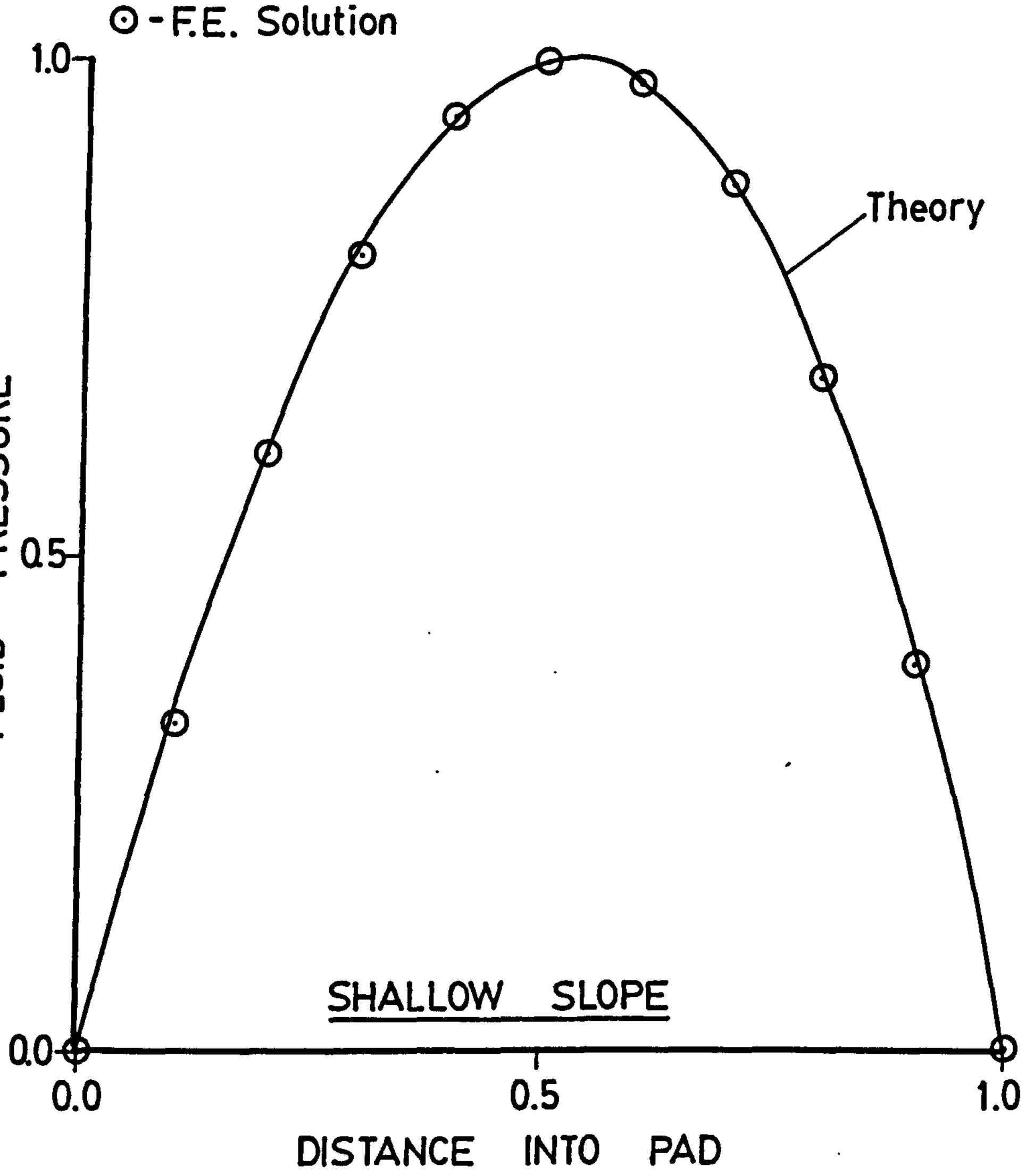

FIGURE 4.2.8a - 1-DIMENSIONAL SQUEEZING - COMPARISON BETWEEN THEORETICAL AND NUMERICAL SOLUTIONS

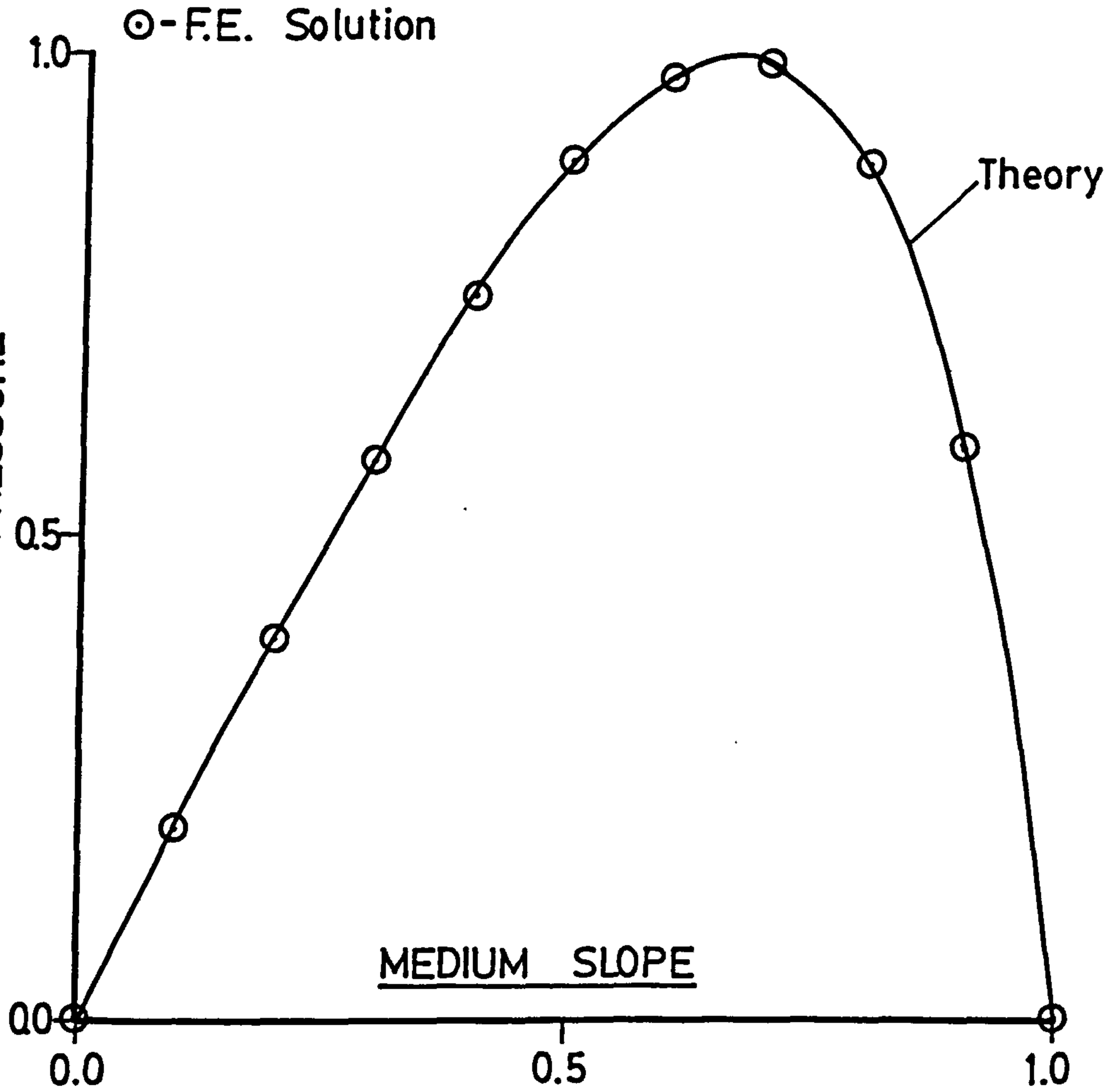

FIGURE 4.2.8b - 1-DIMENSIONAL SQUEEZING - COMPARISON BETWEEN THEORETICAL AND NUMERICAL SOLUTIONS

4.3 2 DIMENSIONAL VERIFICATION OF THE FINITE ELEMENT COMPUTER PROGRAMS

There is no general analytical solution for Reynolds equation in two dimensions; however, under certain circumstances a solution can be found by an approximate method. Two separate cases will be considered; 2-dimensional rectangular sliders and a circular pressurised pad. The solutions for 2-dimensional sliders presented here are in terms of the load carrying capacity only. This is defined as the integral of pressure over the area of the slider, i.e.

$$W = \int_A p dA$$

4.3.1 2-Dimensional Rectangular Slider

Three slightly different methods of finding the load carrying capacity were used from the literature and compared with a fourth, from the finite element model presented here.

In his book (33), Fuller presented two similar methods of finding the load carrying capacity of rectangular bearings with side leakage. The first, originally by Kingsbury and Needs, was found by expressing Reynolds equation in terms of electrical units and building a corresponding model to measure the relationship among the variables. The second method presented by Fuller (33) is by Michell who was able to solve Reynolds equation for a few particular cases by using a special co-ordinate system and expanding the relationship into an infinite series.

The third method is by Jakobsson and Floberg (35), who used a relaxation solution by the finite difference method to obtain the load capacity of various bearings. The bearing used in all these cases (including the present finite element solution) is shown in figure 4.3.1.

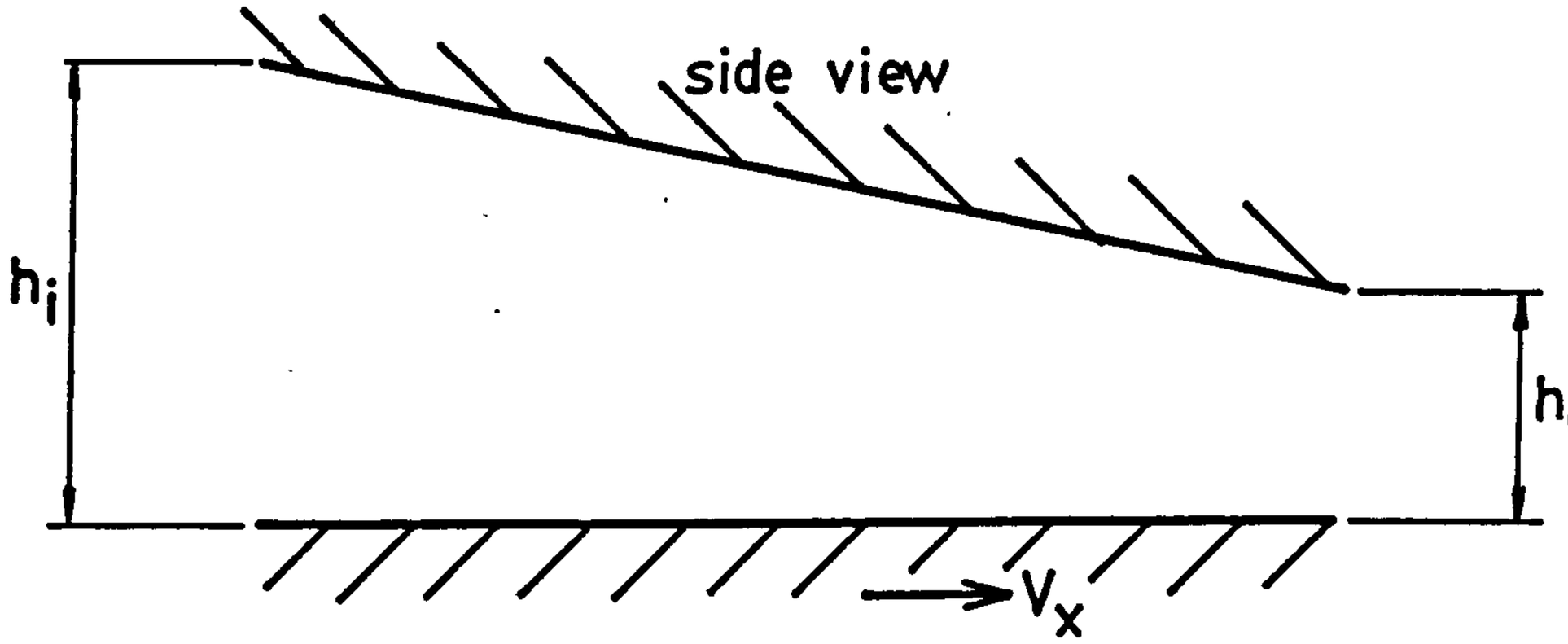

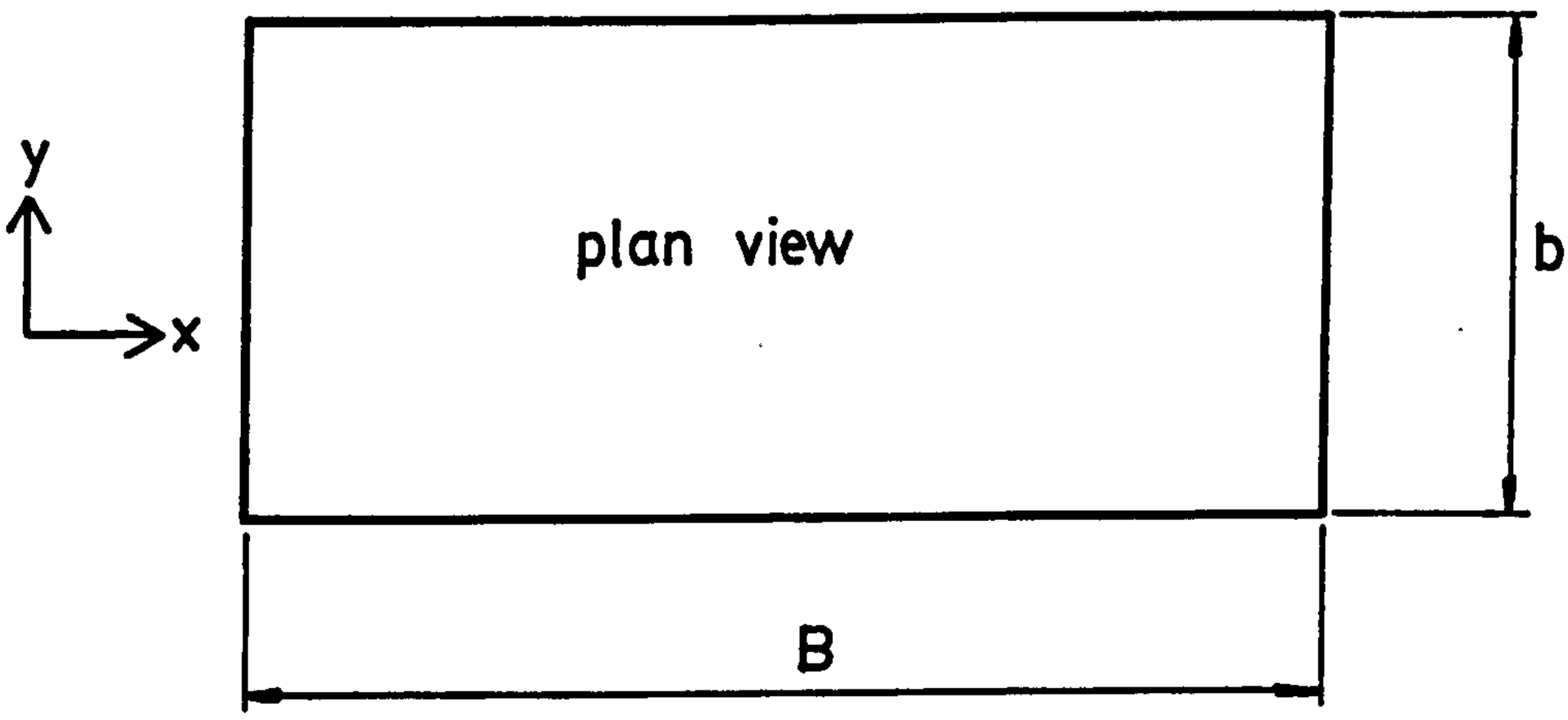

FIGURE 4.3.1 - 2-DIMENSIONAL SLIDER-GEOMETRY AND NOTATION

In all the cases considered here, the viscosity was taken as the laminar viscosity, i.e. no allowance was made for turbulence; the sliding velocity used was 1000mm/s. The values chosen for h_o and B (the length of the bearing) will affect the magnitude of the pressure and thus the load carrying capacity; however, they will not affect the characteristics of the bearing which are determined by the ratios h_i/h_o and b/B. The values of h_o and B were arbitrarily taken as 0.1mm and 100mm respectively.

Alternatively, these verification tests could have been performed in terms of non-dimensional load carrying capacity, removing the need to make assumptions about viscosity, velocity, film thickness and bearing length. However, as the purpose of this section was to verify the results of a computer program, it was felt important to use realistic numerical values in as many cases as possible so that the program was being checked under near normal operating conditions.

The actual load carrying capacity for a 2-dimensional rectangular slider bearing is given by (33),

$$W = \frac{6\mu V B^2 b}{h_o^2} \cdot \eta \, K_p \qquad \text{---------4.3.1}$$

where η (eta) and K_p are factors, dependent on the width/length ratio and the slope of the slider respectively. The factor K_p can be found by the analysis of a slider neglecting side leakage and the factor η "corrects" the result to account for side leakage.

Fuller (33) calculates the following values of K_p,

$m' = \frac{h_i}{h_o} - 1 = \bar{h}_i - 1$	K_p
0.6	0.0235
0.7	0.0247
0.8	0.0255
0.9	0.0261
1.0	0.0265
1.2	0.0267
1.4	0.0265
1.5	0.0263
2.0	0.0246

From the above it can be seen that the load carrying capacity is relatively insensitive to changes in the slope of the slider. The factor η was determined by Kingsbury and Needs for various ratios of b/B for the case when $m' = 1$ ($h_i = 2h_o$). These values of η are shown in the table below

b/B	η (m' = 1)
0.25	0.060
0.33	0.090
0.50	0.185
0.67	0.278
1.00	0.440
1.33	0.550
2.00	0.680
4.00	0.835
5.75	0.920
∞	1.000

Michell obtained values of η for two different values of m', although for fewer values of b/B. The values of η by Michell are shown over.

b/B	η (m' = 1)	η (m' = 2)
0.5	0.19	0.22
1.0	0.44	0.45
2.0	0.69	0.71
4.0	0.84	0.85
∞	1.00	1.00

It can be seen that the values of η found by Michell (for $m' = 1$) agree very well with those found by Kingsbury and Needs.

In the work by Jakobsson and Floberg (35), the results are presented in a slightly different manner. The load carried by a 2-dimensional rectangular slider is defined as

$$W = \frac{\mu V B^2 b}{h_o^2} \cdot \bar{W} \qquad \text{----------4.3.2}$$

where $\bar{W}$ is a non-dimensional load carrying capacity and is, in effect, a combination of the factors η and K_p (and the constant '6'). The values for $\bar{W}$ are shown below (35) where $\bar{h}_i$ is as defined in equation 4.2.1 ($\bar{h}_i = h_i/h_o$).

	$\bar{W}$					
b/B	$\bar{h}_i$= 1.0	$\bar{h}_i$= 1.5	$\bar{h}_i$= 2.0	$\bar{h}_i$= 2.5	$\bar{h}_i$= 3.0	$\bar{h}_i$= 4.0
0.50	0	0.0229	0.0289	0.0301	0.0295	0.0268
0.75	0	0.0404	0.0504	0.0516	0.0498	0.0441
1.00	0	0.0558	0.0689	0.0700	0.0670	0.0584
1.50	0	0.0772	0.0946	0.0950	0.0900	0.0769
2.00	0	0.0900	0.1096	0.1095	0.1032	0.0872
∞	0	0.1312	0.1589	0.1577	0.1479	0.1242

The load carrying capacities predicted by the above methods can now be compared with the load carrying capacity preducted by the current finite element model for various values of b/B and $\bar{h}_i$. As the values of η are only given for m' = 1.0 ($\bar{h}_i$ = 2.0) by Kingsbury and Needs, $\bar{h}_i$ = 2.0 will be used for the initial set of comparisons. In the table in figure 4.3.2, the load carrying capacity predicted by the method of Kingsbury and Needs, is denoted as W_{KN}: by the method of Michell on W_M, and by the method of Jakobsson and Floberg as W_{JF}. The finite element solution is denoted by W_{FE} and the % error is given by,

$$\% \text{ error} = \left(\frac{W_{FE} - \text{mean load capacity by KN, M and JF}}{\text{mean load capacity by KN, M and JF}} \right) \times 100$$

The load carrying capacities are in each case given in Newtons, but as was discussed earlier, their actual value is not as important here as the error existing between the different methods, in particular, between the methods from the literature and the finite element solution.

Figure 4.3.2 shows that the load carrying capacity predicted by the finite element model agrees closely with that predicted by the three methods from the literature.

The load capacities predicted by the three methods from the literature are very similar. Therefore, a further set of comparisons with the finite element method can be justified for $\bar{h}_i$ = 4.0, where only the Jakobsson and Floberg solution is available. The results of this are shown in figure 4.3.3 and, again, the load capacities are shown in Newtons, and the percentage error is defined as

$$\% \text{ error} = \left(\frac{W_{FE} - W_{JF}}{W_{JF}} \right) \times 100$$

Once again there is close agreement between the finite element model and the results from the literature. A typical 2-dimensional pressure

b/B	W_{KN}	W_{M}	W_{JF}	W_{FE}	% error
0.50	1.6840	1.7295	1.6545	1.6436	-2.71
0.75	-	-	4.3281	4.2926	-0.82
1.00	8.0104	8.0104	7.8891	7.8295	-1.76
1.50	-	-	16.248	16.133	-0.71
2.00	24.759	25.124	25.098	24.949	-0.18
4.00	60.806	61.170	-	60.550	-0.72

FIGURE 4.3.2 - LOAD CARRYING CAPACITIES $\bar{h}_c = 2.0$

b/B	W_{JF}	W_{FE}	% error
0.50	1.5343	1.5127	-1.41
0.75	3.7871	3.7332	-1.42
1.00	6.6868	6.5886	-1.47
1.50	13.208	13.115	-0.70
2.00	19.969	19.959	-0.05

FIGURE 4.3.3 - LOAD CARRYING CAPACITIES $\bar{h}_c = 4.0$

distribution, as predicted by the finite element model is shown in figure 4.3.4. This pressure distribution was produced using triangular finite elements based on a rectangular grid, and the diagonals forming the triangles have been omitted from figure 4.3.4 in the interests of clarity. Figure 4.3.4 clearly shows the loss in load carrying capacity due to side leakage as the pressure falls to atmospheric at the sides of the bearing. This loss in load carrying capacity is, of course, beneficial in the case of a tyre on wet roads.

4.3.2. Circular Pressurised Pad

The circular pressurised pad is a special case of 2-dimensional flow, for which an analytical solution exists and can be found in (33),

$$p = \frac{6\mu Q}{\pi h^3} \cdot \ln\left(\frac{r_o}{r}\right) \qquad \text{--------4.3.3}$$

where p = pressure at radius r

h = constant film thickness

r_o = outside radius of the pad

r_i = inside radius of the pad

and Q = volume flow rate.

as shown in figure 4.3.5

The inlet pressure (from 4.3.3) is, therefore, given by

$$p_i = \frac{6\mu Q}{\pi h^3} \cdot \ln\left(\frac{r_o}{r_i}\right) \qquad \text{-------4.3.4}$$

and the non-dimensional pressure (with respect to inlet pressure) at any point in the pad is given by

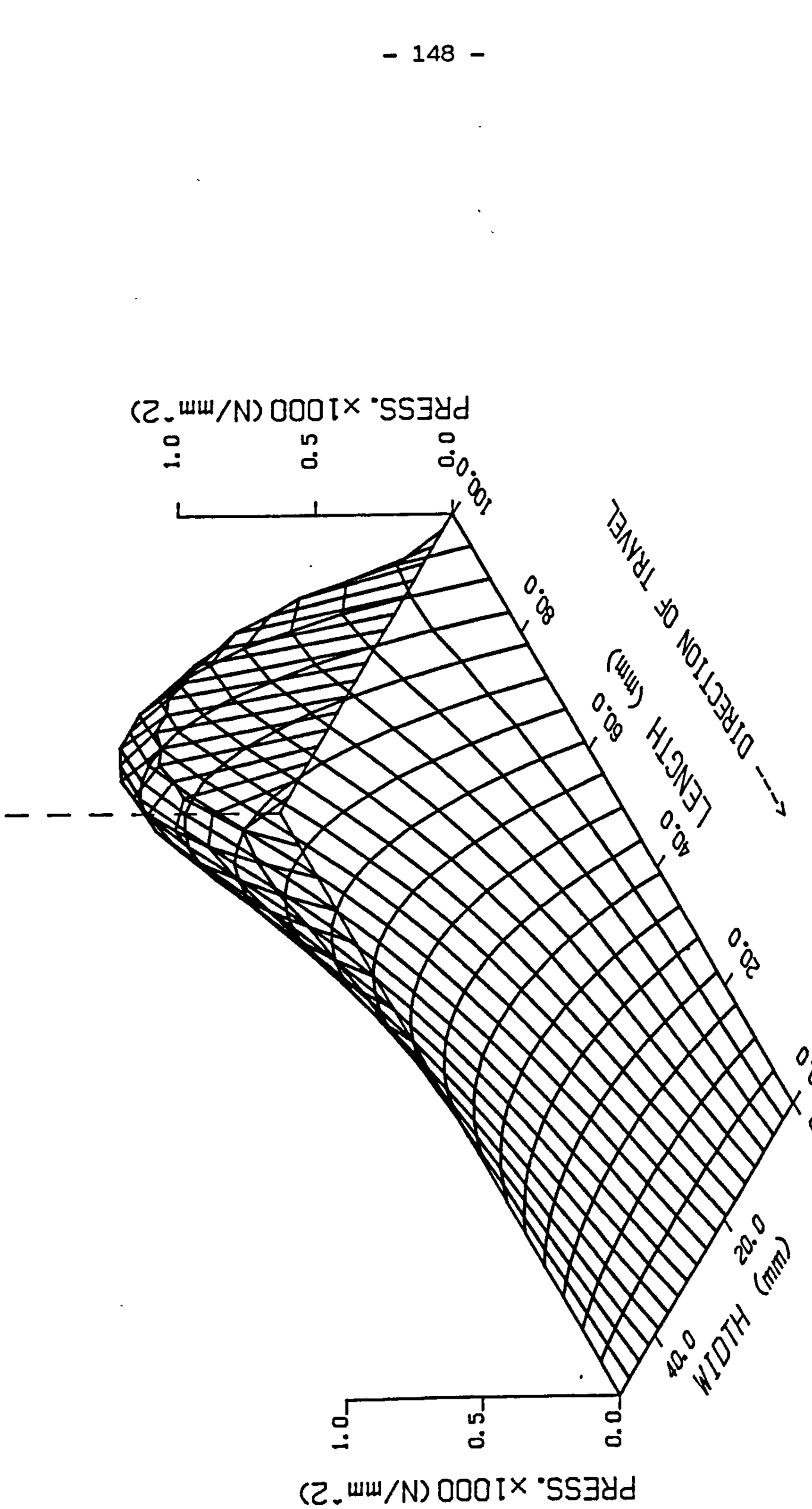

FIGURE 4.3.4 - RIGID RECTANGULAR SLIDER

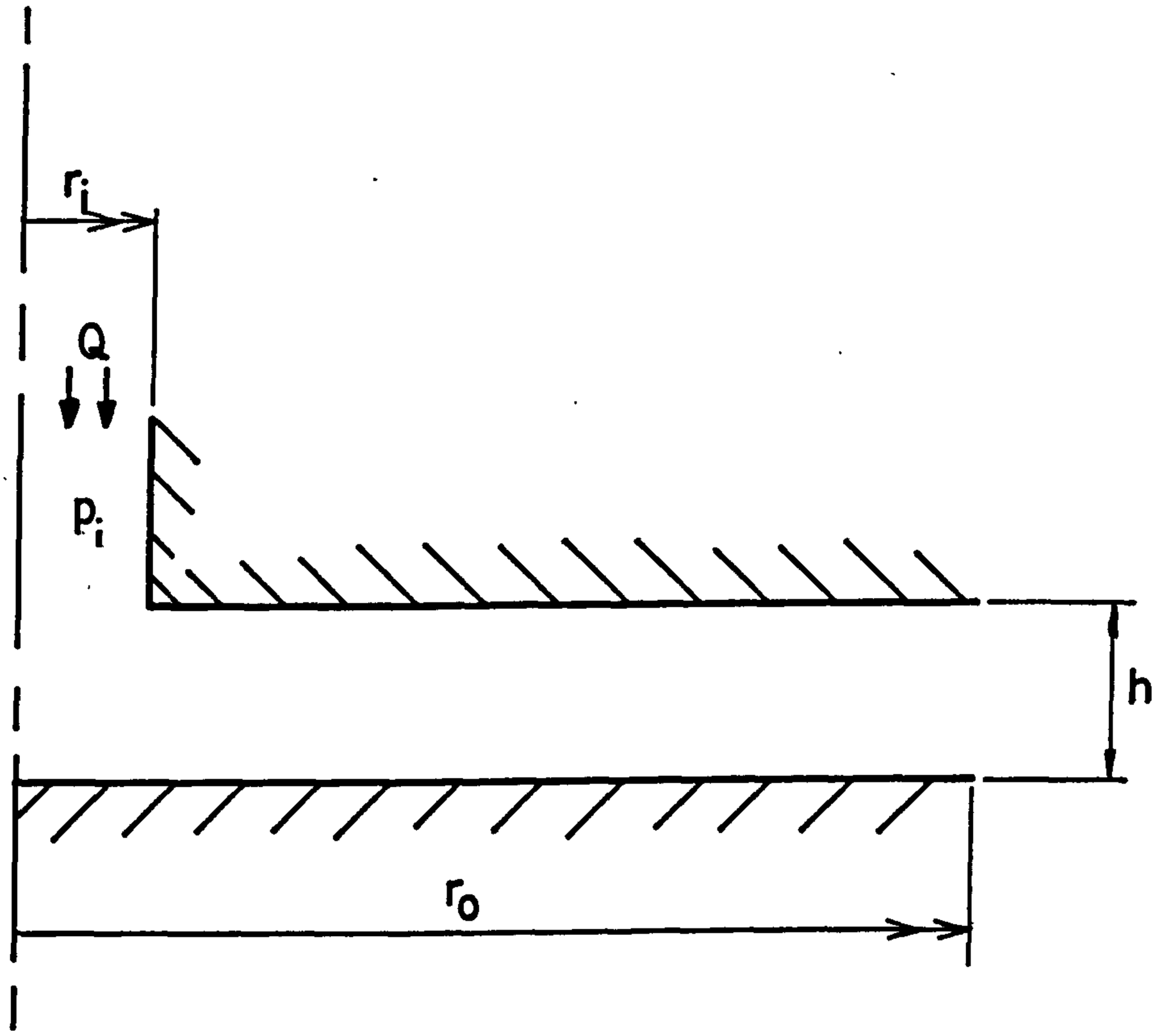

FIGURE 4.3.5 - CIRCULAR PRESSURIZED PAD - GEOMETRY AND NOTATION

$$\bar{p} = \frac{p}{p_i} = \frac{\ln\left(\frac{r_o}{r}\right)}{\ln\left(\frac{r_o}{r_i}\right)} \qquad \text{------4.3.5}$$

For the sake of comparison, a pad with r_i = 2mm and r_o = 100mm was considered. Figure 4.3.6 shows the analytical curve given by equation 4.3.5, together with points from two finite element solutions. The finite element solutions differ only in the type of mesh that they used. FE SOL. 1 used a mesh with nodes spaced uniformly in the radial direction every 10mm (except the centre most nodes at r = 2mm). FE SOL. 2 is the same as FE SOL. 1, except that extra nodes are placed at radii of 5, 15 and 25mm in the area of high pressure gradient. The use of these extra nodes improves the accuracy of the solution and demonstrates the need to have sufficient nodes in areas of high pressure gradient. Normally, however, the areas of high pressure gradient would not be known and the mesh could not be arranged for greatest accuracy. It is important, therefore, that a simple uniform mesh will give adequately accurate results. If required, the mesh can then be subsequently refined based on the results of the uniform mesh.

In the example shown, the largest errors are in the region r = 10mm to r = 40mm (figure 4.3.6). The values of $\bar{p}$ in this region are shown together with the percentage error for each of the two finite element solutions. The percentage error is defined as

$$\% \text{ error} = \left(\frac{\text{FE Solution} - \text{theoretical Solution}}{\text{theoretical Solution}}\right) \times 100$$

r(mm)	Analytical $\bar{p}$	FE SOL. 1 $\bar{p}$	FE SOL. 2 $\bar{p}$	FE SOL. 1 % error	FE SOL. 2 % error
10	0.5886	0.6296	0.6005	6.97	2.02
20	0.4114	0.4444	0.4206	8.02	2.24
30	0.3078	0.3333	0.3147	8.28	2.24
40	0.2342	0.2540	0.2398	8.45	2.39

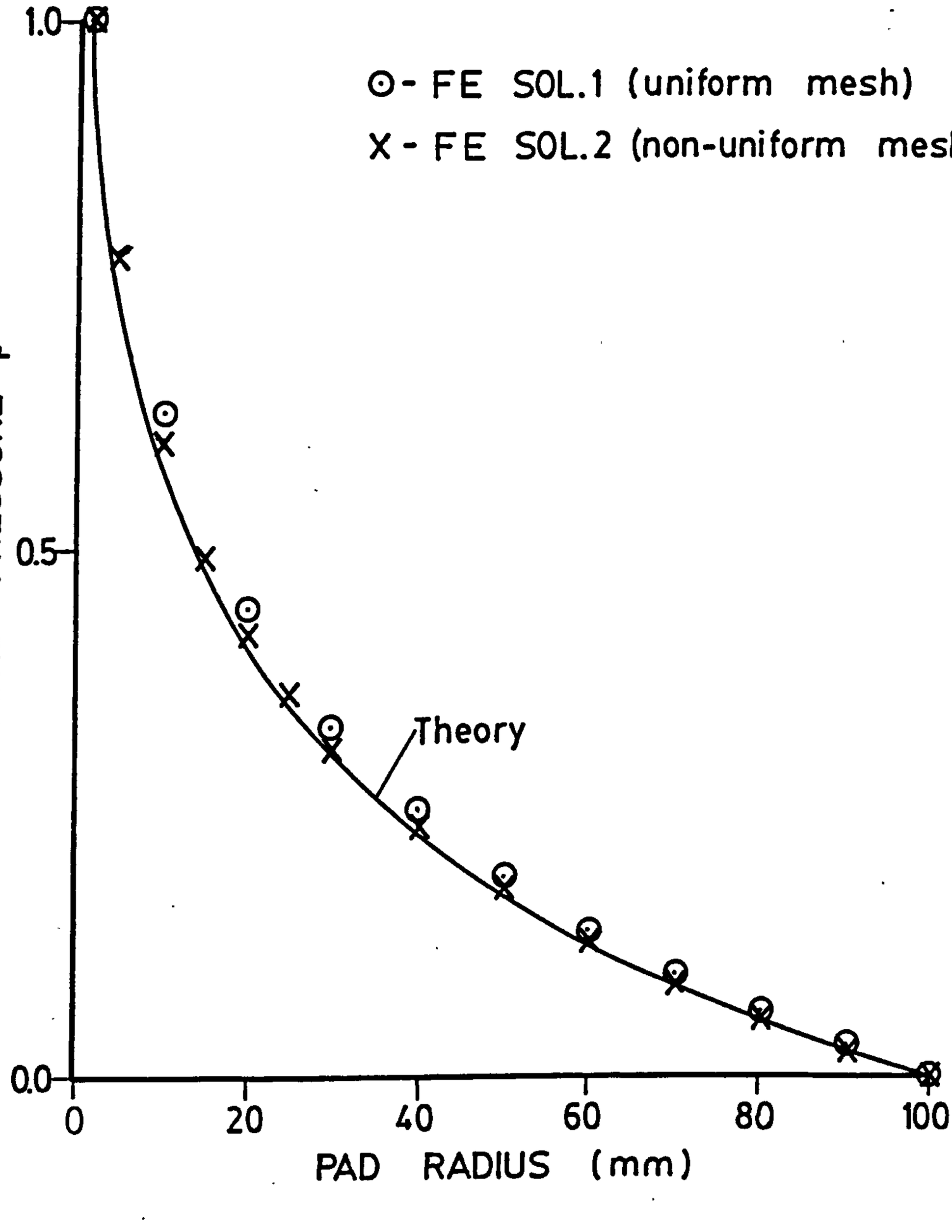

FIGURE 4.3.6 - CIRCULAR PRESSURIZED PAD - COMPARISON BETWEEN THEORETICAL AND NUMERICAL SOLUTIONS

From the table above it can be seen that the errors from FE SOL. 2 are smaller than those from FE SOL. 1, but both would be acceptable, as the errors shown are only for the worst region of this case with a very high pressure gradient.

4.4 DISCUSSION OF PROGRAM VERIFICATION

The preceding sections have presented a number of test cases which were performed to allow verification of the computer programs. These have shown that this implementation of the finite element method is capable of solving Reynolds equation and giving answers which agree well with analytical solutions. During the development of these computer programs many aspects were tested and verified, but it would not be appropriate to cover all these details here. One important aspect of the program operation is the application of boundary conditions. The pressure boundary conditions are used on the ends of the 1-dimensional sliders and on all edges of the 2-dimensional sliders, described in the previous sections.

The correct application of flow boundary conditions is slightly less easy to verify and a number of test cases of flow through wide slots were considered.

Flow through a wide slot is given by (33) and also section 3.9 as,

$$Q = \frac{\Delta P b h^3}{12 \mu B} \qquad \text{--------4.4.1}$$

where Q = total volume flow

b = width of slot

B = length of slot

h = thickness of slot

and ΔP = pressure drop over the length of the slot.

Equation 4.4.1 assumes that the width is very large compared to the film thickness, and that the length is also very large. By using an infinite width parallel slider bearing with zero sliding velocity, and specifying a volume flow per unit width into this bearing, the case of viscous flow through a slot can be modelled by the finite

element method. As the infinite width case is to be considered to remove the effect of bearing width, equation 4.4.1 can be modified to

$$q = \frac{\Delta P h^3}{12 \mu B} \qquad \text{-------4.4.2}$$

where q is the volume flow/unit width. The pressure at the exit of the slot can be considered zero; therefore, ΔP is equal to the inlet pressure. This inlet pressure is not specified, but from 4.4.2 is a function of flow, slot dimensions and viscosity. Comparing the inlet pressure given by equation 4.4.2 with that given by the finite element solution for a number of test cases, shows that the error in all cases is much less than 0.1%. The computer programs therefore apply the flow boundary conditions correctly.

The finite element computer programs have been verified in all aspects of their operation related to fluid mechanics. The various details of the finite element method, such as the solution of the simultaneous equations, are also verified in the process of solving the test cases in this and previous sections. The computer programs use three subroutines which have been derived from ones published in the literature (49). These subroutines perform the routine functions of assembling the local element matrices into the global matrices, adding the geometric (pressure) boundary conditions and solving the simultaneous equations by the Gauss-Doolittle method of back substitution.

The verification of the tyre contact patch deflection model is only possible to the extent that the computer implementation of the theory derived in section 3.10 has been checked and agrees with hand calculated values. As was stated in section 3.10, the tyre contact patch deflection model is not intended to model accurately the behaviour of the tyre due to changes in construction, etc..

The calculation of the fluid flow velocities and subsequently the effective viscosities were checked with hand calculated values and found to be in agreement.

4.5 DESCRIPTION OF THE FINITE ELEMENT COMPUTER PROGRAMS

The discussion so far in this chapter on the verification of the finite element computer programs has been equally valid for both the block design program and the contact patch analysis program. This work is aimed at producing a computer program to analyse the behaviour of the tyre contact patch under wet conditions. However, it was realised that to assist in the design process (see Chapter 2) it would be useful if a program were available to help in the detailed design of individual tyre tread blocks.

The differences between the two finite element programs can be seen from the following two sections where the flow diagrams for each are presented and discussed. These differences are mainly limited to the boundary conditions and the type of loading involved.

The Block Design Program analyses the effects of fluid pressure and block deformation for an individual tyre tread block, such as the one shown in figure 4.5.1.

This analysis is valid if the grooves within the tyre contact patch are not filled with water, i.e. the tyre is not flooded. This condition is met in many cases when the amount of water on the road surface is small due to either low rainfall or a well drained road surface. As the grooves are not filled with water, the pressure in the interfacial fluid will drop to atmospheric (zero) at the edges of the tread blocks and, because of this, there is no interaction within the fluid between adjacent blocks and the behaviour of each block can be analysed separately. The contact patch analysis computer program also allows the situation of an unflooded tyre to be modelled by making the pressure at all nodes within grooves zero.

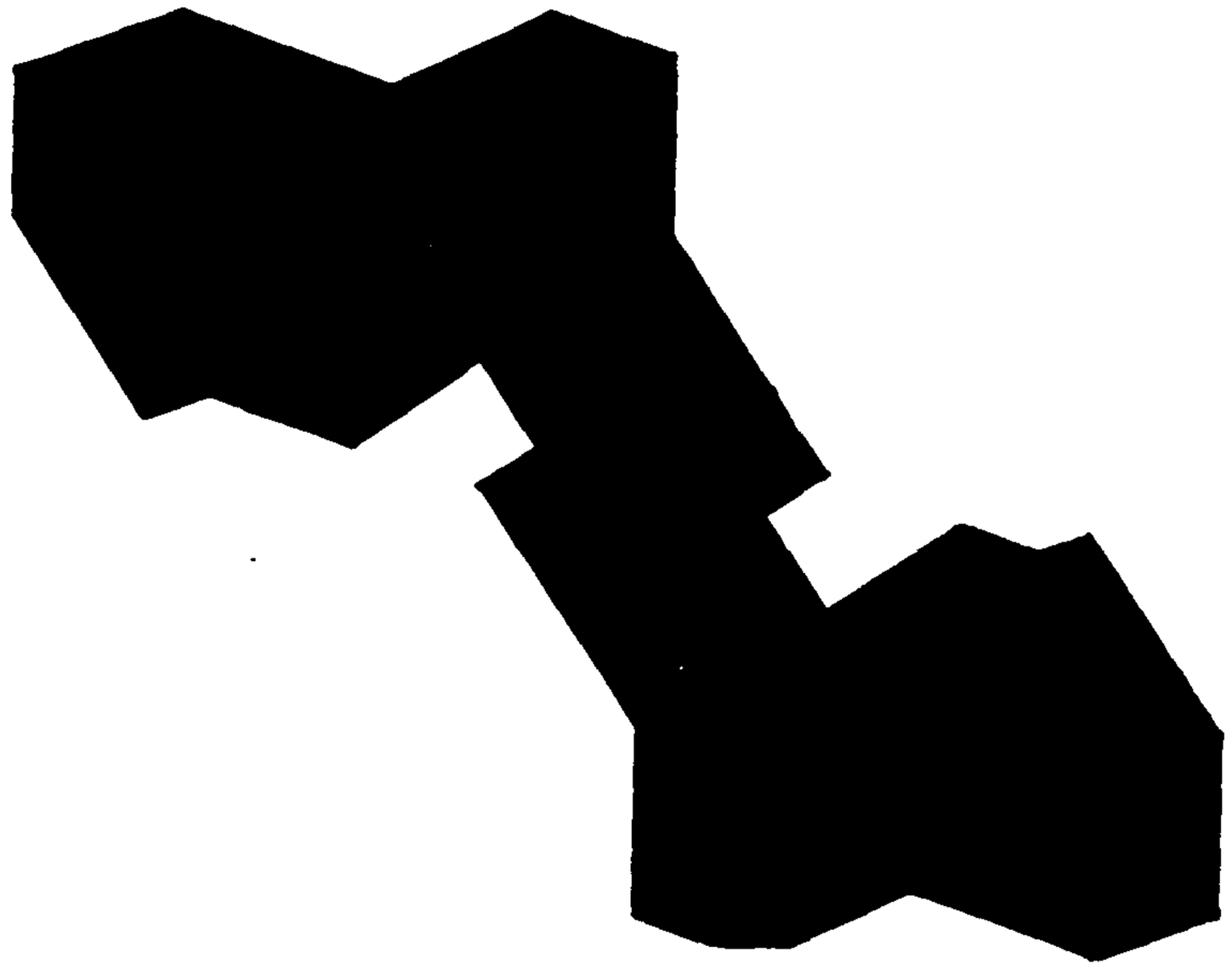

DUNLOP SP ELITE - Centre Block
(2 x actual size)

FIGURE 4.5.1 - TYPICAL TYRE TREAD BLOCK

If the contact patch computer program is to be used to model accurately the behaviour of a commercial tread pattern, then this would require the use of very many nodes and elements within the finite element mesh. This would cause problems both in the effort involved in the generation of the mesh and in the amount of computer time required to obtain a solution. By using the block design computer program where only one block is modelled, a mesh which will give accurate results can be used without imposing large penalties on mesh generation and computer time.

Both the block and the contact patch computer programs allow calculations to be made at a series of 'time' steps. Each step is actually a steady state condition, but allows variation of a number of factors to be studied by using a different value at each step.

The present uses of the contact patch analysis program are seen in the areas of broad research into various simple tread patterns and the shape of the contact patch, whilst the block design program can be used for the detailed analysis of specific tyre tread blocks. Both of the programs are written in a modular form so that as research into the modelling of tyres on wet roads advances, the programs can easily be modified to take advantage of new techniques. For example, if a new contact patch deflection model were developed, this could be incorporated into a FORTRAN subroutine and substituted for the original deflection subroutine without affecting the operation of other parts of the computer program. Whilst this type of modular programming also makes the testing and de-bugging processes much simpler, it is particularly relevant in this case, as the computer model here only represents the first stage in the development of computer modelling techniques for tyres on wet roads.

4.5.1 The Tread Block Design Program

The flow diagram showing the overall structure of the tread block design program is shown in figure 4.5.2. The intention of this section is to show the logic of the computer program and not to deal with the details of the implementation into FORTRAN.

FIGURE 4.5.2 - FLOW DIAGRAM OF THE BLOCK DESIGN PROGRAM

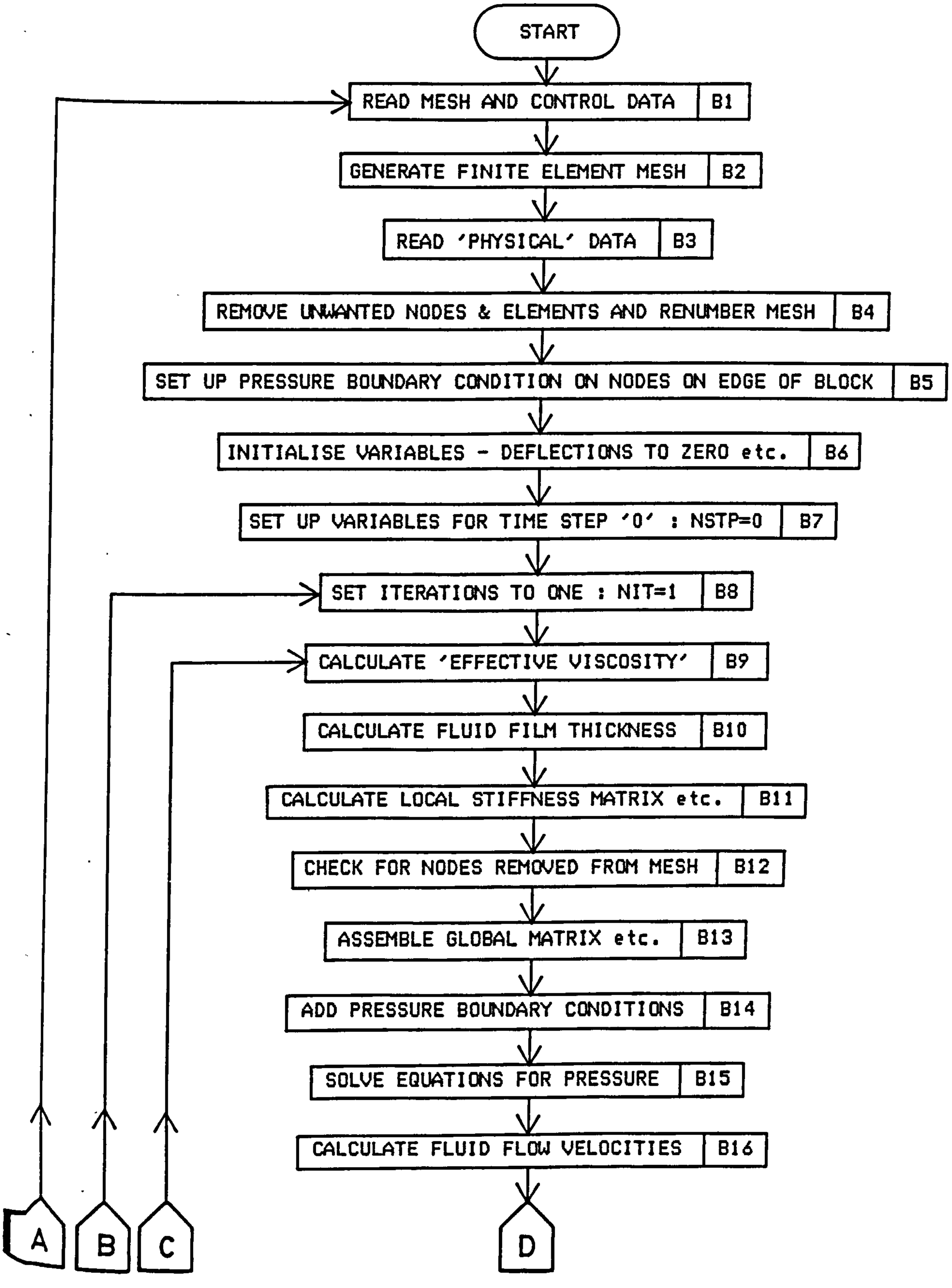

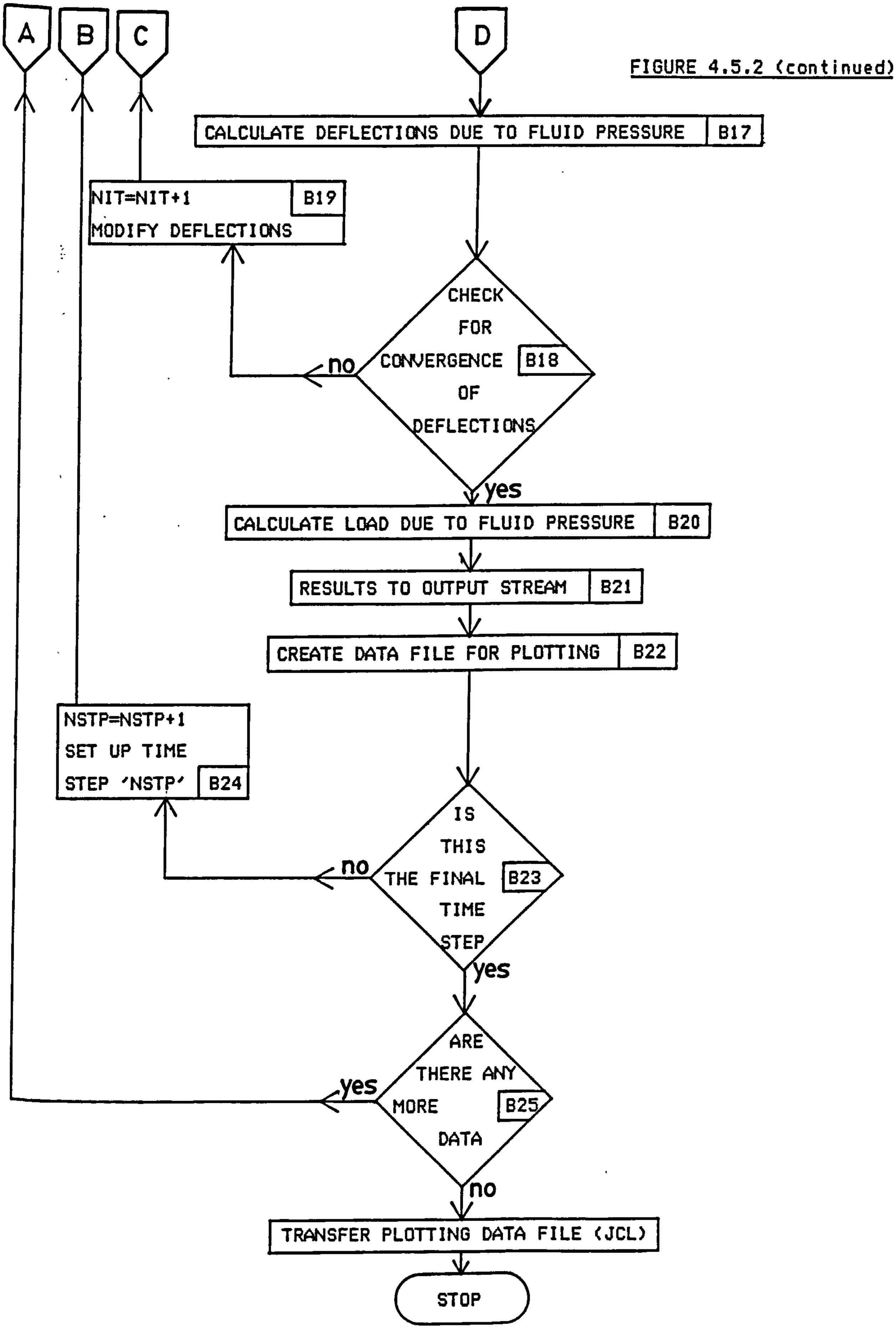

FIGURE 4.5.2 (continued)

The actual source listing can be found in Appendix B along with the user guide, which explains in detail the input variable usage.

The various sections in figure 4.5.2 are explained below:

B1 The title of the job is written on the program output and also as the title to the graphs for the plotting programs. The control data set up the maximum number of iterations that will be allowed, the final convergence criteria and the damping and limiting factors to aid convergence (discussed later). The mesh data set up the mesh type that will be used (see section 4.6.1) and the number of nodes in the x and y directions.

B2 The node and element numbering is performed for the reference mesh from the data given in B1 . The details of this are given in section 4.6.1.

B3 The 'physical' data gives the details of the length and width of the block or the spacing of the x and y node rows, the position of nodes if they are not on the grid, the elements which are in grooves and the groove widths. The details of any time stepping are also given here, as are the sliding and squeezing velocities and details of nodes which are in sipes or on axes of symmetry.

B4 Because of the way the mesh is generated, some elements will need to be removed from the reference mesh and the nodes and elements will then be renumbered.

B5 The pressure on all nodes on the edge of the block will be zero, and this is automatically set, without the user needing to know which nodes are actually on the edge.

If sipes are required then the nodes defined as being in sipes will also have a zero pressure boundary condition. Nodes on an axis of symmetry do not have zero pressure boundary conditions applied.

B6 The deflections are initialised to zero and various other variables are also initialised to their starting values.

B7 The first set of calculations is always at time step '0' and the various factors which can vary with time steps are initialised to their step '0' values. The time step number 'NSTP' is initialised to zero.

B8 The number of iteration counter, 'NIT', is initialised to one.

B9 The effective viscosity is calculated which allows for the effects of turbulence, as shown in section 3.6. The velocities and film thicknesses from the previous iteration are used in the calculation of Reynolds Number. On the first iteration, the effective viscosity is set to the laminar viscosity of water.

B10 Based on the block deflections and any grooves, etc. set up in section B3 , the fluid film thickness at each node of each element is calculated. Calculating a film thickness for the local node within each element rather than a value for each global node number allows discontinuities in film thickness between elements to exist such as is required to model the geometry of a groove.

B11 The local stiffness matrix and generalised force vector for each element are calculated. If the fluid film thickness over a particular element is zero, then the pressure from Reynolds equation would be indeterminate; therefore, elements of this type are removed from the mesh and their local stiffness matrix and generalised force vector are not calculated.

For elements within a groove, the 'groove flow factor' developed in section 3.9 will be calculated and used in the formulation of the local stiffness matrix.

B12 A check is made for any nodes which need to be removed from the mesh due to the removal of elements in section B11 , and any such nodes have a "dummy" boundary condition applied to them. This will not affect any other part of the mesh as, by definition, these nodes are unconnected. The boundary condition is needed because the unconnection to the mesh means that the pressure at these nodes cannot be found and an error would occur in the solution method if a "dummy" boundary condition were not used.

B13 The local stiffness matrices are assembled into their correct position in the global stiffness matrix. Similarly, for the generalised force vector. Any element which has been removed from the mesh in B11 is not added to the global stiffness matrix or force vector.

B14 The geometric (pressure) boundary conditions are added into the global stiffness matrix and force vector.

B15 The system of simultaneous equations formed by B13 and B14 is solved for the unknown pressures by the Gauss-Doolittle back substitution method.

B16 From the now known pressures (and hence pressure gradients) and the fluid film thicknesses, the fluid flow velocities can be calculated. As well as being useful output data, these are required by B9 in the calculation of effective viscosity on the next iteration. The fluid flow velocities are calculated at the element centroids for reasons discussed in section 3.5.

B17 Using the deflection model developed in section 3.10, the deflection at each node is calculated from the fluid pressures found in section B15 .

B18 The deflections calculated in section B17 are compared with those from the last iteration and if they agree to within the convergence criteria defined in section B1 at all nodes, then control is passed to section B20 , otherwise control is passed to section B19 .

B19 If the deflections have not converged, then this section increments the iteration counter 'NIT', and damps and limits the deflections as described in section 4.5.3, to help convergence. Control is then passed to section B9 and the iterative process repeated through to section B18 where the convergence is again checked.

B20 When the deflections have converged, the total load due to the fluid pressure is found by the method described in section 4.3. This load can be used as a measure of the blocks wet grip properties, i.e. low load is good for wet grip, high load is bad.

B21 The bulk of the results are written to the output stream for printing or display on a VDU. Histograms are produced showing the distribution of pressure and fluid film thickness. Tables are produced showing fluid pressure, block deflection, film thickness and flow velocity.

B22 A data file is produced with the data for the plotting programs to give graphical output of pressure, film thickness and flow velocity as well as a plot of the finite element mesh if required.

B23 The current time step number 'NSTP' is compared with the required number of time steps and if the maximum has been reached the program passes control to section B25 , otherwise control is passed to section B24 .

B24 Another time step is required so the time step counter 'NSTP' is incremented and the various factors which can change with time steps are set to the appropriate values; control is passed to section B8 , from where the whole solution procedure can be repeated.

B25 This set of results is now complete. The program allows concatenation of data files so that within one job there can be a number of different problems considered. If there is a further set of data, control is passed back to section B1 and the complete program is repeated with the new data. If there are no further data, the program is halted and the plotting file is transferred to a special storage area, so that it can be accessed by the PDP11 at a later stage. The job then terminates.

4.5.2 The Contact Patch Analysis Program

The operation of the contact patch analysis computer program will now be described in a similar way to the block design program. When modules are the same or similar to those used in the block design program reference will be made to the appropriate 'B' number in section 4.5.1. The flow diagram of the contact patch analysis program is shown in figure 4.5.3 and the source listing is given in Appendix B.

The various sections in figure 4.5.3 are explained below:

C1 Similar to B1 , where title, number of iterations, convergence criteria, mesh type,nodes in x and y directions, etc., are set up.

C2 Same as B2 , mesh is generated.

FIGURE 4.5.3 - FLOW DIAGRAM OF THE CONTACT PATCH ANALYSIS PROGRAM

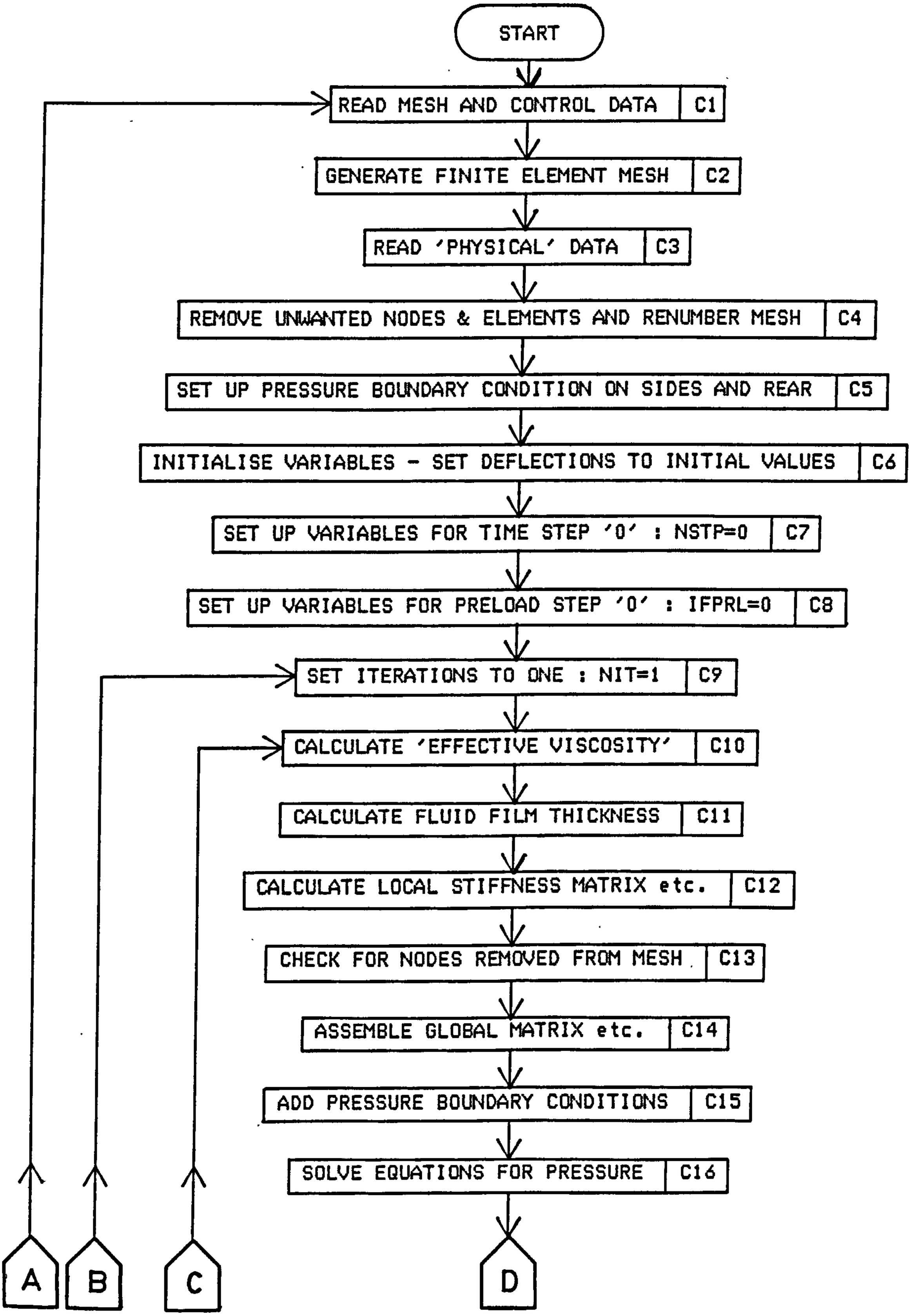

FIGURE 4.5.3 (continued)

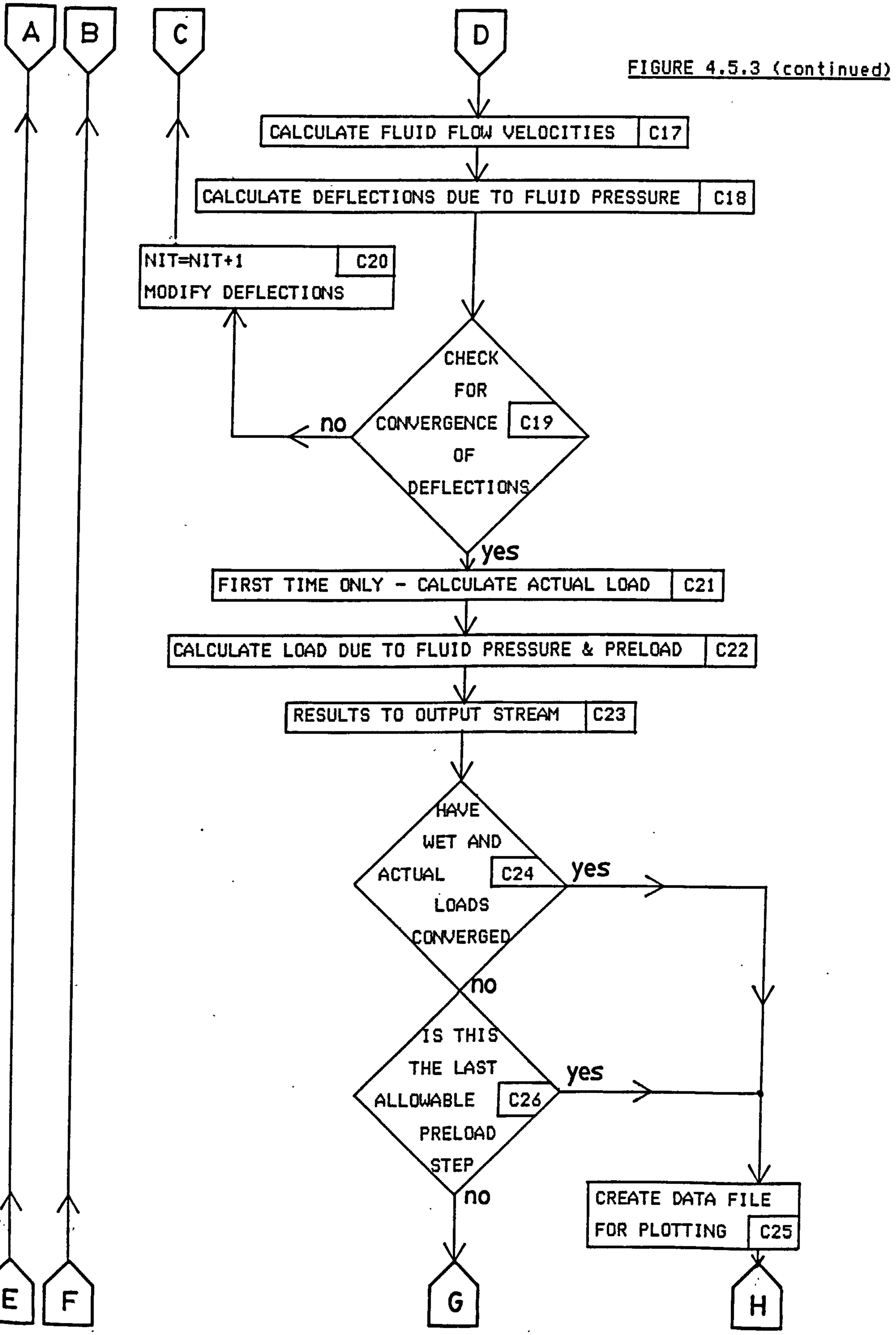

FIGURE 4.5.3 (continued)

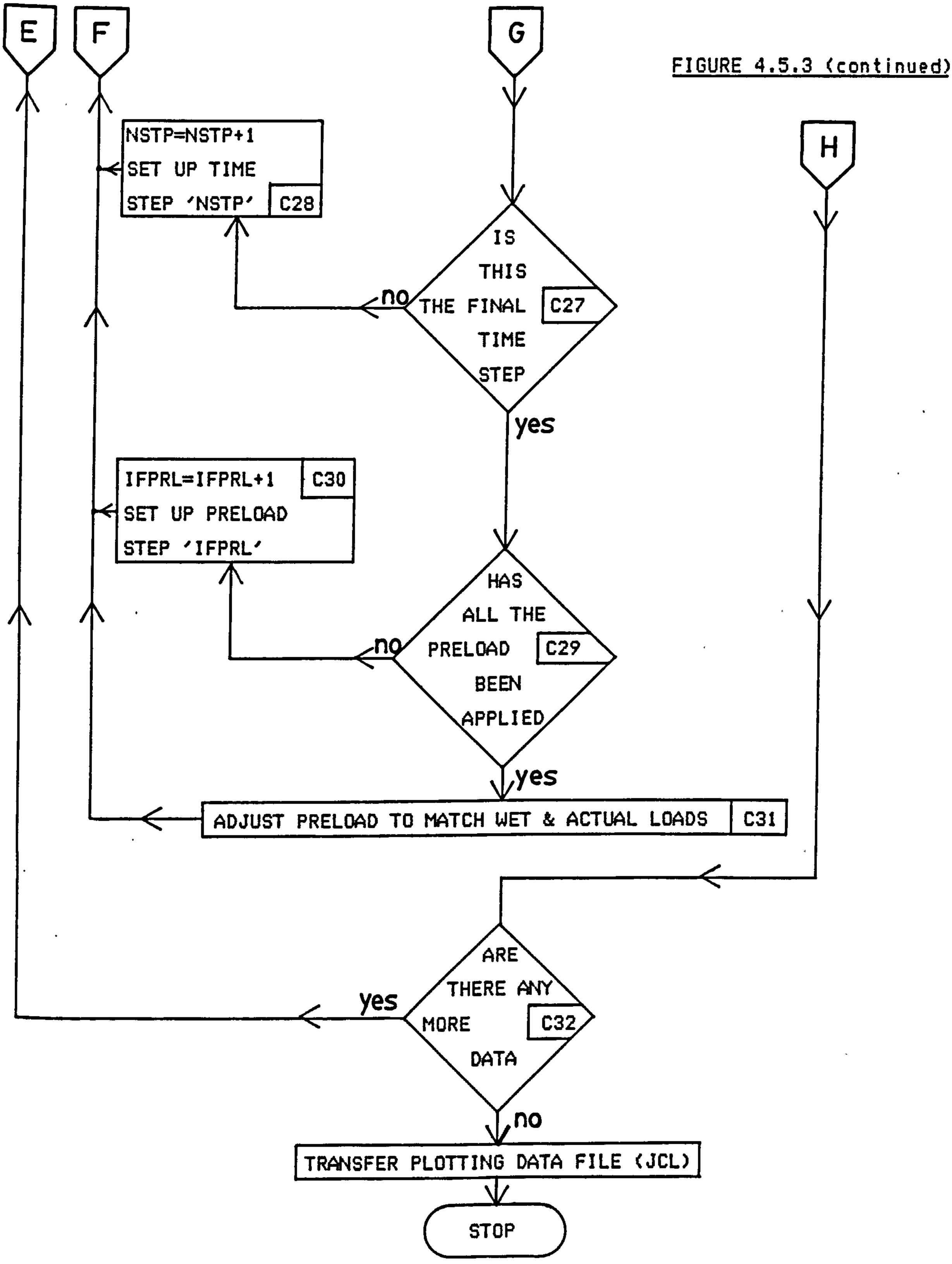

C3 Similar to B3 , with the addition of data on tyre dry contact pressures, slip and slip angle, vehicle road speed, and the nodes which are on the front edge of the contact patch (to allow the application of flow boundary conditions, section 3.7.4).

C4 Same as B4 , unwanted elements removed.

C5 Similar to B5 , except that no pressure boundary condition is placed on nodes on the front edge of the contact patch, to allow the application of flow boundary conditions. The contact patch can also be symmetrical in which case no pressure boundary condition is placed on nodes on the axis of symmetry.

C6 Similar to B6 , except that in this case the deflections are not initialised to zero. An initial slope of 0.2mm is superimposed on the film thickness distribution. This has been found to give a solution more quickly than starting the problem with the whole of the dry contact area in contact with the road surface. The starting value taken for the slope does not affect the results.

C7 Same as B7 , the time varying factors are set to their step '0' values and the time step number 'NSTP' is initialised to zero.

C8 The values of the preload due to the dry contact patch are initalised to zero. The preload will be applied in a series of steps, as an aid to convergence (see section 4.5.3). Initially, this will be preload '0' and the preload number 'IFPRL' is set to zero.

C9 Same as B8 , iteration counter initialised to one.

C10 Same as B9 , effective viscosity calculated.

C11 Same as B10 , fluid film thickness calculated.

C12 Similar to B11 , except that the fluid flow boundary conditions are added to the local generalised force vector.

C13 Same as B12 , check for nodes not connected to mesh.

C14 Same as B13 , assemble global matrix, etc.

C15 Same as B14 , add in pressure boundary conditions.

C16 Same as B15 , solve equations.

C17 Same as B16 , calculate fluid flow velocities.

C18 Similar to B17 , except that the preload on the contact patch must be taken into account as discussed in section 3.11.

C19 Similar to B18 , convergence of deflections is checked. If converged control is passed to section C21 otherwise to section C20 .

C20 Similar to B19 , deflections have not converged; therefore increment counter 'NIT' and damp & limit deflections. Control is then passed to section C10 and the iterative process through to section C19 is repeated.

C21 If this is the first preload and the first time step, then the actual load on the tyre in the dry, due to dry contact pressure is calculated. This is used as a 'target' for the wet load of subsequent preload iterations.

C22 Similar to B20 , except that the load due to both the fluid pressure (the wet load) and due to the applied preload at this preload step (the dry load) are calculated, by the method shown in section 4.3.

C23 Similar to B21 , output tables of fluid pressure, contact pressure, deflection, water depth and fluid velocity are written to the output stream.

C24 Test to see if the wet load calculated in section C22 is within 2% of the actual tyre load found in section C21 . If it is, then control is transferred to the plotting data file creation section C25 . If the loads have not converged, control is passed to C26 .

C25 Same as B22 ; a data file to be used with the plotting programs is created; control is then passed to section C32 .

C26 Test to see if this is the last allowable preload step. A number of steps are used to apply the tyre preload for reasons discussed in section 4.5.5. The allowable number of preload steps is always greater than the number of steps taken to apply the contact pressure preload. This allows the wet and actual loads to converge, even after the full load is applied to the tyre. If this is the last allowable preload step, then there will be no fully converged solution; however, it is useful if these results are fully available and, therefore, control is passed to section C25 to create a plotting data file. If this is not the last allowable preload step control passes directly to section C27.

C27 Same as B23 ; check to see if the maximum number of time steps has been reached, and if it has pass control to section C29 otherwise to section C28 .

C28 Same as B24 , set up for further time step and pass control to section C9 .

C29 Check to see if all the required preload has been applied; if it has, pass control to section C31 otherwise to section C30 .

C30 A further preload step is to be performed; therefore, the preload counter 'IFPRL' is incremented and the contact patch preload is set up for the next step. Control is then passed to section C9 .

C31 All the preload from contact pressure is now applied; therefore, need to modify preload in an attempt to match wet load with actual tyre load on the next iteration. Control is then passed to section C9 .

C32 Same as B25 , a check is made to see if there are more data; if there are then control is passed to section C1 , otherwise the program is halted, the plotting file is transferred and the job terminated.

A comparison of the flow diagrams for the block design program (figure 4.5.2) and the contact patch analysis program (figure 4.5.3) shows the main difference to be the use of a preload in the latter case. The majority of the program modules are either the same or very similar for the two programs.

In both the flow diagrams, the action when the program will terminate abnormally is not shown. Abnormal termination will take place if the maximum specified number of iterations are used without a converged solution being found or by error in the input data.

In both the finite element computer programs a certain amount of remedial action has been taken to improve the convergence speed of the deflections, and in the case of the contact patch analysis program also the preloading. This is described in the following section.

Two further common aspects of the two programs are mesh generation and plotting and these are covered in sections 4.6 and 4.7 respectively.

4.5.3 Modifications to the Finite Element Computer Programs to Improve Convergence

Modifications to improve convergence were made in two areas of the computer programs. The first, which is common to both programs, affects the value of the deflection which is passed on to the subsequent iteration. The second area affects the contact patch analysis program only and relates to the way the preload is applied. These two areas will now be dealt with separately.

4.5.4 Modifications to Deflections

Two forms of modifications are made to the deflections. If one assumes that the initial film thickness is small compared to the film thickness at the converged solution, then the pressures calculated from this initial film thickness will be very large and overestimate the true pressures. Then on the following iteration these exaggerated pressures will, in turn, exaggerate the displacements. The displacements will now be highly over-estimated; therefore, the next set of pressures calculated will be highly underestimated, then the following deflections underestimated followed by overestimated pressures, and so on. This situation is highly unstable and can be avoided by limiting the change in nodal displacement on any one iteration. Oh and Huebner (60) discuss this type of problem and use a similar solution. The method used here is that the deflection at a node can only change by a fixed percentage of the deflection at the previous iteration. Usually, it is sufficient to use 100% as the limit, that is to say, in one iteration the deflection due to fluid pressure may either double its value or be reduced to zero. This limiting is only needed in the first few iterations when the solution at that particular iteration is a long way from the converged solution.

The other way in which the deflections are modified is by damping. This is also discussed by Oh and Huebner (60) and by Taylor and O'Callaghan (59). If the simple method of taking the actual predicted deflections (allowing for any limiting) and using them as the basis of the next iteration is used, then an underdamped response with oscillations about the converged solution will result. Typically, this would yield the response shown in figure 4.5.4.

The convergence (if any) is necessarily very slow in this case. The speed of convergence can be improved if each new deflection is weighted with the deflection from the previous iteration, thus preventing a large change of film profile in one iteration. This can be expressed as follows:

$$d_{I+1} = d_I + \delta(d - d_I) \quad \text{------4.5.1}$$

where 'd_{I+1}' is the new deflection that will be used on the next iteration, 'd_I' is the deflection found by applying equation 4.5.1 on the previous iteration and 'd' is the actual deflection predicted by the pressures resulting from the deflection 'd_I'. Equation 4.5.1 can be applied to the deflections at each node. The factor δ is chosen between 0 and 1 to give the fastest convergence and would, typically, be about 0.2.

An alternative to using a damping factor 'δ' is suggested by Oh and Heubner (60). This involves weighting the new deflection with the deflections from a number of previous iterations. The new deflection in this case would be given by

$$d_{I+1} = \frac{1}{n}\left[d + \sum_{i=I-n+2}^{i=I} d_i\right] \quad \text{----------4.5.2}$$

where n-1 is the number of previous iterations to be used in the weighting.

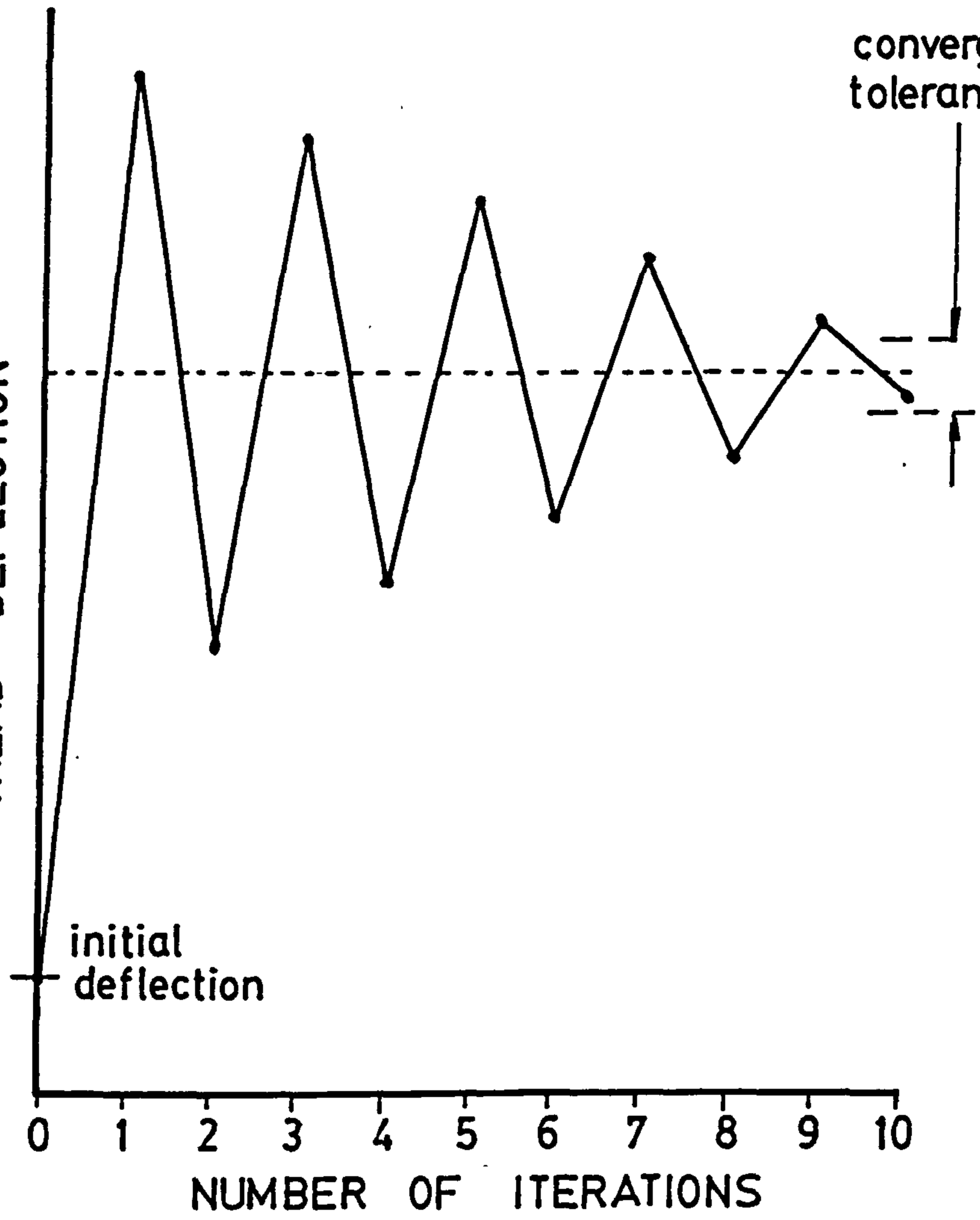

FIGURE 4.5.4 - UNDERDAMPED ITERATION/ TREAD DEFLECTION RESPONSE

The predicted deflection 'd' is also used in the averaging, making a total of 'n' deflections from which the new deflection is to be found. 'n' has to be kept relatively small, otherwise the estimated solution will become very insensitive to the deflections of the immediately preceding iteration. In practice it is found that 'n' should be less than 6 for the best results.

The actual damping method used in section B19 and C20 of the computer programs is a combination of the above two methods. This was found to give a good compromise between stopping wild oscillations and making the solution too insensitive to the last iteration. Equations 4.5.1 and 4.5.2 can be combined to give

$$d_{I+1} = d_I + \delta\left(\frac{1}{n}\left[d + \sum_{i=I-n+2}^{i=I} d_i\right] - d_I\right) \qquad \text{-----4.5.3}$$

Because in this case an averaged deflection is being used in place of the actual predicted deflection in equation 4.5.1, the damping required is much less. A value of 0.8 for 'δ' is typical. The value of 'n', the number of deflections that are to be averaged (including the current predicted one), would typically be 3. This means that averaging is taking place between the current predicted deflection, the last iteration and the iteration previous to that.

When a preloaded case, such as a tyre contact patch is being modelled, the solution is more unstable than without a preload. This requires more careful choosing of the damping factor 'δ'. It was found that the convergence was improved if the value of 'δ' was reduced (i.e. damping increased) as the preload was increased. Oh and Huebner (60) applying their averaging of previous estimates method to a journal bearing, suggest that the value of 'n' (equation 4.5.2) should be dependent on the eccentricity ratio of the bearing. Increasing the eccentricity ratio of a journal bearing makes the solution more unstable and, from that point of view, is similar to increasing the preload in the contact patch model. Therefore, the value of 'n' can be increased as the

preload is increased. Both this, and the reduction in 'δ', make the new deflection less sensitive to the deflection of the previous iteration and slows the rate of change of deflection between successive iterations.

This damping, and the limiting of initial iterations, was found to be very effective in speeding convergence in most problems. However, in some cases of a plain tread tyre on a smooth road, the damping factor has to be chosen carefully to ensure convergence. This type of problem is the worst for the instability of the solution, because any film thickness existing will be due entirely to tyre deflection and, therefore, the fluid pressure is very sensitive to changes in the contact patch deflections. The situation of all film thickness being due to deflection can also exist with the block design program, when a block that would just be touching a smooth road surface (had there been no water in the interface), is being modelled. However, this poses no convergence problem because the block is not preloaded, and it is the combination of high sensitivity to pressure/deflection changes with a preload that gives rise to convergence problems.

4.5.5 Modifications to Preload

Because non-preloaded solutions were found to pose no convergence problem, a scheme was devised for preloaded problems to reduce the effect of preload on the solution technique. This was done by finding an initial solution with no preload and then applying the preload due to contact pressure in a number of steps, specified by the user. This eases the problem because the starting point for each solution is the result from the previous preload step, and, therefore, the solution at one preload step is never very far from the starting point at that step. Once the full amount of preload has been added (or the actual tyre load has been exceeded by the wet load), the preload is modified to match the actual and wet loads on the next iteration. This is required because in the case of a tyre on a vehicle, the total load on that tyre is fixed, whilst the axle height can vary. It is also possible to model the fixed axle

height case by taking the final solution at the point when the full preload has been applied and the wet load will be greater than the actual load. This difference in the actual and wet loads can be used as a measure of that tyre's wet grip performance.

4.5.6 Conclusions on Computer Program Instabilities

From the information available at present it is not possible to determine the exact nature of instabilities in the computer program. Two main possibilities exist:-

i) The instabilities are caused by the numerical solution process, whereby the combined fluid/structural problem is split up and successive solutions are obtained, first for the fluid problem and then for the structural problem. This process could introduce instabilities into an otherwise physically stable problem.

ii) The problem is inherently physically unstable, at least under certain conditions and the computer program reflects this.

It should be emphasised, however, that these instabilities only manifest themselves under certain conditions, such as a smooth tyre on a smooth road surface and can be overcome by modifications to the damping factor 'δ' and/or the number of iterations to be averaged 'n' (equation 4.5.3). If the instabilities are physically based, then there exists the possibility that they may be utilised in the design of tyres for improved wet grip. Further work, therefore, needs to be done in this area and this is discussed in section 8.3.1.

4.6 MESH GENERATION

The problem of mesh generation was recognised early on in the project, as a particular barrier to the use of a finite element

based model within the tyre design process. The methods of mesh generation discussed in the literature were thought to be unsuitable for this application (section 1.2.3), because they still required a relatively large amount of data to be provided by the user. It was therefore decided to approach the mesh generation problem from a different point of view and develop a method with the specific case of tyre tread patterns in mind. The method is, in fact, a computerisation of a manual method developed early in the project.

4.6.1 Principles of the Mesh Generation Method

The required result of any mesh generation process is a list containing the co-ordinates of all the nodes within the mesh and the element connectivity data, i.e. which nodes are in which elements and, therefore, which elements are connected to each other. Also required are the details of which nodes are to have boundary conditions applied and the value of those boundary conditions. Various other pieces of information, such as material properties, are also required, but as these are not dependent on the finite element mesh, they will not be considered as part of the mesh generation process.

In this particular case, the boundary condition specification can be simplified somewhat, as it is known that in the case of pressure boundary conditions, the value on the boundary will always be 0.0 N/mm^2 (i.e. atmospheric). This is not necessary for the finite element solution, but as in all envisaged problems, this will be the case, the program has been designed to assume pressure boundary conditions of zero pressure (this could easily be changed if required). The nodes on which the zero pressure condition is to be applied still have to be defined, although this is relatively simple. For a tread block it is known that zero pressure boundary conditions need to be applied to all nodes on the edge of the block, and to nodes which are specified as being in sipes. The nodes

which are in sipes are supplied by the user by interactively selecting them at the time of mesh generation on the image analyser. The nodes on the edge of the block are defined in the finite element programs (section B5 or C5). This is achieved by working through the elements and selecting the edges which are only in one 'included' element ('included'means an element which is actually part of the block as discussed later). These will then form the edge of the block and the nodes on these edges are those on which the boundary conditions are applied.

In the contact patch analysis program, the procedure is modified slightly to account for nodes on the front of the contact patch. As discussed in section 3.7.4, the boundary conditions on the front edge of the contact patch are specified in terms of volume flow. Therefore, no pressure boundary conditions are required on these nodes. Section C5 of the contact patch analysis program uses a user supplied list of nodes which are on the front of the contact patch and applies pressure boundary conditions only to nodes on the side and rear edges of the contact patch.

The application of the boundary conditions (except for specifying the nodes in sipes or on the front of the contact patch) takes place within the finite element programs, and, therefore, the mesh generation program is left with the task of providing data on the x-y co-ordinates of the nodes and on element connectivity. The mesh generation program used on the image analyser outputs a data file which is used to direct the mesh generation process in the finite element programs (sections B2 , B3 , B4 and C2 , C3 , C4).Whilst this means that each time a finite element job is run a certain amount of mesh generation has to be performed (automatically with no user intervention); the amount of time used to do this is negligible compared with that taken by the finite element solution procedure. This arrangement allows the input data files to be kept relatively small.

The mesh generation program is based on generating a rectangular grid which covers the area of the block (or contact patch) for which the mesh is required. The spacing of this grid can either be uniform or be set in any way by the user to give a mesh with elements concentrated in a particular area of interest or to fit an unusual geometry. Figure 4.6.1(a) shows the grid and is the first stage of the mesh generation process.

The actual positioning of the 'x' and 'y' rows (if a non-uniform spacing is required) is performed interactively on the image analyser by moving each of the rows in turn to its required position, viewed superimposed over an image of the block. Once the rectangular grid is specified, it is divided into triangles to yield the typical result shown in figure 4.6.1(b).

The positioning of the diagonals to form the triangles can be performed in a number of different ways, shown in figure 4.6.2 and these are known as 'node numbering methods'. (Note: that node numbering method 1 denotes user input mesh data).

There now exists a valid finite element mesh of a rectangular area which covers the required block area. All elements which have more than half their area actually on the block are then 'included' in the mesh and other elements are 'not included'. In practice, this procedure is modified in an attempt to prevent a 'saw-tooth' edge to the mesh being formed. The mesh (with only 'included' elements) now approximately fits the area for which it is required. The nodes on the edge of this modified mesh are then moved until they are on the edge of the block and the mesh accurately fits the block.

When a node is to be moved to fit the edge of the block, a search is made PIXEL by PIXEL until the transition from block to no block(or no blockto block) is found. This search is performed in eight directions simultaneously as shown in figure 4.6.3.

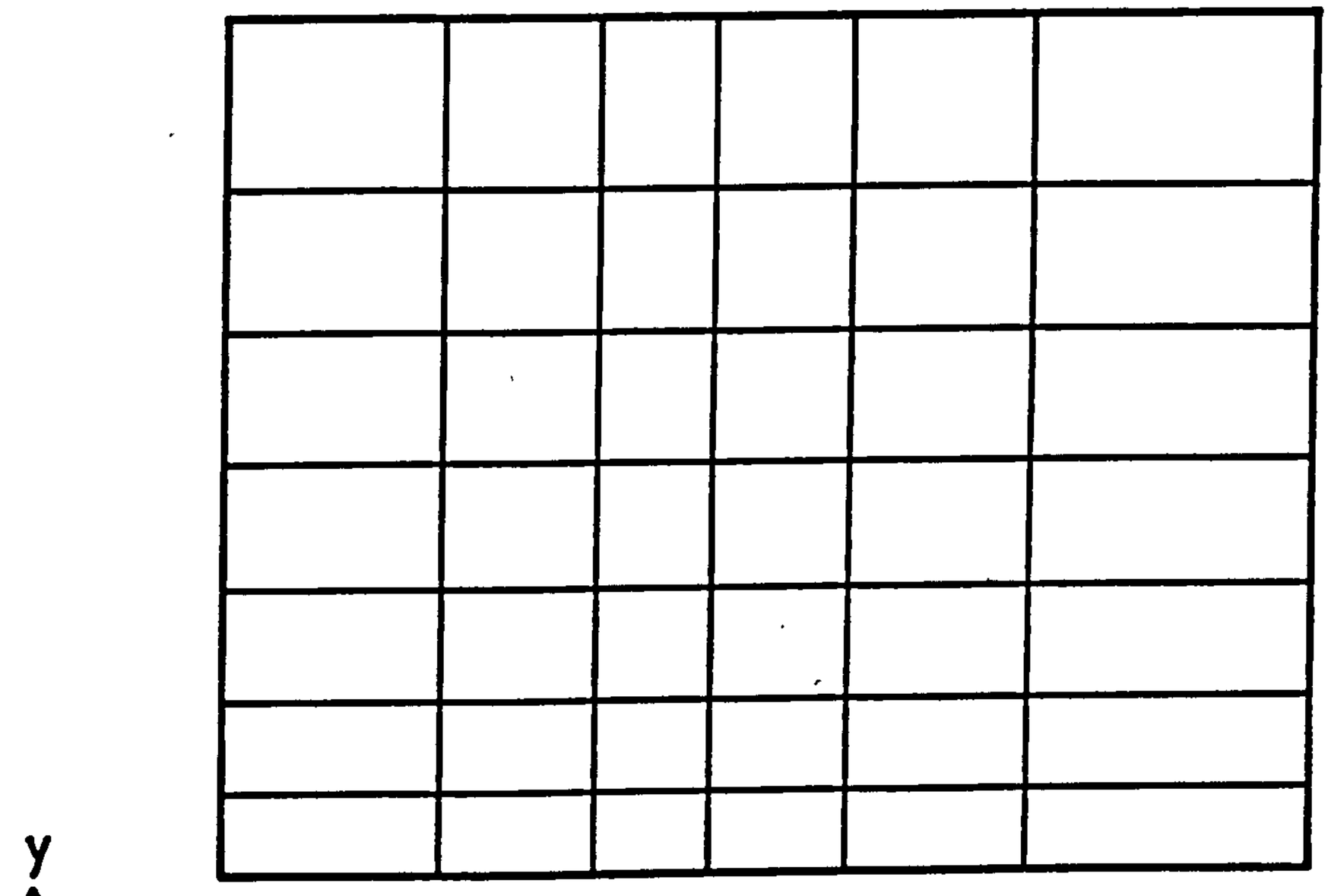

a)

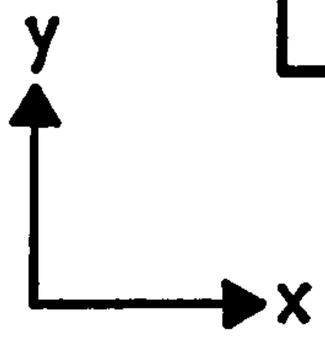

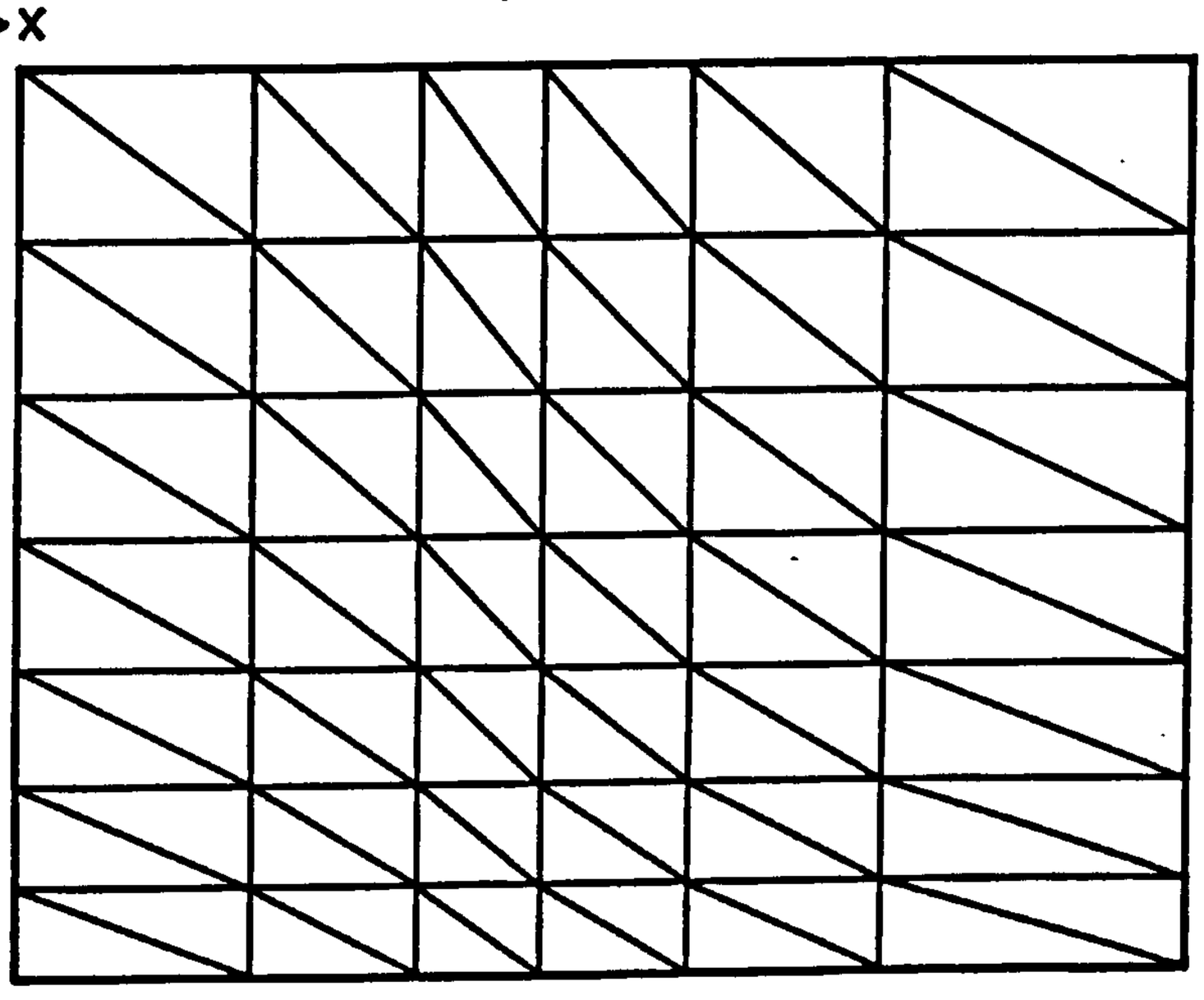

b)

FIGURE 4.6.1 - MESH GENERATION PROCEDURE

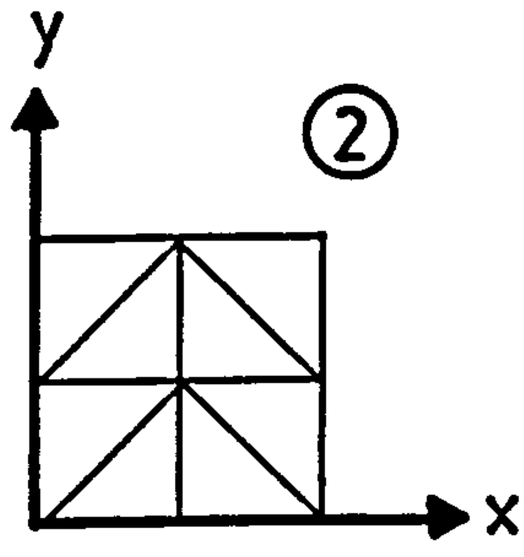

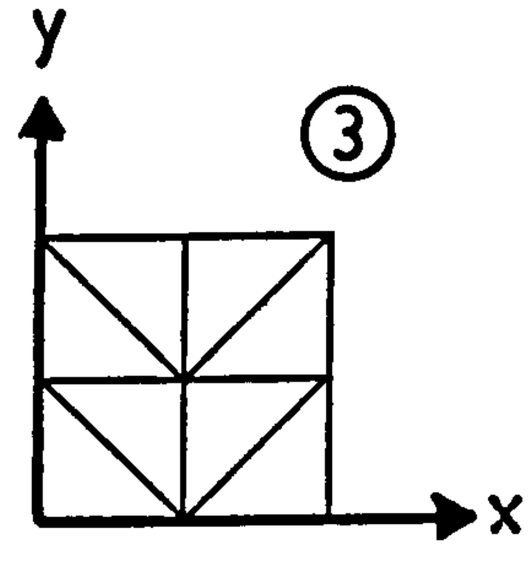

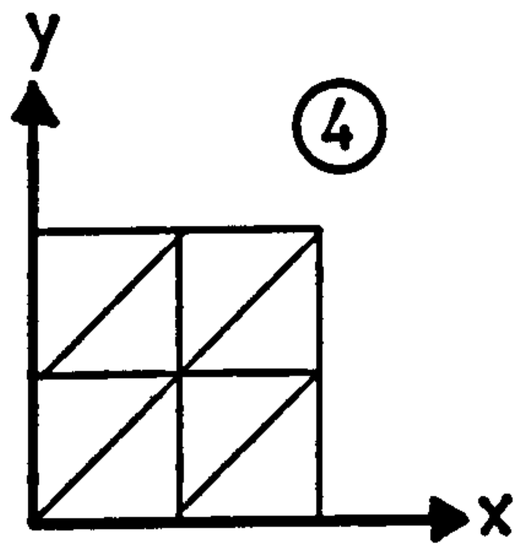

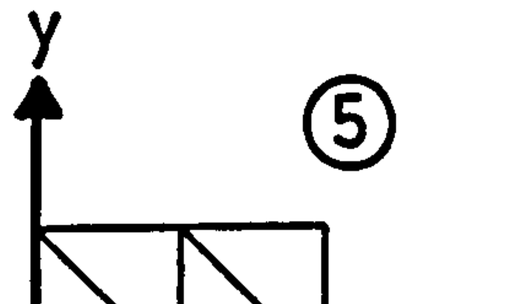

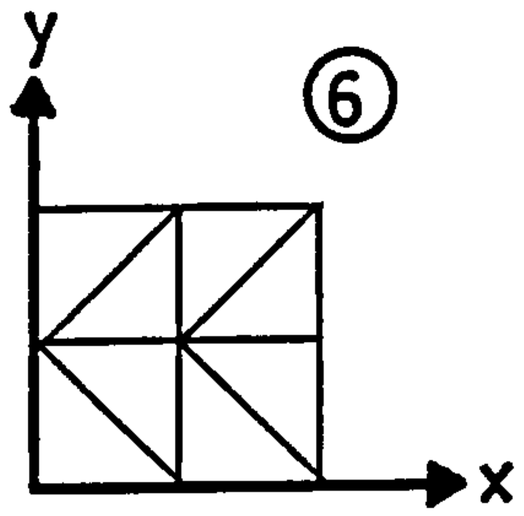

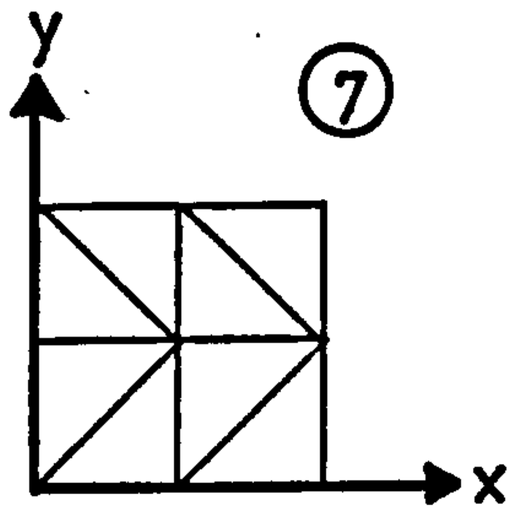

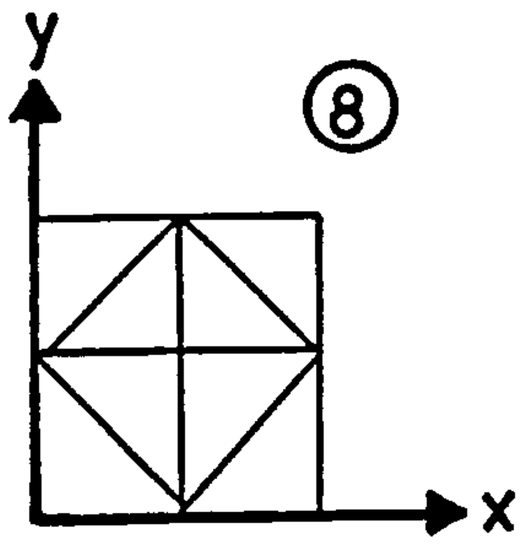

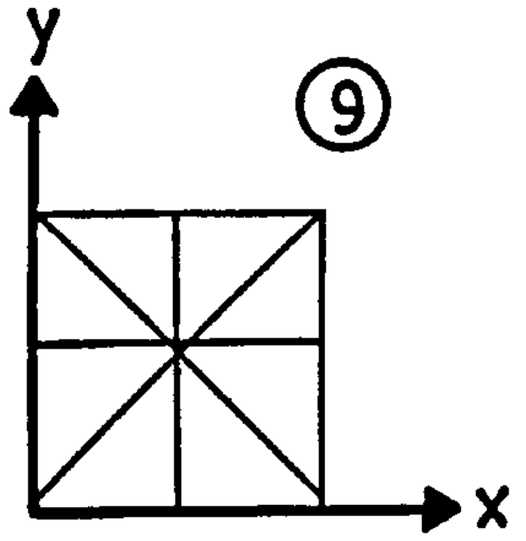

FIGURE 4.6.2 - NODE NUMBERING METHODS

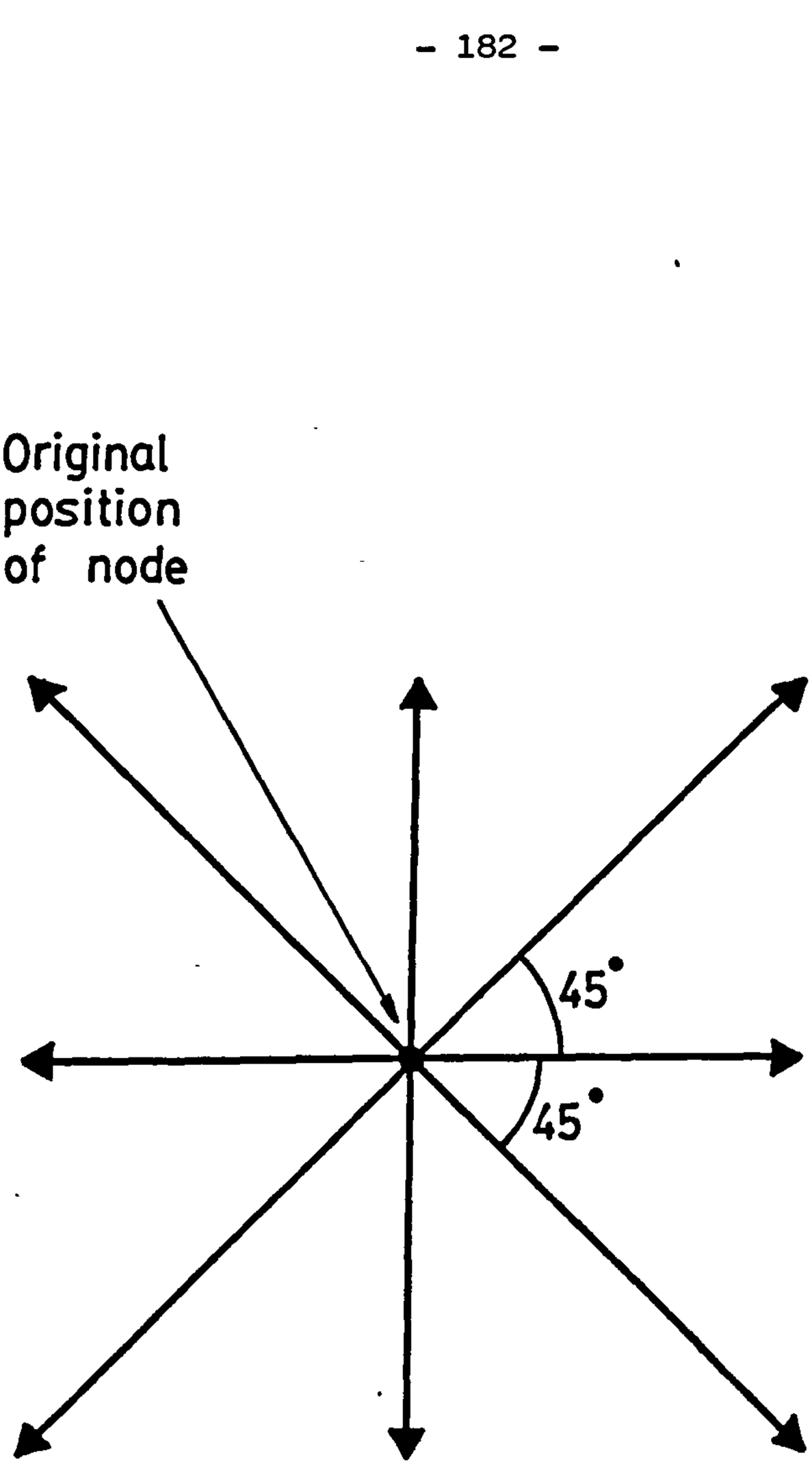

FIGURE 4.6.3 - NODE MOVING DIRECTIONS

The shortest distance to the edge of the block from the original node position is found, taking into account that moving one PIXEL diagonally is a greater absolute distance than moving one PIXEL horizontally or vertically.

The user may then make any modifications to this mesh by moving nodes or by inserting/deleting elements until a satisfactory mesh is produced. Usually there are very few modifications to be made by the user. Any sipes required can now be specified and these will be used in the generation of the boundary conditions, as already discussed. All that now remains is for the data file to be created which will be used (together with data on material properties, speeds, etc.) as input to the finite element programs. The mesh generation procedure described here can be used to generate meshes for either tyre tread blocks or tyre contact patches.

The mesh generation program does not specify the fluid film thickness, and if a number of different film thicknesses are required, such as when different depth grooves are present, these must be specified on the input to the finite element programs by treating the elements within the groove as a specific element type. The element types possible are shown below:-

0 - element not to be included in mesh.
1 - normal element on a block.
2 - 9 - element is in a groove.

During the mesh generation procedure and until section B4 / C4 in the finite element programs, the mesh is considered to be the whole of the rectangular grid based mesh, and any elements within the grid which are not required have their element type set to '0'. These elements are then removed in section B4 / C4 . Normal elements, whose film thickness will be specified by the base-line film thickness and deflections, have the type '1' and all 'included' elements have this type set by the mesh generation program. If an element is required to be in a groove or at a step depth, then its

type can be set to '2' - '9'. The step depth for the appropriate element type is set in the finite element programs (section B3 / C3) as well as the width of the groove. The groove width is used in the calculation of the groove flow factor which was developed in section 3.9. The use of the groove flow factor can be suppressed when, for example, a cut-out in a block is being modelled.

4.7 THE PLOTTING SYSTEM

Two special purpose plotting programs were developed to provide graphical output of the results from the finite element programs. This was found necessary because of the difficulty in interpreting the large amount of data produced in tabular form by the programs. In particular, it was difficult to picture the 3-dimensional shape of the contact patch (or tread block) surface when it had been deformed by fluid pressure.

Ideally, some form of graphical output directly from the finite element program was required, but this was not possible because of hardware limitations. Therefore, a plotting system was developed on a PDP11 computer, and a data file produced by the finite element programs (section B22 / C25) was made available for transmission to the PDP11 from the IBM. It was also found most convenient to divide the plotting function between two separate computer programs. This was partly due to the limited amount of memory available on the PDP11, and the large amount of data required to perform the plotting. One of the plotting programs produces output of the finite element mesh (with node and/or element numbers), the flow velocities at element centroids, and the volume flow velocities at element centroids. The other plotting program provides output of a 3-dimensional representation of the contact patch or block, showing either fluid pressure or film thickness. The source listings of these two programs are given in Appendix B.

CHAPTER 5 - EXPERIMENTAL DEVELOPMENT

5.1 INTRODUCTION TO EXPERIMENTAL DEVELOPMENT

There are two main testing facilities used at Fort Dunlop to evaluate the wet grip performance of tyres. These are a glass-plate, and an external drum machine. The results from the external drum machine could also be obtained from either an internal drum, or a flat belt machine, and the relative merits of these machines were discussed in section 1.2.1. Because of the very high cost, it was not possible to design and build a machine specifically for this project, and the available external drum machine was used for the test work. The main purpose of the test work was to indicate the level of success of the mathematical model, although the techniques developed can be used to increase the amount of information available from routine testing.

5.2 ROUTINE USE OF TESTING FACILITIES

The routine uses of the glass plate facility and the High Speed Cornering Force Machine are described in the following two sections.

5.2.1 Glass Plate Facility

The glass plate is situated on the proving ground at Fort Dunlop, Birmingham.

The glass plate itself is mounted level and flush with the road surface, and is approximately two metres in length and half a metre in width. Beneath the glass plate is a pit approximately half a metre in depth and when a photograph is to be taken the camera is placed on the base of the pit facing upwards at the glass plate. The photograph is taken by the vehicle breaking a light beam, which then triggers both the camera shutter and the high speed flash gun.

Glass plate photographs are usually used to assess performance in the wet, the glass plate being covered by a specified (usually 2mm) thickness of water before the vehicle starts its run. To make the water visible on the photographs fluorescein is added to it. Fluorescein is a very strong fluorescent indicator which shows up as green on the photographs. Figure 5.3.1 shows typical glass plate photographs and the penetration of water into the contact patch can be clearly seen as the green area. The dark areas within the tyre contact patch are what are normally considered as dry contact between the tyre and the glass plate. However, the current work tends to suggest that this is not in fact dry contact, but merely a film thickness of perhaps one order of magnitude less than the film thickness which shows up as green. The concentration of fluoresœin added to the water is uncontrolled; therefore no conclusions can be drawn from the differences in light intensity between different photographs.

The glass plate photographs are used purely to give a qualitative judgement of wet grip performance. An attempt to obtain more quantitative measurements will be discussed in section 5.3.

5.2.2 High Speed Cornering Force Machine

The cornering force machine is situated within the Indoor Tyre Testing Department at Fort Dunlop, Birmingham, and, as already mentioned is an external drum type machine. The overall layout of the machine is shown in figure 5.2.1.

Figures 5.2.2 (a) and (b) show general views of the machine and the control room.

As its name suggests one of the main uses of this machine is in the measurement of cornering force. This is the sideways force developed by a tyre when a slip angle is applied. The machine can also be used for the measurement of braking force, aligning torque etc.. These measurements can be carried out under any combination of slip angles, camber angles and loading conditions, and can be performed in the wet or in the dry. However, dry testing is

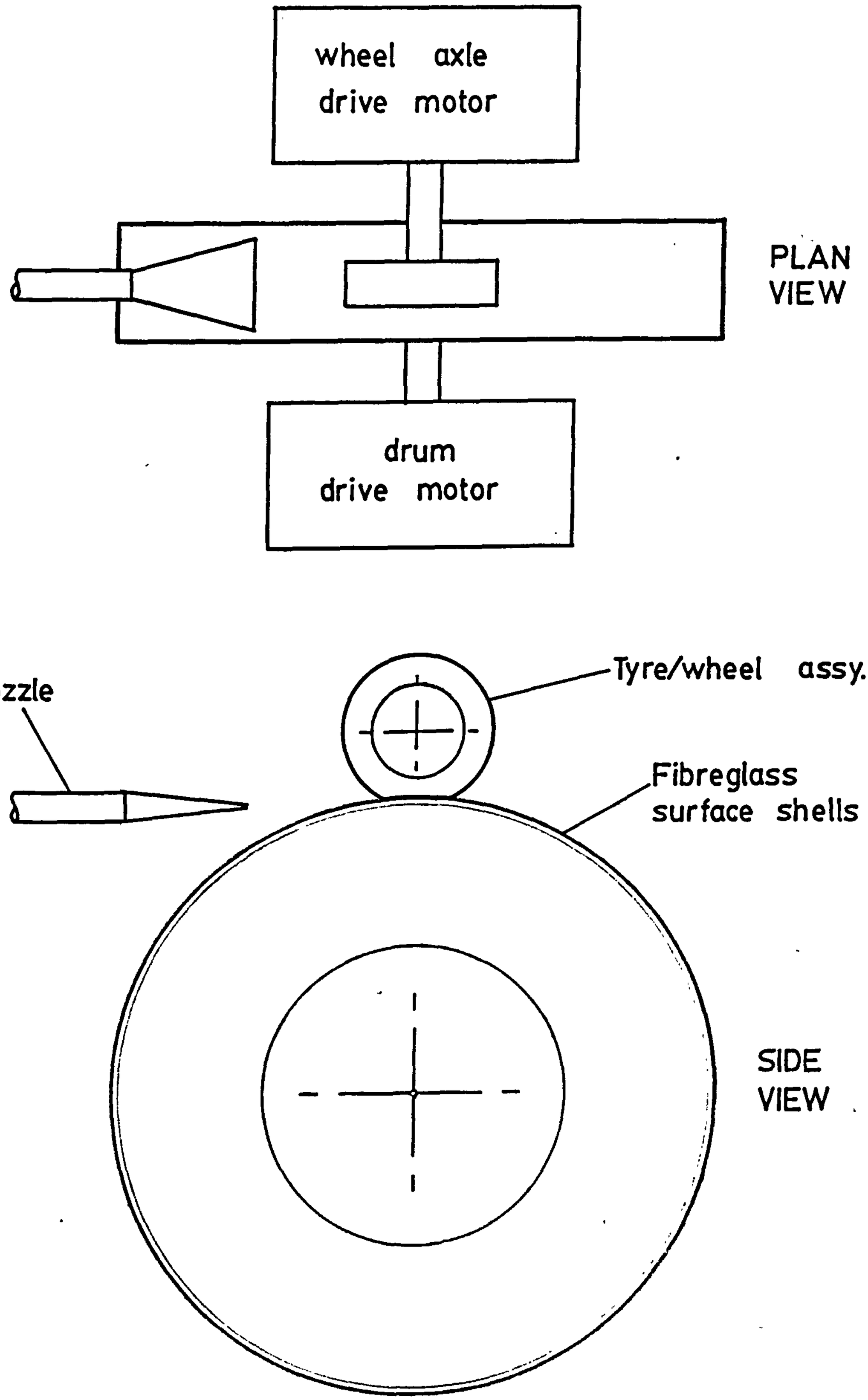

FIGURE 5.2.1 - CORNERING FORCE MACHINE

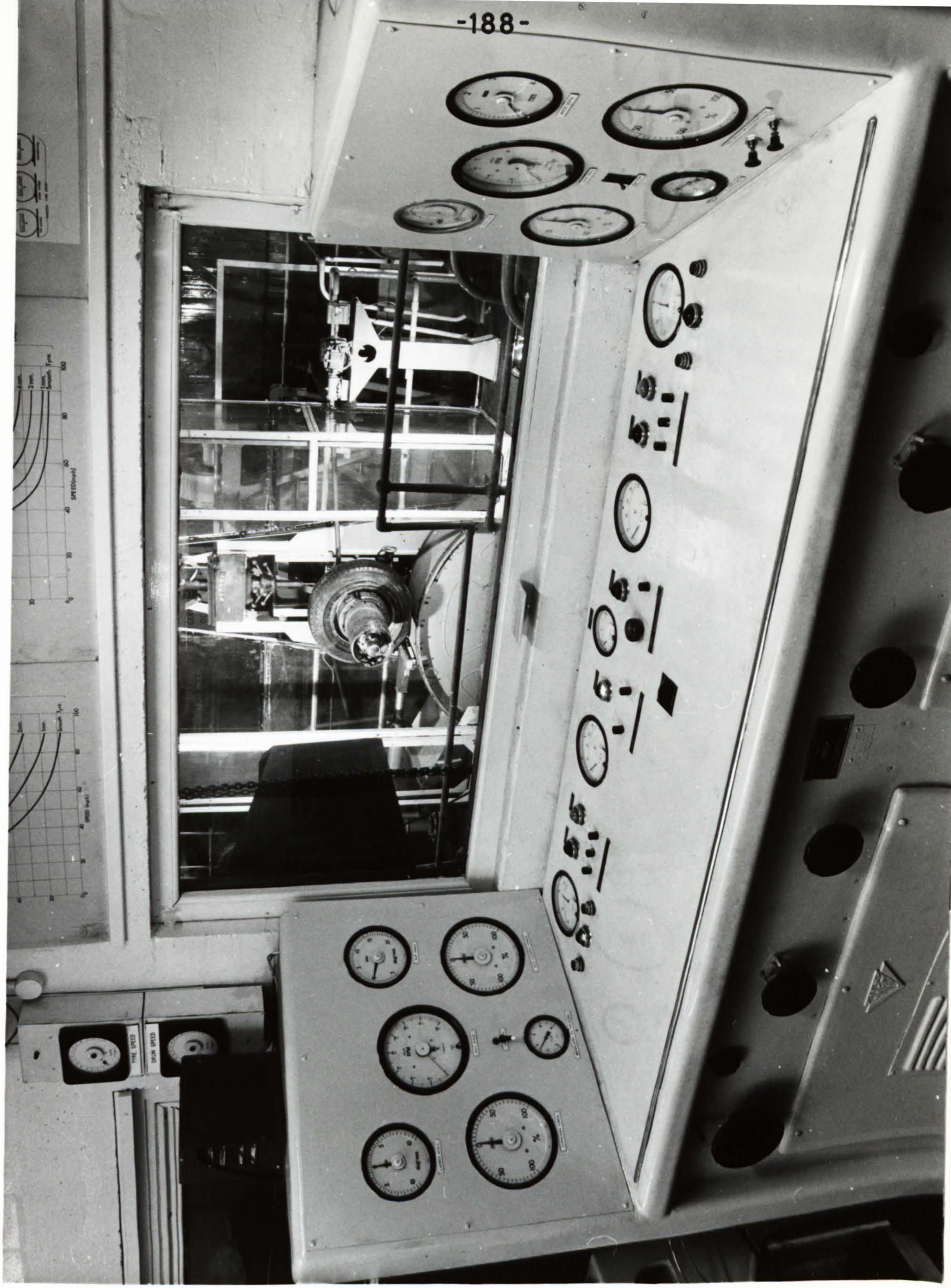

FIGURE 5.2.2a - CORNERING FORCE MACHINE

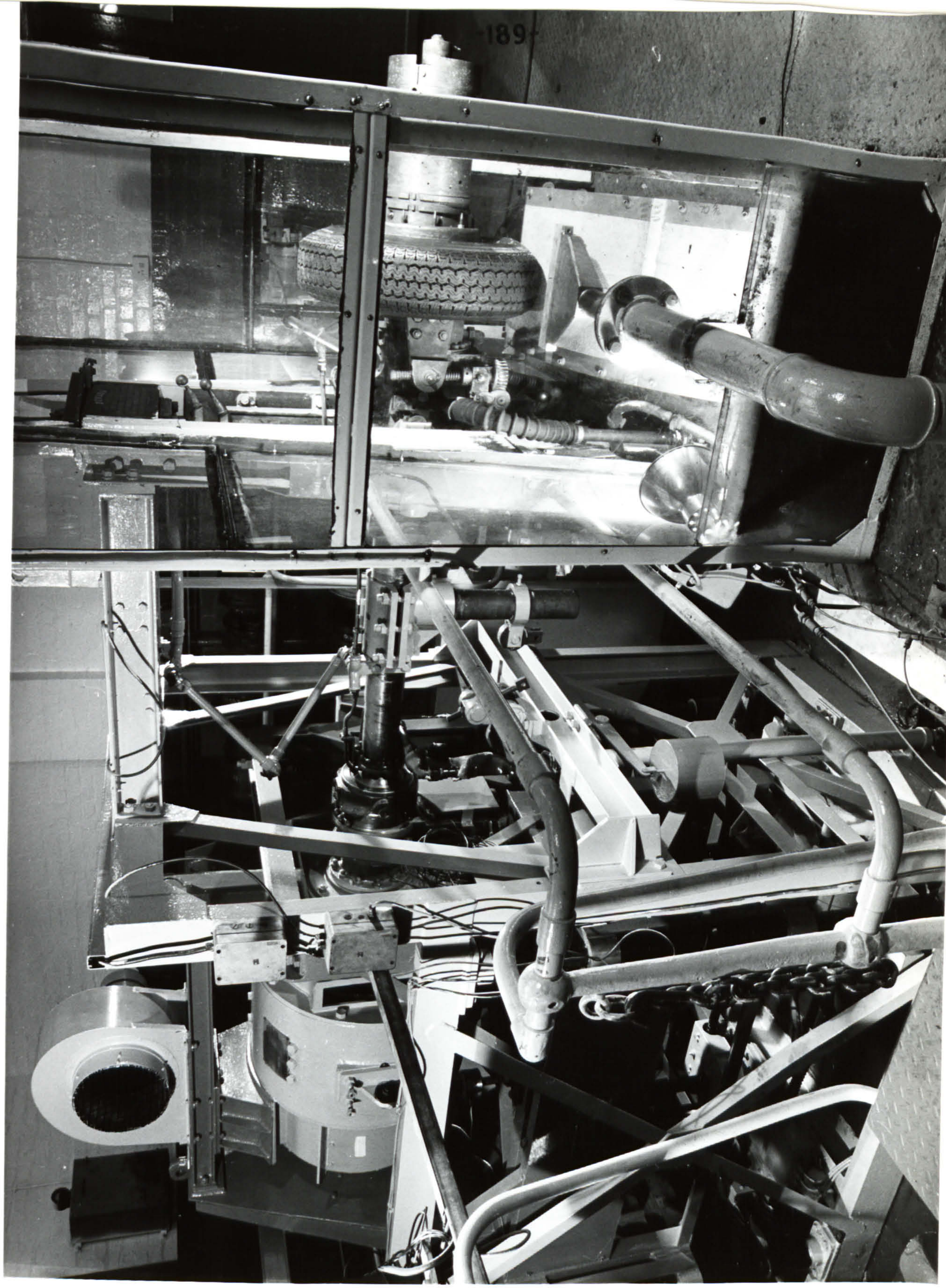

FIGURE 5.2.2b - CORNERING FORCE MACHINE

limited because the level of forces developed in the dry by modern tyres is greater than anticipated by the machines designers some twenty five years ago. The original design of this machine did not allow for the application of water for testing in the wet; this was added approximately twenty years ago, and is the only major change to the original machine. This machine is one of only a small number which allow the testing of full size tyres at high speeds under wet conditions.

There are available a number of fibreglass replica road surfaces which can be fitted to the machine's drum. Real road surfaces can not be used because of the effects of centrifugal force, as discussed in section 1.2.1. These fibreglass surfaces provide a realistic amount of macrotexture, giving the approximate drainage capacity of an actual road surface of that type. However, they do not provide any significant microtexture , and therefore the friction level attainable on these fibreglass surfaces is very much lower than that on a real road surface. It has been shown in the past that, whilst the correlation between the forces predicted on the cornering force machine and those measured on the road is poor, the actual ranking of tyres is broadly similar. As most tyre testing involves comparing the results of tests with the results on a control tyre, the overall values of forces etc. are less important than the correct ranking, and therefore the cornering force machine can be used to perform comparative tests. Because of the lack of microtexture on the fibreglass replica surfaces, there will be a tendency for a very thin film of water to exist between the tyre and the surface which would under normal circumstances be broken up by contact with the road surface asperities. A tyre tread pattern can be made to remove this very thin film by the use of sipes; therefore on the cornering force machine the effect of sipes will tend to be exaggerated and any comparison of highly siped with sparsely siped tyres should be treated with caution.

The application of water to the tyre/drum interface on an external drum machine poses a number of problems. Normally the road surface and the water on the road surface are stationary. In the case of the external drum machine the road surface (drum periphery) is

moving at the linear speed of that particular test condition, i.e. the speed that would normally be the vehicle road speed. The water should be stationary relative to the drum surface, so a jet of water has to be applied to the tyre/drum interface. As well as being at the correct speed this water jet must also be of the correct depth required for the test condition. The test methods normally used on the cornering force machine do not attempt to simulate realistic conditions for the application of water. Two types of water test conditions are used. If only a small amount of water is required, 'damp conditions', the water is applied to the drum via a spray bar with a number of small holes. If a greater amount of water is required it is applied through a nozzle of the type specified in reference (68). With this nozzle the water is directed, as a number of small jets, at the front of the tyre contact patch. These small jets are produced by a nozzle having 37 holes of two different diameters. Reference (68) sets out a complete standard for the testing of tyres using a trailer towed behind a vehicle, and the above described nozzle is the one specified for this testing. However no reasons for the specification of a nozzle of this type are given. This nozzle with an uncontrolled flow velocity and water depth was thought unsuitable for the current work, and the design of a new nozzle is described in section 5.4.6.

5.3 DEVELOPMENTS MADE TO GLASS PLATE PHOTOGRAPH TECHNIQUES

As was mentioned in the previous section, glass plate photographs are currently only used to provide a qualitative estimate of water penetration into the tyre contact patch. To obtain more information from these photographs, developments were made in two areas; improvements to the photographs themselves, and the development of an analysis technique using an image analyser. These areas will now be dealt with separately.

5.3.1 Improvements to Photographs

One of the main problems with the photographs is that a large amount of spurious light is included. The majority comes from the

flash which is used to take the photograph. This light is reflected from the underside of the glass plate directly into the camera lens. The required light is that which has been absorbed and then re-emitted by the fluorescein, where the amount re-emitted will depend on the quantity of fluorescein which in turn depends upon the thickness of the water film.

The quality of the glass plate photographs could therefore be improved by removing the effects of light reflected from the underside of the glass plate. To achieve this use was made of the fact that when un-polarized light is incident on the surface of any transparent material the reflected beam of light will be partially plane polarized (69).

A polarizing filter placed over the camera lens will therefore remove a large proportion of the reflected light from the photograph. Figure 5.3.1 shows a comparison between photographs taken with and without a polarizing filter. Because more of the light on the photograph taken with the polarizing filter is due to emission from the fluorescein, then more water penetration can be seen compared to the photograph taken without a polarizing filter.

5.3.2 Improvements to the Analysis Technique

In theory it would seem that it should be possible to obtain actual fluid film thicknesses from glass plate photographs. In practice it was found that problems in controlling the absolute value of light intensity, both when the photograph was taken and when it was viewed, meant that this was not possible. Glass plate photographs can however be used to obtain estimates of the fluid film thickness shape.

One problem with obtaining fluid film shapes in this way is that there is a distribution of light over the photograph which is not due to changes in the fluid film thickness, but is due to the distribution of light from the flash gun. The distribution of light due to the flash gun is of much greater magnitude than any

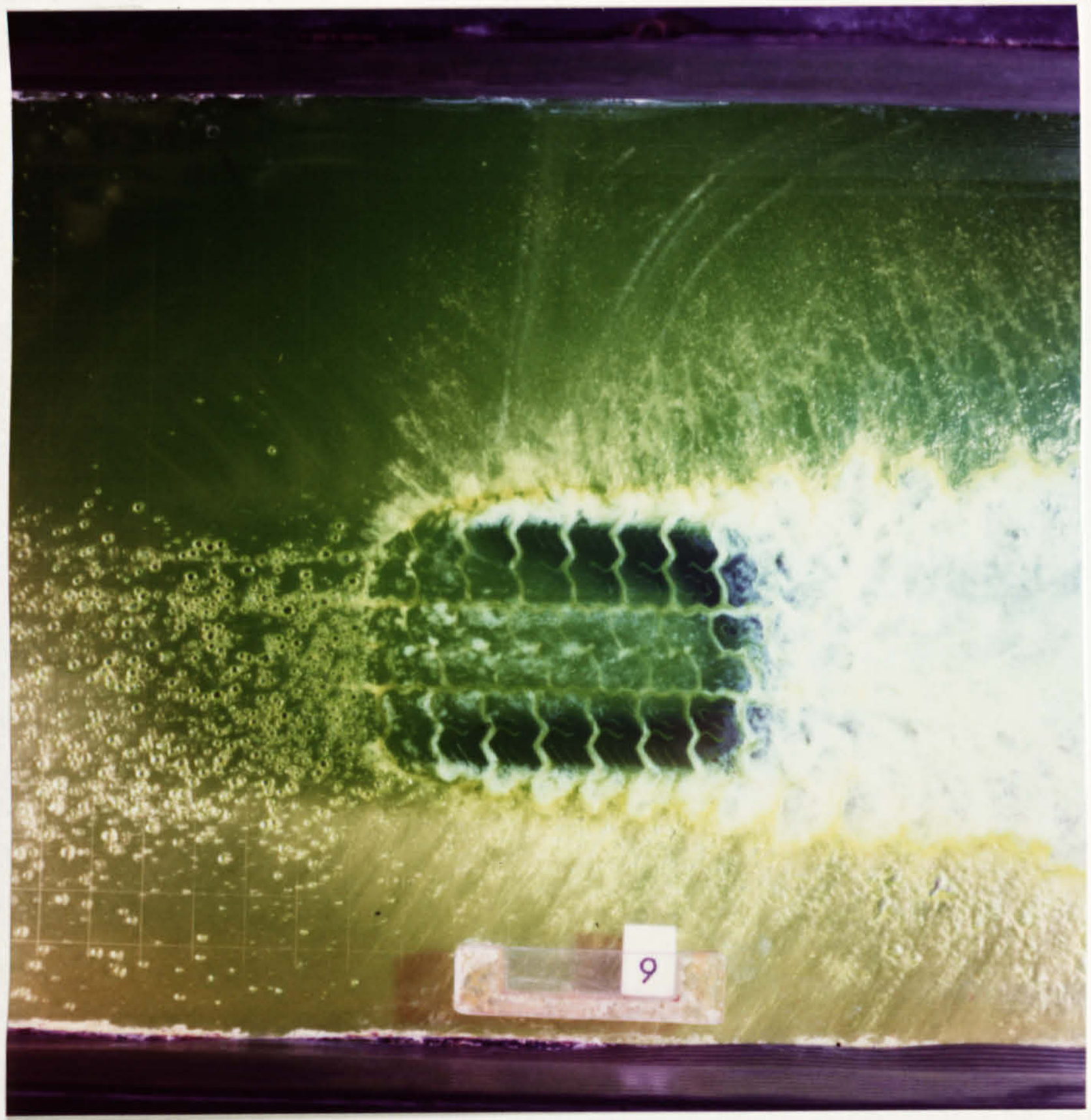

WITH FILTER

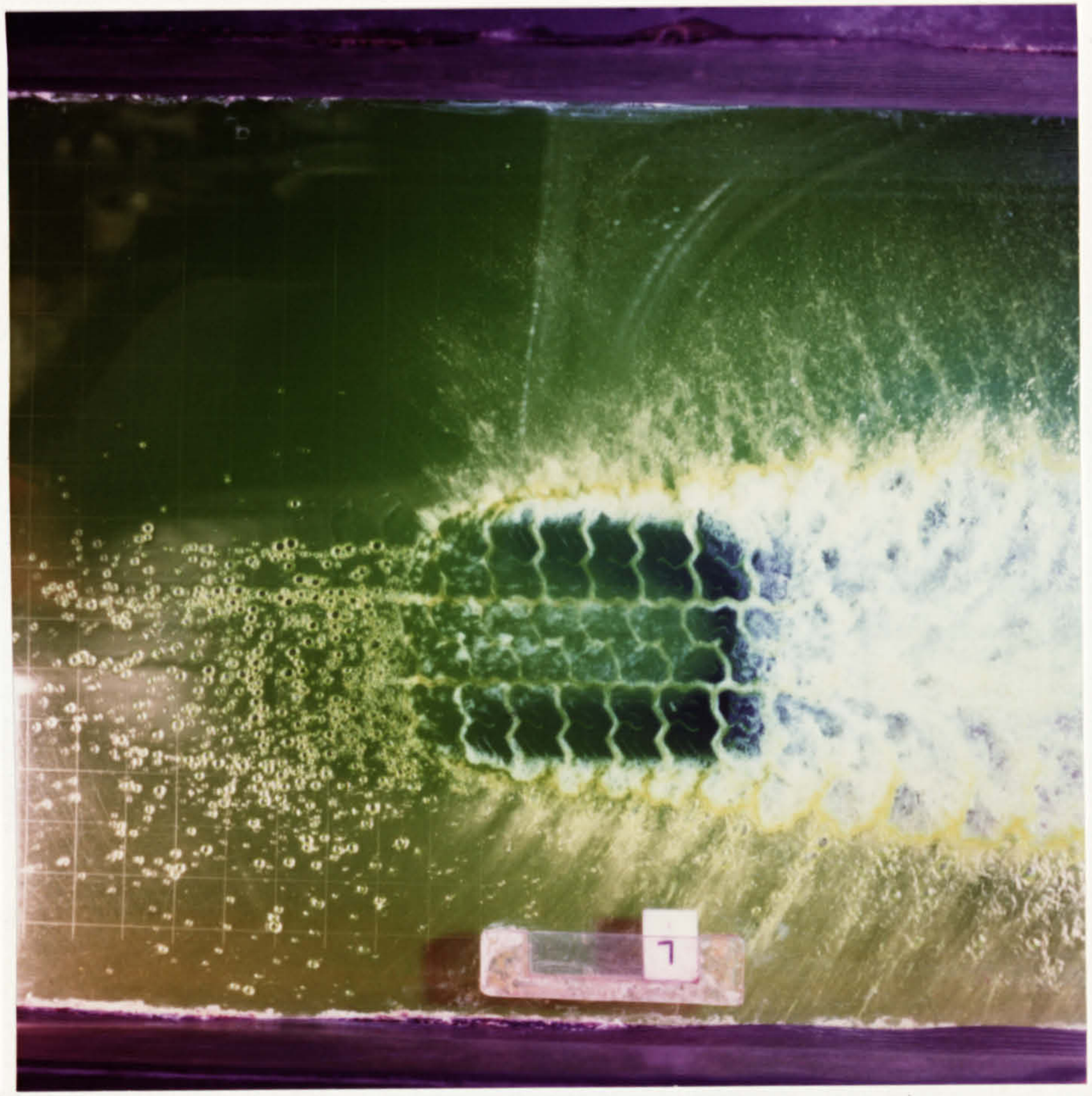

WITHOUT FILTER

FIGURE 5.3.1 - GLASS PLATE PHOTOGRAPHS

distribution of light due to variations in water film thickness; therefore it must be removed before glass plate photographs can be used to estimate fluid film thickness shape.

This was done by utilizing the fact that with a parallel film the changes in light intensity are due only to lighting distribution. Therefore, the difference in grey levels (intensity) between photographs of parallel and varying films will represent changes due only to the variation in fluid film thickness. This subtraction between images was performed using an image analyser.

When the above technique is applied to glass plate photographs of tyres under wet conditions, the static tyre photograph is used to obtain the lighting distribution due to the flash. To improve the visability of the variation in light distribution every 10 by 10 square of pixels was averaged, and the result of this averaging on a static photograph of a plain treaded tyre is shown in figure 5.3.2(a). The lighting distribution manifests itself as an apparent water penetration into the rear of the contact patch, but as the tyre is static it is known that there can be no actual water penetration. Figure 5.3.2(b) shows the same tyre but this time moving from left to right. It would appear that there is a large amount of water penetration into the rear of the contact patch, but with reference to figure 5.3.2(a) it is known that this is largely due to the light distribution from the flash gun. By subtracting one image from the other, thus obtaining the difference in grey levels and then performing the pixel averaging the effects of lighting distribution were removed. The resulting image is shown in figure 5.3.2(c), and shows a more realistic water penetration shape into the front of the contact patch. There also appears to be an area at the rear of the contact patch where the water film thickness is large. By examining results presented in chapter 6 it can be seen that this would appear to be correct.

Because of the difficulty in obtaining actual film thickness measurements from glass plate photographs, techniques on the high speed cornering force machine were developed (section 5.4.5). However the techniques developed here for use with glass plate

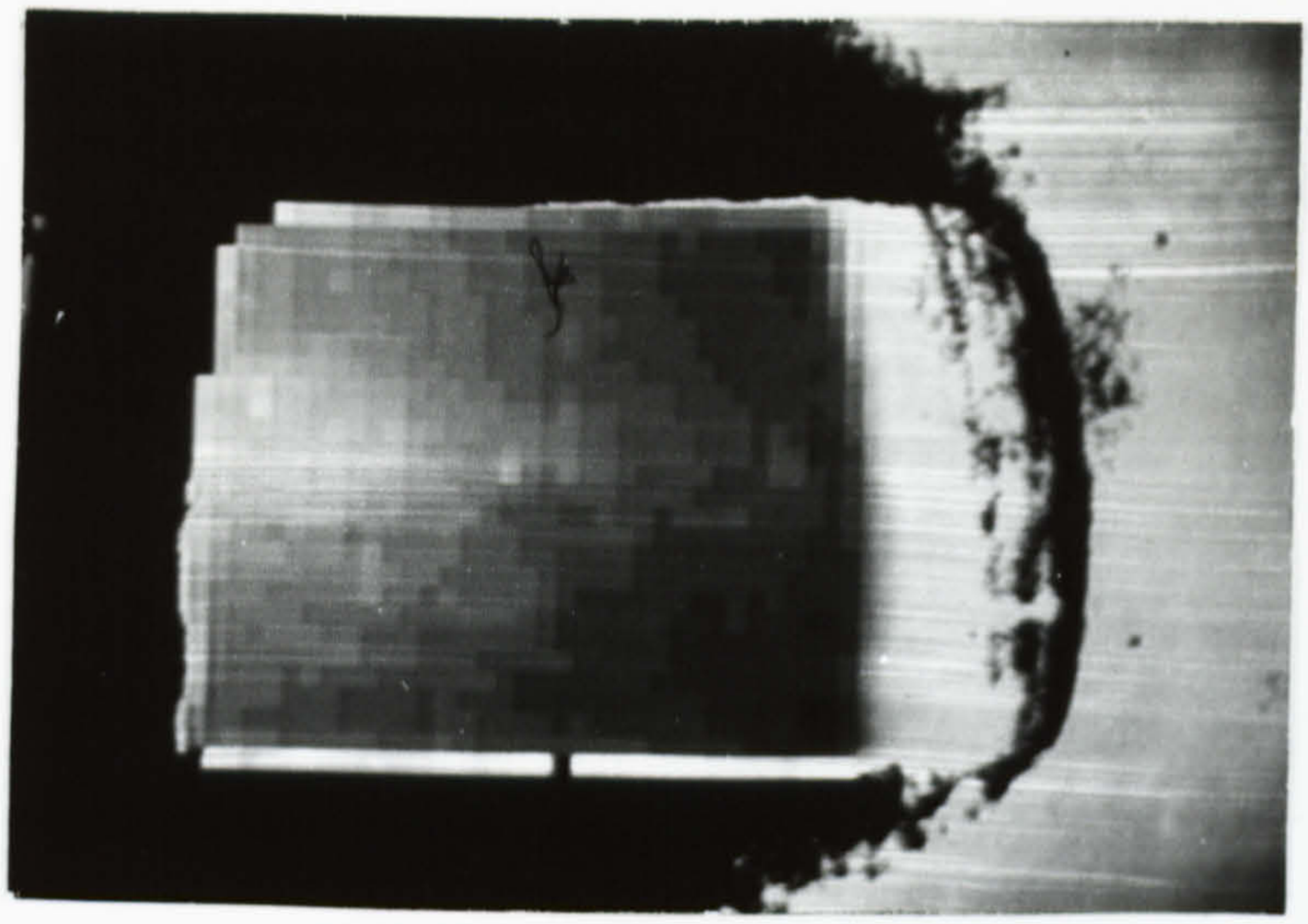

(a)
STATIONARY

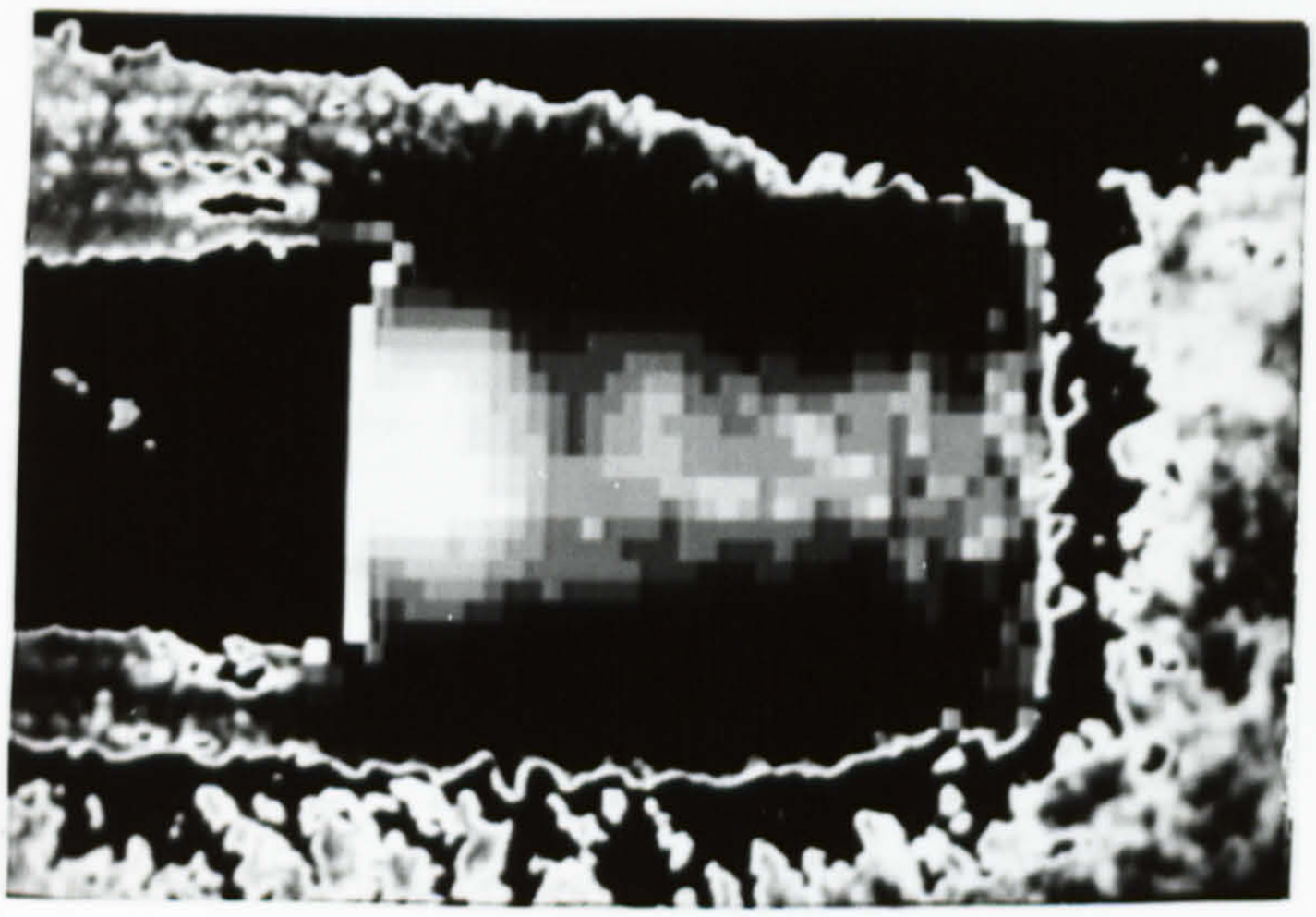

(b)
100 Kph

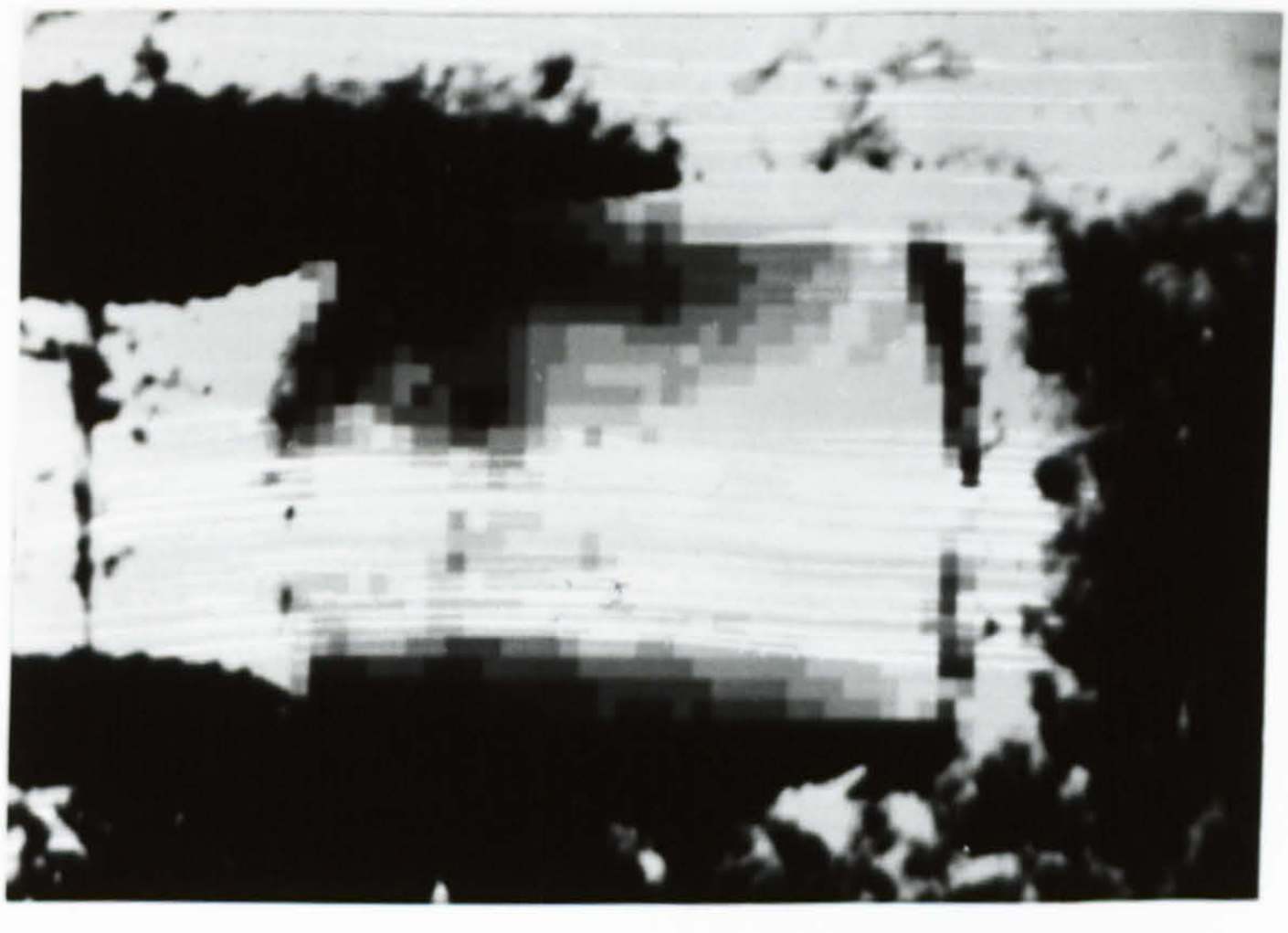

(c)
SUBTRACTION

FIGURE 5.3.2- IMAGE PROCESSED GLASS PLATE PHOTOGRAPHS

photographs, show a qualitative correlation with fluid film thickness shapes found by both the fibre optic probe and analytical methods, and as such show that the glass plate can reasonably be used in the evaluation of tyres for wet grip.

5.4 DEVELOPMENTS MADE TO TESTING ON THE HIGH SPEED CORNERING FORCE MACHINE

The object of developing new experimental techniques using the High Speed Cornering Force Machine was to allow the measurement of fluid pressure and film thickness distributions within the tyre contact patch. To achieve this a number of modifications and additions were made to the machine:

1. Smooth road surface
2. Pressure transducer
3. Radio telemetry
4. Data logging
5. Fluid film thickness probe
6. Nozzle.

The instrumentation to allow the measurement of fluid pressure was developed first. To allow the measurement of fluid film thickness the pressure transducer was replaced by the fluid film thickness probe and the rest of the instrumentation remained unchanged.

The instrumentation as developed here is suitable for measurements on any tyre tread pattern under locked wheel conditions. However when the tyre is rotating, measurements can only be made on tyres with plain tread patterns or circumferential grooves. This is because the rotational position of the tyre is not recorded. The addition of an encoder to the wheel axle would remove this restriction, and this is discussed in section 8.3.2. For the purpose of the work here it was required to obtain pressure and film thickness distributions for plain and simple patterned tyres, therefore the lack of an encoder on the wheel axle did not pose any limitations on the results presented in chapter 6.

5.4.1 Smooth Road Surface

As was discussed in section 5.2.2 there are a number of fibre glass replica road surfaces available to fit the cornering force machine drum. However, as the purpose of the current work is to study the effect of tyre tread patterns on fluid pressure and film thickness, a smooth road surface was required. A set of surface shells with a completely smooth surface was manufactured specifically for this project.

As well as providing the correct type of surface for the tyre to run on, the surface shells also have to provide the mounting for both the pressure and fluid depth transducers. This was achieved by moulding a threaded insert into each of the three sections of the surface shells. It was not possible to make any modifications to the actual machine drum, therefore all the instrumentation had to fit inside the thickness of the fibre glass surface shells (20 mm).

5.4.2 Pressure Transducer

The pressure transducer must measure the interfacial fluid pressure between the tyre tread and the drum surface, and must fit into the limited space available.

The size of the active area of the pressure transducer was very important as the requirement of this work was to gain details of the pressure distribution within the contact patch.

The frequency response of the pressure transducer had also to be considered carefully. When the tyre/wheel assembly is locked the pressure transducer (or film thickness transducer) is moving past the tyre tread surface at the full test speed, and must be able to respond to the sharp drop in pressure as a lateral groove is passed. A typical lateral groove would be 4 to 6 mm wide, and it was decided that the frequency response should be such that the output could respond to changes occurring within 1 to 2 mm movement

through the contact patch. If a maximum test speed of 100 Kph is assumed, then this requires a frequency response in the range 13.5 to 27 KHz.

The typical maximum fluid pressure expected from a car tyre is 0.69 N/mm^2 (100 psi), but after discussion with manufacturers of pressure transducers it was thought safe if a transducer with a rated maximum pressure of 500 psi was used. This was so that the transducer would be more physically robust against possible damage caused by the tyre passing over it. The disadvantage of this was that the accuracy of the pressure transducer would be reduced, and this is discussed in section 5.5.

A pressure transducer was obtained which met all the above criteria. The active pressure sensing area was 2.54 mm in diameter; which it was thought would give good discrimination for the measurement of pressure distributions. The frequency response was easily met as this transducer had a usable flat response to 40 KHz.

Because of the size limitation imposed by the requirement to fit the transducer into the fibre glass surface shells, a special version of the pressure transducer was supplied. This consisted of the measurement module normally fitted into a threaded type of transducer, and was 12.7 mm from the pressure sensing surface to its rear. The transducer was supplied by Kulite Sensors under their reference number XCQM-1-147-500, and was mounted by bonding into a threaded plug. This plug could then be inserted into the hole provided in the surface shells.

As the pressure transducer is effectively a full strain gauge bridge, a stabilized power supply is required. In this case this can be supplied directly from the radio telemetry transmitter.

5.4.3 Radio Telemetry

Because both the pressure and film thickness transducers are mounted on a rotating drum, the resulting electrical signal must be taken to a stationary point. The traditional method of achieving this is by the use of slip rings, and many excellent units such as those discussed in (70), are available. However, the use of a pre-packaged slip ring assembly was not possible in this case for a number of reasons. It is most convenient when using slip rings if the slip ring assembly can be mounted on the end of a shaft. Whilst there is a shaft end available on the High Speed Cornering Force Machine, any connections between the drum and the shaft end would have to pass through one of the drum support bearings. This would have necessitated drilling the main drum support shaft which was not possible. Also, the drum support bearings are mounted close (approximately 50 mm) to the drum which gives little room for a slip ring assembly to be mounted around the shaft, between the bearing and drum.

The use of slip rings was therefore not possible in this case and an alternative method of transferring the electrical signal from the rotating drum to a stationary point had to be found.

The use of a radio telemetry system is the main alternative to slip rings, and uses either capacitive or inductive coupling. This transfers the required signal, which has been used to modulate a carrier, across a small air gap between an aerial fixed to the rotating drum and a stationary receiver.

The specification of the radio telemetry system was based on fluid pressure measurement. For convenience, when the fluid film thickness measurement system was designed it was made to produce an output which looked to the transmitter like the pressure transducer output. This meant that no modifications needed to be made to the transmitter. Details of the fluid film thickness measurement system are given in section 5.4.5.

Remembering the system frequency response requirement (section 5.4.2) of 27 KHz, it was found that 'Astech Electronics' could supply a special version of their transmitter which would have a bandwidth of 70 KHz. This system was obtained and may be considered as two main units:

i) The transmitter, with associated components and transmitting aerial.

ii) The pickup aerial unit and receiver (indicator) unit.

A schematic of the radio telemetry system is shown in figure 5.4.1.

The mode of operation of the radio telemetry system is as follows. As the pressure transducer is behaving (as far as the transmitter is concerned) as a full strain gauge bridge, its output is a voltage of the order of a few millivolts. The pressure transducer excitation voltage is supplied directly from the transmitter.

The output voltage of the transducer controls the frequency of a square wave oscillator, whose output is applied to the transmitting aerial mounted on the rotating drum. As the aerial is driven by the oscillator an electric field is generated around it. A receiving aerial is placed in the vicinity of this (alternating) electric field and will experience small voltage changes with respect to earth, since it becomes the second 'plate' of what is in effect a very low value capacitor.

The pickup unit amplifies this small voltage and feeds it to the indicator unit via co-axial cable. The indicator unit then converts this signal, which is in the form of a frequency, back to a voltage which is directly proportional to the output voltage from the transducer. As the signal is passed from the moving drum to the stationary pickup in the form of a frequency modulated signal then any variation in the signal strength will not effect the output. This means that variations in the distance between the moving transmitting aerial and the pickup aerial will not cause errors. Also variations in signal strength due to battery voltage

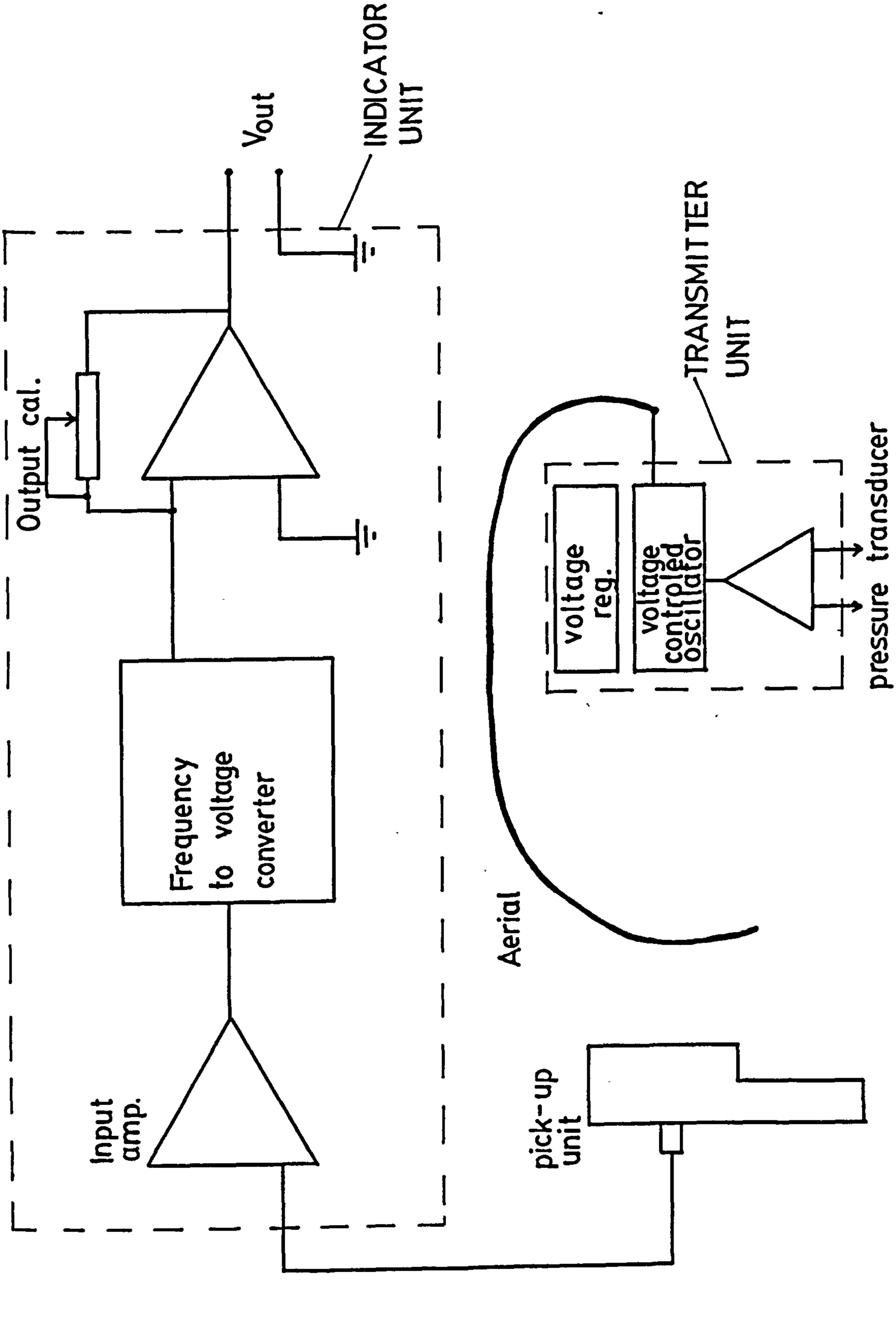

FIGURE 5.4.1 - SCHEMATIC OF THE RADIO TELEMETRY SYSTEM

fluctuations (strain gauge bridge supply is stabilized) will not affect the output.

The transmitter has facilities for changing the input sensitivity and this was set so that full scale output was obtained at a pressure of 0.69 N/mm^2 (100 psi). The indicator unit has a zero offset and gain adjustment facility for the analogue voltage output, and this was set so that 0.69 N/mm^2 was represented by an output voltage of 4 volts. The output from the indicator unit was fed to a data tape recorder for later analysis.

As the tests to be performed were concerned with the measurement of dynamic values of pressure and fluid film thickness, the radio telemetry system was bench tested on its ability to handle high frequency signals. It was found that the manufacturer's estimated bandwidth of 70 KHz was reasonable, and that the radio telemetry system would easily be able to cope with the required frequency response.

A number of problems with the mounting of the transmitter and its associated battery pack on the drum had to be overcome. It was not possible to make any modifications to the drum itself, therefore the transmitter and battery pack could not be mounted directly. Special mountings were designed which allowed the transmitter and battery pack to be fixed to the drum using the existing bolts which attach the fibre glass surface shells.

The other major problem associated with the mounting of the radio telemetry system was the ingress of water into the telemetry electronics. A large amount of water (see section 5.4.6) is applied to the drum surface at high velocity which makes the protection of the transmitter and batteries very difficult.

The prevention of water ingress was achieved by mounting the transmitter and batteries (and the electronics associated with the film thickness probe), in water-proof enclosures, and using water proof connectors for all electrical interconnections between the different units.

5.4.4 Data Logging and Analysis

The voltage signal representing either fluid pressure or film thickness from the radio telemetry system was recorded on magnetic tape. The tape recorder used was a Racal Store 7 model, which provides seven data channels plus one voice channel. One channel was used to record the signal from the radio telemetry and a second channel to record a synchronizing pulse. This synchronizing pulse was obtained by using a reflective switch, and reflective tape on the cornering force machine drum. One pulse was obtained for each revolution of the drum. The position of the pulse was set so that it occurred just before the transducer in use entered the front of the tyre contact patch.

The bandwidth of the tape recorder is determined by the tape speed, and 15 ips (inches per second) was used, which gave a bandwidth of 10 KHz on the wideband setting. As the tyres tested here(with one exception) did not have lateral grooves, it was not necessary to use a bandwidth of the maximum value (27 KHz). The one test case that did have lateral grooves was a tyre with a tread pattern made up of blocks 25 mm square, which was tested under locked wheel conditions. However, the test speed was only 50 Kph, therefore the tape bandwidth met the criteria, set out in section 5.4.2, for the measurement of changes in 1 to 2 mm movement through the contact patch. The bandwidth of the tape recorder can be improved simply by increasing the tape speed, and if tyres with lateral grooves are to be tested at high speeds, then there is no alternative but to do this.

Initial proposals for the experimental work on the cornering force machine were to use a computer with a high speed Analogue to Digital Convertor, which would directly sample the pressure or film thickness signal and store it in computer memory for immediate analysis. This would overcome any problem of tape recorder bandwidth and make the results available immediately; however, there was not time for this to be achieved within the scope of this project. The subject of data capture by computer is discussed in section 8.3.2.

Once the test data had been stored on magnetic tape they were analysed using a Nicolet 660A spectral analyser. Use of the Nicolet allowed the individual test samples, taken for each pass of the transducer through the contact patch, to be averaged. For each test condition, of tyre type, test speed, and lateral position, a number (say 50) samples were recorded by allowing the tape recorder to record the output from the transducer continuously over a period of time. This was then played back into the Nicolet and by using the synchronizing pulse to trigger each sample, the Nicolet could be made to average automatically all the samples. The results presented in chapter 6 are as a result of this averaging process.

When the signal being analysed is a pressure signal there is very little difference between successive samples. Figure 5.4.2(a) shows a number of individual pressure samples for one test condition, and figure 5.4.2(b) shows the averaged value obtained from the values in figure 5.4.2(a) and others. It can be seen that the pressure measurements obtained are extremely repeatable between successive samples.

The fluid film thickness measurement system (see section 5.4.5) utilizes the reflectivity of the tyre tread surface. As this may vary around the tyre circumference, owing to variations in surface finish, it is necessary to average a number of samples taken at different positions on the tyre. The calibration of the film thickness measurement system was also performed at a number of positions around the tyre circumference, and is discussed in section 5.6. When the test being performed is with the wheel rolling, then each time the transducer passes through the tyre contact patch it will be at a different point on the tyre circumference, and therefore the correct samples for averaging the effects of reflectivity will automatically be obtained. When the test being performed is with the wheel locked, then the same point on the tyre circumference will be met at each subsequent sample. Therefore, on locked wheel tests a small number of samples were taken with the wheel in one position, and then the wheel rotated and another set of samples taken at a second wheel position. This procedure was repeated a number of times until samples at

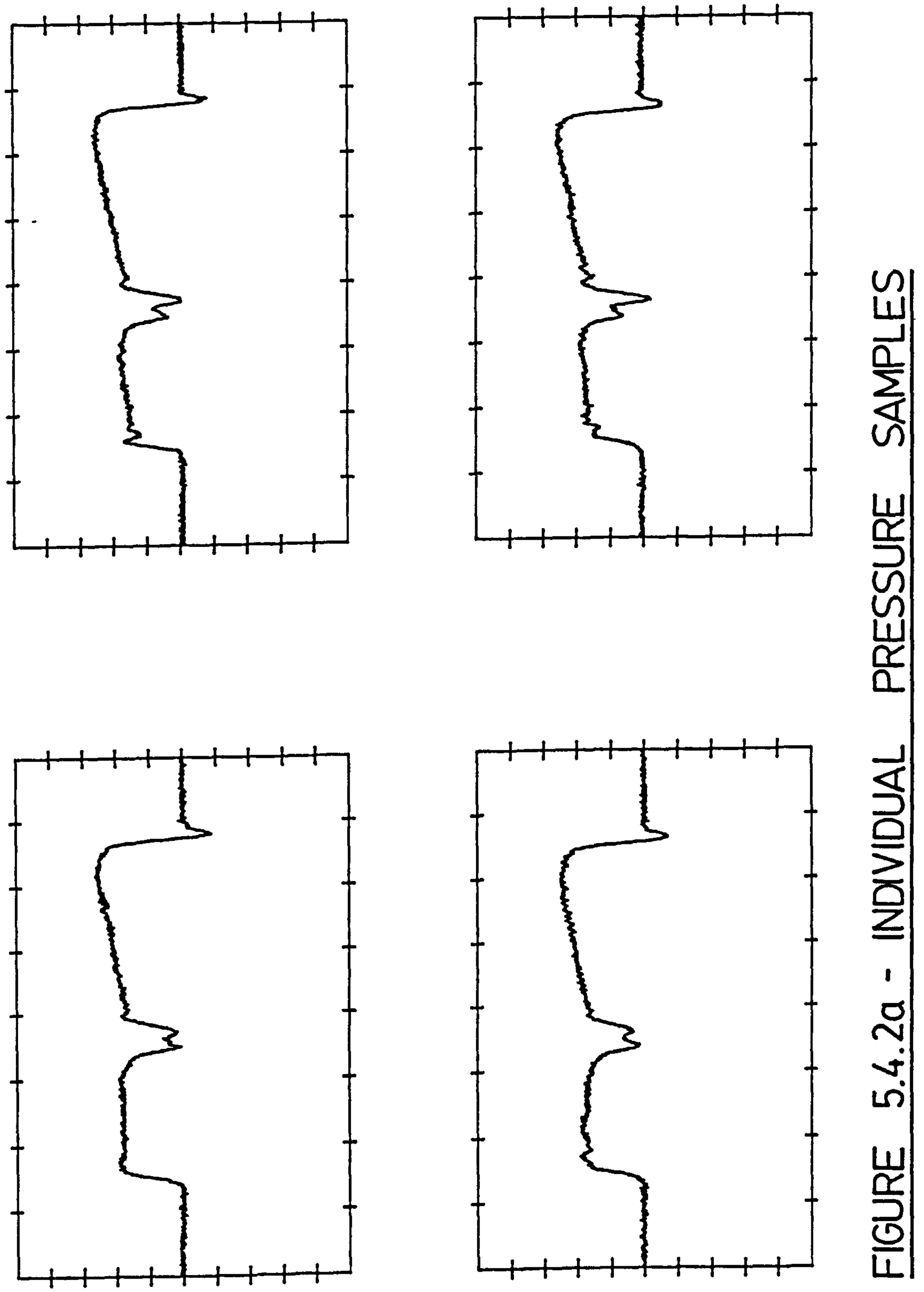

FIGURE 5.4.2a - INDIVIDUAL PRESSURE SAMPLES

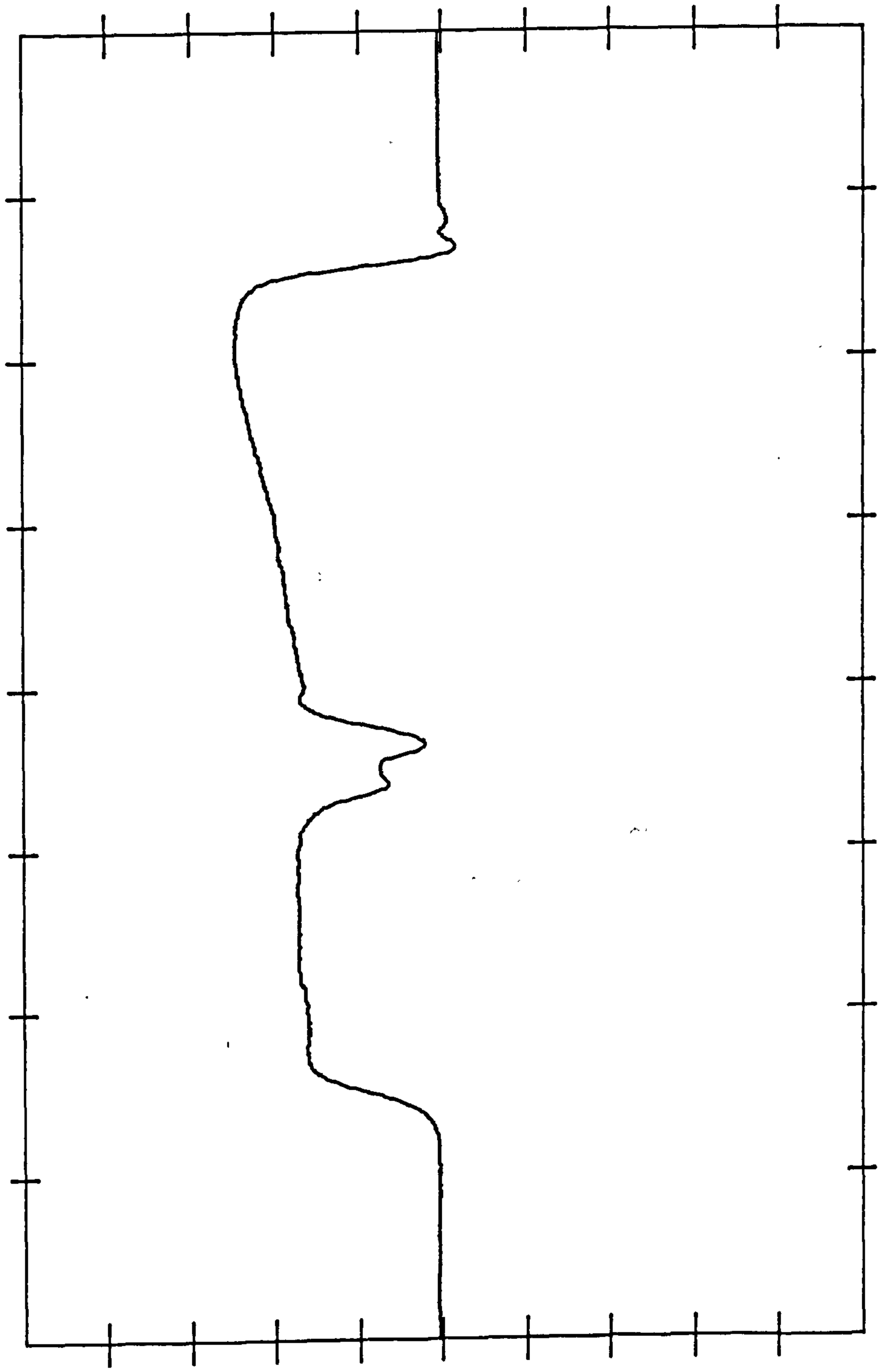

FIGURE 5.4.2b - AVERAGE OF A NUMBER OF PRESSURE SAMPLES

sufficient positions to average the effects of reflectivity, had been made.

In the case of fluid pressure measurements the voltage which is recorded on magnetic tape is directly proportional to the fluid pressure in the tyre/surface interface. The voltage which is recorded when fluid film thickness measurements are being made, however is not directly proportional to the fluid film thickness (see section 5.6). The output plot from the Nicolet (after averaging) is one of transducer output voltage. This plot is then digitized and the voltage converted to a depth value by use of an equation derived from the calibration procedure described in section 5.6. The resulting data can then be replotted as a fluid depth plot.

The data logging and analysis system is therefore able to handle information gained both from the pressure transducer discussed in section 5.4.2, and from the fluid film thickness transducer to be described in section 5.4.5.

5.4.5 Fluid Film Thickness Transducer

One method of fluid film thickness measurement has already been discussed (see section 5.3), whereby the glass plate facility was utilized. As this method was unable to provide actual film thickness values, a further method was developed on the cornering force machine.

There are various physical phenomena which could be utilized to provide a measurement of the thickness of the fluid film existing between a tyre and the surface of the drum. These include capacitance, inductance, mechanical, and optical methods. Of these the first was used by Benson et at (14) in their tyre tread deflection measurement system.

Their system basically consisted of a specially modified tyre which had a number of capacitor plates mounted on its inside surface, with a second plate for the capacitors mounted on the wheel rim. The separation between these plates can be measured indirectly as a function of their capacitance. The fluid film thickness itself is not measured directly, but is obtained from simultaneous measurement of tread deflection and the wheel rim vertical displacement. This highlights one of the serious faults in this technique, in that a fluid film thickness of perhaps 0.1 mm or less is being derived from measurements of the axle height and tread deflection, the combined errors of which could be of the same order of magnitude as the fluid film thickness which is being measured.

It would also be very difficult to use a method, such as that used by Benson et al, on a rolling tyre. The ultimate objective (outside the scope of this thesis) of this development of testing facilities on the High Speed Cornering Force Machine, is that routine measurements of fluid pressure and film thickness can be made on standard production tyres. Therefore certain features, such as bandwidth and the ability to test rotating tyres, were specified with this ultimate objective in mind.

If an inductive method were to be utilized in the measurement of fluid film thickness, then similar problems to those encountered in a capacitive method would be found. A mechanical system where a probe would be mounted in the drum surface would not be able to provide the frequency response required. There would also be problems with the discontinuity in film thickness at grooves, and the probe itself would disturb the fluid film.

The major alternative to the above methods of film thickness measurement was to use an optical device. Because of the limited space available at the position where the measurement was to be made, it would have been difficult to position an actual film thickness measuring device in situ. The method chosen was to use fibre optics so that the transducer could be positioned remotely from the point of measurement.

A fibre optic element is a flexible glass (or plastic)rod capable of transmitting light along its length by maintaining near total internal reflection of the input light source. In practice a large number of fibres are used together to form a bundle. The fibre optic probe which was utilized in the film thickness measurement system developed here, was of the bifurcated type (figure 5.4.3).

In this type of unit one group of fibres is used to transmit light from a stable source, onto the target surface. The second group of fibres receives light which has been reflected from the target, and converts it via a photosensitive detector into an electrical signal which is proportional to the intensity of reflected light.

The actual response of the intensity of reflected light to changes in the distance to the target surface, can be explained with reference to the action of an adjacent pair of fibre optic light transmitters and receivers, as shown in figure 5.4.4.

As the surface moves away from the fibres, the area A which is illuminated by the transmitting optical fibre will become larger. The lighted area in the interface B_1, which is giving light to the surface of the receiving element as B_2 will also grow larger. There is a rapid growth in the signal output as more of the surface C is illuminated. This section of the output/displacement curve is usually referred to as the frontslope region. The point when all the area C is just illuminated is referred to as the optical peak and is the point of maximum output. As the surface moves further away the size of the area B_2 will become larger than area C, and therefore the intensity of the detected light will fall. This is usually referred to as the backslope region. The full curve showing output against displacement for a bifurcated type probe is shown in figure 5.4.5, from reference (71).

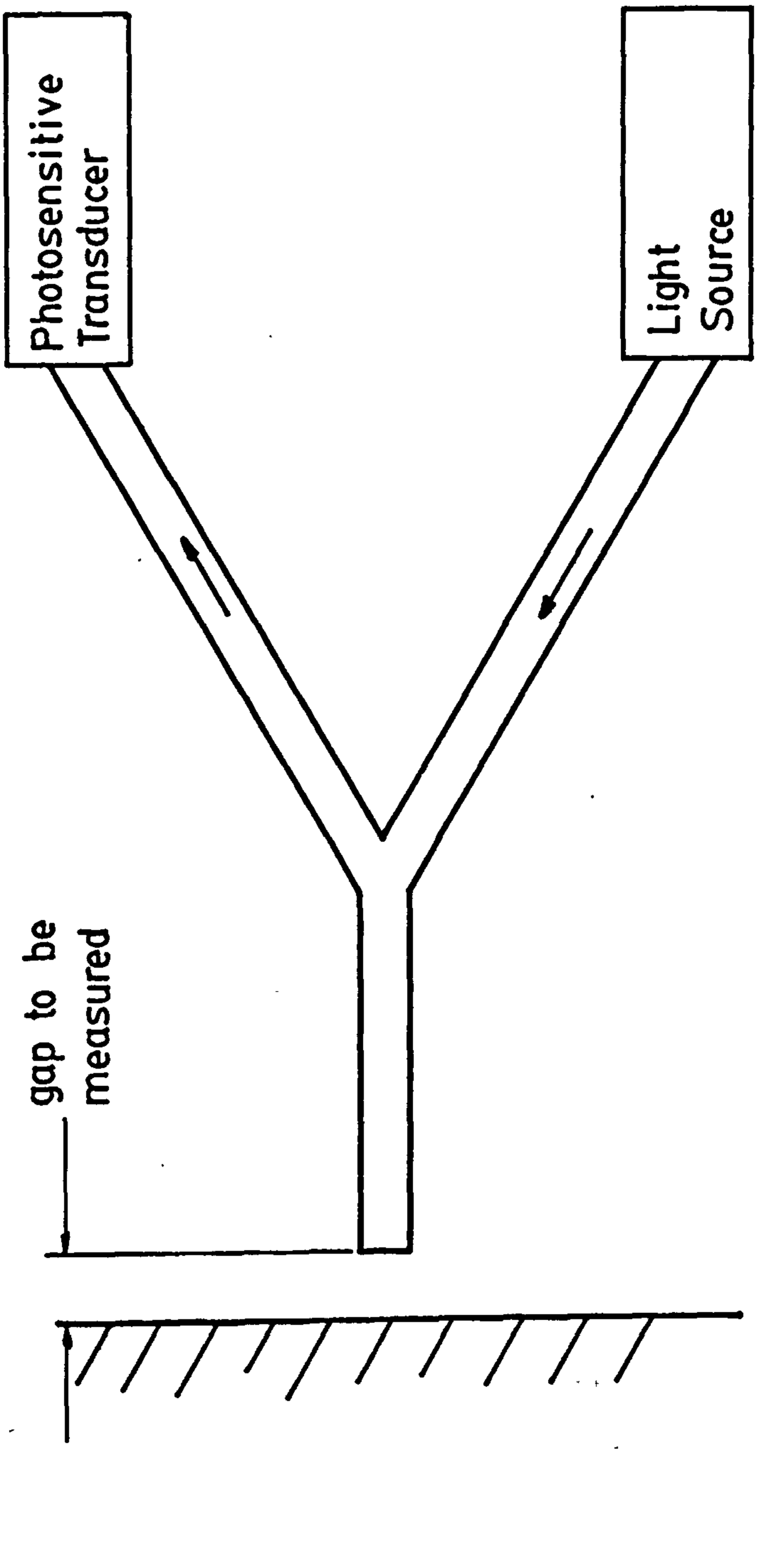

FIGURE 5.4.3- BIFURCATED FIBRE OPTIC PROBE

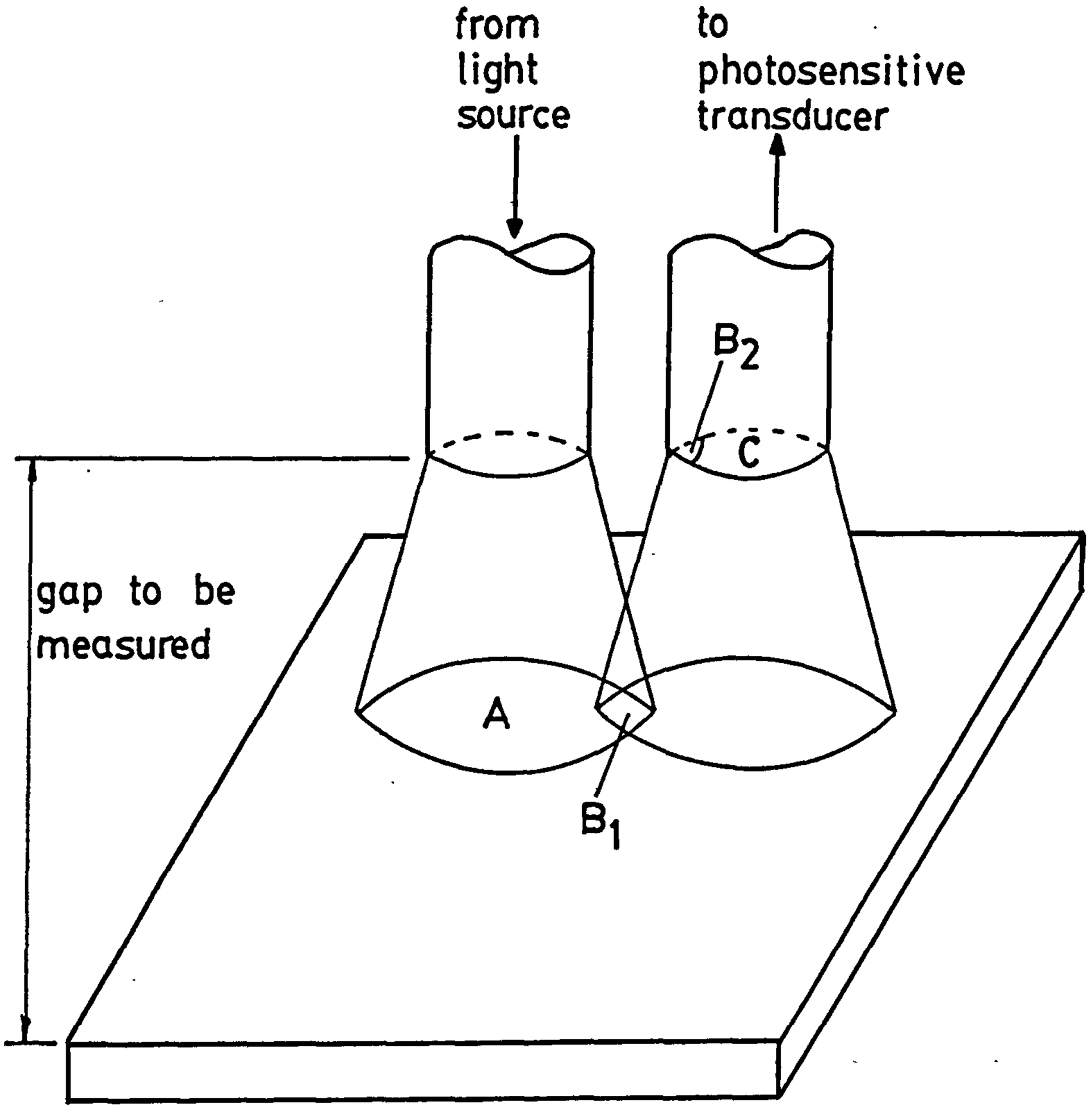

FIGURE 5.4.4 - PRINCIPLE OF OPERATION OF FIBRE OPTIC PROBE

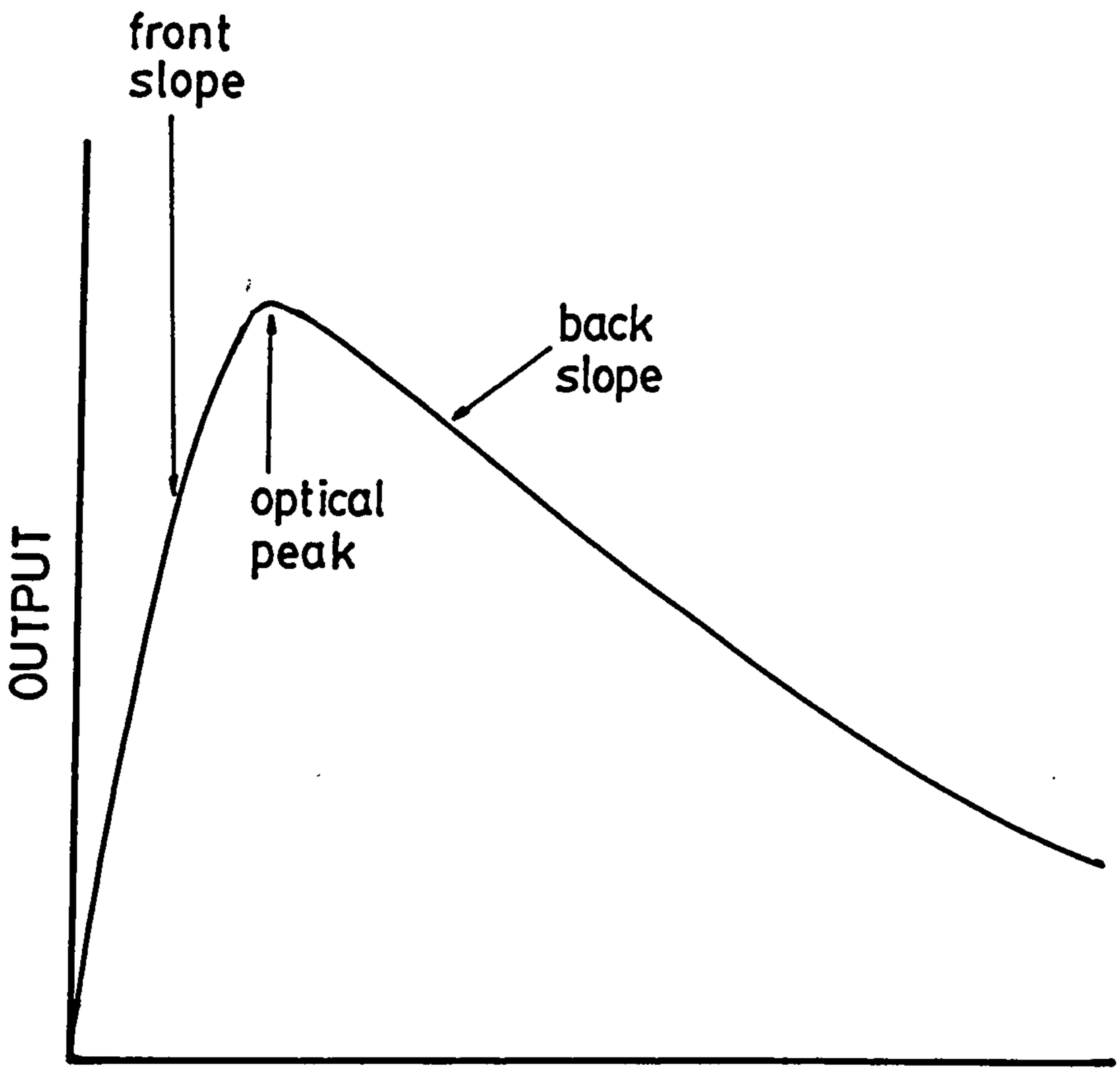

FIGURE 5.4.5 - TYPICAL OUTPUT/ DISPLACEMENT RESPONSE FOR A FIBRE OPTIC PROBE

The sensitivity of the output, and the position of the optical peak are determined primarily by the distribution of fibres at the common end of the probe. The size and number of fibres used will also have some effect on sensitivity. Changing the distribution of transmit and receive fibres from hemispherical (figure 5.4.6) to random will cause a reduction in the stand-off distance of the optical peak by a factor of approximately 8 (reference (71)). Because of the position of the optical peak, a probe with a random distribution of fibres will only have a limited measuring range, and for this reason a probe with a hemispherical distribution was chosen. It was found, after water film thickness measurements had been made, that under some circumstances the response of a random distribution probe would be more appropriate, and this is further discussed in chapters 6 and 8.

The actual probe used was manufactured by Dolen Jenner and included a right angle bend at the common end as shown in figure 5.4.7. This right angle bend allowed the whole of the probe to be contained within the fibre glass road surface shells.

As the probe would be viewing the tyre surface through a film of water, an infrared light source was used so that the variation in light level received would be further enhanced by the fact that some of the infrared light would be absorbed by the water, the level of absorption depending on the thickness of the water. An infrared phototransistor was used as the sensing element on the end of the receive fibres. The output from this was then amplified to give a strain gauge level output over the required measuring range, which allowed direct interchangeability between depth and pressure measurement without modifications to the sensitivity of the telemetry transmitter. The infrared source and sensor were mounted in a water-proof enclosure, along with a stabilizer for the source power supply and the amplifier for the output signal.

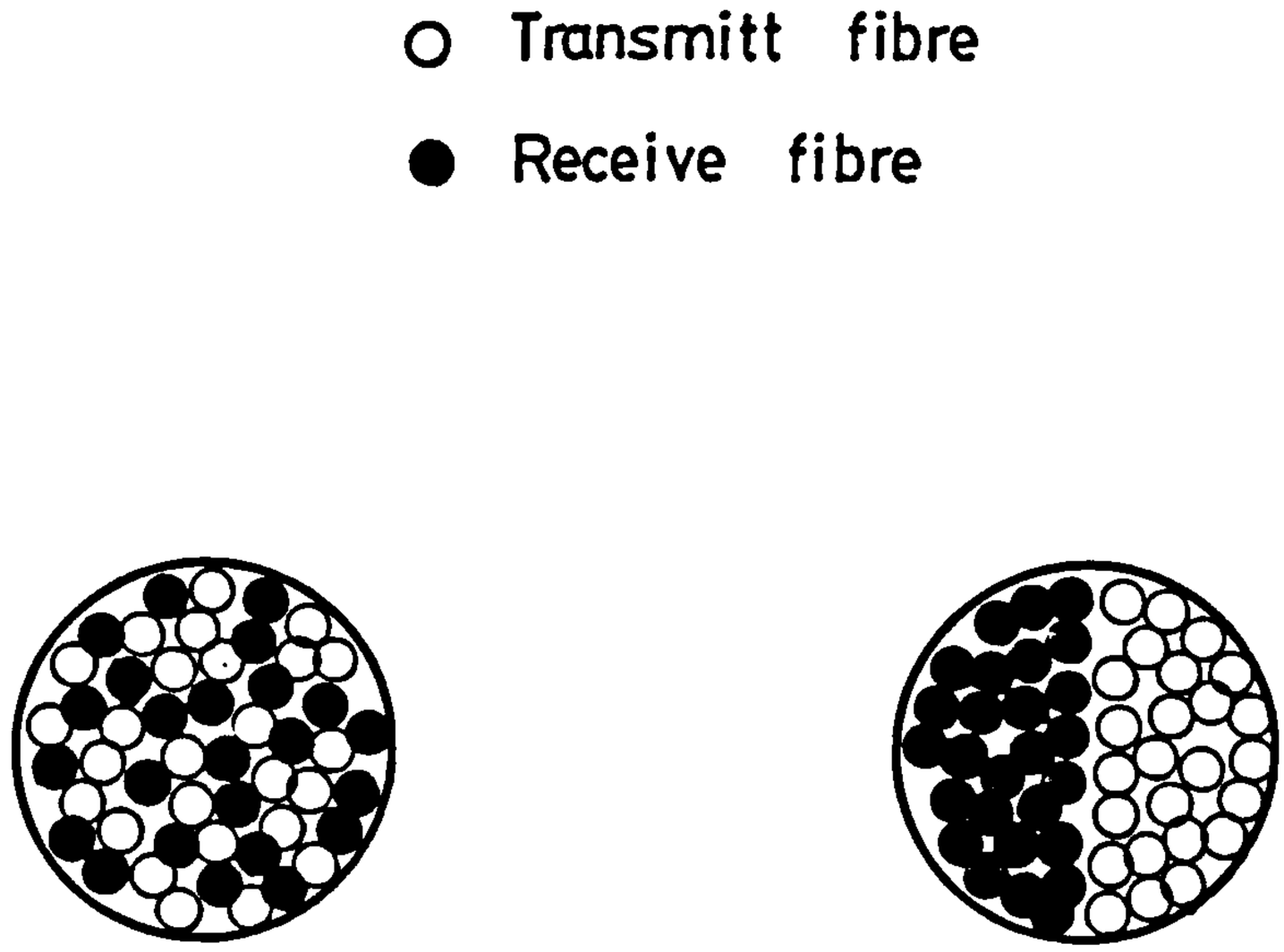

FIGURE 5.4.6 - DISTRIBUTION OF FIBRES AT THE COMMON END OF PROBE

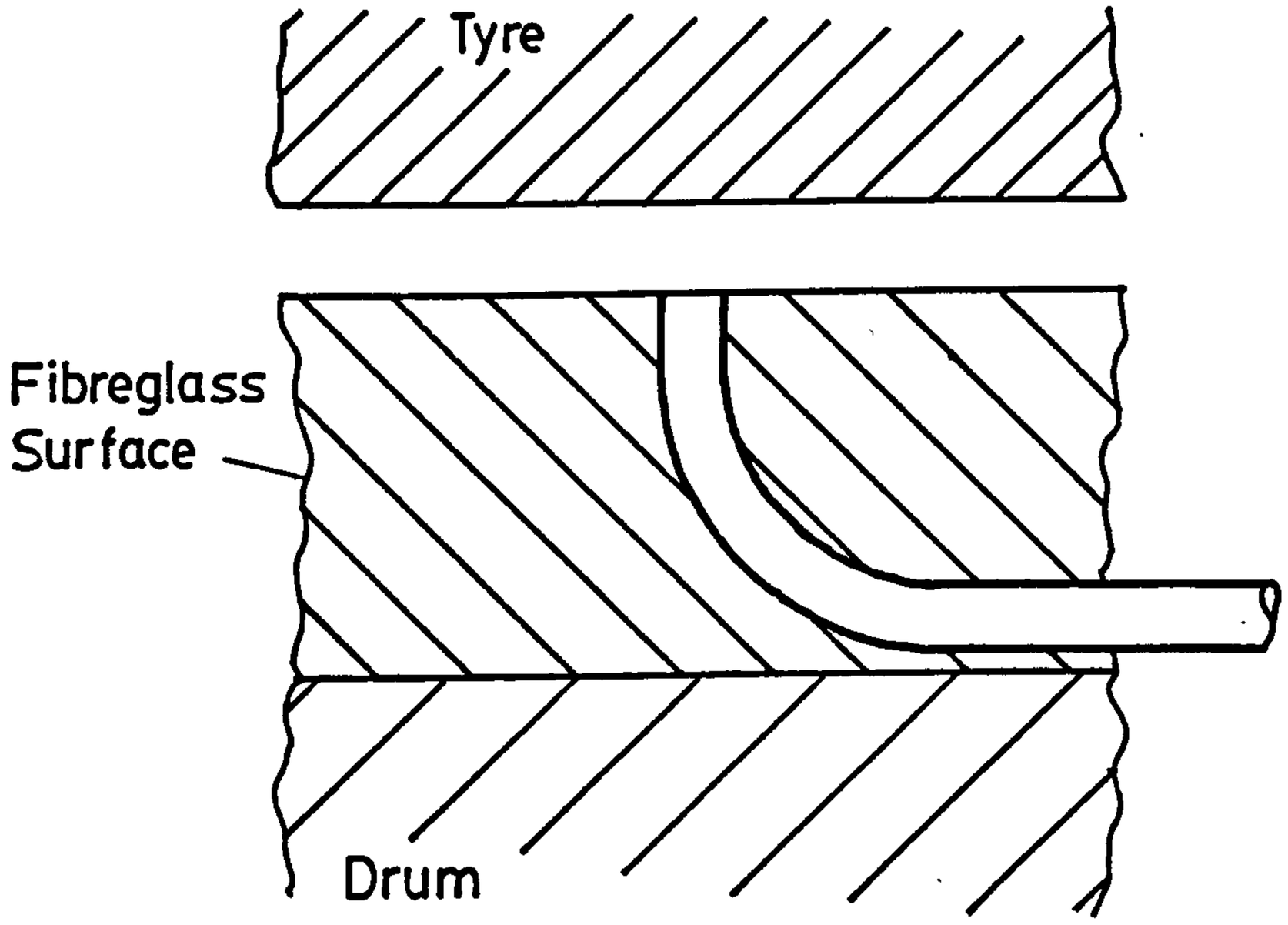

FIGURE 5.4.7 - RIGHT-ANGLE BEND AT COMMON END OF PROBE

Once built, the depth measurement system was bench tested to obtain the position of the optical peak and the degree of nonlinearity in the system. The relationship between output and stand-off distance is shown in figure 5.4.8, and is of the shape expected from reference (71).

The optical peak can be seen to be situated at a stand-off distance of 2.1 mm. Checks were carried out to ensure that this peak position was independent of such factors as source supply current and surface reflectivity. At this stage it was noted that the output was approximately linear, with respect to changes in deflection, over the range 0.5 mm to 1.5 mm. The nonlinearity outside this range (particularly below 0.5 mm) is discussed in section 5.6. The actual output level was found to be sensitive to changes in the reflectivity of the tyre surface, and the test procedure used to cope with this was discussed in section 5.4.4.

5.4.6 Nozzle

As was discussed in section 5.2.2 a nozzle has to be used to apply water to the periphery of the cornering force machine drum. The requirement for this work was for a nozzle which would produce a flow of water at the same velocity as the drum surface and with the required depth. The water supply for the nozzle is direct from the mains and no reliable method of flow measurement was available. The nozzle design therefore had to include a method of measuring the volume flow and hence the mean velocity of the water.

The width of the nozzle had to be large enough to cover the range of car tyre widths commonly tested and allow for the lateral movement of the tyre for positioning over the pressure or depth transducer. A width of 250 mm was chosen as being suitable. It was thought desirable that the depth of water should be capable of being varied up to 3 mm, which would cover most conditions found on British roads. Initially the nozzle was intended to produce a water depth which could be continuously varied up to the above maximum. The resulting design proved to be unnecessarily complex

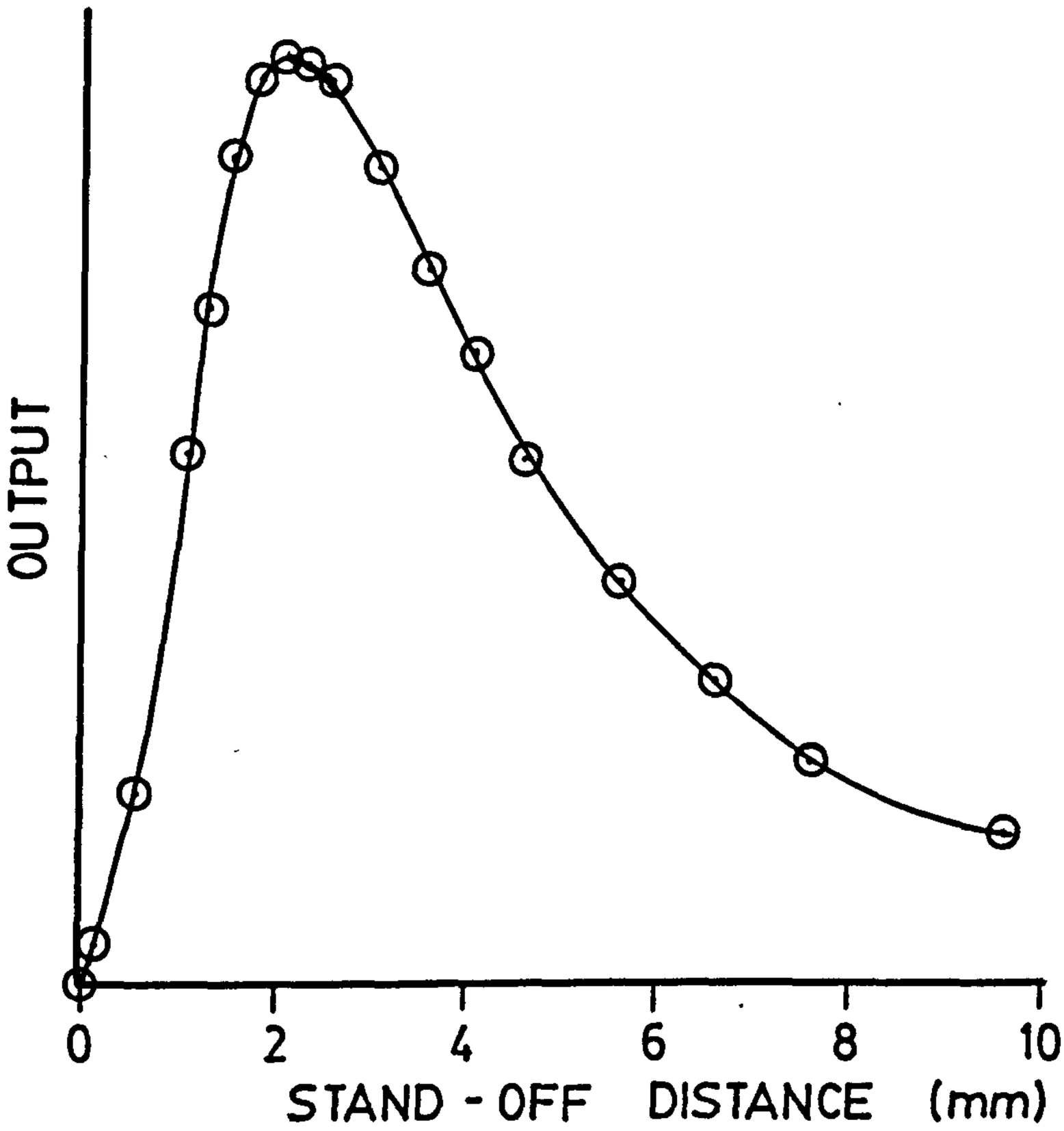

FIGURE 5.4.8- OUTPUT / DISPLACEMENT RESPONSE OF THE PROBE USED IN THE EXPERIMENTS

and it was decided to design a nozzle with a fixed geometry body, with separate 'outlet ends' which would provide alternative water depths of 1,2 or 3 mm. In this respect the nozzle would be similar to that in reference (68), except that in the outlet would be a slot rather than a series of holes. The resulting design is shown in figure 5.4.9. Particular care was taken to produce as constant a reduction in cross-sectional area as possible, to improve the stability of the outlet jet of water.

The requirement for the measurement of flow volume (velocity) through the nozzle was met by the installation of a pressure transducer in the nozzle inlet pipe. The pressure indicated by this transducer will be related to the volume flow by the characteristics of the nozzle. Because of the unusual shape of the nozzle there was no information available in the literature which would allow the accurate prediction of pressure drop for a given volume flow. It was therefore necessary to conduct experiments to calibrate the pressure indicated by the transducer with the actual volume flow. This was achieved by utilizing a test rig at Cranfield Institute of Technology. This rig is normally used for the calibration of flow meters, but it was modified to allow the flow through the nozzle to be measured using an ultrasonic flow meter. The results of this calibration procedure are shown in figures 5.4.10(a), (b) and (c) for the nozzle set for 1, 2 and 3 mm water depths respectively. The volume flow measured was converted into average flow velocity simply by dividing by the appropriate cross-sectional area of the nozzle outlet (at 1, 2 or 3 mm water depth).

When in use on the high speed cornering force machine the flow through the nozzle is controlled so the average flow velocity of water exiting the nozzle is matched to the speed of the drum periphery.

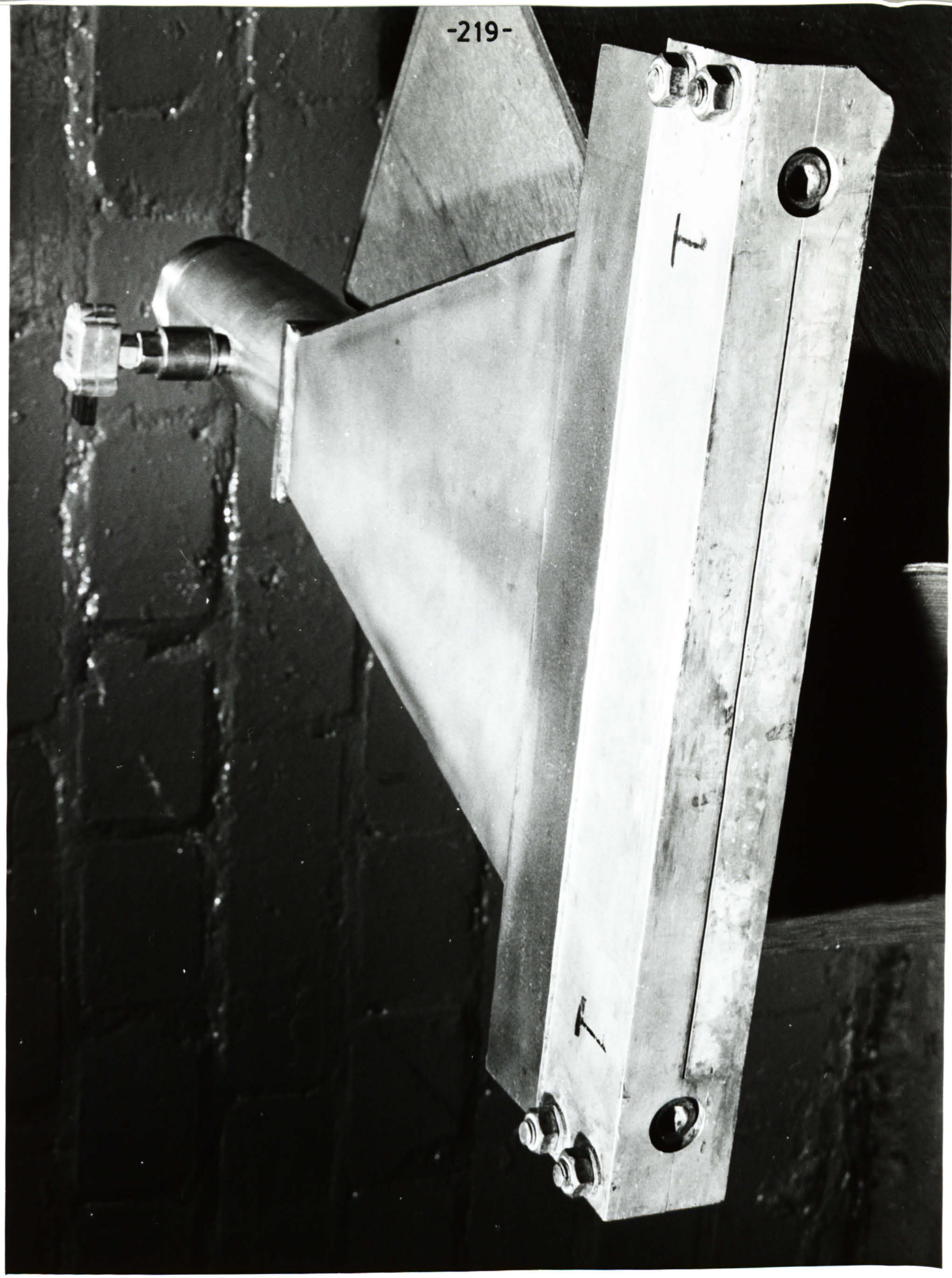

FIGURE 5.4.9 - NOZZLE

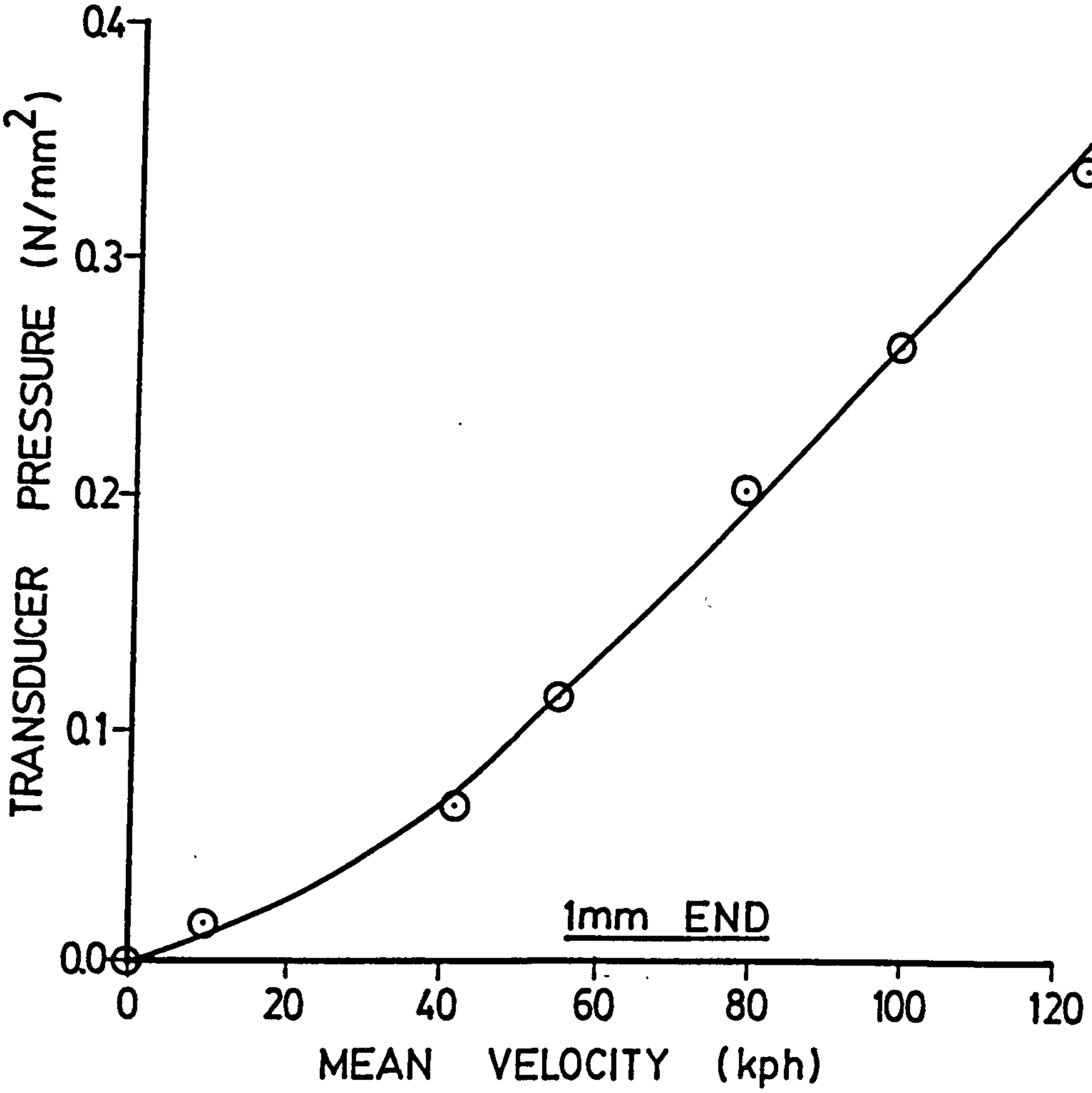

FIGURE 5.4.10a - NOZZLE CALIBRATION

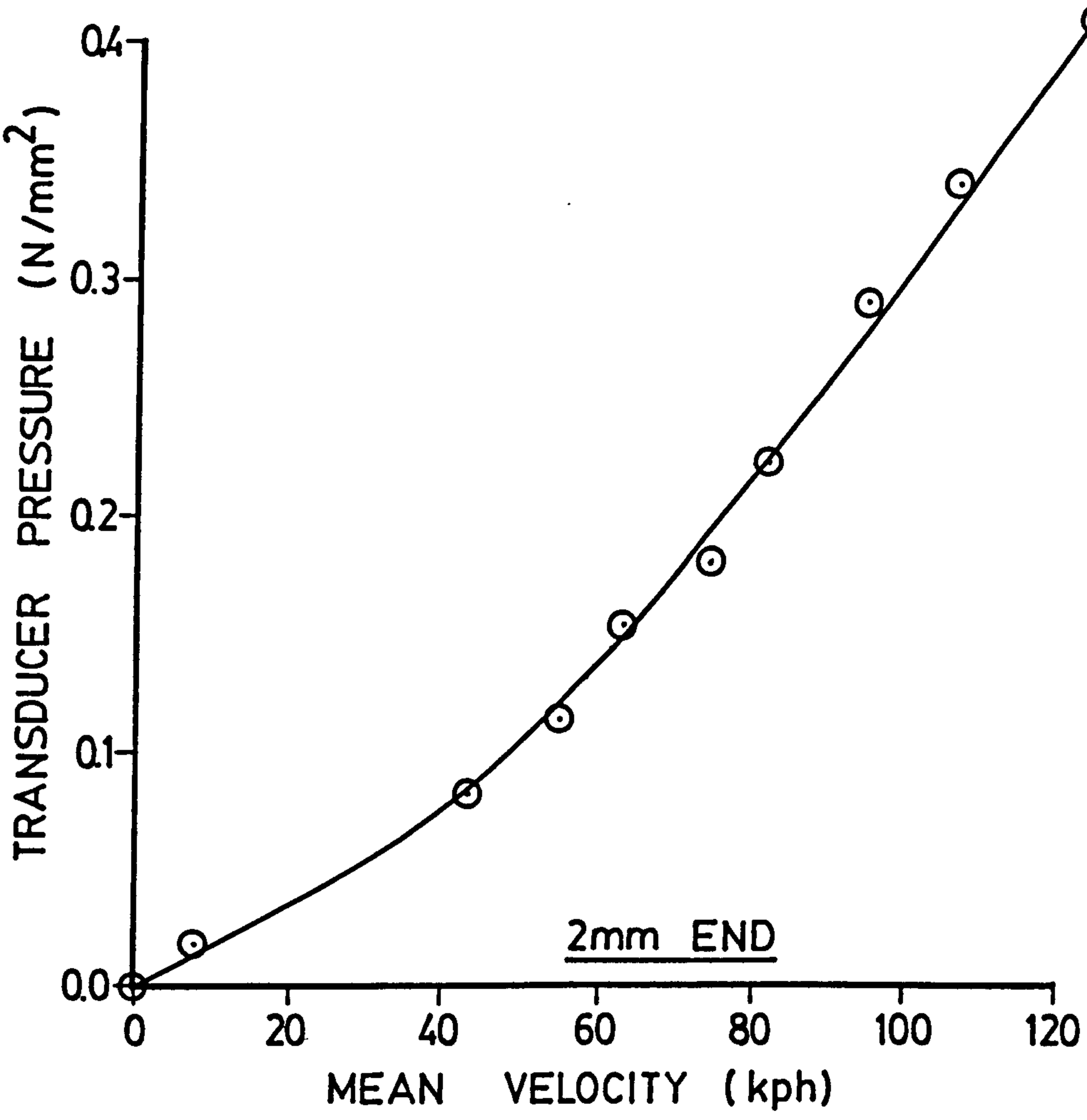

FIGURE 5.4.10b - NOZZLE CALIBRATION

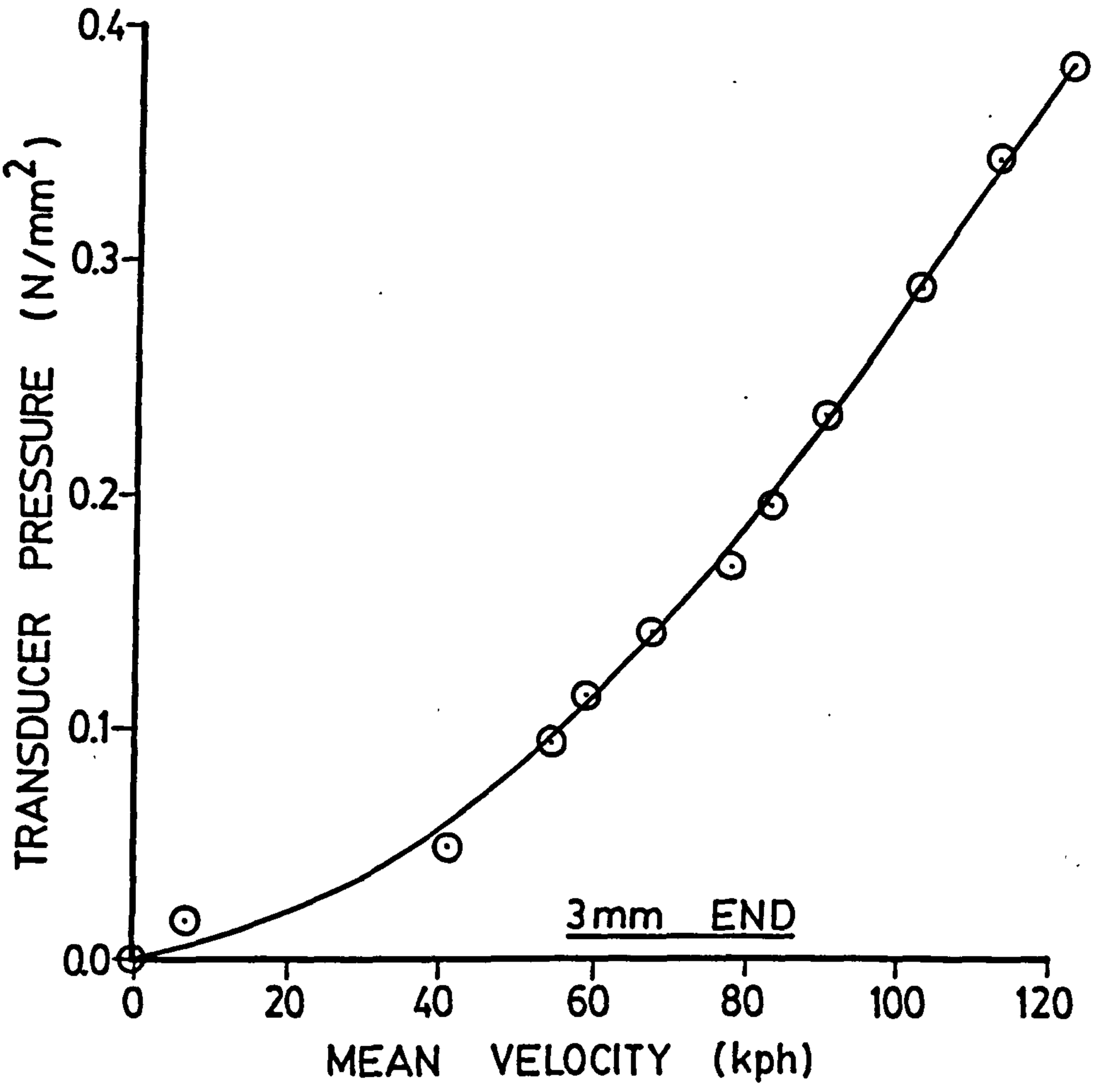

FIGURE 5.4.10c - NOZZLE CALIBRATION

5.5 CALIBRATION OF THE PRESSURE MEASUREMENT SYSTEM

To allow the calibration of the pressure measurement system, comprising the pressure transducer, the telemetry transmitter, and the telemetry receiver, it was necessary to be able to apply a known pressure to the transducer whilst measuring the output voltage from the telemetry. To account for installation effects, such as pre-stresses on the pressure transducer diaphragm, it was necessary to be able to apply a known pressure to the transducer whilst it was mounted in the cornering force machine drum. A calibration rig (shown in figure 5.5.1) was designed to allow this.

A chamber is clamped in position over the pressure transducer and air pressure applied via a regulator. As this calibration is performed with the drum stationary, any effects of acceleration on the pressure transducer are neglected. When the drum is rotating the transducer will be subject to perpendicular (radial) acceleration, and the pressure transducer manufacturer's quoted sensitivity to perpendicular acceleration is 0.0003% FS/g_2. As the pressure transducer used is rated to 500 psi and the pressure measurement system is set up for 100 psi full scale, then the accelerationsensitivity is 0.0015% of system full scale per g. The acceleration acting on the pressure transducer at theperipheral speed of 96 Kph is 84g, therefore the effect on the transducer output will be 0.13% of system fullscale i.e. 0.13 psi maximum. As this is negligible to the accuracy that these measurements are required, the method of calibration outlined above will provide a satisfactory calibration of the pressure measurement system.

The relationship between applied pressure and telemetry system output voltage is shown in figure 5.5.2. The assumed relationship is linear with 4 volts equal to 0.69 N/mm^2 (100 psi), and it can be seen that this gives close agreement with calibration values taken at various times during the testing programme.

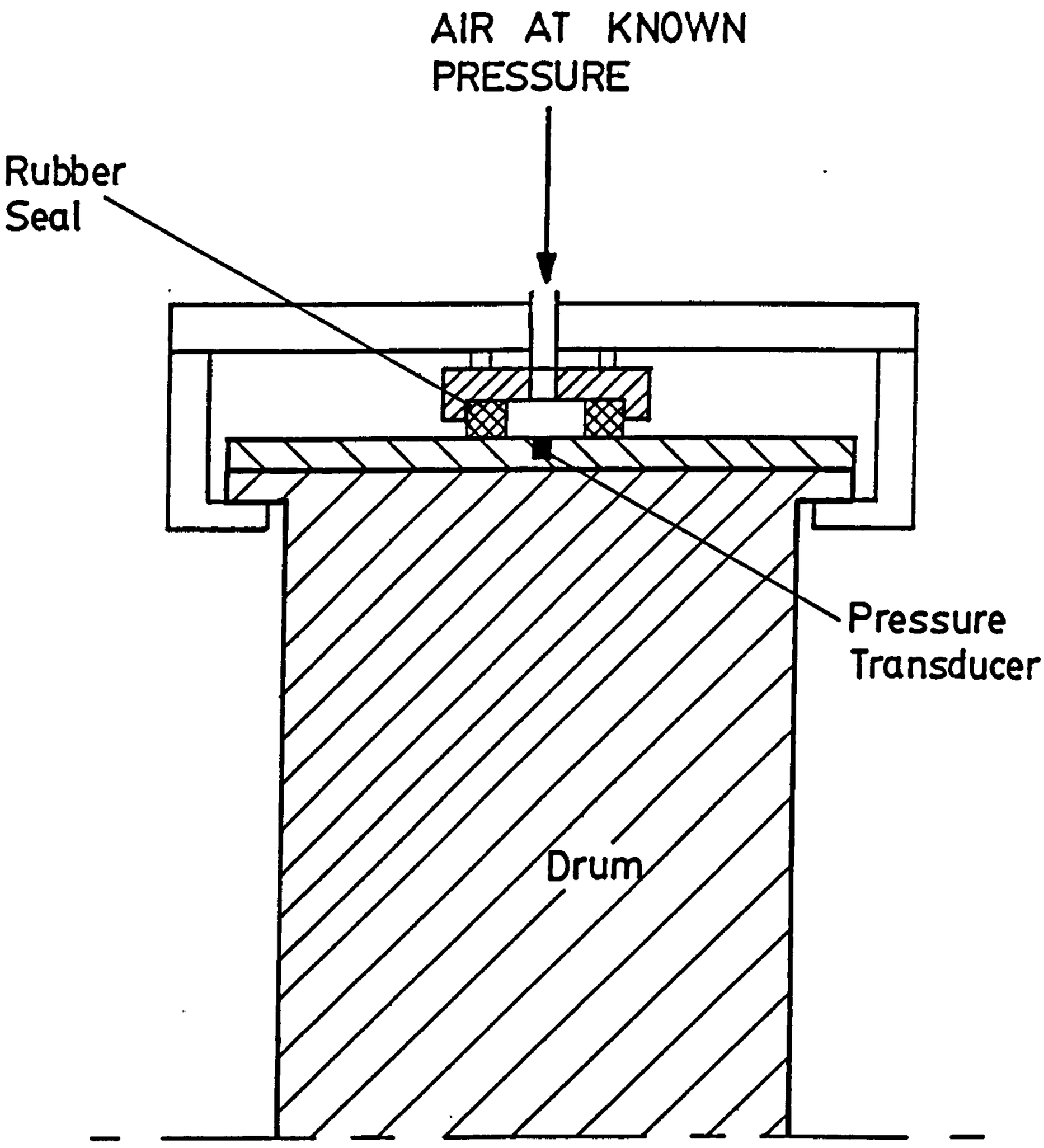

FIGURE 5.5.1 - PRESSURE CALIBRATION RIG

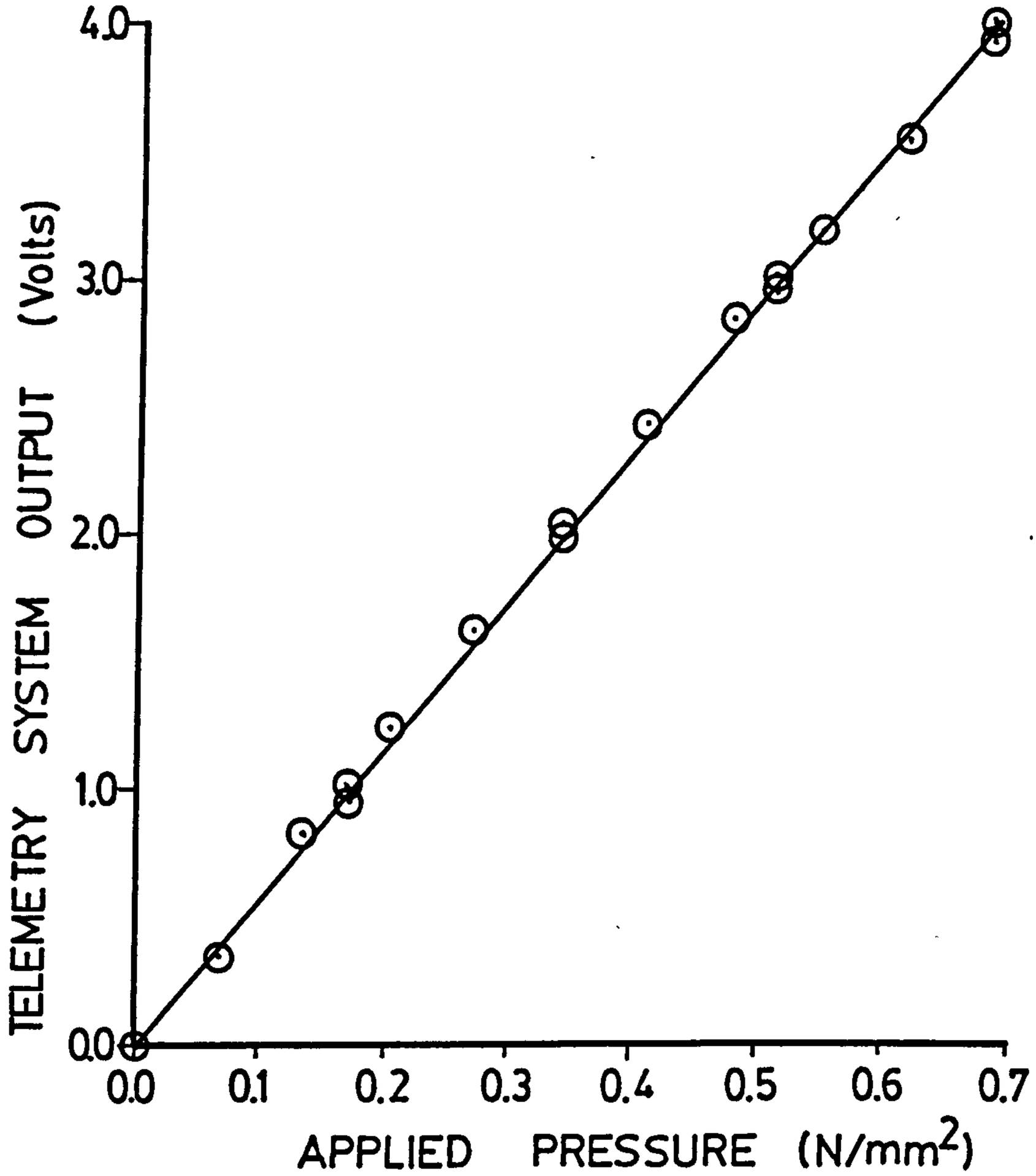

FIGURE 5.5.2 - CALIBRATION OF THE PRESSURE MEASUREMENT SYSTEM

5.6 CALIBRATION OF THE FILM THICKNESS MEASUREMENT SYSTEM

In a similar way to the calibration of the pressure measurement system, the requirement to calibrate the water film thickness measurement system was to provide a known water film thickness between a tyre and the drum surface, whilst measuring the output voltage from the telemetry.

The known water depth was obtained by using two shims, one either side of the depth probe, to support a tyre. The whole of the tyre contact patch area was immersed in water during the calibration procedure. A cross-section through the contact patch showing the tyre supported above the depth probe is shown in figure 5.6.1.

There will be a certain amount of 'sagging' of the tyre tread surface between the two supports owing to the loading applied by the tyre contact pressure. By considering the portion of the tyre between the two shims as a beam, built in at both ends and carrying a uniformly distributed load, the amount of this 'sag' has been estimated, and found to be of the order of 0.0004 mm. This amount of 'sag' is negligibly small and can be neglected for the purpose of calibrating the fluid film thickness measurement system.

As has been mentioned in section 5.4.4 the gain of the fluid film thickness measurement system is affected by the reflectivity of the tyre tread surface. Because of this, calibration readings with each set of shim thicknesses were taken at a large number of points around the tyre circumference. The spread of values for each calibration point is shown on figure 5.6.2. This spread of values is not too great a disadvantage as when a test is being performed a number of samples are taken at different points on the tyre circumference (see section 5.4.4).

In a similar way to this, the calibration of the film thickness measurement system is made by averaging the values for each calibration film thickness (shown in figure 5.6.2). The resulting averaged values are shown on figure 5.6.3. A curve was fitted to these points to give the relationship between telemetry output

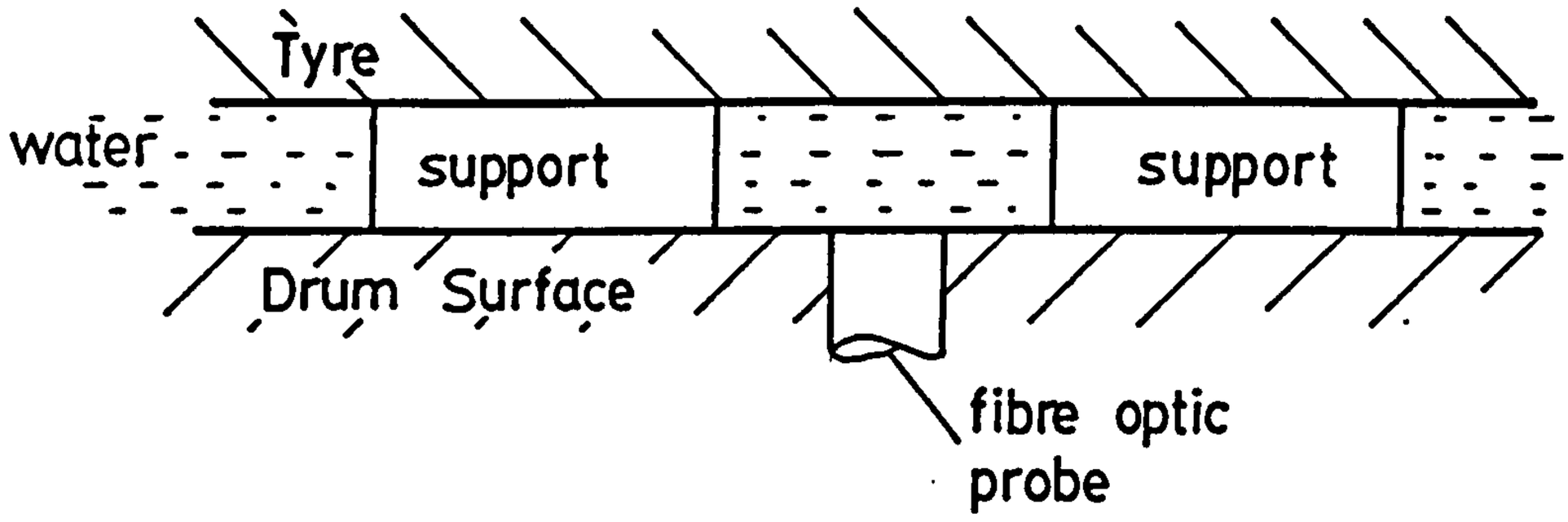

FIGURE 5.6.1 - CALIBRATION SET-UP FOR FILM THICKNESS

FIGURE 5.6.2 - FILM THICKNESS CALIBRATION - SPREAD OF POINTS

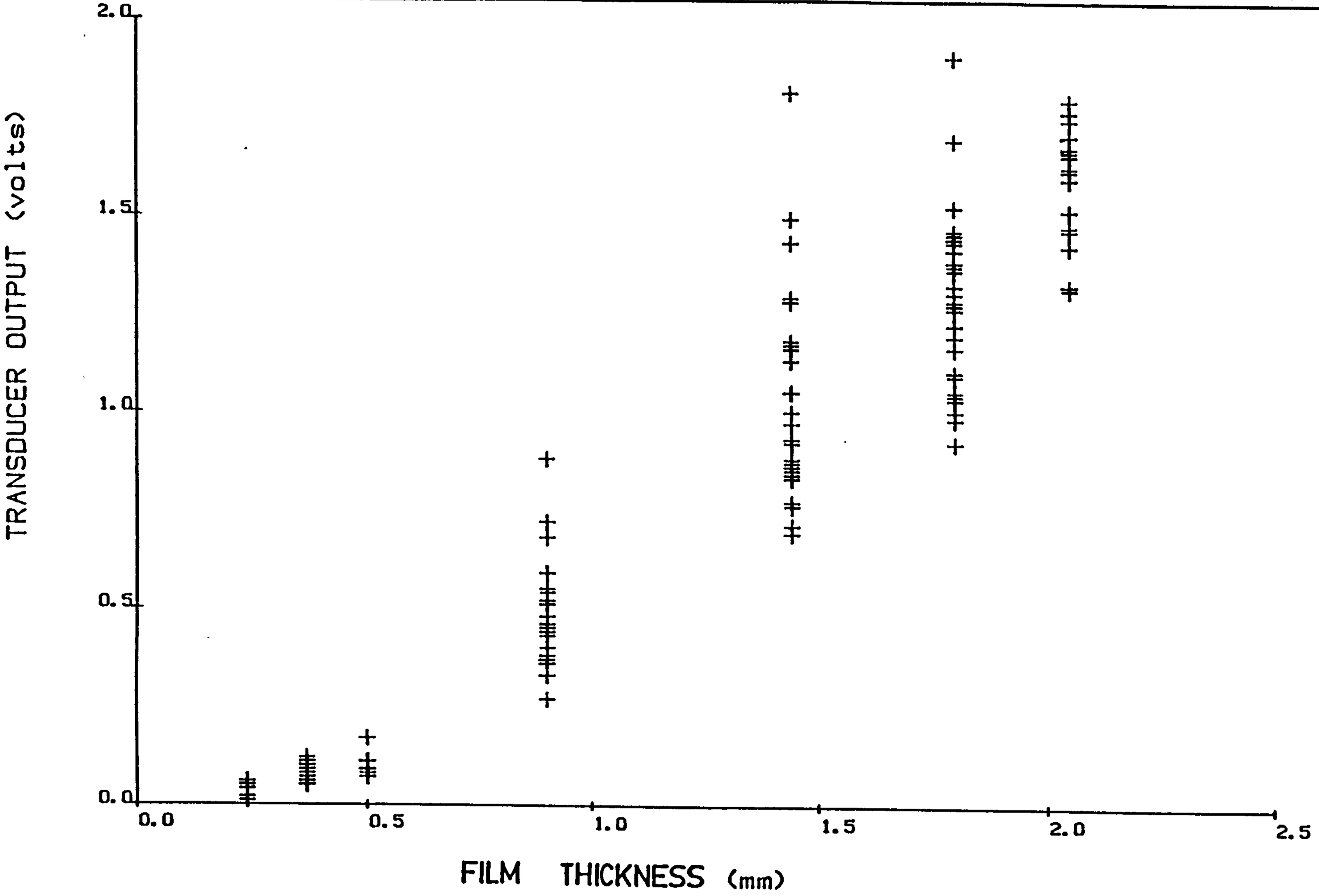

FIGURE 5.6.3 - FILM THICKNESS CALIBRATION CURVE

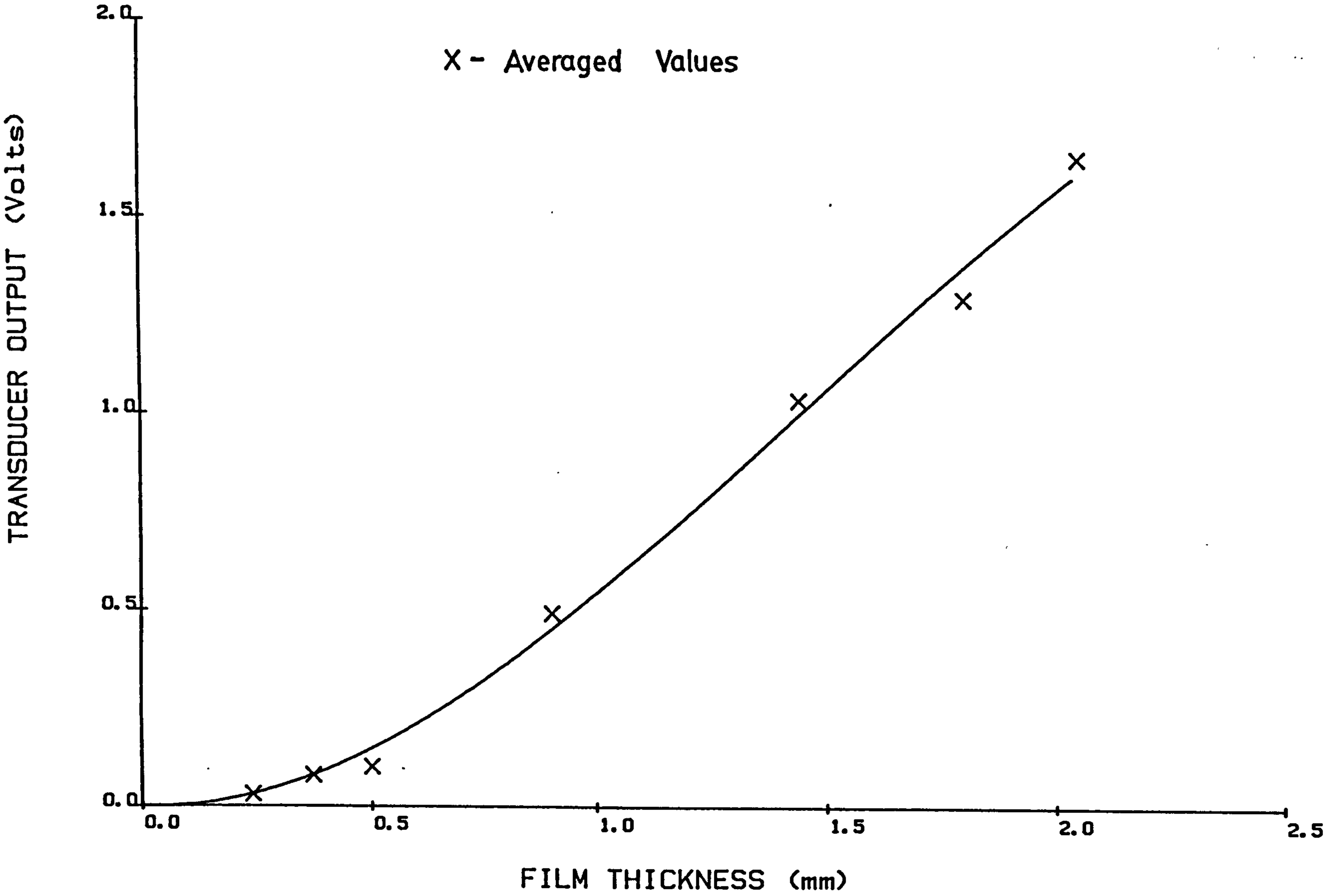

voltage and fluid film thickness, for any value of output voltage within the required range. This relationship can be expressed as:

$$v = -0.03482d + 0.74975d^2 - 0.17150d^3 \qquad \text{----------5.6.1}$$

where v = telemetry output voltage and d = water film thickness, and was obtained by using a standard curve fitting technique. This curve is shown on figure 5.6.3 and it can be seen that it closely fits the averaged points. Equation 5.6.1 can therefore be solved for any value of v. It can be seen from the curve in figure 5.6.3, that at low water film thicknesses (less than 0.1 mm) there is very little output from the system. This caused problems in tests at 50 Kph where the water film thickness expected is of the order of 0.1 mm, and this signal was almost totally lost in system noise. The remedy for this problem has already been discussed in section 5.4.5, and involves the use of a random rather than hemispherical distribution of fibres in the measurement probe. To allow the voltage output from the telemetry system to be converted into fluid film thickness via equation 5.6.1, a computer program was written which takes the digitized form of the voltage/time output and converts it to film thickness/distance data ready for plotting.

CHAPTER 6 - EXPERIMENTAL AND ANALYTICAL RESULTS

6.1 INTRODUCTION TO EXPERIMENTAL AND ANALYTICAL RESULTS

In this chapter the results of some of the experiments which were performed are presented. Tests were carried out on tyres at a number of different road speeds, namely 8, 16, 24, 32, 50 and 100 Kph. The results of only the 50 and 100 Kph tests are presented here. The low speed tests were performed because, the road surface used was completely smooth; therefore there would be no drainage from the road and particularly when a plain tread tyre was used, the tyre would completely aquaplane at low speed. However, examining the results of these low speed tests shows that they do not differ significantly from the 50 Kph results, but are merely scaled down in terms of the fluid pressure levels etc. (more contact). The 50 and 100 Kph results show differences in the shape of the pressure distributions etc., therefore the presentation here concentrates on these two speeds. Tests were performed with the tyre both freely rolling and locked and results are given for both these cases. As the tyres tested here were symmetrical about the contact patch centre-line, the experimental results are presented for only half the contact patch. Tests were performed in some cases over the whole width of the contact patch, and the results showed symmetry.

The problems encountered in the measurement of fluid film thickness, have already been discussed in section 5.4.5. The distribution of fibres in the common end of the probe meant that it was only suitable for measurements on tyres travelling at 100 Kph, when the magnitude of the film thickness being measured was greatest. To allow measurements at lower speeds (film thickness) an alternative distribution of fibres is required and this is discussed in section 8.3.2. The second problem of the film thickness measurement system, that of the tyre 'polishing' under locked wheel conditions, meant that only results on free rolling tyres were available. The experimental film thickness results presented here are therefore only for the case of 100 Kph free rolling.

The experimental measurements were performed mainly for two different tyres. One was completely smooth (plain tread) and the other had two circumferential grooves. The contact patch prints showing the contact patch shape and the position and size of the grooves are shown in figures 6.1.1 and 6.1.2 for the plain and grooved tyres respectively. The measurement of fluid film thickness was made only for the case of the plain tread tyre.

There are six different test conditions which will be considered here:

1. 50 Kph plain tyre - free rolling.
2. 50 Kph plain tyre - locked.
3. 100 Kph plain tyre - free rolling.
4. 100 Kph plain tyre - locked.
5. 50 Kph grooved tyre - locked.
6. 100 Kph grooved tyre - locked.

The analytical results produced by the contact patch computer program are also presented for these 6 test conditions. In addition to these analytical results, an example of the detailed flow on a single tyre tread block, from the block analysis computer program, is given.

Experimental results showing the fluid pressure distribution over square blocks of a locked tyre are also presented and show the pressure measurement system's capacity to handle the pressure variations due to lateral grooves.

The static contact patch shapes for the plain and grooved tyres are shown in figures 6.1.1 and 6.1.2. However, it is not known exactly what effect speed will have on this shape, although inevitably the experimental results will be affected. A more serious effect on the experimental results is due to testing the tyres on a drum, rather than on a flat road surface. Drum curvature presents two problems as far as wet grip testing is concerned. The first is that the contact pressure distribution is

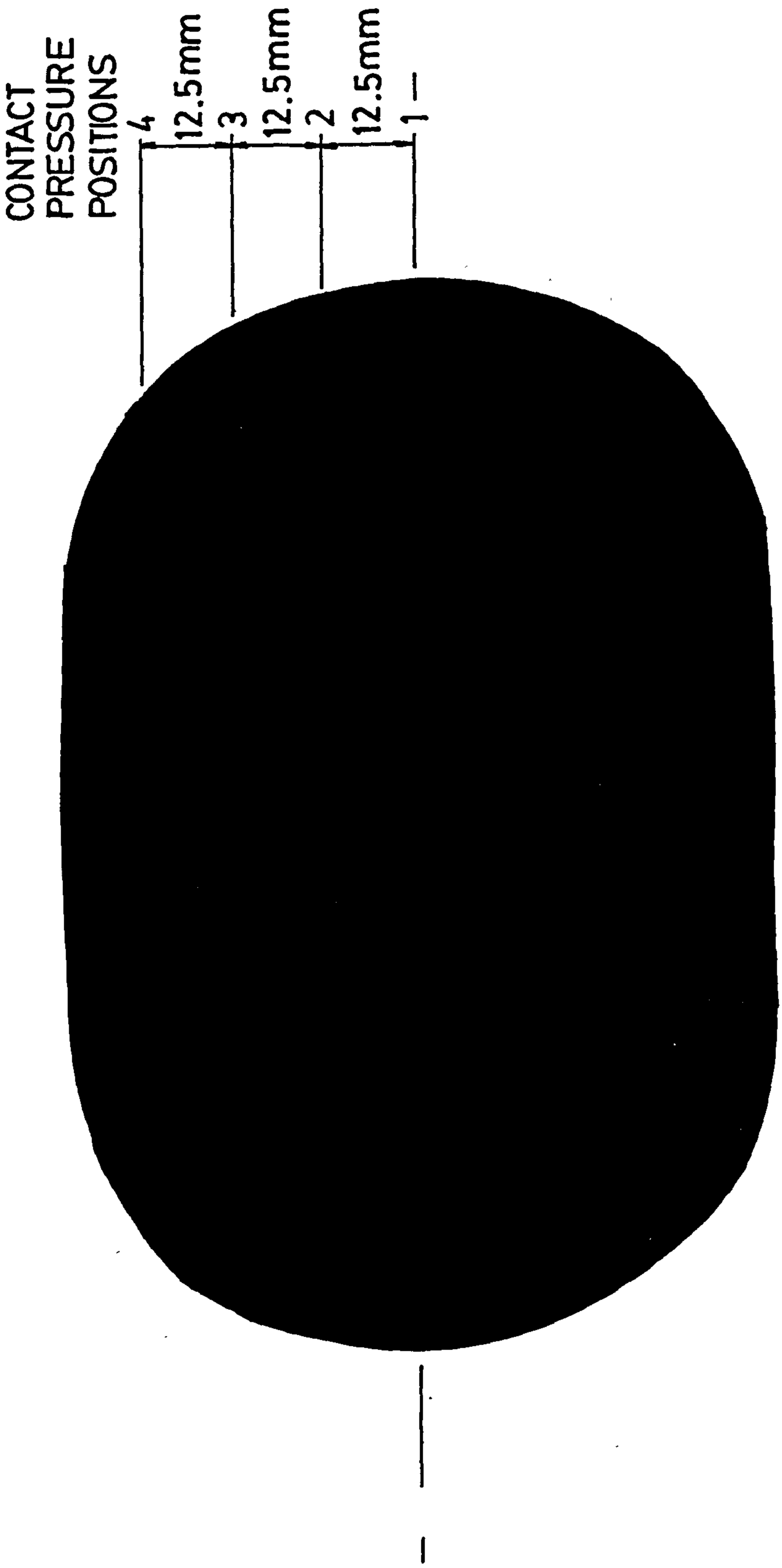

FIGURE 6.1.1- PLAIN TREAD TYRE - CONTACT PRINT

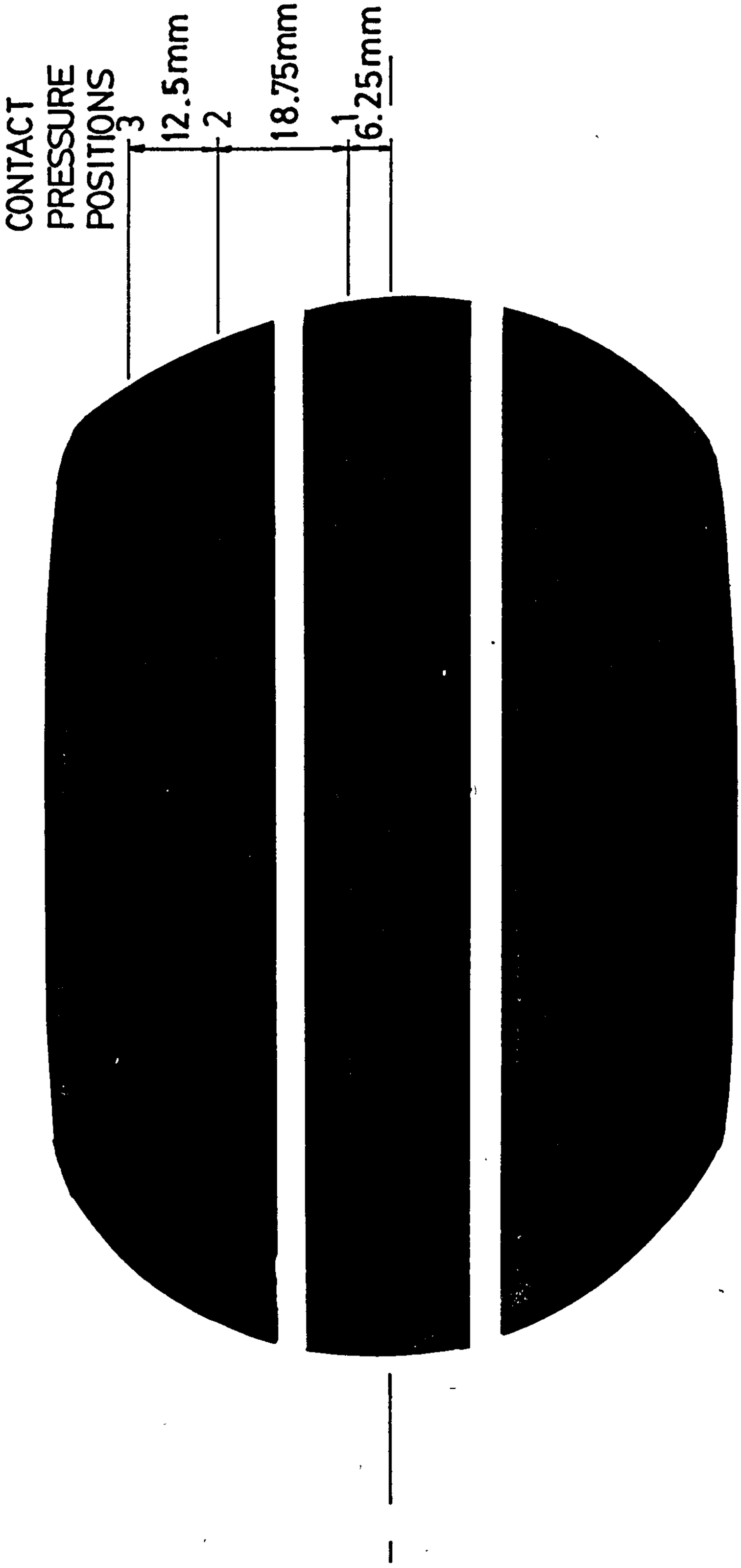

FIGURE 6.1.2 - GROOVED TYRE - CONTACT PRINT

modified from that found on a flat surface. There is little information available on this, therefore the contact pressure distribution used to produce the analytical results is based on the 'static' distribution measured on a flat surface. The contact pressure distributions for the plain and grooved tyres are shown in figures 6.1.3 and 6.1.4 respectively. These contact pressure distributions were actually obtained by rolling at 0.01 Kph over a load transducer mounted flush with a smooth surface. The lateral positions on the tyres at which dry contact pressure measurements were taken, are shown on figures 6.1.1 and 6.1.2. The measurements were actually made for positions over the full width of the tyres, but as these showed symmetry (as did the fluid pressure measurements), results for only one half of each tyre are shown. Some care must be taken when interpreting dry contact pressure measurements, particularly in the shoulder regions, as the magnitude can be very sensitive to lateral position. The contact pressure distributions used in the analytical solutions were derived from those in figures 6.1.3 and 6.1.4.

The second effect due to drum curvature is the shortening of the contact patch length. This is due to the road surface (drum periphery) curving away from the tyre at both the front and rear of the contact patch. As has already been discussed in sections 3.7.4 and 3.8.2 there is an area ahead of the front of the dry contact patch which can support a load in the wet. This area is formed as the tyre approaches the road surface, from the point at which the gap between the tyre and the road is equal to the road surface water depth. This additional length to the wet contact patch will also be shortened by the effect of drum curvature.

The overall static contact patch length is approximately 150 mm and the additional length in the wet was estimated to be approximately 40 mm (section 3.8.2). Examining the fluid pressure and film thickness experimental results shows that the contact patch length is substantially shortened to approximately 120 mm due to curvature effects at both the front and rear of the contact patch.

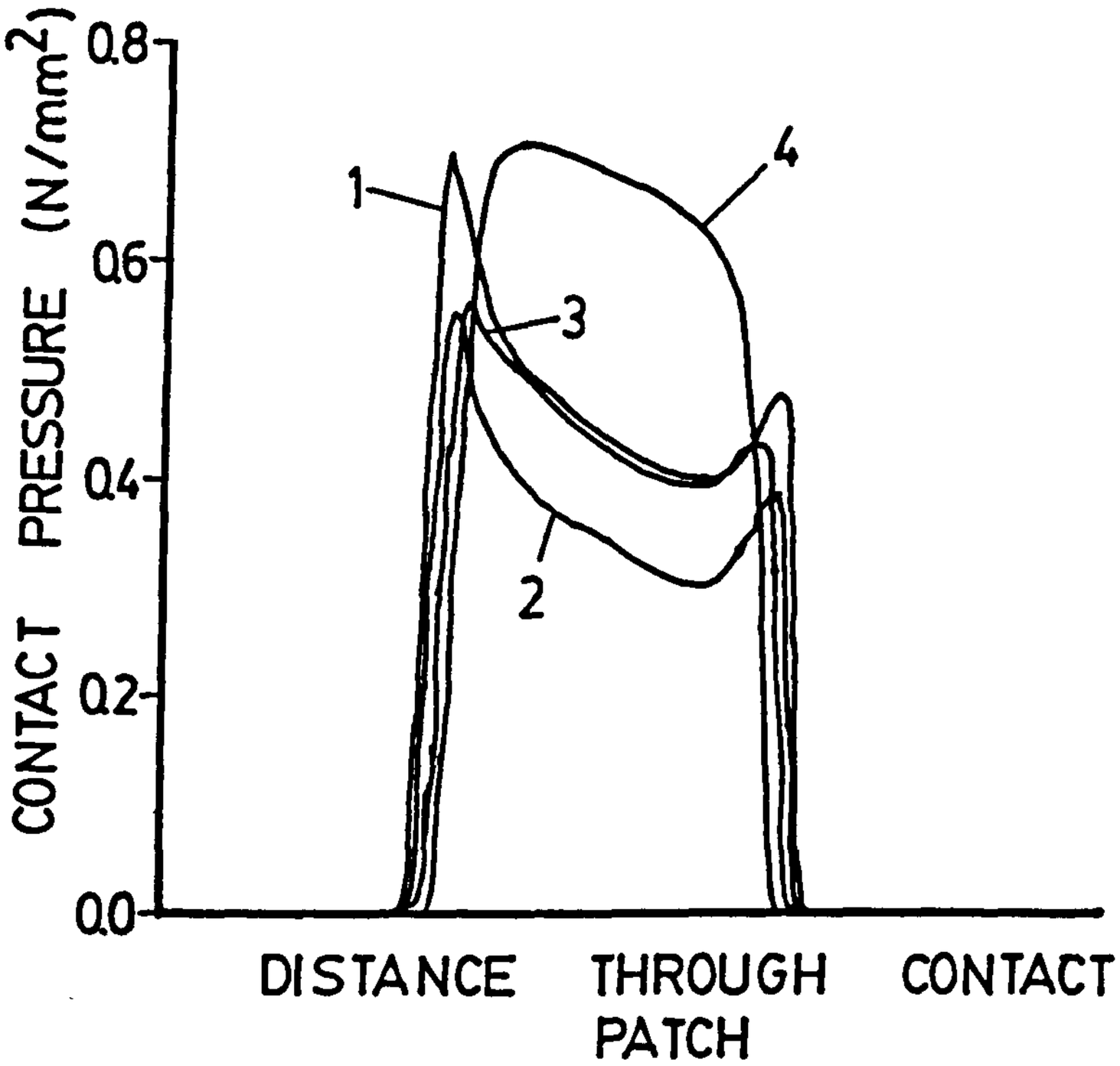

FIGURE 6.1.3 - PLAIN TREAD TYRE - DRY CONTACT PRESSURES

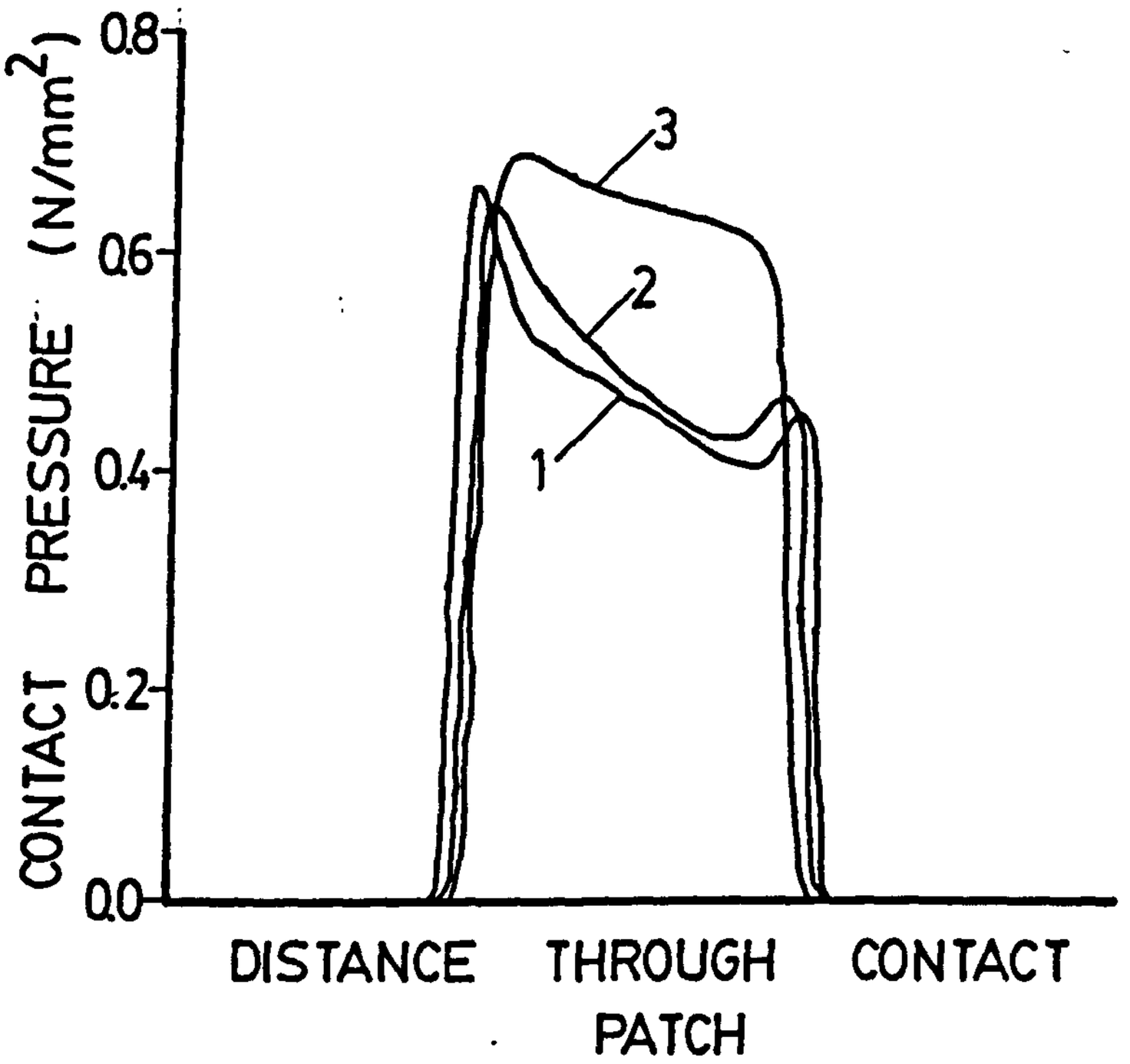

FIGURE 6.1.4 - GROOVED TYRE - DRY CONTACT PRESSURES

The low pressure area at the leading edge of the contact patch allows the size of the additional length to be estimated as 30 mm, giving an overall contact patch length in the wet of 150 mm.

As the purpose of the analytical results for contact patches presented here, is comparison with experimental results, the above values for lengths were used to model the situation on the drum. Analytical results can be found for the case of a tyre on a flat road surface by using contact patch and additional lengths based on measurements on a flat surface.

As was discussed in section 5.4.1 the tests on the cornering force machine were carried out on a smooth surface. The analytical results are also for a tyre on a smooth surface, although the effect of a road surface can easily be added by specifying its drainage capacity.

When the grooved tyre was modelled no allowance was made for groove closure. It is possible that under high speed conditions the grooves within the contact patch will close up, effectively reducing their width. As no information is available on the extent of this, the widths of the grooves were considered not to change from their static values.

In addition to the distribution of contact pressure it is also thought that the vertical stiffness of the tyre will vary within the contact patch. No information is available on this, and suggestions as to how this could be obtained are made in section 8.3.1. The analytical results were obtained using a uniform vertical stiffness at all points within the contact patch, and inevitably this will cause there to be some differences between the analytical and experimental results.

The experimental pressure distributions for the plain and grooved tyres are presented in two forms; both for half the contact patch width. The first is a set of individual pressure profiles obtained as the transducer in the drum surface moved from front to rear of

the contact patch. In all cases the front of the contact patch is to the left hand side of the diagram. The lateral positions of these pressure profiles are shown in the relevant sections. The vertical axis shows fluid pressure with a centre zero (atmospheric) and a full scale of 0.689 N/mm^2 (6.89 Bar). The horizontal axis represents distance through the contact patch (200 mm full scale). The positioning of the 200 mm length for which the pressures are presented, is determined by a trigger pulse which was generated once per revolution of the drum. The second method of presenting the pressure distributions is as a three-dimensional plot showing the pressure distribution over half the width of the contact patch. The axis, at width equal to zero, represents the contact patch centre-line. The values at widths from 0 to 50 mm on the experimental pressure distributions, correspond to values at widths from 50 to 100 mm on the analytical pressure distributions. Therefore, the half of the contact patch furthest from the point of viewing is represented in the experimental cases. The three-dimensional plots were formed by taking pressure values from the individual pressure profiles at different points in the contact patch. To achieve clarity, in the three-dimensional plots, only a limited number of points could be used; there is therefore inevitably some loss of detail. The individual profiles should therefore be used if details are required, and the three-dimensional plots if an overview of the distribution is required. The three-dimensional plots also give a more direct comparison with the results from the computer program.

Unless otherwise stated, the figures showing pressure, film thickness and flows are analytically predicted values.

6.2 RESULTS FOR THE PLAIN TREAD TYRE

The analytical and experimental results of pressure and film thickness for the following four cases with a plain tread 155SR13 tyre will be considered.

1. 50 Kph free rolling.
2. 50 Kph locked.
3. 100 Kph free rolling.
4. 100 Kph locked.

In all cases the tyre was loaded to 385 Kg with an inflation pressure of 1.9 Bar. The water depth on the road surface was 1 mm. In addition to film thickness and pressure results, analytically predicted values of flow velocity and volumetric flow per unit width are presented.

Figure 6.2.1 shows the positions within the contact patch where the experimental pressure measurements, presented as individual profiles, were taken. These positions are used for all cases of measurements on the plain tread tyre.

The analytical results were obtained by using a rectangular finite element mesh of the whole of the contact patch, as shown in figure 6.2.2.

As was discussed in section 6.1, the first 30 mm at the front of the wet contact patch is considered to be sloping in its undeformed state. The film thickness in this area is therefore of a greater magnitude than the film thickness in the rest of the contact patch. To allow the film thicknesses in each of these areas to be seen clearly, they are shown on separate figures.

All the three-dimensional plots of results for tyre contact patches are with a finite element mesh based on a rectangular grid. In the interests of clarity the diagonals which divide this rectangular grid into triangles are omitted from the plots.

The plots showing fluid flow velocity and volumetric flow per unit width give values at element centroids for the reasons discussed in section 3.5. By considering the volumetric flow, an indication can be gained as to where the largest amounts of water are flowing, and by considering flow velocity areas of high fluid velocity can be identified.

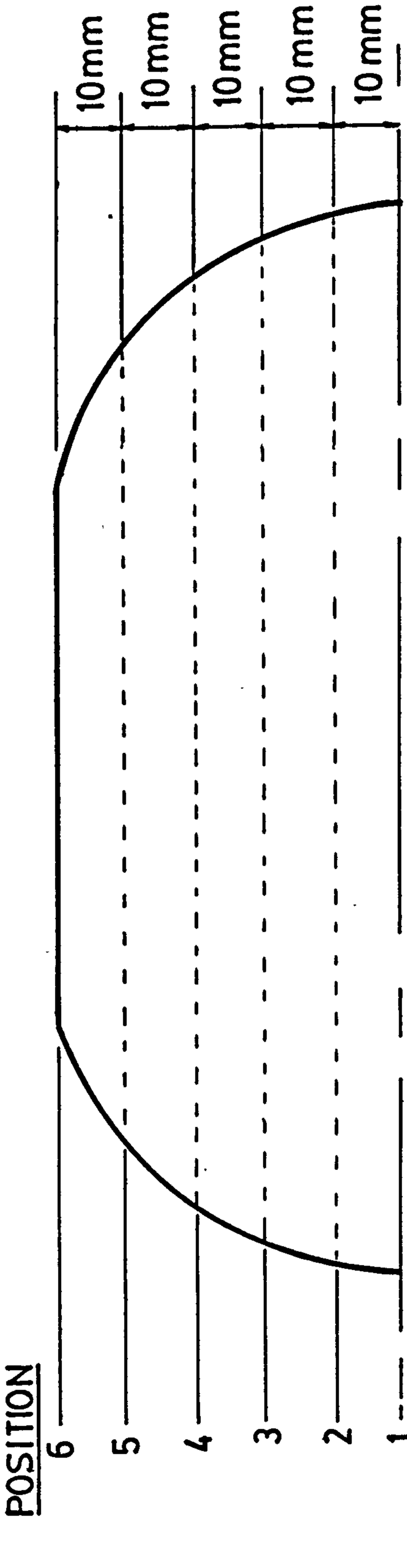

FIGURE 6.2.1 - PLAIN TREAD TYRE - TEST POSITIONS

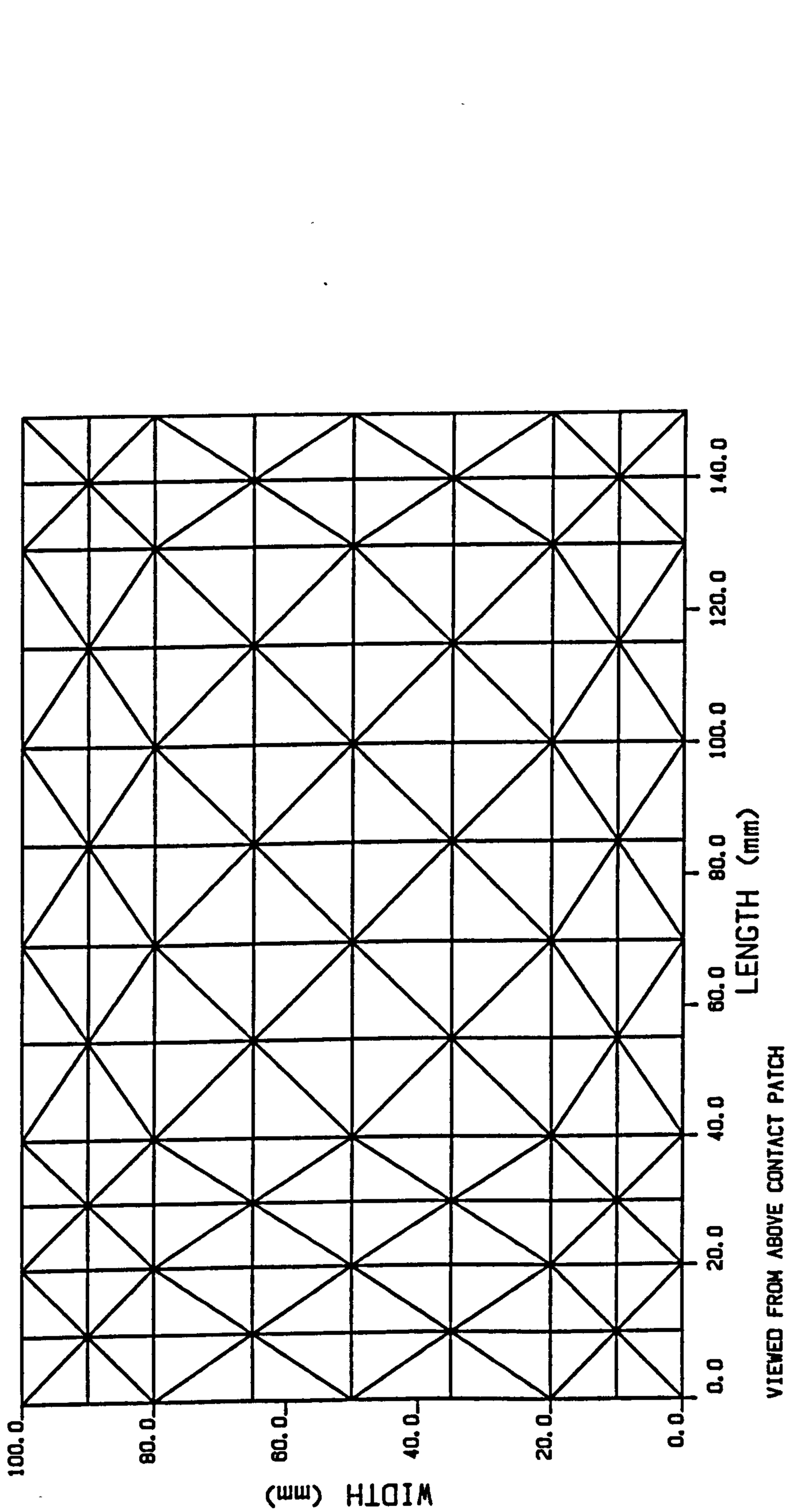

FIGURE 6.2.2 -- MESH FOR PLAIN TREAD TYRE

6.2.1 50 Kph Free Rolling

The individual experimental pressure profiles for the case of 50 Kph free rolling are shown in figures 6.2.3 and 6.2.4. The pressure distribution predicted by the contact patch computer program is shown in figure 6.2.5. As can be seen from the computer predicted fluid film thicknesses (figure 6.2.6a), the tyre is in contact with the road in much of the contact patch. The pressures shown in figure 6.2.5 are therefore fluid pressures in the areas where there is water penetration, and in the areas of tyre/road contact the pressures are the proportion of the dry contact pressures which are applied by the load stepping procedure (section 4.5.5). The computed film thicknesses in the front 30 mm of the wet contact patch are shown in figure 6.2.6b.

When it was attempted to measure experimentally the fluid film thicknesses under this condition no significant voltage output was obtained from the instrumentation. With reference to the calibration of the film thickness measurement system (figure 5.6.3) the film thickness under these conditions would be less than 0.2mm. The error between the analytical results where an amount of tyre/road contact is shown and the experimental results where fluid pressures were measured at all points within the contact patch are therefore not great in terms of the magnitude of the fluid film thicknesses. In fact it is possible that there could be some tyre/road contact in the experimental results and that the fluid pressure measured is that in the 0.25 mm deep cavity above the pressure transducer. The pressure transducer had to be recessed slightly from the road surface to prevent physical damage as the tyre passed over it.

Figure 6.2.7 shows the analytically predicted fluid flow velocities, and figure 6.2.8 the volumetric flows per unit width.

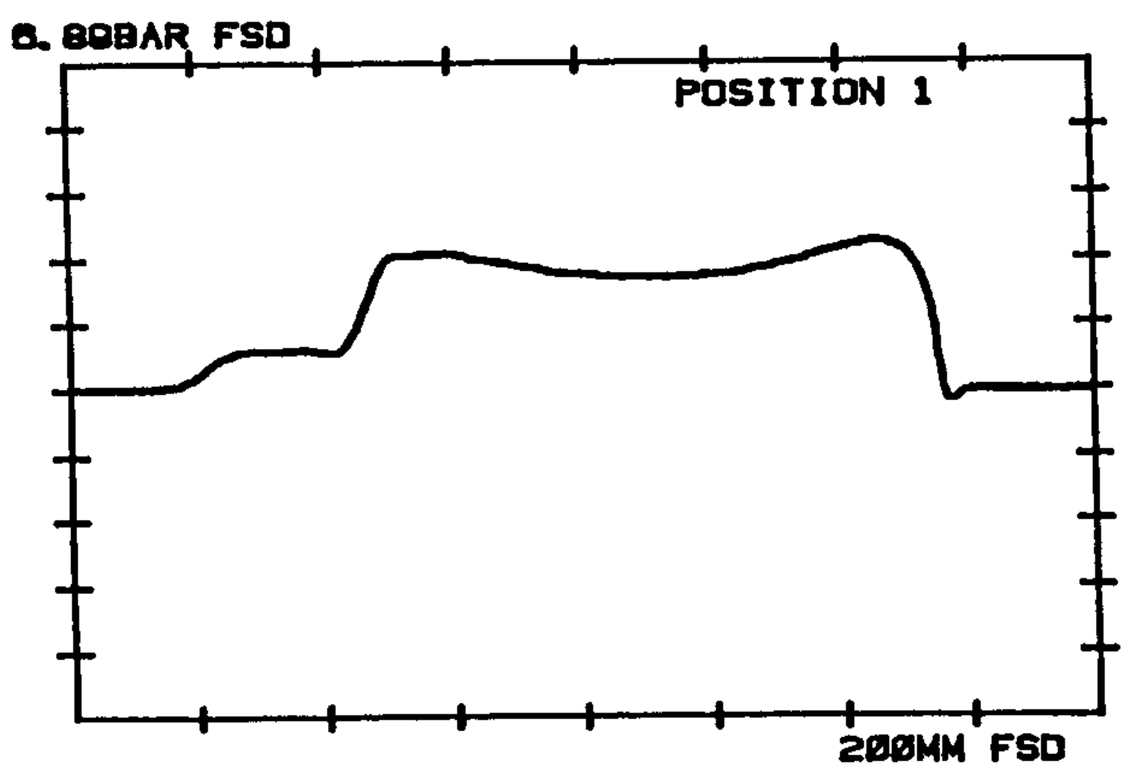

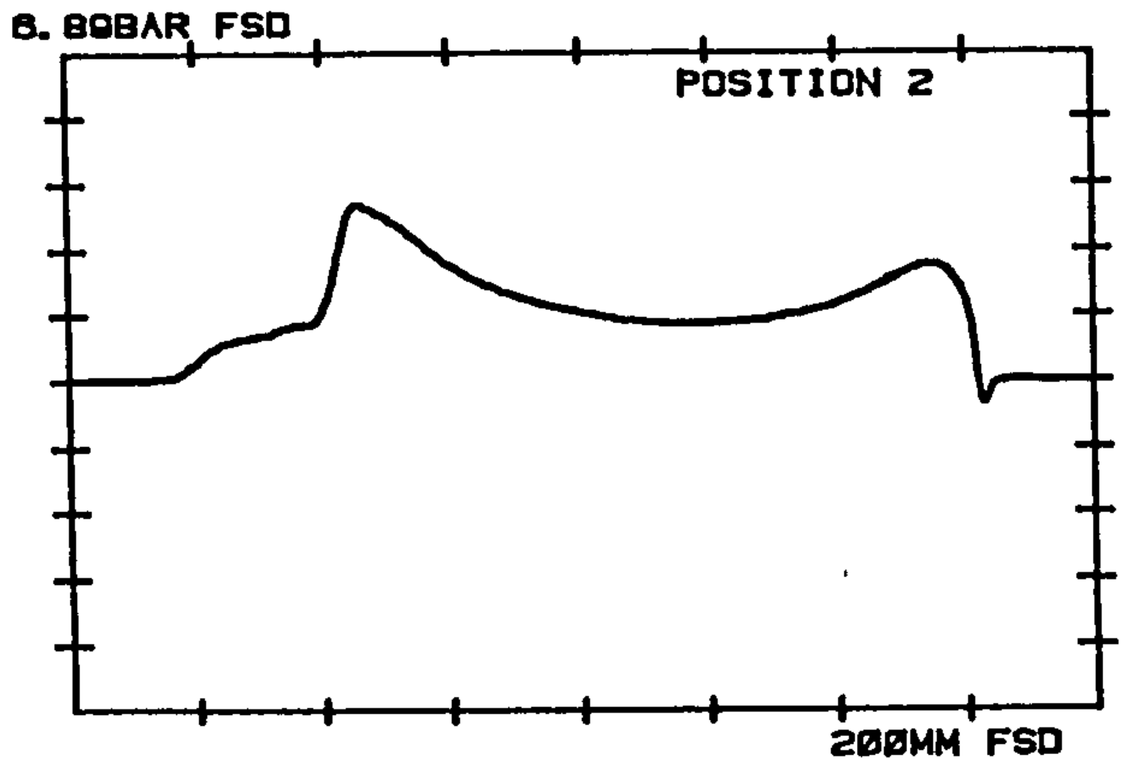

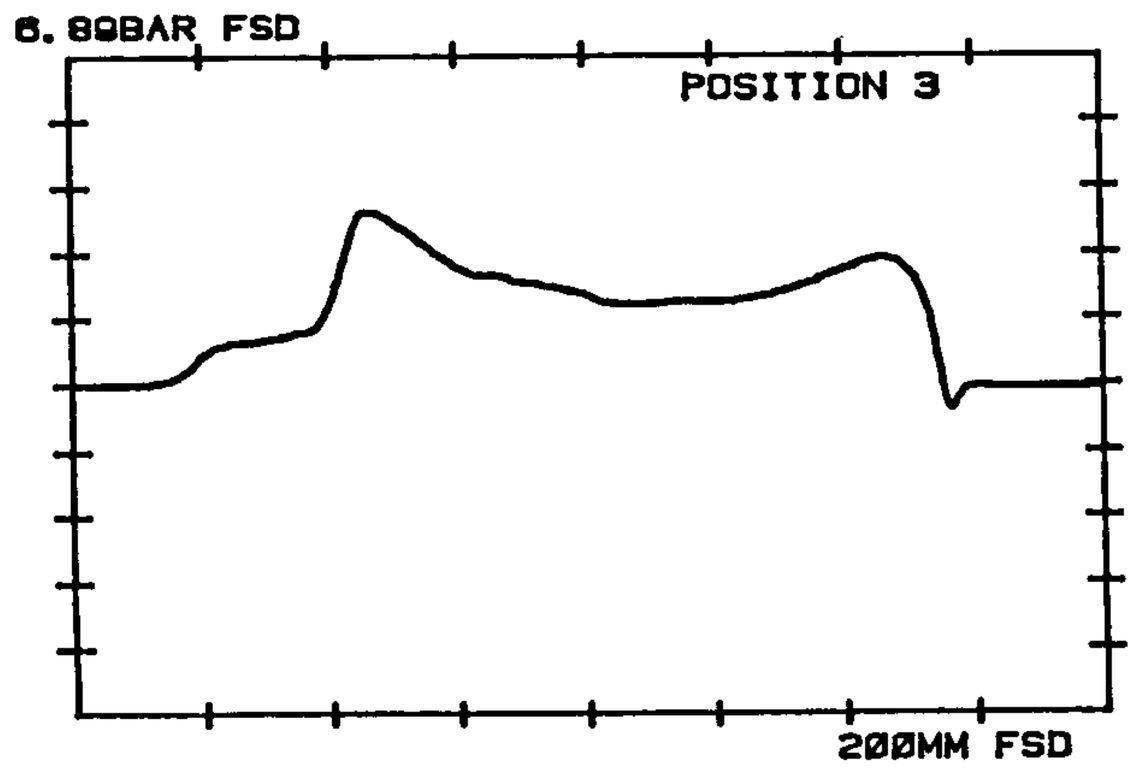

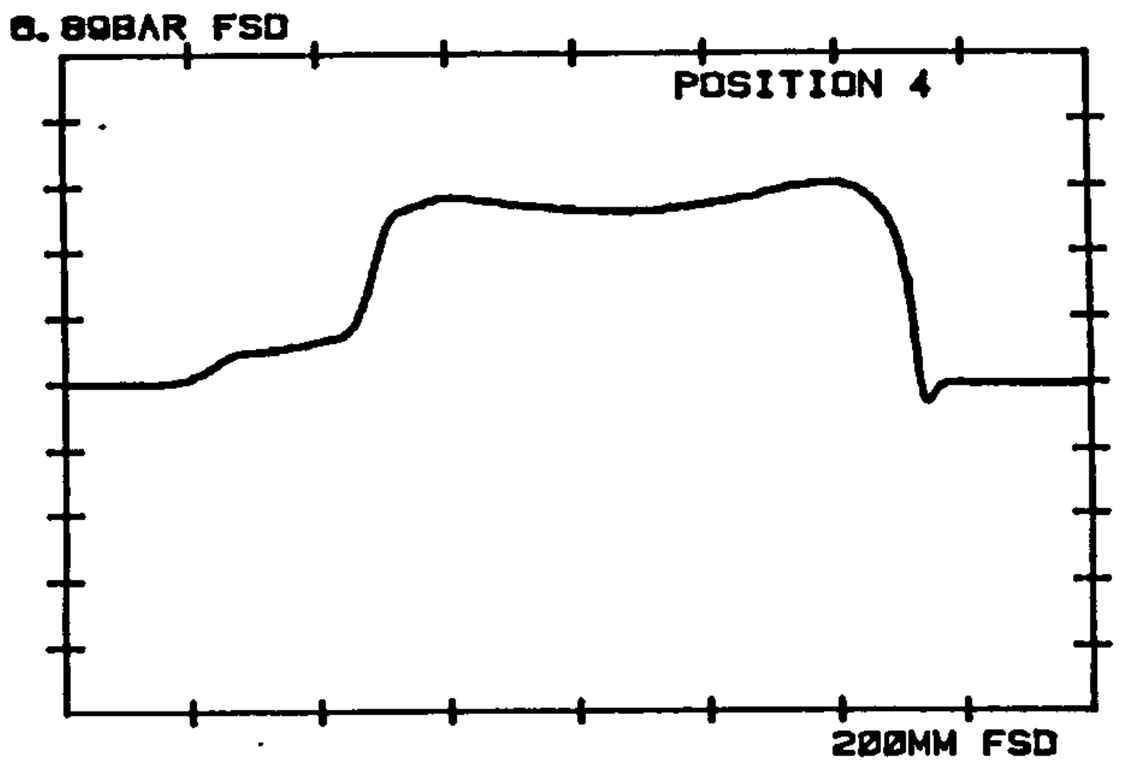

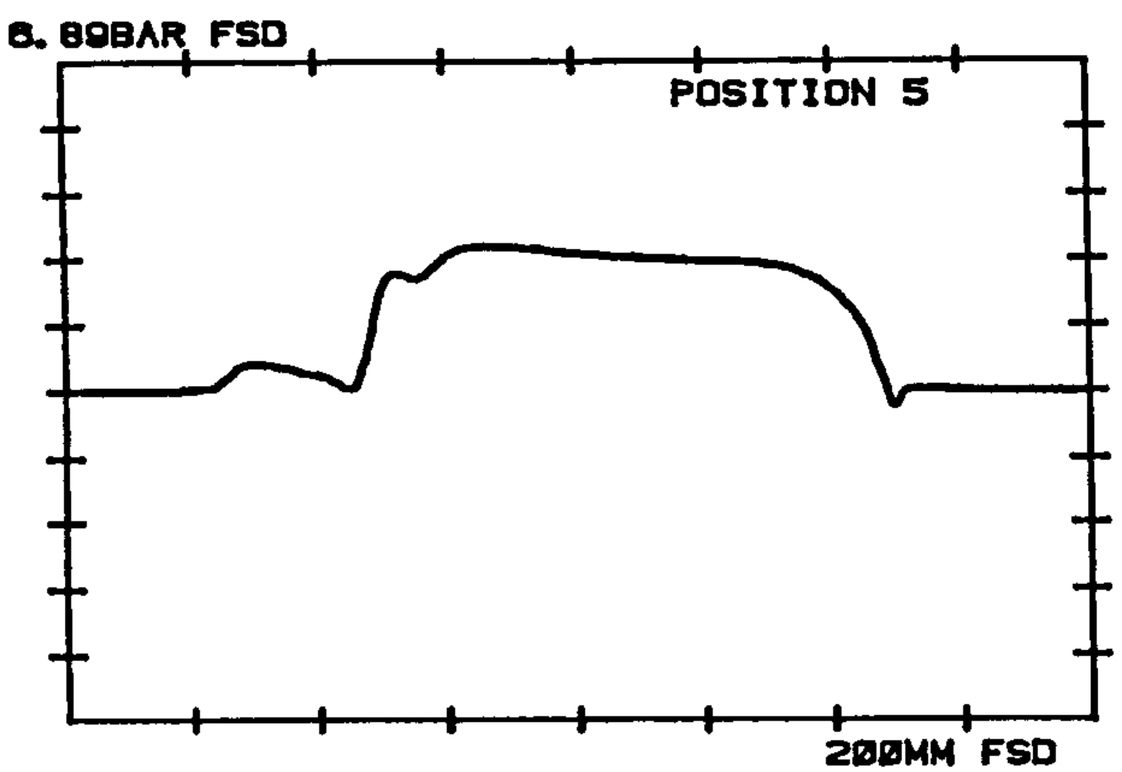

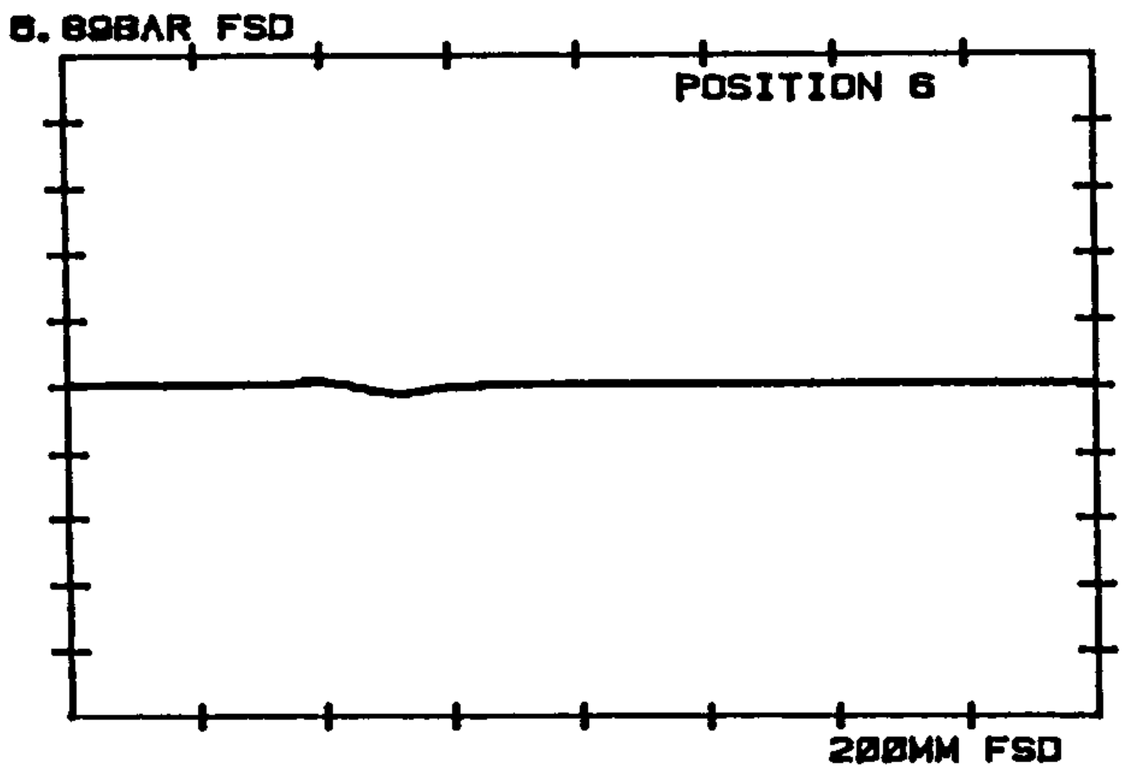

FIGURE 6.2.3 - EXPERIMENTAL FLUID PRESSURES - PLAIN TYRE 50 KPH ROLLING

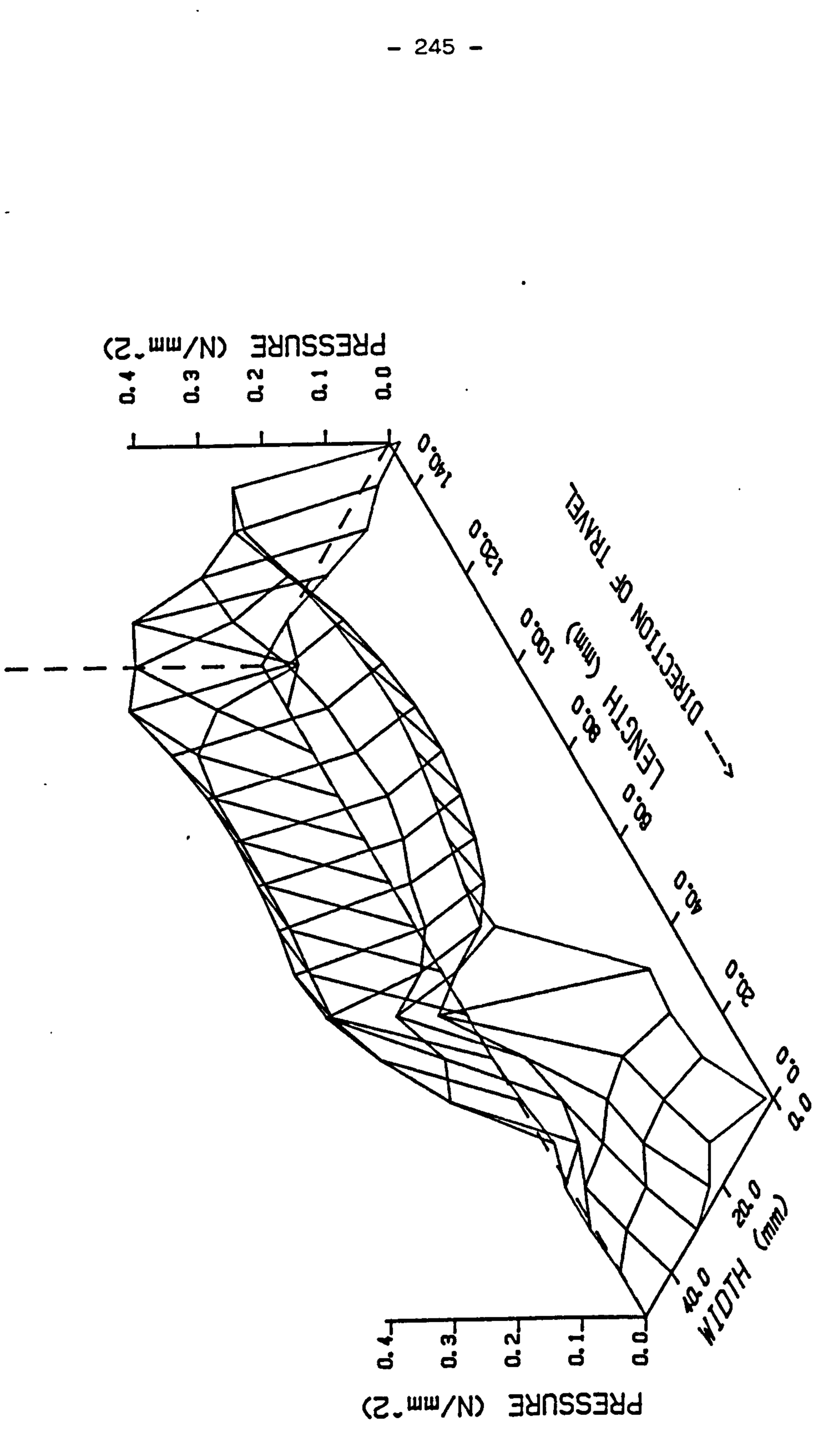

FIG 6.2.4 – PLAIN TYRE 50 KPH ROLLING (EXPERIMENTAL)

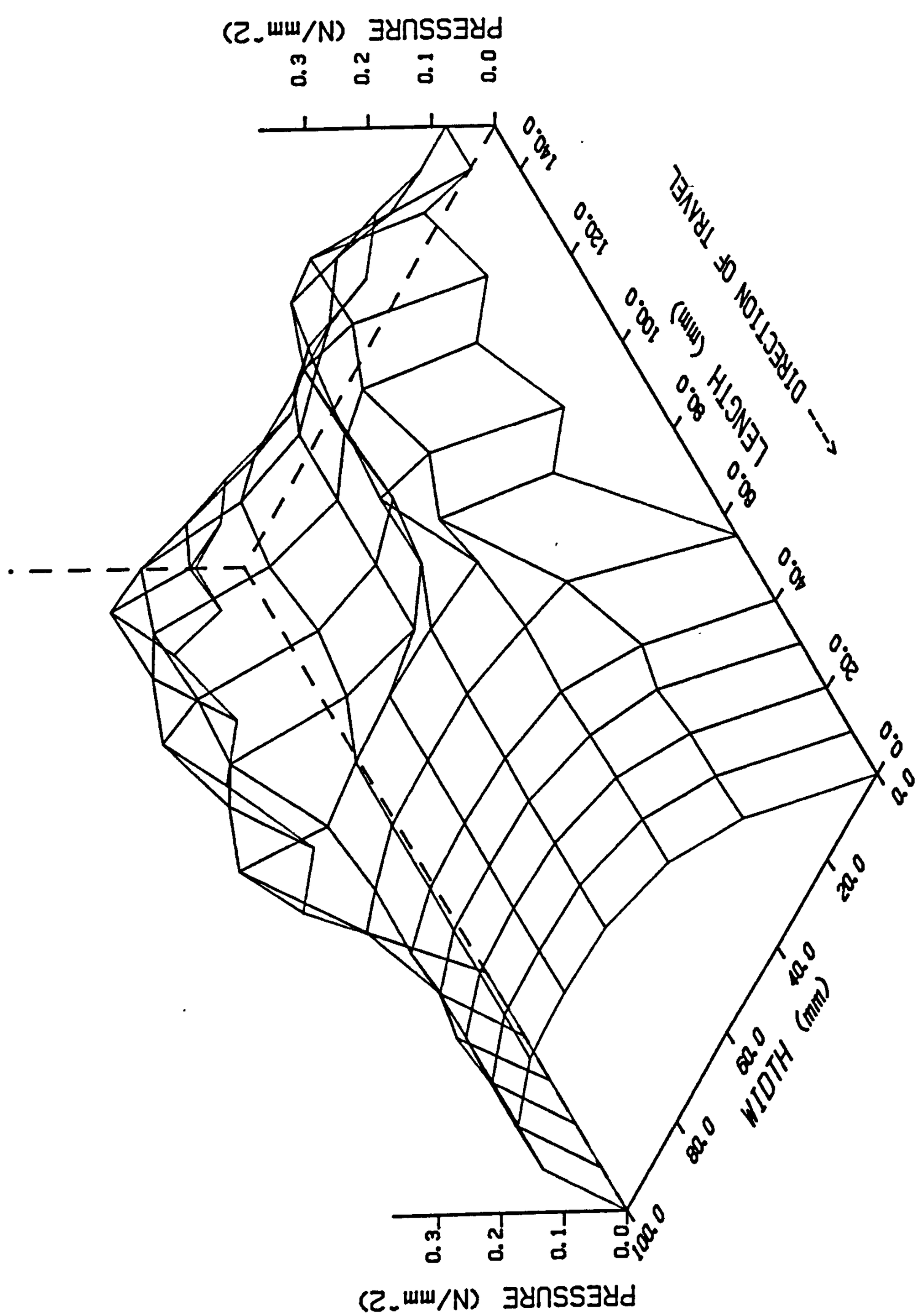

FIGURE 6.2.5 - PLAIN TYRE 50 Kph ROLLING

FIGURE 6.2.6a -PLAIN TYRE 50 Kph ROLLING

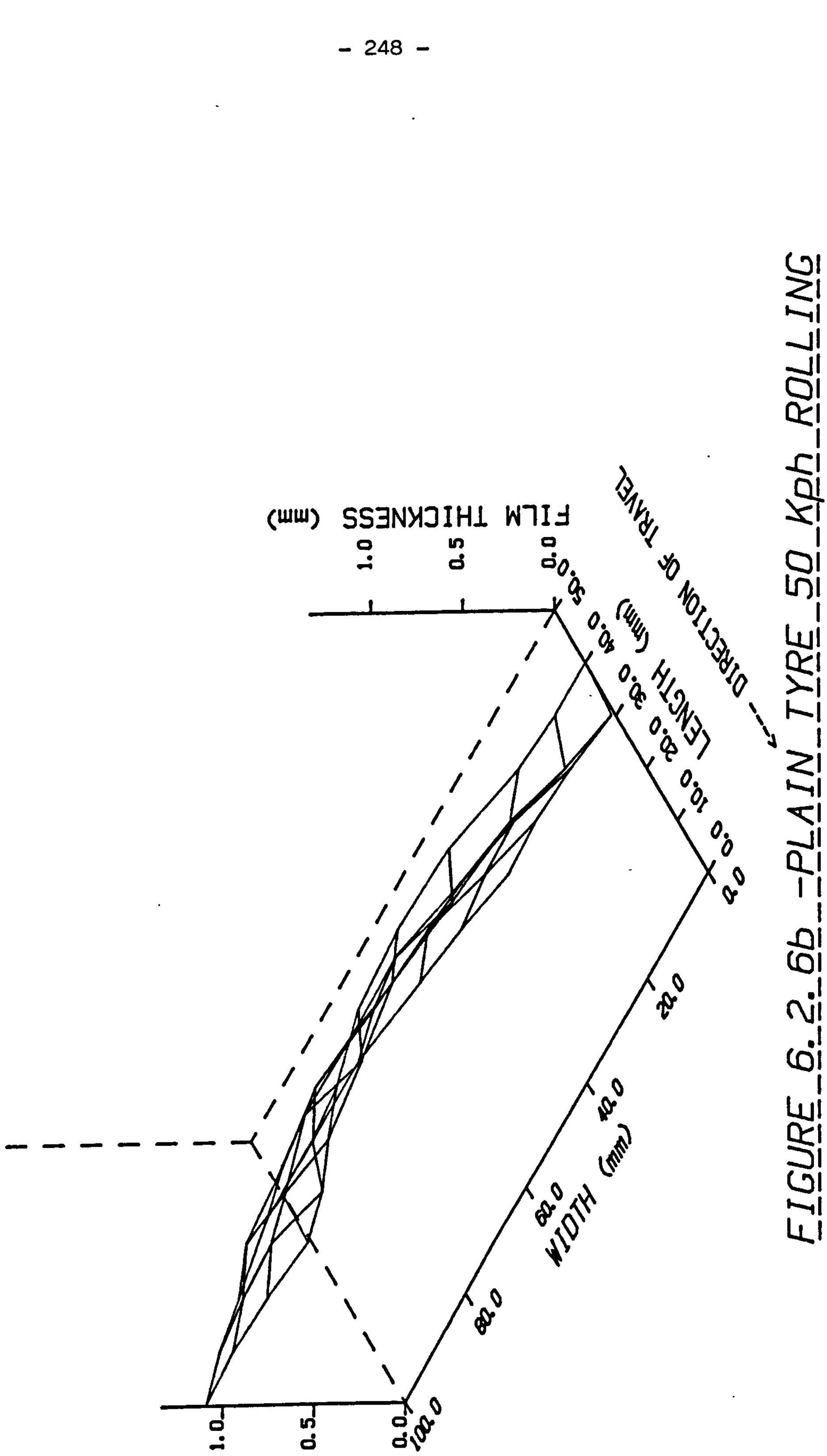

FIGURE 6.2.6b -PLAIN TYRE 50 Kph-ROLLING

FIGURE 6.2.7 = PLAIN TYRE 50 Kph ROLLING

FLOW VELOCITY
5000 mm/s= 2.500mm

<--- DIRECTION OF TRAVEL

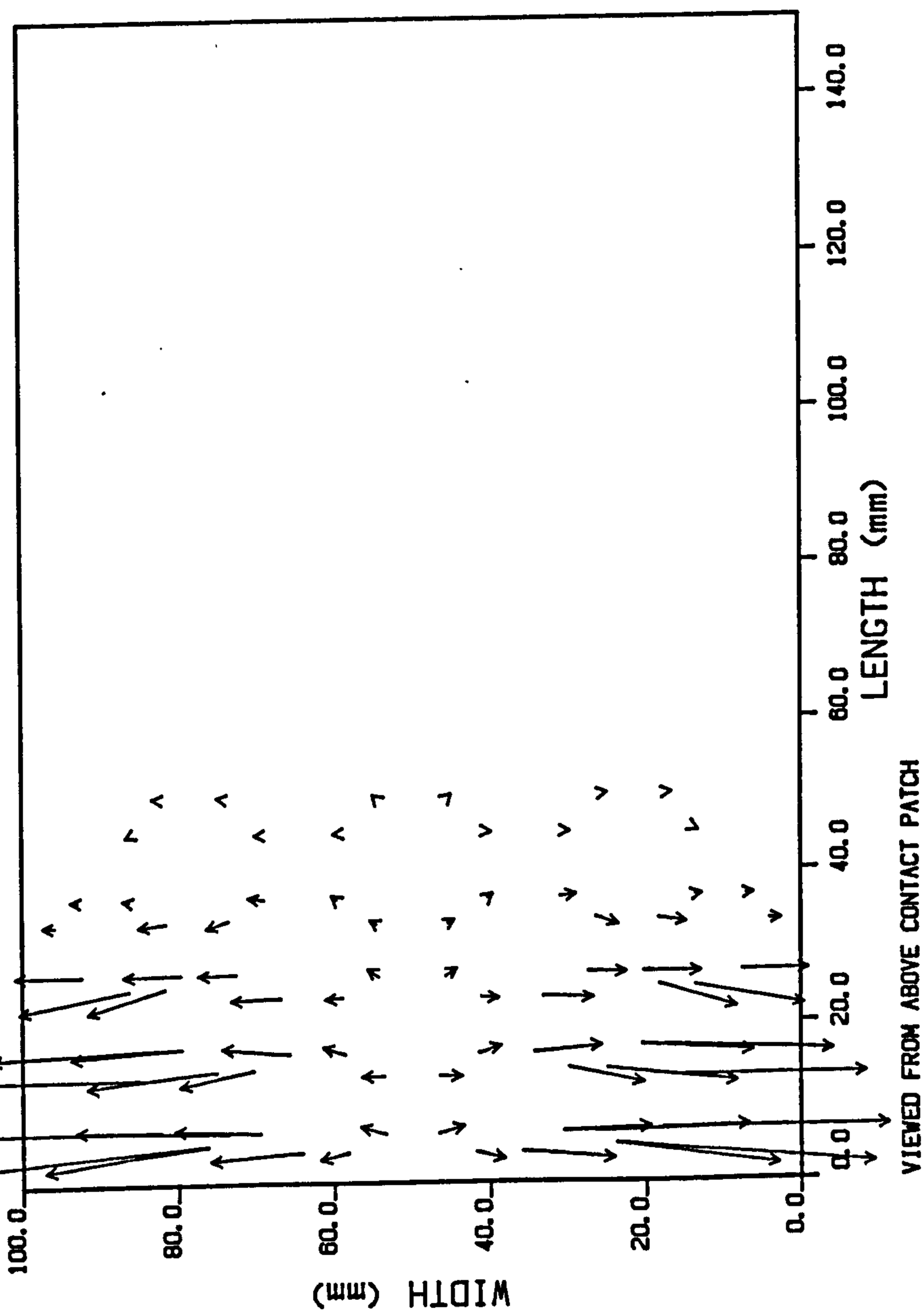

FIGURE 6.2.8 = PLAN VIEW OF CONTACT PATCH

ROLLING <--- DIRECTION OF TRAVEL

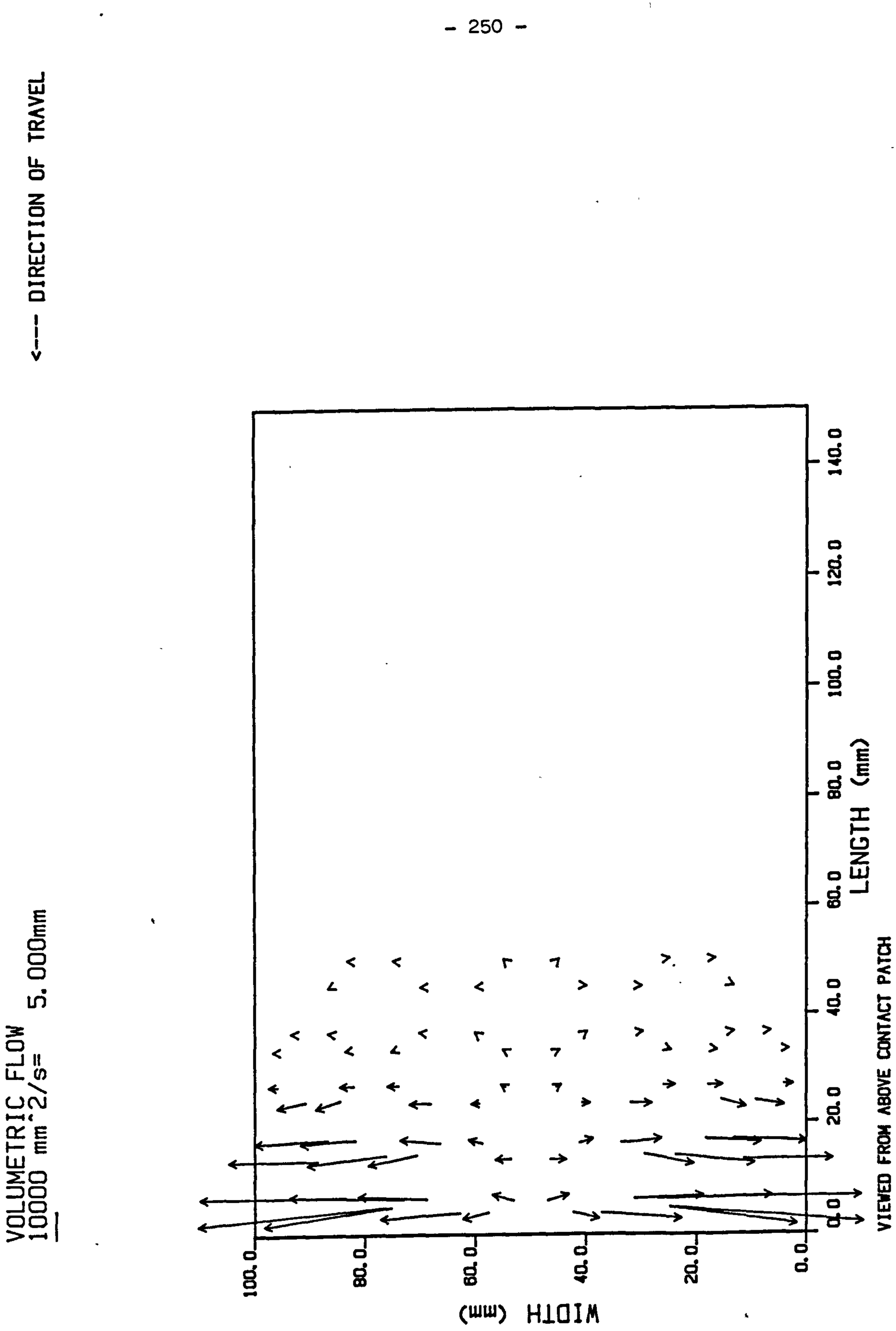

IN TYRE 50 Kph

6.2.2 50 Kph Locked

Figure 6.2.9 shows the individual experimental pressure profiles for the case of 50 Kph with a locked (sliding) tyre. These results are combined to give a three-dimensional plot in figure 6.2.10. The analytically predicted pressure distribution is shown in figure 6.2.11. In this case a fluid film exists over virtually the whole of the contact patch; therefore the pressures shown are fluid pressures. The magnitude of this theoretical fluid film thickness in the main part of the contact patch is shown in figure 6.2.12a and in the front of the contact patch in figure 6.2.12b.

There are no experimental values of fluid film thickness for this case, but as in the previous case their values are known to be less than approximately 0.2 mm. There was however, the additional problem of the tyre surface polishing whilst the film thickness measurements were being made.

The calculated distributions of fluid flow velocity and volumetric flow per unit width are shown in figures 6.2.13 and 6.2.14 respectively. Figure 6.2.13 shows a small area towards the rear of the shoulders where there is tyre/road contact (no flow velocities).

6.2.3 100 Kph Free Rolling

The individual experimental pressure profiles for 100 Kph with a free rolling tyre are shown in figure 6.2.15. These results are combined into a three-dimensional plot in figure 6.2.16. The pressure distribution produced by the computer program is shown in figure 6.2.17. As with the case of 50 Kph free rolling there is a significant area of the tyre which is in contact with the road surface: the rear most part of each of the shoulders. The pressures in this area are therefore derived from the loading on the contact patch and not fluid pressures. The fluid film thickness predicted by the computer program is shown in figures 6.2.18a and 6.2.18b and the above areas of tyre/road contact can be seen.

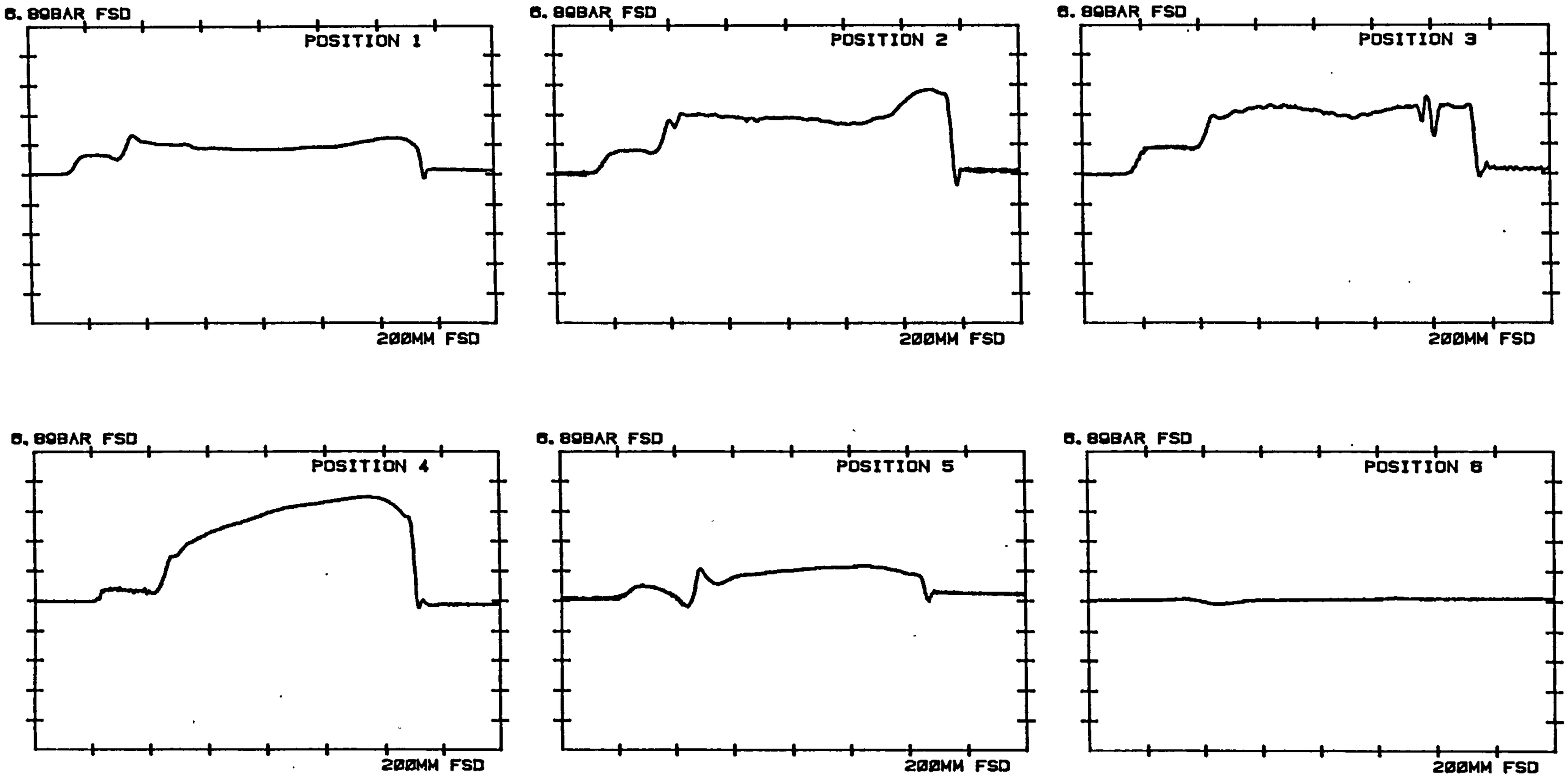

FIGURE 6.2.9 - EXPERIMENTAL FLUID PRESSURES -

PLAIN TYRE 50 KPH LOCKED

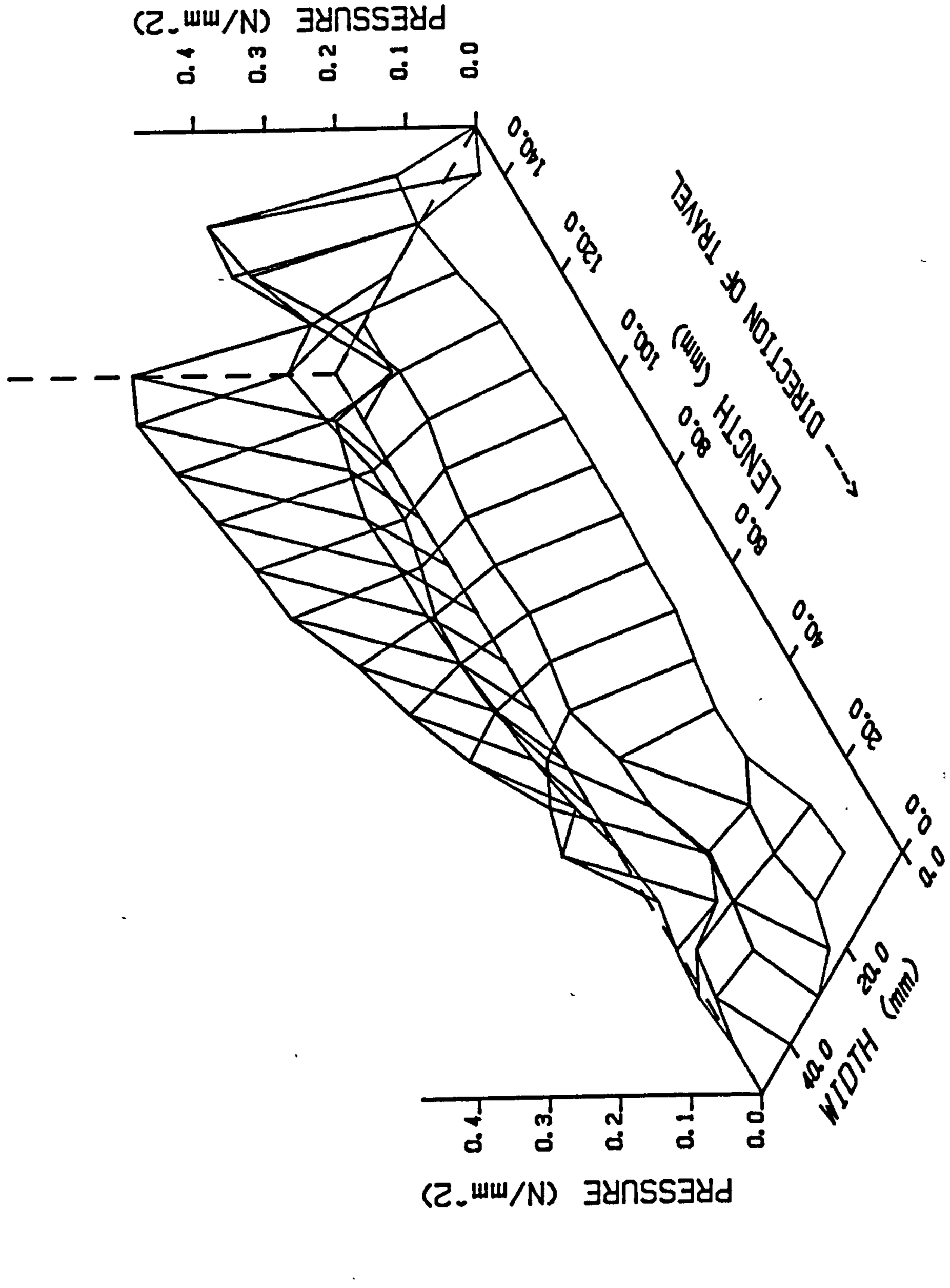

FIGURE 6.2.10 - PLAIN TYRE 50 KPH LOCKED (EXPERIMENTAL)

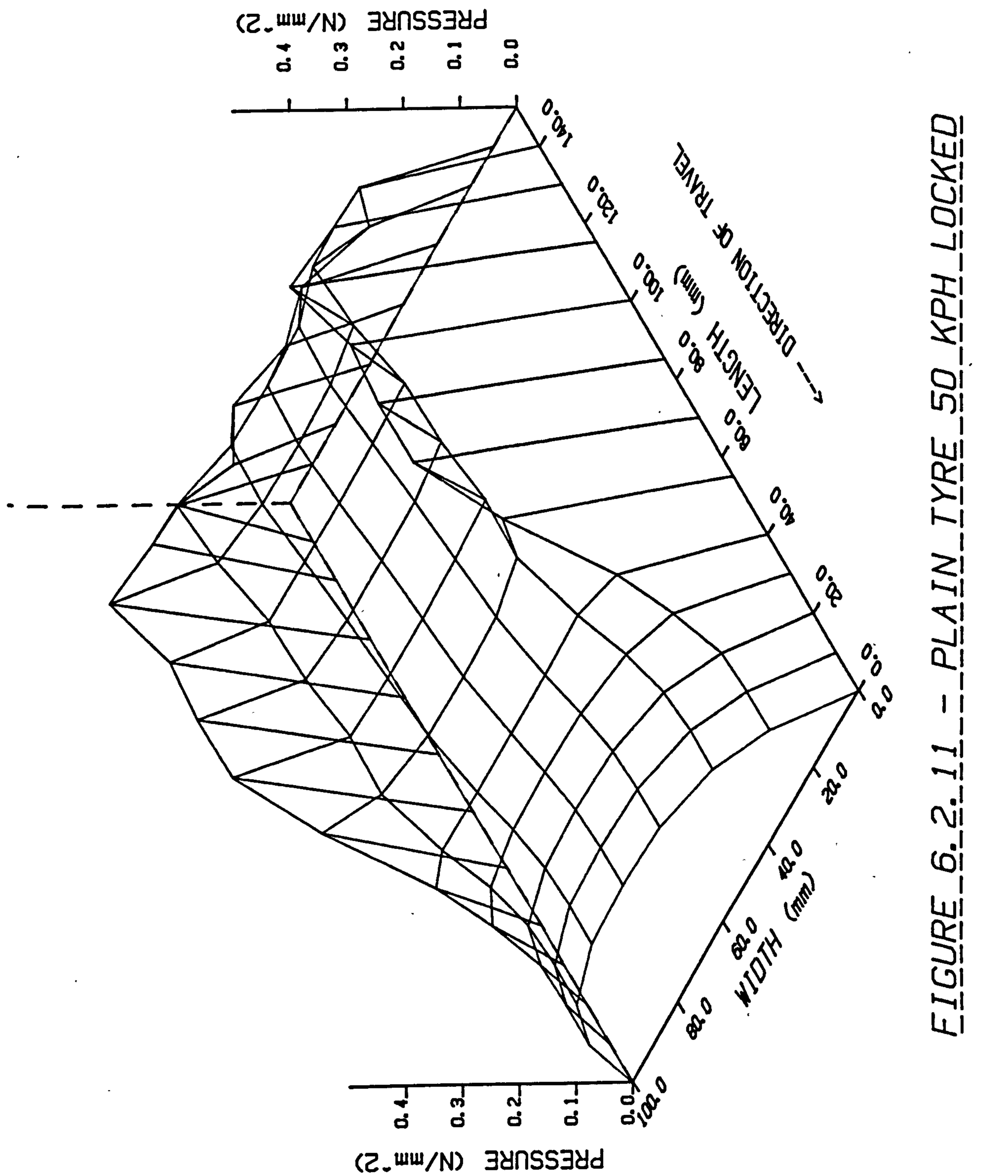

FIGURE 6.2.11 – PLAIN TYRE 50 KPH LOCKED

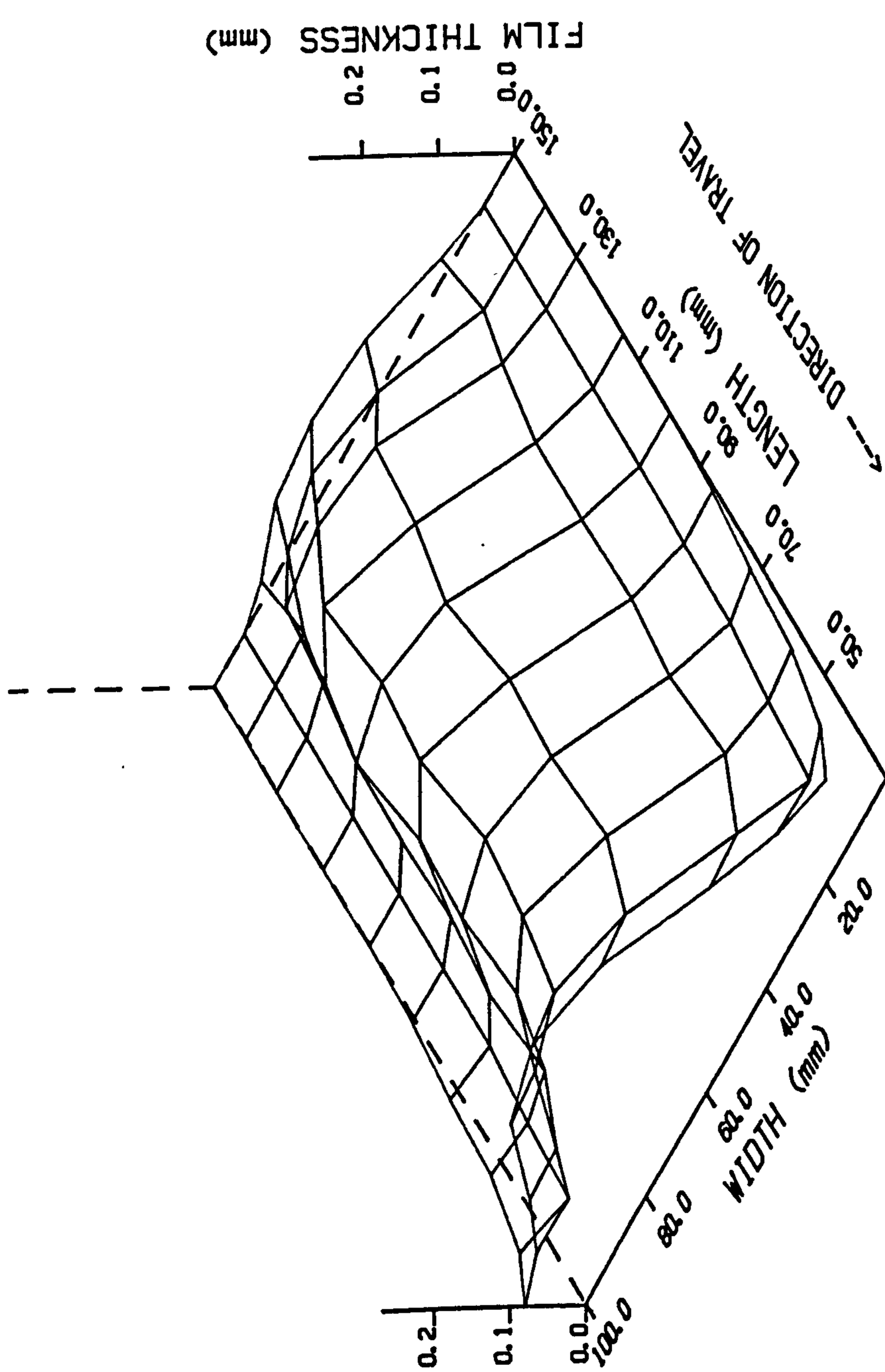

FIGURE 6.2.12a -PLAIN TYRE 50 KPH LOCKED

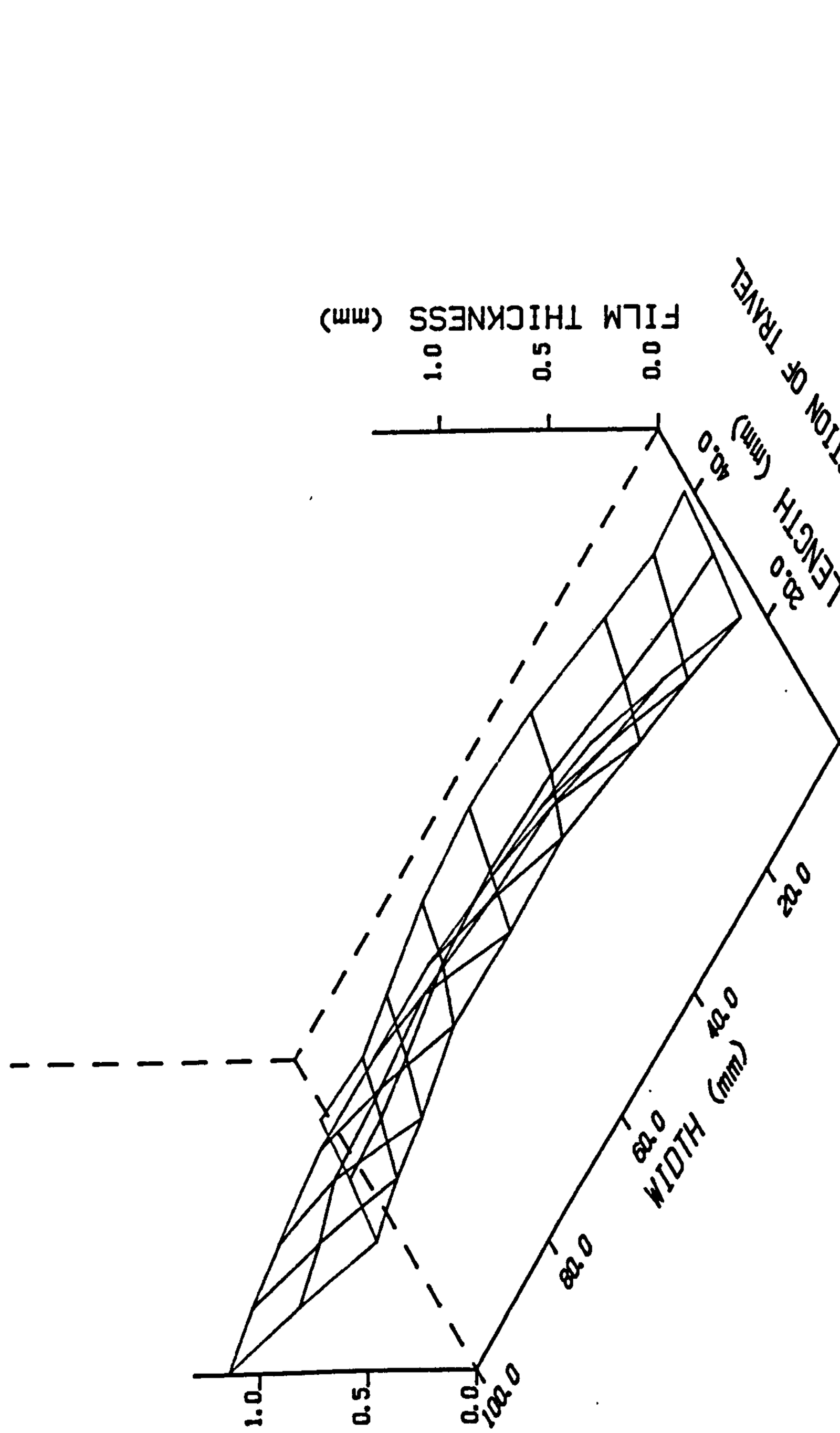

FIGURE 6.2.12b -PLAIN TYRE 50 KPH LOCKED

FIGURE 6.2.13 - PLAIN TYRE 50 KPH LOCKED

FLOW VELOCITY
5000 mm/s= 2.500mm

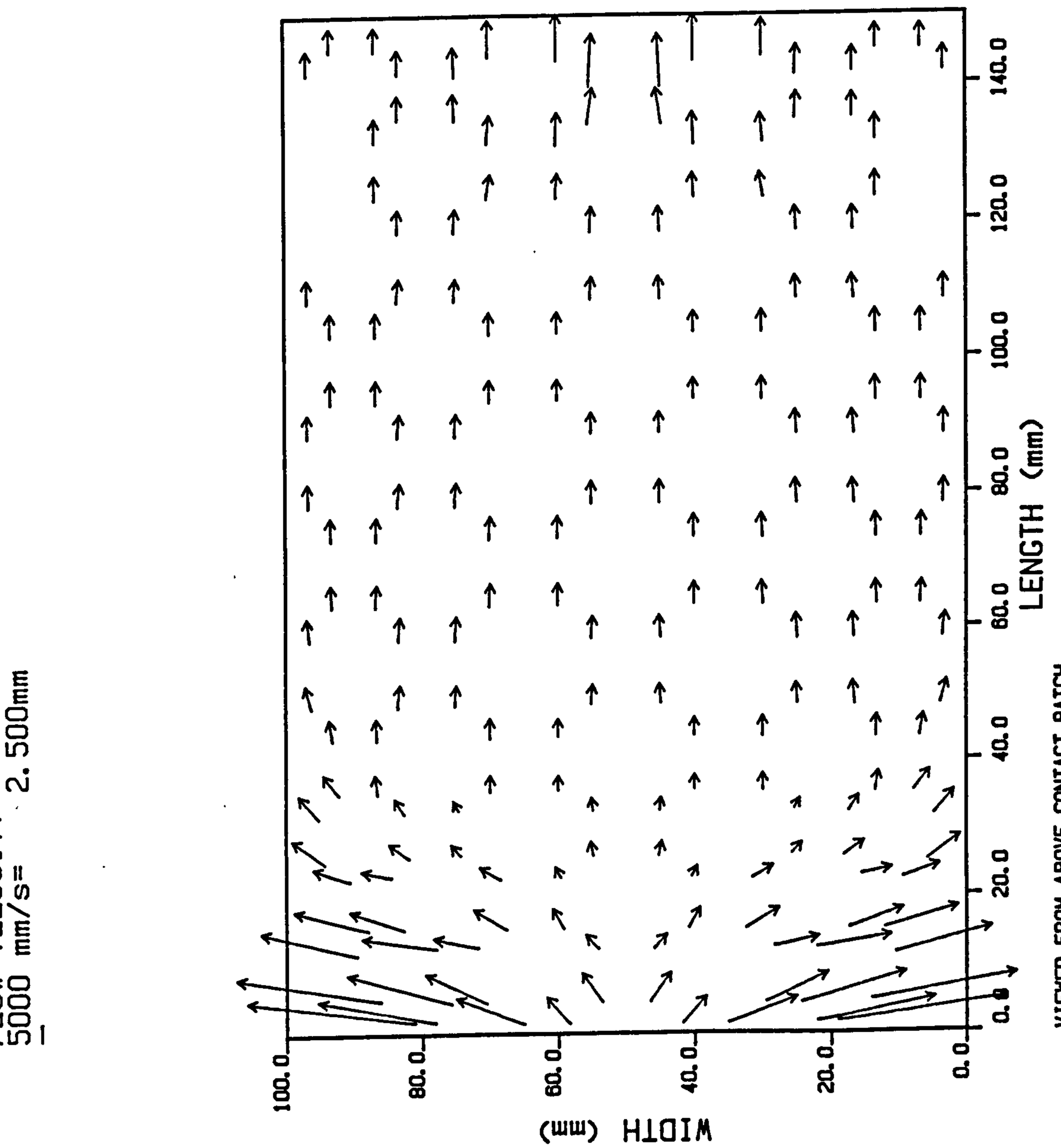

FIGURE 6.2.14 - PLAN VIEW OF FLOW IN TYRE 50 KPH LOCKED

VOLUMETRIC FLOW
10000 mm^2/s= 5.000mm

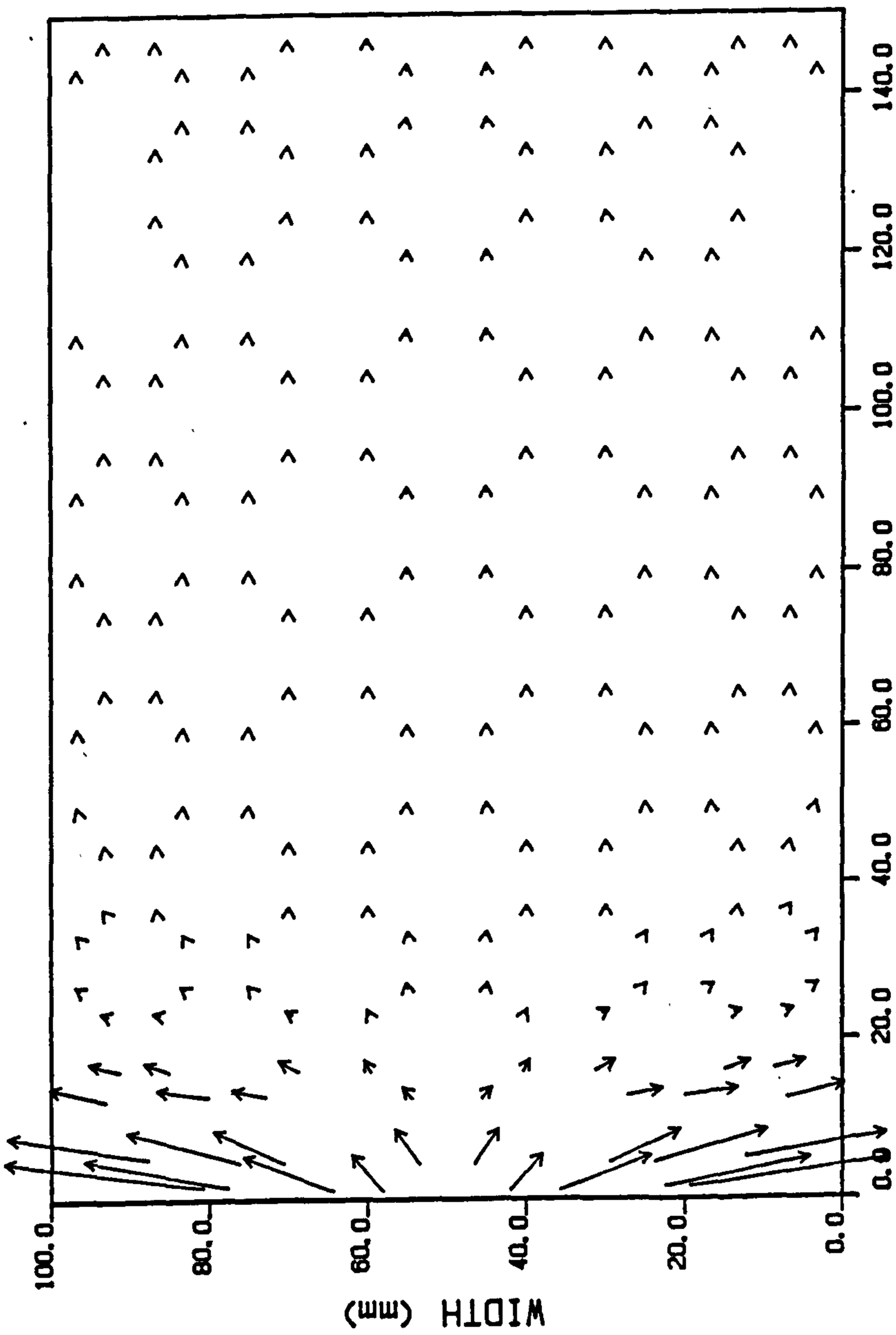

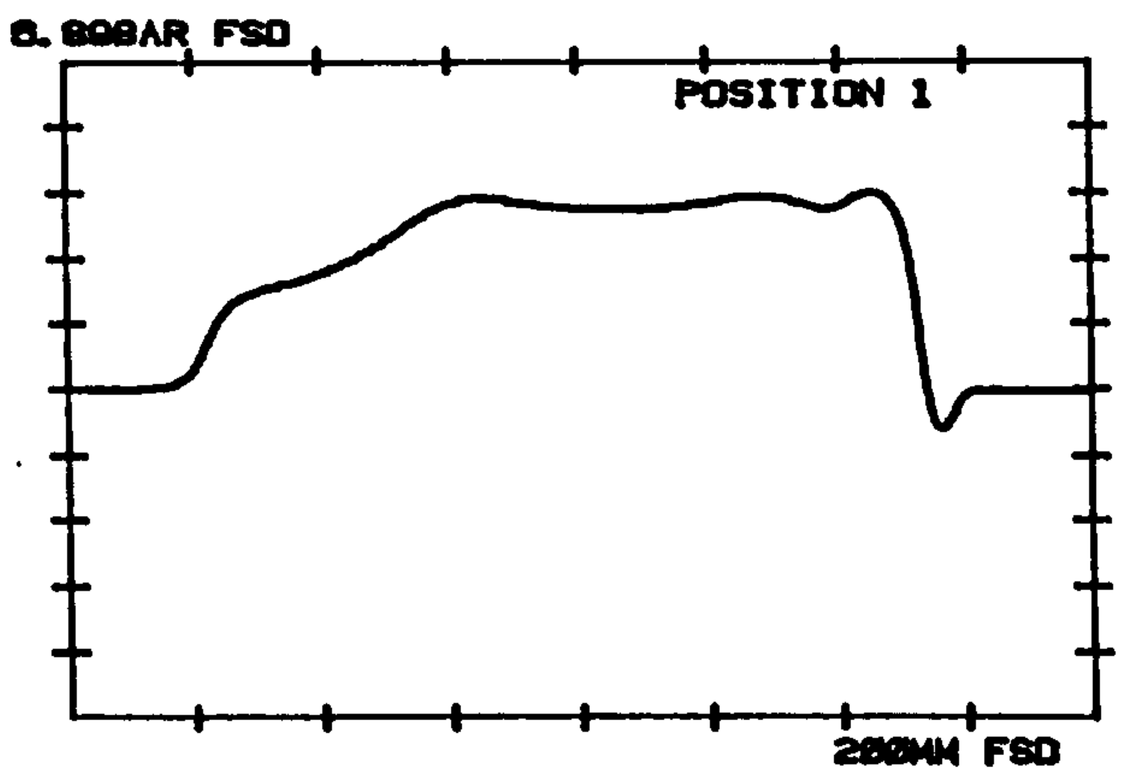

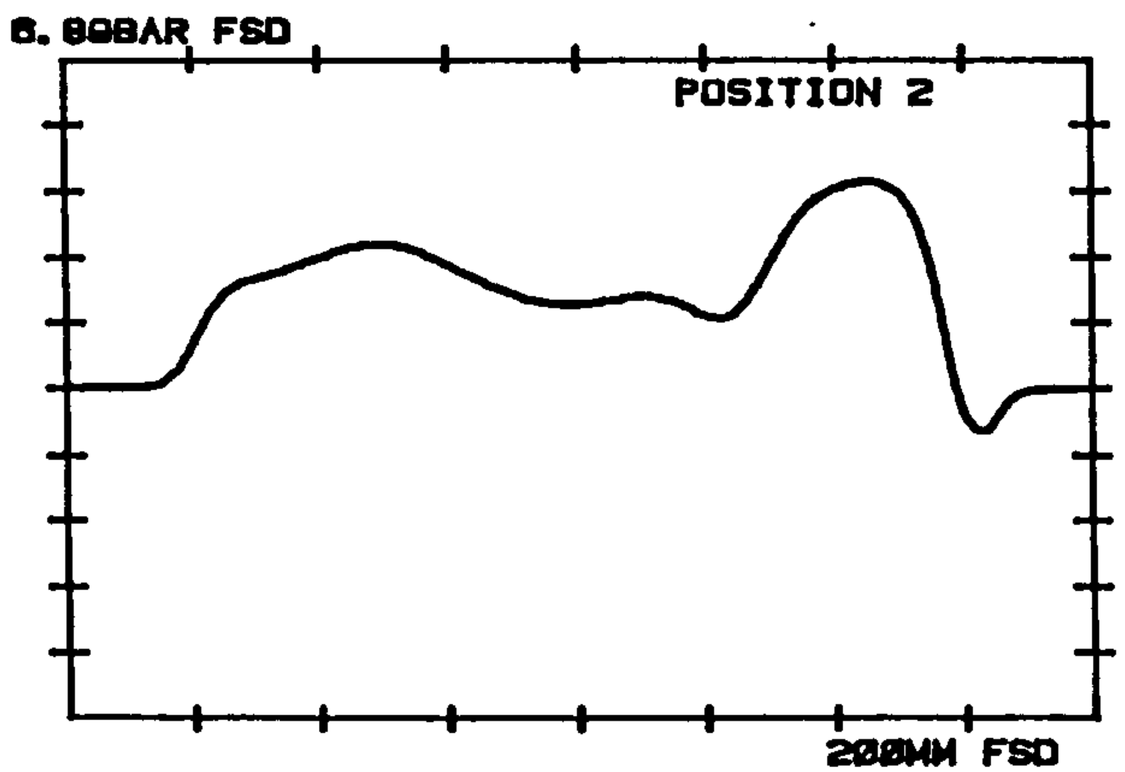

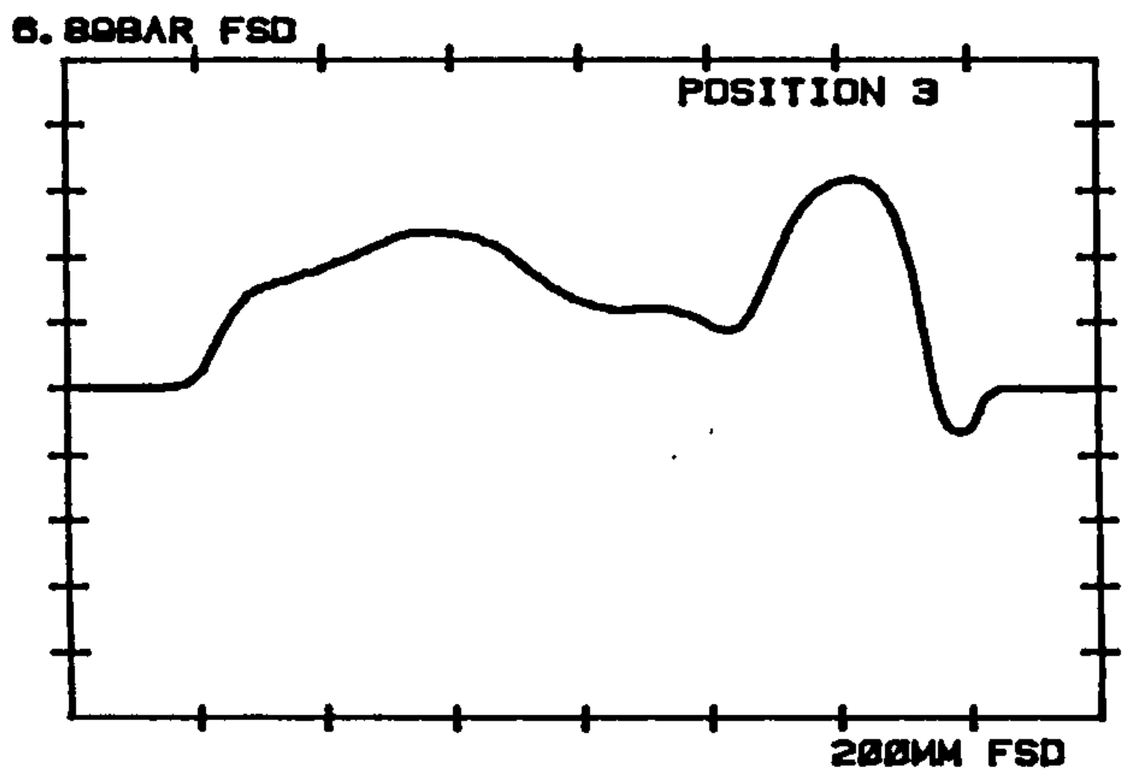

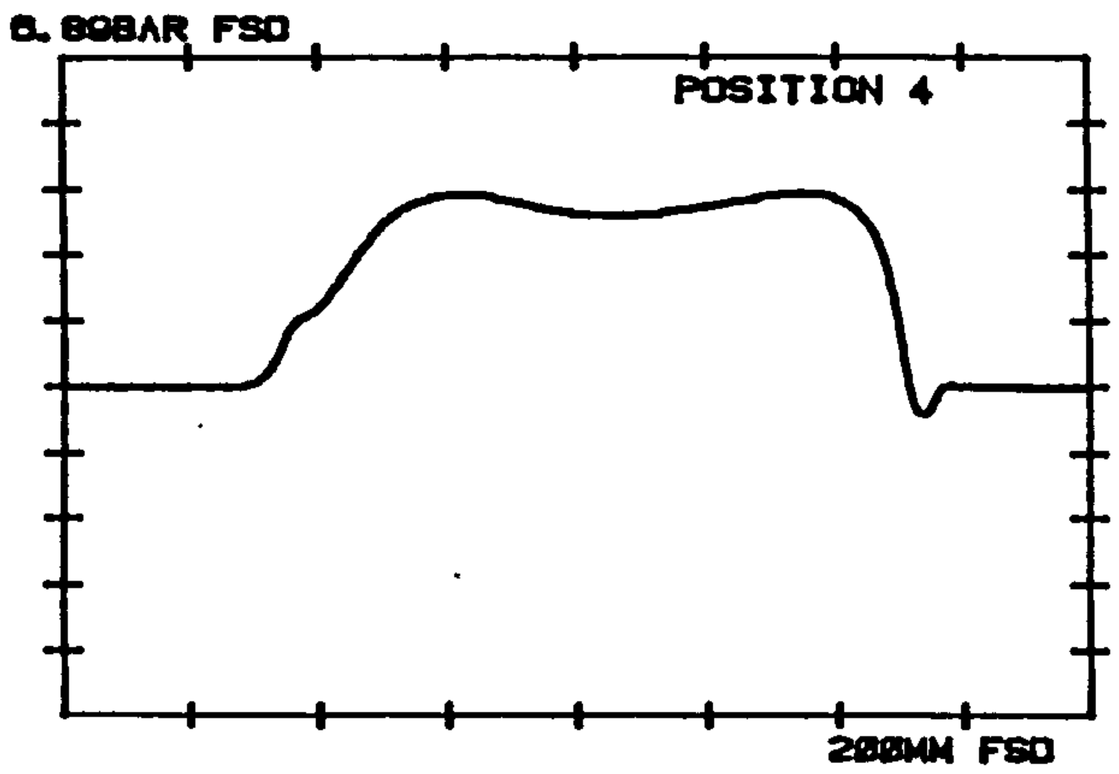

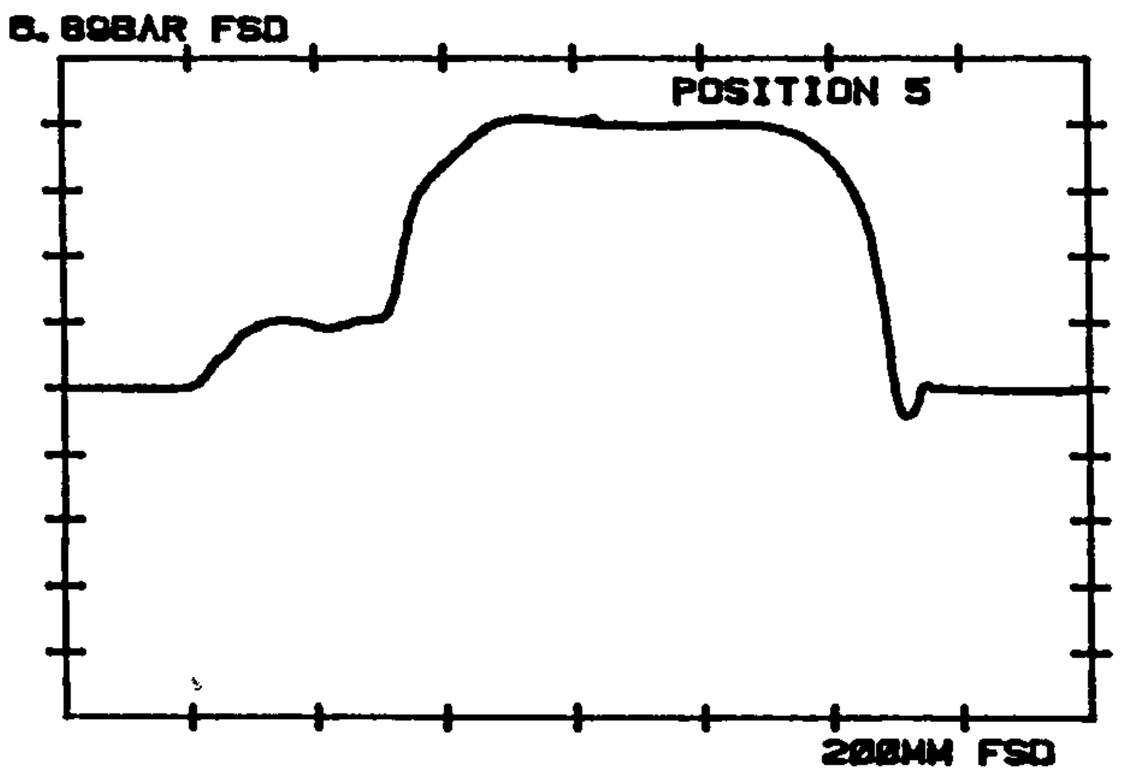

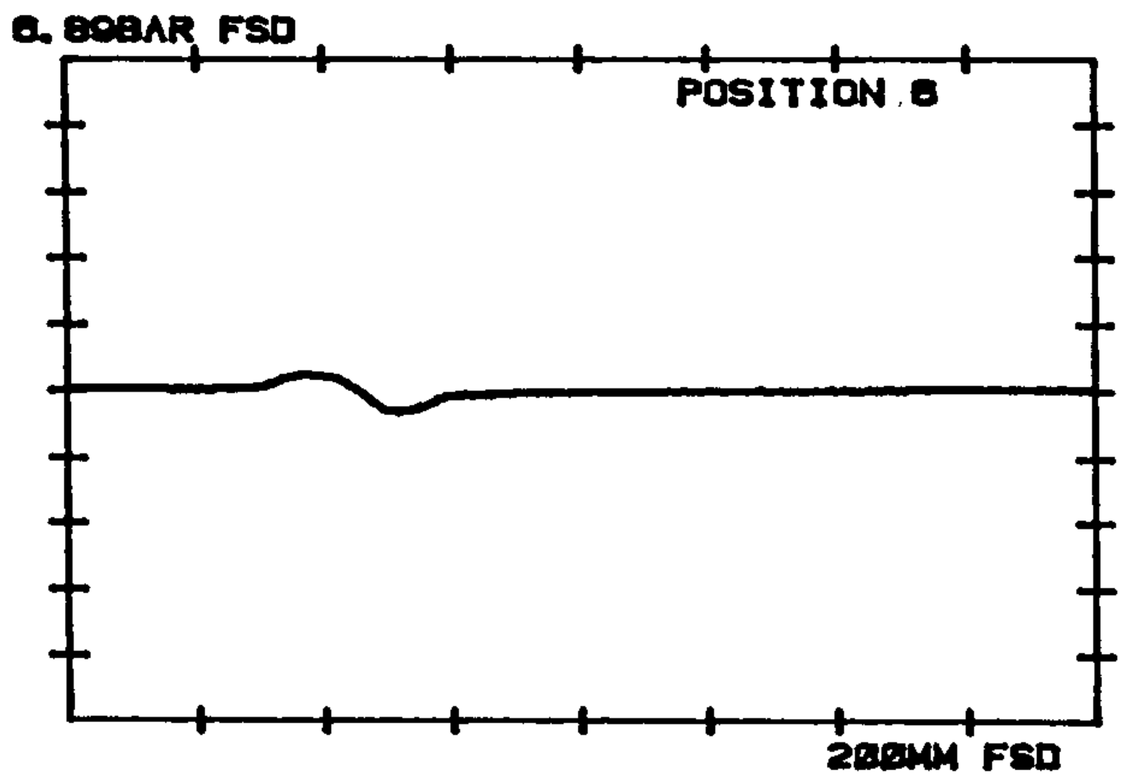

FIGURE 6.2.15 - EXPERIMENTAL FLUID PRESSURES -

PLAIN TYRE 100 KPH ROLLING

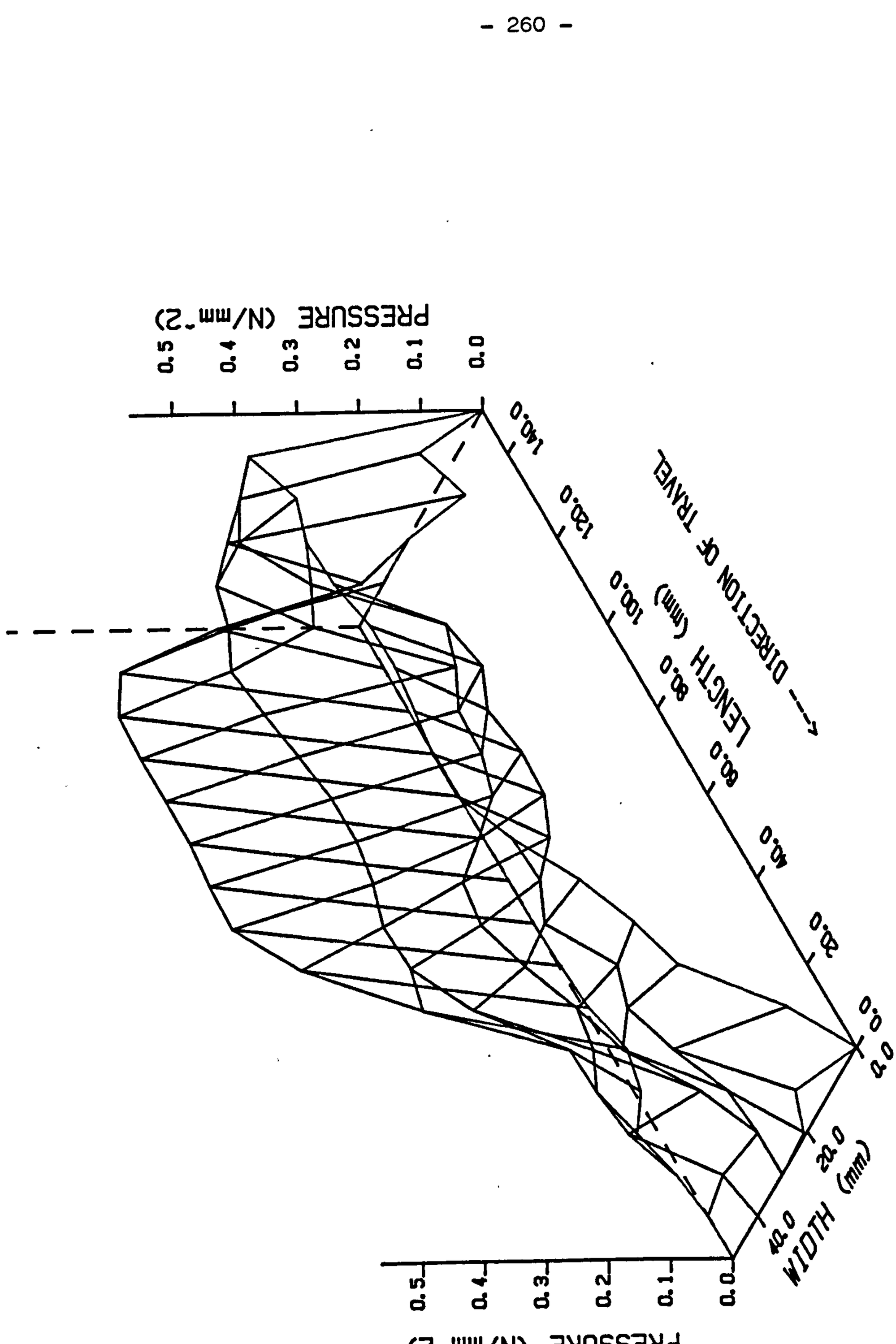

FIG 6.2.16 – PLAIN TYRE 100 KPH ROLLING (EXPERIMENTAL)

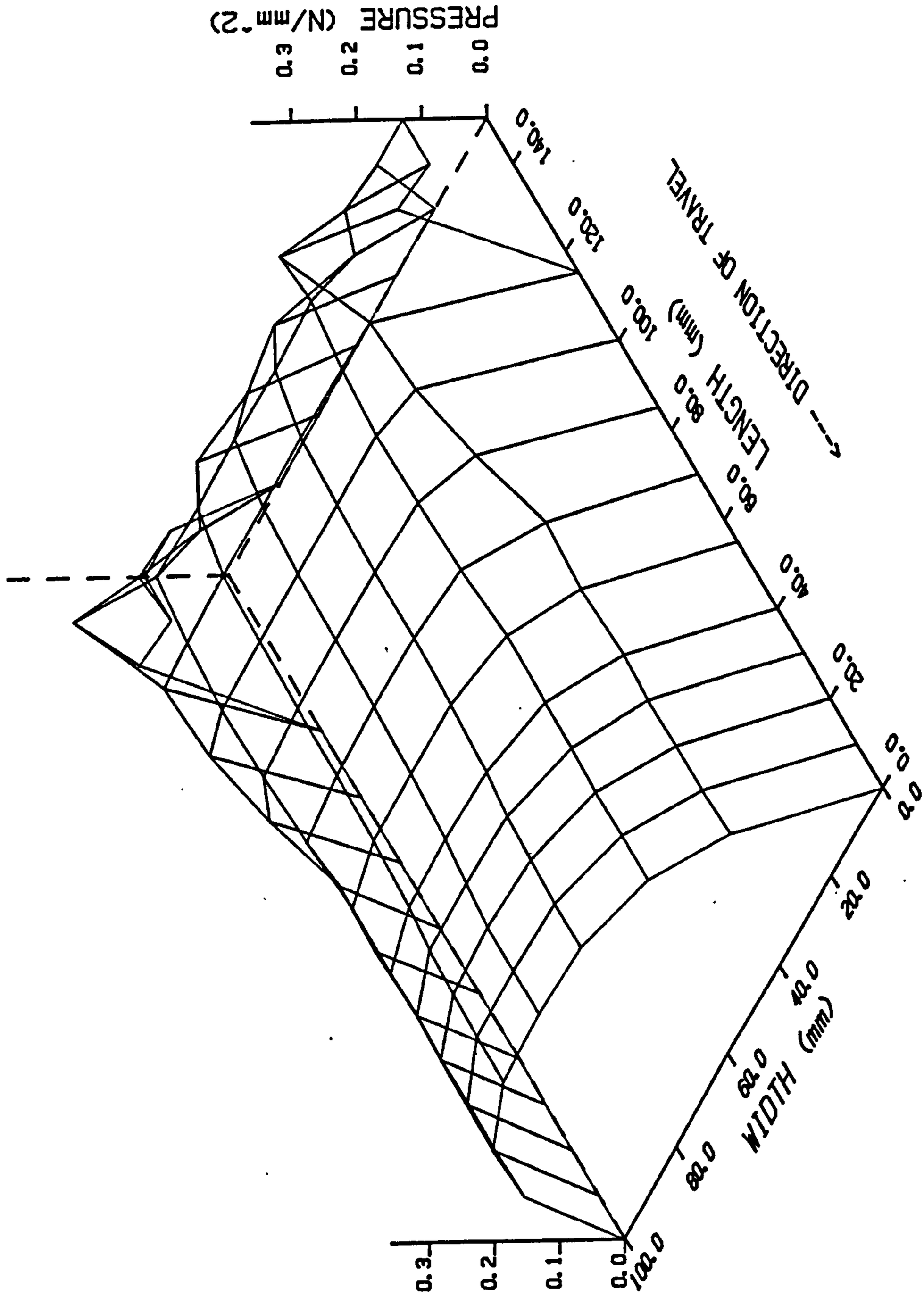

FIG 6.2.17 – PLAIN TYRE 100 KPH ROLLING

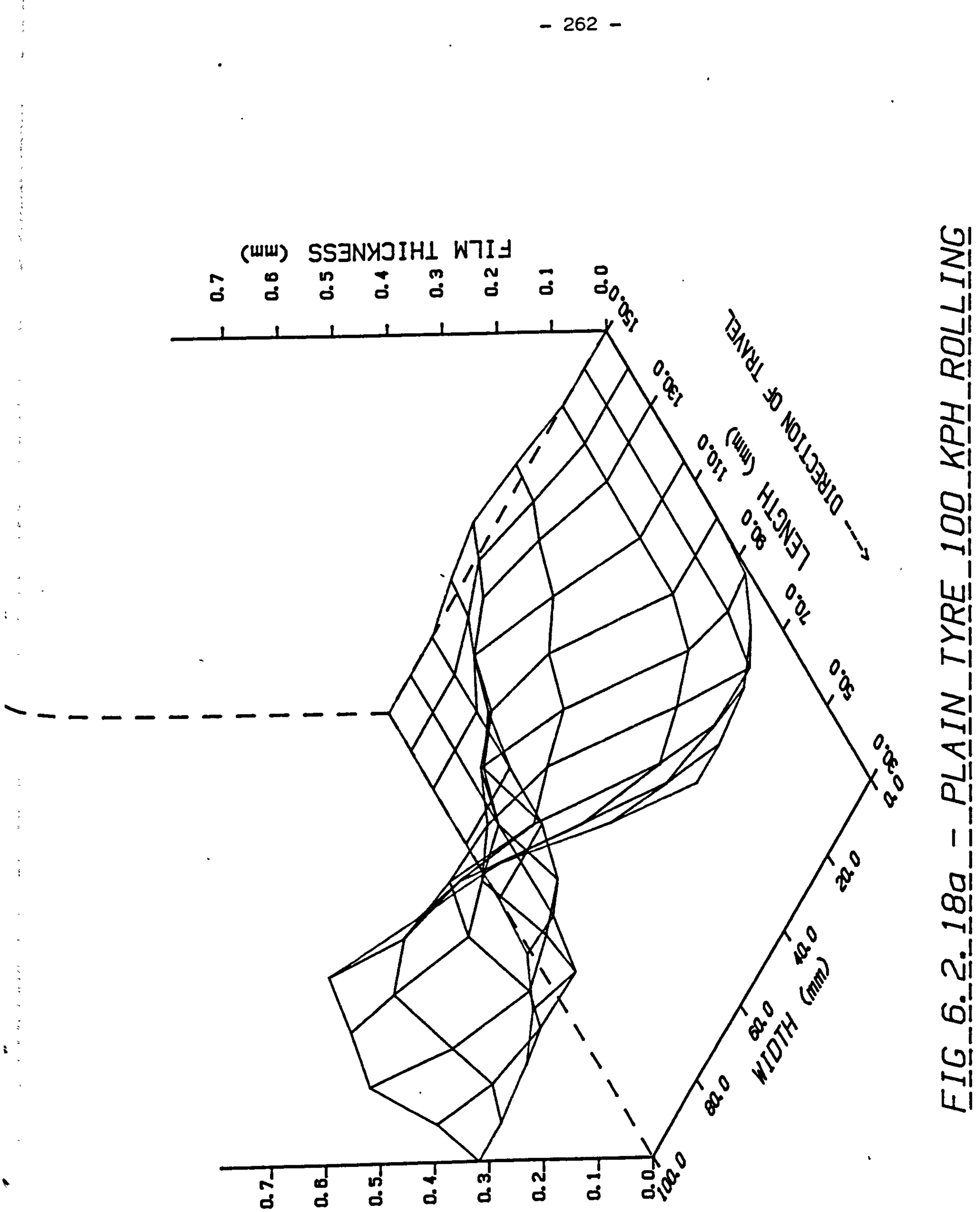

FIG 6.2.18a - PLAIN TYRE 100 KPH ROLLING

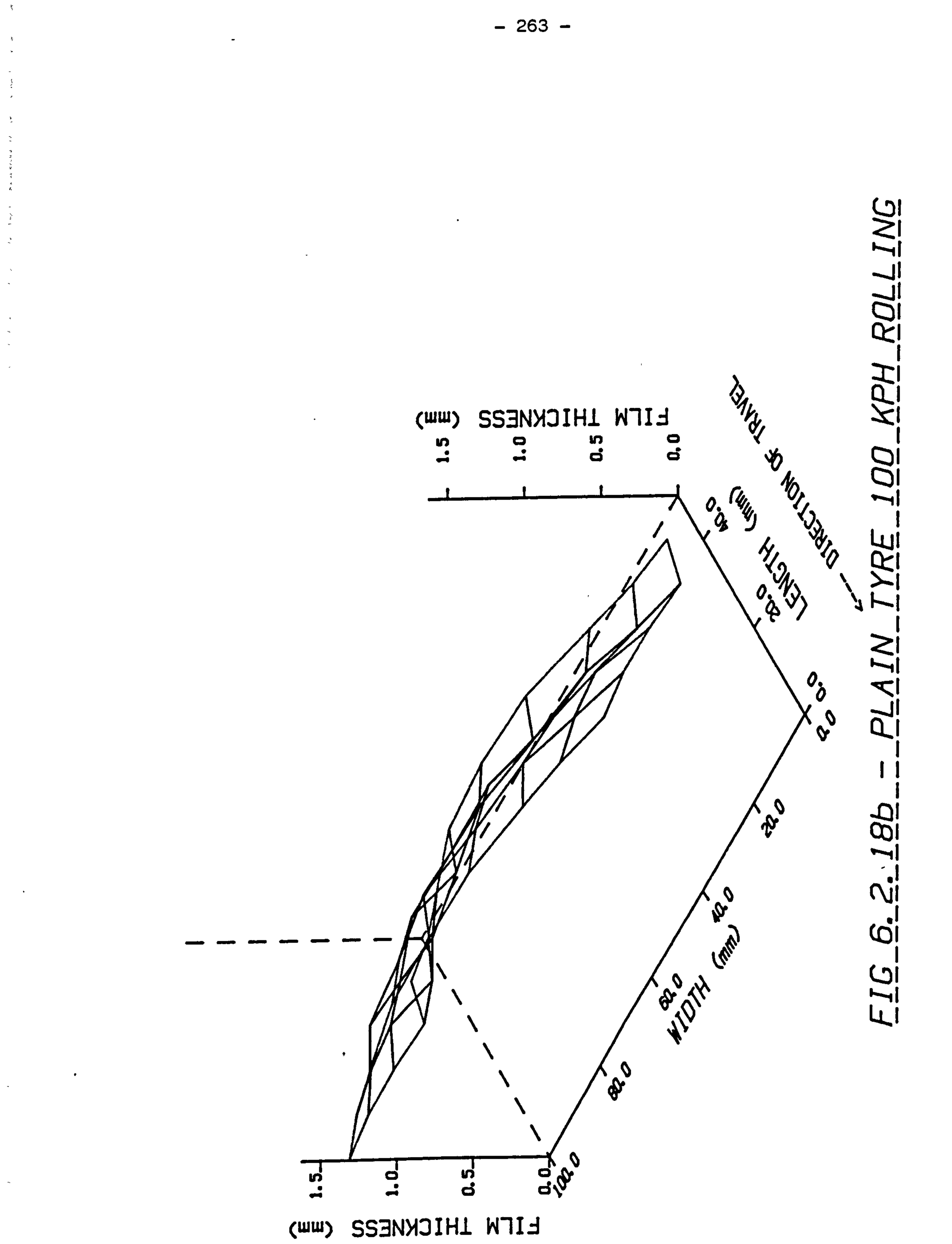

FIG 6.2.18b - PLAIN TYRE 100 KPH

The experimentally measured fluid film thicknesses are shown in figure 6.2.19. The reference positions are the same as those used for the pressure measurements. The magnitudes of these film thicknesses are different from those predicted by the computer program and this is discussed in section 6.6.

The fluid flow velocities and volumetric flows per unit width are shown in figures 6.2.20 and 6.2.21.

6.2.4 100 Kph Locked

The individual experimental pressure profiles for the case of 100 Kph with a locked (sliding) tyre are shown in figure 6.2.22. For this case, experimental pressure values are only available at positions 1, 3 and 5. This was due to a problem with the instrumentation when these measurements were made. The pressure at position 6 (the edge of the contact patch) is in all cases almost atmospheric at all points; therefore no useful information is lost by its omission. In producing the three-dimensional plot of the experimental pressures (figure 6.2.23) the pressure values for the case of 100 Kph free rolling were used for position 6. Suggested explanations for the sharp dip in the measured pressure at the centre of the contact patch are given in section 6.6.

The fluid pressures predicted by the computer program are shown in figure 6.2.24 and the corresponding film thicknesses in figures 6.2.25a and 6.2.25b. In this case there is a water film between the tyre and road at all points within the contact patch. The fluid flow velocities and the volumetric flows per unit width are shown in figures 6.2.26 and 6.2.27 respectively.

6.3 RESULTS FOR THE GROOVED TYRE

The grooved tyre which was used for this work was identical in construction and size to the plain tread tyre, but had two 5 mm wide by 8 mm deep grooves hand cut circumferentially. The position of these grooves can be seen from the contact print, figure 6.1.2.

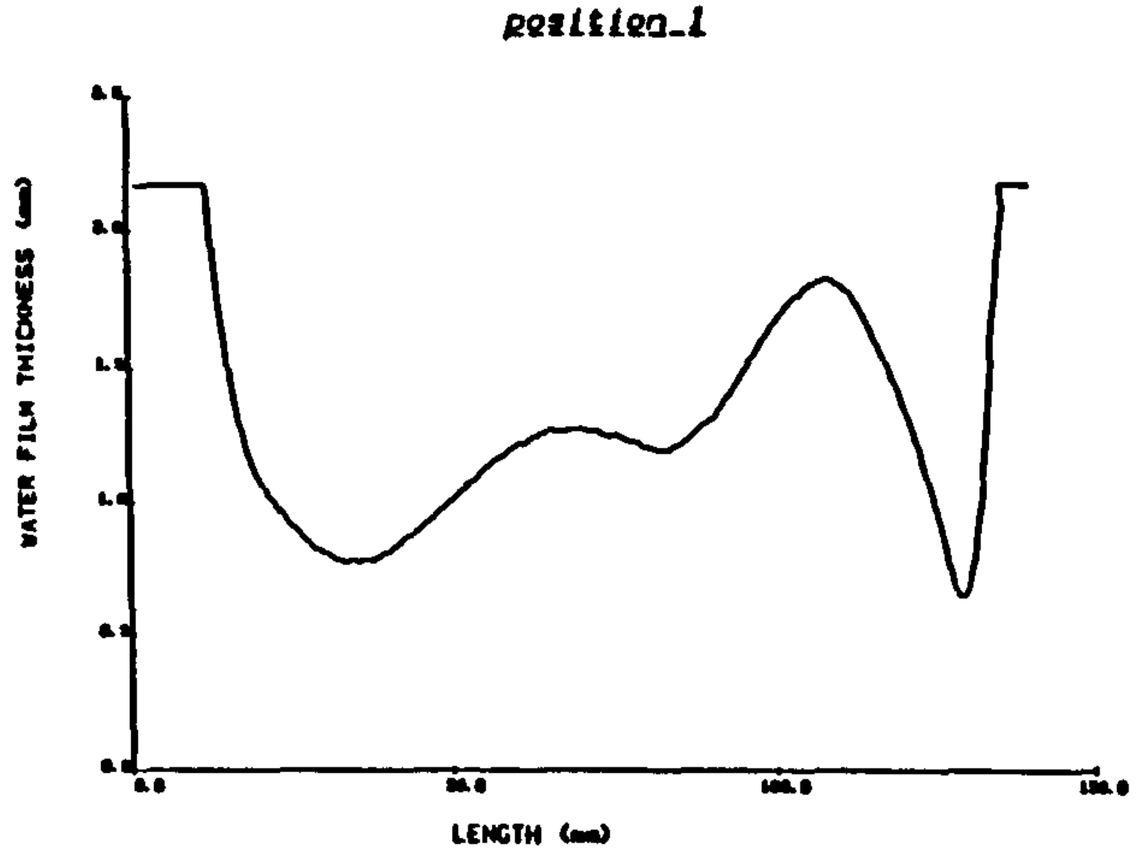

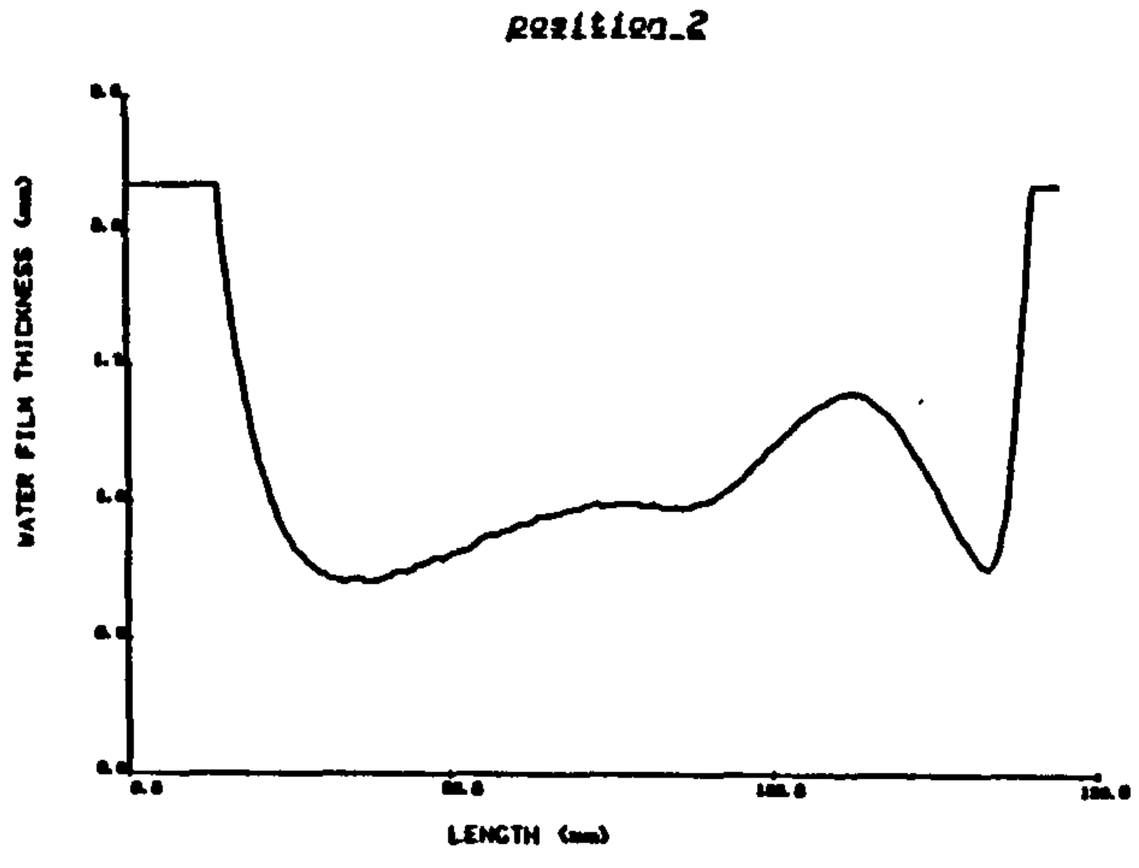

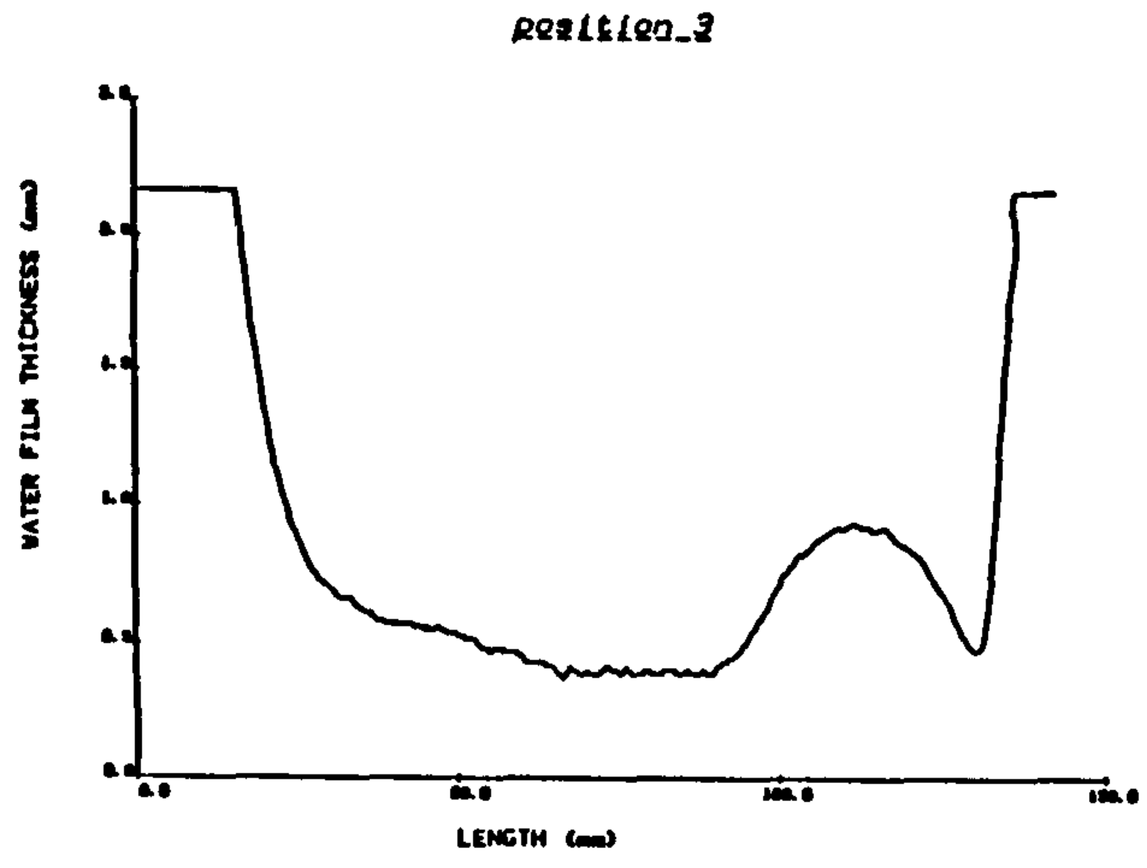

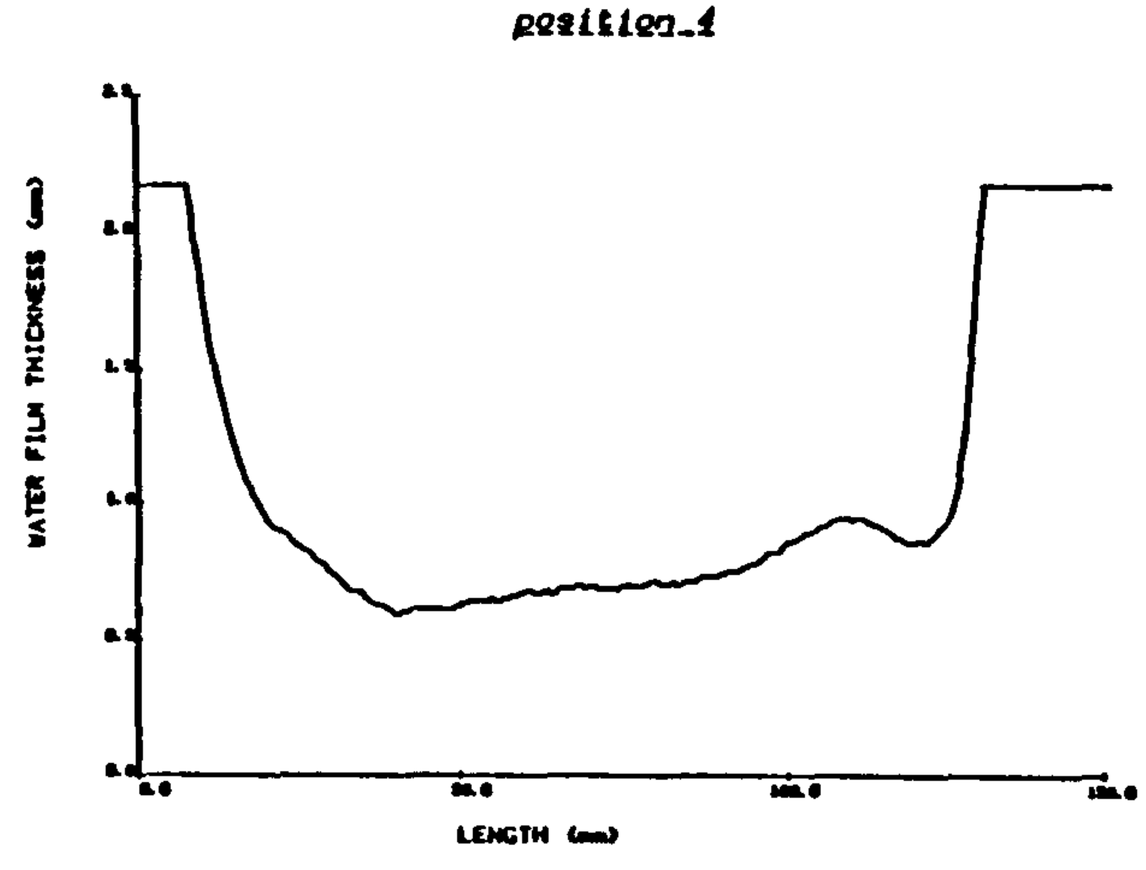

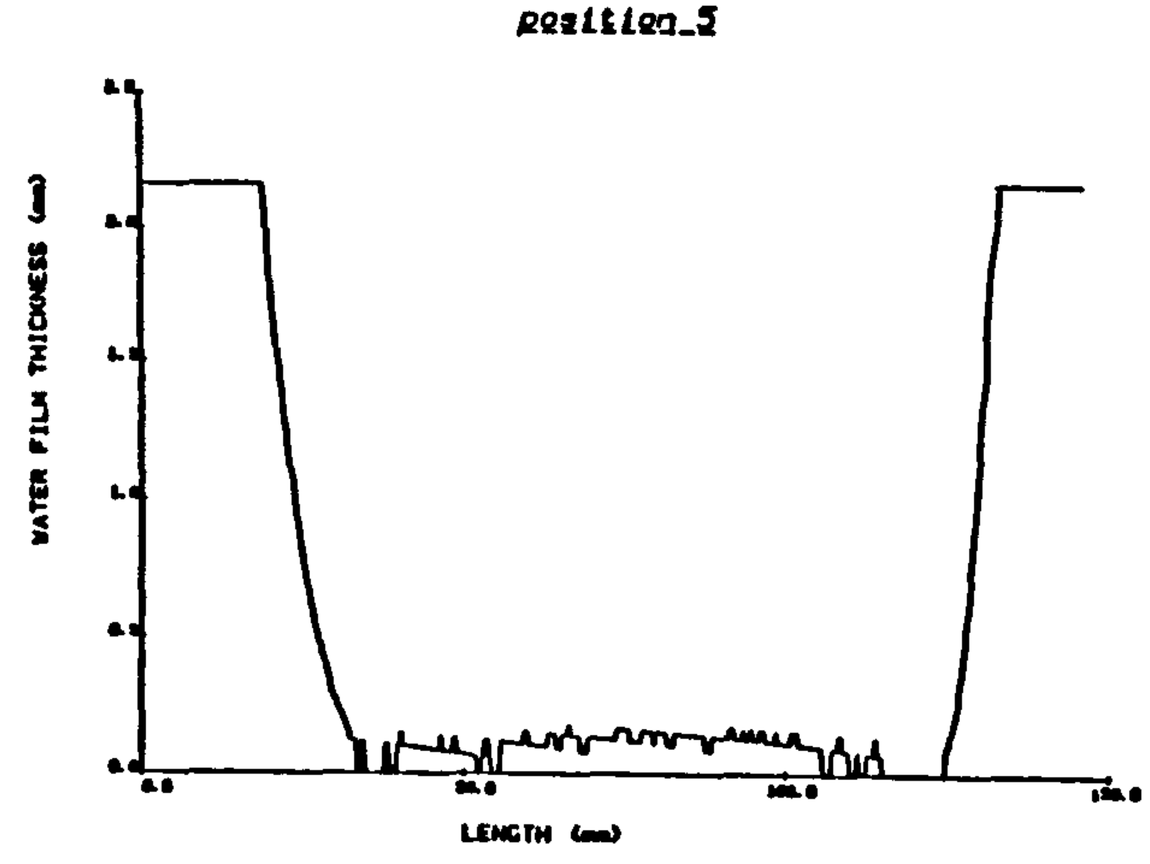

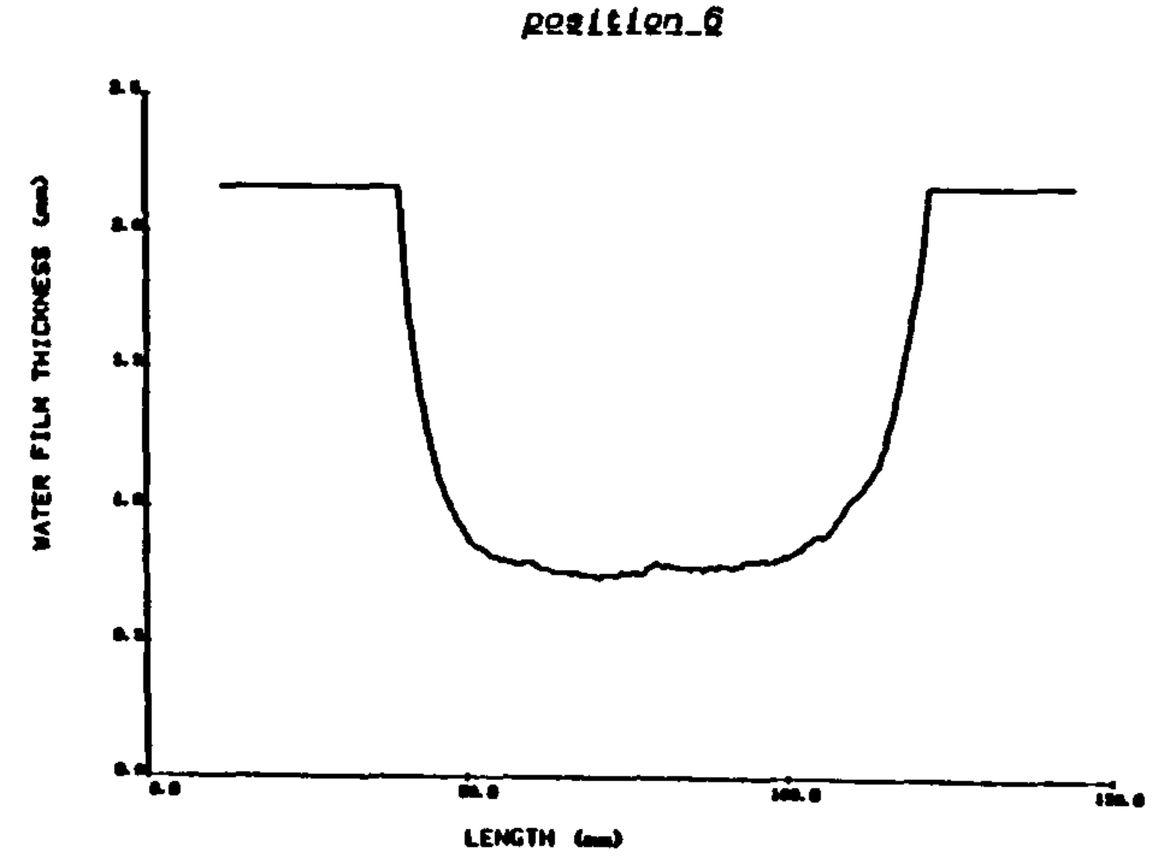

FIGURE 6.2.19 - EXPERIMENTAL FLUID FILM THICKNESSES - PLAIN TYRE 100 KPH ROLLING

FIG 6.2.20 - PLAIN TYRE 100 KPH ROLLING

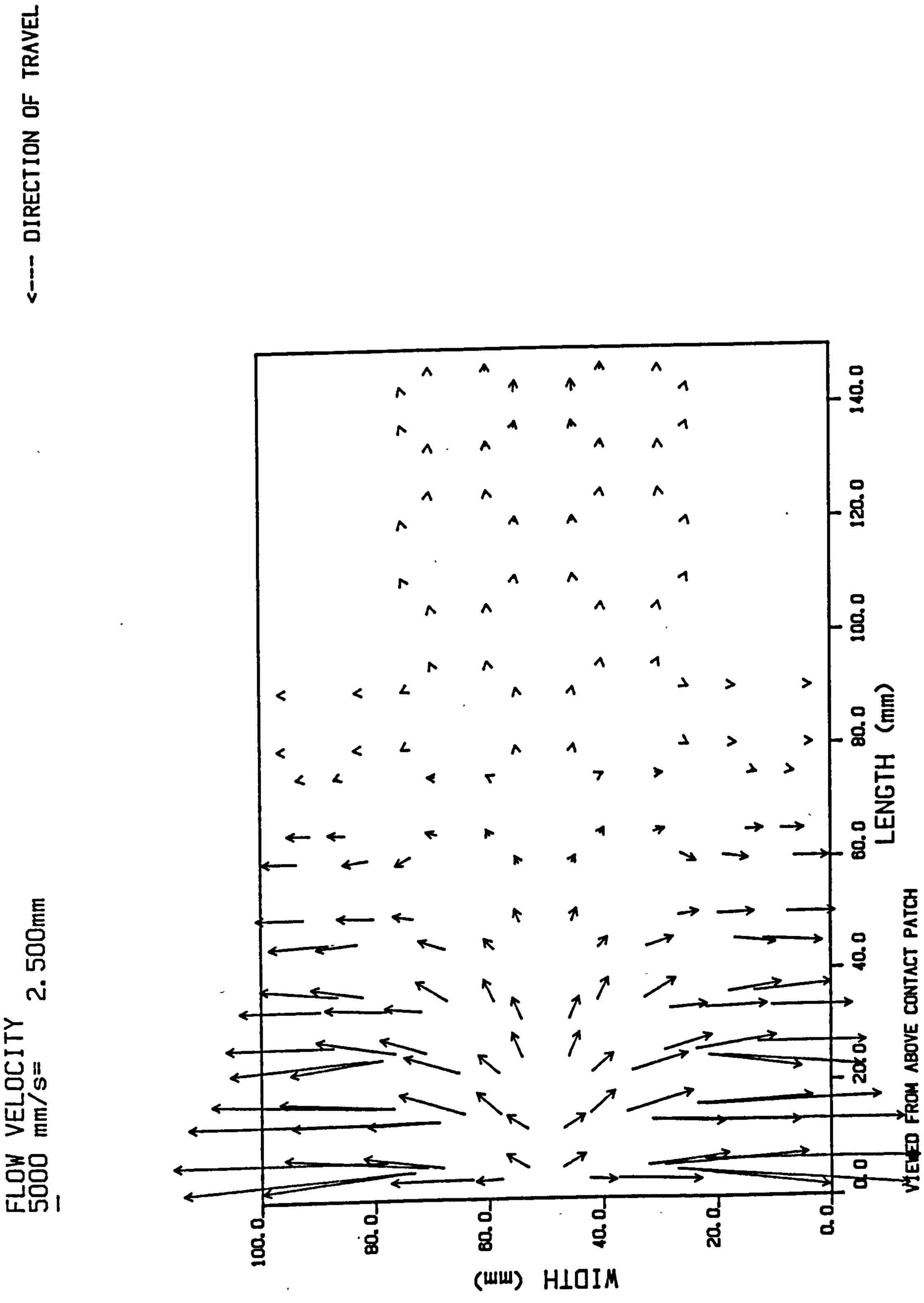

FIG_6.2.21 - PLAIN_TYRE_100_KPH_ROLLING

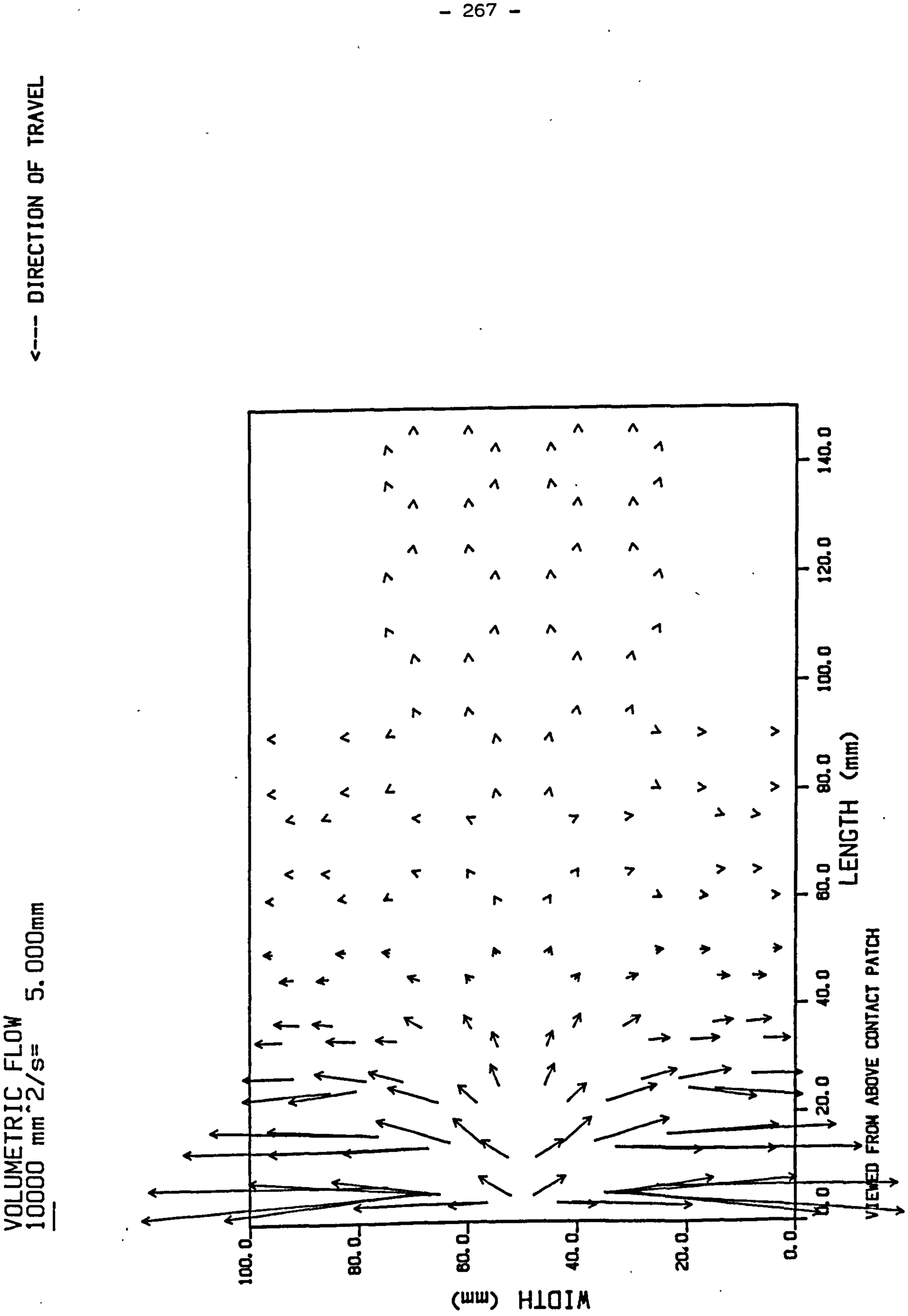

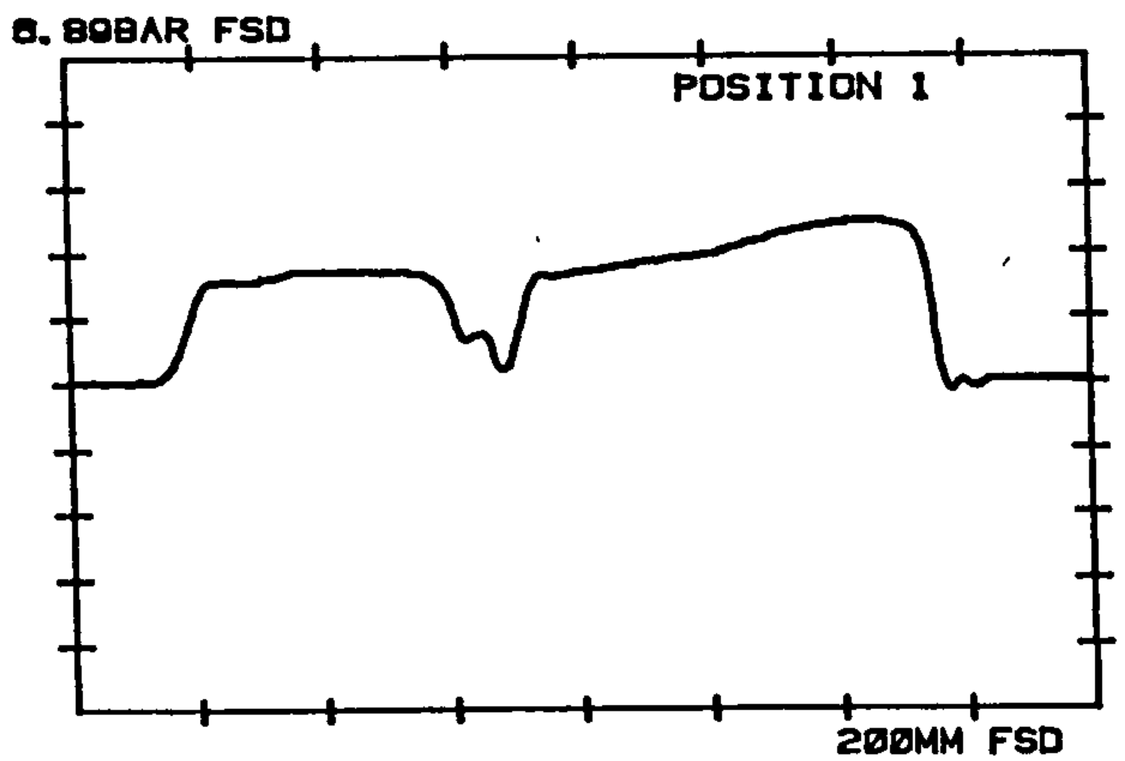

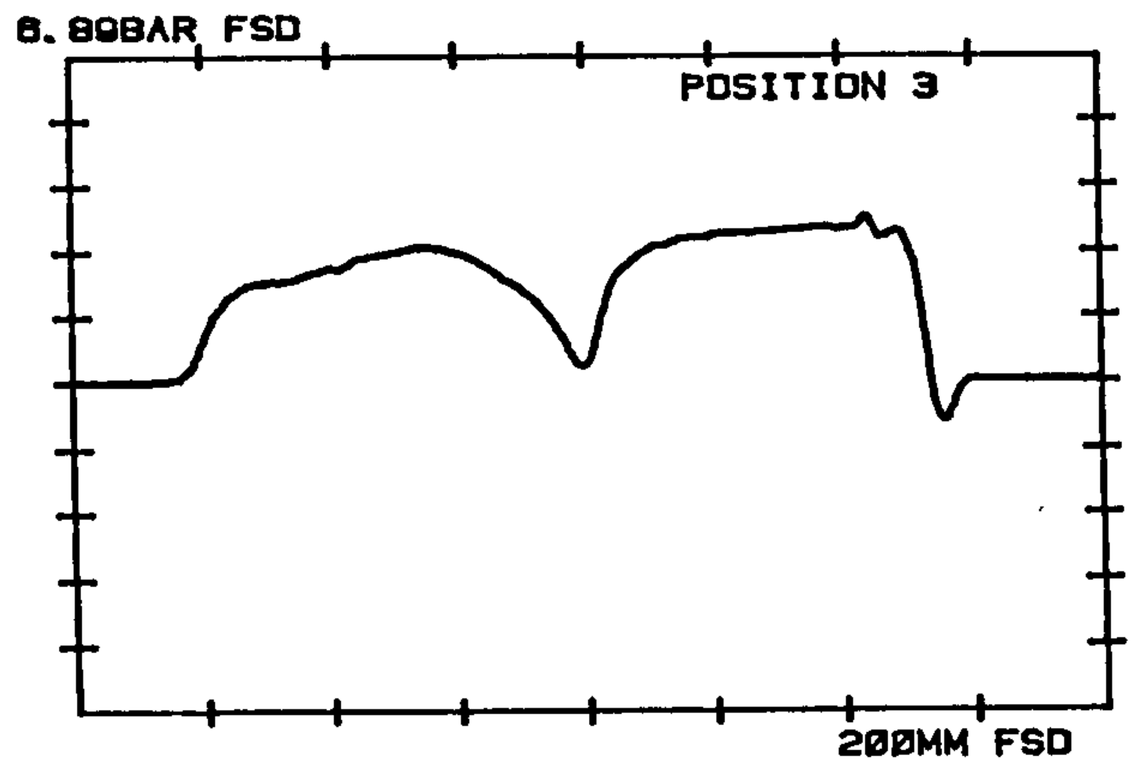

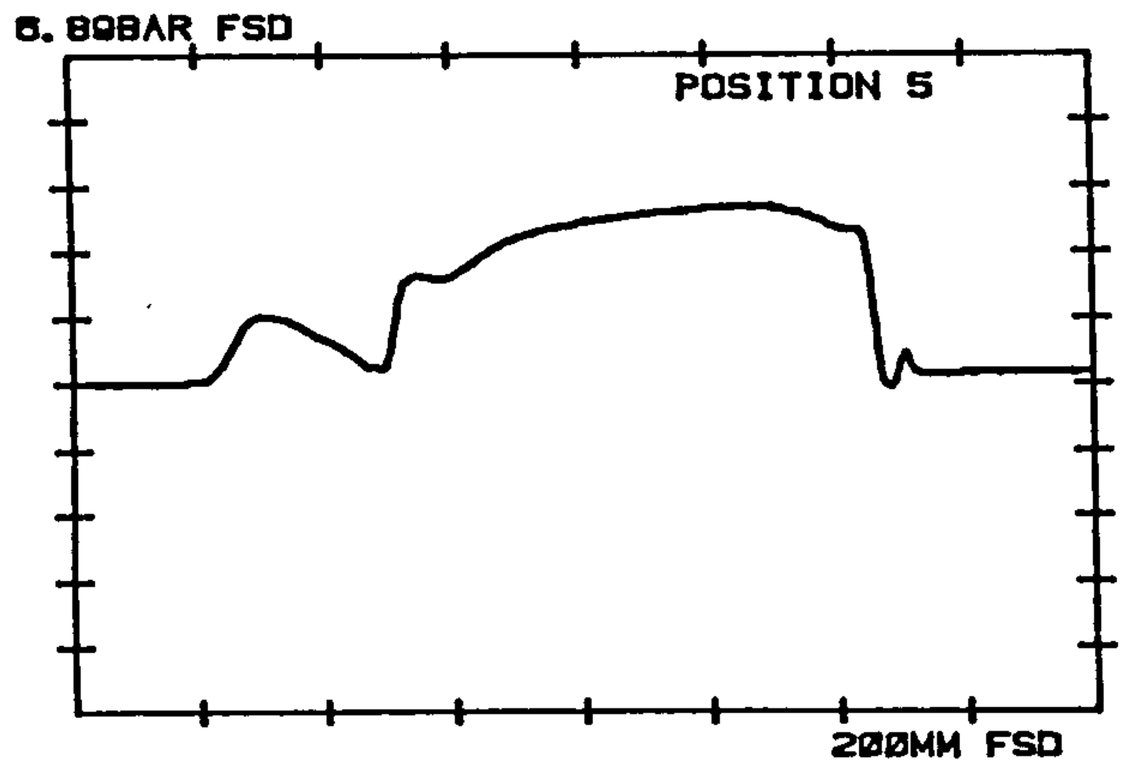

FIGURE 6.2.22 - EXPERIMENTAL FLUID PRESSURES - PLAIN TYRE 100 KPH LOCKED

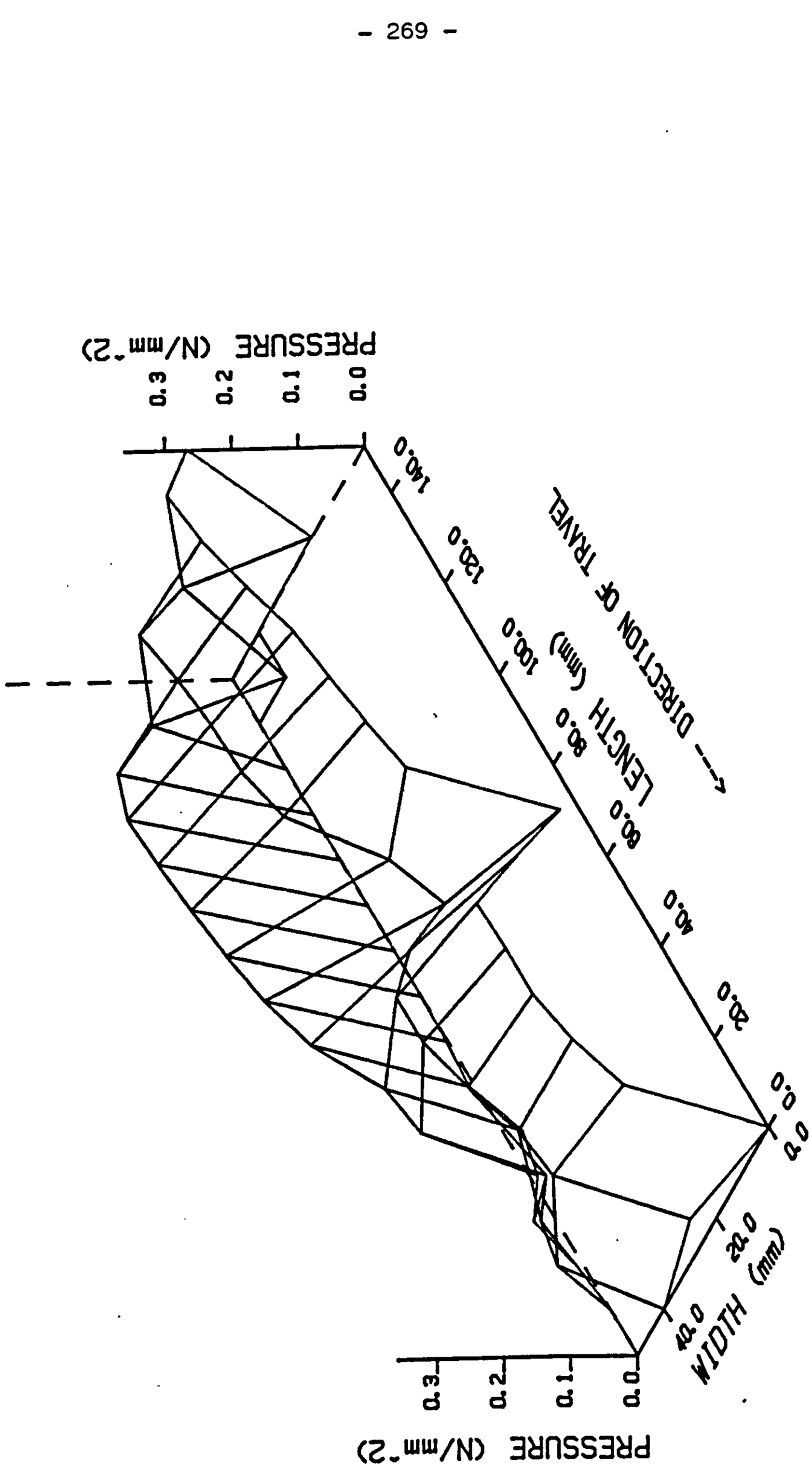

FIG 6.2.23 - PLAIN TYRE 100 KPH LOCKED (EXPERIMENTAL)

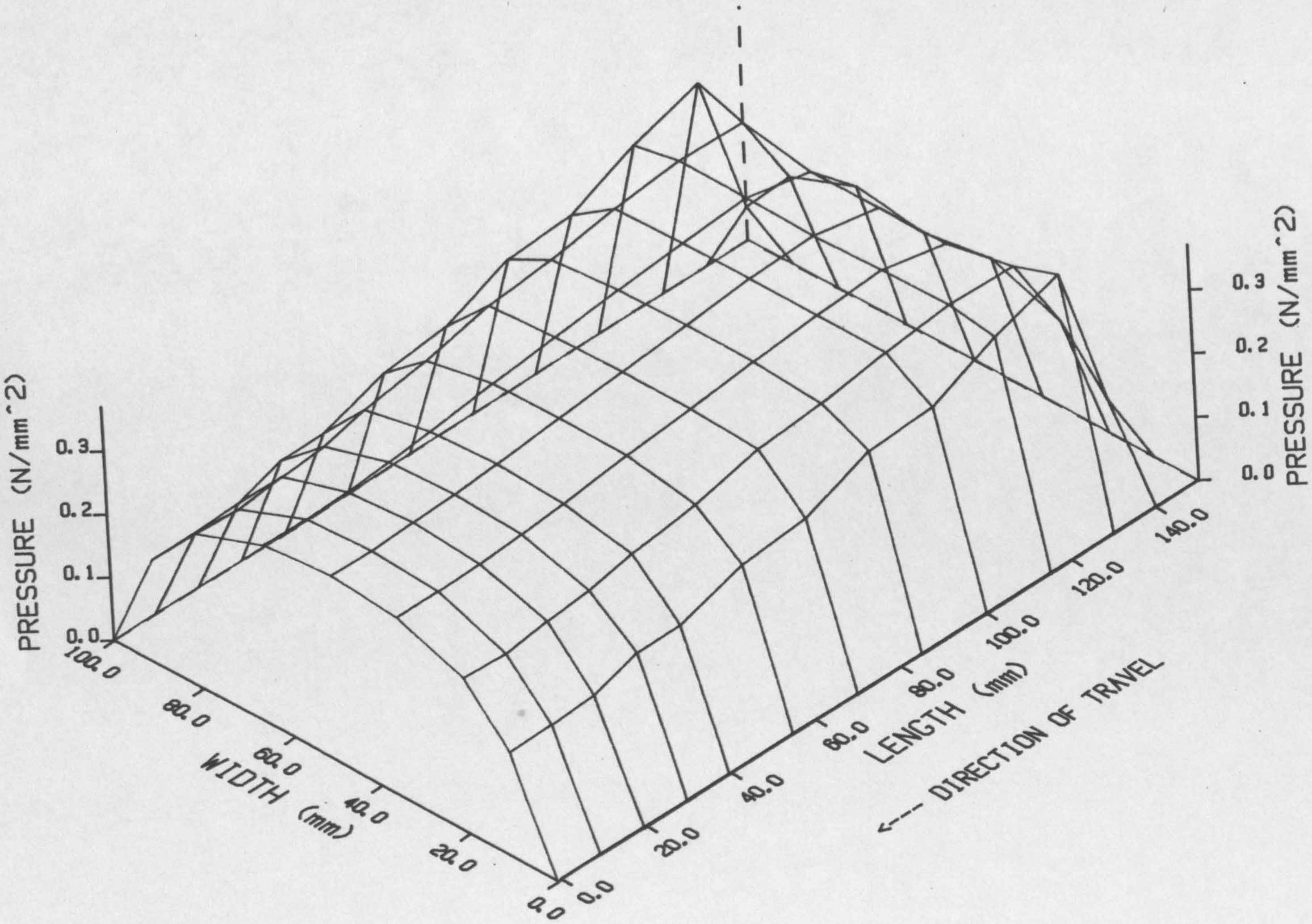

FIG 6.2.24 - PLAIN TYRE 100 KPH LOCKED

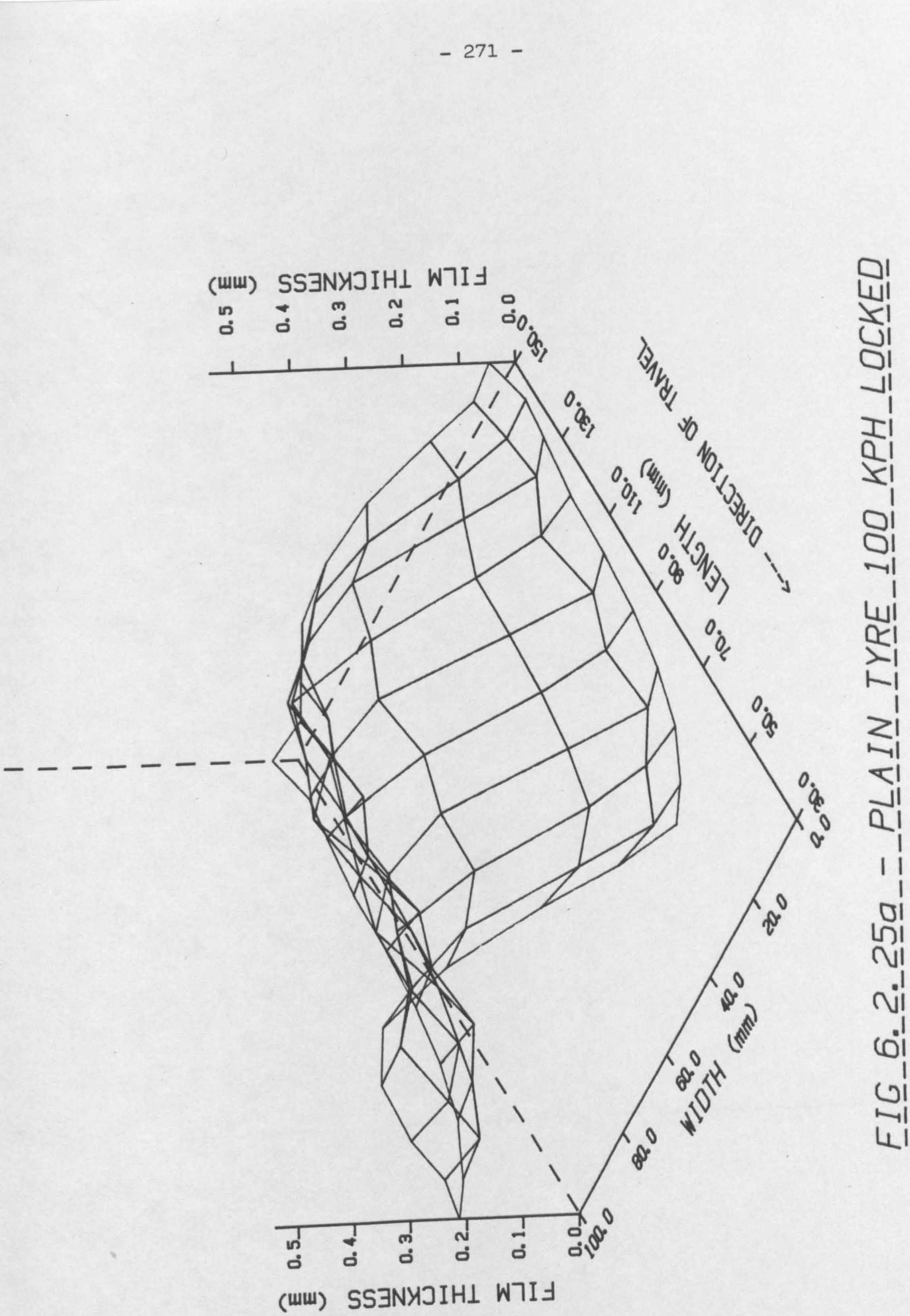

FIG 6.2.25a - PLAIN TYRE 100 KPH LOCKED

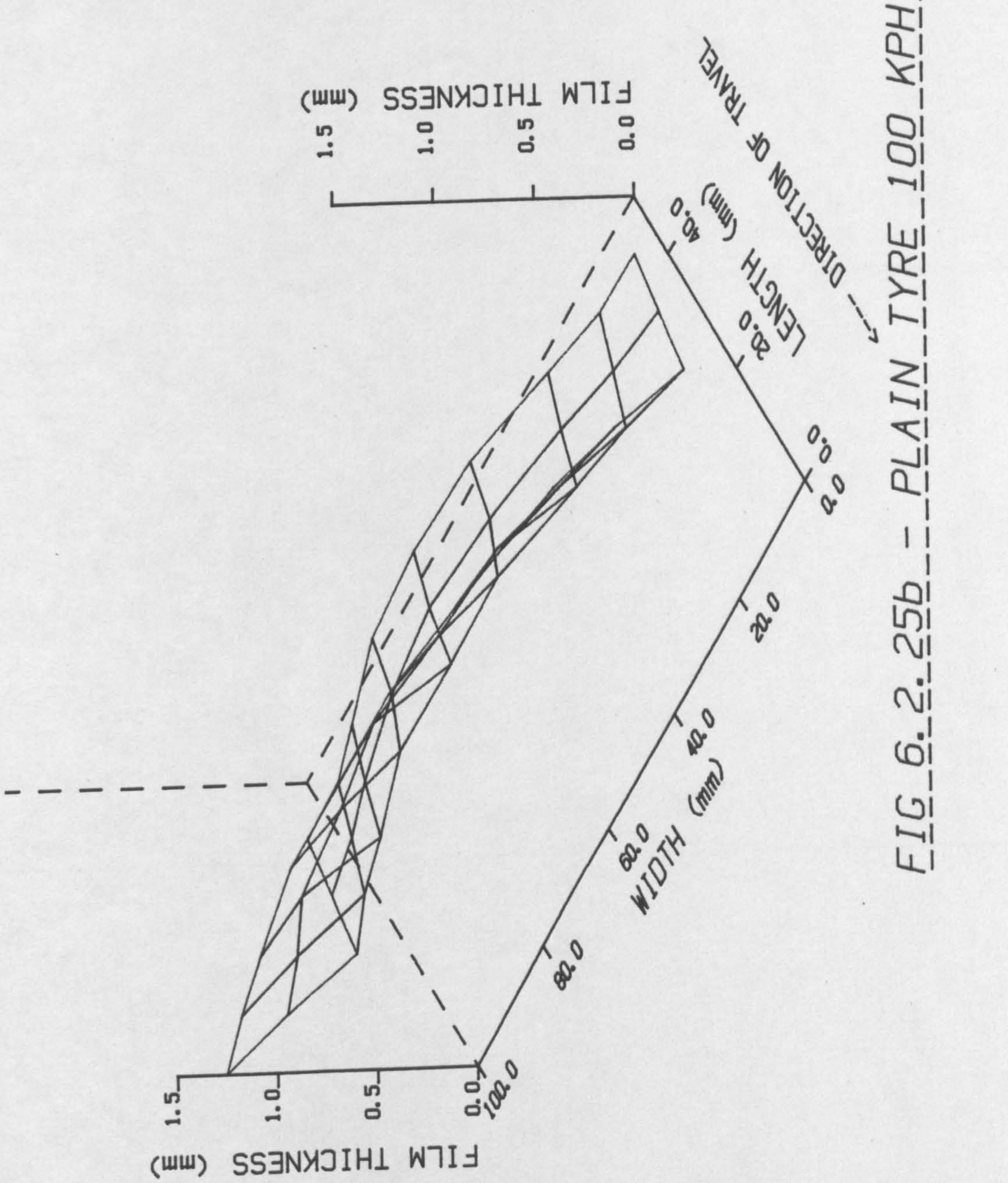

FIG 6.2.25b - PLAIN TYRE 100 KPH LOCKED

FIG 6.2.26 - PLAIN TYRE 100 KPH LOCKED

FLOW VELOCITY
5000 mm/s= 2.500mm

<--- DIRECTION OF TRAVEL

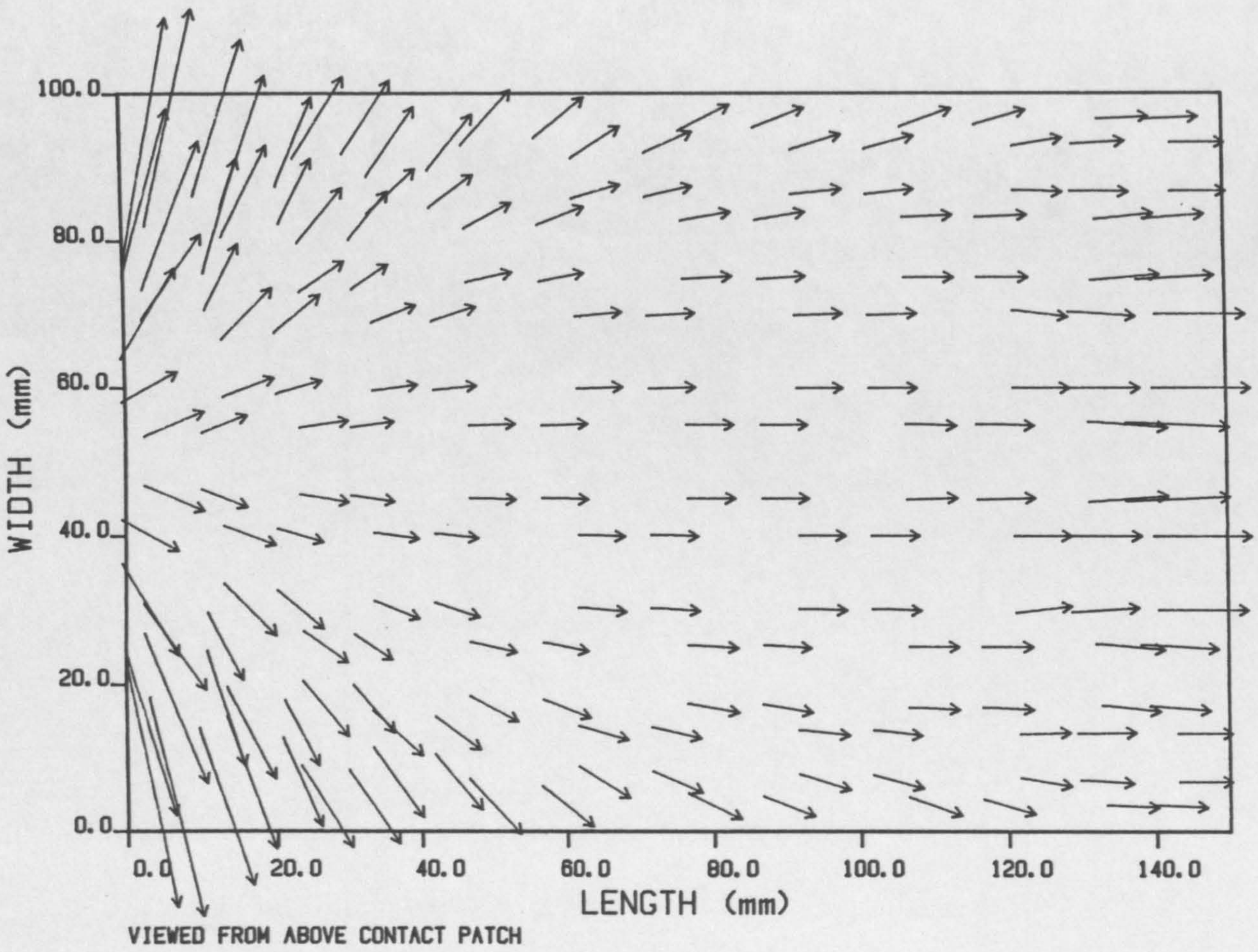

FIG 6.2.27 - PLAIN TYRE 100 KPH LOCKED

VOLUMETRIC FLOW
10000 mm^2/s= 5.000mm

<--- DIRECTION OF TRAVEL

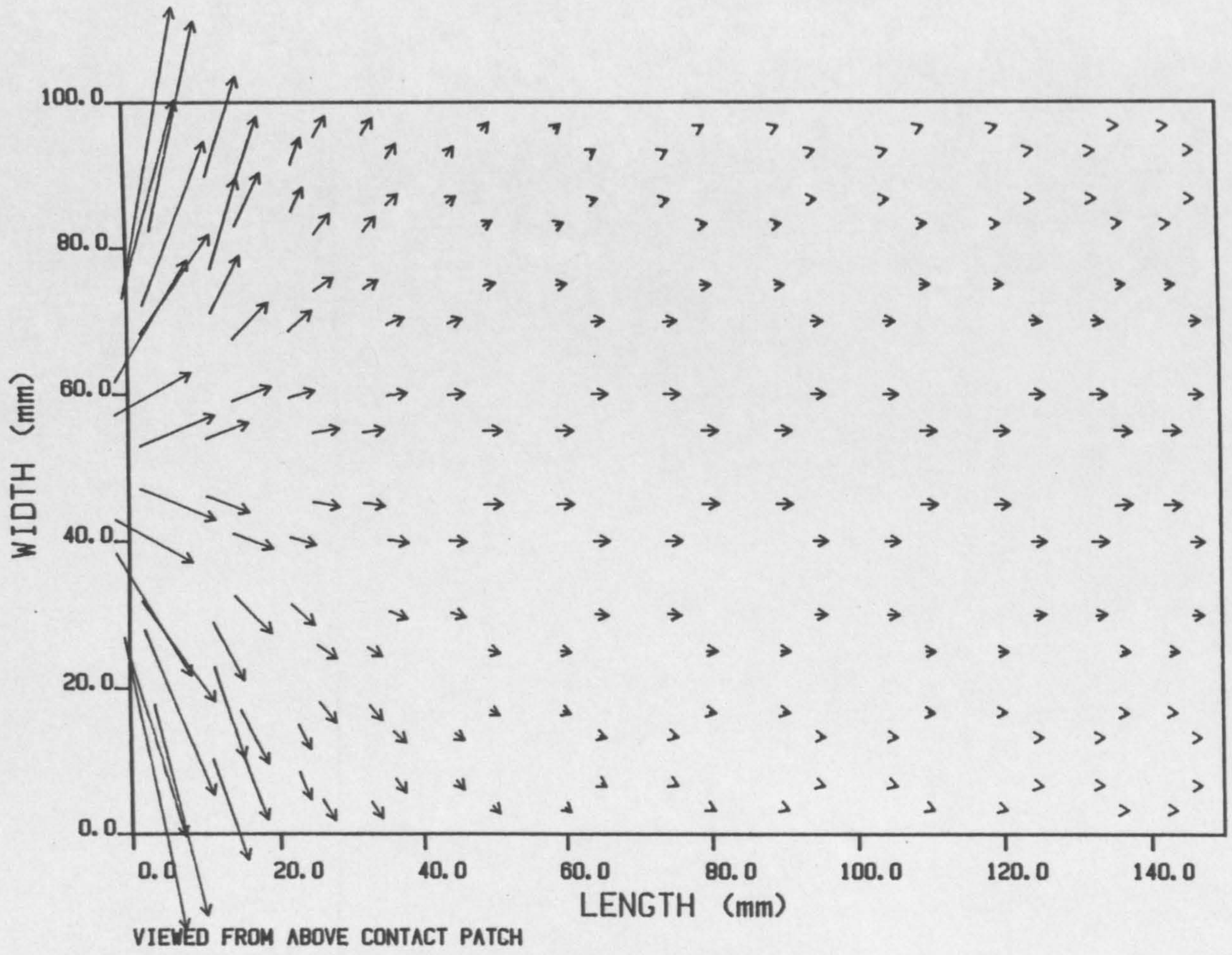

Two cases for both experimental and analytical results will be considered.

1. 50 Kph locked.
2. 100 Kph locked.

The load, inflation pressure, and road surface water depth were as for the plain tread tyre. The instrumentation in its present form is capable of producing results for this type of tyre under free rolling conditions, but due to limitations on the cornering force machine when these experiments were undertaken, only locked wheel testing was performed.

Figure 6.3.1 shows the positions within the contact patch where the experimental pressure measurements were taken. Position 2A is in the centre of the groove. Results in these cases were not obtained for position 6, for the reasons discussed in section 6.2.4, and the values of pressure at position 6 used when constructing the three-dimensional plots are taken from the plain tread tyre at the appropriate speed.

As in the case of the plain tyre the analytical results were obtained by using a rectangular mesh of the whole of the contact patch. This finite element mesh for the grooved tyre is shown in figure 6.3.2, and the elements that define the grooves are shown shaded.

6.3.1 50 Kph Locked

The experimentally measured fluid pressure profiles for the grooved tyre moving at 50 Kph with the wheel locked are shown in figure 6.3.3. By comparing this with figure 6.2.9, for a plain tread tyre under the same conditions, it can be seen that the grooves have a very large effect on the pressure distribution. The individual pressure profiles are combined into a three-dimensional plot in

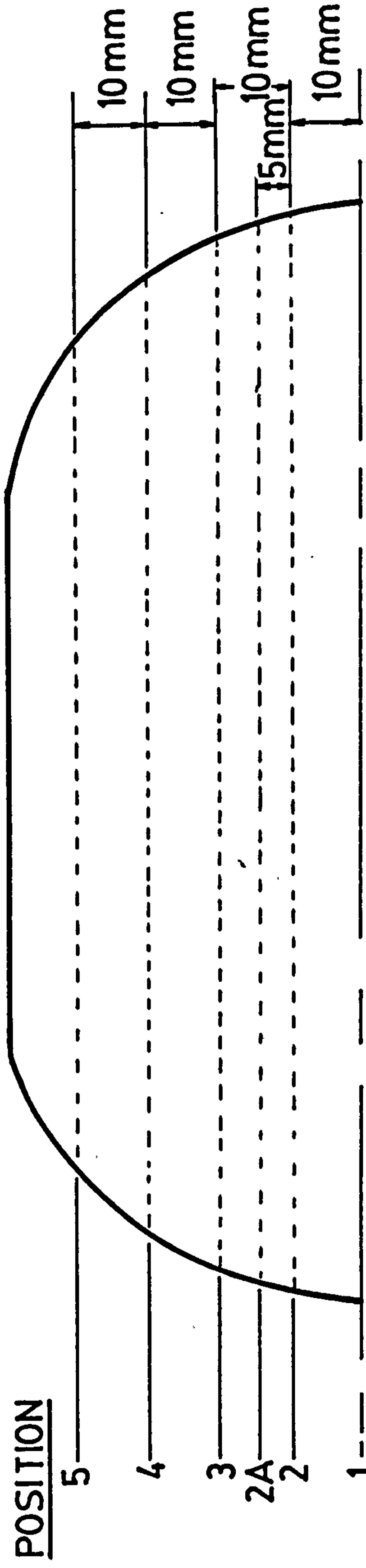
10 mm
10 mm
10 mm
15mm
10 mm
REAR
TEST POSITIONS
GROOVED TYRE -
centre-line
Tyre
FRONT
POSITION
5
4
3
2A
2
1

FIGURE 6.3.1 - G

FIGURE 6.3.2 - MESH FOR GROOVED TYRE

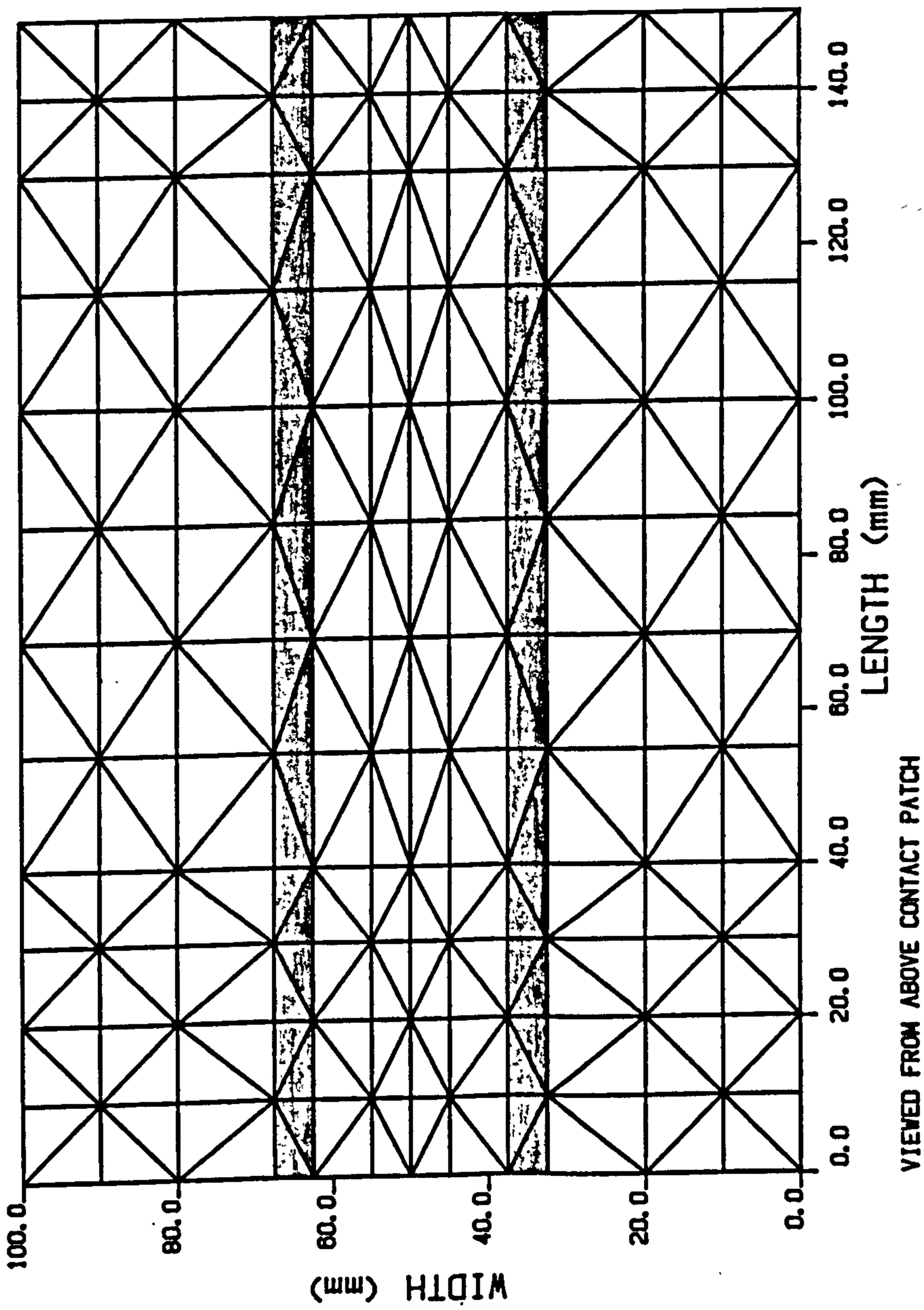

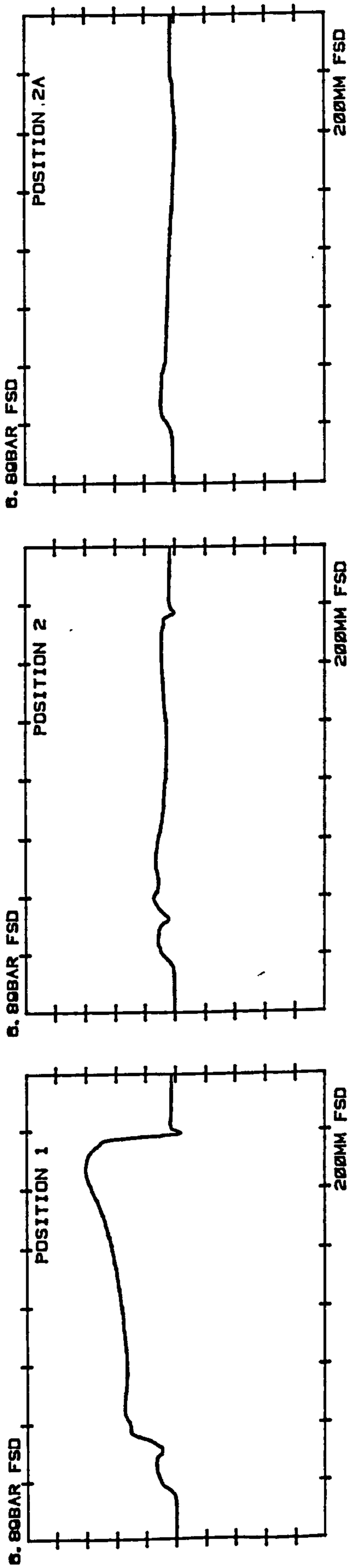

FIGURE 6.3.3 - EXPERIMENTAL FLUID PRESSURE

GROOVED TYRE 50 KPH LOCKED

figure 6.3.4. As with the plain tread tyre, the experimental three-dimensional plots for the grooved tyre are for half the contact patch and the zero width axis represents the tyre centre-line.

The analytically predicted pressure distribution is shown in figure 6.3.5, and the fluid film thickness distribution in figures 6.3.6a and 6.3.6b. In the fluid film thickness plots the elements which define the grooves of the tyre are not shown. This is because the thickness of water for these elements is much larger than that on the surrounding ribs of the tyre. The grooves in this tyre were 8 mm deep and a plot which would allow this thickness to be shown would not allow the film thickness on the ribs (0.01 mm) to be seen. This large difference in the film thickness between blocks (ribs) and grooves had to be given special attention in the development of the analytical model (section 3.9).

One interesting feature of the analytical results for film thickness is that there is no area of actual tyre/road contact, as there was in the case of a plain tread tyre under the same conditions. The actual magnitudes of the film thicknesses in the case of the grooved tyre are approximately one tenth those of the plain tyre. It is this which is important for improved wet grip, not having small areas of tyre/road contact (with a relatively thick film of water in the major part of the contact patch). This is further discussed in section 6.6.

The analytically predicted fluid flow velocity and fluid volumetric flow per unit width distributions are shown in figures 6.3.7 and 6.3.8 respectively. The difference that the grooves make to the way in which water is removed from the contact patch can be cearly seen by comparison with the corresponding plots for the plain tread tyre (figures 6.2.13 and 6.2.14).

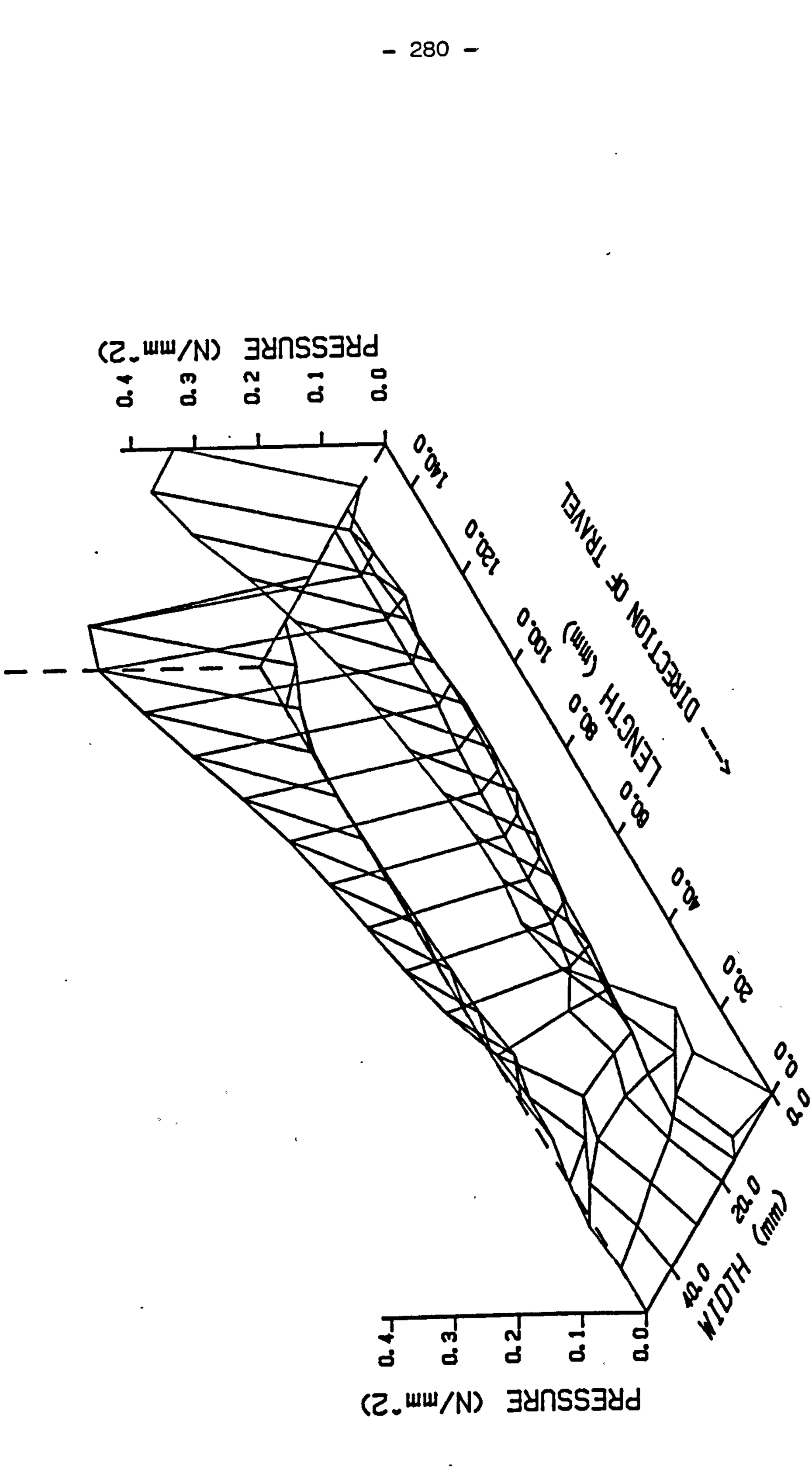

FIG. 6.3.4 - GROOVED TYRE 50 KPH LOCKED (EXPERIMENTAL)

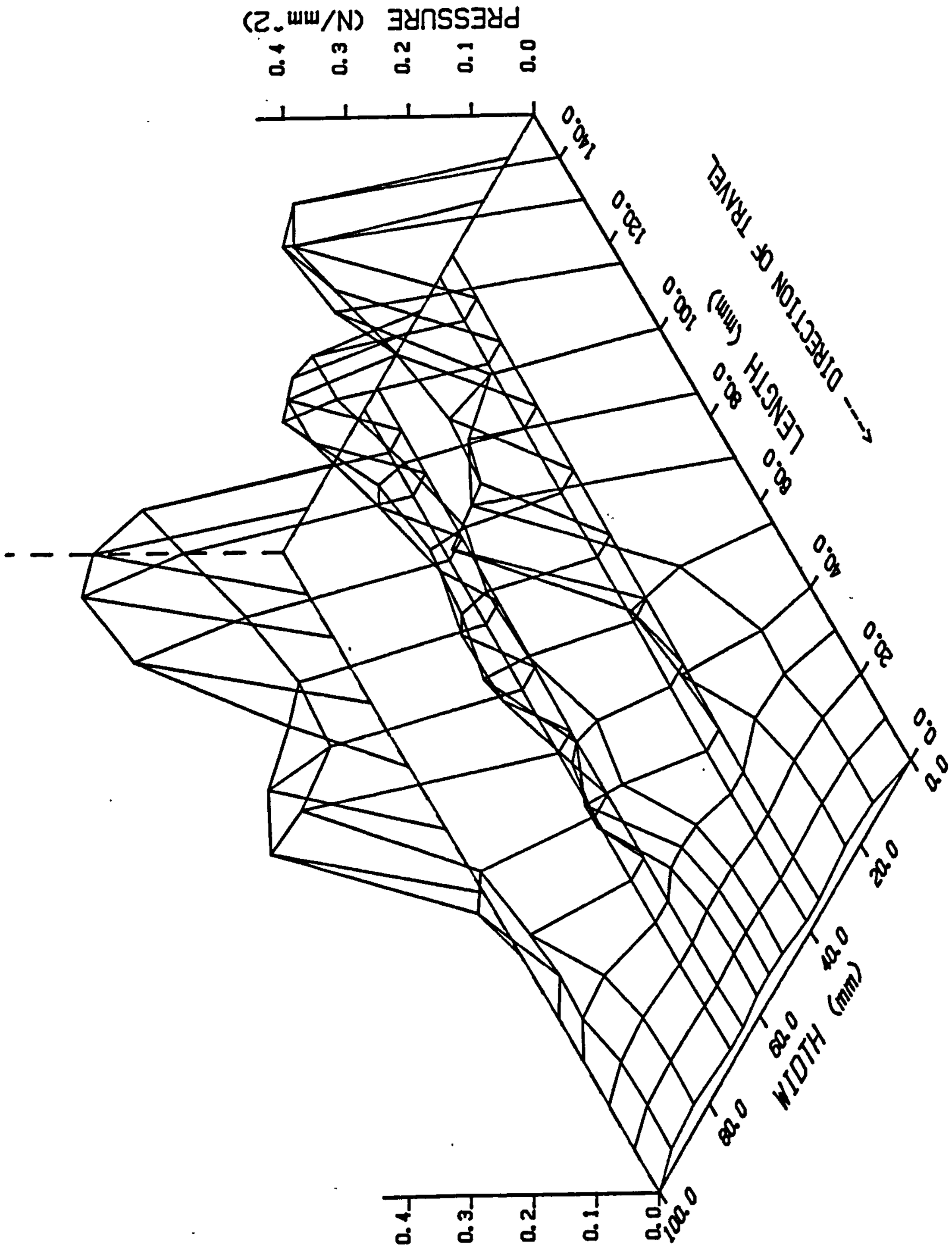

FIG 6.3.5 – GROOVED TYRE 50 KPH LOCKED

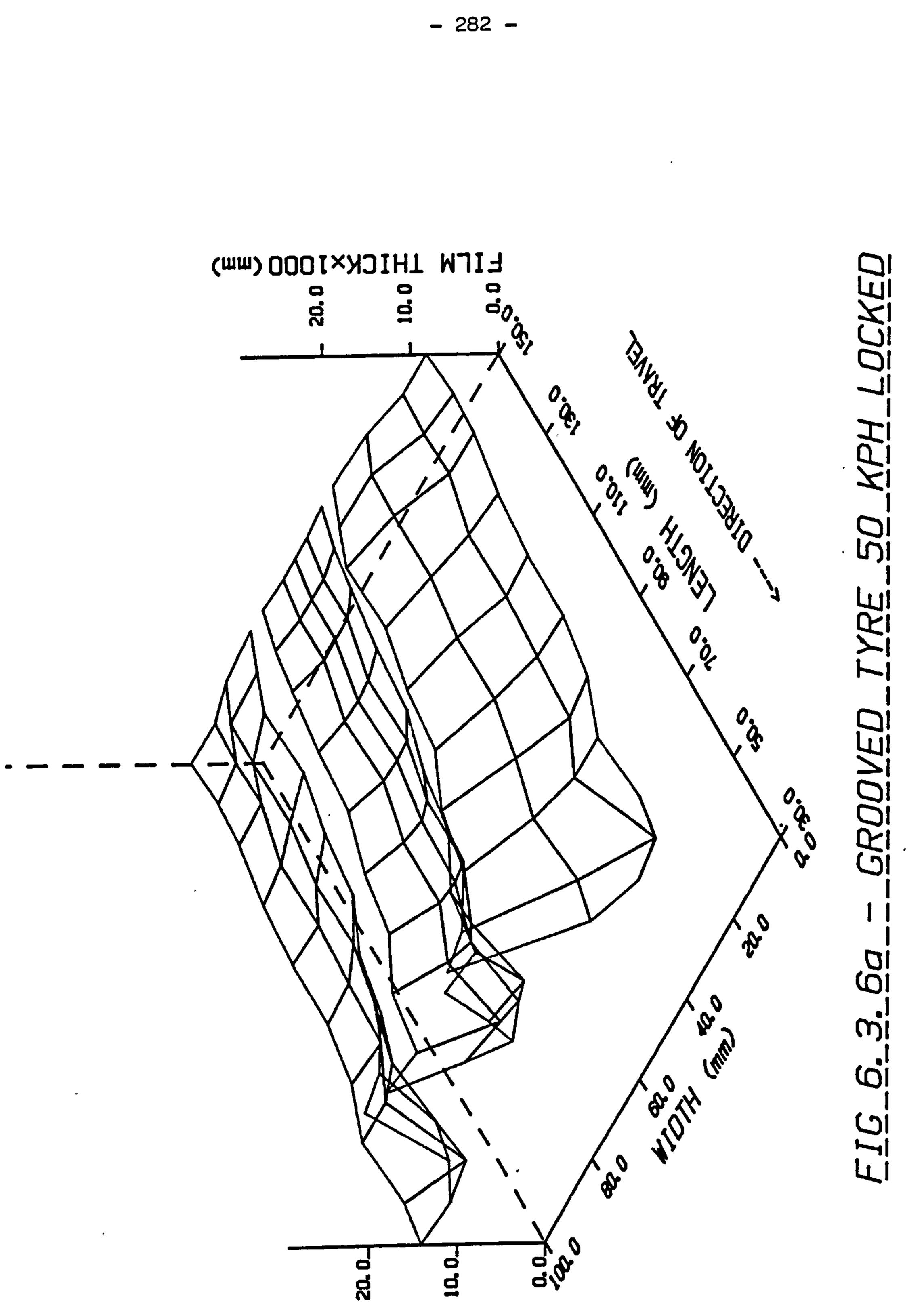

FIG 6.3.6a - GROOVED TYRE 50 KPH LOCKED

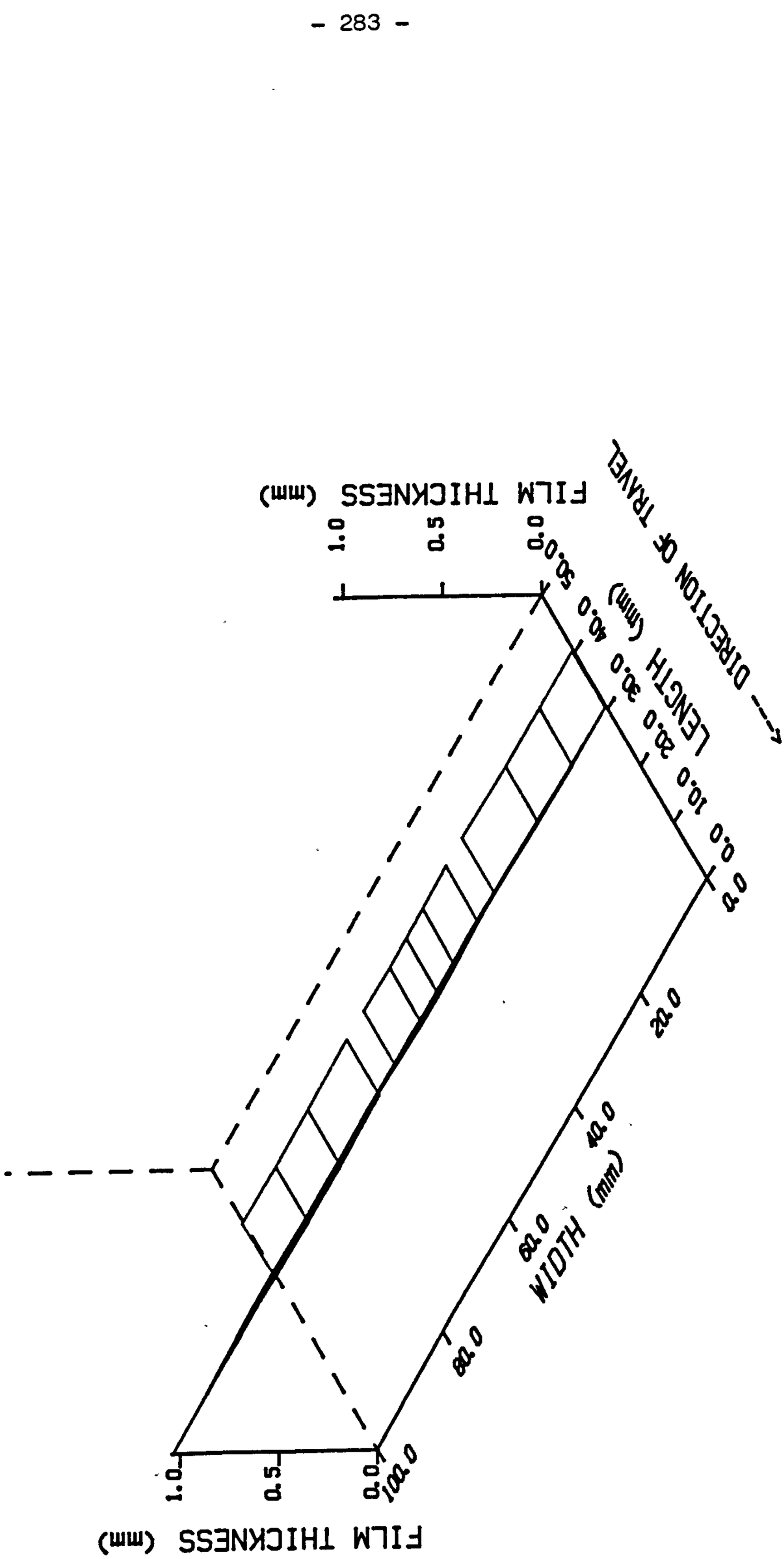
LOCKED
GROOVED TYRE 50 KPH
DIRECTION OF TRAVEL
FILM THICKNESS (mm)
1.0
0.5
0.0
50.0
40.0
30.0
20.0
10.0
0.0
LENGTH (mm)
0.0
20.0
40.0
60.0
80.0
100.0
WIDTH (mm)
1.0
0.5
0.0
FILM THICKNESS (mm)

FIG 6.3.6b - C

FIG 6.3.7 - GROOVED TYRE 50 KPH LOCKED

FLOW VELOCITY
5000 mm/s= 2.500mm

<--- DIRECTION OF TRAVEL

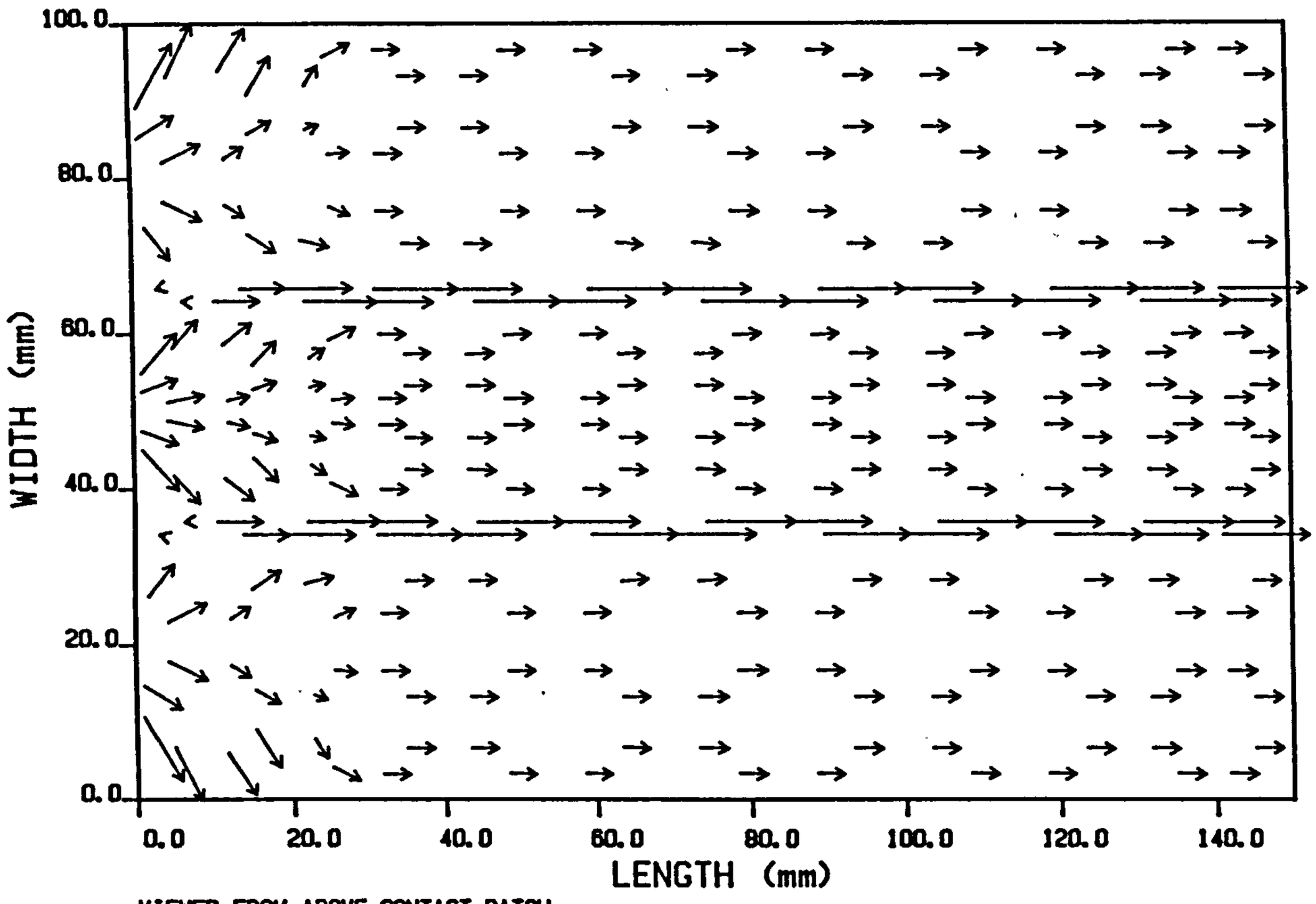

VIEWED FROM ABOVE CONTACT PATCH

FIG 6.3.8 - GROOVED TYRE 50 KPH LOCKED

VOLUMETRIC FLOW
10000 mm^2/s= 1.000mm

<--- DIRECTION OF TRAVEL

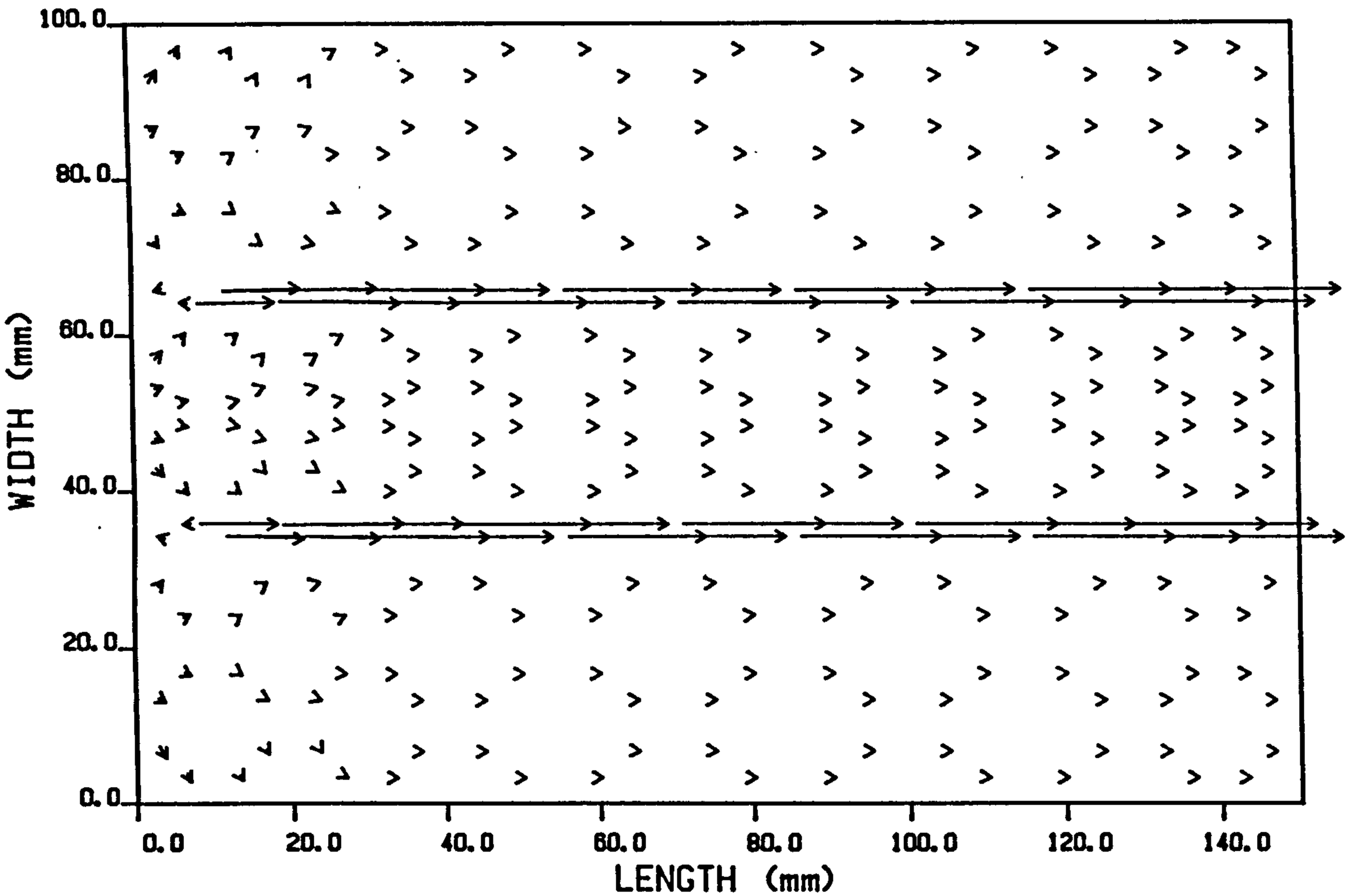

VIEWED FROM ABOVE CONTACT PATCH

6.3.2 100 Kph Locked

The pressure profiles measured experimentally, for the condition of 100 Kph with a locked wheel, are shown in figure 6.3.9. Again it can be seen that the grooves have a very large effect on the fluid pressure distribution, compared to a plain tread tyre (figure 6.2.22). Position 2A is for the centre of the groove and it can be seen that in this case there is a build-up of pressure at the front of the groove. This is due to the larger volume flow of water which must be handled at this higher speed. The three-dimensional plot of experimental fluid pressures is shown in figure 6.3.10, and as usual this is for half the contact patch width only.

The analytically predicted fluid pressure distribution is shown in figure 6.3.11 and is for the complete contact patch. The analytically predicted fluid film thicknesses are shown in figures 6.3.12a and 6.3.12b for the main part and the front of the contact patch respectively. As in the 50 Kph case with the grooved tyre, the elements which define the grooves are not shown in the film thickness plots because of the difference in the order of magnitude of the film thickness in grooves and on the ribs of the tyre.

The analytically predicted fluid flow velocities at element centroids are shown in figure 6.3.13, and the analytically predicted volume flows per unit width in figure 6.3.14. Because of the very high volume of water flowing in the grooves, the scale of the volumetric flow vectors (in figure 6.3.14) was reduced from that used in the case of the plain tread tyre under the same conditions. To allow easy comparison between the plain and grooved tyres the volumetric flows per unit width for all parts of the grooved tyre except the grooves themselves, are shown in figure 6.3.15, on the same scale as those for the plain tread tyre.

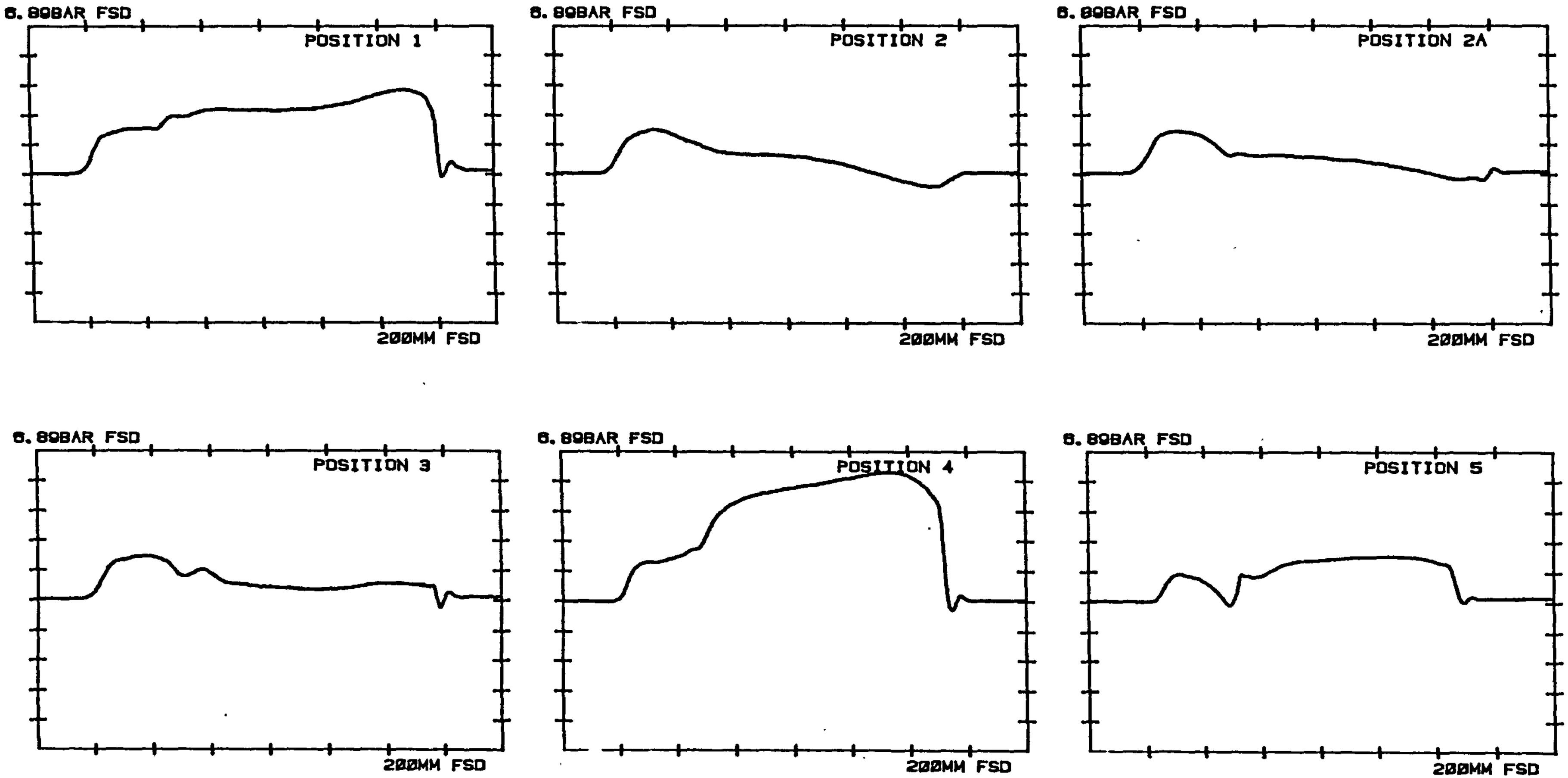

FIGURE 6.3.9 - EXPERIMENTAL FLUID PRESSURES -

GROOVED TYRE 100 KPH LOCKED

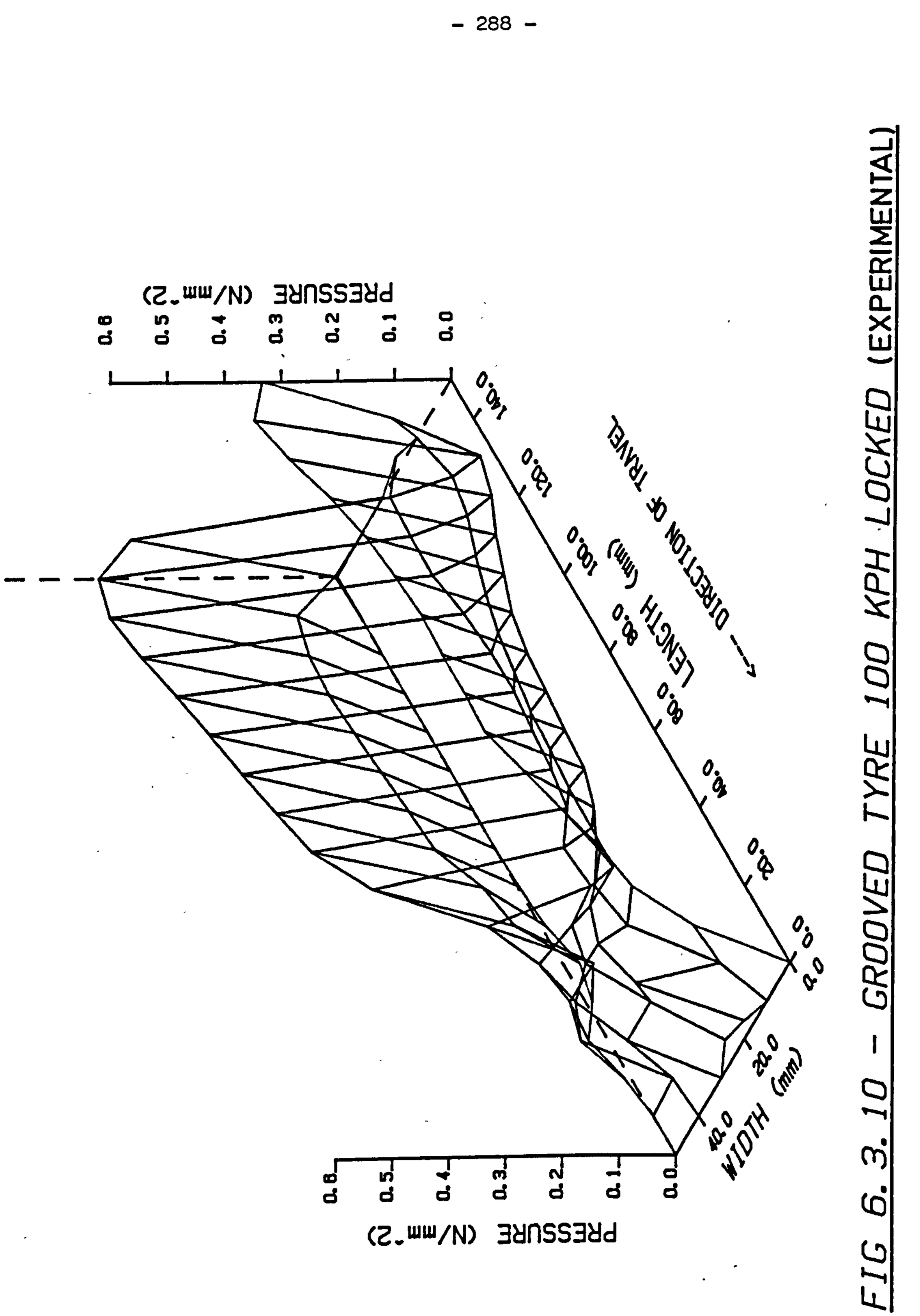

FIG 6. 3. 10 - GROOVED TYRE 100 KPH LOCKED (EXPERIMENTAL)

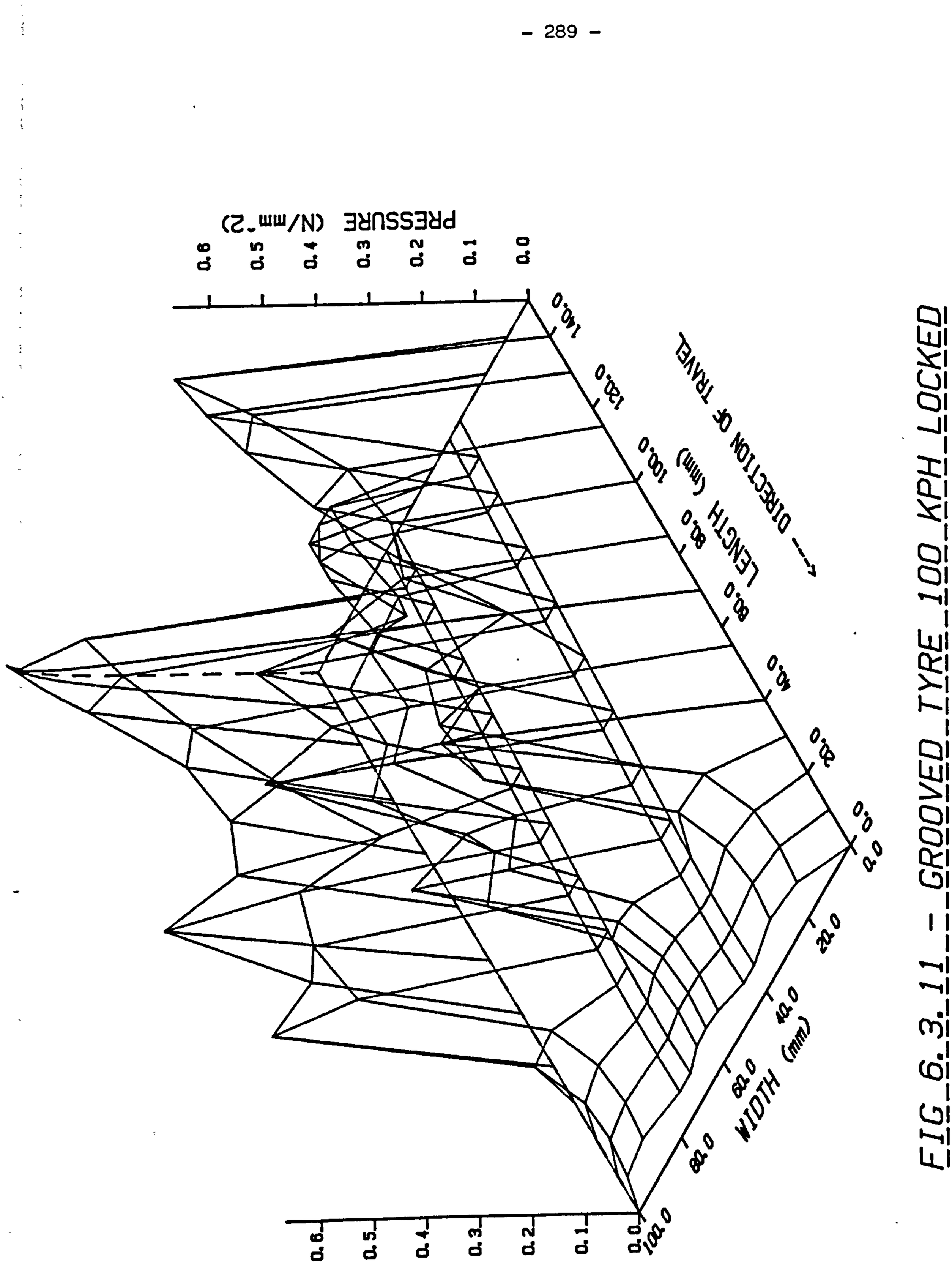

FIG 6.3.11 - GROOVED TYRE 100 KPH LOCKED

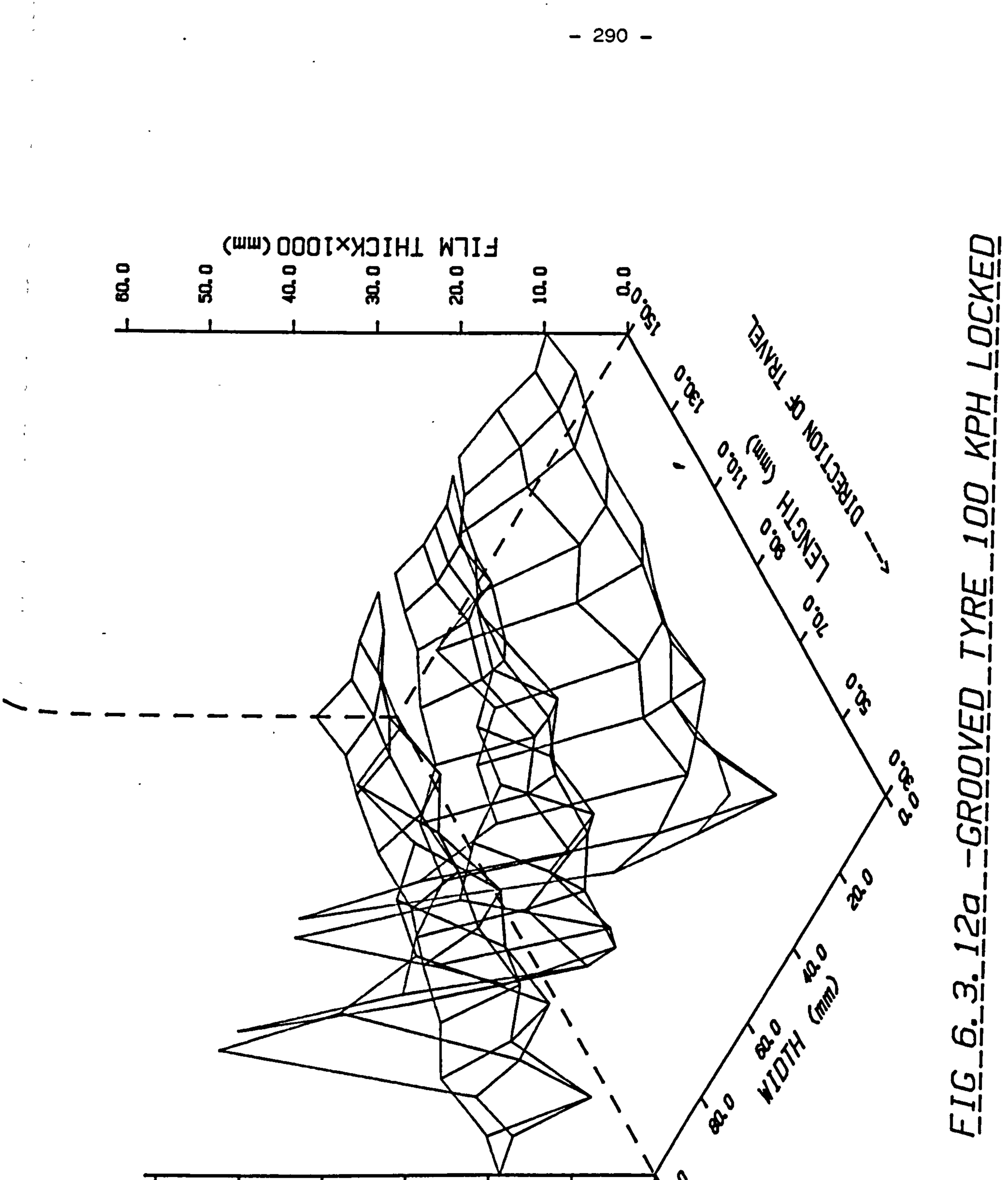

FIG 6.3.12a -GROOVED TYRE 100 KPH LOCKED

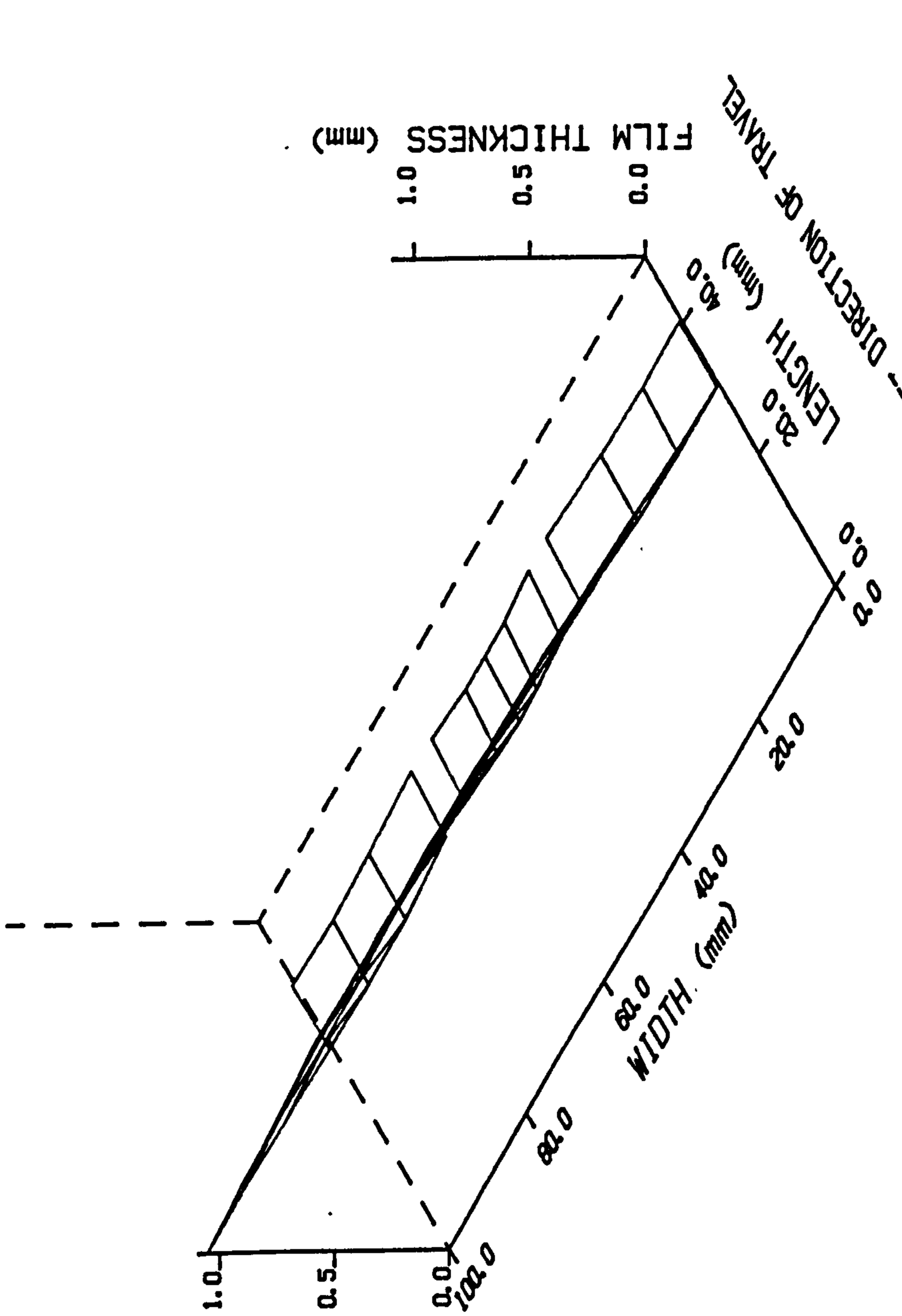

FIG 6.3.12b -GROOVED TYRE 100 KPH LOCKED

FIG_6._3._13_-_GROOVED_TYRE_100_KPH_LOCKED

FLOW VELOCITY 2.500mm
5000 mm/s=

<--- DIRECTION OF TRAVEL

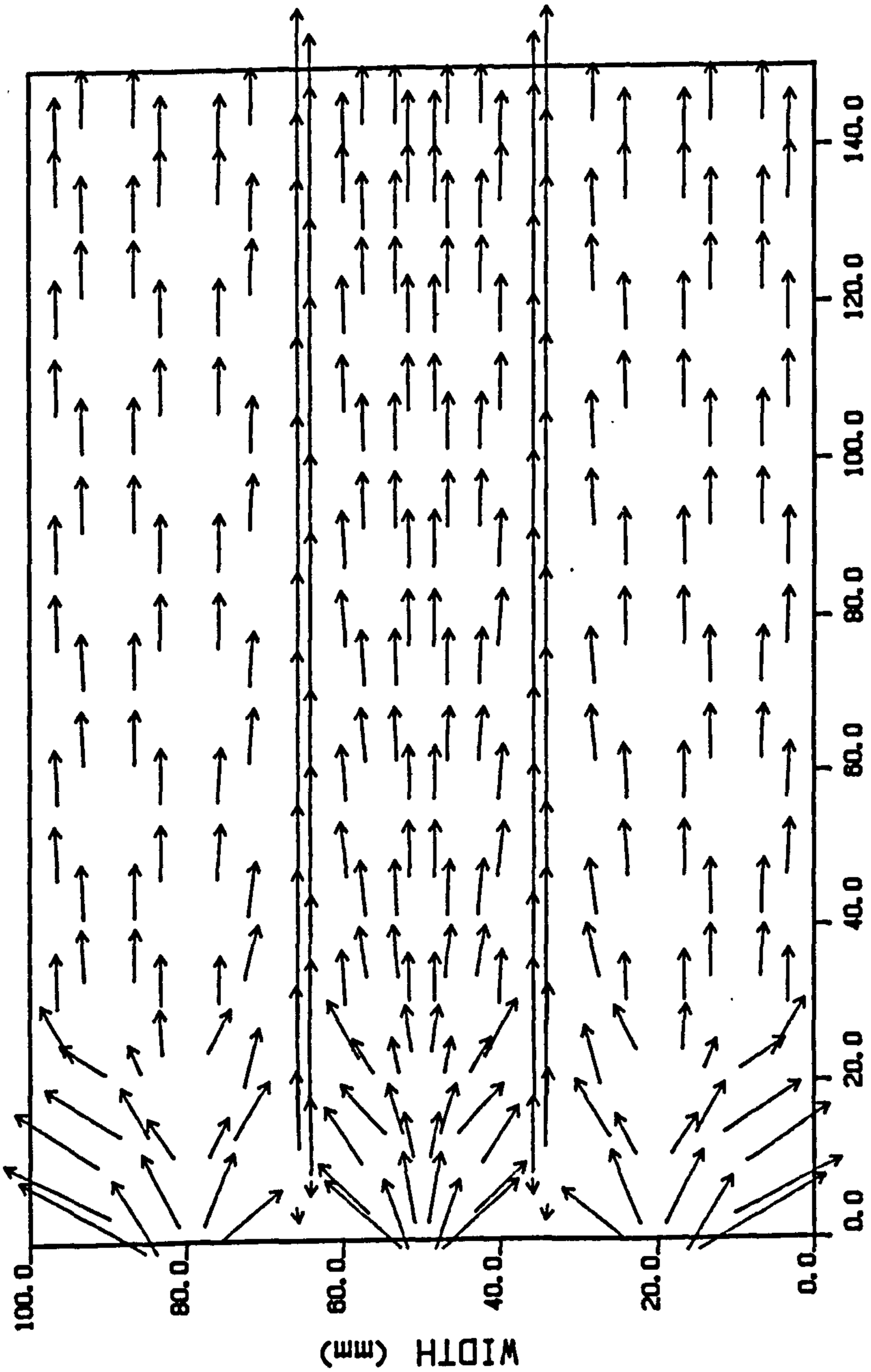

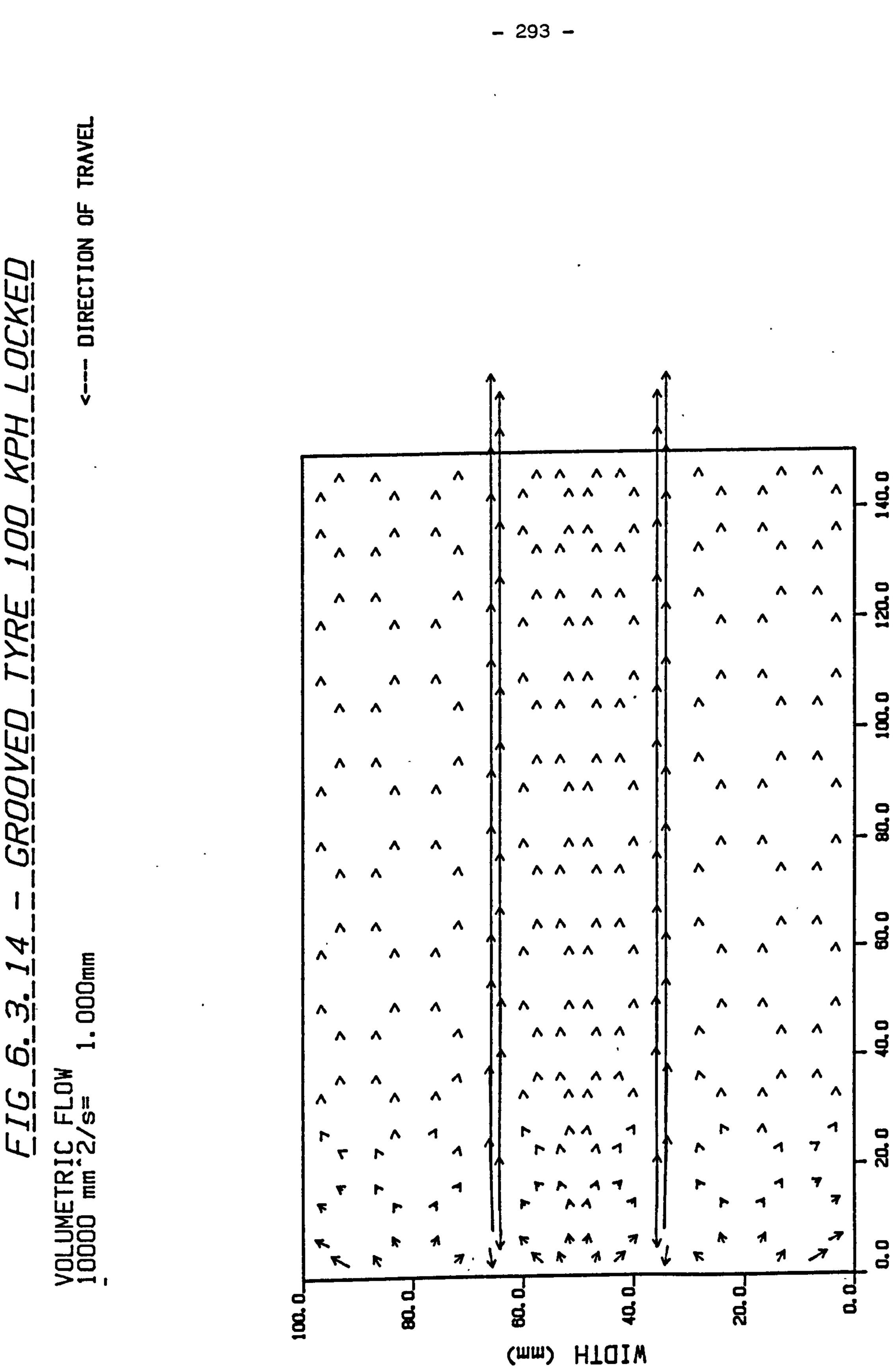
FIG 6.3.14 - GROOVED TYRE 100 KPH LOCKED
VOLUMETRIC FLOW
10000 mm^2/s= 1.000mm
<-- DIRECTION OF TRAVEL
140.0
120.0
100.0
80.0
60.0
40.0
20.0
0.0
LENGTH (mm)
100.0
80.0
60.0
40.0
20.0
0.0
WIDTH (mm)
VIEWED FROM ABOVE CONTACT PATCH

FIG 6.3.15 - GROOVED TYRE 100 KPH LOCKED

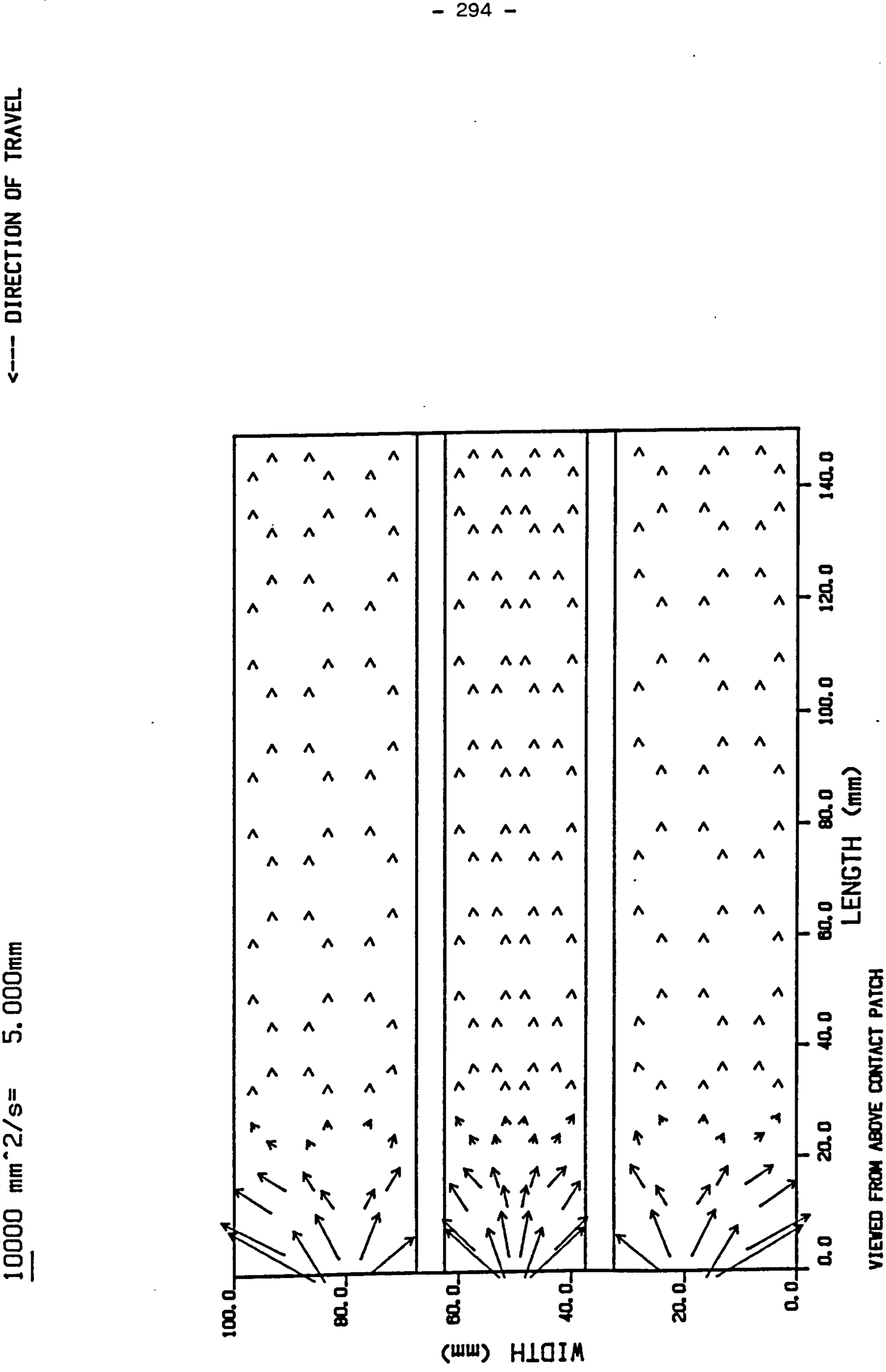

6.4 SQUARE TREAD BLOCK

Experimental measurements were made on a tyre whose tread pattern was composed of 25 mm square blocks separated by 5 mm wide grooves. These were made only for the central row of blocks within the contact patch, as shown in figure 6.4.1. Also shown in figure 6.4.1 are the actual positions where the experimental measurements were made. The pressure profiles presented in figure 6.4.2 are for half the width of the central blocks at 2.5 mm spacing. Figure 6.4.2 shows that there are six individual blocks from front to rear at the centre of the contact patch. The pressure measurements on this tyre were made at 50 Kph with the wheel locked, and a road surface water depth of 1 mm. Only locked wheel measurements could be made because of the lateral grooves, and the lack of any measurement of tyre angular position with the present experimental set-up. The addition of this facility is discussed in section 8.3.2.

As can be seen from figure 6.4.2 the pressure distribution on the same shape block at different longitudinal positions within the contact patch is different. This is owing to a number of factors, the main one being that there will be differing amounts of water flowing into the block in different parts of the contact patch. The magnitude of this flow is not known, although future studies utilizing the contact patch computer program may be able to help in this. At present therefore, when using the block analysis computer program, flow boundary conditions are not specified. A second difference between the conditions under which the different blocks in figure 6.4.2 are operating is their inclination relative to the horizontal. There will be a general reduction in the film thickness from the front to rear of the contact patch with the tyre operating under locked conditions (figures 6.2.12 and 6.2.25), although under free rolling condition there tends to be an area of thicker film towards the rear of the contact patch (figures 5.3.2 and 6.2.19). In the case of a locked tyre there must be this reduction in film thickness as this is the only means of developing hydrodynamic pressures, because there is no squeezing, as there is in the case of a rolling tyre.

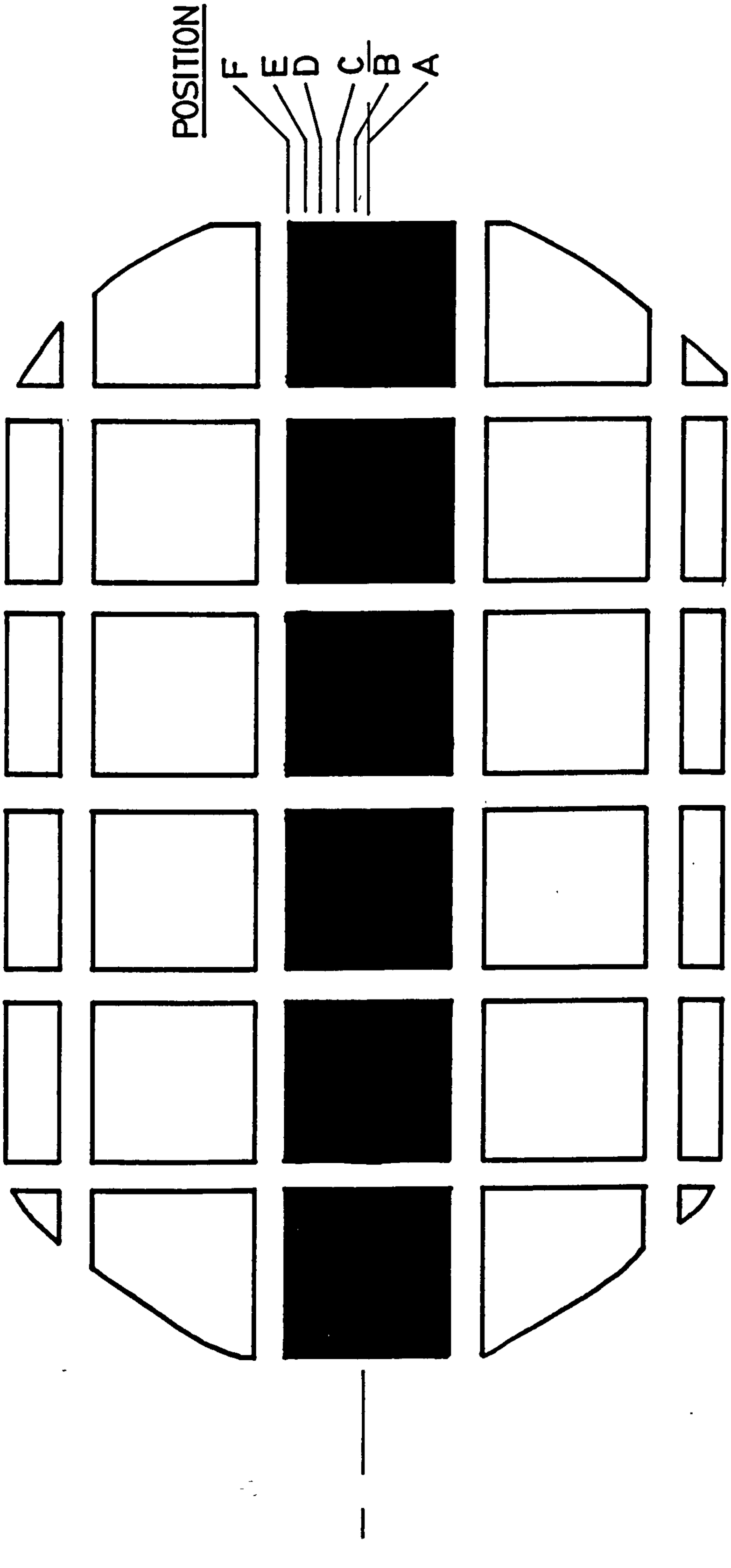

FIGURE 6.4.1 - 'BLOCKY' TYRE - TEST POSITIONS

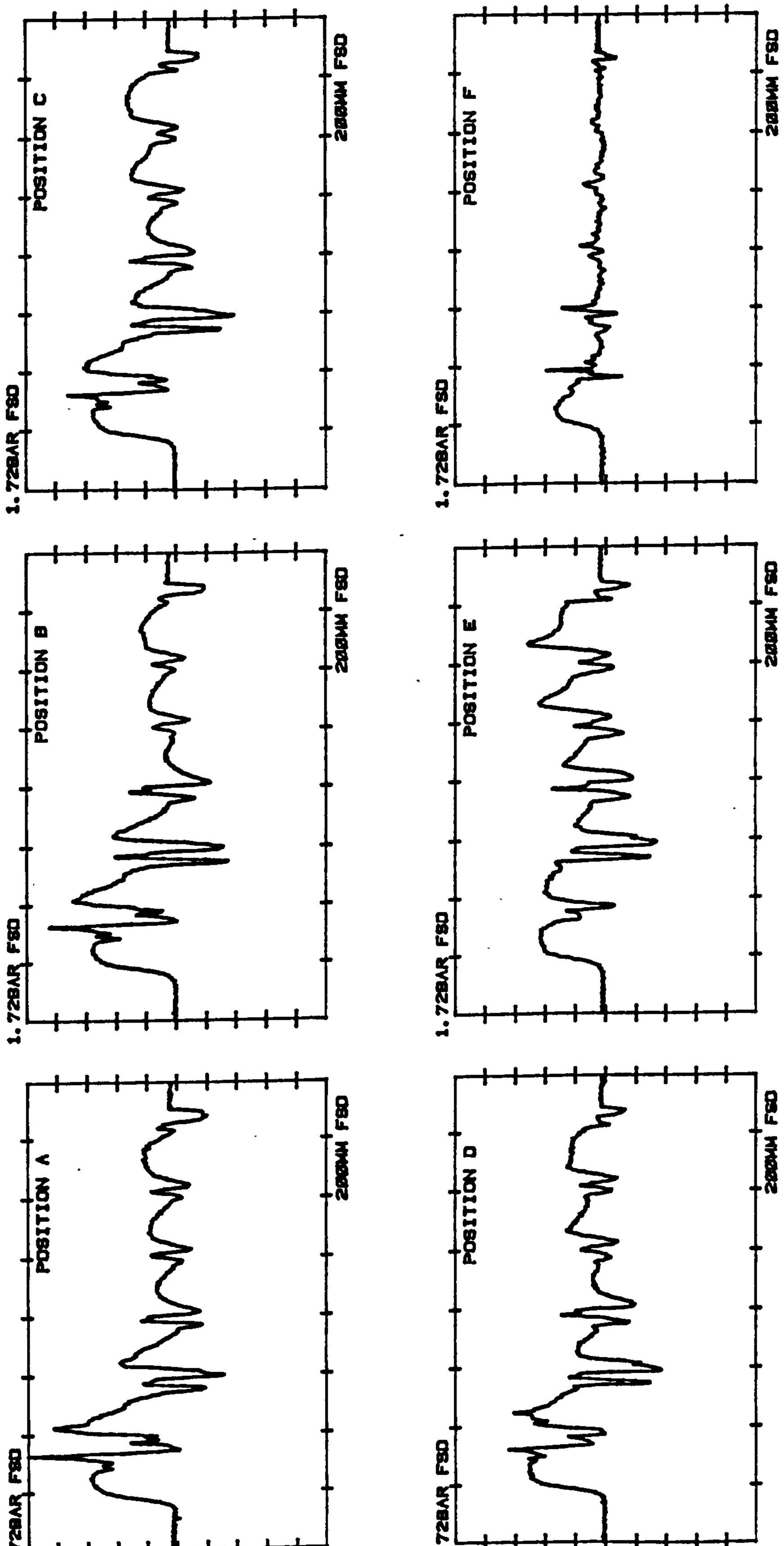

FIGURE 6.4.2 - EXPERIMENTAL FLUID PRESSURE

'BLOCKY' TYRE 50 KPH LOCKED

The block analysis computer program has been used to assess the effects of different inclinations on a single block of the type used in the tyre which produced the results in figure 6.4.2. For the purpose of this exercise it was assumed that the edge of the block nearest the rear of the contact patch would, if there were no deformation, just touch the road surface. The height of the front of the block from the road surface was varied. It must be stressed that this inclination of the block is only for its undeformed shape and that under the action of fluid pressure the block will deform.

To assess the effect of inclination, various values of undeformed 'inlet' film thicknesses, ranging from 0.02 mm to 0.30 mm, were used in a series of examples. The total load carrying capacity of the block was used an an indication of the effect of inclination and values are shown in figure 6.4.3. In each of these cases the pressures at edges of the block were taken to be atmospheric.

It can be seen that the load carrying capacity of this square tread block is sensitive to its inclination to the road surface. The peak load capacity is with an undeformed 'inlet' film thickness of approximately 0.07 mm.

The fluid pressure distribution predicted by the block analysis computer program is shown in figure 6.4.4, and is for the case with the inclination to give the maximum load capacity. If this pressure distribution is compared with those measured experimentally (shown in figure 6.4.2), it can be seen that the predicted pressure distribution builds up much more slowly to a maximum than the measured distribution. This is due to the lack of flow boundary conditions specifying flow into the front edge of the block. The analytically predicted fluid film thickness distribution is shown in figure 6.4.5. This shows the extent to which the block has deformed from its original shape (tapering from 0.07 mm to zero film thickness).

FIG. 6.4.3 - SQUARE BLOCK - LOAD CAPACITY

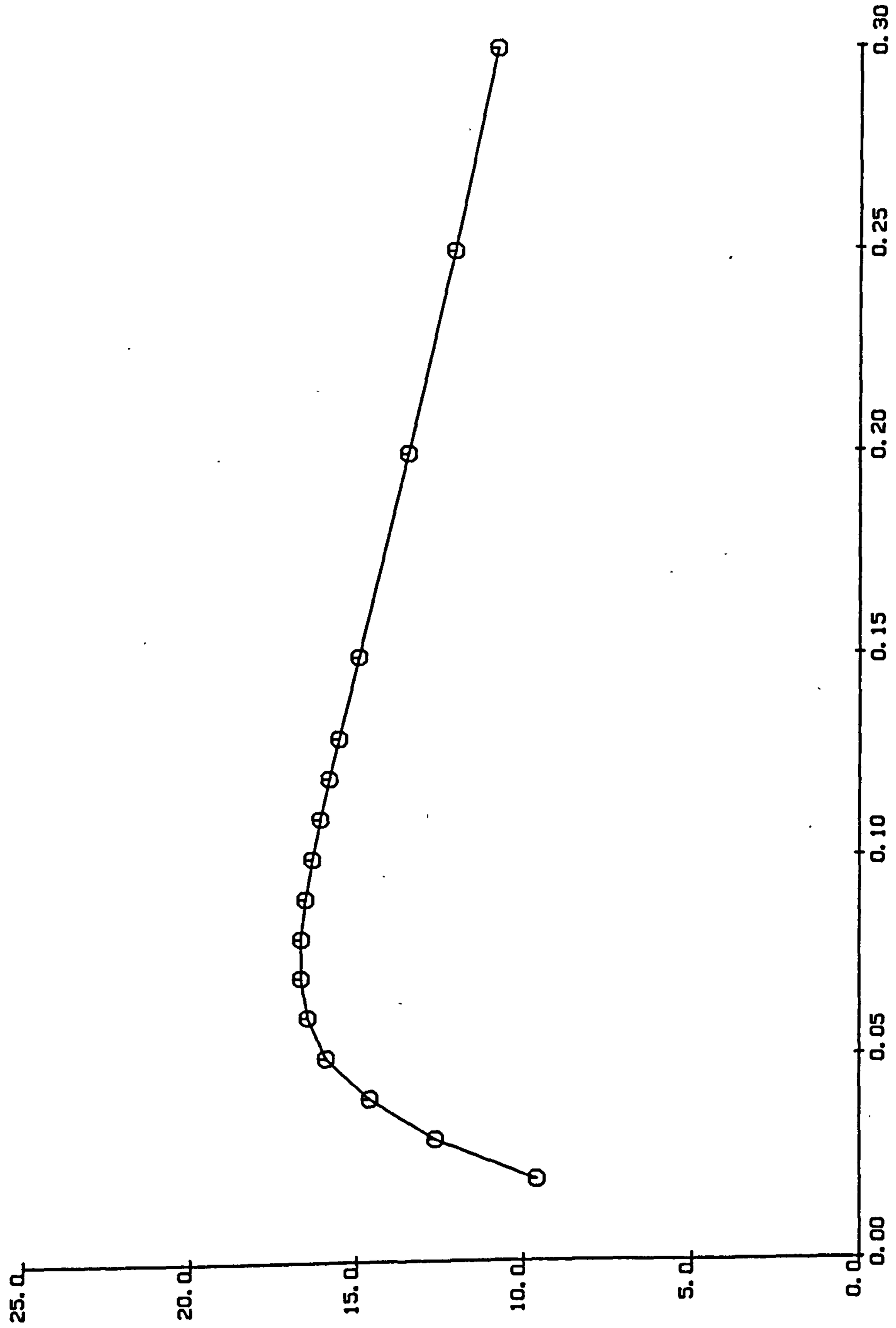

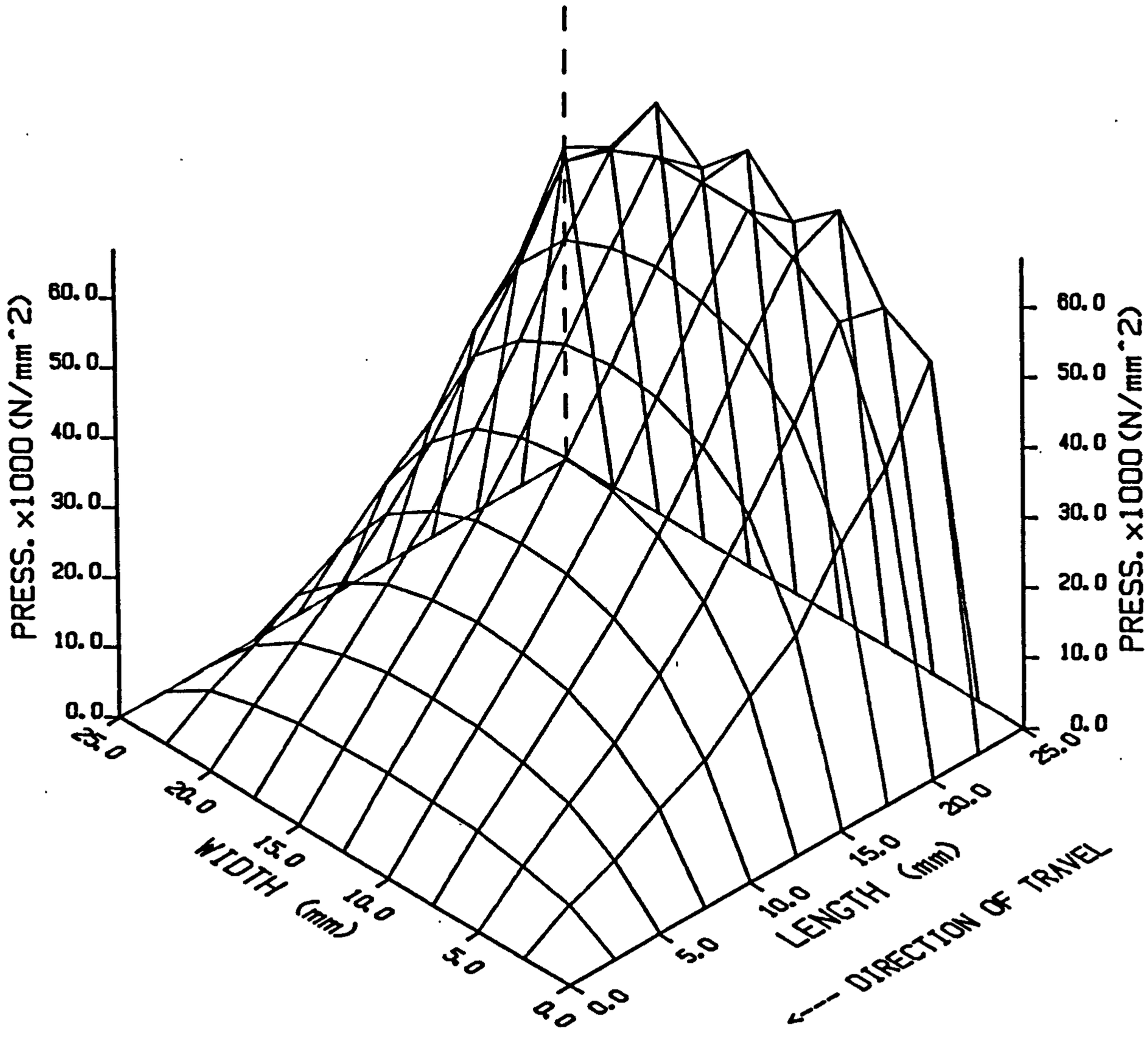

FIGURE 6.4.4 - SQUARE TREAD BLOCK

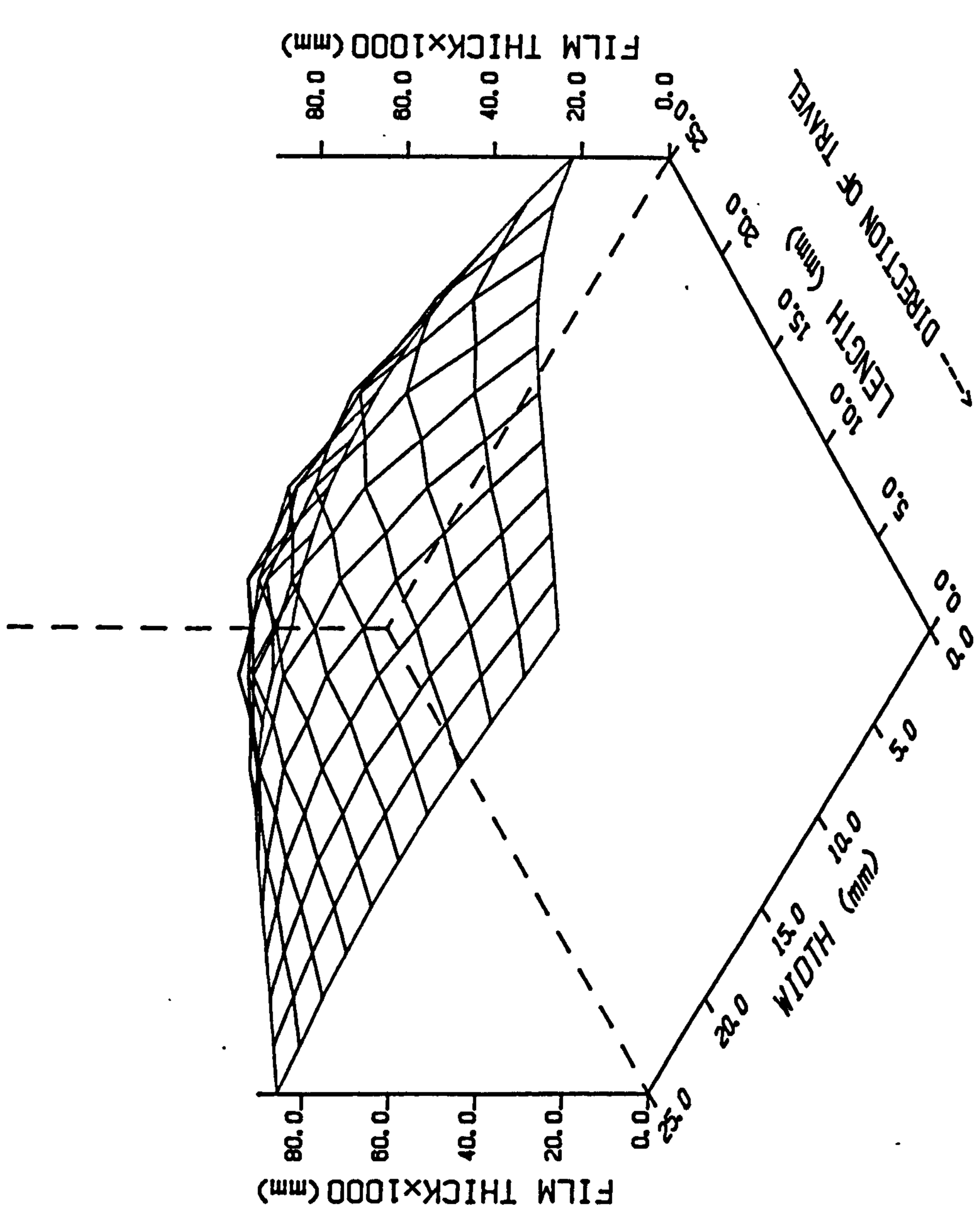

FIGURE 6.4.5 -- SQUARE TREAD BLOCK

An alternative method of using the block design program, which lessens the problem of specifying flow boundary conditions, is discussed in the following section.

6.5 DUNLOP SP ELITE TREAD BLOCK

To illustrate the capability of the tread block analysis computer program to analyse actual tyre tread blocks, an example is presented here which shows results for a Dunlop SP Elite centre block. The actual shape of this block was shown in figure 4.5.1, and the finite element mesh which was used to represent this is shown in figure 6.5.1.

In the previous section it was shown how the block analysis program could be used to analyse a block under sliding conditions. An alternative is to consider a block 'squeezing' towards the road surface. This squeezing condition for a single tread block corresponds to the situation with a free rolling tyre when the block is within the contact patch, with a water film separating it from the road surface. To gain contact with the road the block must be able to squeeze through this water film, and the design of block which is able to achieve this with the least application of load will provide the best performance in the wet. On a tyre this load is provided by the contact pressure and there will therefore tend to be some squeezing at all points within the contact patch; not only in the additional area in front of the dry contact patch. This is discussed in sections 6.6 and 8.3.1, with reference to the contact patch results presented in section 6.2.

By considering the block under squeezing conditions the problem, mentioned in the previous section, with the specification of flow boundary conditions is lessened. This is because when there is no relative velocity (in the plane of the contact patch) between the tyre and the road then the fluid flow velocities are also of a lower magnitude.

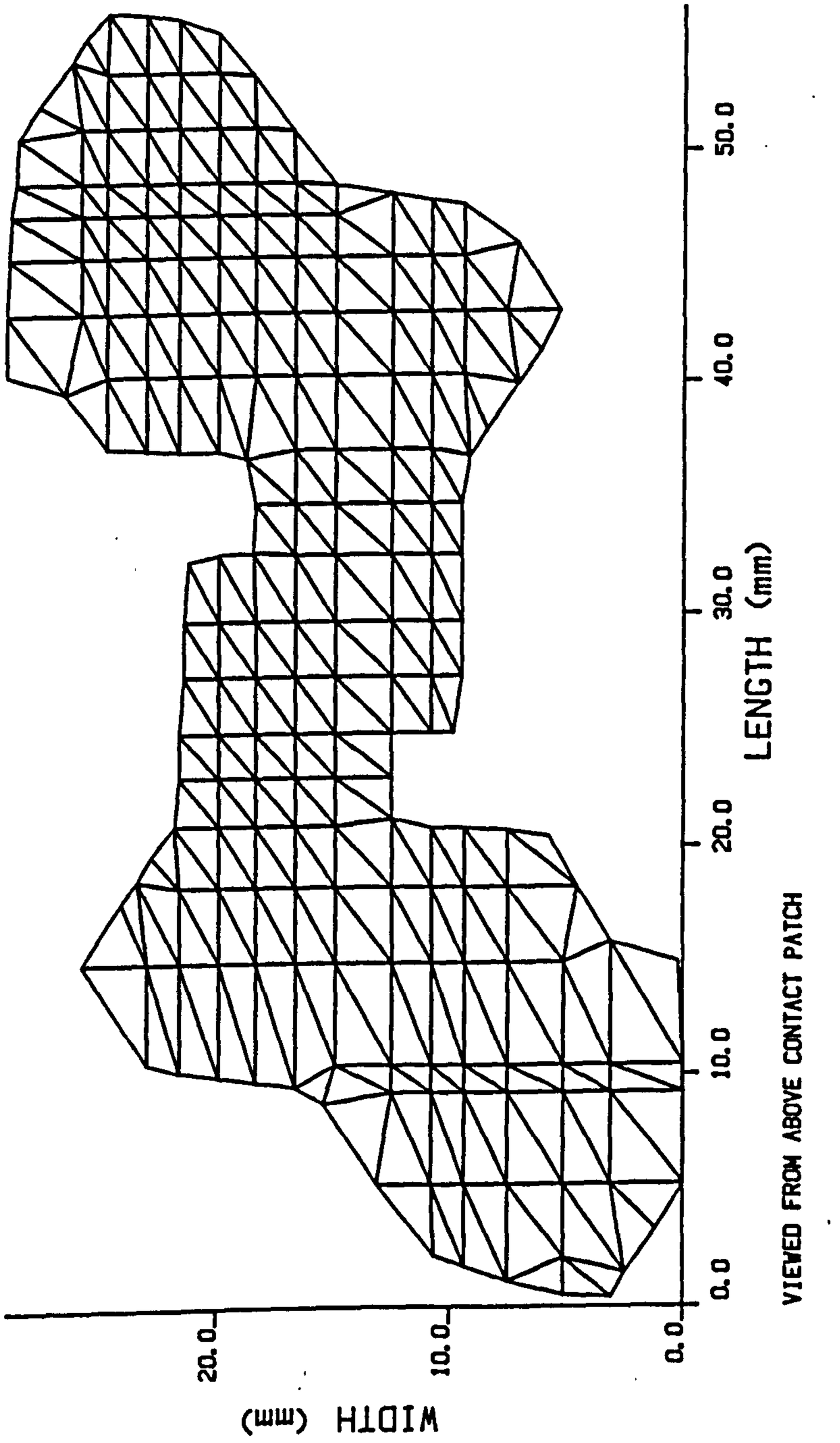

FIGURE 6.5.1 - DUNLOP SP ELITE BLOCK

The magnitude of the squeezing velocity used in this example was determined by considering the situation when a block is just entering the front of the wet contact patch, with a road surface water depth of the maximum normally found: 3 mm. To achieve contact with the road surface without any loss of contact area this block must move vertically downwards a distance of 3 mm in the time taken for the tyre to move forward 40 mm (the length of the additional part of the contact patch). The average vertical velocity is therefore given by 0.075x V_{ROAD}. If a road speed of say 100 Kph is considered then this gives a mean vertical velocity of approximately 2000 mm/s, which was used in this example. As the purpose of the block analysis computer program is to allow comparisons to be made between alternative block designs, the actual value of the velocity is not critical provided it remains consistant.

Because the analysis is provided at one instant in time, the height above the road surface of the block must be specified. If a number of different positions above the road surface are required then the 'time stepping' facility within the program can be utilized. As the worst case for vertical velocity was used, then the worst case for film thickness was also used. This is when there would be no film thickness between the block and the road surface if there were no deformation of the block. All film thickness is therefore due to block deformation, and the amount of this deformation gives a measure of how near to the required situation, of no film thickness, that particular block design comes. There are two simple ways of characterising this, maximum film thickness and total volume of 'trapped' water. As well as using these as a measure of a particular block's performance the load carrying capacity generated by that block can be compared with that of other alternative designs to assess which is most suitable. It is obviously desirable to have a low film thickness (trapped volume) and a low load carrying capacity. As with the square tread block, the fluid pressures at the edges of the ELITE block were assumed to be atmospheric. This models the case when the grooves of the tyre are not filled with water.

The fluid pressure distribution predicted for the ELITE block is shown in figure 6.5.2. Because the mesh in this case is not based on a rectangular grid, it is not possible to remove the 'diagonals' from the plots of pressure and film thickness. The fluid film thickness distribution is shown in figure 6.5.3 and is relatively large considering that the block should now be in contact with the road surface. The fluid flow velocities are shown in figure 6.5.4 and the volumetric flows per unit width in figure 6.5.5.

6.6 DISCUSSION OF EXPERIMENTAL AND ANALYTICAL RESULTS

This discussion is divided into three sections. The first two will deal with results for whole tyre contact patches, and the third with results for individual tread blocks.

The results (both analytical and experimental) presented here are for the two extreme cases of locked wheel and free rolling. In actual fact, under operating conditions, a tyre will develop its peak brake force coefficient at a slip of between 10% and 20% under straight ahead braking. Under cornering, where there are large sideways forces, the situation will be even more complex. The contact patch computer program has been designed so that any slip condition between free rolling and locked wheel can be specified. Also a slip angle can be specified. If it is required to model a tyre under cornering conditions, as well as specifying a slip angle, because a significant amount of the cornering effects will be due to a change in the contact pressure distribution, this must also be modified. The test conditions used here are only those for which experimental results are available (i.e. zero slip angle, free rolling or locked).

Because the main purpose of the analytical results is to show the areas of agreement (and disagreement) with the experimental results, the contact patch lengths, etc. were those that were found when testing on the drum (see section 6.1). There will still be some discrepancy between the conditions for the analytical and

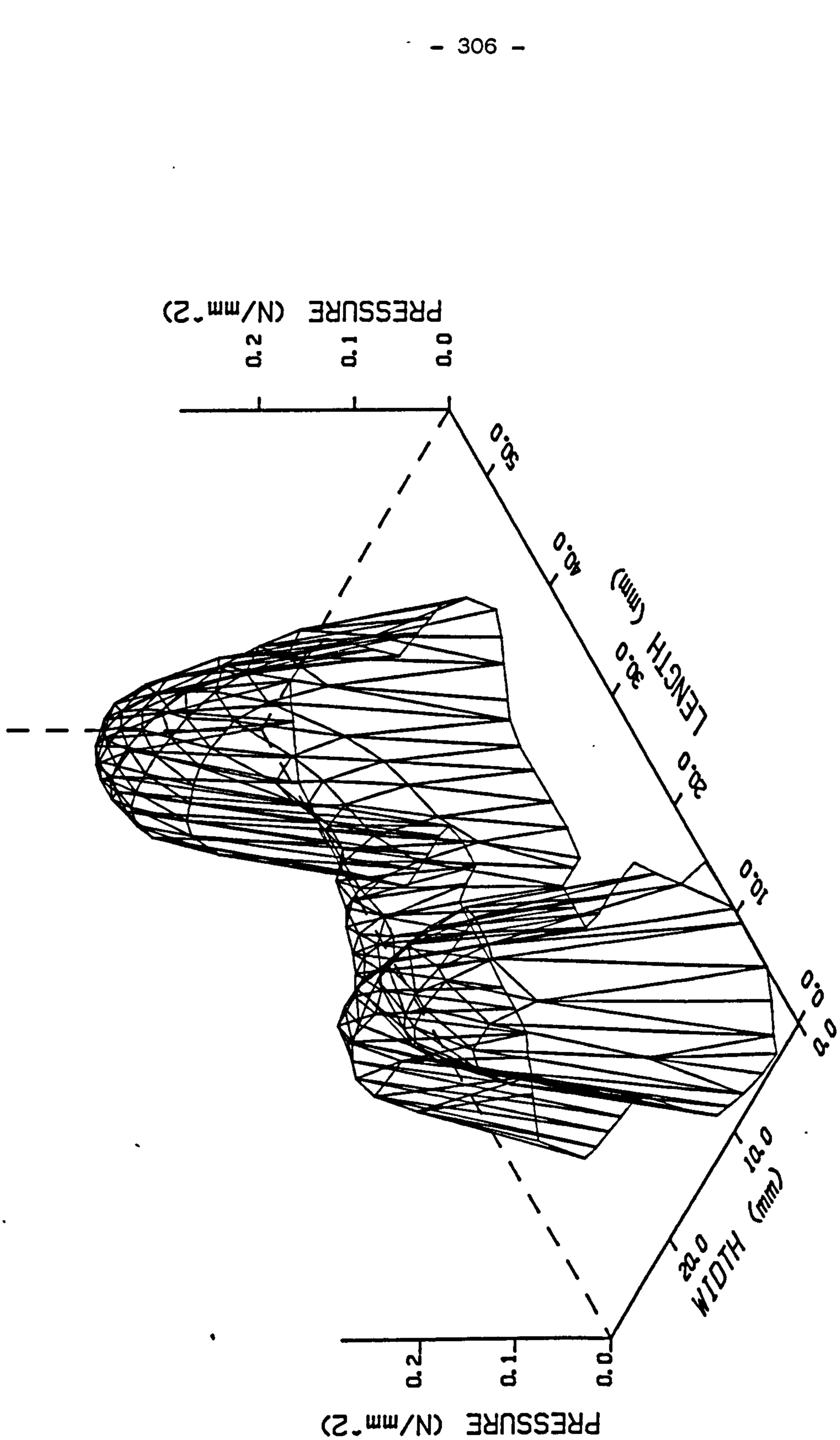

FIGURE 6.5.2 = DUNLOP SP ELITE BLOCK

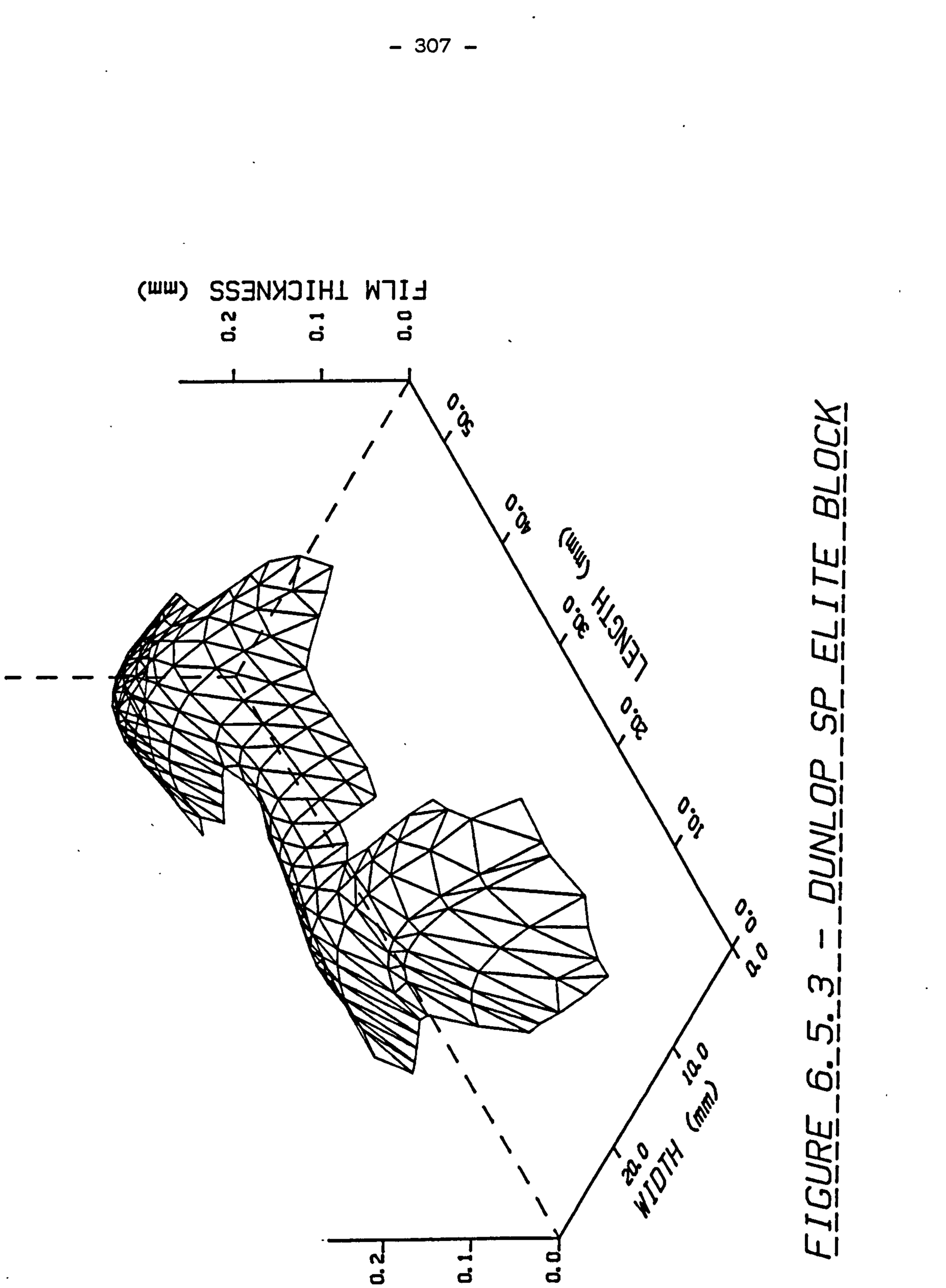

FIGURE 6.5.3 - DUNLOP SP ELITE BLOCK

FIGURE 6.5.4 - DUNLOP SP ELITE BLOCK

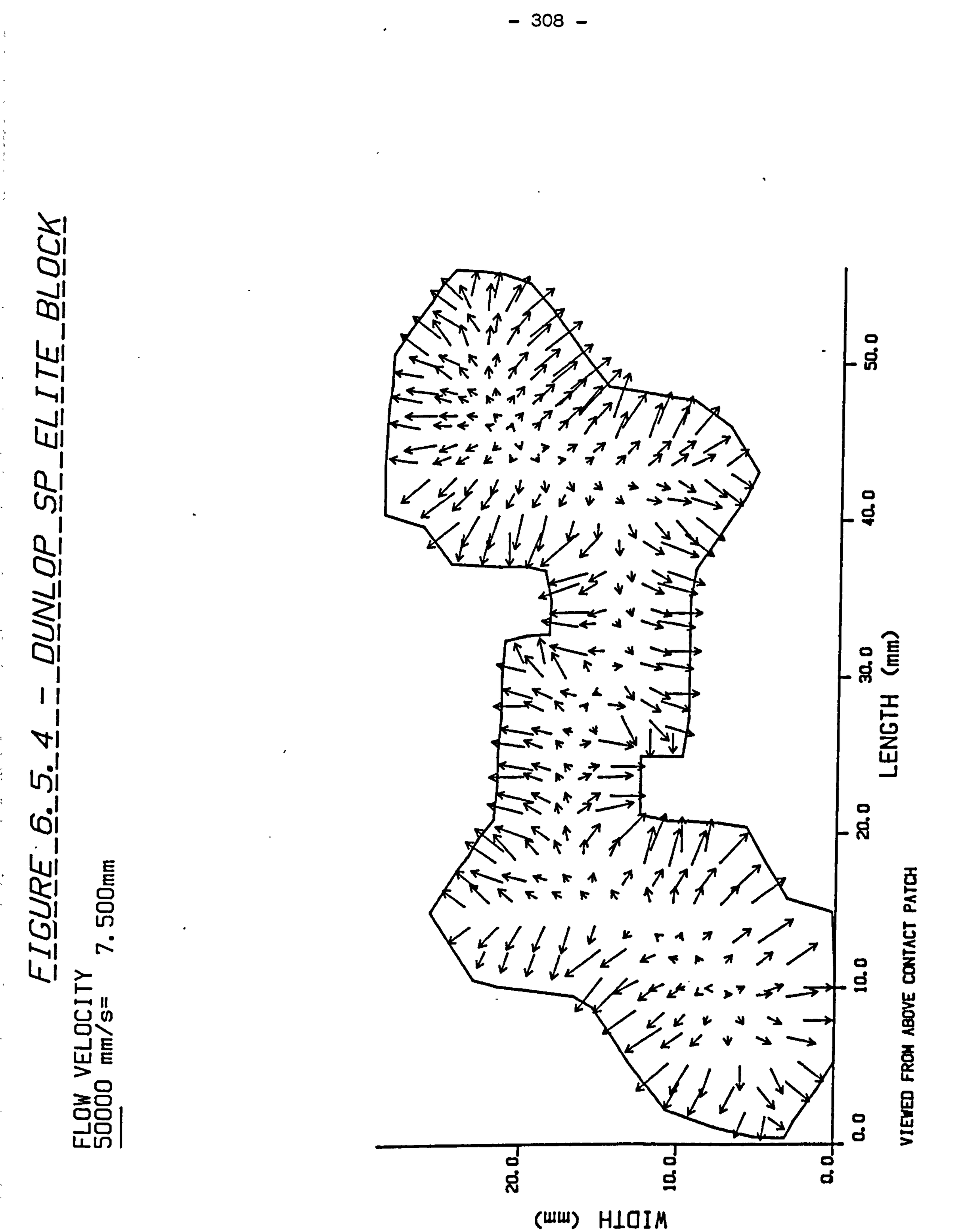

FIGURE 6.5.5 - DUNLOP SP ELITE BLOCK

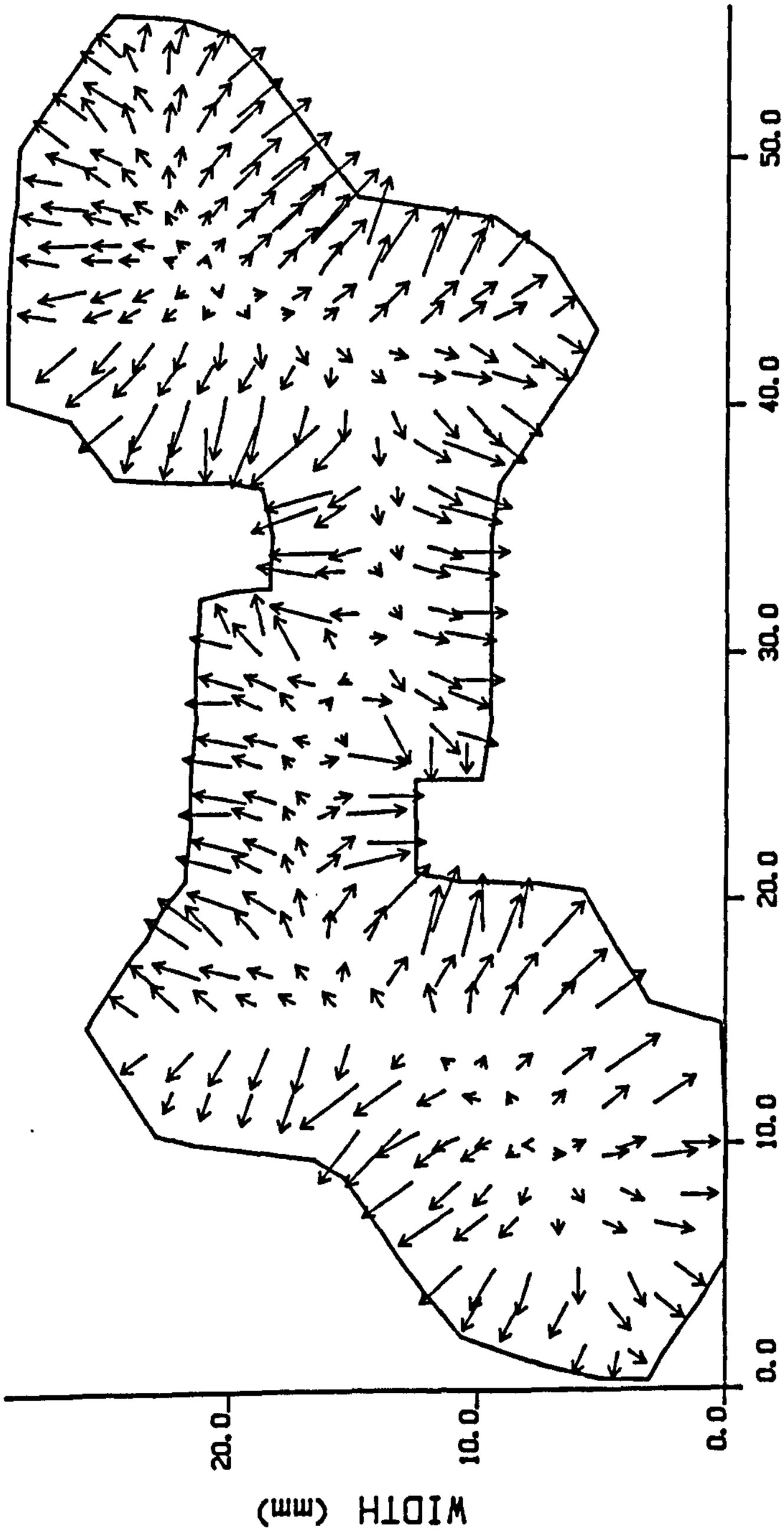

experimental results because the analytical results assume a flat road surface. Further areas of the analytical solution where there is not accurate modelling of the actual situation, are for the contact pressure distribution, and the contact patch vertical stiffnesses. As has already been discussed the contact pressure distribution will be modified from that measured, owing to both drum curvature and speed. No information is at present available on the distribution of contact patch vertical stiffness and a possible method of measuring this is discussed in section 8.3.1.

For both the plain and the grooved tyres the analytical representation of the contact patch is as a rectangle. This was done for simplicity, but the method allows contact patches with rounded ends to be modelled. However, with reference to figures 6.1.1 and 6.1.2 it can be seen that the actual contact patch shapes are not very rounded and it is thought that the mesh used here will give a reasonable representation of this.

6.6.1 Discussion of Tyre Contact Patch Results (50 Kph)

For the case of the plain tread tyre under free rolling conditions, the experimental pressure distribution is shown in figures 6.2.3 and 6.2.4. It can be seen that there tends to be an area of higher pressure at the front of the dry contact patch (i.e. approximately 30 mm into the front of the wet contact patch). This is due to the squeezing action as the forward part of the contact patch attempts to make contact with the road surface.

When the contact patch program was used to model this condition it was found that a large part of the contact patch was predicted to be in contact with the road surface. This obviously has an effect on the predicted pressures as it is not possible to have a fluid pressure where there is no actual fluid film thickness. The result (figure 6.2.5) therefore shows the proportion of the dry contact pressure that was applied in the region of tyre/road contact when the converged solution was obtained. The actual film thickness between the tyre and the road surface was measured using the fibre optic probe, but it was found that no significant output could be obtained under these conditions. This suggests that the magnitude

of the fluid film thickness is such that it is in the area where the sensitivity of the film thickness measurement system is poor (figure 5.6.3), and that the film thickness is therefore less than 0.2 mm.

As has already been discussed, in section 3.8.2, the subject of tread movements under free rolling conditions is little understood. The analytical model is therefore thought to be poorest at modelling the condition of a free rolling tyre. Some suggestions as to how this should be improved are made in sections 3.8.2 and 8.3.1.

As would be expected, from the fact that the tyre is predicted to be in contact with the road in much of the contact patch, the fluid flow velocities (figure 6.2.7) are very high as water is 'squeezed' out of the sides of the front section of the contact patch. Similarily the volumetric flows per unit width show a large quantity of water exiting from the contact patch in the front region. As has already been discussed the experimental fluid film thicknesses within the contact patch were very small, therefore the volumetric flows would not be greatly different to those predicted. This ejection of large quantities of water in the front of the contact patch can be seen in glass plate photographs, such as figure 5.3.1.

With the tyre moving at 50 Kph, but now with the wheel locked, the experimentally measured pressures (figures 6.2.9 and 6.2.10) show a general rise in pressure level towards the rear of the contact patch. This would be expected as the tyre is acting, to some extent, as a slider bearing. The low pressure area at the front of the contact patch is the additional contact patch length, where the fluid film thickness is greatest (due to the sloping of the tread surface). The pressure levels are shown to be higher in the shoulders than the centre of the contact patch. This is also shown in the analytically predicted fluid pressure distribution, which shows good agreement with the measured values. This analytical

solution shows small areas towards the rear of the shoulders which are in contact with the road surface. The film thickness predicted throughout the centre of the contact patch is however relatively large (0.1 mm), and shows an area towards the rear of the contact patch where the film thickness becomes larger. This is similar to the situation shown when a glass plate photograph was analysed (section 5.3.2), although in this case the wheel was not locked.

The effect of adding grooves to the plain tread tyre can be seen by comparing the above discussed case of 50 Kph locked wheel, with the grooved tyre under the same conditions. The film thickness distribution predicted for the grooved tyre is very different to that predicted for the plain tyre. With the grooved tyre the film thickness is one order of magnitude lower (0.01 mm rather than 0.1 mm) in general, than those for the plain tread tyre. However, the film thickness in the case of the grooved tyre is very much more uniform over the contact patch, i.e. no significantly lower films in the shoulders. In fact with the grooved tyre there are no areas of actual tyre/road contact, as these were with the plain tread tyre. For improved wet grip it is felt that it is important to have a low film thickness over the whole of the contact patch, because with a real road surface this film would then be broken-up by the road surface asperities (microtexture). It is this general reduction in fluid film thicknesses that gives the grooved tyre its improved wet grip level over that of the plain tread tyre.

The fluid pressure distribution which was measured for the grooved tyre shows that the grooves have a large effect on pressures, and that the pressures are very low within the grooves themselves. The pressure levels in the shoulder and the centre of the contact patch are broadly similar for plain and grooved tyres, although because the load capacity must be the same in both cases, the high shoulder pressures are maintained over a greater width in the case of the grooved tyre. This compensates for the lack of load capacity in the groove areas. The experimental measurement of

pressure shows that the pressure in the centre of the contact patch is raised slightly in the case of the grooved tyre. The analytically predicted pressure distribution for the grooved tyre shows good agreement with the measured values. The analytically predicted pressures show a dip in the shoulders which is not present in the measurements. This is probably due to the discretization of the contact pressure into values at nodes.

The flows of water within the contact patch, as analytically predicted, are as would be expected, very different for the grooved and plain tyres. Figure 6.2.13 shows the flow velocities for the plain tyre and figure 6.3.7 for the grooved tyre. The velocity of water ejected from the side of the contact patch is reduced by over 50% for the grooved tyre, as some of the water flows towards the grooves. By considering the volumetric flows per unit width (figures 6.2.14 and 6.3.8) a greater insight to the differences in flow can be gained. With the grooved tyre (noting the different volumetric flow scales) the volume of water exiting the contact patch to the sides can be seen to be approximately 25% of that in the case of the plain tyre. This is because the water in the centre of the contact patch passes through the grooves. In both cases the volume of water flowing in the main part of the contact patch (excluding grooves) is small compared to that in the front section.

Because, with the grooved tyre, the water does not mainly get removed from the side, there is very little deformation of the front of the contact patch (6.3.6b). This in itself is beneficial as it prevents the formation of a 'pocket' where water can become trapped in the front of the contact patch, and if the tyre had a tread pattern with blocks, it would reduce the inclination of those blocks (section 6.6.3).

6.6.2 Discussion of Tyre Contact Patch Results (100 Kph)

For the case of 100 Kph free rolling with the plain tread tyre, the experimental pressure distribution is shown in figures 6.2.15 and 6.2.16. In the centre of the contact patch there are high pressures towards the front which are due to the squeezing action. However, there are also high pressures at the rear of the contact patch. This coincides with the area of high film thickness which was measured in the centre rear of this tyre under this condition.

The measured fluid film thicknesses are larger than those predicted by the computer program, particularly towards the rear of the contact patch. This is thought to be due to the poor modelling of contact patch movements under rolling conditions as already discussed. As the film thickness measurement system relied on the tyre surface reflectivity remaining constant for the duration of the test, it is possible that the measured values are also in error. The effect of tyre polishing would be to increase the gain of the measurement system and therefore exaggerate the results. The presence of an area of thicker film towards the rear of the contact patch would not be affected by this. This area coincides with that shown by the glass plate/image analysis method discussed in section 5.3.2. The fluid film thickness shape measured by Browne, figure 1.2.3, shows film thicknesses even higher than those that have been measured here. Browne's results are for a plain tyre travelling at 68 Kph, but as was discussed in section 1.2.1, the tread was made from white sidewall rubber and the tyre was under inflated. The shape of the film measured by Browne is very close to that measured here. It is thought that the film thicknesses measured here are closer to being correct than those measured by Browne as the tyre is under the correct conditions and the only errors involved are those due to the measurement method (and drum curvature).

A further reason for the analytical film thicknesses not coinciding well with the experimental ones is the tyre vertical stiffness being considered uniform over the contact patch. It is felt that if measurements were made, the stiffness would be lower in the centre of the contact patch than in the shoulders. This would allow the analytically predicted film thicknesses to be greater for the same level of fluid pressure distribution in the centre of the contact patch.

Because of the relatively large film thickneses predicted at the front of the contact patch there are flow velocities showing a loss of water to the side in the front half of the contact patch. The rear of the shoulders are in contact with the road surface, therefore no flow velocities (figure 6.2.20) or volumetric flows per unit width (figure 6.2.21) are shown in these regions.

Figure 6.2.22 shows the individual pressure profiles for the case of 100 Kph locked with the plain tread tyre. As has already been discussed pressure values are only available for three lateral positions on the tyre, owing to a problem with the instrumentation. From figures 6.2.22 and 6.2.23 it can be seen that there is a general increase in pressure towards the rear of the contact patch. The pressure is also very even across the width of the contact patch, and this is also reflected in the analytically predicted pressures (figure 6.2.24). However as there are only a limited number of experimental pressure profiles available, it is possible that a high area of pressure has been missed (position 4). If one compares this 100 Kph locked pressure distribution with the corresponding one at 50 Kph, it can be seen that at the higher speed both analytical and experimental pressures show a much more even distribution over the contact patch. Reference (21) presents pressure profiles for the centre and shoulders of a rolling tyre at 40, 50 and 60 Mph, and this also shows that there is some evening up of pressures at the high speed, compared to the lower speed distribution with high shoulder pressures (as shown here in figure 6.2.11).

The experimental pressure profiles (figure 6.2.22) show a sharp drop in pressure (almost to atmospheric) in the centre of the contact patch. This would appear to be due to some form of buckling of the contact patch surface under these conditions. It should be remembered that the pressure profiles presented here are as a result of averaging the values from a number of consecutive passes of the pressure transducer through the contact patch. This sharp drop in pressure appeared on all these different samples.

It is thought that this type of buckling of the contact patch would only occur for plain tread tyres (it did not appear with the grooved tyre), and that it is due to the effect of 'straightening' the tyre tread surface from the curved shape outside the contact patch. This would cause the tread surface to be under compression. In a tyre with a tread pattern this effect would be prevented by closure of the grooves.

The experimental pressures for the grooved tyre under the same conditions (figure 6.3.9) show, by comparison with figure 6.2.22, the difference that the grooves make to the pressure distribution. Apart from the lack of any dip in the pressure, the distribution in the very centre of the contact patch is virtually unaffected by the addition of the grooves. However, near to the grooves the pressure falls and this loss of load capacity is compensated by higher pressures in the shoulders.

Compared to the grooved tyre at 50 Kph, at 100 Kph the pressures in the grooves are much higher. This is due to the extra volume of water which has to be removed from the contact patch at the higher speed, which causes a pressure build-up in the grooves as they fill with water.

The analytically predicted pressure distribution for the grooved tyre at 100 Kph (figure 6.3.11) shows good agreement with the measured values. In the shoulder regions the analytical distribution has a number of peaks. It is thought that this is due to

the discretization of the contact pressure into values at nodes, and that if more nodes were used then these peaks would at least be smoothed. At 100 Kph the pressures at the front of the grooves are predicted to be higher than at 50 Kph, but are lower than those measured. Examining the predicted film thickness distribution for the grooved tyre at 100 Kph (figure 6.3.12a) shows that there are relatively large film thicknesses in the areas at the front of the grooves. This is probably the reason why the pressures in this area are predicted lower than those that were measured.

Comparing the analytical film thickness distributions for the plain and grooved tyres at 100 Kph with locked wheels shows, as would be expected, that the film thicknesses for the grooved tyre are generally lower than those for the plain tyre. The distribution of film thickness is also much more even for the grooved tyre; although it is not as even as the grooved tyre at 50 Kph, indicating that the grooved tyre at 100 Kph is losing some of the advantage in wet grip level given by the grooves. The film thickness distribution for the plain tread tyre shows low film thickness in the shoulder regions with a large film thickness from front to rear of the contact patch in the centre. The actual shape of this distribution is almost identical to that measured by Browne (figure 1.2.3) although in this case the tyre is locked. This film thickness also shows the area of thicker film towards the rear of the contact patch as shown from glass plate photographs in section 5.3.2. Again the glass plate photographs are for free rolling whilst figure 6.2.25a is for locked wheel. However as glass plate photographs are taken with the tyre mounted on a vehicle, the amount of slip can not be guaranteed to be zero, and the tyre may have been sliding to some extent. This area of deeper water to the rear of the contact patch, therefore, may exist under both rolling and sliding conditions.

Figure 6.3.12b shows that the deformation of the tyre at the front of the contact patch is very much lower for the grooved tyre than for the plain tread tyre (figure 6.2.25b). This is due to the

ability of water to flow through the contact patch (down grooves) rather than having to flow out of the side.

The analytically predicted fluid flow velocities show that the velocity at which water is ejected from the sides of the contact patch, is reduced in the case of the grooved tyre (figure 6.3.13) compared to the plain tyre (figure 6.2.26), as was also found at 50 Kph. With the plain tread tyre some water flows through the centre of the contact patch (figure 6.2.27) because of the high deformation there. There is also some water flowing out of the side, throughout the whole length of the contact patch, in the case of the plain tread tyre. The volumetric flow velocities for the grooved tyre are shown in figures 6.3.14 and 6.3.15. Figure 6.3.15 has the volumetric flows in the grooves omitted so that they can be plotted on the same scale as the volumetric flows for the plain tyre (figure 6.2.27) to allow easier comparison. The volume of water flowing out of the side of the contact patch is substantially reduced for the case of the grooved tyre. Water flows down the grooves (figure 6.3.14) rather than out of the side of the contact patch. With the plain tread tyre there is also some water which flows out of the side, well into the contact patch. With the grooved tyre all water which passes past the front portion of the contact patch, passes out of the rear.

The grooves therefore encourage water to pass through the contact patch rather than out of the sides. Whilst in overall terms the grooves improve performance in the wet, they do appear to have some detrimental effects, as well as beneficial ones. The challenge to the tyre designer is to gain the benefits only, without the detrimental effects of grooves. It would seem, from examining the results here, that the most advantage could be gained from the two grooves if it were possible to arrange that the grooves were closed at the front, preventing water flow into the main body of the contact patch, and to have the grooves open in the main body of the contact patch to allow what water was there to flow easily so as to reduce fluid pressures and, it would be hoped, film

thickness. It is this reduction in film thickness that must be the overall aim to improve wet grip levels.

6.6.3 Discussion of Results for Individual Tread Blocks

The experimental pressures for the central row of blocks, with the 'blocky' tyre are shown in figure 6.4.2. The pressure at the lateral grooves falls very rapidly, in some cases to below atmospheric. The pressure also builds up very quickly at the front edges of the blocks. This is because of the flow of water into the front of each block, as was discussed in section 6.4. The variation of the amount of this flow is one of the major features which causes different pressures on the same size block in different parts of the contact patch.

The analytically predicted fluid pressure distribution for a single tread block of the type used in the 'blocky' tyre is shown in figure 6.4.4. The pressure builds up slowly in this case as no flow velocities are specified into the front of the block.

By considering different inclinations to the horizontal, it was shown (figure 6.4.3) that as the block becomes more parallel to the road surface then the load carrying capacity will drop rapidly. This reduction in inclination would be achieved if the deformation of the tyre is reduced at the front of the contact patch. In fact if the contact patch deformation is made more even, then it would appear to be beneficial to the load capacity of individual blocks.

Because the block deforms under the action of fluid pressure (figure 6.4.5) the amount of water lost from the edge of the block will be less than in the rigid case, and the pressure will be more even across the width of the block.

As was noted in section 6.4, before the block analysis computer program can be used to assess block characteristics under sliding conditions more information has to be gained on the flow

characteristics into blocks at different parts of the contact patch.

An alternative method of assessing block performance is to consider the block under squeezing. Normal operating conditions for a tyre are with predominant rolling, therefore there is squeezing in the front of the contact patch. The Dunlop SP ELITE centre block analysis shown here is an example of an analysis on an actual production tread block. The finite element mesh (figure 6.5.1) for this block was produced by using the mesh generation program, described in section 4.6.

In the example shown, the block would be touching the road surface if it were not for the water film. The analytical pressure distribution shows very even pressures over the block with a sharp drop at the edges. This is because the deformation of the block (figure 6.5.2) is less at the edges, which in turn causes the pressure at the edges to be higher than would be expected for a rigid block.

Figure 6.5.4 shows the flow velocities and it can be seen that these are relatively high at the edges of the block, and into the two 'cut-outs'. The volumetric flows per unit width (figure 6.5.5) show that a large volume of water is flowing into the cut-outs. To assess the effect on load capacity of these cut-outs, the block was modelled under the same conditions but without the cut-outs. The load capacity in this case was increased by approximately 20% from the load found for the standard block. A number of alternative positions for the two cut-outs were investigated and it was found that a 15% to 20% improvement (reduction) in load capacity could be gained over the standard design.

The overall effect of this on a tyre's performance is difficult to determine, but it is safe to assume that a reduction in load capacity for an individual tread block will cause an improvement in the wet grip performance of the tyre as a whole.

In modelling the SP ELITE, sipes were not considered. This is because the sipes in an ELITE are closed-ended, and therefore by not considering them it is the same as assuming that they are filled with water.

A different tread block, which had open ended sipes was modelled. The sipes were considered to be completely drained and therefore the pressure was atmospheric within the whole of the sipes. The same block was also modelled without the sipes and it was found that the sipes caused a 25% reduction in the wet load capacity of the block. Treating the sipes in this way gives the best possible effect which could be gained, and it is likely that in practice the pressure will not be completely zero within the sipes. A method of improving the modelling of sipes is suggested in section 8.3.1.

It can be seen from the above that the use of sipes, particularly if placed in the optimum positions, can give very large improvements in wet grip levels. The major problem with sipes is that they tend to close owing to the loading on the block. One way of reducing the effects of closure on sipes is to make them wider, when they in effect become narrow cut-outs of the type shown in the ELITE block. Another method of reducing closure is to reduce the depth of the sipe, but this will cause problems when the tyre is partly worn.

The performance of blocks can be improved by the use of cut-outs and/or sipes which give low resistance to flow paths to allow water to reach the edges of the block. If one considers the context in which the block is being used, then to some extent the size of the grooves should be taken into account when positioning cut-outs etc. so that the additional flow of water at that point will not cause problems by filling the grooves.

CHAPTER 7 - NETWORK ANALYSIS

7.1 INTRODUCTION TO NETWORK ANALYSIS

Network Analysis is a technique that can be used in the planning and control of projects. The basic principle is that the project is split into a number of activities, and the interconnections (constraints) between these activities determine the order in which the activities must be undertaken. In very large projects the level of subdivision (into individual activities) necessary can be difficult to determine, and often an overall network of the project is produced, with subnetworks detailing areas which were shown as only one activity on the main network.

This level of detail of the network obviously varies depending on the type of activity being represented. If for example a network was being produced to assist in the planning of the assembly of a car, then the level of detail would be great and the activities would be well defined, and importantly the time to undertake each activity would also be well defined. In the case of a research project, such as here, the activities are not well defined and may change as the project progresses. The time assigned to each activity in this case is therefore very much a rough estimate. To allow network analysis to be useful in this type of project regular updating is necessary.

The updating of the network serves two purposes, the activities which have been completed can be deleted and new activities can be added, and also the time for all the activities can be reassessed. This allows the anticipated finish date to be continuously updated. By using the information on activity times, the critical patch for the network can be found. Activities on the critical path have no slack (or float) and any increase in their event time will cause a corresponding increase in the total project time. Knowing which activities are on the critical path allows work to be scheduled so that these activities are given the most priority. During the life

of the project the activities which are on the critical path may change and by updating the network this can be seen and the priority of activities modified accordingly.

A further problem in research projects is that some activities will be outside direct control, and network analysis allows these to be closely monitored and other work to be rescheduled to best fit in with them.

7.2 THE USE OF NETWORK ANALYSIS FOR THE WET GRIP PROJECT

To allow the monitoring of progress on the wet grip project a network was produced and then updated at regular (6 monthly) intervals. To illustrate this the original network and one updated network will be shown, along with charts showing the earliest start date and total float for each activity. The notation used in figures 7.2.2 and 7.2.4 is as follows:-

I - start node for activity
J - end node for activity
DU - duration of activity (weeks)
TF - total float for activity (weeks)
ES - earliest start for activity (weeks from start of project)
A - ascending order.

7.2.1 Original Network

The original network was produced some time after the start of the project, after the first major problem had occurred. This was a fault in the radio telemetry system which necessitated its return to the manufacturer. The activity "have fault repaired" represents this and the estimated time to repair was 18 weeks. In reality this took longer, but considering the original network (figures 7.2.1 and 7.2.2), it can be seen that this activity was not on the critical path, with its time at 18 weeks, and that there was a total float of 14 weeks (figure 7.2.2). The total

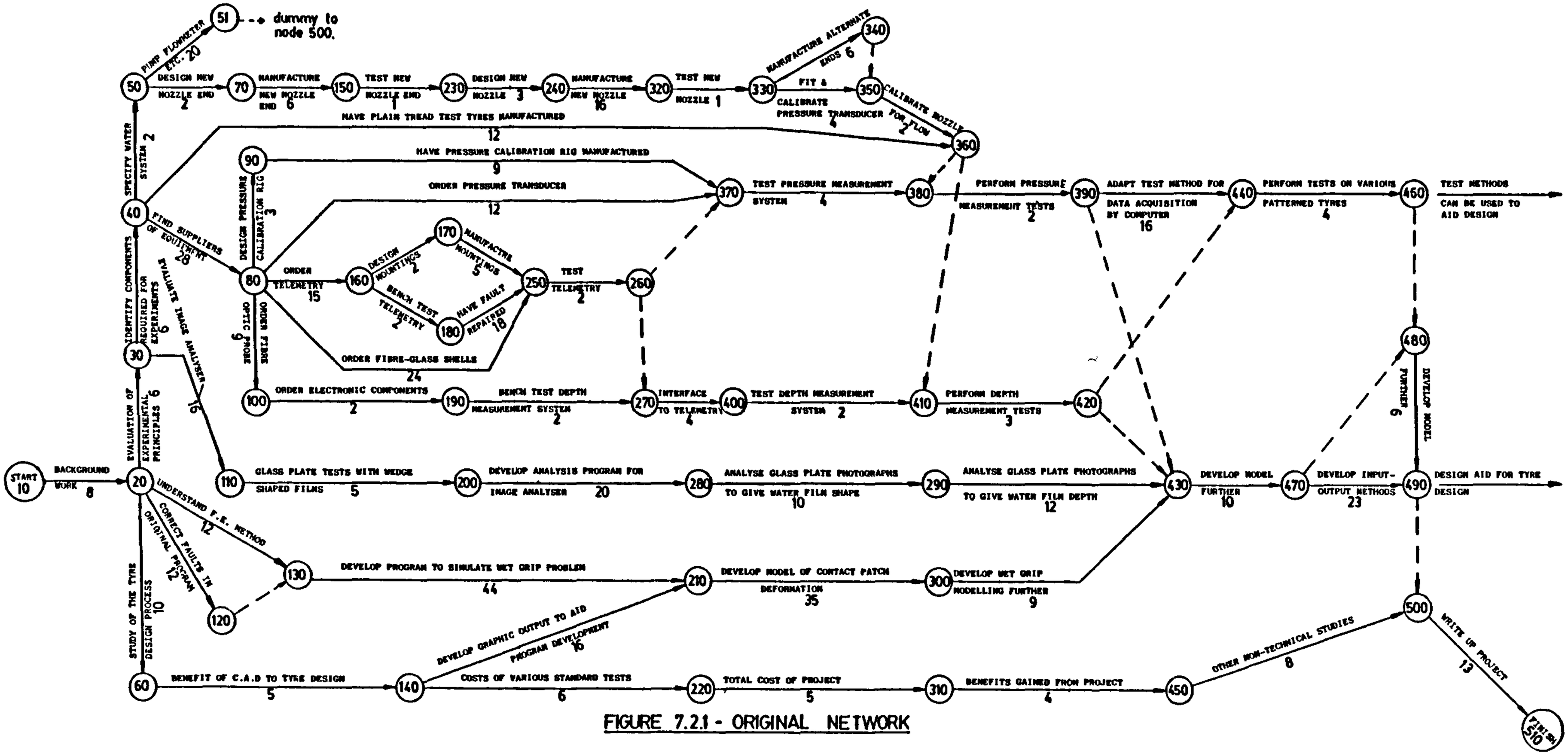

FIGURE 7.2.1 - ORIGINAL NETWORK

FIGURE 7.2.2 - TIME ANALYSIS OF ORIGINAL NETWORK

SCHEDULE BY TF [illegible] THEN ES [illegible]

I	J	DU	TF	ES	DESCRIPTION
10	20	8	0	0	[illegible]
20	130	12	0	8	[illegible]
20	120	12	0	8	[illegible]
130	210	44	0	20	[illegible]
120	130	0	0	20	[illegible]
210	300	35	0	64	[illegible]
300	430	9	0	99	[illegible]
430	470	10	0	108	[illegible]
470	490	23	0	118	[illegible]
500	510	13	0	141	[illegible]
490	500	0	0	141	[illegible]
20	30	6	14	8	A12-EVAL PRIN
30	40	6	14	14	A13-ID COMP
40	80	28	14	20	A24-FIND SUPLI
80	160	15	14	48	A14-ODR TELEM
160	180	2	14	63	A15-BEN TES TEL
180	250	18	14	65	A16-FAULT
250	260	2	14	83	A17 TES TELEM
270	400	4	14	85	A30-INTER TO TEL

SCHEDULE BY TF [illegible] THEN ES [illegible]

I	J	DU	TF	ES	DESCRIPTION
260	270	0	14	85	DUMMY
400	410	2	14	89	A31-T DEP MEAS
410	420	3	14	91	A32-DEPTH TESTS
420	430	0	14	94	DUMMY
370	380	4	17	85	A21-T P MEAS SY
260	370	0	17	85	DUMMY
380	390	2	17	89	A22-P MEAS TEST
390	430	0	17	91	DUMMY
480	490	6	17	118	A56-DEV MODEL
470	480	0	17	118	DUMMY
390	440	16	24	91	A23-DAT ACQ COM
440	460	4	24	107	A26-PATTERN TEST
460	480	0	24	111	DUMMY
20	60	10	25	8	A50-STD DES PROC
60	140	5	25	18	A53-CAD TO DES
140	210	16	25	23	A48-GRA OUT
80	250	24	25	48	A25-ORD SHELLS
160	170	2	27	63	A18-D MOUNT
170	250	5	27	65	A19-M MOUNT

(continued)

FIGURE 7.2.2 - continued

SCHEDULE BY TF ▣ THEN ES ▣

I	J	DU	TF	ES	DESCRIPTION
30	110	16	31	14	A36-EVAL IMANAL
110	200	5	31	30	A37-WEDGE FILM
200	280	20	31	35	A38-ANALYS PRO
280	290	10	31	55	A39-ANAL FIL SHP
290	430	12	31	65	A40-ANAL DEPTH
420	440	0	37	94	DUMMY
80	100	9	38	48	A27-ORD IB PROB
100	190	2	38	57	A28-ORD ELEC COMP
190	270	2	38	59	A29-BEN T DEPTH
80	90	3	42	48	A33-D P CAL RIG
80	370	12	42	48	A20-ORD P TRANS
90	370	9	42	51	A34-M P CAL RIG
40	50	2	46	20	A1-SPEC WATER
50	70	2	46	22	A2-D NOZ END
70	150	6	46	24	A3-M NOZ END
150	230	1	46	30	A4-T NOZ END
230	240	3	46	31	A5-D NEW NOZ
240	320	16	46	34	A6-M NEW NOZ
320	330	1	46	50	A7-T NEW NOZ

SCHEDULE BY TF ▣ THEN ES ▣

I	J	DU	TF	ES	DESCRIPTION
330	340	6	46	51	A10-M ALT END
350	360	2	46	57	A11-CAL NOZ
340	350	0	46	57	DUMMY
360	410	0	46	59	DUMMY
360	380	0	47	59	DUMMY
330	350	4	48	51	A8-F&CAL P T
40	360	12	73	20	A35-TEST TYRES
140	220	6	95	23	A52-COS TESTS
220	310	5	95	29	A54-COS PROJECT
310	450	4	95	34	A55-BEN PROJECT
450	500	8	95	38	A57-OTH NONTEC
50	51	20	99	22	A9-SPEC PUMP
51	500	0	99	42	DUMMY

(TIME UNITS = WEEKS)

time for this activity could therefore have increased to as much as 32 weeks before affecting the critical path at which point all the activities shown in figure 7.2.2 with a total float of 14 weeks would have been on the critical path. In reality it did not take 32 weeks to have the telemetry repaired, therefore the critical path was unaffected.

From figure 7.2.2 it can be seen that the critical path was through the development of the computer model, but it should be borne in mind that time estimates for computer programming are very difficult to determine accurately.

The networks shown here do not take account of the resources required, and in certain cases this will delay the time from that given. Many of the activities rely on human resources which in this case amounted to one person. There inevitably had to be some trade-off in the scheduling of activities to allow for this, and whenever possible activities with the least amount of float were undertaken first. Some of the activities rely on items being manufactured or delivered and in this case no resource is being utilized during that activity. The fault in the telemetry system also falls into this category as it was possible to perform different activities whilst waiting for it to be repaired.

7.2.2 Updated Network

The updated network presented here is one of a number that were produced throughout the project. The updated network shown in figure 7.2.3 was produced at the time when the second major set-back in the experimental programme had taken place. This was a breakdown of the cornering force machine on which the tests were to take place. The machine had in fact been broken down a number of weeks when this network was drawn up and the time of 8 weeks was an estimate for the remaining time. However the fault on the machine turned out to be more serious than was thought at this time and the actual time to repair (from week 100) was in fact

FIGURE 7.2.3 - UPDATED NETWORK (AT WEEK 100)

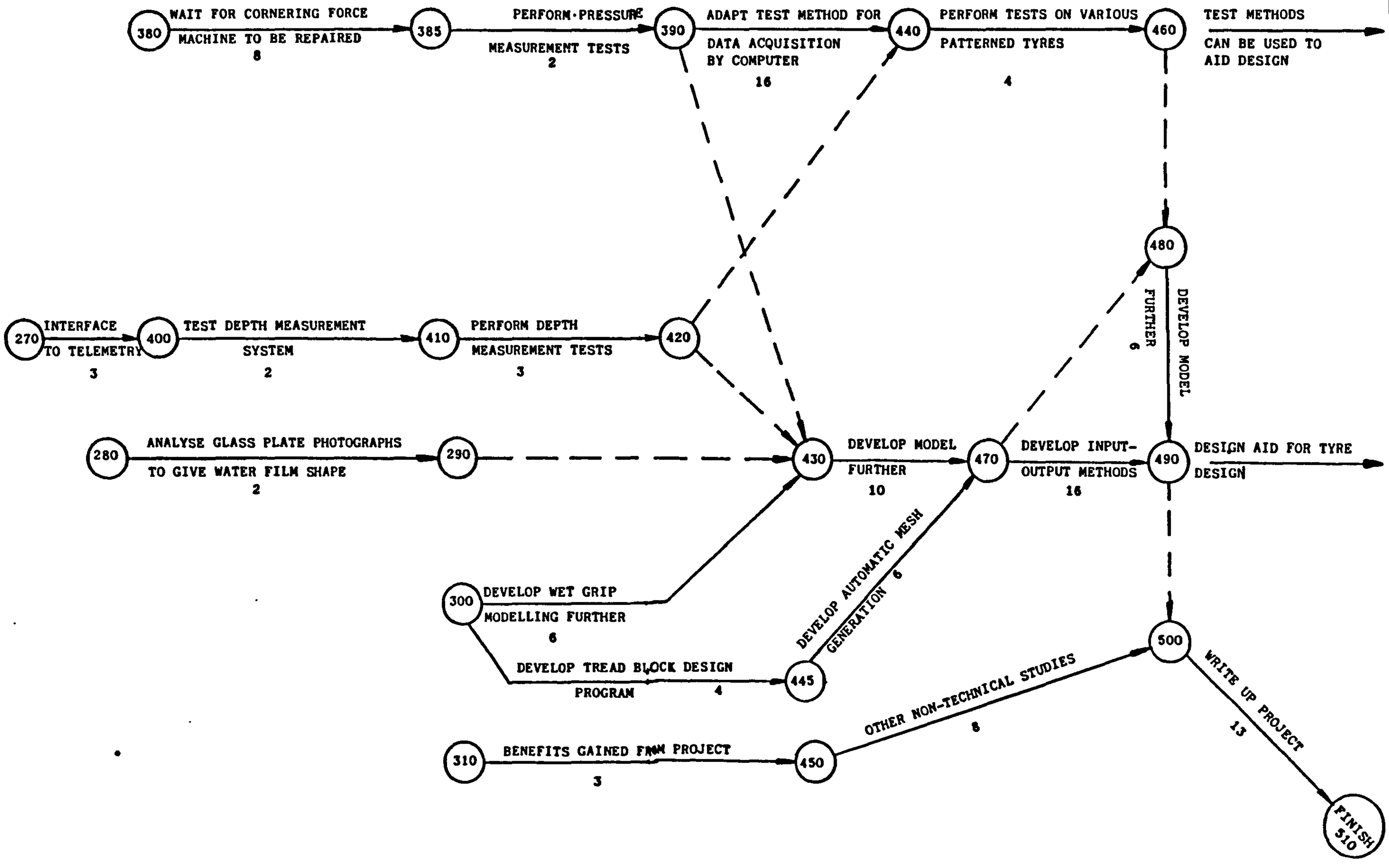

Text cut off in original

20 weeks, and even then this was only a temporary repair which allowed limited testing on locked tyres. Some testing was carried out with this temporary repair, but it was a further 10 weeks before the machine was completely repaired. The machine had then been out of commission for a total of 36 weeks, and understandably a considerable backlog of work had built up. This meant that the rest of the testing could not be carried out immediately and "data acquisition by computer" could not be achieved, as discussed in section 5.4.4. Because the repair to the cornering force machine was on the critical path (figure 7.2.4) then all delays outlined above would have affected the finish date of the project. However, as the acquisition of data by computer was not performed this saved time, as did the activity "develop input-output methods" which was shortened considerably. The finish date for the project was still delayed and this was largely due to the breakdown of the cornering force machine.

The updated network (figure 7.2.3) shows two activities which have been added, and these are "develop tread block design program" and "develop automatic mesh generation". These activities resulted from the study of the tyre design process (see chapter 2), and were carried out whilst waiting for the temporary repair to be made to the cornering force machine.

From figure 7.2.4 it can be seen that all the main items of the project have very little float and with the errors in time estimating, and possible delays, virtually any activity could have gone on to the critical path.

7.3 CONCLUSIONS FROM THE USE OF NETWORK ANALYSIS ON THE WET GRIP PROJECT

By comparing the two networks shown in figures 7.2.1 and 7.2.3 and detailed in figures 7.2.2 and 7.2.4 respectively, it can be seen that the large amount of float available on many activities early in the project was lost by the time the update shown here was produced. This can be attributed to a number of factors, the fault on the telemetry, the breakdown on the cornering force

FIGURE 7.2.4 - TIME ANALYSIS OF UPDATED NETWORK (AT WEEK 100)

SCHEDULE BY TF ▒ THEN ES ▒

I	J	DU	TF	ES	DESCRIPTION
380	385	8	0	100	▒▒▒▒▒▒▒▒▒▒▒▒
385	390	2	0	108	▒▒▒▒▒▒▒▒▒▒▒▒
390	440	16	0	110	▒▒▒▒▒▒▒▒▒▒▒▒
430	470	10	0	110	▒▒▒▒▒▒▒▒▒▒▒▒
390	430	0	0	110	▒▒▒▒▒
470	490	16	0	120	▒▒▒▒▒▒▒▒▒▒▒▒
440	460	4	0	126	▒▒▒▒▒▒▒▒▒▒▒▒
480	490	6	0	130	▒▒▒▒▒▒▒▒▒▒▒▒
460	480	0	0	130	▒▒▒▒▒
500	510	13	0	136	▒▒▒▒▒▒▒▒▒▒▒▒
490	500	0	0	136	▒▒▒▒▒
270	400	3	2	100	A30-INTER TO TEL
400	410	2	2	103	A31-T DEP MEAS
410	420	3	2	105	A32-DEPTH TESTS
420	430	0	2	108	DUMMY
300	430	6	4	100	A46-DEL MOD FUR
280	290	2	8	100	A39-ANAL FIL SHP
290	430	0	8	102	DUMMY
300	445	4	10	100	A81-DEV TR BLK

SCHEDULE BY TF ▒ THEN ES ▒

I	J	DU	TF	ES	DESCRIPTION
445	470	6	10	104	A82-DEV MESH GEN
470	480	0	10	120	DUMMY
420	440	0	18	108	DUMMY
310	450	3	25	100	A55-BEN PROJECT
450	500	8	25	103	A57-OTH NONTEC

(TIME UNITS = WEEKS)

machine, and poor time estimating. This highlights the problem of using network analysis on research projects, as by their very nature they are unique, and therefore time estimates are difficult to predict accurately.

As has been mentioned the allocation of resources has not been considered here, and in practice this is probably a further reason why the initial completion date was not met. However, despite all the problems it is felt that the use of network analysis on this project was useful, particularly when discussing progress with other people, as this allowed them to build up a picture of the project and the remaining activities. The network was also useful when adding extra activities, such as the block design and mesh generation computer programs, so that their effect on the rest of the project could be seen.

CHAPTER 8 - CONCLUSIONS AND SUGGESTIONS FOR FURTHER WORK

8.1 INTRODUCTION TO CONCLUSIONS AND SUGGESTIONS FOR FURTHER WORK

The work undertaken in this project represents the first stage of development in computer modelling of wet grip for use in the tyre design process. Also, the experimental techniques developed here are the first stage in the development of tests which will allow the routine testing of tyres during the design process. The tests also provide verification of the mathematical model. The "suggestions for further work" section is particularly important as it gives the author's views on what developments should be made both to the mathematical model and to the experimental facilities.

Whilst the broad aim of this project was to produce a computer model of a tyre operating under wet conditions, it was clearly not possible to achieve this completely in the duration of this project. The conclusions therefore reflect the success achieved in progressing towards this overall aim.

8.2 CONCLUSIONS

The computer models that have been developed, allow the further study of many aspects of tyre wet grip. The contact patch model allows research in the area of broad contact patch features, such as the effects of contact patch shape, the number and size of grooves, the amount of lateral drainage, etc.. The practical use of the contact patch program to analyse car tyre contact patches is limited by the complexity of the mesh required (and hence the computer time for solution). The contact patch program can, however, certainly be used to model truck tyres, as the tread patterns are much simpler and therefore the finite element mesh required to model them is also simpler.

To gain the most benefit from the contact patch computer program in its present form it would be desirable that the contact patch stiffnesses, for any tyre that was to be modelled, were measured. Once typical values for the variation in contact patch stiffnesses are known, these could be used on new tyre designs of similar size and construction, to allow the prediction of the properties before any new tyre is manufactured.

The contact patch computer program produces results which are in closest agreement with those measured experimentally for the case of tyres under locked conditions. As will be discussed in section 8.3.1 this is thought to be due to the method of modelling the contact patch movements in this case. The results for both the plain and grooved tyres show good agreement with measured values under locked conditions.

The results that were presented in chapter 6 allow some conclusions on the behaviour of tyre contact patches to be made. The fluid pressures in the tyre/road interface are not of primary importance in determining the wet grip level. The important feature is the fluid film thickness. As has been discussed in sections 6.6.1 and 6.6.2, the effect of adding grooves to a plain tyre is to reduce the general level of film thickness in the tyre/road interface. If this is achieved, then in practice, the microtexture of the road surface will have a greater opportunity of breaking-down this film and establishing tyre/road contact. In section 1.2.1, the relationship between tyre/road friction and the actual area of tyre/road contact was discussed, and it was shown in (4) that the friction is proportional to the area of contact. Therefore, by maximizing the area of actual contact (lower film thicknesses) the friction level will also be maximized, assuming that the tyre tread compound and road surface microtexture effects remain constant.

By comparing the results for the grooved and plain tyres it can be seen that, whilst the grooves improve the wet grip level, they do encourage more of the water in the path of the tyre to pass through the contact patch. A design of tread pattern which provides the benefits of grooves within the contact patch, whilst preventing the flow of water into the front of the contact patch would seem attractive. In practice this could possibly mean reducing the amount of longitudinal grooving in favour of more lateral grooving. Lateral grooves also have the advantage that they allow water to escape out of the side of the contact patch. Without lateral grooves this is restricted because of the low film thicknesses in the shoulder regions. A tread pattern design which allows the longitudinal grooves to close-up at the front of the contact patch and open within the contact patch would also reduce the amount of water passing through the contact patch.

The block analysis computer program allows the detailed study of tyre tread blocks. The example shown of a square tread block shows poor agreement with measured values. This is because of the lack of flow boundary conditions in the case of a sliding block. Further work needs to be performed (possibly with the contact patch program) to allow the specification of flow boundary conditions for a sliding block.

The analysis of blocks under squeezing conditions allows the evaluation of block performance without the problems associated with flow boundary conditions. The analysis of the effects of cut-outs and sipes on blocks is an important area of use for this model. It was shown for the ELITE block that the addition of cut-outs provided a significant improvement in the wet grip level. At present these cut-outs are often included for aesthetic reasons, and not to improve the wet grip level. In future, the size, position, and number of these cut-outs should be considered carefully from the point of view of improving wet grip.

The block analysis program, when used in conjunction with the mesh generation program, provides a useful tool which the designer can use without specialist knowledge of the finite element method. The results of such an analysis can easily be displayed in graphical form, such as the results presented in chapter 6. This allows a comparison to be made between alternative block designs.

The experimental techniques which have been developed here, allow the routine measurement of fluid presure for all tread patterns under locked conditions, and with the extensions suggested in section 8.3.2 also for all rolling tyres. The technique developed for the measurement of fluid film thickness, given that there are still a number of problems, is capable of measuring film thickness on unmodified tyres. This is something which does not appear to have been possible with other methods (discussed in section 1.2.1). As the level of fluid film thickness is thought to be very important in determining wet grip level, the development of a technique for measuring this is also very important.

8.3 SUGGESTIONS FOR FURTHER WORK

The further work to extend that performed in this project can be split into two categories:

Computer Model
Experimental Techniques

These will now be dealt with separately.

8.3.1 Computer Model

The computer programs presented in chapter 4 could be extended in many ways. The following suggestions are mainly concerned with areas of tyre wet grip behaviour which are little understood, and therefore, for which the greatest assumptions had to be made in developing the mathematical model.

As was discussed in the conclusions (section 8.2), the area where the results of the analytical solution differ most from those of the experiments, is for free rolling tyres. The reasons for this appear to be in the assumptions made about the movements within the contact patch, particularly vertical movements. In section 3.8.2 when the method used was being developed, it was realised that it would not be an accurate model, but owing to a lack of any further information some assumptions had to be made.

Suggestions are made in section 3.8.2 as to the possible behaviour of a tyre under free rolling conditions. If experiments are performed to confirm this then the modifications to the computer program would be relatively simple. This would involve there being vertical 'squeezing' velocities at points other than those in the area ahead of the dry contact patch, and those velocities would depend on the deformed shape of the tyre.

The actual movements of the tyre tread surface under both low and high speed conditions could be studied, by recording the path followed by a particular point on the tyre periphery as it entered and left the contact patch. It would also be desirable if a technique were developed so that the movement of a point on the tyre periphery could be studied under wet conditions.

Connected with the above work, to some extent, is the need for further study of the behaviour of water ahead of the front of the contact patch. This is an area which does not appear to have been studied in the past, and if further information were gained, either experimentally or theoretically, then it may be possible to improve the specification of boundary conditions at the front edge of the contact patch.

A second area of the computer model where assumptions are made is in the deflection of the tyre due to fluid pressure. The technique used is based on a semi-infinite method and, as is discussed in

section 3.10.3, gives a good compromise between complexity and accuracy. The method used could be changed to a more complex one, perhaps based on the finite element method, or alternatively the basic method used here could be developed. The second of these alternatives would seem to be the more promising. The area where the semi-infinite technique models the case of a tyre contact patch least well, is in the assumption of infinite thickness of the tread material. The thickness of the tread rubber is actually approximately 15 mm to the breakers, although the breakers are not completely rigid. Experiments could be performed on tyres to give a correction factor to the deflections predicted by the semi-infinite method. This could then be extended to allow the tyre to be stiffer in different parts of the contact patch. A simpler method of obtaining the same result would be to use the facility already built into the contact patch computer program, where the stiffness of the contact patch at each node is supplied as input data, in a similar way to the dry contact pressures. There is then no need for any assumptions about the modulus etc. of the tread material, and also no need for modification of the computer program.

At present no values are available for local vertical stiffnesses at different parts of the contact patch. Experiments would therefore have to be performed, and it is envisaged that the following method would yield the desired results. The tyre could be loaded against a flat plate and a probe in this plate would measure the dry contact pressure. If this probe were then adjusted so that it indented into the contact patch, a higher 'contact pressure' would be measured corresponding to a given local deflection. This could then be repeated for other values of local deflection. If the local deflections (indentations) were kept small (say less than 3 mm), then the response would probably be relatively linear and the stiffness could be found from the slope of the local load/local deflection curve. If the relationship was found not to be linear (to a first approximation) then the computer program could be modified to account for this by using different local stiffnesses for different values of local deformation. By using actual experimental values of stiffness to link fluid

pressure and the tyre deformation, it is thought that a good representation of tyre contact patch behaviour would be given.

At present within the contact patch computer program, instabilities can occur (under certain conditions) in the iterative process between the fluid pressures and contact patch deflections. These could be due to either a physical phenomenon, or the iterative solution technique as discussed in section 4.5.6. The very high repeatability between successive pressure measurements tends to suggest that this is not a physical phenomenon, although further work is required to confirm this conclusively. If one assumes that these instabilities are due to the iterative solution technique, then the problem could be overcome by formulating the complete problem in terms of one differential equation. The appropriate variational principle could then be found and the finite element method used to gain a discrete solution without the pressure/deflection iterations required at present. To enable this to be possible the deflection of the contact patch, as discussed above, would have to be further investigated.

At present the tread block analysis computer program allows the modelling of sipes by a very much simplified method. The pressure within the sipes is taken to be atmospheric (zero). This is the case when sipes will have the most effect, and is the opposite extreme case to neglecting the effect of sipes in the analysis. In the case of a closed end sipe the above assumption is that the sipe is empty of water and that it provides a perfect sink. Whilst this may or may not be true when the sipe enters the contact patch, it is certainly not true for any length of time, as water will quickly flow into the sipe and fill it. An open end sipe will not fill in the same way as a closed end sipe, as it is able to drain some water to the adjacent groove. This drainage of water from an open end sipe means that there is a pressure gradient along the sipe.

Based on the above assumptions about the action of sipes the following modifications could be made to the sipe modelling method:

Closed End Sipes - the 'time' stepping facility could be utilized and the pressure in a closed end sipe allowed to build up to that of the surrounding block in a number of steps.

Open End Sipes - the sipe could be treated as a narrow slot and a pressure distribution from the inner to outer end used. In a narrow slot the pressure drop is linear; therefore an approximation to the behaviour of an open ended sipe could be made by using the surrounding block pressure at the inner end of the sipe, with a linear drop to the groove pressure (atmospheric) at the outer end of the sipe.

Both the above would be relatively simple to incorporate into the block analysis computer program and would give some improvement in sipe modelling, although further experimental work on the fundamental behaviour of sipes is needed before they can be modelled accurately.

In common with all finite element problems the solution here is sensitive to the bandwidth of the finite element mesh. A bandwidth minimization, node renumbering, technique could be incorporated into the computer programs and would give a reduction in the amount of computer time required. This would be important if the computer techniques, particularly the block analysis program, were to be incorporated into a Computer-Aided-Design System, so that analysis could be carried out during the actual design process.

8.3.2 Experimental Techniques

Some future experimental work has already been discussed in the previous section, where that work is required to allow the computer programs to be further developed. The suggestions in this section are for developments to the testing techniques developed in this project, in particular on the High Speed Cornering Force Machine.

As was discussed in section 5.4, the test techniques on the cornering force machine are at present only suitable for free rolling tests on tyres with plain or circumferentially grooved patterns, and for locked wheel tests on any tread pattern. This is because the rotational position of the wheel is not recorded. If the rotational position of the wheel is known then it is possible to build up a "picture" of the pressure (or film thickness) for any tread pattern. This can be achieved by use of a shaft encoder on the wheel axle and also it would be beneficial if an encoder were also used on the drum axle, rather than the present single pulse per revolution. Therefore, with knowledge on the position of both the transducer and the tread pattern a map of the distribution over the contact patch could be built up.

To achieve the most value from the above extension to testing on the cornering force machine, it would also be desirable to improve the data logging and analysis techniques. As was discussed in section 5.4.4 the use of a computer to log the data directly by use of an analogue to digital converter (ADC) was considered, but was not possible because of time constraints. If encoders are added, then their output as well as the pressure or film thickness output could be fed to a computer so that the data could be syncronized and analysed immediately.

The above two extensions to the testing technique would allow the measurement of fluid pressure in the tyre/road contact area on a routine basis on standard tyres. Before this can be achieved with fluid film thickness measurements further developments are required.

In section 5.4.5 the need to use a random distribution of fibres in the common end of the film thickness measurement probe was discussed. This is because at the low film thicknesses found in tyres moving at 50 Kph the signal output is lost in noise. Therefore, to cover the full range of film thicknesses found for tyres moving at all speeds two separate fibre optic probes are required, each with a different distribution of transmit and receive fibres.

An identical fibre optic probe to the one used is available but with a random distribution of fibres; this would be directly interchangeable. However, as there is a spare mounting position available in the surface shells, the second probe could be added (along with the necessary electronics) to allow the selection of the appropriate probe to suit the test conditions.

A further problem with the film thickness measurement method is that it utilizes the reflectivity of the tyre tread surface; therefore a method of monitoring any changes in this is required. This is particularly important when tests with locked tyres are being performed as it was found that under these circumstances the tread surface in the contact patch tended to 'polish', therefore effecting the gain of the film thickness output signal.

When an improved glass plate facility is available, the possibility of gaining quantitative values of fluid film thickness can be further explored. To achieve this there needs to be more control over the lighting conditions both when the photograph is taken, and when it is being analysed.

REFERENCES

(1) ALLBERT, B.J. and WALKER, J.C., "Tyre to Wet Road Friction at High Speeds", Proc. Instn. Mech. Engrs. Vol. 180 Pt.2A No. 4, 1965-66.

(2) BOND, R., "The Optimisation of Tyre-Road Friction", Ph.D Thesis, Department of Transportation and Environmental Planning, University of Birmingham, March 1976.

(3) MOORE, D.F., "Tyre Traction Under Elastohydrodynamic Conditions", Friction and Traction, Proc. 7th Leeds-Lyon Symp. on Tribology, D. Dowson, C.M. Taylor, M. Godet, D. Berthe (eds), Session VIII, Paper VIII(iii), Sept 9-12 1980.

(4) GOUGH, V.E., "Friction of Rubber on Lubricated Surfaces", contribution to discussion of paper by D. Tabor, Rev. Gen. du Caoutchouc., 36 (No. 10) 1409, 1959.

(5) BONESS, R.J., "A Theoretical Treatment of the Aquaplaning Tyre", Automobile Engineer, June 1968.

(6) BATHELT, H., "Calculation of the Aquaplaning Behaviour of Smooth and Profiled Tyres", ATZ Automobiltechnische Zeitschrift, 75 (1973) 10.

(7) GOLDEN, J.M., "A Theory of Wet Road-Tyre Friction", Wear, pp. 307-331, 71 (1981).

(8) LIPPMANN, S.A., and OBLIZAJEK, K.L., "The Distributions of Stress Between the Tread and the Road for Freely Rolling Tires", S.A.E. 740072, Automotive Engineering Congress, Detroit, Mich., February 25-March 1, 1974.

(9) BROWNE, A., CHENG, H. and KISTLER, A., "Dynamic Hydroplaning of Pneumatic Tires", Wear, pp. 1-28, 20 (1972).

(10) BROWNE, A.L., "Tire Deformation During Dynamic Hydroplaning" , Tire Science and Technology,TSTCA, Vol. 3, No. 1, pp. 16-28, Feb. 1975.

(11) BROWNE, A.,L, "Computer-Aided Prediction of the Effect of Tire Tread Pattern Design on Thick Film Wet Traction", General Motors Research Publication GMR-2487, 21 July 1977.

(12) BROWNE, A.L. and WHICKER, D., "An Interactive Tire-Fluid Model for Dynamic Hydroplaning" , Frictional Interaction of Tire and Pavement, ASTM STP 793, W.E. Meyer and J.D. Walter, Eds., American Society for Testing and Materials, pp. 130-150, 1983.

(13) AGRAWAL, S.K. and HENRY, J.J., "A Simple Tire Deformation Model for the Transient Aspect of Hydroplaning" , Tire Science and Technology, Vol. 8, Nos. 3-4, pp. 23-36, July-Dec. 1980.

(14) BENSON,W., HENRY, J.J. and ADAMS, W.S., "A Tread-Deflection Measurement System Utilized in Tire Hydroplaning Studies", S.A.E. 800243, February 1980.

(15) TIMOSHENKO, S.P. and GOODIER, J.N., "Theory of Elasticity", Third Edition, McGraw-Hill Book Company, 1970.

(16) BROWNE, A.L., "Fluid Film Thickness Measurement with Moiré Fringes", Applied Optics, Vol. 11, No. 10, October 1972.

(17) ROBERTS, A.D., "Studies of Lubricated Rubber Friction , Part 2: Optical techniques applied to practical problems", Tribology International, June 1977.

(18) HORNE, W.B. and DREMER, R.C., "Phenomena of Pneumatic Tire Hydroplaning", NASA TN D-2056, National Aeronautics and Space Administration, Washington D.C., Nov. 1963.

(19) ANON, Dunlop Car Tyre Data Book, Tyre Technical Division, Fort Dunlop, Birmingham, April 1981.

(20) BROWNE, A.L., "Mathematical Analysis for Pneumatic Tire Hydroplaning", Surface Texture Versus Skidding: Measurements, Frictional Aspects and Safety Features of Tire-Pavement Interactions, ASTM STP 583, American Society for Testing and Materials, pp. 75-94, 1975.

(21) YEAGER, R.W. and TUTTLE, J.L., "Testing and Analysis of Tire Hydroplaning", S.A.E. 720471, May 1972.

(22) MOSLEY, J.H., "The Improvement of Glass Plate Photograph Techniques by use of a Polarizing Filter and Image Analyser", Dunlop Internal Report, TD1307, November 1982.

(23) BROWNE, A.L., WHICKER, D. and ROHDE, S.M., "The Significance of Tread Element Flexibility to Thin Film Wet Traction", Tire Science and Technology, TSTCA, Vol. 3, No. 4, pp. 215-234, Nov. 1975.

(24) BROWNE, A.L. and WHICKER, D., "Design of Tire Tread Elements for Optimum Thin Film Wet Traction", S.A.E. 770278, March 1977.

(25) ROHDE, S.M. WHICKER, D. and BROWNE, A.L., "Dynamic Analysis of Elastohydrodynamic Squeeze Films", Transactions of The ASME, Journal of Lubrication Technology, Vol. 98, No. 3, July 1976.

(26) WHICKER, D., BROWNE, A.L. and ROHDE, S.M. "Some Effects of Inclination on Elastohydrodynamic squeeze film Problems", J. Fluid Mech., Vol. 78, part 2, pp. 247-260, 1976.

(27) BIRD, K.D. and MARTIN, J.K., "The Calspan Tire Research Facility: Design, Development and Initial Test Results", S.A.E. 730582, May 1973.

(28) NILSSON, N., "Air Resonant and Vibrational Radiation-Possible Mechanisms for Noise from Cross-Bar Tires", International Tire Noise conference, Stockholm, August 28-31, 1979.

(29) HENRY, J.J. and HEGMON, R.R., "Pavement Texture Measurement and Evaluation", Surface Texture Versus Skidding: Measurements, Frictional Aspects, and Safety Features of Tire-Pavement Interactions, ASTM STP 583, American Society for Testing and Materials, pp. 3-17, 1975.

(30) DOTY, R.N., "Study of the Sand Patch and Outflow Meter Methods of Pavement Surface Texture Measurement", Surface Texture Versus Skidding: Measurements, Frictional Aspects and Safety Features of Tire-Pavement Interactions, ASTM STP 583, American Society for Testing and Materials, pp. 42-61, 1975.

(31) CAMERON, A., "Basic Lubrication Theory", Second Edition, John Wiley and Sons, ISBN 853120579, 1976.

(32) GROSS, W.A., et al., "Fluid Film Lubrication", John Wiley and Sons, 1980.

(33) FULLER, D.D., "Theory and Practice of Lubrication for Engineers", John Wiley and Sons, 1956.

(34) MASSEY, B.S., "Mechanics of Fluids", 3rd Edition, Van Nostrand Reinhold Company Ltd., ISBN 0 442 30021 2, 1975.

(35) JAKOBSSON, D. and FLOBERG, L., "The Rectangular Pad Bearing", Transactions of Chalmers University of Technology, Gothenburg, Nr. 203 (Report No. 5, Institute of Machine Elements) 1958.

(36) DOWSON, D. and HIGGINSON, G.R., "A Numerical Solution To The Elasto-Hydrodynamic Problem", Journal of Mechanical Engineering Science, Vol. 1, No. 1, pp. 6-15, 1959.

(37) DOWSON, D. and TAYLOR C.M., "Elastohydrostatic Lubrication of Circular Plate Thrust Bearings", Transactions of the ASME, Journal of Lubrication Technology, July 1967.

(38) CASTELLI, V., RIGHTMIRE, G.K. and FULLER, D.D., "On the Analytical and Experimental Investigation of a Hydrostatic Axisymmetric Compliant-Surface Thrust Bearing", Transactions of the ASME, Journal of Lubrication Technology, October 1967.

(39) GUPTA, P.K., "Incipient Lift-Off in Preloaded Plane Externally-Pressurized Compliant Surface Bearings", Proc. Instn. Mech. Engrs. Vol. 188 42/74, 1974.

(40) ELROD, H.G. and NG, C.W., "A Theory for Turbulent Fluid Films and Its Application to Bearings", Transactions of the ASME, Journal of Lubrication Technology, July 1967.

(41) CONSTANTINESCU, V.N., "Basic Relationships in Turbulent Lubrication and Their Extension to Include Thermal Effects", Transactions of the ASME, Journal of Lubrication Technology, Paper No. 72-Lub-16, 1972.

(42) TAYLOR, C.M. and DOWSON, D., "Turbulent Lubrication Theory-Application to Design", Transactions of the ASME, Journal of Lubrication Technology, January 1974.

(43) CAPITAO, J.W., "Influence of Turbulence on Performance Characteristics of the Tilting Pad Thrust Bearing", Transactions of the ASME, Journal of Lubrication Technology, January 1974.

(44) WILCOCK, D.F., "Turbulent Lubrication - It's Genesis and Role in Modern Design", Transactions of the ASME, Journal of Lubrication Technology, January 1974.

(45) WILCOCK, D.F., "Designing Turbulent Bearings for Reduced Power Loss", Paper X(i), Proceedings of the Leeds-Lyons Symposium, Sept. 1975.

(46) WILCOCK, D.F., "Design of Efficient Turbulent Thrust Bearings", Transactions of the ASME, Journal of Lubrication Technology, January 1977.

(47) CONSTANTINESCU, V.N., PAN, C.H.T. SMALLEY, A.J. and VOHR, J.H., "Lubrication Phenomena in a film of Low Kinematic Viscosity", Romanian Journal of Technical Sciences, Rev. Roum. Sci. Techn.-Mec. Appl., Tome 15, No. 2, pp. 479-502, 1970.

(48) ZIENKIEWICZ, O.C., "The Finite Element Method", Third Edition, McGraw-Hill Book Company Ltd., 1977.

(49) DESAI, C.S. and ABEL, J.F., "Introduction to the Finite Element Method: A Numerical Method for Engineering Analysis", Van Nostrand Reinhold Company, 1972.

(50) SEGERLIND, L.J., "Applied Finite Element Analysis", John Wiley and Sons, 1976.

(51) TAYLOR, C. and HUGHES, T.G., "Finite Element Programming of the Navier-Stokes Equations", Pineridge Press Ltd., 1981.

(52) HINTON, E. and OWEN, D.R.J., "An Introduction to Finite Element Computations", Pineridge Press Ltd., 1979.

(53) REDDI, M.M., "Finite-Element Solution of the Incompressible Lubrication Problem", Transactions of the ASME, Journal of Lubrication Technology, July 1969.

(54) REDDI, M.M. and CHU, T.Y., "Finite Element Solution of the Steady-State Compressible Lubrication Problem", Transactions of the ASME, Journal of Lubrication Technology, July 1970.

(55) BOOKER, J.K. and HUEBNER, K.H., "Application of Finite Element Methods to Lubrication: An Engineering Approach", Transactions of the ASME, Journal of Lubrication Technology, October 1972.

(56) WADA, S., HAYASHI, H. and MIGITA, M., "Application of Finite-Element Method to Hydrodynamic Lubrication Problems (Part 1)", Bulletin of the JSME, Vol. 14, No. 77, pp. 1222-1233, 1971.

(57) WADA, S. and HAYASHI, H., "Application of Finite-Element Method to Hydrodynamic Lubrication Problems (Part 2: Finite-Width Bearings)", Bulletin of the JSME, Vol. 14, No. 77, pp. 1234-1243, 1971.

(58) ALLAIRE, P.E., NICHOLAS, J.C. and GUNTER, E.J., "Systems of Finite Elements for Finite Bearings", Transactions of the ASME, Journal of Lubrication Technology, April 1977.

(59) TAYLOR, C. and O'CALLAGHAN, J.F., "A Numerical Solution of the Elastohydrodynamic Lubrication Problem Using Finite Elements", Journal of Mechanical Engineering Science, Vol. 14, No. 4, 1972.

(60) OH, K.P. and HUEBNER, K.H., "Solution of the Elastohydrodynamic Finite Journal Bearing Problem", Transactions of the ASME, Journal of Lubrication Technology, July 1973.

(61) ROHDE, S.M. and OH, K.P., "A Unified Treatment of Thick and Thin Film Elastohydrodynamic problems by Using Higher Order Element Methods", Proc. R. Soc. Lond. A. 343, pp. 315-331 (1975).

(62) FREDERICK, C.O., WONG, Y.C. and EDGE, F.W., "Two-Dimensional Automatic Mesh Generation for Structural Analysis", International Journal for Numerical Methods in Engineering, Vol. 2, pp. 133-144 (1970).

(63) ANDERSON, J., "True Integration of FEA and CAD/CAM", Computer Systems, Techpress Publishing Company Ltd., Bromley, March 1982.

(64) STRICKLIN, J.A., "Integration of Area Coordinates in Matrix Structural Analysis", AIAA Journal, Vol. 6, No. 10, pp. 2023, 1968.

(65) HINTON, E. and CAMPBELL, J.S., "Local and Global Smoothing of Discontinuous Finite Element Functions Using a Least Squares Method", International Journal for Numerical Methods in Engineering, Vol. 8, pp. 461-480, 1974.

(66) TAYLOR, C.M. "Turbulent Lubrication Theory Applied to Fluid Film Bearing Design", Tribology Convention, Procedures of the Institution of Mechanical Engineers, at Brighton, Vol. 18A, Part 3L, 1970.

(67) TAVAZZA, G. and CERVI, E., "Finite Element Techniques to Design Tyres", ISATA 80, International Symposium on Automotive Technology and Automation-Turin, September 1980.

(68) ANON, "Standard Test Method for Skid Resistance of Paved Surfaces Using a Full-Scale Tire", American National Standard, ANSI/ASTM E274, 1979.

(69) LONGHURST, R.S., "Geometrical and Physical Optics", Longmans, 1964.

(70) GALL, M.H.W., "Recent Applications of Slip Ring Assemblies", Strain, November 1981.

(71) LAGACE, L.J. and KISSINGER, C.D., "Non-Contact Displacement and Vibration Measurement Systems Employing Fiber Optic and Capacitance Transducers", Instrument Society of America, ISBN 87664-362-4, 23rd International Instrumentation Symposium, Las Vegas, Nevada, 1-5 May, 1977.

(72) CLARK, S.K. (editor), "Mechanics of Pneumatic Tires", U.S. Department of Transportation, National Highway Traffic Safety Administration, Washington D.C., 1981.

(73) ANON, "Road Accidents Great Britain 1981", Department of Transport; Scottish Development Department; Welsh Office, HMSO, London, 1982.

APPENDIX A - FORMULATION OF THE GOVERNING EQUATIONS

As was stated in section 3.3 the equation governing the fluid flow between a tyre and a road surface will be represented by Reynolds equation in the form:

$$\frac{\partial}{\partial x}\left(\frac{h^3}{12\mu_x}\cdot\frac{\partial p}{\partial x}\right) + \frac{\partial}{\partial y}\left(\frac{h^3}{12\mu_y}\cdot\frac{\partial p}{\partial y}\right) = \frac{1}{2}\frac{\partial}{\partial x}(V_x h) + \frac{1}{2}\frac{\partial}{\partial y}(V_y h) + \frac{\partial h}{\partial t} \qquad \text{——A.1}$$

To solve this equation using the Finite Element method a functional 'I' is found such that the pressure which minimizes it satisfies equation A.1 and the boundary conditions. This functional is widely quoted in the literature and its proof is shown in Reddi (53) in particular.

For Reynolds equation with sliding in both the x and y directions and squeezing in the h direction this functional is given by:

$$I = \int_R \left[\frac{h^3}{24\mu_x}\left(\frac{\partial p}{\partial x}\right)^2 + \frac{h^3}{24\mu_y}\left(\frac{\partial p}{\partial y}\right)^2 - \frac{1}{2}hV_x\frac{\partial p}{\partial x} - \frac{1}{2}hV_y\frac{\partial p}{\partial y} + p\frac{\partial h}{\partial t}\right] dA + \int_C qp\, dS \qquad \text{——A.2}$$

where R is the whole of the region in question, and c that part of its boundary on which flow boundary conditions are required. It is possible in certain cases to asign a physical significance to the functional I, especially in solids problems where the case of minimum potential energy for the system is being found, but in this case no such physical significance will be used and I will be treated purely as a convenient mathematical formulation of the problem.

The second integral in equation A.2

i.e. $$I_{FB} = \int_C qp\, dS$$

allows the specification of flow boundary conditions (53). 'q' is the outward normal volumetric flow per unit width, and it will be shown later that the discretization of the problem into elements allows the value of 'q' to be specified differently for different elements on the edge of the domain.

The remaining portion of the boundary (i.e. not c) may have pressure boundary conditions applied; that is to say the value of 'p' may be specified explicitly, and typically in this application:

$p = 0$ on the boundary

However if no boundary condition is specified on a portion of the boundary this implies that there is zero flow ($q = 0$) across that boundary.

This is a very useful feature of the finite element method, which allows an axis of symmetry to be modelled simply by leaving an edge of the domain with no boundary conditions. This can be utilized in the current application when the contact patch of a tyre is symmetric about its centre line, allowing solution by discretising only half of the contact patch.

The value of 'p' which minimizes the functional I is the solution to equation A.1, therefore equation A.2 must now be differentiated with respect to P_i, where i is a global node number.

$$\frac{\partial I}{\partial P_i} = \int_R \left\{ \frac{h^3}{24} \left[\frac{2}{\mu_x} \frac{\partial p}{\partial x} \frac{\partial}{\partial P_i} \left(\frac{\partial p}{\partial x} \right) + \frac{2}{\mu_y} \frac{\partial p}{\partial y} \frac{\partial}{\partial P_i} \left(\frac{\partial p}{\partial y} \right) \right] - \frac{h}{2} V_x \frac{\partial}{\partial P_i} \left(\frac{\partial p}{\partial x} \right) \right.$$

$$\left. - \frac{h}{2} V_y \frac{\partial}{\partial P_i} \left(\frac{\partial p}{\partial y} \right) + \frac{\partial h}{\partial t} \frac{\partial p}{\partial P_i} \right\} dA + \int_c q \frac{\partial p}{\partial P_i} \, dS \qquad \text{------A.3}$$

I is a minimum when

$$\frac{\partial I}{\partial P_i} = 0 \; ; \quad i = 1,2,3,\ldots,n : \quad n = \text{total number of nodes}$$

i.e.

$$\int_R \frac{h^3}{12}\left[\frac{1}{\mu_x}\cdot\frac{\partial p}{\partial x}\cdot\frac{\partial}{\partial P_i}\left(\frac{\partial p}{\partial x}\right) + \frac{1}{\mu_y}\cdot\frac{\partial p}{\partial y}\cdot\frac{\partial}{\partial P_i}\left(\frac{\partial p}{\partial y}\right)\right] dA$$

$$= \int_R \left\{ \frac{h}{2}\left[V_x \frac{\partial}{\partial P_i}\left(\frac{\partial p}{\partial x}\right) + V_y \frac{\partial}{\partial P_i}\left(\frac{\partial p}{\partial y}\right)\right] - \frac{\partial h}{\partial t}\cdot\frac{\partial p}{\partial P_i} \right\} dA$$

$$- \int_C q \frac{\partial p}{\partial P_i} \, dS \qquad \text{------A.4}$$

The solution to equation A.4, is the required solution over the whole domain R in terms of the general pressure 'p'.

The functional I is the sum, over the whole of the domain, of functionals I_E; where I_E is defined similarly to I in equation A.2 except that it now refers to one element only. The values of I_E can be evaluated for each element, and then summed to allow the solution over the whole domain.

If we consider equation A.3 as being for one node of one element, and calculate each of the terms for the three nodes within that element we can find $[K_L]$ the local stiffness matrix, and $\{F_L\}$ the local generalized force vector for that element. When these are combined with the local stiffness matrices and force vectors for all other elements which include the same node, then

$$\frac{\partial I}{\partial P_i} = 0$$

at that node i.

In the assembly of the global stiffness matrix and force vector this is repeated for each node such that

$$\frac{\partial I}{\partial P_i} = 0 \qquad i = 1,2,3,\ldots,n$$

is true and an equation of the form of A.4 can be written for the whole of the domain. This equation is normally expressed in matrix form as

$$[K].\{p\} = \{F\}$$

where $[K]$ is the global stiffness matrix, $\{p\}$ is a column vector of the unknown pressures, and $\{F\}$ is the global force vector.

Therefore we shall consider equation A.3 for one element where P_i represents one of the three nodes within that element. The pressure at any point within that element can be expressed by the interpolation function, and for three noded triangular elements this is given by (50),

$$p = N_1P_1 + N_2P_2 + N_3P_3$$

where $N_i = \frac{1}{2A}.\left[a_i + b_ix + c_iy\right]$; $i = 1,2,3$ ------A.5

and a_i, b_i, c_i are as defined in (50); the nodes for the element in question are now numbered 1,2 and 3 for convenience.

Therefore $\frac{\partial p}{\partial x} = \frac{\partial N_1}{\partial x} P_1 + \frac{\partial N_2}{\partial x} P_2 + \frac{\partial N_3}{\partial x} P_3$ ------A.6

and, $\frac{\partial p}{\partial y} = \frac{\partial N_1}{\partial y} P_1 + \frac{\partial N_2}{\partial y} P_2 + \frac{\partial N_3}{\partial y} P_3$ ------A.7

and, $\frac{\partial p}{\partial P_i} = N_1 \frac{\partial P_1}{\partial P_i} + N_2 \frac{\partial P_2}{\partial P_i} + N_3 \frac{\partial P_3}{\partial P_i}$ ------A.8

Equation A.5 gives

$$\frac{\partial N_i}{\partial x} = \frac{b_i}{2A} \quad ; \qquad i = 1,2,3 \qquad \text{------A.9}$$

and,

$$\frac{\partial N_i}{\partial y} = \frac{c_i}{2A} \quad ; \qquad i = 1,2,3 \qquad \text{------A.10}$$

Substituting equation A.9 into equation A.6 gives

$$\frac{\partial p}{\partial x} = \frac{b_1P_1 + b_2P_2 + b_3P_3}{2A} \qquad \text{------A.11}$$

and substituting equation A.10 into equation A.7 gives

$$\frac{\partial p}{\partial y} = \frac{c_1P_1 + c_2P_2 + c_3P_3}{2A} \qquad \text{------A.12}$$

Equation A.3 can now be expressed in terms of nodal pressures for one element within the domain by substituting equations A.11, A.12 and A.8 into equation A.3 (i = 1,2 or 3 representing one node of the element).

$$\frac{\partial I_E}{\partial P_i} = \int \frac{h^3}{12} \left[\left(\frac{b_1P_1 + b_2P_2 + b_3P_3}{2A\mu_x}\right) \cdot \frac{\partial}{\partial P_i}\left(\frac{b_1P_1 + b_2P_2 + b_3P_3}{2A}\right) + \left(\frac{c_1P_1 + c_2P_2 + c_3P_3}{2A\mu_y}\right) \cdot \frac{\partial}{\partial P_i}\left(\frac{c_1P_1 + c_2P_2 + c_3P_3}{2A}\right)\right] dA$$

$$- \int \left\{ \frac{h}{2}\left[V_x \frac{\partial}{\partial P_i}\left(\frac{b_1P_1 + b_2P_2 + b_3P_3}{2A}\right) + V_y \frac{\partial}{\partial P_i}\left(\frac{c_1P_1 + c_2P_2 + c_3P_3}{2A}\right)\right] + \frac{1}{2A}\frac{\partial h}{\partial t}\left[(a_1 + b_1x + c_1y)\frac{\partial P_1}{\partial P_i} + (a_2 + b_2x + c_2y)\frac{\partial P_2}{\partial P_i} + (a_3 + b_3x + c_3y)\frac{\partial P_3}{\partial P_i}\right]\right\} dA$$

$$+ \int \frac{q}{2A}\left[(a_1 + b_1x + c_1y)\frac{\partial P_1}{\partial P_i} + (a_2 + b_2x + c_2y)\frac{\partial P_2}{\partial P_i} + (a_3 + b_3x + c_3y)\frac{\partial P_3}{\partial P_i}\right] dS$$

------A.13

Equation A.13 applies to the three nodes of the element, and 'dA' now refers to the area of that element and not the area of the domain. Similarly 'dS' refers to the edge of the element (if any) which is on that part of the boundary which is to have flow boundary conditions applied.

Simplifying gives,

$$\frac{\partial I_E}{\partial P_i} = \int \frac{h^3}{12}\left[\frac{(b_1P_1 + b_2P_2 + b_3P_3)}{2A\mu_x}\cdot\frac{b_i}{2A} + \frac{(c_1P_1 + c_2P_2 + c_3P_3)}{2A\mu_y}\cdot\frac{c_i}{2A}\right] dA$$

$$- \int \frac{h}{2}\left[V_x\,\frac{b_i}{2A} + V_y\,\frac{c_i}{2A}\right] dA + \int \frac{\partial h}{\partial t}\cdot\frac{(a_i + b_ix + c_iy)}{2A} \quad dA$$

$$+ \int q.\frac{(a_i + b_ix + c_iy)}{2A}\, dS \qquad \text{------A.14}$$

Equation A.14 initially looks rather difficult to integrate explicitly, but the only variables involved are x, y and h.

Once again the linear interpolation function is (50),

$$p = N_1P_1 + N_2P_2 + N_3P_3$$

where N_1, N_2 and N_3 are known as the area coordinates of the element. The fluid film thickness variation throughout the element can also be expressed in terms of area coordinates i.e.

$$h = N_1H_1 + N_2H_2 + N_3H_3 \qquad \text{------A.15}$$

A useful property of area coordinates which was shown by Stricklin (64) and is quoted in many referances such as (50) or (54), is that integrals of the form

$$I = \int_A N_i^l\, N_j^m\, N_k^n \quad dA$$

where N_i, N_j, N_k are the area coordinates, l, m, n, are integers and A is the area of the triangular element, have a closed-form solution:

$$I = \frac{(l!\ m!\ n!).2A}{(l+m+n+2)!} \qquad \text{------A.16}$$

This solution was obtained by Stricklin by inspection and can easily be verified.

It is convenient to consider equation A.14 as

$$\frac{\partial I_E}{\partial P_i} = I_{①} - I_{②} + I_{③} + I_{④}$$

and perform each of the integrals separately.

Integral $I_{①}$:

Consider $I_{①}$ to be

$$I_{①} = K_k \int h^3 \ dA \qquad \text{------A.17}$$

where K_k is a constant, given by

$$K_k = \frac{1}{12}\left[\frac{(b_1P_1 + b_2P_2 + b_3P_3)}{2A\mu_x}.\frac{b_i}{2A} + \frac{(c_1P_1 + c_2P_2 + c_3P_3)}{2A\mu_y}.\frac{c_i}{2A}\right]$$

Substituting A.15 into A.17 gives

$$I_{①} = K_k\int(N_1H_1 + N_2H_2 + N_3H_3).(N_1H_1 + N_2H_2 + N_3H_3).(N_1H_1 + N_2H_2 + N_3H_3)\,dA$$

Expanding and collecting terms gives

$$I_{①} = K_k\int(N_1^3H_1^3 + N_2^3H_2^3 + N_3^3H_3^3 + 3N_1^2N_2H_1^2H_2 + 3N_1^2N_3H_1^2H_3$$
$$+ 3N_2^2N_1H_2^2H_1 + 3N_2^2N_3H_2^2H_3 + 3N_3^2N_1H_3^2H_1$$
$$+ 3N_3^2N_2H_3^2H_2 + 6N_1N_2N_3H_1H_2H_3)\ dA \qquad \text{------A.18}$$

Using the closed-form solution given in A.16, A.18 can now be integrated to give,

$$I_{①} = 2AK_k\left[\frac{3!}{5!}H_1^3 + \frac{3!}{5!}H_2^3 + \frac{3!}{5!}H_3^3 + 3.\frac{2!1!}{5!}H_1^2H_2 + 3.\frac{2!1!}{5!}H_1^2H_3\right.$$

$$+ \quad 3.\frac{2!1!}{5!}H_2^2H_1 + 3.\frac{2!1!}{5!}H_2^2H_3 + 3.\frac{2!1!}{5!}H_3^2H_1$$

$$\left. + \quad 3.\frac{2!1!}{5!}H_3^2H_2 + 6.\frac{1!1!1!}{5!}H_1H_2H_3\right]$$

Therefore,

$$I_{①} = \frac{AK_k}{10}\left[H_1^3 + H_2^3 + H_3^3 + H_1^2H_2 + H_1^2H_3 + H_2^2H_1 + H_2^2H_3\right.$$

$$\left. + \quad H_3^2H_1 + H_3^2H_2 + H_1H_2H_3\right] \qquad \text{------A.19}$$

For the sake of simplicity we shall define $\overline{h^3}$ as,

$$\overline{h^3} = (H_1^3 + H_2^3 + H_3^3 + H_1^2H_2 + H_1^2H_3 + H_2^2H_1 + H_2^2H_3$$

$$+ H_3^2H_1 + H_3^2H_2 + H_1H_2H_3)/10$$

which makes equation A.19

$$I_{①} = AK_k\overline{h^3} \qquad \text{------A.20}$$

Integral $I_{②}$:

$$I_{②} = \frac{(V_xb_i + V_yc_i)}{4A}\int h\,dA \qquad \text{------A.21}$$

(assuming that V_x and V_y are uniform across the element)

Substituting A.15 into A.21 gives,

$$I_{②} = \frac{(V_xb_i + V_yc_i)}{4A}\int(N_1H_1 + N_2H_2 + N_3H_3)\,dA \qquad \text{------A.22}$$

Using A.16, A.22 can now be integrated:

$$I_{②} = \frac{(V_x b_i + V_y c_i)}{4A} \cdot 2A \left[\frac{1!}{3!} H_1 + \frac{1!}{3!} H_2 + \frac{1!}{3!} H_3 \right]$$

Therefore,

$$I_{②} = \frac{(V_x b_i + V_y c_i)}{4} \left[\frac{H_1 + H_2 + H_3}{3} \right] \qquad \text{------A.23}$$

It can be seen that the term in square brackets in equation A.23 is the mean fluid film thickness of the element, which we shall represent by $\bar{h}$, where,

$$\bar{h} = \frac{H_1 + H_2 + H_3}{3} \qquad \text{------A.24}$$

Therefore substituting A.24 into A.23 gives,

$$I_{②} = \frac{(V_x b_i + V_y c_i)}{4} \bar{h} \qquad \text{------A.25}$$

Integral $I_{③}$:

$$I_{③} = \int \frac{\partial h}{\partial t} \cdot \frac{(a_i + b_i x + c_i y)}{2A} \, dA \qquad \text{------A.26}$$

but $\frac{(a_i + b_i x + c_i y)}{2A} = N_i$, from A.5

Therefore A.26 becomes,

$$I_{③} = \frac{\partial h}{\partial t} \int N_i \, dA \qquad \text{------A.27}$$

and using A.16, A.27 can be integrated:

$$I_{③} = \frac{\partial h}{\partial t} \left[\frac{1!}{3!} \right] 2A$$

Therefore,

$$I_{③} = \frac{\partial h}{\partial t} \cdot \frac{A}{3} \qquad \text{------A.28}$$

Integral $I_{④}$:

Integral $I_{④}$, which represents the flow boundary conditions on specified sides of certain elements, cannot be treated in the same manner as integrals $I_{①}$, $I_{②}$ and $I_{③}$, as $I_{④}$ is to be integrated with respect to 'S', the edge of the element and not the area of the element as in the other cases.

$$I_{④} = \int q \left(\frac{a_i + b_i x + c_i y}{2A}\right) \quad dS \qquad \text{------A.29}$$

Also q is the outward normal flow across the boundary S, and it would be more covenient in this application to have separate x and y components of q, so that as is discussed in section 3.7.4, q can be easily related to vehicle motion.

Figure A.1 shows a typical element. If edge 1-3 is on the edge of the region where a flow boundary condition is imposed, it can be seen that

$$qdS = -q_x dy + q_y dx$$

$$\text{therefore} \qquad qdS = \left(\frac{-q_x L_y}{L} + \frac{q_y L_x}{L}\right) dS \qquad \text{------A.30}$$

where L is the length of the side, and L_x and L_y are the projections of the side on the two coordinate axes.

We shall assume that the flow across the edge of one element is constant over that edge.

As before,

$$\frac{a_i + b_i x + c_i y}{2A} = N_i \quad ;$$

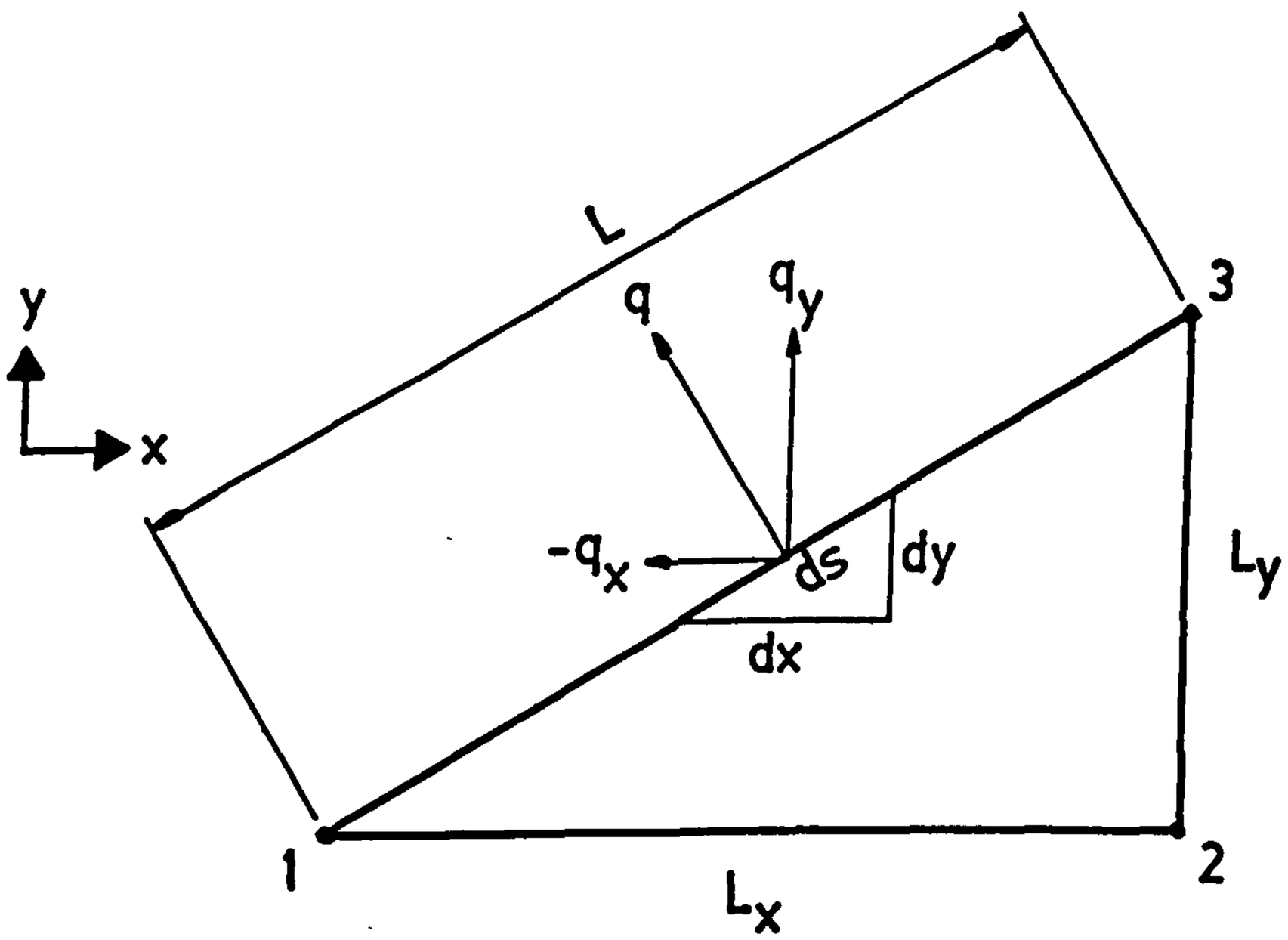

FIGURE A.1 - FLOW BOUNDARY CONDITIONS FOR A TYPICAL ELEMENT

therefore A.29 becomes,

$$I_{④} = \left(\frac{-q_x L_y + q_y L_x}{L}\right) \int_{1-3} N_i \quad dS \qquad \text{------A.31}$$

A second identity, similar to the one (A.16) which allowed integration over the area of the element, exists and is quoted in Segerlind (50); this allows integration along the edge of an element for an expression in terms of area coordinates:

$$I = \int_{\text{edge } ij} N_i^l \, N_j^m \quad dS \qquad \text{------A.32}$$

where N_i and N_j are area coordinates, and l and m are integers. The closed-form solution is given by,

$$I = \frac{(l!\ m!)}{(l + m + 1)!} \, L \qquad \text{------A.33}$$

where L is the length of the edge i,j. A.31 can thus be integrated to give,

$$I_{④} = \frac{1}{2}\left(q_y L_x - q_x L_y\right) \qquad \text{------A.34}$$

<u>Assembly of the Integrated Form of Equation A.14</u>

The four integrals can now be assembled in the form

$$\frac{\partial I_E}{\partial P_i} = I_{①} - I_{②} + I_{③} + I_{④}$$

to give the integrated form of equation A.14.

$$\frac{\partial I_E}{\partial P_i} = \frac{\overline{h^3}}{48A}\left[\frac{(b_1P_1 + b_2P_2 + b_3P_3).b_i}{\mu_x} + \frac{(c_1P_1 + c_2P_2 + c_3P_3).c_i}{\mu_y}\right]$$

$$- \frac{\overline{h}}{4}.(V_x b_i + V_y c_i) + \frac{A}{3}.\frac{\partial h}{\partial t} + \left\{\frac{1}{2}.(q_y L_x - q_x L_y)\right\} \qquad \text{------A.35}$$

A.35 is for one node of one element, and there will be a total of three equations of this type for each element. The term in $\{\}$ brackets will only be applied in elements which have an edge on the edge of the domain and then only to nodes which lie on that edge (provided that portion of the edge of the domain is to have flow boundary conditions applied).

Equation A.35 must therefore be evaluated for each node of each element within the mesh, so then when combined

$$\frac{\partial I}{\partial P_i} = 0 \quad \text{at every node} \quad i = 1,2,3,\ldots,n$$

The equations governing the complete system can then be expressed as

$$[K] \cdot \{p\} = \{F\} \qquad \text{------A.36}$$

where $[K]$ is made up of the first term on the RHS of equation A.35, for each node of each element. $\{F\}$ is made up of the remaining terms on the RHS of equation A.35.

The resulting system of simultaneous equations can then be solved by one of the standard methods.

APPENDIX B - SOURCE LISTINGS OF COMPUTER PROGRAMS

FOR REFERENCE ONLY - IN SEPARATE FOLDER IN DEPARTMENT OF FLUID ENGINEERING AND INSTRUMENTATION.